BaBar Analysis Document #1586, Version 8
March 11, 2008

Global Fit for Branching Fractions of $B \to D^{(*)}\ell\nu$ Decays and Form Factor Slope of $B \to D\ell\nu$ Decays

Kenji Hamano (University of Victoria)
Robert V. Kowalewski (University of Victoria)

Abstract

We present details of our Global fit analysis in $B \to D^{(*,**)}(\pi)\ell\nu$ decays. We use 86×10^6 $B\bar{B}$ events collected by the Babar detector. The primary target of this analysis is to determine the branching fractions and form factor parameters of $B \to D\ell\nu$ and $B \to D^*\ell\nu$ decays and to extract $\mathcal{G}(1)|V_{cb}|$ and $\mathcal{F}(1)|V_{cb}|$.

Main changes from previous version

- Calculation of $\cos\theta_{B-Dl}$ in section 3
- Inclusive $B \to D(D_s)$ re-weighting is reviewed. See section 9.1.4 and 9.4
- Beam energy correction in section 9
- Test fit resluts and the process to reach nominal fit configuration is explainde in section 12 - 18

To Do list

- See postings on review HN.

Contents

List of Figures

List of Tables

1 Introduction

The Cabbibo-Kobayashi-Maskawa (CKM) Matrix [1][2] plays an important role in quark mixing and CP violation. The matrix elements of it are free parameters of the Standard Model of particle physics. They need to be determined by experiments. As a B-factory, Babar can measure some of the CKM matrix elements, such as $|V_{ub}|$ and $|V_{cb}|$, in a good precision. To extract $|V_{cb}|$, semileptonic $B \to X_c \ell \nu$ decays have been used. Here, X_c denotes a charmed meson or a particle system including a charmed meson, and ℓ an electron or a muon. Especially two exclusive decay modes, $B \to D^* \ell \nu$ and $B \to D \ell \nu$ have been very useful. A study of these decay modes are also important to measure $|V_{ub}|$ because these are the biggest background of $B \to X_u \ell \nu$ decays. However, there are still unresolved problems in these decay modes such as

- $B^0 \to D^{*-} \ell^+ \nu$ decay [1] branching fraction measurements disagreement.
- Discrepancy between inclusive and sum of exclusive branching fractions.
- $B \to D \ell \nu$ decay form factor slope is not well measured.
- HQET inspired model for $B \to D^{**} \ell \nu$ decays has not been used to evaluate the contribution from these decays.

In existing measurements, each decay mode is reconstructed exclusively to measure branching fractions or form factor parameters. However, the above problems are related with each other and cannot be easily solved by looking at a single decay mode. It is better to look at all semileptonic $B \to D^{(*,**)}(\pi) \ell \nu$ decay modes at the same time. We use a global fit method which simultaneously determine contributions from D, D^* and $D^{**}(D^{(*)}\pi)$. One analysis from Babar [3][4] has similar goals, and can also reconstruct the full set of $B \to D^{(*,**)}(\pi) \ell \nu$ decays. The analysis is complementary because the ability to distinguish among the different channels is better than in our work but the statistics are much lower since they use hadronic B-tag. Another important point of our fitting method is an ability to access form factor parameters. We implement this by Monte Carlo re-weighting method as explained later. Since it is not easy to determine a correct contribution from a decay mode without using a sufficient form factor, an ability to simultaneously measure branching fractions and form factor parameters is essential.

1.1 Problems in $B \to D^{(*,**)}(\pi) \ell \nu$ decays

There are still problems in semileptonic B to charmed meson decays even though many measurements have been done. We list important ones below.

- $B^0 \to D^{*-} \ell^+ \nu$ decay branching fraction measurements disagreement
  There ia s disagreement between $B^0 \to D^{*-} \ell^+ \nu$ decay branching fraction measurements. Those are summarized in Table 1. The results vary from 0.0459 (BELLE) to 0.0609 (CLEO), and those measurements are not consistent with each other.

[1] Charge conjugate modes are implied throughout this text

- Inclusive-exclusive disagreement
  There are mainly 10 exclusive decay modes of the type $B \to X_c \ell\nu$ (see Appendix A)
  - $B \to D\ell\nu$
  - $B \to D^*\ell\nu$
  - $B \to D_0^*\ell\nu$
  - $B \to D_1\ell\nu$
  - $B \to D_1'\ell\nu$
  - $B \to D_2^*\ell\nu$
  - $B \to D\pi^+\ell\nu$ (non-resonant)
  - $B \to D\pi^0\ell\nu$ (non-resonant)
  - $B \to D^*\pi^+\ell\nu$ (non-resonant)
  - $B \to D^*\pi^0\ell\nu$ (non-resonant)

  The D_0^*, D_1, D_1' and D_2^* are called D^{**} as a whole (see Appendix B).
  The sum of the branching fractions of these exclusive decays is supposed to be consistent with the inclusive $B \to X_c\ell\nu$ branching fractions (this X_c denotes a particle system including a charm quark such as D^* or $D\pi$ etc.). Those branching fractions are summarized in Table 2. In this table, non-resonant $B \to D^{(*)}\pi\ell\nu$ decays and $B \to D^{**}\ell\nu$ decays are combined (see Appendix D). The sum of exclusive modes is consistent with the inclusive branching fraction in case of B^+ decays. However, there is a disagreement in B^0 decays. If $\mathcal{B}(B^0 \to D^{*-}\ell^+\nu)$ is as large as to satisfy isospin symmetry with $\mathcal{B}(B^+ \to \bar{D}^{*0}\ell^+\nu)$, the inclusive and exclusive branching fractions agree. Note that the decay modes which include more than 2 pions such as $D^*\pi\pi\ell\nu$ mode or include D_s such as $D_sK\ell\nu$ mode are not included in the table; however, those contributions are expected to be too small [12] to explain the inclusive exclusive difference.

- $B \to D\ell\nu$ decay form factor slope and $G(1)|V_{cb}|$
  $B \to D\ell\nu$ decay form factor slope, ρ_D^2 (see Appendix H), has never been well measured. Existing measurements are listed in Table 3. The best measurement from BELLE has a 23 % uncertainty. Consequently, the uncertainty on $G(1)|V_{cb}|$ is much larger than $F(1)|V_{cb}|$. More precise measurement is necessary also to address the above issues.

- HQET inspired model for $B \to D^{**}\ell\nu$ decays.
  HQET inspired model for $B \to D^{**}\ell\nu$ decays (see Appendix H) is to describe these decays better. But, the HQET model has not been used in existing measurements.

In this analysis, we address these problems. We use a global fit technique to determine relative exclusive branching fractions, $\mathcal{B}(B \to D\ell\nu)$, $\mathcal{B}(B \to D^*\ell\nu)$ and

Branching Fraction	Experiment (year)	Decay mode
$0.0459 \pm 0.0023 \pm 0.0040$	BELLE (2002) [5]	$B^0 \to D^{*-}\ell^+\nu$
$0.0470 \pm 0.0013^{+0.0036}_{-0.0031}$	DELPHI (2001) [6]	$B^0 \to D^{*-}\ell^+\nu$
$0.0490 \pm 0.0007^{+0.0036}_{-0.0035}$	BABAR (2005) [7]	$B^0 \to D^{*-}\ell^+\nu$
$0.0526 \pm 0.0020 \pm 0.0046$	OPAL (2000) [8]	$B^0 \to D^{*-}\ell^+\nu$
$0.0553 \pm 0.0026 \pm 0.0052$	ALEPH (1997) [9]	$B^0 \to D^{*-}\ell^+\nu$
$0.0590 \pm 0.0022 \pm 0.0050$	DELPHI (2004) [10]	$B^0 \to D^{*-}\ell^+\nu$
$0.0609 \pm 0.0019 \pm 0.0040$	CLEO (2003) [11]	$B^0(B^+) \to D^{*-}(\bar{D}^{*0})\ell^+\nu$

Table 1: [$B^0 \to D^*\ell\nu$ **BF**] $B^0 \to D^{*-}\ell^+\nu$ branching fractions from different experiments. The first uncertainty is statistical and the second one is systematic. In the most right column, the decay modes measured in each analysis are listed. Only CLEO (2003) measured both $B^0 \to D^{*-}\ell^+\nu$ and $B^+ \to \bar{D}^{*0}\ell^+\nu$ modes.

$\mathcal{B}(B \to D^{**}\ell\nu) + \mathcal{B}(B \to D^{(*)}\pi\ell\nu)$, and form factor parameters of $B \to D\ell\nu$ and $B \to D^*\ell\nu$ decays. Using these results along with $\mathcal{G}(1)$ and $\mathcal{F}(1)$, we can also extract $|V_{cb}|$ as explained in section 20. We do not explicitly reconstruct D^* or D^{**}. Thus, we do not have to rely on slow pion reconstruction. We also do not have to determine the efficiency to reconstruct and detect a specific decay mode, wich is usually done by Monte Carlo simulation (MC). This is a different approach from the existing measurements listed above. We, however, depend on MC to construct the probability density functions (PDF) to be used in the fit. Details of our fit technique is explained in section 3. Since we use a different approach, our results are useful to address the above problems.

Decay mode (B^+)	Branching Fraction (%)	Reference
$B^+ \to \bar{D}^0 \ell^+ \nu$	2.15 ± 0.22	[12]
$B^+ \to \bar{D}^{*0} \ell^+ \nu$	6.5 ± 0.5	[12]
$B^+ \to D^- \pi^+ \ell^+ \nu$	0.53 ± 0.10	[12]
$B^+ \to \bar{D}^0 \pi^0 \ell^+ \nu$	0.265 ± 0.05	Isospin symmetry
$B^+ \to D^{*-} \pi^+ \ell^+ \nu$	0.64 ± 0.15	[12]
$B^+ \to \bar{D}^{*0} \pi^0 \ell^+ \nu$	0.32 ± 0.075	Isospin symmetry
Sum of exclusive modes	10.41 ± 0.61	
Inclusive $B^+ \to X_c \ell^+ \nu$	10.8 ± 0.4	[12]
Decay mode (B^0)	Branching Fraction (%)	Reference
$B^0 \to D^- \ell^+ \nu$	2.13 ± 0.18	[12]
$B^0 \to D^{*-} \ell^+ \nu$	5.20 ± 0.24	[12]
$B^0 \to \bar{D}^0 \pi^- \ell^+ \nu$	0.32 ± 0.095	[12]
$B^0 \to D^- \pi^0 \ell^+ \nu$	0.16 ± 0.0475	Isospin symmetry
$B^0 \to \bar{D}^{*0} \pi^- \ell^+ \nu$	0.65 ± 0.16	[12]
$B^0 \to D^{*-} \pi^0 \ell^+ \nu$	0.325 ± 0.08	Isospin symmetry
Sum of exclusive modes	8.79 ± 0.41	
Inclusive $B^0 \to X_c \ell^+ \nu$	10.1 ± 0.4	[12]

Table 2: [**Exclusive-Inclusive comparison**] Branching fractions of $B \to X_c \ell \nu$ type of decays. $B \to D^{(*)} \pi \ell \nu$ decays include not only non-resonant $B \to D^{(*)} \pi \ell \nu$ decays but also $B \to D^{**} \ell \nu$ decays.

ρ_D^2	Experiment (year)	Decay mode
$0.97 \pm 0.98 \pm 0.38$	ALEPH (1997) [9]	$B^0 \to D^- \ell^+ \nu$
$1.12 \pm 0.22 \pm 0.14$	BELLE (2002) [13]	$B^0 \to D^- \ell^+ \nu$
$1.27 \pm 0.25 \pm 0.14$	CLEO (1999) [14]	$B^0 \to D^- \ell^+ \nu$ and $B^+ \to \bar{D}^0 \ell^+ \nu$

Table 3: [$B \to D \ell \nu$ **FF slope**] Form factor slope ρ_D^2 from different experiments. The first uncertainty is statistic and the second one is systematic.

1.2 Structure of this document

- Section 2 : **Signals and Backgrounds**
  Events or decay modes in the signals and backgrounds are explained.

- Section 3 to 5 : **Fitting Method**
  Overview of our fitting method is described in section 3.
  Detailed description of the coefficients in our fit is in section 4.
  The constraints we apply in the fit is discussed in section 5.

- Section 6 : **Event Selection**
  The data set used in this analysis and selection methods to extract $B \to D^{(*,**)}(\pi)\ell\nu$ events are explained.

- Section 7 : **Tracking Efficiency and PID corrections**
  The effect of Tracking Efficiency and PID corrections are shown.

- Section 8 : **D mass sideband subtraction**
  The validity of D mass sideband subtraction is discussed.

- Section 9 to 11 : **Monte Carlo Re-weighting**
  Overview of our Monte Carlo (MC) re-weighting method and Branching Fraction (BF) re-weighting is described in section 9.
  $B \to D^{(*,**)}(\pi)\ell\nu$ Form Factor (FF) re-weighting method is shown in section 10.
  The method to perform FF parameter fitting is explained in section 11.

- Section 12 : **Test Fit**
  The results of test fit using full kinematic rage are shown.

- Section 13 : **Lepton momentum, D momentum and $\cos\theta_{B-Dl}$ cuts**
  To improve χ^2, lepton momentum, D momentum and $\cos\theta_{B-Dl}$ cuts are applied.
  The details of these cuts are explained.

- Section 14 : **Bin by bin D mass sideband subtraction**
  The validity of bin by bin D mass sideband subtraction is discussed.

- Section 15 : **Fit Validation**
  Fit validation is done using MC. Validation fit results are shown.

- Section 16 : **Fit Result**
  Our fit result and discussion is given.

- Section 17 : **Cross Checks**
  Some cross checks of the fit result are given.

- Section 20 : **Calculation of $\mathcal{G}(1)|V_{cb}|$ and $\mathcal{F}(1)|V_{cb}|$**
  Calculation of $\mathcal{G}(1)|V_{cb}|$ and $\mathcal{F}(1)|V_{cb}|$ is shown.

- Section 21 : **Systematic Uncertainty**
  The results of systematic study is explained.

- Section 22 : **Full Covariance Matrix**
  We give full covariance matrix to keep track of correlations.
- Section 23 : **Discussions**
  We compare our results with previous Babar measurements.
- Section 24 : **Conclusion**
  We summarize our final results.

Appendix

- Appendix A : B decay modes
- Appendix B : Classification of D^{**}
- Appendix C : Isospin symmetry
- Appendix D : Values in MC and Fit
- Appendix E : BToDlnu skims
- Appendix F : $\cos\theta_{BY}$
- Appendix G : Velocity transfer w
- Appendix H : Form Factors of $B \to D^{(*,**)}X\ell\nu$ decays

2 Signal and Background Events

2.1 Signal

We are interested in $B \to D^{(*,**)}(\pi)\ell\nu$ decays. We reconstruct either D^0 or D^+ and a lepton (electron or muon) to form a Dl candidate as a candidate of a B meson. We do not explicitly reconstruct D^* or D^{**}. However, we can access those higher charmed meson states because, as described in Appendix A, D^* and D^{**} eventually decay into either D^0 or D^+. We separate decay modes into two categories: the decay modes to produce D^0 and the ones to produce D^+. Contributions of each component can be seen in Fig 1.

2.1.1 D^0 modes

The decay processes to produce D^0 are

- $B^+ \to \bar{D}^0\ell^+\nu$
- $B^+ \to \bar{D}^{*0}\ell^+\nu$ with $\bar{D}^{*0} \to \bar{D}^0\pi^0$ or $\bar{D}^{*0} \to \bar{D}^0\gamma$
- $B^0 \to D^{*-}\ell^+\nu$ with $D^{*-} \to \bar{D}^0\pi^-$
- $B^+ \to \bar{D}^{**0}\ell^+\nu$ with $\bar{D}^{**0} \to D^0\pi^0$
  $B^+ \to \bar{D}^{**0}\ell^+\nu$ with $\bar{D}^{**0} \to D^{*0}\pi^0$ and $D^{*0} \to \bar{D}^0\pi^0$ or $D^{*0} \to \bar{D}^0\gamma$
  $B^+ \to \bar{D}^{**0}\ell^+\nu$ with $\bar{D}^{**0} \to D^{*-}\pi^+$ and $D^{*-} \to \bar{D}^0\pi^-$
- $B^0 \to D^{**-}\ell^+\nu$ with $D^{**-} \to \bar{D}^0\pi^-$
  $B^0 \to D^{**-}\ell^+\nu$ with $D^{**-} \to \bar{D}^{*0}\pi^-$ and $\bar{D}^{*0} \to \bar{D}^0\pi^0$ or $\bar{D}^{*0} \to \bar{D}^0\gamma$
  $B^0 \to D^{**-}\ell^+\nu$ with $D^{**-} \to D^{*-}\pi^0$ and $D^{*-} \to \bar{D}^0\pi^-$
- $B^+ \to \bar{D}^0\pi^0\ell^+\nu$
- $B^0 \to \bar{D}^0\pi^-\ell^+\nu$
- $B^+ \to \bar{D}^{*0}\pi^0\ell^+\nu$ with $\bar{D}^{*0} \to \bar{D}^0\pi^0$ or $\bar{D}^{*0} \to \bar{D}^0\gamma$
  $B^+ \to D^{*-}\pi^+\ell^+\nu$ with $D^{*-} \to \bar{D}^0\pi^-$
- $B^0 \to \bar{D}^{*0}\pi^-\ell^+\nu$ with $\bar{D}^{*0} \to \bar{D}^0\pi^0$ or $\bar{D}^{*0} \to \bar{D}^0\gamma$
  $B^0 \to D^{*-}\pi^0\ell^+\nu$ with $D^{*-} \to \bar{D}^0\pi^-$

2.1.2 D^+ modes

The decay processes to produce D^+ are

- $B^0 \to D^-\ell^+\nu$
- $B^0 \to D^{*-}\ell^+\nu$ with $D^{*-} \to D^-\pi^0$ or $D^{*-} \to D^-\gamma$
- $B^0 \to D^{**-}\ell^+\nu$ with $D^{**-} \to D^-\pi^0$
  $B^0 \to D^{**-}\ell^+\nu$ with $D^{**-} \to D^{*-}\pi^0$ and $D^{*-} \to D^-\pi^0$ or $D^{*-} \to D^-\gamma$

- $B^+ \to \bar{D}^{**0}\ell^+\nu$ with $\bar{D}^{**0} \to D^-\pi^+$
  $B^+ \to \bar{D}^{**0}\ell^+\nu$ with $\bar{D}^{**0} \to D^{*-}\pi^+$ and $D^{*-} \to D^-\pi^0$ or $D^{*-} \to D^-\gamma$
- $B^0 \to D^-\pi^0\ell^+\nu$
- $B^+ \to D^-\pi^+\ell^+\nu$
- $B^0 \to D^{*-}\pi^0\ell^+\nu$ with $D^{*-} \to D^-\pi^0$ or $D^{*-} \to D^-\gamma$
- $B^+ \to D^{*-}\pi^+\ell^+\nu$ with $D^{*-} \to D^-\pi^0$ or $D^{*-} \to D^-\gamma$

2.2 Backgrounds

Backgrounds are categorized as described in the following subsections. Contributions of each component can be seen in Fig 1. Some of backgrounds are non-peaking backgrounds in D mass plots and almost disappear after D mass sideband subtraction. However, some are peaking backgrounds and remain after D mass sideband subtraction as can be seen in Figure 19 - 21 in section 8. D mass sidebands are defined in section 8.1. The composition of major tree backgrounds after sideband subtraction is given in Tables 4 - 6

2.2.1 UncorrDL and UncorrDLMix: peaking background from $B\bar{B}$

D and ℓ come from different B (Uncorrelated), and ℓ come directly from B (DL = Direct Lepton). (Table 4)
One example of this background is the following $B \to D^{(*)}\bar{D}^{(*)}X$ (One of D may be D_s) type :

- $B^+ \to \bar{D}^0\ell^+\nu$
- $B^- \to D^{(*)0}D^{*-}K^0$ with $D^{*-} \to D^-\pi^0$ or $D^{*-} \to D^-\gamma$

These ℓ^+ from B^+ and D^- from B^- form a Dl candidate.
Another example is $B^0\bar{B}^0$ mixing. We separate $B^0\bar{B}^0$ mixing as **UncorrDLMix**

2.2.2 UncorrCL : peaking background from $B\bar{B}$

D and ℓ come from different B (Uncorrelated), and ℓ does not directly come from B (CL = Cascade Lepton). (Table 5)
Main source of this background is semileptonic D decays such as

- $B^+ \to \bar{D}^0X_1$
- $B^- \to D^0X_2$ with $D^0 \to K^-\ell^+\nu$

These $\bar{D}^0$ from B^+ and ℓ^+ from $B^-(D^0)$ form a Dl candidate.

2.2.3 CascL and CascLTau: peaking background from $B\bar{B}$

D and ℓ come from same B (Correlated), and ℓ does not directly come from B (Cascade Lepton). (Table 6)
One example of this background is the following $B \to D^{(*)}\bar{D}^{(*)}X$ (One of D may be D_s) type :

- $B^+ \to \bar{D}^0 D^{*0} K^+$
  with $\bar{D}^0 \to K^+\ell^-\bar{\nu}$ and $D^{*0} \to D^0\pi^0$

These ℓ^- and D^0 form a Dl candidate.
Another example of this background is $B \to X\tau\nu$ type. For example,

- $B^+ \to \bar{D}^0\tau^+\bar{\nu}$
  with $\tau^+ \to \mu^+\bar{\nu}_\mu\nu_\tau$

These $\bar{D}^0$ and μ^+ form a Dl candidate. We separate this type as **CascLTau**

2.2.4 FakeL : peaking background from $B\bar{B}$

The lepton in a Dl candidate is a mis-identified K, π or p.
90 % of mis identification is between μ and π.
We do not float this component in the fit.

2.2.5 CombRL : non-peaking background from $B\bar{B}$

Combinatorial background from $B\bar{B}$ events. This is the case that reconstructed D is not real. Typical mis-reconstructions are that the kaon and the pion do not come from same D or not directly come from D. In our analysis, D^0 has much less combinatorial background than D^+ because D^0 is reconstructed from two particles (one K and one π) whereas D^+ is reconstructed from three particles (one K and two π) (see section 6.1.1).
This component almost disappear after D mass sideband subtraction. Thus, we do not float this component in the fit.

2.2.6 CombFL : non-peaking background from $B\bar{B}$

D is mis-reconstructed (Combinatorial) and ℓ is mis-identified (Fake Lepton).
This component almost disappear after D mass sideband subtraction. Thus, we do not float this component in the fit.

2.2.7 OffPeak : OffPeak data

OffPeak data. The main contribution to OffPeak data is $c\bar{c}$, $s\bar{s}$, $u\bar{u}$, $d\bar{d}$ and $\tau^+\tau^-$ events. This can be separated into two category : continuum background and "$c\bar{c}$ with true D" background. Continuum background can be subtracted out by D mass sideband subtraction. "$c\bar{c}$ with true D" background is a peaking background in the D mass distribution and does not disappear after sideband subtraction.

process	B^+	B^0
$B \to D^{(*)}\bar{D}^{(*)}X$ (One of D may be D_s)	96 %	45 %
$B^0\bar{B}^0$ mixing	0	53 %

Table 4: [**UncorrDL backgroubd processes**] The compositin of UncorrDL backgrounds. Numbers are approximate because compositions are different for D^0 and D^+.

process	B^+	B^0
lepton from γ	4 %	3 %
lepton from τ	5 %	7 %
lepton from uds (K, π, etc.)	3 %	2 %
lepton from $D^{(*)}$ or $D_s^{(*)}$	86 %	87 %

Table 5: [**UncorrCL backgroubd processes**] The compositin of UncorrCL backgrounds. Numbers are approximate because compositions are different for D^0 and D^+.

process	B^+	B^0
lepton from γ	4 %	3 %
lepton from τ	40 %	43 %
lepton from uds (K, π, etc.)	5 %	4 %
lepton from $D^{(*)}$ or $D_s^{(*)}$ ($B \to D^{(*)}\bar{D}^{(*)}X$ (One of D may be D_s))	52 %	49 %

Table 6: [**CascL backgroubd processes**] The compositin of CascL backgrounds. Numbers are approximate because compositions are different for D^0 and D^+.

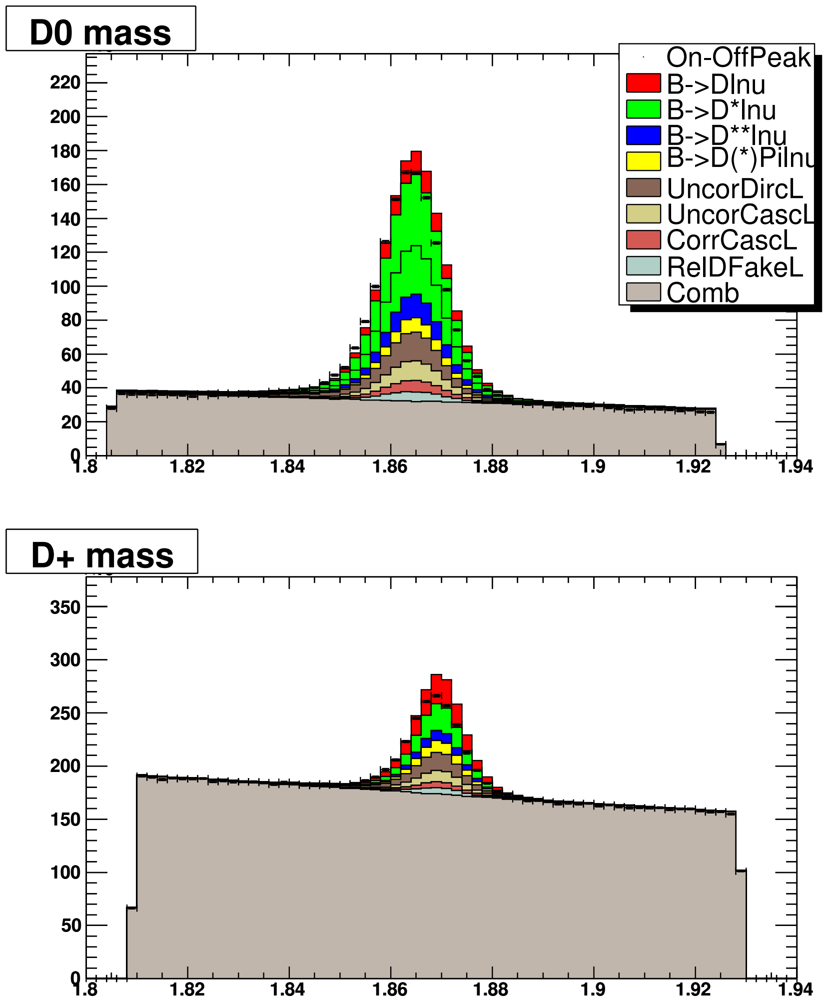

Figure 1: [D **mass plot**] An example of D mass plot showing all components of signal and backgroud. The top is D^0 and the bottom is D^+. Black line with error bar is OnPeak data. Red is $B \to D\ell\nu$, green is $B \to D^*\ell\nu$, blue is $B \to D^{**}\ell\nu$, yellow is non-resonant $B \to D^{(*)}\pi\ell\nu$, and the rest is background. Dark brown is UncorrDL, light brown is UncorrCL, dark red is CascL, blue gray is FakeL, light gray is Comb, and dark gray is OffPeak.

3 Fitting Method

We use binned χ^2 fitting.

3.1 3D binning (i)

We use 3D binning by three variables :

- lepton momentum in the CM frame p_ℓ^*
- D momentum in the CM frame p_D^*
- $\cos\theta_{B-Dl}$ (see below)

The reason of this choice is the following. In the $B \to D\ell\nu$ decays, there are only three independent kinematic variables. For example, in Figure 62, supposing D^* is D and does not decay, independent variables can be

- The magnitude of lepton momentum
- The magnitude of D momentum
- The angle θ_ℓ

because χ and θ_V are irrelevant. The same is true also in other decay modes when we reconstruct only $D\ell$. We chose three variables, p_ℓ^*, p_D^* and $\cos\theta_{B-Dl}$, because this combination is simple, well known and useful to separate each signal decay modes and backgrounds. As you can see from Figures 19-21 in section 8, the shape of the histogram of each MC mode is quite different. We also tried $\cos\theta_{D-\ell}$ (the cosine of the angle between D and ℓ in the CM frame) instead of $\cos\theta_{B-Dl}$ to assure that $\cos\theta_{B-Dl}$ is a better parameter.

3.2 Calculation of $\cos\theta_{B-Dl}$

$\cos\theta_{B-Dl}$ is given by (see Appendix F)

$$\cos\Theta_{B-Dl} = \frac{2E_B E_{Dl} - m_B^2 - m_{Dl}^2}{2|\vec{p}_B||\vec{p}_{Dl}|} \tag{1}$$

where E_B and $p_B = |\vec{p}_B|$ are calculated from beam energy E_{beam} by

$$\begin{aligned} E_B &= E_{beam}/2 \\ p_B &= \sqrt{E_B^2 - m_B^2} \end{aligned} \tag{2}$$

because we don not reconstruct B. We use

$$\begin{aligned} E_{beam} &= E_{\text{data}} \text{ in Table 23} \\ m_B &= m_{B^0} = 5.2795\,\text{GeV} \end{aligned} \tag{3}$$

for both data and MC (both BpBm and B0B0bar MC) because we do not know whether the B in data is B^0 or B^+. Here E_{data} is given in Table 23 in section 9.6. Thus,

$$\cos\Theta_{B-Dl} = \frac{E_{beam}E_{Dl} - m_{B^0}^2 - m_{Dl}^2}{2\sqrt{(E_{beam}/2)^2 - m_{B^0}^2}\,|\vec{p}_{Dl}|} \tag{4}$$

$D\ell$ mass, momentum and energy are reconstructed values.

3.2.1 $\cos\theta_{B-Dl}$ of OffPeak data

OffPeak data is taken at the energy 39MeV below the OnPeak data energy. Thus, the $D\ell$ mass, momentum and energy are different from the continuum background in OnPeak data. In order to get similar $\cos\theta_{B-Dl}$ distribution to OnPeak data, we need to do a modification.

One idea is to scale up $D\ell$ mass, momentum and energy by the ratio of beam energies

$$r_{\mathrm{beam}} = \frac{E_{\mathrm{data}}^{OnPeak}}{E_{\mathrm{data}}^{OffPeak}} = \frac{E_{\mathrm{data}}}{E_{\mathrm{data}} - 0.039\ \mathrm{GeV}} \tag{5}$$

where E_{data} is given in Table 23 in section 9.6. Thus

$$\cos\Theta_{B-Dl} = \frac{E_{beam}(r_{\mathrm{beam}}E_{Dl}) - m_{B^0}^2 - (r_{\mathrm{beam}}\,m_{Dl})^2}{2\sqrt{(E_{beam}/2)^2 - m_{B^0}^2}\,|r_{\mathrm{beam}}\,\vec{p}_{Dl}|} \tag{6}$$

In reality, $D\ell$ mass, momentum and energy do not have to scale as the same rate to beam energy. Thus, we introduce scale modification factors x_E and x_p for $D\ell$ energy and momentum, respectively. Then, scale factors for $D\ell$ energy is given by

$$r_{\mathrm{beam}}^E = \frac{E_{\mathrm{data}}}{E_{\mathrm{data}} - 0.039x_E} \tag{7}$$

and for $D\ell$ momentum is given by

$$r_{\mathrm{beam}}^p = \frac{E_{\mathrm{data}}}{E_{\mathrm{data}} - 0.039x_p} \tag{8}$$

$D\ell$ mass is calculated from these energy and momentm

$$m_{Dl}^{corrected} = \sqrt{(r_{\mathrm{beam}}^E)^2E_{Dl}^2 - (r_{\mathrm{beam}}^p)^2p_{Dl}^2} \tag{9}$$

Thus, $\cos\theta_{B-Dl}$ is given by

$$\cos\Theta_{B-Dl} = \frac{E_{beam}(r_{\mathrm{beam}}^E E_{Dl}) - m_{B^0}^2 - (m_{Dl}^{corrected})^2}{2\sqrt{(E_{beam}/2)^2 - m_{B^0}^2}\,|r_{\mathrm{beam}}^p\,\vec{p}_{Dl}|} \tag{10}$$

We use $x_E = 1$ and $x_p = 1$ in our nominal fit and, for systematic study, we use the following three combinations :

- $x_E = 1$ and $x_p = 0$
- $x_E = 0$ and $x_p = 1$
- $x_E = 0$ and $x_p = 0$

3.3 χ^2

The χ^2 is given by

$$\chi^2 = \sum_{i=\text{bin}}^{D^0} \frac{(N_i^{OnPeak} - N_i^{OffPeak} - \sum_j C_j^{MC} N_{ij}^{MC})^2}{(\sigma_i^{OnPeak})^2 + (\sigma_i^{OffPeak})^2 + \sum_j (C_j^{MC} \sigma_{ij}^{MC})^2} + \sum_{i=\text{bin}}^{D^+} \frac{(N_i^{OnPeak} - N_i^{OffPeak} - \sum_j C_j^{MC} N_{ij}^{MC})^2}{(\sigma_i^{OnPeak})^2 + (\sigma_i^{OffPeak})^2 + \sum_j (C_j^{MC} \sigma_{ij}^{MC})^2} \quad (11)$$

where,

- i represents each bin
- j represents each MC mode.

MC modes are listed in section 4 separately for D^0 and D^+ modes. See also Appendix A and section 2.
Quantities in the χ^2 are:

- N_i^{OnPeak}
  The number of OnPeak data candidates in the i-th bin.
- $N_i^{OffPeak}$
  The number of OffPeak data candidates in the i-th bin, luminosity normalized to OnPeak data.
- N_{ij}^{MC}
  The number of j-th MC mode candidates in the i-th bin, luminosity normalized to OnPeak data. Details are in section 3.4. The effect of data MC differences from tracking and PID are corrected (see section 7). MC re-weighting is also done. We can fit for form factor parameters through MC re-weighting (see sections 9 and 10)
- C_j^{MC}
  The coefficient of each MC mode (j). These include branching fractions to be determined in the fit. Details are in section 4.
- σ_i^{OnPeak}
  The statistical uncertainty of N_i^{OnPeak}. $\sigma_i^{OnPeak} = \sqrt{N_i^{OnPeak}}$.
- $\sigma_i^{OffPeak}$
  The statistical uncertainty of $N_i^{OffPeak}$. Details are in section 3.5.
- σ_{ij}^{MC}
  The statistical uncertainty of N_{ij}^{MC}. Details are in section 3.5.

We use bins which have more than 10 expected candidates

$$\sum_j C_j^{MC} N_{ij}^{MC} > 10 \quad (12)$$

and neglect other bins. The number 10 can be changed for systematic study.

3.4 Number of MC Candidates N_{ij}^{MC}

We calculate the number of candidates from MC using MC truth information. We use five generic MC samples: BpBm, B0B0bar, ccbar, uds and tautau. Note that ccbar, uds and tautau MCs are used only for validation of the fit. Tracking efficiency and PID corrections are applied to adjust MC to OnPaek data (see section 7). MCs are also luminosity normalized to OnPeak data.

3.4.1 Luminosity normalization

All MC and OffPeak data are normalized to OnPeak data by luminosity. Supposing OnPeak luminosity is $\mathcal{L}^{OnPeak}$ and MC (mode j) luminosity is $\mathcal{L}_j^{MC}$, the normalization factor r_j^{Lumi} is given by

$$r_j^{Lumi} = \frac{\mathcal{L}^{OnPeak}}{\mathcal{L}_j^{MC}} \tag{13}$$

where the luminosity of $B\bar{B}$ MC is calculated by the generated number of events and B counting number from OnPeak data. For the luminosity of ccbar, uds and tautau MC, their cross sections are used. Details are in Appendix E. Note that depending on the given MC mode j, luminosity is given. For example, when j=1,2,6,8,etc., $\mathcal{L}_j^{MC}$ is the luminosity of BpBm MC and when j=3,5,7,9,etc., $\mathcal{L}_j^{MC}$ is the luminosity of B0B0bar MC (see section 4 for details of MC modes j).
Note that, the luminosity calculation was done based on the assumption that produced number of B^+B^- and $B^0\bar{B}^0$ are equal. The decay rate difference is taken into account in the coefficients (see section 4).
In case of OffPeak data, since OffPeak data is taken at 40 MeV lower energy than OnPeak data, we need to correct for $1/s$ dependence of cross section, where s is the square of CM energy :

$$\begin{aligned} s_{OnPeak} &= 10.58^2 \ \text{GeV} \\ s_{OffPeak} &= (10.58 - 0.04)^2 = 10.54^2 \ \text{GeV} \end{aligned} \tag{14}$$

Thus, correction factor is

$$r_{OffPeak}^{Lumi} = \frac{\mathcal{L}^{OnPeak} s_{OffPeak}}{\mathcal{L}^{OffPeak} s_{OnPeak}} \tag{15}$$

3.4.2 N_{ij}^{MC}

The number of MC candidates N_{ij}^{MC} is given by

$$N_{ij}^{MC} = r_j^{Lumi} \sum_k r_k^{Trk} r_k^{KPID} r_k^{LPID} W_{jk}^{MC} \tag{16}$$

where

- k represents the k-th candidate in i-th bin and MC mode j.

and

- r_k^{Trk} is the tracking efficiency correction factor (⇒ section 7)
- r_k^{KPID} is the kaon PID correction factor (⇒ section 7)
- r_k^{LPID} is the lepton PID correction factor (⇒ section 7)
- W_{jk}^{MC} is the MC weight (⇒ sections 9 and 10)

Tracking efficiency and PID corrections are described in section 7. MC weights are described in sections 9 and 10.

3.5 Statistical uncertainty $\sigma_i^{OffPeak}$ and σ_{ij}^{MC}

Statistical uncertainty of OnPeak data is given by

$$\sigma_i^{OnPeak} = \sqrt{N_i^{OnPeak}} \tag{17}$$

However, since statistical uncertainty of OffPeak data and MCs are luminosity normalized and re-weighted, statistical uncertainties are not simply given by $\sigma_i = \sqrt{N_i}$. In this section, we explain how the statistical uncertainty of OffPeak data and MCs are calculated.

3.5.1 Luminosity normalization and statistical uncertainty

OffPeak and MCs are luminosity normalized to OnPeak data. We take OffPeak data as an example. If the number of OffPeak candidate in i-th bin is N_i^0, the number of luminosity normalized candidate in the bin is given by

$$N_i^{OffPeak} = r_{OffPeak}^{Lumi} N_i^0 \tag{18}$$

and the statistical uncertainty of the bin is given by

$$\sigma_i^{OffPeak} = r_{OffPeak}^{Lumi} \sqrt{N_i^0} \tag{19}$$

3.5.2 MC re-weighting and statistical uncertainty

Supposing the total weight of the k-th candidate of MC mode j is

$$w_{jk}^T \equiv r_k^{Trk} r_k^{KPID} r_k^{LPID} W_{jk}^{MC} \tag{20}$$

The number of candidate in the i-th bin is given by

$$N_{ij}^{MC} = r_j^{Lumi} \sum_k w_{jk}^T \tag{21}$$

We add statistical uncertainty quadratically. Thus,

$$\sigma_{ij}^{MC} = r_j^{Lumi} \sqrt{\sum_k \left(w_{jk}^T\right)^2} \tag{22}$$

4 Coefficients in the fitting C_j^{MC}

Coefficients consist of branching fractions, some of which are to be determined by the fit. Coefficients are given by taking ratios between new branching fractions and the ones used in SP5/SP6 MC (the ones with superscript 0 in the following subsections). The decays contributing to each MC mode are shown in Appendix A and B. New measurements of branching fractions and constraints that we use in our fit are explained in section 5.

4.1 Number of produced B

Branching fractions of B^+B^- and $B^0\bar{B}^0$ of $\Upsilon(4S)$ resonance are denoted by

$$\begin{aligned} f_{+-} &= \mathcal{B}(\Upsilon(4S) \to B^+B^-) \\ f_{00} &= \mathcal{B}(\Upsilon(4S) \to B^0\bar{B}^0) \end{aligned} \tag{23}$$

We define the ratio of these two branching fractions

$$f_{+0} \equiv \frac{f_{+-}}{f_{00}} \tag{24}$$

In the first approximation, $f_{+-} = f_{00} = 0.5$ and $f_{+0} = 1$. In SP5/SP6 MC

$$f_{+0}^0 = 1 \tag{25}$$

is used [2]. The number of produced B is related to this ratio. Supposing $N_{B\bar{B}}$ of $B\bar{B}$-pairs are produced, the number of produced neutral B is

$$N_{neut}^{prod} = 2f_{00}N_{B\bar{B}} \tag{26}$$

and the number of produced charged B is

$$N_{chrg}^{prod} = 2f_{+-}N_{B\bar{B}} = f_{+0}N_{neut}^{prod} \tag{27}$$

Thus,

$$2N_{B\bar{B}} = N_{neut}^{prod} + N_{chrg}^{prod} = N_{neut}^{prod} + f_{+0}N_{neut}^{prod} \tag{28}$$

We get

$$N_{neut}^{prod} = \frac{2}{1+f_{+0}}N_{B\bar{B}} \tag{29}$$

and

$$N_{chrg}^{prod} = \frac{2f_{+0}}{1+f_{+0}}N_{B\bar{B}} \tag{30}$$

This f_{+0} can be floated in the fit.

[2] In this section the superscript "0" is used to denote SP5/SP6 values. For example, the BF that have a superscript "0" after the closing parenthesis are the values from the SP5/SP6 MC

4.2 $B\bar{B}$ luminosity correction

As explained in section 3.4.1, we assumed $f_{+0} = 1$, namely, the same number of B^+B^- and $B^0\bar{B}^0$ to calculate luminosity. We need to correct these. The correction factors are given by

$$C_{B^+} = \frac{2f_{+0}}{1+f_{+0}} \quad \text{for BpBm MC}$$
$$C_{B^0} = \frac{2}{1+f_{+0}} \quad \text{for B0B0bar MC} \tag{31}$$

The coefficients C_j^{MC} include the factor C_{B^+} if those are of BpBm MC and C_{B^0} if those are of B0B0bar MC.

4.3 D^0 MC modes

4.3.1 Coefficients for signals : $j = 1 - 15$

There are 15 signal MC modes.

- $j = 1 : B^+ \to \bar{D}^0\ell^+\nu$
  Number of produced events is

$$N = N_{chrg}^{prod}\mathcal{B}(B^+ \to \bar{D}^0\ell^+\nu)B_{D0} = N_{B\bar{B}}C_{B^+}\mathcal{B}(B^+ \to \bar{D}^0\ell^+\nu)B_{D0} \tag{32}$$

  As $N_{B\bar{B}}$ is common, it will be canceled by taking a ratio. Thus, the coefficient is given by

$$C_1^{MC} = \frac{C_{B^+}\mathcal{B}(B^+ \to \bar{D}^0\ell^+\nu)\mathcal{B}(D^0 \to K^-\pi^+)}{\mathcal{B}(B^+ \to \bar{D}^0\ell^+\nu)^0\mathcal{B}(D^0 \to K^-\pi^+)^0} \tag{33}$$

- $j = 2 : B^+ \to \bar{D}^{*0}\ell^+\nu$ with $\bar{D}^{*0} \to \bar{D}^0 + \gamma/\pi^0$
  Number of produced events is

$$\begin{aligned} N &= N_{chrg}^{prod}\mathcal{B}(B^+ \to \bar{D}^{*0}\ell^+\nu)[\mathcal{B}(D^{*0} \to D^0\pi^0) + \mathcal{B}(D^{*0} \to D^0\gamma)]\mathcal{B}(D^0 \to K^-\pi^+) \\ &= N_{B\bar{B}}C_{B^+}\mathcal{B}(B^+ \to \bar{D}^{*0}\ell^+\nu)\mathcal{B}(D^0 \to K^-\pi^+) \end{aligned} \tag{34}$$

  Thus

$$C_2^{MC} = \frac{C_{B^+}\mathcal{B}(B^+ \to \bar{D}^{*0}\ell^+\nu)\mathcal{B}(D^0 \to K^-\pi^+)}{\mathcal{B}(B^+ \to \bar{D}^{*0}\ell^+\nu)^0\mathcal{B}(D^0 \to K^-\pi^+)^0} \tag{35}$$

- $j = 3 : B^0 \to D^{*-}\ell^+\nu$ with $D^{*-} \to \bar{D}^0\pi^-$
  Number of produced events is

$$N = N_{B\bar{B}}C_{B^0}\mathcal{B}(B^0 \to D^{*-}\ell^+\nu)\mathcal{B}(D^{*+} \to D^0\pi^+)\mathcal{B}(D^0 \to K^-\pi^+) \tag{36}$$

  Thus

$$C_3^{MC} = \frac{C_{B^0}\mathcal{B}(B^0 \to D^{*-}\ell^+\nu)\mathcal{B}(D^{*+} \to D^0\pi^+)\mathcal{B}(D^0 \to K^-\pi^+)}{\mathcal{B}(B^0 \to D^{*-}\ell^+\nu)^0\mathcal{B}(D^{*+} \to D^0\pi^+)^0\mathcal{B}(D^0 \to K^-\pi^+)^0} \tag{37}$$

- $j = 4:\ B^+ \to \bar{D}_0^{*0}\ell^+\nu$ with $\bar{D}_0^{*0} \to \bar{D}^0\pi^0$
  The coefficient is

$$C_4^{MC} = \frac{C_{B^+}\mathcal{B}(B^+ \to \bar{D}_0^{*0}\ell^+\nu)\mathcal{B}(D_0^{*0} \to D^0\pi^0)\mathcal{B}(D^0 \to K^-\pi^+)}{\mathcal{B}(B^+ \to \bar{D}_0^{*0}\ell^+\nu)^0\mathcal{B}(D_0^{*0} \to D^0\pi^0)^0\mathcal{B}(D^0 \to K^-\pi^+)^0} \tag{38}$$

- $j = 5:\ B^0 \to D_0^{*-}\ell^+\nu$ with $D_0^{**-} \to \bar{D}^0\pi^-$
  The coefficient is

$$C_5^{MC} = \frac{C_{B^0}\mathcal{B}(B^0 \to D_0^{*-}\ell^+\nu)\mathcal{B}(D_0^{*+} \to D^0\pi^+)\mathcal{B}(D^0 \to K^-\pi^+)}{\mathcal{B}(B^0 \to D_0^{*-}\ell^+\nu)^0\mathcal{B}(D_0^{*+} \to D^0\pi^+)^0\mathcal{B}(D^0 \to K^-\pi^+)^0} \tag{39}$$

- $j = 6:\ B^+ \to \bar{D}_1^0\ell^+\nu$
  The decays contribute to this mode are
  $B^+ \to \bar{D}_1^0\ell^+\nu$ with $\bar{D}_1^0 \to D^{*-}\pi^+$ and $D^{*-} \to \bar{D}^0\pi^-$
  $B^+ \to \bar{D}_1^0\ell^+\nu$ with $\bar{D}_1^0 \to \bar{D}^{*0}\pi^0$ and $\bar{D}^{*0} \to \bar{D}^0 + \gamma/\pi^0$
  Number of produced events is

$$\begin{aligned}
N &= N_{B\bar{B}}C_{B^+}\mathcal{B}(B^+ \to \bar{D}_1^0\ell^+\nu)\mathcal{B}(D_1^0 \to D^{*+}\pi^-)\mathcal{B}(D^{*+} \to D^0\pi^+)\mathcal{B}(D^0 \to K^-\pi^+) \\
&\quad + N_{B\bar{B}}C_{B^+}\mathcal{B}(B^+ \to \bar{D}_1^0\ell^+\nu)\mathcal{B}(D_1^0 \to D^{*0}\pi^0) \\
&\qquad \times[\mathcal{B}(D^{*0} \to D^0\pi^0) + \mathcal{B}(D^{*0} \to D^0\gamma)]\mathcal{B}(D^0 \to K^-\pi^+) \\
&= N_{B\bar{B}}C_{B^+}\mathcal{B}(B^+ \to \bar{D}_1^0\ell^+\nu) \\
&\qquad \times[\mathcal{B}(D_1^0 \to D^{*+}\pi^-)\mathcal{B}(D^{*+} \to D^0\pi^+) + \mathcal{B}(D_1^0 \to D^{*0}\pi^0)]\mathcal{B}(D^0 \to K^-\pi^+)
\end{aligned} \tag{40}$$

  The coefficient is

$$C_6^{MC} = \frac{\begin{array}{l} C_{B^+}\mathcal{B}(B^+ \to \bar{D}_1^0\ell^+\nu)\times \\ {[\mathcal{B}(D_1^0 \to D^{*+}\pi^-)\mathcal{B}(D^{*+} \to D^0\pi^+) + \mathcal{B}(D_1^0 \to D^{*0}\pi^0)]\mathcal{B}(D^0 \to K^-\pi^+)} \end{array}}{\begin{array}{l} \mathcal{B}(B^+ \to \bar{D}_1^0\ell^+\nu)^0\times \\ {[\mathcal{B}(D_1^0 \to D^{*+}\pi^-)^0\mathcal{B}(D^{*+} \to D^0\pi^+)^0 + \mathcal{B}(D_1^0 \to D^{*0}\pi^0)^0]\mathcal{B}(D^0 \to K^-\pi^+)^0} \end{array}} \tag{41}$$

- $j = 7:\ B^0 \to D_1^-\ell^+\nu$
  The decays contribute to this mode are
  $B^0 \to D_1^-\ell^+\nu$ with $D_1^- \to D^{*-}\pi^0$ and $D^{*-} \to \bar{D}^0\pi^-$
  $B^0 \to D_1^-\ell^+\nu$ with $D_1^- \to \bar{D}^{*0}\pi^-$ and $\bar{D}^{*0} \to \bar{D}^0 + \gamma/\pi^0$
  Number of produced events is

$$\begin{aligned}
N &= N_{B\bar{B}}C_{B^0}\mathcal{B}(B^0 \to D_1^-\ell^+\nu)\mathcal{B}(D_1^+ \to D^{*+}\pi^0)\mathcal{B}(D^{*+} \to D^0\pi^+)\mathcal{B}(D^0 \to K^-\pi^+) \\
&\quad + N_{B\bar{B}}C_{B^0}\mathcal{B}(B^0 \to D_1^-\ell^+\nu)\mathcal{B}(D_1^+ \to D^{*0}\pi^+) \\
&\qquad \times[\mathcal{B}(D^{*0} \to D^0\pi^0) + \mathcal{B}(D^{*0} \to D^0\gamma)]\mathcal{B}(D^0 \to K^-\pi^+) \\
&= N_{B\bar{B}}C_{B^0}\mathcal{B}(B^0 \to D_1^-\ell^+\nu) \\
&\quad \times[\mathcal{B}(D_1^+ \to D^{*+}\pi^0)\mathcal{B}(D^{*+} \to D^0\pi^+) + \mathcal{B}(D_1^+ \to D^{*0}\pi^+)]\mathcal{B}(D^0 \to K^-\pi^+)
\end{aligned} \tag{42}$$

The coefficient is

$$C_7^{MC} = \frac{\begin{array}{l} C_{B^0}\mathcal{B}(B^0 \to D_1^- \ell^+ \nu)\times \\ {[\mathcal{B}(D_1^+ \to D^{*+}\pi^0)\mathcal{B}(D^{*+} \to D^0\pi^+) + \mathcal{B}(D_1^+ \to D^{*0}\pi^+)]\mathcal{B}(D^0 \to K^-\pi^+)} \end{array}}{\begin{array}{l} \mathcal{B}(B^0 \to D_1^- \ell^+ \nu)^0 \times \\ {[\mathcal{B}(D_1^+ \to D^{*+}\pi^0)^0\mathcal{B}(D^{*+} \to D^0\pi^+)^0 + \mathcal{B}(D_1^+ \to D^{*0}\pi^+)^0]\mathcal{B}(D^0 \to K^-\pi^+)^0} \end{array}} \tag{43}$$

- $j = 8:\ B^+ \to \bar{D}_1'^0 \ell^+ \nu$
  The decays contribute to this mode are
  $B^+ \to \bar{D}_1'^0 \ell^+ \nu$ with $\bar{D}_1'^0 \to D^{*-}\pi^+$ and $D^{*-} \to \bar{D}^0\pi^-$
  $B^+ \to \bar{D}_1'^0 \ell^+ \nu$ with $\bar{D}_1'^0 \to \bar{D}^{*0}\pi^0$ and $\bar{D}^{*0} \to \bar{D}^0 + \gamma/\pi^0$
  Number of produced events is

$$\begin{aligned} N &= N_{B\bar{B}}C_{B^+}\mathcal{B}(B^+ \to \bar{D}_1'^0 \ell^+ \nu)\mathcal{B}(D_1'^0 \to D^{*+}\pi^-)\mathcal{B}(D^{*+} \to D^0\pi^+)\mathcal{B}(D^0 \to K^-\pi^+) \\ &\quad + N_{B\bar{B}}C_{B^+}\mathcal{B}(B^+ \to \bar{D}_1'^0 \ell^+ \nu)\mathcal{B}(D_1'^0 \to D^{*0}\pi^0) \\ &\qquad \times[\mathcal{B}(D^{*0} \to D^0\pi^0) + \mathcal{B}(D^{*0} \to D^0\gamma)]\mathcal{B}(D^0 \to K^-\pi^+) \\ &= N_{B\bar{B}}C_{B^+}\mathcal{B}(B^+ \to \bar{D}_1'^0 \ell^+ \nu) \\ &\quad \times[\mathcal{B}(D_1'^0 \to D^{*+}\pi^-)\mathcal{B}(D^{*+} \to D^0\pi^+) + \mathcal{B}(D_1'^0 \to D^{*0}\pi^0)]\mathcal{B}(D^0 \to K^-\pi^+) \end{aligned} \tag{44}$$

  The coefficient is

$$C_8^{MC} = \frac{\begin{array}{l} C_{B^+}\mathcal{B}(B^+ \to \bar{D}_1'^0 \ell^+ \nu)\times \\ {[\mathcal{B}(D_1'^0 \to D^{*+}\pi^-)\mathcal{B}(D^{*+} \to D^0\pi^+) + \mathcal{B}(D_1'^0 \to D^{*0}\pi^0)]\mathcal{B}(D^0 \to K^-\pi^+)} \end{array}}{\begin{array}{l} \mathcal{B}(B^+ \to \bar{D}_1'^0 \ell^+ \nu)^0 \times \\ {[\mathcal{B}(D_1'^0 \to D^{*+}\pi^-)^0\mathcal{B}(D^{*+} \to D^0\pi^+)^0 + \mathcal{B}(D_1'^0 \to D^{*0}\pi^0)^0]\mathcal{B}(D^0 \to K^-\pi^+)^0} \end{array}} \tag{45}$$

- $j = 9:\ B^0 \to D_1'^- \ell^+ \nu$
  The decays contribute to this mode are
  $B^0 \to D_1'^- \ell^+ \nu$ with $D_1'^- \to D^{*-}\pi^0$ and $D^{*-} \to \bar{D}^0\pi^-$
  $B^0 \to D_1'^- \ell^+ \nu$ with $D_1'^- \to \bar{D}^{*0}\pi^-$ and $\bar{D}^{*0} \to \bar{D}^0 + \gamma/\pi^0$
  Number of produced events is

$$\begin{aligned} N &= N_{B\bar{B}}C_{B^0}\mathcal{B}(B^0 \to D_1'^- \ell^+ \nu)\mathcal{B}(D_1'^+ \to D^{*+}\pi^0)\mathcal{B}(D^{*+} \to D^0\pi^+)\mathcal{B}(D^0 \to K^-\pi^+) \\ &\quad + N_{B\bar{B}}C_{B^0}\mathcal{B}(B^0 \to D_1'^- \ell^+ \nu)\mathcal{B}(D_1'^+ \to D^{*0}\pi^+) \\ &\qquad \times[\mathcal{B}(D^{*0} \to D^0\pi^0) + \mathcal{B}(D^{*0} \to D^0\gamma)]\mathcal{B}(D^0 \to K^-\pi^+) \\ &= N_{B\bar{B}}C_{B^0}\mathcal{B}(B^0 \to D_1'^- \ell^+ \nu) \\ &\quad \times[\mathcal{B}(D_1'^+ \to D^{*+}\pi^0)\mathcal{B}(D^{*+} \to D^0\pi^+) + \mathcal{B}(D_1'^+ \to D^{*0}\pi^+)]\mathcal{B}(D^0 \to K^-\pi^+) \end{aligned} \tag{46}$$

$$C_9^{MC} = \frac{\begin{array}{l} C_{B^0}\mathcal{B}(B^0 \to D_1'^{-}\ell^+\nu)\times \\ {[}\mathcal{B}(D_1'^{+} \to D^{*+}\pi^0)\mathcal{B}(D^{*+} \to D^0\pi^+) + \mathcal{B}(D_1'^{+} \to D^{*0}\pi^+)]\mathcal{B}(D^0 \to K^-\pi^+) \end{array}}{\begin{array}{l} \mathcal{B}(B^0 \to D_1'^{-}\ell^+\nu)^0\times \\ {[}\mathcal{B}(D_1'^{+} \to D^{*+}\pi^0)^0\mathcal{B}(D^{*+} \to D^0\pi^+)^0 + \mathcal{B}(D_1'^{+} \to D^{*0}\pi^+)^0]\mathcal{B}(D^0 \to K^-\pi^+)^0 \end{array}} \tag{47}$$

- $j = 10 :\ B^+ \to \bar{D}_2^{*0}\ell^+\nu$
  The decays contribute to this mode are
  $B^+ \to \bar{D}_2^{*0}\ell^+\nu$ with $\bar{D}_2^{*0} \to D^{*-}\pi^+$ and $D^{*-} \to \bar{D}^0\pi^-$
  $B^+ \to \bar{D}_2^{*0}\ell^+\nu$ with $\bar{D}_2^{*0} \to \bar{D}^{*0}\pi^0$ and $\bar{D}^{*0} \to \bar{D}^0 + \gamma/\pi^0$
  $B^+ \to \bar{D}_2^{*0}\ell^+\nu$ with $\bar{D}_2^{*0} \to \bar{D}^0\pi^0$
  Number of produced events is

$$\begin{aligned} N &= N_{B\bar{B}}C_{B^+}\mathcal{B}(B^+ \to \bar{D}_2^{*0}\ell^+\nu)\mathcal{B}(D_2^{*0} \to D^{*+}\pi^-)\mathcal{B}(D^{*+} \to D^0\pi^+)\mathcal{B}(D^0 \to K^-\pi^+) \\ &\quad + N_{B\bar{B}}C_{B^+}\mathcal{B}(B^+ \to \bar{D}_2^{*0}\ell^+\nu)\mathcal{B}(D_2^{*0} \to D^{*0}\pi^0) \\ &\quad\quad \times[\mathcal{B}(D^{*0} \to D^0\pi^0) + \mathcal{B}(D^{*0} \to D^0\gamma)]\mathcal{B}(D^0 \to K^-\pi^+) \\ &\quad + N_{B\bar{B}}C_{B^+}\mathcal{B}(B^+ \to \bar{D}_2^{*0}\ell^+\nu)\mathcal{B}(D_2^{*0} \to D^0\pi^0)\mathcal{B}(D^0 \to K^-\pi^+) \\ &= N_{B\bar{B}}C_{B^+}\mathcal{B}(B^+ \to \bar{D}_2^{*0}\ell^+\nu) \\ &\quad \times[\mathcal{B}(D_2^{*0} \to D^{*+}\pi^-)\mathcal{B}(D^{*+} \to D^0\pi^+) + \mathcal{B}(D_2^{*0} \to D^{*0}\pi^0) + \mathcal{B}(D_2^{*0} \to D^0\pi^0)] \\ &\quad \times\mathcal{B}(D^0 \to K^-\pi^+) \end{aligned} \tag{48}$$

  The coefficient is

$$C_{10}^{MC} = \frac{\begin{array}{l} C_{B^+}\mathcal{B}(B^+ \to \bar{D}_2^{*0}\ell^+\nu)\times \\ {[}\mathcal{B}(D_2^{*0} \to D^{*+}\pi^-)\mathcal{B}(D^{*+} \to D^0\pi^+) + \mathcal{B}(D_2^{*0} \to D^{*0}\pi^0) + \mathcal{B}(D_2^{*0} \to D^0\pi^0)] \\ \times\mathcal{B}(D^0 \to K^-\pi^+) \end{array}}{\begin{array}{l} \mathcal{B}(B^+ \to \bar{D}_2^{*0}\ell^+\nu)^0\times \\ {[}\mathcal{B}(D_2^{*0} \to D^{*+}\pi^-)^0\mathcal{B}(D^{*+} \to D^0\pi^+)^0 + \mathcal{B}(D_2^{*0} \to D^{*0}\pi^0)^0 + \mathcal{B}(D_2^{*0} \to D^0\pi^0)^0] \\ \times\mathcal{B}(D^0 \to K^-\pi^+)^0 \end{array}} \tag{49}$$

- $j = 11 :\ B^0 \to D_2^{*-}\ell^+\nu$
  The decays contribute to this mode are
  $B^0 \to D_2^{*-}\ell^+\nu$ with $D_2^{*-} \to D^{*-}\pi^0$ and $D^{*-} \to \bar{D}^0\pi^-$
  $B^0 \to D_2^{*-}\ell^+\nu$ with $D_2^{*-} \to \bar{D}^{*0}\pi^-$ and $\bar{D}^{*0} \to \bar{D}^0 + \gamma/\pi^0$
  $B^0 \to D_2^{*-}\ell^+\nu$ with $D_2^{*-} \to \bar{D}^0\pi^-$

Number of produced events is

$$
\begin{aligned}
N &= N_{B\bar{B}} C_{B^0} \mathcal{B}(B^0 \to D_2^{*-}\ell^+\nu)\mathcal{B}(D_2^{*+} \to D^{*+}\pi^0)\mathcal{B}(D^{*+} \to D^0\pi^+)\mathcal{B}(D^0 \to K^-\pi^+) \\
&\quad + N_{B\bar{B}} C_{B^0} \mathcal{B}(B^0 \to D_2^{*-}\ell^+\nu)\mathcal{B}(D_2^{*+} \to D^{*0}\pi^+) \\
&\qquad \times [\mathcal{B}(D^{*0} \to D^0\pi^0) + \mathcal{B}(D^{*0} \to D^0\gamma)]\mathcal{B}(D^0 \to K^-\pi^+) \\
&\quad + N_{B\bar{B}} C_{B^0} \mathcal{B}(B^0 \to D_2^{*-}\ell^+\nu)\mathcal{B}(D_2^{*+} \to D^0\pi^+)\mathcal{B}(D^0 \to K^-\pi^+) \\
&= N_{B\bar{B}} C_{B^0} \mathcal{B}(B^0 \to D_2^{*-}\ell^+\nu) \\
&\quad \times [\mathcal{B}(D_2^{*+} \to D^{*+}\pi^0)\mathcal{B}(D^{*+} \to D^0\pi^+) + \mathcal{B}(D_2^{*+} \to D^{*0}\pi^+) + \mathcal{B}(D_2^{*+} \to D^0\pi^+)] \\
&\quad \times \mathcal{B}(D^0 \to K^-\pi^+)
\end{aligned} \tag{50}
$$

The coefficient is

$$
C_{11}^{MC} = \frac{\begin{array}{l} C_{B^0}\mathcal{B}(B^0 \to D_2^{*-}\ell^+\nu)\times \\ {[\mathcal{B}(D_2^{*+} \to D^{*+}\pi^0)\mathcal{B}(D^{*+} \to D^0\pi^+) + \mathcal{B}(D_2^{*+} \to D^{*0}\pi^+) + \mathcal{B}(D_2^{*+} \to D^0\pi^+)]} \\ \times\mathcal{B}(D^0 \to K^-\pi^+) \end{array}}{\begin{array}{l} \mathcal{B}(B^0 \to D_2^{*-}\ell^+\nu)^0\times \\ {[\mathcal{B}(D_2^{*+} \to D^{*+}\pi^0)^0\mathcal{B}(D^{*+} \to D^0\pi^+)^0 + \mathcal{B}(D_2^{*+} \to D^{*0}\pi^+)^0 + \mathcal{B}(D_2^{*+} \to D^0\pi^+)^0)} \\ \times\mathcal{B}(D^0 \to K^-\pi^+)^0 \end{array}} \tag{51}
$$

- $j = 12 :\ B^+ \to \bar{D}^0\pi^0\ell^+\nu$
  The coefficient is

$$
C_{12}^{MC} = \frac{C_{B^+}\mathcal{B}(B^+ \to \bar{D}^0\pi^0\ell^+\nu)\mathcal{B}(D^0 \to K^-\pi^+)}{\mathcal{B}(B^+ \to \bar{D}^0\pi^0\ell^+\nu)^0\mathcal{B}(D^0 \to K^-\pi^+)^0} \tag{52}
$$

- $j = 13 :\ B^0 \to \bar{D}^0\pi^-\ell^+\nu$
  The coefficient is

$$
C_{13}^{MC} = \frac{C_{B^0}\mathcal{B}(B^0 \to \bar{D}^0\pi^-\ell^+\nu)\mathcal{B}(D^0 \to K^-\pi^+)}{\mathcal{B}(B^0 \to \bar{D}^0\pi^-\ell^+\nu)^0\mathcal{B}(D^0 \to K^-\pi^+)^0} \tag{53}
$$

- $j = 14 :\ B^+ \to D^*\pi\ell^+\nu$
  The decays contribute to this mode are
  $B^+ \to D^{*-}\pi^+\ell^+\nu$ with $D^{*-} \to \bar{D}^0 + \pi^-$
  $B^+ \to \bar{D}^{*0}\pi^0\ell^+\nu$ with $\bar{D}^{*0} \to \bar{D}^0 + \gamma/\pi^0$
  Number of produced events is

$$
\begin{aligned}
N &= N_{B\bar{B}} C_{B^+} \mathcal{B}(B^+ \to D^{*-}\pi^+\ell^+\nu)\mathcal{B}(D^{*+} \to D^0\pi^+)\mathcal{B}(D^0 \to K^-\pi^+) \\
&\quad + N_{B\bar{B}} C_{B^+} \mathcal{B}(B^+ \to \bar{D}^{*0}\pi^0\ell^+\nu)[\mathcal{B}(D^{*0} \to D^0\pi^0) + \mathcal{B}(D^{*0} \to D^0\gamma)]\mathcal{B}(D^0 \to K^-\pi^+) \\
&= N_{B\bar{B}} C_{B^+} [\mathcal{B}(B^+ \to D^{*-}\pi^+\ell^+\nu)\mathcal{B}(D^{*+} \to D^0\pi^+) + \mathcal{B}(B^+ \to \bar{D}^{*0}\pi^0\ell^+\nu)] \\
&\quad \times \mathcal{B}(D^0 \to K^-\pi^+)
\end{aligned} \tag{54}
$$

The coefficient is

$$C_{14}^{MC} = \frac{C_{B^+}[\mathcal{B}(B^+ \to D^{*-}\pi^+\ell^+\nu)\mathcal{B}(D^{*+} \to D^0\pi^+) + \mathcal{B}(B^+ \to \bar{D}^{*0}\pi^0\ell^+\nu)] \times\mathcal{B}(D^0 \to K^-\pi^+)}{[\mathcal{B}(B^+ \to D^{*-}\pi^+\ell^+\nu)^0\mathcal{B}(D^{*+} \to D^0\pi^+)^0 + \mathcal{B}(B^+ \to \bar{D}^{*0}\pi^0\ell^+\nu)^0] \times\mathcal{B}(D^0 \to K^-\pi^+)^0} \tag{55}$$

- $j = 15:\ B^0 \to D^*\pi\ell^+\nu$
  The decays contribute to this mode are
  $B^0 \to D^{*-}\pi^0\ell^+\nu$ with $D^{*-} \to \bar{D}^0 + \pi^-$
  $B^0 \to \bar{D}^{*0}\pi^-\ell^+\nu$ with $\bar{D}^{*0} \to \bar{D}^0 + \gamma/\pi^0$
  Number of produced events is

$$\begin{aligned} N &= N_{B\bar{B}}C_{B^0}\mathcal{B}(B^0 \to D^{*-}\pi^0\ell^+\nu)\mathcal{B}(D^{*+} \to D^0\pi^+)\mathcal{B}(D^0 \to K^-\pi^+) \\ &\quad +N_{B\bar{B}}C_{B^0}\mathcal{B}(B^0 \to \bar{D}^{*0}\pi^-\ell^+\nu)[\mathcal{B}(D^{*0} \to D^0\pi^0) + \mathcal{B}(D^{*0} \to D^0\gamma)]\mathcal{B}(D^0 \to K^-\pi^+) \\ &= N_{B\bar{B}}C_{B^0}[\mathcal{B}(B^0 \to D^{*-}\pi^0\ell^+\nu)\mathcal{B}(D^{*+} \to D^0\pi^+) + \mathcal{B}(B^0 \to \bar{D}^{*0}\pi^-\ell^+\nu)] \\ &\quad \times\mathcal{B}(D^0 \to K^-\pi^+) \end{aligned} \tag{56}$$

  The coefficient is

$$C_{15}^{MC} = \frac{C_{B^0}[\mathcal{B}(B^0 \to D^{*-}\pi^0\ell^+\nu)\mathcal{B}(D^{*+} \to D^0\pi^+) + \mathcal{B}(B^0 \to \bar{D}^{*0}\pi^-\ell^+\nu)] \times\mathcal{B}(D^0 \to K^-\pi^+)}{[\mathcal{B}(B^0 \to D^{*-}\pi^0\ell^+\nu)^0\mathcal{B}(D^{*+} \to D^0\pi^+)^0 + \mathcal{B}(B^0 \to \bar{D}^{*0}\pi^-\ell^+\nu)^0] \times\mathcal{B}(D^0 \to K^-\pi^+)^0} \tag{57}$$

4.3.2 Coefficients for backgrounds : $j = 16 - 27$

There are 12 background MC modes. The coefficient of each mode is

- $j = 16$, UncorrDL from B^+B^-

$$C_{16}^{MC} = C_{UncorDL}^{D^0}\frac{C_{B^+}\mathcal{B}(D^0 \to K^-\pi^+)}{\mathcal{B}(D^0 \to K^-\pi^+)^0} \tag{58}$$

- $j = 17$, UncorrDL from $B^0\bar{B}^0$

$$C_{17}^{MC} = C_{UncorDL}^{D^0}\frac{C_{B^0}\mathcal{B}(D^0 \to K^-\pi^+)}{\mathcal{B}(D^0 \to K^-\pi^+)^0} \tag{59}$$

- $j = 18$, UncorrCL from B^+B^-

$$C_{18}^{MC} = C_{UncorCL}^{D^0}\frac{C_{B^+}\mathcal{B}(D^0 \to K^-\pi^+)}{\mathcal{B}(D^0 \to K^-\pi^+)^0} \tag{60}$$

- $j = 19$, UncorrCL from $B^0\bar{B}^0$

$$C_{19}^{MC} = C_{UncorCL}^{D^0}\frac{C_{B^0}\mathcal{B}(D^0 \to K^-\pi^+)}{\mathcal{B}(D^0 \to K^-\pi^+)^0} \tag{61}$$

- $j = 20$, CascL from B^+B^-

$$C_{20}^{MC} = C_{CascL}^{D^0}\frac{C_{B^+}\mathcal{B}(D^0 \to K^-\pi^+)}{\mathcal{B}(D^0 \to K^-\pi^+)^0} \tag{62}$$

- $j = 21$, CascL from $B^0\bar{B}^0$

$$C_{21}^{MC} = C_{CascL}^{D^0}\frac{C_{B^0}\mathcal{B}(D^0 \to K^-\pi^+)}{\mathcal{B}(D^0 \to K^-\pi^+)^0} \tag{63}$$

- $j = 22$, FakeL from B^+B^-

$$C_{22}^{MC} = C_{FakeL}^{D^0}\frac{C_{B^+}\mathcal{B}(D^0 \to K^-\pi^+)}{\mathcal{B}(D^0 \to K^-\pi^+)^0} \tag{64}$$

- $j = 23$, FakeL from $B^0\bar{B}^0$

$$C_{23}^{MC} = C_{FakeL}^{D^0}\frac{C_{B^0}\mathcal{B}(D^0 \to K^-\pi^+)}{\mathcal{B}(D^0 \to K^-\pi^+)^0} \tag{65}$$

- $j = 24$, CombRL from B^+B^-

$$C_{24}^{MC} = \frac{C_{B^+}\mathcal{B}(D^0 \to K^-\pi^+)}{\mathcal{B}(D^0 \to K^-\pi^+)^0} \tag{66}$$

- $j = 25$, CombRL from $B^0\bar{B}^0$

$$C_{25}^{MC} = \frac{C_{B^0}\mathcal{B}(D^0 \to K^-\pi^+)}{\mathcal{B}(D^0 \to K^-\pi^+)^0} \tag{67}$$

- $j = 26$, CombFL from B^+B^-

$$C_{26}^{MC} = \frac{C_{B^+}\mathcal{B}(D^0 \to K^-\pi^+)}{\mathcal{B}(D^0 \to K^-\pi^+)^0} \tag{68}$$

- $j = 27$, CombFL from $B^0\bar{B}^0$

$$C_{27}^{MC} = \frac{C_{B^0}\mathcal{B}(D^0 \to K^-\pi^+)}{\mathcal{B}(D^0 \to K^-\pi^+)^0} \tag{69}$$

The factors such as $C_{UncorDL}^{D^0}$ are free parameters to be floated with constraints in the fit. See section 5.3 for details of constraints.

4.4 D^+ MC modes

4.4.1 Coefficients for signals : $j = 1 - 14$

There are 14 signal MC modes.

- $j = 1$: $B^0 \to D^-\ell^+\nu$
  The coefficient is

$$C_1^{MC} = \frac{C_{B^0}\mathcal{B}(B^0 \to D^-\ell^+\nu)\mathcal{B}(D^+ \to K^-\pi^+\pi^+)}{\mathcal{B}(B^0 \to D^-\ell^+\nu)^0\mathcal{B}(D^+ \to K^-\pi^+\pi^+)^0} \tag{70}$$

- $j = 2$: $B^0 \to D^{*-}\ell^+\nu$ with $D^{*-} \to D^- + \gamma/\pi^0$
  The coefficient is

$$C_2^{MC} = \frac{\begin{array}{l} C_{B^0}\mathcal{B}(B^0 \to D^{*-}\ell^+\nu)\times \\ {[\mathcal{B}(D^{*+} \to D^+\pi^0) + \mathcal{B}(D^{*+} \to D^+\gamma)]\mathcal{B}(D^+ \to K^-\pi^+\pi^+)} \end{array}}{\begin{array}{l} \mathcal{B}(B^0 \to D^{*-}\ell^+\nu)^0\times \\ {[\mathcal{B}(D^{*+} \to D^+\pi^0)^0 + \mathcal{B}(D^{*+} \to D^+\gamma)^0]\mathcal{B}(D^+ \to K^-\pi^+\pi^+)^0} \end{array}} \tag{71}$$

- $j = 3$: $B^+ \to \bar{D}_0^{*0}\ell^+\nu$ with $\bar{D}_0^{*0} \to D^- + \pi^+$
  The coefficient is

$$C_3^{MC} = \frac{C_{B^+}\mathcal{B}(B^+ \to \bar{D}_0^{*0}\ell^+\nu)\mathcal{B}(D_0^{*0} \to D^+\pi^-)\mathcal{B}(D^+ \to K^-\pi^+\pi^+)}{\mathcal{B}(B^+ \to \bar{D}_0^{*0}\ell^+\nu)^0\mathcal{B}(D_0^{*0} \to D^+\pi^-)^0\mathcal{B}(D^+ \to K^-\pi^+\pi^+)^0} \tag{72}$$

- $j = 4$: $B^0 \to D_0^{*-}\ell^+\nu$ with $D_0^{*-} \to D^-\pi^0$
  The coefficient is

$$C_4^{MC} = \frac{C_{B^0}\mathcal{B}(B^0 \to D_0^{*-}\ell^+\nu)\mathcal{B}(D_0^{*+} \to D^+\pi^0)\mathcal{B}(D^+ \to K^-\pi^+\pi^+)}{\mathcal{B}(B^0 \to D_0^{*-}\ell^+\nu)^0\mathcal{B}(D_0^{*+} \to D^+\pi^0)^0\mathcal{B}(D^+ \to K^-\pi^+\pi^+)^0} \tag{73}$$

- $j = 5$: $B^+ \to \bar{D}_1^0\ell^+\nu$ with $\bar{D}_1^0 \to D^{*-} + \pi^+$ and $D^{*-} \to D^- + \pi^0/\gamma$
  The coefficient is

$$C_5^{MC} = \frac{\begin{array}{l} C_{B^+}\mathcal{B}(B^+ \to \bar{D}_1^0\ell^+\nu)\mathcal{B}(D_1^0 \to D^{*+}\pi^-)\times \\ {[\mathcal{B}(D^{*+} \to D^+\pi^0) + \mathcal{B}(D^{*+} \to D^+\gamma)]\mathcal{B}(D^+ \to K^-\pi^+\pi^+)} \end{array}}{\begin{array}{l} \mathcal{B}(B^+ \to \bar{D}_1^0\ell^+\nu)^0\mathcal{B}(D_1^0 \to D^{*+}\pi^-)^0\times \\ {[\mathcal{B}(D^{*+} \to D^+\pi^0)^0 + \mathcal{B}(D^{*+} \to D^+\gamma)^0]\mathcal{B}(D^+ \to K^-\pi^+\pi^+)^0} \end{array}} \tag{74}$$

- $j = 6$: $B^0 \to D_1^-\ell^+\nu$ with $D_1^- \to D^{*-}\pi^0$ and $D^{*-} \to D^- + \pi^0/\gamma$
  The coefficient is

$$C_6^{MC} = \frac{\begin{array}{l} C_{B^0}\mathcal{B}(B^0 \to D_1^-\ell^+\nu)\mathcal{B}(D_1^+ \to D^{*+}\pi^0)\times \\ {[\mathcal{B}(D^{*+} \to D^+\pi^0) + \mathcal{B}(D^{*+} \to D^+\gamma)]\mathcal{B}(D^+ \to K^-\pi^+\pi^+)} \end{array}}{\begin{array}{l} \mathcal{B}(B^0 \to D_1^-\ell^+\nu)^0\mathcal{B}(D_1^+ \to D^{*+}\pi^0)^0\times \\ {[\mathcal{B}(D^{*+} \to D^+\pi^0)^0 + \mathcal{B}(D^{*+} \to D^+\gamma)^0]\mathcal{B}(D^+ \to K^-\pi^+\pi^+)^0} \end{array}} \tag{75}$$

- $j = 7:\ B^+ \to \bar{D}_1'^0 \ell^+ \nu$ with $\bar{D}_1'^0 \to D^{*-} + \pi^+$ and $D^{*-} \to D^- + \pi^0/\gamma$
  The coefficient is

$$C_7^{MC} = \frac{\begin{array}{l} C_{B^+}\mathcal{B}(B^+ \to \bar{D}_1'^0 \ell^+ \nu)\mathcal{B}(D_1'^0 \to D^{*+}\pi^-)\times \\ [\mathcal{B}(D^{*+} \to D^+\pi^0) + \mathcal{B}(D^{*+} \to D^+\gamma)]\mathcal{B}(D^+ \to K^-\pi^+\pi^+) \end{array}}{\begin{array}{l} \mathcal{B}(B^+ \to \bar{D}_1'^0 \ell^+ \nu)^0 \mathcal{B}(D_1'^0 \to D^{*+}\pi^-)^0\times \\ [\mathcal{B}(D^{*+} \to D^+\pi^0)^0 + \mathcal{B}(D^{*+} \to D^+\gamma)^0]\mathcal{B}(D^+ \to K^-\pi^+\pi^+)^0 \end{array}} \tag{76}$$

- $j = 8:\ B^0 \to D_1'^- \ell^+ \nu$ with $D_1'^- \to D^{*-}\pi^0$ and $D^{*-} \to D^- + \pi^0/\gamma$
  The coefficient is

$$C_8^{MC} = \frac{\begin{array}{l} C_{B^0}\mathcal{B}(B^0 \to D_1'^- \ell^+ \nu)\mathcal{B}(D_1'^+ \to D^{*+}\pi^0)\times \\ [\mathcal{B}(D^{*+} \to D^+\pi^0) + \mathcal{B}(D^{*+} \to D^+\gamma)]\mathcal{B}(D^+ \to K^-\pi^+\pi^+) \end{array}}{\begin{array}{l} \mathcal{B}(B^0 \to D_1'^- \ell^+ \nu)^0 \mathcal{B}(D_1'^+ \to D^{*+}\pi^0)^0\times \\ [\mathcal{B}(D^{*+} \to D^+\pi^0)^0 + \mathcal{B}(D^{*+} \to D^+\gamma)^0]\mathcal{B}(D^+ \to K^-\pi^+\pi^+)^0 \end{array}} \tag{77}$$

- $j = 9:\ B^+ \to \bar{D}_2^{*0} \ell^+ \nu$
  The decays contribute to this mode are
  $B^+ \to \bar{D}_2^{*0} \ell^+ \nu$ with $\bar{D}_2^{*0} \to D^{*-} + \pi^+$ and $D^{*-} \to D^- + \pi^0/\gamma$
  $B^+ \to \bar{D}_2^{*0} \ell^+ \nu$ with $\bar{D}_2^{*0} \to D^- + \pi^+$
  The coefficient is

$$C_9^{MC} = \frac{\begin{array}{l} C_{B^+}\mathcal{B}(B^+ \to \bar{D}_2^{*0} \ell^+ \nu)\times \\ \{\mathcal{B}(D_2^{*0} \to D^{*+}\pi^-)[\mathcal{B}(D^{*+} \to D^+\pi^0) + \mathcal{B}(D^{*+} \to D^+\gamma)] + \mathcal{B}(D_2^{*0} \to D^+\pi^-)\} \\ \times\mathcal{B}(D^+ \to K^-\pi^+\pi^+) \end{array}}{\begin{array}{l} \mathcal{B}(B^+ \to \bar{D}_2^{*0} \ell^+ \nu)^0\times \\ \{\mathcal{B}(D_2^{*0} \to D^{*+}\pi^-)^0[\mathcal{B}(D^{*+} \to D^+\pi^0)^0 + \mathcal{B}(D^{*+} \to D^+\gamma)^0] + \mathcal{B}(D_2^{*0} \to D^+\pi^-)^0)\} \\ \times\mathcal{B}(D^+ \to K^-\pi^+\pi^+)^0 \end{array}} \tag{78}$$

- $j = 10:\ B^0 \to D_2^{*-} \ell^+ \nu$
  The decays contribute to this mode are
  $B^0 \to D_2^{*-} \ell^+ \nu$ with $D_2^{*-} \to D^{*-}\pi^0$ and $D^{*-} \to D^- + \pi^0/\gamma$
  $B^0 \to D_2^{*-} \ell^+ \nu$ with $D_2^{*-} \to D^-\pi^0$

The coefficient is

$$C_{10}^{MC} = \frac{\begin{array}{l} C_{B^0}\mathcal{B}(B^0 \to D_2^{*-}\ell^+\nu)\times \\ \{\mathcal{B}(D_2^{*+} \to D^{*+}\pi^0)[\mathcal{B}(D^{*+} \to D^+\pi^0) + \mathcal{B}(D^{*+} \to D^+\gamma)] + \mathcal{B}(D_2^{*+} \to D^+\pi^0)\} \\ \times\mathcal{B}(D^+ \to K^-\pi^+\pi^+) \end{array}}{\begin{array}{l} \mathcal{B}(B^0 \to D_2^{*-}\ell^+\nu)^0\times \\ \{\mathcal{B}(D_2^{*+} \to D^{*+}\pi^0)^0[\mathcal{B}(D^{*+} \to D^+\pi^0)^0 + \mathcal{B}(D^{*+} \to D^+\gamma)^0] + \mathcal{B}(D_2^{*+} \to D^+\pi^0)^0)\} \\ \times\mathcal{B}(D^+ \to K^-\pi^+\pi^+)^0 \end{array}} \quad (79)$$

- $j = 11: \ B^+ \to D^-\pi^+\ell^+\nu$
  The coefficient is

$$C_{11}^{MC} = \frac{C_{B^+}\mathcal{B}(B^+ \to D^-\pi^+\ell^+\nu)\mathcal{B}(D^+ \to K^-\pi^+\pi^+)}{\mathcal{B}(B^+ \to D^-\pi^+\ell^+\nu)^0\mathcal{B}(D^+ \to K^-\pi^+\pi^+)^0} \quad (80)$$

- $j = 12: \ B^0 \to D^-\pi^0\ell^+\nu$
  The coefficient is

$$C_{12}^{MC} = \frac{C_{B^0}\mathcal{B}(B^0 \to D^-\pi^0\ell^+\nu)\mathcal{B}(D^+ \to K^-\pi^+\pi^+)}{\mathcal{B}(B^0 \to D^-\pi^0\ell^+\nu)^0\mathcal{B}(D^+ \to K^-\pi^+\pi^+)^0} \quad (81)$$

- $j = 13: \ B^+ \to D^{*-}\pi^+\ell^+\nu$ with $D^{*-} \to D^- + \gamma/\pi^0$
  The coefficient is

$$C_{13}^{MC} = \frac{\begin{array}{l} C_{B^+}\mathcal{B}(B^+ \to D^{*-}\pi^+\ell^+\nu)\times \\ [\mathcal{B}(D^{*+} \to D^+\pi^0) + \mathcal{B}(D^{*+} \to D^+\gamma)]\mathcal{B}(D^+ \to K^-\pi^+\pi^+) \end{array}}{\begin{array}{l} \mathcal{B}(B^+ \to D^{*-}\pi^+\ell^+\nu)^0\times \\ [\mathcal{B}(D^{*+} \to D^+\pi^0)^0 + \mathcal{B}(D^{*+} \to D^+\gamma)^0]\mathcal{B}(D^+ \to K^-\pi^+\pi^+)^0 \end{array}} \quad (82)$$

- $j = 14: \ B^0 \to D^{*-}\pi^0\ell^+\nu$ with $D^{*-} \to D^- + \gamma/\pi^0$
  The coefficient is

$$C_{14}^{MC} = \frac{\begin{array}{l} C_{B^0}\mathcal{B}(B^0 \to D^{*-}\pi^0\ell^+\nu)\times \\ [\mathcal{B}(D^{*+} \to D^+\pi^0) + \mathcal{B}(D^{*+} \to D^+\gamma)]\mathcal{B}(D^+ \to K^-\pi^+\pi^+) \end{array}}{\begin{array}{l} \mathcal{B}(B^0 \to D^{*-}\pi^0\ell^+\nu)^0\times \\ [\mathcal{B}(D^{*+} \to D^+\pi^0)^0 + \mathcal{B}(D^{*+} \to D^+\gamma)^0]\mathcal{B}(D^+ \to K^-\pi^+\pi^+)^0 \end{array}} \quad (83)$$

4.4.2 Coefficients for backgrounds : $j = 15 - 26$

There are 16 background MC modes (j). The coefficient of each mode is

- $j = 15$, UncorrDL B^+B^-

$$C_{15}^{MC} = C_{UncorDL}^{D^+} \frac{C_{B^+}\mathcal{B}(D^+ \to K^-\pi^+\pi^+)}{\mathcal{B}(D^+ \to K^-\pi^+\pi^+)^0} \tag{84}$$

- $j = 16$, UncorrDL from $B^0\bar{B}^0$

$$C_{16}^{MC} = C_{UncorDL}^{D^+} \frac{C_{B^0}\mathcal{B}(D^+ \to K^-\pi^+\pi^+)}{\mathcal{B}(D^+ \to K^-\pi^+\pi^+)^0} \tag{85}$$

- $j = 17$, UncorrCL from B^+B^-

$$C_{17}^{MC} = C_{UncorCL}^{D^+} \frac{C_{B^+}\mathcal{B}(D^+ \to K^-\pi^+\pi^+)}{\mathcal{B}(D^+ \to K^-\pi^+\pi^+)^0} \tag{86}$$

- $j = 18$, UncorrCL from $B^0\bar{B}^0$

$$C_{18}^{MC} = C_{UncorCL}^{D^+} \frac{C_{B^0}\mathcal{B}(D^+ \to K^-\pi^+\pi^+)}{\mathcal{B}(D^+ \to K^-\pi^+\pi^+)^0} \tag{87}$$

- $j = 19$, CascL from B^+B^-

$$C_{19}^{MC} = C_{CascL}^{D^+} \frac{C_{B^+}\mathcal{B}(D^+ \to K^-\pi^+\pi^+)}{\mathcal{B}(D^+ \to K^-\pi^+\pi^+)^0} \tag{88}$$

- $j = 20$, CascL from $B^0\bar{B}^0$

$$C_{20}^{MC} = C_{CascL}^{D^+} \frac{C_{B^0}\mathcal{B}(D^+ \to K^-\pi^+\pi^+)}{\mathcal{B}(D^+ \to K^-\pi^+\pi^+)^0} \tag{89}$$

- $j = 21$, FakeL from B^+B^-

$$C_{21}^{MC} = C_{FakeL}^{D^+} \frac{C_{B^+}\mathcal{B}(D^+ \to K^-\pi^+\pi^+)}{\mathcal{B}(D^+ \to K^-\pi^+\pi^+)^0} \tag{90}$$

- $j = 22$, FakeL from $B^0\bar{B}^0$

$$C_{22}^{MC} = C_{FakeL}^{D^+} \frac{C_{B^0}\mathcal{B}(D^+ \to K^-\pi^+\pi^+)}{\mathcal{B}(D^+ \to K^-\pi^+\pi^+)^0} \tag{91}$$

- $j = 23$, CombRL from B^+B^-

$$C_{23}^{MC} = \frac{C_{B^+}\mathcal{B}(D^+ \to K^-\pi^+\pi^+)}{\mathcal{B}(D^+ \to K^-\pi^+\pi^+)^0} \tag{92}$$

- $j = 24$, CombRL from $B^0\bar{B}^0$

$$C_{24}^{MC} = \frac{C_{B^0}\mathcal{B}(D^+ \to K^-\pi^+\pi^+)}{\mathcal{B}(D^+ \to K^-\pi^+\pi^+)^0} \tag{93}$$

- $j = 25$, CombFL from B^+B^-

$$C_{25}^{MC} = \frac{C_{B^+}\mathcal{B}(D^+ \to K^-\pi^+\pi^+)}{\mathcal{B}(D^+ \to K^-\pi^+\pi^+)^0} \tag{94}$$

- $j = 26$, CombFL from $B^0\bar{B}^0$

$$C_{26}^{MC} = \frac{C_{B^0}\mathcal{B}(D^+ \to K^-\pi^+\pi^+)}{\mathcal{B}(D^+ \to K^-\pi^+\pi^+)^0} \tag{95}$$

5 Constraints on variables in the fit

5.1 $B \to D^{**}\ell\nu$ and $B \to D^{(*)}\pi\ell\nu$ decay branching fractions

[Note] The calculated results in this subsection are not used in our fit as explained later. We keep this section for the following purposes :

- **to show the origin of our parametrization.**
- **to keep the original numbers for a reference.**

Our fitting method does not have the sensitivity to determine all 16 branching fractions of $B \to D^{**}\ell\nu$ and $B \to D^{(*)}\pi\ell\nu$ (non-resonant) decays. Thus, we need constraints to reduce free parameters. Available measurements of these decay modes are very limited. Currently we have only four usable results. The first is from PDG [12]

$$\mathcal{B}(B^+ \to \bar{D}_1^0\ell^+\nu) = 0.0056 \pm 0.0013 \pm 0.0009 = 0.0056 \pm 0.00158 \tag{96}$$

The next is from the most recent Babar measurement [15]

$$\begin{aligned}
\mathcal{B}(B^+ \to \bar{D}_1^0\ell^+\nu) &= 0.00448 \pm 0.00026 \pm 0.00035 = 0.00448 \pm 0.000436 \\
\mathcal{B}(B^+ \to \bar{D}_2^{*0}\ell^+\nu) &= 0.00354 \pm 0.00032 \pm 0.00054 = 0.00354 \pm 0.000627 \\
\mathcal{B}(B^0 \to D_1^-\ell^+\nu) &= 0.00364 \pm 0.00032 \pm 0.00049 = 0.00364 \pm 0.000585 \\
\mathcal{B}(B^0 \to D_2^{*-}\ell^+\nu) &= 0.00270 \pm 0.00035 \pm 0.00043 = 0.00270 \pm 0.000554
\end{aligned} \tag{97}$$

The third is from the most recent DELPHI measurement [16]

$$\begin{aligned}
&\mathcal{B}(B^0 \to D_0^{*-}\ell^+\nu) = 0.0042 \pm 0.0033 \pm 0.0022 = 0.0042 \pm 0.0040 \\
&\mathcal{B}(B^0 \to D_1'^-\ell^+\nu) = 0.0124 \pm 0.0025 \pm 0.0027 = 0.0124 \pm 0.0037 \\
&\mathcal{BT}(B^0 \to D^{**-}\ell^+\nu) \\
&\equiv \mathcal{B}(B^0 \to D_0^{*-}\ell^+\nu) + \mathcal{B}(B^0 \to D_1'^-\ell^+\nu) + \mathcal{B}(B^0 \to D_1^-\ell^+\nu) + \mathcal{B}(B^0 \to D_2^{*-}\ell^+\nu) \\
&= 0.027 \pm 0.007 \pm 0.002 = 0.027 \pm 0.073
\end{aligned} \tag{98}$$

The last is also from PDG [12]

$$\begin{aligned}
\mathcal{BT}(B^+ \to D^-\pi^+\ell^+\nu) &= 0.0053 \pm 0.0009 \pm 0.0005 = 0.0053 \pm 0.0010 \\
\mathcal{BT}(B^+ \to D^{*-}\pi^+\ell^+\nu) &= 0.0064 \pm 0.0015 \pm 0.0002 = 0.0064 \pm 0.0015 \\
\mathcal{BT}(B^0 \to \bar{D}^0\pi^-\ell^+\nu) &= 0.0032 \pm 0.0009 \pm 0.0003 = 0.0032 \pm 0.00095 \\
\mathcal{BT}(B^0 \to \bar{D}^{*0}\pi^-\ell^+\nu) &= 0.0065 \pm 0.0015 \pm 0.0005 = 0.0065 \pm 0.0016
\end{aligned} \tag{99}$$

These values are based on a BELLE measurement [17] and $B \to D^{**}\ell\nu$ decays are included in these branching fractions.
As we show in the following sections, it is convenient to divide $B \to D^{**}\ell\nu$ and $B \to D^{(*)}\pi\ell\nu$ (non-resonant) decay branching fractions into three categories : "$B \to D_1\ell\nu$ and $B \to D_2^*\ell\nu$", "$B \to D_0^*\ell\nu$ and $B \to D\pi\ell\nu$", and "$B \to D_1'\ell\nu$ and $B \to D^*\pi\ell\nu$".

5.1.1 $B \to D_1 \ell\nu$ and $B \to D_2^* \ell\nu$

There are 4 branching fractions in these decay modes : $\mathcal{B}(B^+ \to \bar{D}_1^0 \ell^+\nu)$, $\mathcal{B}(B^0 \to D_1^- \ell^+\nu)$, $\mathcal{B}(B^+ \to \bar{D}_2^{*0} \ell^+\nu)$ and $\mathcal{B}(B^0 \to D_2^{*-} \ell^+\nu)$. We define two parameters, one total branching fraction and one branching fraction ratio, and relate the 4 branching fractions to the parameters. Based on isospin symmetry

$$\begin{aligned} \mathcal{B}(B^+ \to \bar{D}_1^0 \ell^+\nu) &= t_{+0}\mathcal{B}(B^0 \to D_1^- \ell^+\nu) \\ \mathcal{B}(B^+ \to \bar{D}_2^{*0} \ell^+\nu) &= t_{+0}\mathcal{B}(B^0 \to D_2^{*-} \ell^+\nu) \end{aligned} \tag{100}$$

The Babar results (Equation (97)) show that isospin symmetry holds. Thus, we take averages. As we do not know the correlation between these branching fractions, we take a conservative side and assume the maximum correlation

$$\begin{aligned} \mathcal{B}(B^+ \to \bar{D}_1^0 \ell^+\nu) &= \tfrac{1}{2}\left[(0.00448 \pm 0.000436) + (0.00364 \pm 0.000585) \times (1.071 \pm 0.009)\right] \\ &= \tfrac{1}{2}\left[(0.00448 \pm 0.000436) + (0.003898 \pm 0.0006274)\right] \\ &= 0.00419 \pm 0.000532 \end{aligned} \tag{101}$$

and

$$\begin{aligned} \mathcal{B}(B^+ \to \bar{D}_2^{*0} \ell^+\nu) &= \tfrac{1}{2}\left[(0.00354 \pm 0.000627) + (0.00270 \pm 0.000554) \times (1.071 \pm 0.009)\right] \\ &= \tfrac{1}{2}\left[(0.00354 \pm 0.000627) + (0.002892 \pm 0.0005938)\right] \\ &= 0.003215 \pm 0.0006104 \end{aligned} \tag{102}$$

Thus, if we define a total branching fraction

$$\begin{aligned} \mathcal{BT}(B^+ \to \bar{D}_1^0/\bar{D}_2^{*0} \ell^+\nu) &\equiv \mathcal{B}(B^+ \to \bar{D}_1^0 \ell^+\nu) + \mathcal{B}(B^+ \to \bar{D}_2^{*0} \ell^+\nu) \\ &= (0.00419 \pm 0.000532) + (0.003215 \pm 0.0006104) \\ &= 0.007405 \pm 0.0011874 \end{aligned} \tag{103}$$

and a branching fraction ratio

$$\begin{aligned} f_{D_2^*/D_1} \equiv \frac{\mathcal{B}(B^+ \to \bar{D}_2^{*0} \ell^+\nu)}{\mathcal{B}(B^+ \to \bar{D}_1^0 \ell^+\nu)} &= \frac{0.003215 \pm 0.0006104}{0.00419 \pm 0.000532} \\ &= 0.767 \pm 0.243 \end{aligned} \tag{104}$$

We can relate 4 branching fractions to $f_{D_2^*/D_1}$ and $\mathcal{BT}(B^+ \to \bar{D}_1^0/\bar{D}_2^{*0} \ell^+\nu)$

$$\mathcal{B}(B^+ \to \bar{D}_1^0 \ell^+\nu) = \frac{1}{1+f_{D_2^*/D_1}} \mathcal{BT}(B^+ \to \bar{D}_1^0/\bar{D}_2^{*0} \ell^+\nu) \tag{105}$$

$$\begin{aligned} \mathcal{B}(B^0 \to D_1^- \ell^+\nu) &= \frac{\mathcal{B}(B^+ \to \bar{D}_1^0 \ell^+\nu)}{t_{+0}} \\ &= \frac{1}{t_{+0}(1+f_{D_2^*/D_1})} \mathcal{BT}(B^+ \to \bar{D}_1^0/\bar{D}_2^{*0} \ell^+\nu) \end{aligned} \tag{106}$$

$$\begin{aligned}
\mathcal{B}(B^+ \to \bar{D}_2^{*0}\ell^+\nu) &= f_{D_2^*/D_1}\mathcal{B}(B^+ \to \bar{D}_1^0\ell^+\nu) \\
&= \frac{f_{D_2^*/D_1}}{1+f_{D_2^*/D_1}}\mathcal{BT}(B^+ \to \bar{D}_1^0/\bar{D}_2^{*0}\ell^+\nu)
\end{aligned} \tag{107}$$

$$\begin{aligned}
\mathcal{B}(B^0 \to D_2^{*-}\ell^+\nu) &= \frac{\mathcal{B}(B^+ \to \bar{D}_2^{*0}\ell^+\nu)}{t_{+0}} \\
&= \frac{\mathcal{B}(B^+ \to \bar{D}_2^{*0}\ell^+\nu)}{t_{+0}(1+f_{D_2^*/D_1})}\mathcal{BT}(B^+ \to \bar{D}_1^0/\bar{D}_2^{*0}\ell^+\nu)
\end{aligned} \tag{108}$$

5.1.2 $B \to D_0^*\ell\nu$ and non-resonant $B \to D\pi\ell\nu$

There are 6 branching fractions in this category : $\mathcal{B}(B^+ \to \bar{D}_0^{*0}\ell^+\nu)$, $\mathcal{B}(B^0 \to D_0^{*-}\ell^+\nu)$, $\mathcal{B}(B^+ \to D^-\pi^+\ell^+\nu)$, $\mathcal{B}(B^0 \to \bar{D}^0\pi^-\ell^+\nu)$, $\mathcal{B}(B^+ \to \bar{D}^0\pi^0\ell^+\nu)$ and $\mathcal{B}(B^0 \to D^-\pi^0\ell^+\nu)$. As in the previous section, we define two parameters, one total branching fraction and one branching fraction ratio, and relate the 6 branching fractions to the parameters. Isospin symmetry gives

$$\begin{aligned}
&\mathcal{B}(B^+ \to \bar{D}_0^{*0}\ell^+\nu) = t_{+0}\mathcal{B}(B^0 \to D_0^{*-}\ell^+\nu) \\
&\mathcal{B}(B^+ \to D^-\pi^+\ell^+\nu) = 2\mathcal{B}(B^+ \to \bar{D}^0\pi^0\ell^+\nu) \\
&\quad = t_{+0}\mathcal{B}(B^0 \to \bar{D}^0\pi^-\ell^+\nu) = 2t_{+0}\mathcal{B}(B^0 \to D^-\pi^0\ell^+\nu) \\
&\mathcal{BT}(B^+ \to D^-\pi^+\ell^+\nu) = t_{+0}\mathcal{BT}(B^0 \to \bar{D}^0\pi^-\ell^+\nu)
\end{aligned} \tag{109}$$

Note that $\mathcal{BT}(B^+ \to D^-\pi^+\ell^+\nu)$ is what is given in Equation (99). This includes not only non-resonant $D^-\pi^+$ mode but also relevant D^{**} modes. Thus,

$$\begin{aligned}
&\mathcal{BT}(B^+ \to D^-\pi^+\ell^+\nu) \\
&= \mathcal{B}(B^+ \to \bar{D}_0^{*0}\ell^+\nu)\mathcal{B}(\bar{D}_0^{*0} \to D^-\pi^+) + \mathcal{B}(B^+ \to \bar{D}_2^{*0}\ell^+\nu)\mathcal{B}(\bar{D}_2^{*0} \to D^-\pi^+) \\
&\quad +\mathcal{B}(B^+ \to D^-\pi^+\ell^+\nu)
\end{aligned} \tag{110}$$

Using the above isospin condition, we can take an average of Equation (99). Here, we also take the maximum correlation

$$\begin{aligned}
&\mathcal{BT}(B^+ \to D^-\pi^+\ell^+\nu) \\
&= \tfrac{1}{2}\left[(0.0053 \pm 0.0010) + (0.00323 \pm 0.00095) \times (1.071 \pm 0.009)\right] \\
&= \tfrac{1}{2}\left[(0.0053 \pm 0.0010) + (0.00346 \pm 0.001018)\right] \\
&= 0.00438 \pm 0.00101
\end{aligned} \tag{111}$$

From Equation (110),

$$\begin{aligned}
&\mathcal{BT}(B^+ \to D^-\pi^+\ell^+\nu) \\
&= \mathcal{B}(B^+ \to \bar{D}_0^{*0}\ell^+\nu) \times \tfrac{2}{3} + \mathcal{B}(B^+ \to \bar{D}_2^{*0}\ell^+\nu)\mathcal{B}(\bar{D}_2^{*0} \to D^-\pi^+) \\
&\quad +\mathcal{B}(B^+ \to D^-\pi^+\ell^+\nu)
\end{aligned} \tag{112}$$

Using equations (196) (in section 9) and (102),

$$\begin{aligned}
&\mathcal{B}(B^+ \to D^-\pi^+\ell^+\nu) + \tfrac{2}{3}\mathcal{B}(B^+ \to \bar{D}_0^{*0}\ell^+\nu) \\
&= \mathcal{BT}(B^+ \to D^-\pi^+\ell^+\nu) - \mathcal{B}(B^+ \to \bar{D}_2^{*0}\ell^+\nu)\mathcal{B}(\bar{D}_2^{*0} \to D^-\pi^+) \\
&= (0.00438 \pm 0.00101) - (0.003215 \pm 0.0006104) \times (0.452 \pm 0.167) \\
&= (0.00438 \pm 0.00101) - (0.001453 \pm 0.0006036) \\
&= 0.00293 \pm 0.00118
\end{aligned} \tag{113}$$

Thus, if we define a total branching fraction

$$\begin{aligned}
&\mathcal{BT}(B^+ \to \bar{D}_0^{*0}/(D\pi)^0\ell^+\nu) \\
&\equiv \mathcal{B}(B^+ \to \bar{D}_0^{*0}\ell^+\nu) + \mathcal{B}(B^+ \to D^-\pi^+\ell^+\nu) + \mathcal{B}(B^+ \to \bar{D}^0\pi^0\ell^+\nu) \\
&= \mathcal{B}(B^+ \to \bar{D}_0^{*0}\ell^+\nu) + \tfrac{3}{2}\mathcal{B}(B^+ \to D^-\pi^+\ell^+\nu) \\
&= \tfrac{3}{2}(0.00293 \pm 0.00118) = 0.0044 \pm 0.0018
\end{aligned} \tag{114}$$

and a branching fraction ratio

$$f_{D\pi/D_0^*} \equiv \frac{\mathcal{B}(B^+ \to D^-\pi^+\ell^+\nu)}{\mathcal{B}(B^+ \to \bar{D}_0^{*0}\ell^+\nu)} \tag{115}$$

we can relate 6 branching fractions to $\mathcal{BT}(B^+ \to \bar{D}_0^{*0}/(D\pi)^0\ell^+\nu)$ and $f_{D\pi/D_0^*}$.

$$\mathcal{B}(B^+ \to \bar{D}_0^{*0}\ell^+\nu) = \frac{2}{2+3f_{D\pi/D_0^*}}\mathcal{BT}(B^+ \to \bar{D}_0^{*0}/(D\pi)^0\ell^+\nu) \tag{116}$$

$$\begin{aligned}
\mathcal{B}(B^+ \to D^-\pi^+\ell^+\nu) &= f_{D\pi/D_0^*}\mathcal{B}(B^+ \to \bar{D}_0^{*0}\ell^+\nu) \\
&= \frac{2f_{D\pi/D_0^*}}{2+3f_{D\pi/D_0^*}}\mathcal{BT}(B^+ \to \bar{D}_0^{*0}/(D\pi)^0\ell^+\nu)
\end{aligned} \tag{117}$$

$$\begin{aligned}
\mathcal{B}(B^+ \to \bar{D}^0\pi^0\ell^+\nu) &= \frac{\mathcal{B}(B^+ \to D^-\pi^+\ell^+\nu)}{2} \\
&= \frac{f_{D\pi/D_0^*}}{2+3f_{D\pi/D_0^*}}\mathcal{BT}(B^+ \to \bar{D}_0^{*0}/(D\pi)^0\ell^+\nu)
\end{aligned} \tag{118}$$

$$\begin{aligned}
\mathcal{B}(B^0 \to D_0^{*-}\ell^+\nu) &= \frac{\mathcal{B}(B^+ \to \bar{D}_0^{*0}\ell^+\nu)}{t_{+0}} \\
&= \frac{2}{t_{+0}(2+3f_{D\pi/D_0^*})}\mathcal{BT}(B^+ \to \bar{D}_0^{*0}/(D\pi)^0\ell^+\nu)
\end{aligned} \tag{119}$$

$$\begin{aligned}
\mathcal{B}(B^0 \to \bar{D}^0\pi^-\ell^+\nu) &= \frac{\mathcal{B}(B^+ \to D^-\pi^+\ell^+\nu)}{t_{+0}} \\
&= \frac{2f_{D\pi/D_0^*}}{t_{+0}(2+3f_{D\pi/D_0^*})}\mathcal{BT}(B^+ \to \bar{D}_0^{*0}/(D\pi)^0\ell^+\nu)
\end{aligned} \tag{120}$$

$$\begin{aligned}
\mathcal{B}(B^0 \to D^-\pi^0\ell^+\nu) &= \frac{\mathcal{B}(B^+ \to \bar{D}^0\pi^0\ell^+\nu)}{t_{+0}} \\
&= \frac{f_{D\pi/D_0^*}}{t_{+0}(2+3f_{D\pi/D_0^*})}\mathcal{BT}(B^+ \to \bar{D}_0^{*0}/(D\pi)^0\ell^+\nu)
\end{aligned} \tag{121}$$

Now, let us calculate $f_{D\pi/D_0^*}$. Using Equation (98)

$$\begin{aligned}&\mathcal{B}(B^+ \to \bar{D}_0^{*0}\ell^+\nu) = t_{+0}\mathcal{B}(B^0 \to D_0^{*-}\ell^+\nu)\\ &= (1.071 \pm 0.009)(0.0042 \pm 0.0040) = 0.0045 \pm 0.0043\end{aligned} \tag{122}$$

Thus, from Equation (113),

$$\begin{aligned}\mathcal{B}(B^+ \to D^-\pi^+\ell^+\nu) &= (0.00293 \pm 0.00118) - \tfrac{2}{3}(0.0045 \pm 0.0043)\\ &= -0.00007 \pm 0.00310\end{aligned} \tag{123}$$

Then, $f_{D\pi/D_0^*}$ is given by

$$f_{D\pi/D_0^*} = \frac{-0.00007 \pm 0.00310}{0.0045 \pm 0.0043} = -0.016 \pm 0.689 \tag{124}$$

The ratio $f_{D\pi/D_0^*}$ cannot be negative. Thus, we take a positive number as described below.

5.1.3 $B \to D_1'\ell\nu$ and non-resonant $B \to D^*\pi\ell\nu$.

There are also 6 branching fractions in this category : $\mathcal{B}(B^+ \to \bar{D}_1'^0\ell^+\nu)$, $\mathcal{B}(B^0 \to D_1'^-\ell^+\nu)$, $\mathcal{B}(B^+ \to D^{*-}\pi^+\ell^+\nu)$, $\mathcal{B}(B^0 \to \bar{D}^{*0}\pi^-\ell^+\nu)$, $\mathcal{B}(B^+ \to \bar{D}^{*0}\pi^0\ell^+\nu)$ and $\mathcal{B}(B^0 \to D^{*-}\pi^0\ell^+\nu)$. Again, we define two parameters, one total branching fraction and one branching fraction ratio, and relate the 6 branching fractions to the parameters. From isospin symmetry

$$\begin{aligned}&\mathcal{B}(B^+ \to \bar{D}_1'^0\ell^+\nu) = t_{+0}\mathcal{B}(B^0 \to D_1'^-\ell^+\nu)\\ &\mathcal{B}(B^+ \to D^{*-}\pi^+\ell^+\nu) = 2\mathcal{B}(B^+ \to \bar{D}^{*0}\pi^0\ell^+\nu)\\ &\quad = t_{+0}\mathcal{B}(B^0 \to \bar{D}^{*0}\pi^-\ell^+\nu) = 2t_{+0}\mathcal{B}(B^0 \to D^{*-}\pi^0\ell^+\nu)\\ &\mathcal{BT}(B^+ \to D^{*-}\pi^+\ell^+\nu) = t_{+0}\mathcal{BT}(B^0 \to \bar{D}^{*0}\pi^-\ell^+\nu)\end{aligned} \tag{125}$$

Note that $\mathcal{BT}(B^+ \to D^{*-}\pi^+\ell^+\nu)$ is what is given in Equation (99). This includes not only non-resonant $D^{*-}\pi^+$ mode but also relevant D^{**} modes. Thus,

$$\begin{aligned}&\mathcal{BT}(B^+ \to D^{*-}\pi^+\ell^+\nu)\\ &= \mathcal{B}(B^+ \to \bar{D}_1^0\ell^+\nu)\mathcal{B}(D_1^0 \to D^{*+}\pi^-) + \mathcal{B}(B^+ \to \bar{D}_1'^0\ell^+\nu)\mathcal{B}(D_1'^0 \to D^{*+}\pi^-)\\ &\quad + \mathcal{B}(B^+ \to \bar{D}_2^{*0}\ell^+\nu)\mathcal{B}(D_2^{*0} \to D^{*+}\pi^-) + \mathcal{B}(B^+ \to D^{*-}\pi^+\ell^+\nu)\end{aligned} \tag{126}$$

Using the above isospin condition, we can take an average of Equation (99). Again, assuming the maximum correlation,

$$\begin{aligned}&\mathcal{BT}(B^+ \to D^{*-}\pi^+\ell^+\nu)\\ &= \tfrac{1}{2}\left[(0.0064 \pm 0.0015) + (0.0065 \pm 0.0016) \times (1.071 \pm 0.009)\right]\\ &= \tfrac{1}{2}\left[(0.0064 \pm 0.0015) + (0.00696 \pm 0.00171)\right]\\ &= 0.00668 \pm 0.00161\end{aligned} \tag{127}$$

From Equation (126),

$$\begin{aligned}
&\mathcal{BT}(B^+ \to D^{*-}\pi^+\ell^+\nu) \\
&= \tfrac{2}{3}\mathcal{B}(B^+ \to \bar{D}_1^0\ell^+\nu) + \tfrac{2}{3}\mathcal{B}(B^+ \to \bar{D}_1'^0\ell^+\nu) \\
&\quad +\mathcal{B}(B^+ \to \bar{D}_2^{*0}\ell^+\nu)\mathcal{B}(D_2^{*+} \to D^{*0}\pi^+) + \mathcal{B}(B^+ \to D^{*-}\pi^+\ell^+\nu)
\end{aligned} \tag{128}$$

Using equations (101), (198) (in section 9) and (102),

$$\begin{aligned}
&\mathcal{B}(B^+ \to D^{*-}\pi^+\ell^+\nu) + \tfrac{2}{3}\mathcal{B}(B^+ \to \bar{D}_1'^0\ell^+\nu) \\
&= \mathcal{BT}(B^+ \to D^{*-}\pi^+\ell^+\nu) - \tfrac{2}{3}\mathcal{B}(B^+ \to \bar{D}_1^0\ell^+\nu) - \mathcal{B}(B^+ \to \bar{D}_2^{*0}\ell^+\nu)\mathcal{B}(D_2^{*+} \to D^{*0}\pi^+) \\
&= (0.00668 \pm 0.00161) - \tfrac{2}{3} \times (0.00419 \pm 0.000532) \\
&\qquad -(0.003215 \pm 0.0006104) \times (0.215 \pm 0.045) \\
&= (0.00668 \pm 0.00161) - (0.00279 \pm 0.0003547) - (0.000691 \pm 0.0001953) \\
&= 0.00319 \pm 0.00166
\end{aligned} \tag{129}$$

Thus, if we define a total branching fraction

$$\begin{aligned}
&\mathcal{BT}(B^+ \to \bar{D}_1^{*0}/(D^*\pi)^0\ell^+\nu) \\
&\equiv \mathcal{B}(B^+ \to \bar{D}_1'^0\ell^+\nu) + \mathcal{B}(B^+ \to D^{*-}\pi^+\ell^+\nu) + \mathcal{B}(B^+ \to \bar{D}^{*0}\pi^0\ell^+\nu) \\
&= \mathcal{B}(B^+ \to \bar{D}_1'^0\ell^+\nu) + \tfrac{3}{2}\mathcal{B}(B^+ \to D^{*-}\pi^+\ell^+\nu) \\
&= \tfrac{3}{2}(0.00319 \pm 0.00166) = 0.0048 \pm 0.0025
\end{aligned} \tag{130}$$

and a branching fraction ratio

$$f_{D^*\pi/D_1'} \equiv \frac{\mathcal{B}(B^+ \to D^{*-}\pi^+\ell^+\nu)}{\mathcal{B}(B^+ \to \bar{D}_1'^0\ell^+\nu)} \tag{131}$$

We can relate the 6 branching fractions to $\mathcal{BT}(B^+ \to \bar{D}_1^{*0}/(D^*\pi)^0\ell^+\nu)$ and $f_{D^*\pi/D_1'}$

$$\mathcal{B}(B^+ \to \bar{D}_1'^0\ell^+\nu) = \frac{2}{2+3f_{D^*\pi/D_1'}}\mathcal{BT}(B^+ \to \bar{D}_1^{*0}/(D^*\pi)^0\ell^+\nu) \tag{132}$$

$$\begin{aligned}
\mathcal{B}(B^+ \to D^{*-}\pi^+\ell^+\nu) &= f_{D^*\pi/D_1'}\mathcal{B}(B^+ \to \bar{D}_1'^0\ell^+\nu) \\
&= \frac{2f_{D^*\pi/D_1'}}{2+3f_{D^*\pi/D_1'}}\mathcal{BT}(B^+ \to \bar{D}_1^{*0}/(D^*\pi)^0\ell^+\nu)
\end{aligned} \tag{133}$$

$$\begin{aligned}
\mathcal{B}(B^+ \to \bar{D}^{*0}\pi^0\ell^+\nu) &= \frac{\mathcal{B}(B^+ \to D^{*-}\pi^+\ell^+\nu)}{2} \\
&= \frac{f_{D^*\pi/D_1'}}{2+3f_{D^*\pi/D_1'}}\mathcal{BT}(B^+ \to \bar{D}_1^{*0}/(D^*\pi)^0\ell^+\nu)
\end{aligned} \tag{134}$$

$$\begin{aligned}
\mathcal{B}(B^0 \to D_1'^-\ell^+\nu) &= \frac{\mathcal{B}(B^+ \to \bar{D}_1'^0\ell^+\nu)}{t_{+0}} \\
&= \frac{2}{t_{+0}(2+3f_{D^*\pi/D_1'})}\mathcal{BT}(B^+ \to \bar{D}_1^{*0}/(D^*\pi)^0\ell^+\nu)
\end{aligned} \tag{135}$$

$$\begin{aligned}\mathcal{B}(B^0 \to \bar{D}^{*0}\pi^-\ell^+\nu) &= \frac{\mathcal{B}(B^+ \to D^{*-}\pi^+\ell^+\nu)}{t_{+0}} \\ &= \frac{2f_{D^*\pi/D_1'}}{t_{+0}(2+3f_{D^*\pi/D_1'})}\mathcal{BT}(B^+ \to \bar{D}_1^{*0}/(D^*\pi)^0\ell^+\nu) \end{aligned} \tag{136}$$

$$\begin{aligned}\mathcal{B}(B^0 \to D^{*-}\pi^0\ell^+\nu) &= \frac{\mathcal{B}(B^+ \to \bar{D}^{*0}\pi^0\ell^+\nu)}{t_{+0}} \\ &= \frac{f_{D^*\pi/D_1'}}{t_{+0}(2+3f_{D^*\pi/D_1'})}\mathcal{BT}(B^+ \to \bar{D}_1^{*0}/(D^*\pi)^0\ell^+\nu) \end{aligned} \tag{137}$$

Now, let us calculate $f_{D^*\pi/D_1'}$. Using Equation (98)

$$\begin{aligned}&\mathcal{B}(B^+ \to \bar{D}_1'^0\ell^+\nu) = t_{+0}\mathcal{B}(B^0 \to D_1'^-\ell^+\nu) \\ &= (1.071 \pm 0.009)(0.0124 \pm 0.0037) = 0.0133 \pm 000725\end{aligned} \tag{138}$$

Thus, by Equation (129),

$$\begin{aligned}&\mathcal{B}(B^+ \to D^{*-}\pi^+\ell^+\nu) = (0.00319 \pm 0.00166) - \tfrac{2}{3}(0.0133 \pm 0.00725) \\ &\quad = -0.005677 \pm 0.00511\end{aligned} \tag{139}$$

Then, $f_{D\pi/D_0^*}$ is

$$f_{D^*\pi/D_1'} = \frac{-0.005677 \pm 0.00511}{0.0133 \pm 0.00725} = -0.427 \pm 0.449 \tag{140}$$

The ratio $f_{D^*\pi/D_1'}$ cannot be negative. Thus, we take a positive number as described below.

5.1.4 $B \to D^{**}\ell\nu$ and non-resonant $B \to D^{(*)}\pi\ell\nu$

We define a total branching fraction

$$\begin{aligned}&\mathcal{BT}(B^+ \to \bar{D}^{**0}/(D\pi)^0\ell^+\nu) \\ &\equiv \mathcal{BT}(B^+ \to \bar{D}_1^0/\bar{D}_2^{*0}\ell^+\nu) + \mathcal{BT}(B^+ \to \bar{D}_0^{*0}/(D\pi)^0\ell^+\nu) + \mathcal{BT}(B^+ \to \bar{D}_1^{*0}/(D^*\pi)^0\ell^+\nu)\end{aligned} \tag{141}$$

We also define two ratios

$$\begin{aligned}f_{D_0^*D\pi T/D_1D_2^*T} &\equiv \frac{\mathcal{BT}(B^+ \to \bar{D}_0^{*0}/(D\pi)^0\ell^+\nu)}{\mathcal{BT}(B^+ \to \bar{D}_1^0/\bar{D}_2^{*0}\ell^+\nu)} = \frac{3}{2}\frac{0.00293 \pm 0.00118}{0.007405 \pm 0.0011874} \\ &= 0.59 \pm 0.26\end{aligned} \tag{142}$$

and

$$\begin{aligned}f_{D_1'D^*\pi T/D_1D_2^*T} &\equiv \frac{\mathcal{BT}(B^+ \to \bar{D}_1^{*0}/(D^*\pi)^0\ell^+\nu)}{\mathcal{BT}(B^+ \to \bar{D}_1^0/\bar{D}_2^{*0}\ell^+\nu)} = \frac{3}{2}\frac{0.00319 \pm 0.00166}{0.007405 \pm 0.0011874} \\ &= 0.65 \pm 0.35\end{aligned} \tag{143}$$

Then, we can relate all 16 branching fractions of $B \to D^{**}\ell\nu$ and non-resonant $B \to D^{(*)}\pi\ell\nu$ decays to $\mathcal{BT}(B^+ \to \bar{D}^{**0}/(D\pi)^0\ell^+\nu)$ and five ratios. First, we have

$$\mathcal{BT}(B^+ \to \bar{D}_1^0/\bar{D}_2^{*0}\ell^+\nu) = \frac{\mathcal{BT}(B^+ \to \bar{D}^{**0}/(D\pi)^0\ell^+\nu)}{1 + f_{D_0^* D\pi T/D_1 D_2^* T} + f_{D_1' D^*\pi T/D_1 D_2^* T}} \tag{144}$$

$$\begin{aligned}\mathcal{BT}(B^+ \to \bar{D}_0^{*0}/(D\pi)^0\ell^+\nu) &= f_{D_0^* D\pi T/D_1 D_2^* T}\mathcal{BT}(B^+ \to \bar{D}_1^0/\bar{D}_2^{*0}\ell^+\nu) \\ &= \frac{f_{D_0^* D\pi T/D_1 D_2^* T}\mathcal{BT}(B^+ \to \bar{D}^{**0}/(D\pi)^0\ell^+\nu)}{1 + f_{D_0^* D\pi T/D_1 D_2^* T} + f_{D_1' D^*\pi T/D_1 D_2^* T}}\end{aligned} \tag{145}$$

$$\begin{aligned}\mathcal{BT}(B^+ \to \bar{D}_1^{*0}/(D^*\pi)^0\ell^+\nu) &= f_{D_1' D^*\pi T/D_1 D_2^* T}\mathcal{BT}(B^+ \to \bar{D}_1^0/\bar{D}_2^{*0}\ell^+\nu) \\ &= \frac{f_{D_1' D^*\pi T/D_1 D_2^* T}\mathcal{BT}(B^+ \to \bar{D}^{**0}/(D\pi)^0\ell^+\nu)}{1 + f_{D_0^* D\pi T/D_1 D_2^* T} + f_{D_1' D^*\pi T/D_1 D_2^* T}}\end{aligned} \tag{146}$$

Substituting these into equations (105)-(108), (116)-(121) and (132)-(137),

$$\mathcal{B}(B^+ \to \bar{D}_1^0\ell^+\nu) = \frac{\mathcal{BT}(B^+ \to \bar{D}^{**0}/(D\pi)^0\ell^+\nu)}{(1 + f_{D_2^*/D_1})(1 + f_{D_0^* D\pi T/D_1 D_2^* T} + f_{D_1' D^*\pi T/D_1 D_2^* T})} \tag{147}$$

$$\mathcal{B}(B^+ \to \bar{D}_2^{*0}\ell^+\nu) = f_{D_2^*/D_1}\mathcal{B}(B^+ \to \bar{D}_1^0\ell^+\nu) \tag{148}$$

$$\mathcal{B}(B^+ \to \bar{D}_0^{*0}\ell^+\nu) = \frac{2f_{D_0^* D\pi T/D_1 D_2^* T}\mathcal{BT}(B^+ \to \bar{D}^{**0}/(D\pi)^0\ell^+\nu)}{(2 + 3f_{D\pi/D_0^*})(1 + f_{D_0^* D\pi T/D_1 D_2^* T} + f_{D_1' D^*\pi T/D_1 D_2^* T})} \tag{149}$$

$$\mathcal{B}(B^+ \to \bar{D}_1'^0\ell^+\nu) = \frac{2f_{D_1' D^*\pi T/D_1 D_2^* T}\mathcal{BT}(B^+ \to \bar{D}^{**0}/(D\pi)^0\ell^+\nu)}{(2 + 3f_{D^*\pi/D_1'})(1 + f_{D_0^* D\pi T/D_1 D_2^* T} + f_{D_1' D^*\pi T/D_1 D_2^* T})} \tag{150}$$

$$\mathcal{B}(B^+ \to D^-\pi^+\ell^+\nu) = f_{D\pi/D_0^*}\mathcal{B}(B^+ \to \bar{D}_0^{*0}\ell^+\nu) \tag{151}$$

$$\mathcal{B}(B^+ \to \bar{D}^0\pi^0\ell^+\nu) = \frac{\mathcal{B}(B^+ \to D^-\pi^+\ell^+\nu)}{2} \tag{152}$$

$$\mathcal{B}(B^+ \to D^{*-}\pi^+\ell^+\nu) = f_{D^*\pi/D_1'}\mathcal{B}(B^+ \to \bar{D}_1'^0\ell^+\nu) \tag{153}$$

$$\mathcal{B}(B^+ \to \bar{D}^{*0}\pi^0\ell^+\nu) = \frac{\mathcal{B}(B^+ \to D^{*-}\pi^+\ell^+\nu)}{2} \tag{154}$$

and

$$\mathcal{B}(B^0 \to D_1^-\ell^+\nu) = \frac{\mathcal{B}(B^+ \to \bar{D}_1^0\ell^+\nu)}{t_{+0}} \tag{155}$$

$$\mathcal{B}(B^0 \to D_2^{*-}\ell^+\nu) = \frac{\mathcal{B}(B^+ \to \bar{D}_2^{*0}\ell^+\nu)}{t_{+0}} \tag{156}$$

$$\mathcal{B}(B^0 \to D_0^{*-}\ell^+\nu) = \frac{\mathcal{B}(B^+ \to \bar{D}_0^{*0}\ell^+\nu)}{t_{+0}} \tag{157}$$

$$\mathcal{B}(B^0 \to D_1'^-\ell^+\nu) = \frac{\mathcal{B}(B^+ \to \bar{D}_1'^0\ell^+\nu)}{t_{+0}} \tag{158}$$

$$\mathcal{B}(B^0 \to \bar{D}^0\pi^-\ell^+\nu) = \frac{\mathcal{B}(B^+ \to D^-\pi^+\ell^+\nu)}{t_{+0}} \tag{159}$$

$$\mathcal{B}(B^0 \to D^-\pi^0\ell^+\nu) = \frac{\mathcal{B}(B^+ \to \bar{D}^0\pi^0\ell^+\nu)}{t_{+0}} \tag{160}$$

$$\mathcal{B}(B^0 \to \bar{D}^{*0}\pi^-\ell^+\nu) = \frac{\mathcal{B}(B^+ \to D^{*-}\pi^+\ell^+\nu)}{t_{+0}} \tag{161}$$

$$\mathcal{B}(B^0 \to D^{*-}\pi^0\ell^+\nu) = \frac{\mathcal{B}(B^+ \to \bar{D}^{*0}\pi^0\ell^+\nu)}{t_{+0}} \tag{162}$$

Thus, we have only one branching fraction, $\mathcal{BT}(B^+ \to \bar{D}^{**0}/(D\pi)^0\ell^+\nu)$, to be determined by the fit. We also have five ratios. Three of them are determined from measurements as described above (Equations (104), (142) and (143)).

$$f_{D_2^*/D_1} = 0.767 \pm 0.243 \tag{163}$$

$$f_{D_0^* D\pi T/D_1 D_2^* T} = 0.59 \pm 0.26 \tag{164}$$

$$f_{D_1' D^*\pi T/D_1 D_2^* T} = 0.65 \pm 0.35 \tag{165}$$

and the other two have negative central numbers (Equations (124) and (140))

$$f_{D\pi/D_0^*} = -0.016 \pm 0.689 \tag{166}$$

$$f_{D^*\pi/D_1'} = -0.427 \pm 0.449 \tag{167}$$

In our fit, we set

$$f_{D\pi/D_0^*} = 0.2 \tag{168}$$

$$f_{D^*\pi/D_1'} = 0.1 \tag{169}$$

and we vary these values from 0 to 2 to get the systematic uncertainty from these ratios.
It is worth noting that our fit does not have the sensitivity to determine these ratios. We tried to float these ratios in our fit, but the results give large statistical uncertainties, for example, values larger than 100 %. Thus, we decided to fix these ratios in our fit.

5.2 New standard branching fractions from Semileotonic AWG

The following are the new branching fraction values recommended by the Semileptonic AWG [18]. We use these values in our fit, instead of the values shown above.

- B^+ decays
  - $\mathcal{B}(B^+ \to \bar{D}_0^{*0}\ell^+\nu) = 0.0045 \pm 0.0009$
  - $\mathcal{B}(B^+ \to \bar{D}_1^0\ell^+\nu) = 0.0054 \pm 0.0006$
  - $\mathcal{B}(B^+ \to \bar{D}_1'^0\ell^+\nu) = 0.0085 \pm 0.0020$
  - $\mathcal{B}(B^+ \to \bar{D}_2^{*0}\ell^+\nu) = 0.0042 \pm 0.0008$
  - $\mathcal{B}(B^+ \to D^-\pi^+\ell^+\nu) = 0.0019 \pm 0.0012$
  - $\mathcal{B}(B^+ \to \bar{D}^0\pi^0\ell^+\nu) = 0.0010 \pm 0.0006$

  - $\mathcal{B}(B^+ \to D^{*-}\pi^+\ell^+\nu) = 0.0006 \pm 0.0004$
  - $\mathcal{B}(B^+ \to \bar{D}^{*0}\pi^0\ell^+\nu) = 0.0003 \pm 0.0002$

- B^0 decays
  - $\mathcal{B}(B^0 \to D_0^{*-}\ell^+\nu) = 0.0043 \pm 0.0009$
  - $\mathcal{B}(B^0 \to D_1^{-}\ell^+\nu) = 0.0050 \pm 0.0008$
  - $\mathcal{B}(B^0 \to D_1'^{-}\ell^+\nu) = 0.0080 \pm 0.0020$
  - $\mathcal{B}(B^0 \to D_2^{*-}\ell^+\nu) = 0.0039 \pm 0.0007$
  - $\mathcal{B}(B^0 \to \bar{D}^{0}\pi^-\ell^+\nu) = 0.0019 \pm 0.0012$
  - $\mathcal{B}(B^0 \to D^{-}\pi^0\ell^+\nu) = 0.0009 \pm 0.0006$
  - $\mathcal{B}(B^0 \to \bar{D}^{*0}\pi^-\ell^+\nu) = 0.0006 \pm 0.0004$
  - $\mathcal{B}(B^0 \to D^{*-}\pi^0\ell^+\nu) = 0.0003 \pm 0.0004$

Here, isospin symmetry is assumed. We calculate the branching fraction ratios by assuming the above branching fractions are independent.

$$
\begin{array}{l}
f_{D_2^*/D_1} \equiv \frac{\mathcal{B}(B^+\to\bar{D}_2^{*0}\ell^+\nu)}{\mathcal{B}(B^+\to\bar{D}_1^{0}\ell^+\nu)} = 0.78 \pm 0.17 \\
f_{D_0^*D\pi T/D_1D_2^*T} \equiv \frac{\mathcal{BT}(B^+\to\bar{D}_0^{*0}/(D\pi)^0\ell^+\nu)}{\mathcal{BT}(B^+\to\bar{D}_1^{0}/\bar{D}_2^{*0}\ell^+\nu)} = 0.77 \pm 0.19 \\
f_{D_1'D^*\pi T/D_1D_2^*T} \equiv \frac{\mathcal{BT}(B^+\to\bar{D}_1^{*0}/(D^*\pi)^0\ell^+\nu)}{\mathcal{BT}(B^+\to\bar{D}_1^{0}/\bar{D}_2^{*0}\ell^+\nu)} = 0.98 \pm 0.24 \\
f_{D\pi/D_0^*} \equiv \frac{\mathcal{B}(B^+\to D^-\pi^+\ell^+\nu)}{\mathcal{B}(B^+\to\bar{D}_0^{*0}\ell^+\nu)} = 0.42 \pm 0.28 \\
f_{D^*\pi/D_1'} \equiv \frac{\mathcal{B}(B^+\to D^{*-}\pi^+\ell^+\nu)}{\mathcal{B}(B^+\to\bar{D}_1^{*0}\ell^+\nu)} = 0.071 \pm 0.050
\end{array}
\tag{170}
$$

5.3 Backgrounds

In our fit there are 8 background coefficients for peaking backgrounds: $C^{D^0}_{UncorDL}$, $C^{D^0}_{UncorCL}$, $C^{D^0}_{CascL}$, $C^{D^0}_{FakeL}$, $C^{D^+}_{UncorDL}$, $C^{D^+}_{UncorCL}$, $C^{D^+}_{CascL}$ and $C^{D^+}_{FakeL}$. We may float some of these and fix the other depending on the fit. Note that combinatorial backgrounds are always fixed.

5.4 Summary of fitting parameters and constraints

As a summary, we are trying to fit for three branching fractions and $\Upsilon(4S)$ decay BF ratio

- $\mathcal{B}(B^+ \to \bar{D}^0\ell^+\nu)$
- $\mathcal{B}(B^+ \to \bar{D}^{*0}\ell^+\nu)$
- $\mathcal{BT}(B^+ \to \bar{D}^{**0}/(D\pi)^0\ell^+\nu)$
- f_{+0}

with isospin constraints

- $\mathcal{B}(B^+ \to \bar{D}^0 \ell^+ \nu) = t_{+0}\mathcal{B}(B^0 \to D^- \ell^+ \nu)$
- $\mathcal{B}(B^+ \to \bar{D}^{*0} \ell^+ \nu) = t_{+0}\mathcal{B}(B^0 \to D^{*-} \ell^+ \nu)$
- $\mathcal{B}(B^+ \to \bar{D}_0^{*0} \ell^+ \nu) = t_{+0}\mathcal{B}(B^0 \to D_0^{*-} \ell^+ \nu)$
- $\mathcal{B}(B^+ \to \bar{D}_1^0 \ell^+ \nu) = t_{+0}\mathcal{B}(B^0 \to D_1^- \ell^+ \nu)$
- $\mathcal{B}(B^+ \to \bar{D}_1^{*0} \ell^+ \nu) = t_{+0}\mathcal{B}(B^0 \to D_1^{\prime -} \ell^+ \nu)$
- $\mathcal{B}(B^+ \to \bar{D}_2^{*0} \ell^+ \nu) = t_{+0}\mathcal{B}(B^0 \to D_2^{*-} \ell^+ \nu)$
- $\mathcal{B}(B^+ \to D^- \pi^+ \ell^+ \nu) = 2\mathcal{B}(B^+ \to \bar{D}^0 \pi^0 \ell^+ \nu)$
  $= t_{+0}\mathcal{B}(B^0 \to \bar{D}^0 \pi^- \ell^+ \nu) = 2t_{+0}\mathcal{B}(B^0 \to D^- \pi^0 \ell^+ \nu)$
- $\mathcal{B}(B^+ \to D^{*-} \pi^+ \ell^+ \nu) = 2\mathcal{B}(B^+ \to \bar{D}^{*0} \pi^0 \ell^+ \nu)$
  $= t_{+0}\mathcal{B}(B^0 \to \bar{D}^{*0} \pi^- \ell^+ \nu) = 2t_{+0}\mathcal{B}(B^0 \to D^{*-} \pi^0 \ell^+ \nu)$

and constraints on relative branching fractions

- $f_{D_2^*/D_1} \equiv \frac{\mathcal{B}(B^+ \to \bar{D}_2^{*0} \ell^+ \nu)}{\mathcal{B}(B^+ \to \bar{D}_1^0 \ell^+ \nu)} = 0.78 \pm 0.17$
- $f_{D_0^* D\pi T/D_1 D_2^* T} \equiv \frac{\mathcal{BT}(B^+ \to \bar{D}_0^{*0}/(D\pi)^0 \ell^+ \nu)}{\mathcal{BT}(B^+ \to \bar{D}_1^0/\bar{D}_2^{*0} \ell^+ \nu)} = 0.77 \pm 0.19$
- $f_{D_1' D^*\pi T/D_1 D_2^* T} \equiv \frac{\mathcal{BT}(B^+ \to \bar{D}_1^{*0}/(D^*\pi)^0 \ell^+ \nu)}{\mathcal{BT}(B^+ \to \bar{D}_1^0/\bar{D}_2^{*0} \ell^+ \nu)} = 0.98 \pm 0.24$
- $f_{D\pi/D_0^*} \equiv \frac{\mathcal{B}(B^+ \to D^- \pi^+ \ell^+ \nu)}{\mathcal{B}(B^+ \to \bar{D}_0^{*0} \ell^+ \nu)} = 0.42 \pm 0.28$
- $f_{D^*\pi/D_1'} \equiv \frac{\mathcal{B}(B^+ \to D^{*-} \pi^+ \ell^+ \nu)}{\mathcal{B}(B^+ \to \bar{D}_1^{*0} \ell^+ \nu)} = 0.071 \pm 0.050$

and floating or fixing background components

- $C^{D^0}_{UncorDL}$
- $C^{D^0}_{UncorCL}$
- $C^{D^0}_{CascL}$
- $C^{D^0}_{FakeL}$
- $C^{D^+}_{UncorDL}$
- $C^{D^+}_{UncorCL}$
- $C^{D^+}_{CascL}$
- $C^{D^+}_{FakeL}$

We also fit for form factor parameters of $B \to D^{(*)} \ell \nu$ decays. See details in section 10.

6 Event Selection

We use the data sample of approximately 230 million $B\bar{B}$-pairs, collected by the BaBar detector. This corresponds to the integrated luminosity of 207 fb^{-1}. A description of the BaBar detector can be found elsewhere [19]. The $B\bar{B}$-pairs are produced from $\Upsilon(4S)$ resonance created by the asymmetric e^+e^- collider, PEP-II [20], at the Stanford Linear Accelerator Center (SLAC). We also use 21.5 fb^{-1} of off-resonance data collected 40 MeV below the resonance. This can be used to subtract non-$B\bar{B}$ background. The package EvtGen [21] is used to generate events and to model decays, and the GEANT4 software [22] is used to simulate the Babar detector in our Monte Carlo simulation. We use analysis-26 (release 16.1.5) to analyze Run1-4 data and SP5/SP6 MC.

We consider the uncertainty on signal to optimize our cuts. We use generic MC (BpBm, B0B0bar, ccbar, uds and tautau) to model OnPeak data. Since we apply D mass sideband subtraction to reduce combinatorial and continuum backgrounds, we need to consider signal yields and background yields in the D mass peak and the D mass sideband regions. We denote those as N^{Sig}_{peak}, N^{Bkg}_{peak}, N^{Sig}_{side} and N^{Bkg}_{side}. We can determine these numbers using MC truth information and luminosity normalization to OnPeak data. The definition of sidebands are given in section 8.1. Since sidebands are larger than peak region, the number of candidates in the sidebands is scaled down to the peak region. The scale factor is

$$\begin{aligned} r^{D^0}_{side} &= \tfrac{1.888-1.840}{(1.840-1.806)+(1.922-1.888)} = 0.7059 \\ r^{D^+}_{side} &= \tfrac{1.890-1.848}{(1.848-1.810)+(1.928-1.890)} = 0.5526 \end{aligned} \tag{171}$$

Expected OnPeak yields, which are determined by MC, are given by

$$\begin{aligned} N^{OnPeak}_{peak} &= N^{Sig}_{peak} + N^{Bkg}_{peak} \\ N^{OnPeak}_{side} &= r_{side}(N^{Sig}_{side} + N^{Bkg}_{side}) \end{aligned} \tag{172}$$

In actual fit, we are interested in (OnPeak - OffPeak) data. The number of events, $N^{OffPeak}$, and uncertainty, $\sigma^{OffPeak}$, of OffPeak data after luminosity normalization to OnPeak data are given by

$$\begin{aligned} N^{OffPeak}_{peak} &= r^{Lumi}_{OffPeak} N^{OffOrg}_{peak} \\ \sigma^{OffPeak}_{peak} &= r^{Lumi}_{OffPeak} \sqrt{N^{OffOrg}_{peak}} \\ N^{OffPeak}_{side} &= r^{Lumi}_{OffPeak} r_{side} N^{OffOrg}_{side} \\ \sigma^{OffPeak}_{side} &= r^{Lumi}_{OffPeak} r_{side} \sqrt{N^{OffOrg}_{side}} \end{aligned} \tag{173}$$

where N^{OffOrg} is the actual yield of OffPeak data before normalization and $r^{Lumi}_{OffPeak}$ is the normalization factor (see section 3.4.1). We do not need to model OffPeak data by MC. This is because we do not need MC truth information to separate OffPaek candidates into signal and background. The signal yield, S, after sideband subtraction (and OffPeak subtraction) is given by

$$S = N^{Sig}_{peak} - r_{side} N^{Sig}_{side} \tag{174}$$

The variance by performing D mass sideband subtraction and OffPeak subtraction is expected to be

$$\begin{aligned}\sigma_S^2 &= (N_{peak}^{OnPeak} + N_{side}^{OnPeak}) + [(\sigma_{peak}^{OffPeak})^2 + (\sigma_{side}^{OffPeak})^2] \\ &= N_{peak}^{Sig} + N_{peak}^{Bkg} + r_{side}^2(N_{side}^{Sig} + N_{side}^{Bkg}) + \left(r_{OffPeak}^{Lumi}\right)^2 (N_{peak}^{OffOrg} + r_{side}^2 N_{side}^{OffOrg})\end{aligned} \tag{175}$$

Therefore, the uncertainty on signal is given by

$$\frac{\sigma_S}{S} = \frac{\sqrt{N_{peak}^{Sig} + N_{peak}^{Bkg} + r_{side}^2(N_{side}^{Sig} + N_{side}^{Bkg}) + \left(r_{OffPeak}^{Lumi}\right)^2 (N_{peak}^{OffOrg} + r_{side}^2 N_{side}^{OffOrg})}}{N_{peak}^{Sig} - r_{side} N_{side}^{Sig}} \tag{176}$$

6.1 BToDlnu skim

First, the collected data is precessed to select only $B \to D^{(*)}\ell\nu$ candidates. This process is done by BaBar collaboration and the produced data set is called BToDlnu skim. In this subsection, we summarize the selection criteria of BToDlnu skim. See also Appendix E.

6.1.1 Reconstruction of D^0 and D^+

D^0 is reconstructed by the following 4 modes:

- $D^0 \to K^-\pi^+$
- $D^0 \to K^-\pi^+\pi^+\pi^-$
- $D^0 \to K^-\pi^+\pi^0$
- $D^0 \to \bar{K}^0\pi^+\pi^-$

D^+ is reconstructed by the following 2 modes:

- $D^+ \to K^-\pi^+\pi^+$
- $D^+ \to \bar{K}^0\pi^+$

Figure 2 is the D^0 mass plots corresponding to four D^0 reconstruction modes. From top to bottom, $D^0 \to K^-\pi^+$, $D^0 \to K^-\pi^+\pi^+\pi^-$, $D^0 \to K^-\pi^+\pi^0$, $D^0 \to \bar{K}^0\pi^+\pi^-$. Figure 3 is the D^+ mass plots corresponding to two D^+ reconstruction modes. From top to bottom, $D^+ \to K^-\pi^+\pi^+$ and $D^+ \to \bar{K}^0\pi^+$. In these plots, star is the On Peak data, green is the B^+B^- MC, yellow is the $B^0\bar{B}^0$ MC, blue is the Off Peak data, magenta is the $c\bar{c}$ MC, cyan is the uds MC, and gray is the $\tau^+\tau^-$ MC. From these plots, we can observe clear peaks only in the top plots. Thus,

- We use only $D^0 \to K^-\pi^+$ and $D^+ \to K^-\pi^+\pi^+$ modes.

For K^- tracks in the skim,

- GoodTracksLoose (GTL) is used to reconstruct D^0
- KLHNotPion selector is used to reconstruct D^+

We apply the same KLHNotPion to D^0 as described in subsection 6.2.
In BToDlnu skim, D^* is also reconstructed, but we do not use them in our analysis. This avoids the problems in the reconstruction of soft pions from D^* decays.

6.1.2 Reconstruction of Dl candidates

Electrons and muons are are selected by PID selectors.

- PidLHElectron selector for electrons
- muNNTight selector for muons

are used in the BToDlnu skims. These leptons are combined with D^0 or D^+ to form Dl candidates. Since neutrinos cannot be detected, we cannot reconstruct B mesons. Thus, these Dl candidates are the candidates of B mesons. Only one true Dl-pair can be produced from one B meson. However, tens of Dl candidates are usually reconstructed in a event. Most of them are combinatorial backgrounds with a misreconstructed D.
The following cuts are also applied

- Lepton momentum cut
  $0.8 < p^* < 3.0$ GeV, where p^* is the lepton momentum in the $\Upsilon(4S)$ rest frame.
- Lepton and kaon charge correlation cut
  The kaon and lepton from the same B meson must have the same sign of charge. See Appendix A.

6.2 Kaon Selection

In BToDlnu skim, for K^-, GoodTracksLoose (GTL) is used to reconstruct D^0, but KLHNotPion is used to reconstruct D^+. We apply KLHNotPion to D^0 reconstruction as well to reduce kaon misidentification. Signal and background yield and the uncertainty on signal in both before and after KLHNotPion are given in Table 7. We can reduce the uncertainty on signal by 43 %. There is no cahnge in D^+ mode because KLHNotPion selector was already applied in the BToDlnu skims.

6.3 Vertexing

No vertexing is done in BToDlnu skim, hence, we apply TreeFitter [23] to D vertex and B vertex. By B vertex, we mean the vertex of Dl combination. We cut on the probability value, $P(\chi^2, dof)$, calculated by the χ^2 and the number of degrees of

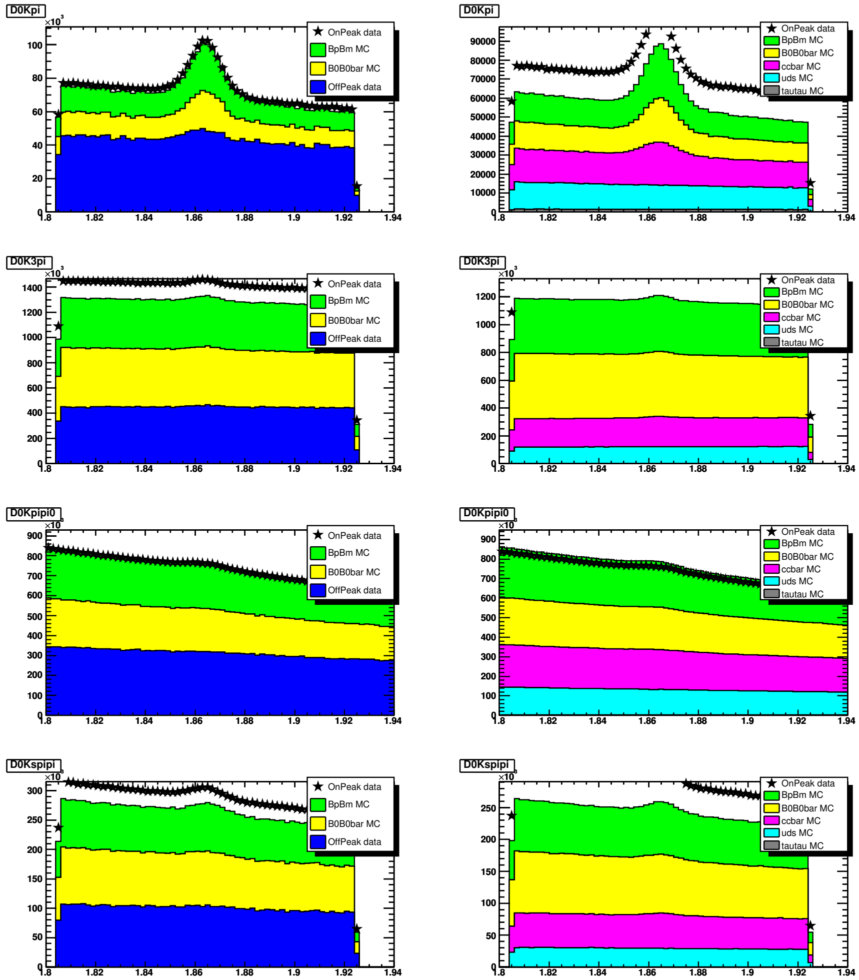

Figure 2: [D^0 **mass plots with 4 reconstruction modes**] D^0 mass plots. From top to bottom, $D^0 \to K^-\pi^+$, $D^0 \to K^-\pi^+\pi^+\pi^-$, $D^0 \to K^-\pi^+\pi^0$, $D^0 \to \bar{K}^0\pi^+$. Left-hand side is the comparison of OnPeak data with $B\bar{B}$ MC + OffPeak data. Right-hand side is of the OnPeak data with $B\bar{B}$ MC + (ccbar, uds and tautau MC). Star is the On Peak data, green is the B^+B^- MC, yellow is the $B^0\bar{B}^0$ MC, blue is the Off Peak data, magenta is the $c\bar{c}$ MC, cyan is the uds MC, and gray is the $\tau^+\tau^-$ MC.

	Before KLHNotPion	After KLHNotPion
D^0 $\frac{\sigma_S}{S}$	0.01152	0.00657
D^+ $\frac{\sigma_S}{S}$	0.01538	0.01538

Table 7: [**KLHNotPion selection**] The uncertainty on signal Signal (σ_S/S) and signal yield in D mass peak region (N^{Sig}_{paek}) before and after KLHNotPion

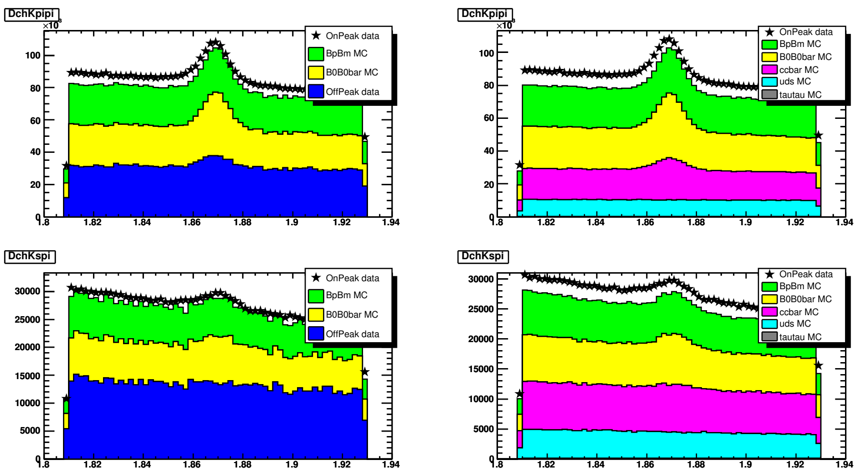

Figure 3: [D^+ **mass plots with 2 reconstruction modes**] D^+ mass plots. From top to bottom, $D^+ \to K^-\pi^+\pi^+$ and $D^+ \to \bar{K}^0\pi^+$. Left-hand side is the comparison of OnPeak data with $B\bar{B}$ MC + OffPeak data. Right-hand side is of the OnPeak data with $B\bar{B}$ MC + (ccbar, uds and tautau MC). Star is the On Peak data, green is the B^+B^- MC, yellow is the $B^0\bar{B}^0$ MC, blue is the Off Peak data, magenta is the $c\bar{c}$ MC, cyan is the uds MC, and gray is the $\tau^+\tau^-$ MC.

freedom (dof) of the vertex fitting. Table 8 shows the uncertainty on signal with variety of $P(\chi^2, dof)$ cuts of D and B vertexing. Tighter cuts give better uncertainties. However, since there is no big difference on uncertainties, we chose looser cuts :

$$P^D(\chi^2, dof) > 0.001, \quad P^B(\chi^2, dof) > 0.01, \tag{177}$$

These cuts improve the uncertainty by 20 % for D^0 mode and 24 % for D^+ mode.

6.4 Thrust cut

$B\bar{B}$ events are isotropic and other $q\bar{q}$ events tend to go back to back in the $\Upsilon(4S)$ rest frame. This is because the mass difference between $\Upsilon(4S)$ and, for example, $D\bar{D}$-pair is big and produced D mesons carry rather large momentum. Thus, we can separate $q\bar{q}$ events from $B\bar{B}$ events using thrust axis. We calculate thrust axis of Dl candidate and "non-Dl" particles in each event. Here, "non-Dl" particles mean all charged tracks and calorimeter energy deposits other than the ones used to reconstruct the Dl candidate. Dl is supposed to be one B in the event; thus, non-Dl should be the other B in the event. However, since we do not reconstruct D^* or D^{**}, soft pions from Dl side are included in non-Dl side. Nevertheless we can achieve a good separation between $B\bar{B}$ events and $q\bar{q}$ events as you can see in the following. We then calculate $|\cos\theta_{Dl-nonDl}|$, which is the cosine of the angle between thrust axis of Dl candidate and non-Dl particles. Those are shown in Figure 4 for D^0 and Figure 5 for D^+. It is almost flat for signal events but peaked at $|\cos\theta_{Dl-nonDl}| = 1$ for $q\bar{q}$ events as expected.

D^0	no cut	$P^D(\chi^2, dof) > 0.0001$	0.001	0.01	0.1
no cut	0.00657	0.00595	0.00589	0.00581	0.00589
$P^B > 0.0001$	0.00549	0.00548	0.00546	0.00542	0.00554
0.001	0.00538	0.00538	0.00537	0.00535	0.00548
0.01	0.00525	0.00525	**0.00525**	0.00525	0.00539
0.1	0.00520	0.00520	0.00520	0.00520	0.00531
D^+	no cut	$P^D(\chi^2, dof) > 0.0001$	0.001	0.01	0.1
no cut	0.01539	0.01283	0.01270	0.01256	0.01274
$P^B > 0.0001$	0.01221	0.01220	0.01212	0.01203	0.01223
0.001	0.01200	0.01200	0.01199	0.01192	0.01214
0.01	0.01174	0.01174	**0.01174**	0.01174	0.01200
0.1	0.01167	0.01167	0.01167	0.01167	0.01181

Table 8: [**Vertex cuts**] The change in the uncertainty on signal, σ_S/S, with variety of $P(\chi^2, dof)$ cuts of D and B vertexing. D^0 , D^+ are shown separately.

To optimize the cut, we calculate the uncertainty on signal by changing cuts. Table 9 show the result. The lowest uncertainty is at $|\cos\theta_{Dl-nonDl}| < 0.80$. However, since no big difference between 0.80 and 0.92, we choose looser cut

$$\cos\theta_{Dl-nonDl} < 0.92 \tag{178}$$

With this cut, we can reduce the uncertainty by 18 % for D^0 and 16 % for D^+.

6.5 Summary of event selection cuts

The cuts we applied, the uncertainty on signal and the number of selected signal candidates in the D mass peak region are summarized in Table 10. We reduced uncertainty by 63 % for D^0 and 36 % for D^+ in total. We also lose 17 % and 18 % of signal candidates by these selection cuts. Tables 11 and 12 are cut-flow tables for D^0 and D^+ respectively. (OnPeak - OffPeak) data and $B\bar{B}$ MC are compared in these tables. Efficiencies show a good agreement.
After event selection cuts, number of candidates per event are

- Signal
  - $B^+ \to D^0/\bar{D}^0 X \ell^+ \nu$ mode : 1.0015
  - $B^+ \to D^+/D^- X \ell^+ \nu$ mode : 1.0012
  - $B^0 \to D^0/\bar{D}^0 X \ell^+ \nu$ mode : 1.0010
  - $B^0 \to D^+/D^- X \ell^+ \nu$ mode : 1.0020

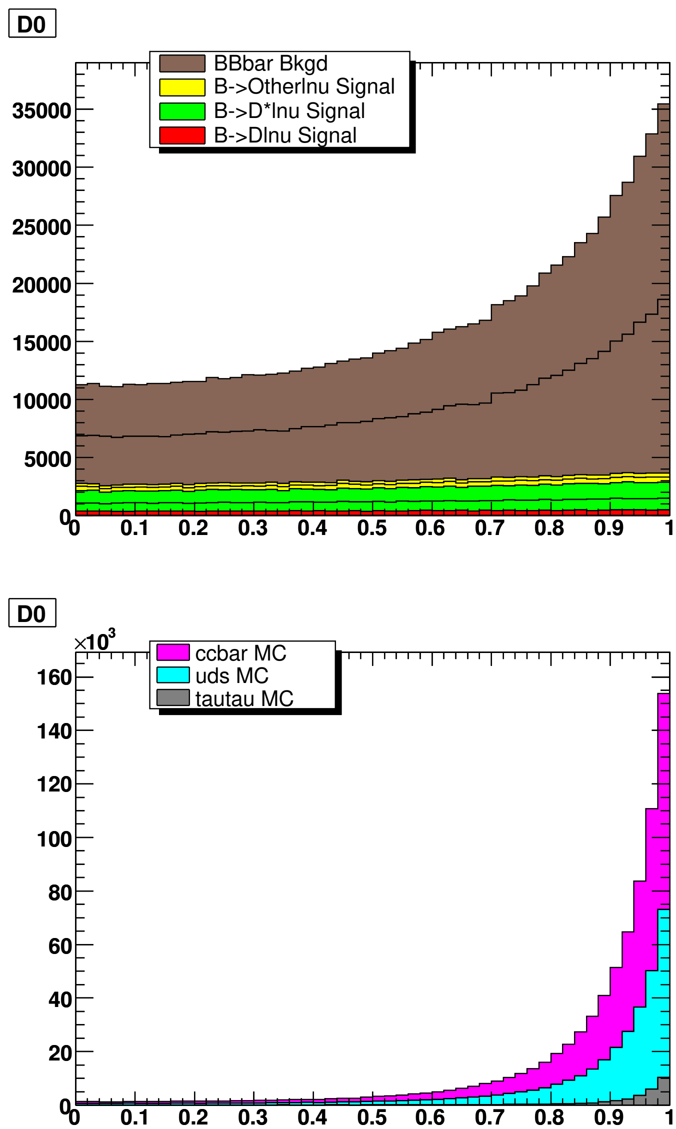

Figure 4: [$|\cos\theta_{Dl-nonDl}|$, D^0] $|\cos\theta_{Dl-nonDl}|$ plot for D^0 case. In the top plot, red is $B \to D\ell\nu$, green is $B \to D^*\ell\nu$, yellow is $B \to D^{**}/(D^{(*)}\pi)\ell\nu$ and brown is $B\bar{B}$ backgrounds. In the bottom plot, magenta is $c\bar{c}$, light blue is uds and gray is $\tau^+\tau^-$.

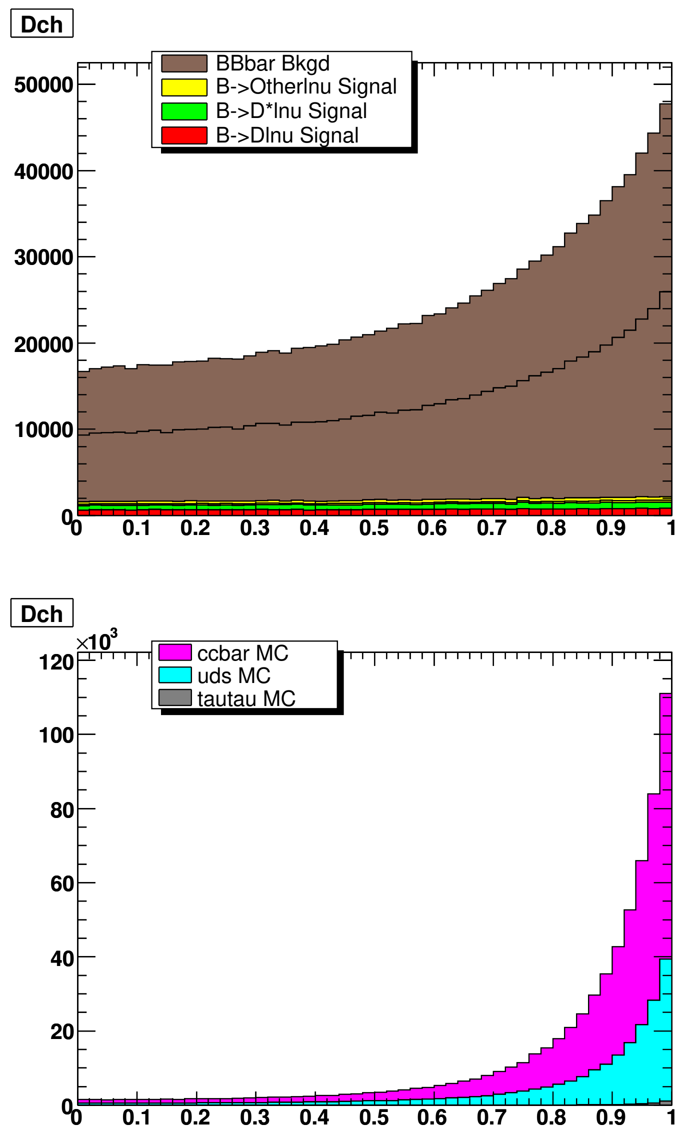

Figure 5: [$|\cos\theta_{Dl-nonDl}|$, D^+] $|\cos\theta_{Dl-nonDl}|$ plot for D^+ case. In the top plot, red is $B \to D\ell\nu$, green is $B \to D^*\ell\nu$, yellow is $B \to D^{**}/(D^{(*)}\pi)\ell\nu$ and brown is $B\bar{B}$ backgrounds. In the bottom plot, magenta is $c\bar{c}$, light blue is uds and gray is $\tau^+\tau^-$.

cuts	D^0	D^+
no cut	0.00525	0.01174
$\lvert\cos\theta_{Dl-nonDl}\rvert < 0.96$	0.00463	0.01063
0.92	**0.00428**	**0.00992**
0.88	0.00405	0.00944
0.84	0.00389	0.00911
0.80	0.00378	0.00890

Table 9: [**Thrust cuts**] The change in the uncertainty on signal, $\frac{\sigma_S}{S}$, with variety of $\lvert\cos\theta_{Dl-nonDl}\rvert$ cuts.

- Backgrounds
  - $B^0 \to D^+/D^- X\ell^+\nu$ Uncorrelated Direct Lepton : 1.0038
  - $B^+ \to D^0/\bar{D}^0 X\ell^+\nu$ Uncorrelated Cascade Lepton : 1.0038
  - $B^0 \to D^0/\bar{D}^0 X\ell^+\nu$ Correlated Cascade Lepton : 1.0038

To understand these numbers, we try to estimate the rate to reconstruct $D\ell$ candidate in the $B^+ \to D^0/\bar{D}^0$ case.

$$\begin{aligned}&\mathcal{B}(B^+ \to X_c\ell^+\nu)\mathcal{B}(X_c \to D^0/\bar{D}^0X)\mathcal{B}(D^0 \to K^+\pi^-) \times (\text{acceptance} \times \text{efficiency})\\ &\simeq 0.1 \times 1 \times 0.04 \times 0.4 = 0.0016\end{aligned} \tag{179}$$

where we assumed $\mathcal{B}(X_c \to D^0/\bar{D}^0X) = 1$, but this number can be lower than 1. Thus, the above number 1.0015 shows that we just reconstructed true $D\ell$ candidate from both B^+ and B^-.

Figure 6 shows the D mass plot before selection cuts are applied. At the bottom of each D^0 and D^+ plot, (number of OnPaek - OffPeak) - (number of $B\bar{B}$ MC) plots are given. Figures 7 - 9 shows the D mass plot after all cuts with all leptons (= electrons + muons), electrons only, and muons only, respectively. There is a significant data-MC disagreement especially in the D^+ case. This is mailnly because D^+ require more chaged tracks to reconstruct than D^0. If you look at Figures 2 and 3, $D^0 \to K^-\pi^+\pi^+\pi^+$ mode shows more data-MC disagreement than $D^+ \to K^-\pi^+\pi^+$ mode. It is understandable that combinatrial bcakground is less well modeled in MC when it requires more tracks. However, since the data-MC difference for combinatrial bckground is flat throughout the D mass region, this difference disappear after D mass sideband subtraction.

	D^0		D^+	
cuts	$\frac{\sigma_S}{S}$	N_{peak}^{Sig}	$\frac{\sigma_S}{S}$	N_{peak}^{Sig}
BToDlnu skim	0.01152	1.0639×10^6	0.01538	628185
KLHNotPion selector	0.00657	1.0349×10^6	0.01538	628170
$P^D(\chi^2, dof) > 0.001$ $P^B(\chi^2, dof) > 0.01$	0.00525	974632	0.01174	568799
$\lvert\cos\theta_{Dl-nonDl}\rvert < 0.92$	0.00428	882038	0.00992	515792

Table 10: [**Event selection cuts**] The summary of event selection cuts.

OnPeak - OffPeak	Yield	Efficiency	Cumulative efficiency
BToDlnu skim	1.3388×10^6		
KLHNotPion selector	1.3410×10^6	1.00	1.00
$P^D(\chi^2, dof) > 0.001$ $P^B(\chi^2, dof) > 0.01$	1.1961×10^6	0.89	0.89
$\lvert\cos\theta_{Dl-nonDl}\rvert < 0.92$	1.0651×10^6	0.89	0.78
$B\bar{B}$ MC	Yield	Efficiency	Cumulative efficiency
BToDlnu skim	1.4679×10^6		
KLHNotPion selector	1.4449×10^6	0.99	0.99
$P^D(\chi^2, dof) > 0.001$ $P^B(\chi^2, dof) > 0.01$	1.3204×10^6	0.92	0.90
$\lvert\cos\theta_{Dl-nonDl}\rvert < 0.92$	1.1789×10^6	0.89	0.80

Table 11: [**Cut-flow Table,** D^0] The cut-flow table for D^0. Yield = number of candidates after D mass sideband subtraction.

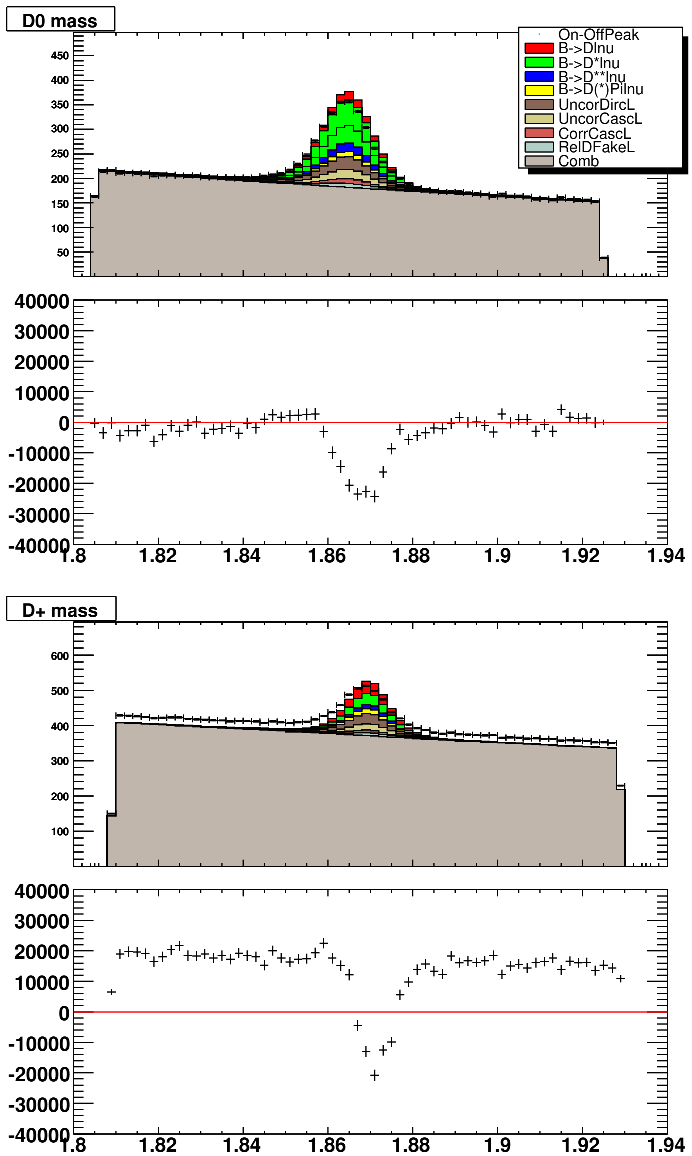

Figure 6: [D **mass before event selection**] D mass plot before applying selection cuts. The top is D^0 and the bottom is D^+. Black line with error bar is (OnPeak - OffPeak) data. Red is $B \to D\ell\nu$, green is $B \to D^*\ell\nu$, blue is $B \to D^{**}\ell\nu$, yellow is non-resonant $B \to D^{(*)}\pi\ell\nu$, and the rest is background. Dark brown is UncorrDL, light brown is UncorrCL, dark red is CascL, blue gray is FakeL, light gray is Comb. Data - MC difference is also plotted.

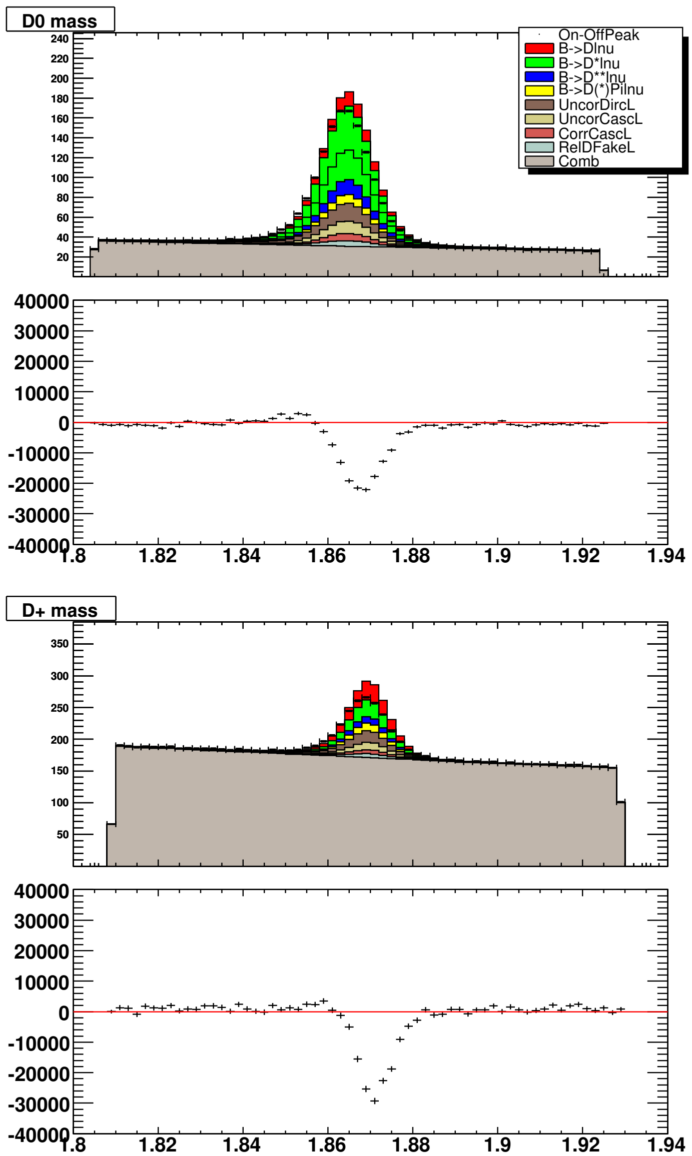

Figure 7: [D **mass after event selection**] D mass plot after all cuts. The top is D^0 and the bottom is D^+. Black line with error bar is (OnPeak - OffPeak) data. Red is $B \to D\ell\nu$, green is $B \to D^*\ell\nu$, blue is $B \to D^{**}\ell\nu$, yellow is non-resonant $B \to D^{(*)}\pi\ell\nu$, and the rest is background. Dark brown is UncorrDL, light brown is UncorrCL, dark red is CascL, blue gray is FakeL, light gray is Comb. Data - MC difference is also plotted.

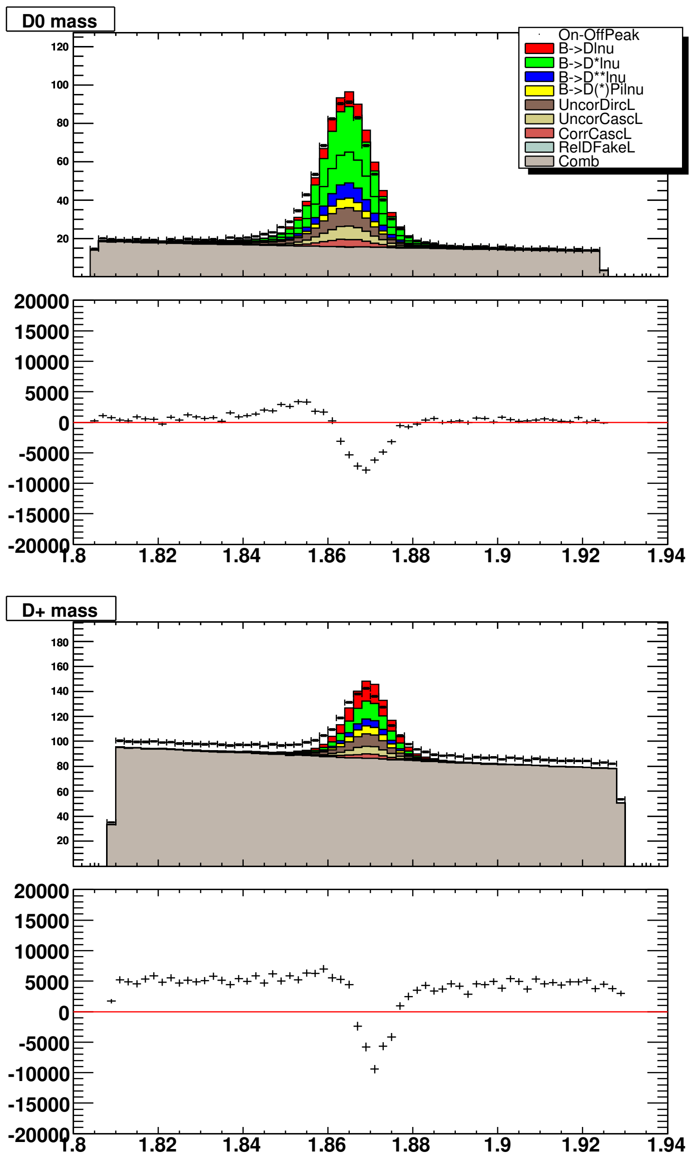

Figure 8: [D **mass after event selection, electron**] D mass plot after all cuts. Only **electrons** are selected. The top is D^0 and the bottom is D^+. Black line with error bar is (OnPeak - OffPeak) data. Red is $B \to D\ell\nu$, green is $B \to D^*\ell\nu$, blue is $B \to D^{**}\ell\nu$, yellow is non-resonant $B \to D^{(*)}\pi\ell\nu$, and the rest is background. Dark brown is UncorrDL, light brown is UncorrCL, dark red is CascL, blue gray is FakeL, light gray is Comb. Data - MC difference is also plotted.

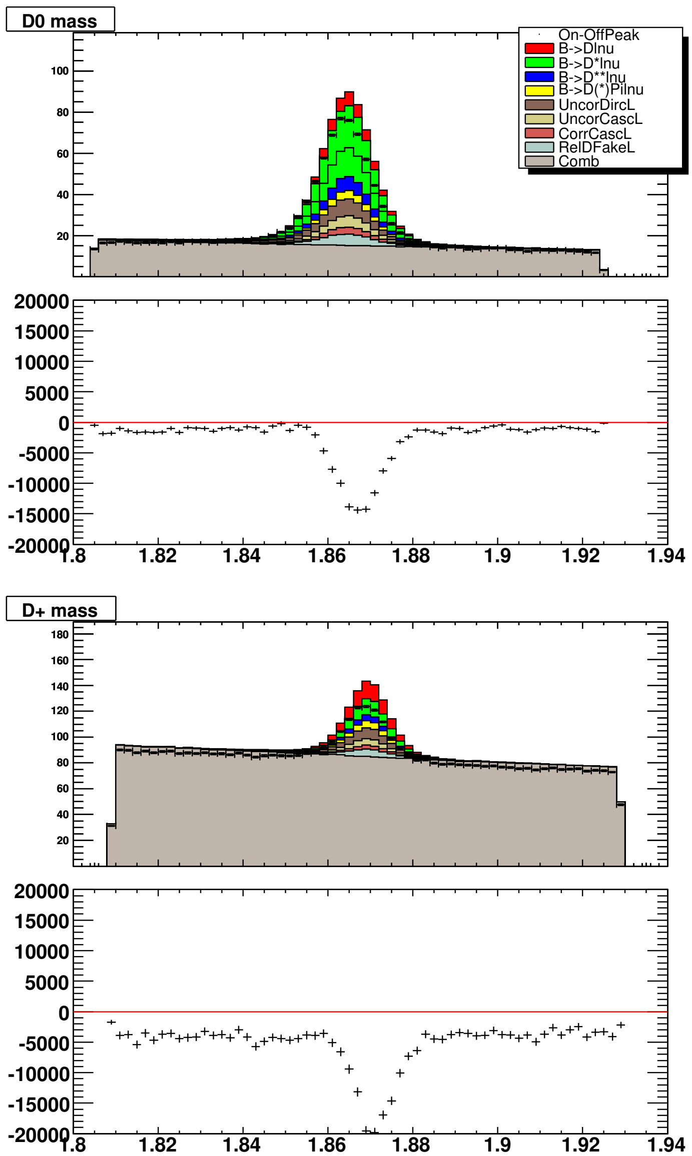

Figure 9: [D **mass after event selection, muon**] D mass plot after all cuts. Only **muons** are selected. The top is D^0 and the bottom is D^+. Black line with error bar is (OnPeak - OffPeak) data. Red is $B \to D\ell\nu$, green is $B \to D^*\ell\nu$, blue is $B \to D^{**}\ell\nu$, yellow is non-resonant $B \to D^{(*)}\pi\ell\nu$, and the rest is background. Dark brown is UncorrDL, light brown is UncorrCL, dark red is CascL, blue gray is FakeL, light gray is Comb. Data - MC difference is also plotted.

OnPeak - OffPeak	Yield	Efficiency	Cumulative efficiency
BToDlnu skim	825616		
KLHNotPion selector	825625	1.00	1.00
$P^D(\chi^2, dof) > 0.001$ $P^B(\chi^2, dof) > 0.01$	700745	0.85	0.85
$\lvert\cos\theta_{Dl-nonDl}\rvert < 0.92$	621453	0.89	0.75
$B\bar{B}$ MC	Yield	Efficiency	Cumulative efficiency
BToDlnu skim	1.0061×10^6		
KLHNotPion selector	1.0061×10^6	1.00	1.00
$P^D(\chi^2, dof) > 0.001$ $P^B(\chi^2, dof) > 0.01$	870188	0.85	0.85
$\lvert\cos\theta_{Dl-nonDl}\rvert < 0.92$	766995	0.88	0.76

Table 12: [**Cut-flow Table,** D^+] The cut-flow table for D^+. Yield = number of candidates after D mass sideband subtraction.

7 Tracking Efficiency and PID correction

Tracking efficiency and PID efficiency are not completely equal in both data and MC. There is always a difference no matter how sophisticated the codes to reconstruct charged tracks and to identify particles are. Tracking efficiency and PID corrections are the corrections to account for the residual difference between data and MC. Both corrections are done in similar way. The correction factors are read out from correction tables stored in the condition database. We use R16 correction tables since we use R16b skims.

7.1 Tracking efficiency correction : r_k^{Trk}

Tracking efficiency correction factors are given for each charged track, depending on its transverse momentum, direction in the LAB frame and the multiplicity of the event. There are 3 charged tracks to reconstruct a $D^0(K\pi)l$ candidate, and 4 charged tracks to reconstruct a $D^+(K\pi\pi)l$ candidate. We multiply those correction factors of charged tracks to get a correction factor r_k^{Trk} for each candidate (k). The distribution of r_k^{Trk} for Run2 BpBm MC is shown in Figure 10 as an example.

7.2 PID correction : r_k^{LPID} and r_k^{KPID}

PID correction factors (called weights) are given one for each PID selector. Thus, we have one factor r_k^{LPID} for lepton (PidLHElectron for electrons and muNNTight for muons) and another factor r_k^{KPID} for kaon (KLHNotPion) for each $D\ell$ candidate (k). When the identified particles are real, r_k^{LPID} and r_k^{KPID} are the factor to correct identification efficiency difference. When the identified particles are fake, r_k^{LPID} and r_k^{KPID} give the factor to correct fake rate difference. The distribution of electron r_k^{LPID} for Run2 BpBm MC, as an example, is shown in Figure 11 and muon r_k^{LPID} in Figure 12. r_k^{KPID} is shown in Figure 13.

7.3 Effect of efficiency correction

Figure 14 show the D mass plots after tracking efficiency and PID corrections. At the bottom of each D^0 and D^+ plot, (number of OnPaek - OffPeak) - (number of $B\bar{B}$ MC) plots are given. Figure 15 and 16 shows the D mass plot of electrons only, and muons only, respectively. These Figures need to be compared with Figures 7 - 9. The data-MC agreement of D^+ mode is significantly improved.

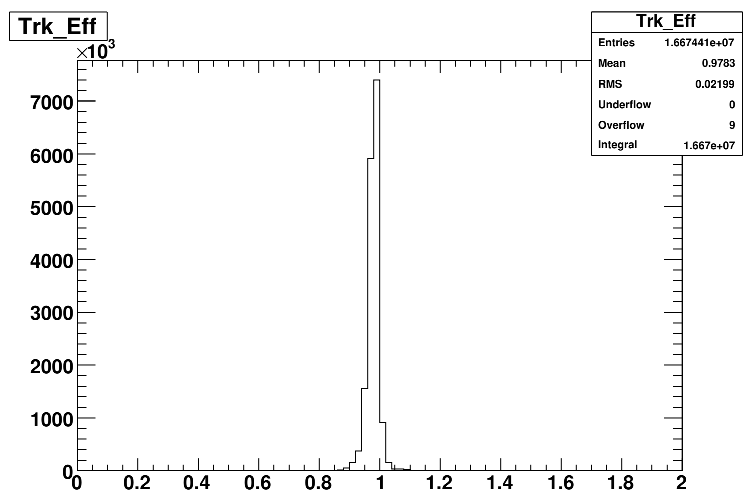

Figure 10: [**TrkEff correction factor**] Tracking efficiency correction factor for each candidate. BpBm MC is used to make this plot.

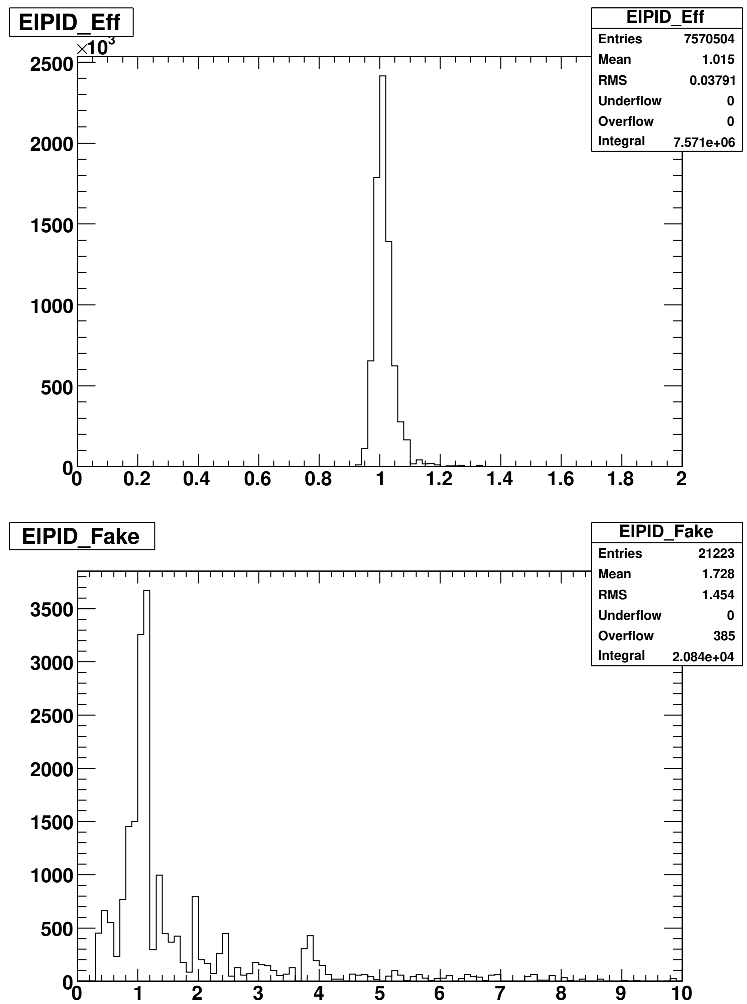

Figure 11: [**Electron PID weight**] Electron PID correction factor for each candidate. BpBm MC is used to make this plot. The top is the efficiency correction factors and the bottom is the fake rate correction factors.

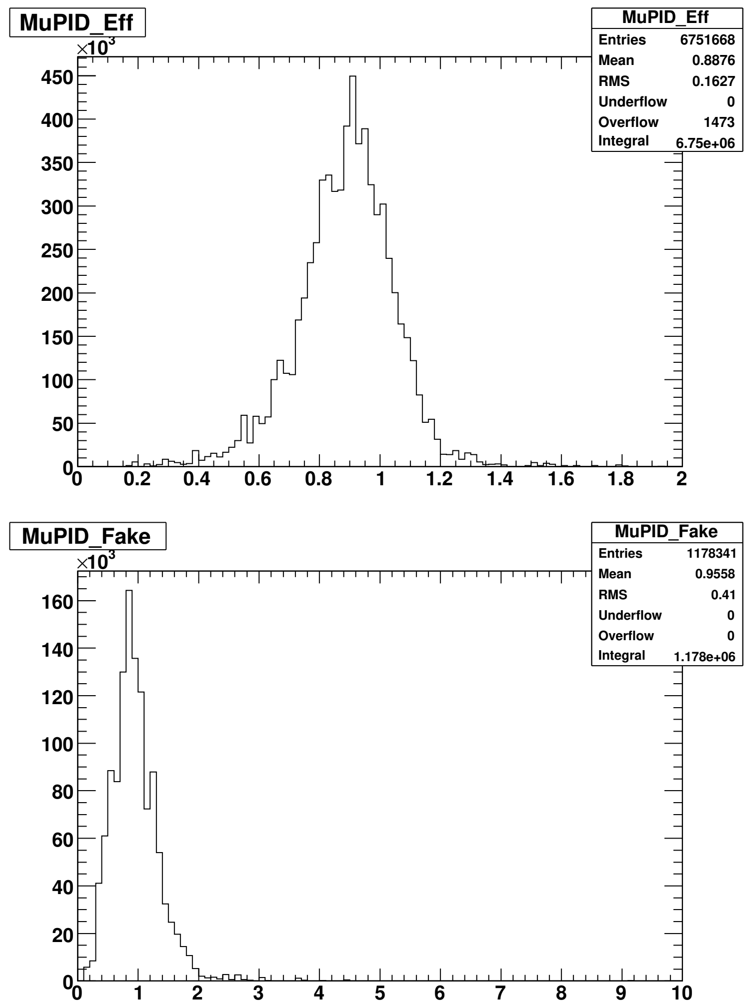

Figure 12: [**Muon PID weight**] Muon PID correction factor for each candidate. BpBm MC is used to make this plot. The top is the efficiency correction factors and the bottom is the fake rate correction factors.

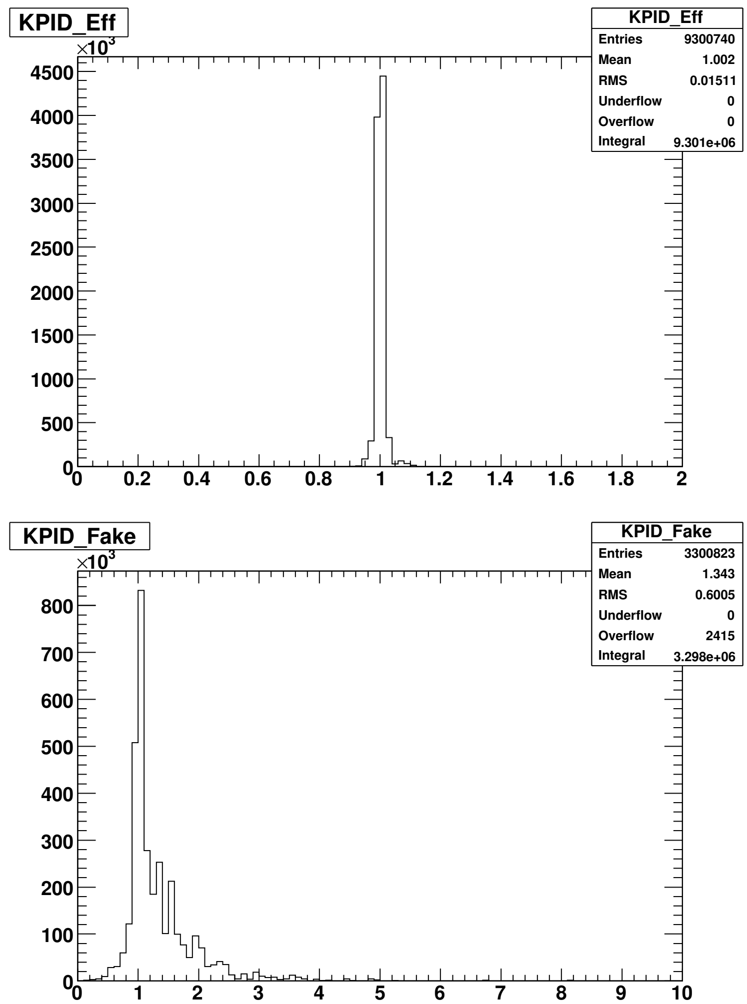

Figure 13: [**Kaon PID weight**] Kaon PID correction factor for each candidate. BpBm MC is used to make this plot. The top is the efficiency correction factors and the bottom is the fake rate correction factors.

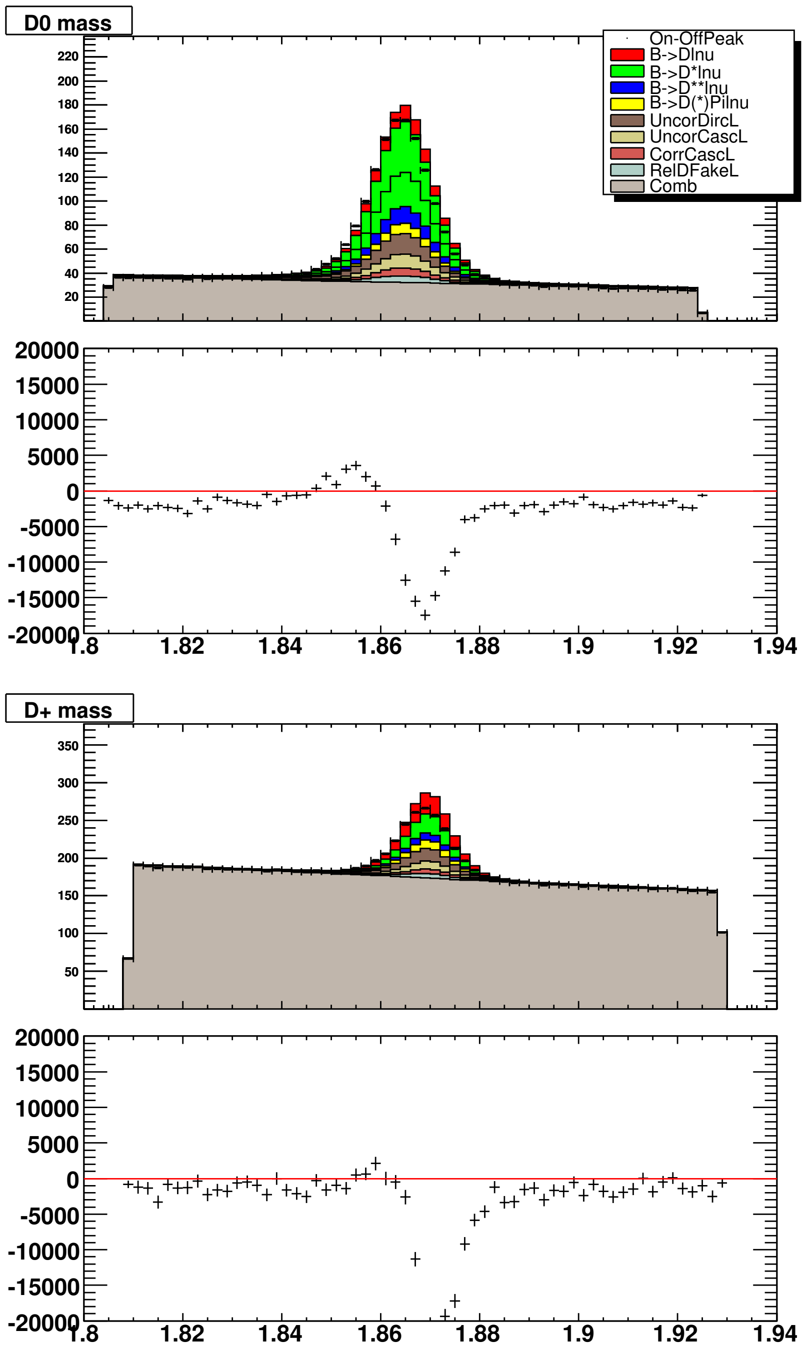

Figure 14: [D **mass after Trk PID correction**] D mass plot after tracking efficiency and PID corrections. The top is D^0 and the bottom is D^+. Black line with error bar is (OnPeak - OffPeak) data. Red is $B \to D\ell\nu$, green is $B \to D^*\ell\nu$, blue is $B \to D^{**}\ell\nu$, yellow is non-resonant $B \to D^{(*)}\pi\ell\nu$, and the rest is background. Dark brown is UncorrDL, light brown is UncorrCL, dark red is CascL, blue gray is FakeL, light gray is Comb. Data - MC difference is also plotted.

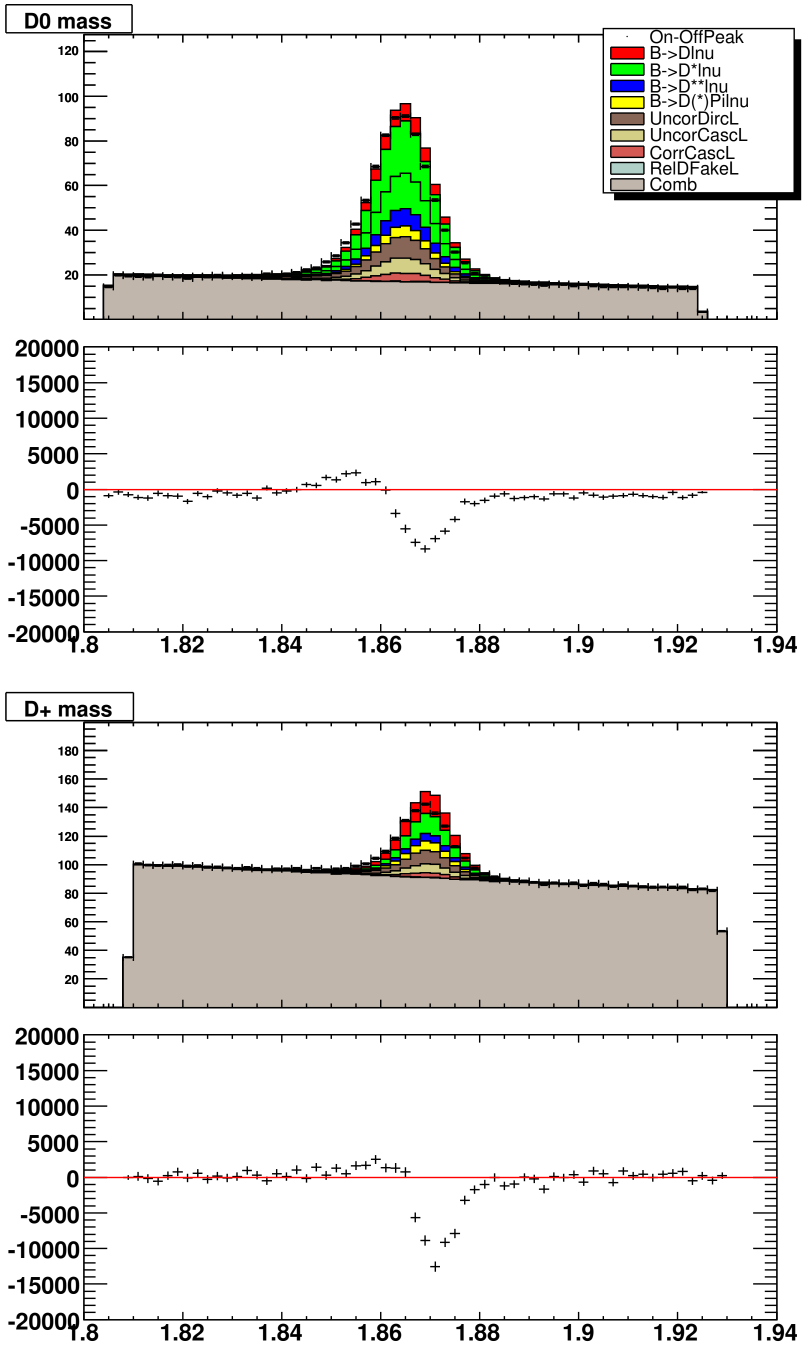

Figure 15: [D **mass after Trk PID correction, Electron**] D mass plot after tracking efficiency and PID corrections in the case $\ell = e$ (Electron only). The top is D^0 and the bottom is D^+. Black line with error bar is (OnPeak - OffPeak) data. Red is $B \to D\ell\nu$, green is $B \to D^*\ell\nu$, blue is $B \to D^{**}\ell\nu$, yellow is non-resonant $B \to D^{(*)}\pi\ell\nu$, and the rest is background. Dark brown is UncorrDL, light brown is UncorrCL, dark red is CascL, blue gray is FakeL, light gray is Comb. Data - MC difference is also plotted.

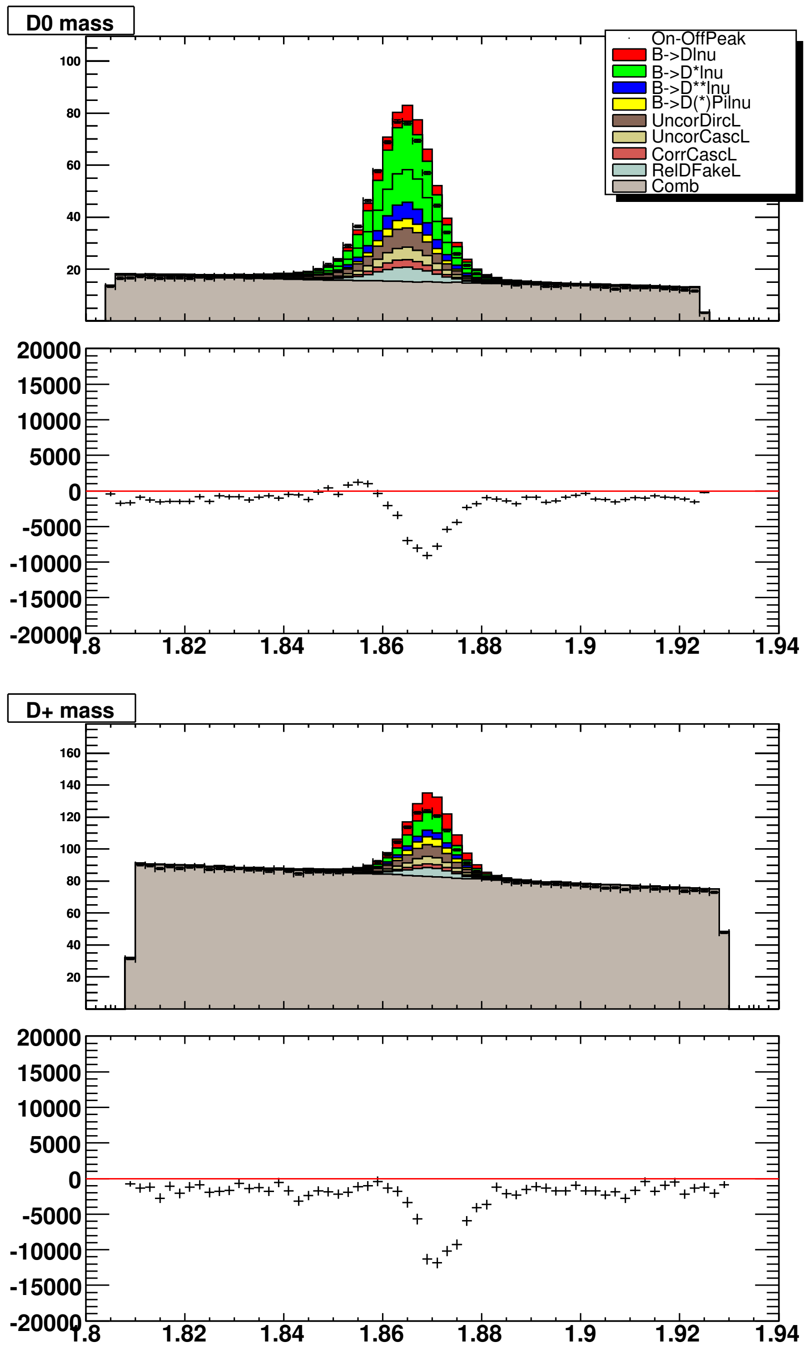

Figure 16: [D **mass after Trk PID correction, Muon**] D mass plot after tracking efficiency and PID corrections in the case $\ell = \mu$ (Muon only). The top is D^0 and the bottom is D^+. Black line with error bar is (OnPeak - OffPeak) data. Red is $B \to D\ell\nu$, green is $B \to D^*\ell\nu$, blue is $B \to D^{**}\ell\nu$, yellow is non-resonant $B \to D^{(*)}\pi\ell\nu$, and the rest is background. Dark brown is UncorrDL, light brown is UncorrCL, dark red is CascL, blue gray is FakeL, light gray is Comb. Data - MC difference is also plotted.

8 D mass sideband subtraction

We assume D mass sideband is flat when we do sideand subtraction. Here we check this assumption.

8.1 Definition of D mass sideband

From D mass plots (Figure 14-16), we decided the range of D mass peak and sidebands as follows

- D^0 mass
  Peak : 1.840 - 1.888 GeV
  Side bands : 1.806 - 1.840 and 1.888 - 1.922 GeV

- D^+ mass
  Peak : 1.848 - 1.890 GeV
  Side bands : 1.810 - 1.848 and 1.890 - 1.928 GeV

Approximately 4.6 % of signal candidates goes into sideband.

8.2 Linearlity of D mass sideband

8.2.1 D mass fit

We try to fit OnPeak D mass plot with the following two combinations :

- 2 Gaussian + a linear function

- 2 Gaussina + a quadratic function

We use two Gaussinas with different width for the peak : one for signal and the other for peaking backgroud. We compare the yeild of sideband from linear and quadratic functions to make sure we get the similar results in both cases. Fitted plots are shown in Figure 17 for D^0 and in Figure 18 for D^+. Yeldsare given in Table 13. Yeilds difference is very small.

D^0	Linear	Quadratic
Peak yield	719.9	719.1
Combinatrial yield	693.9	694.7
D^+	Linear	Quadratic
Peak yield	450.3	448.6
Combinatrial yield	2602.7	2604.7

Table 13: [D **mass fit**] D mass fit results.

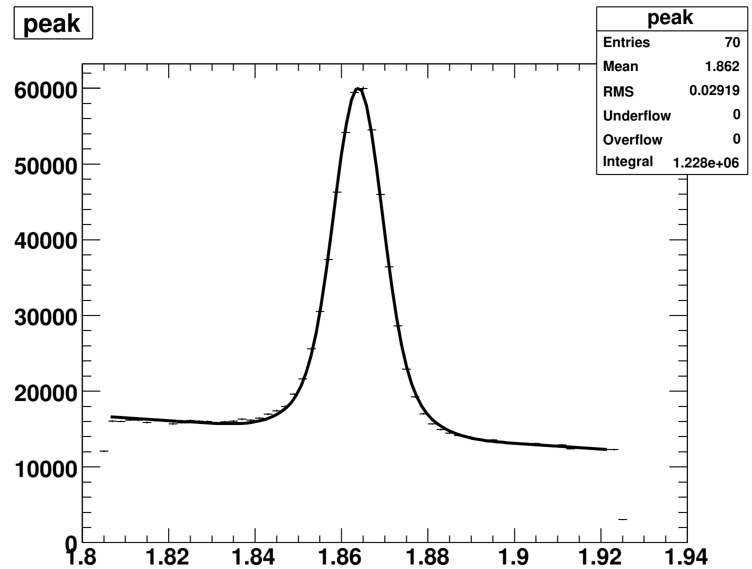

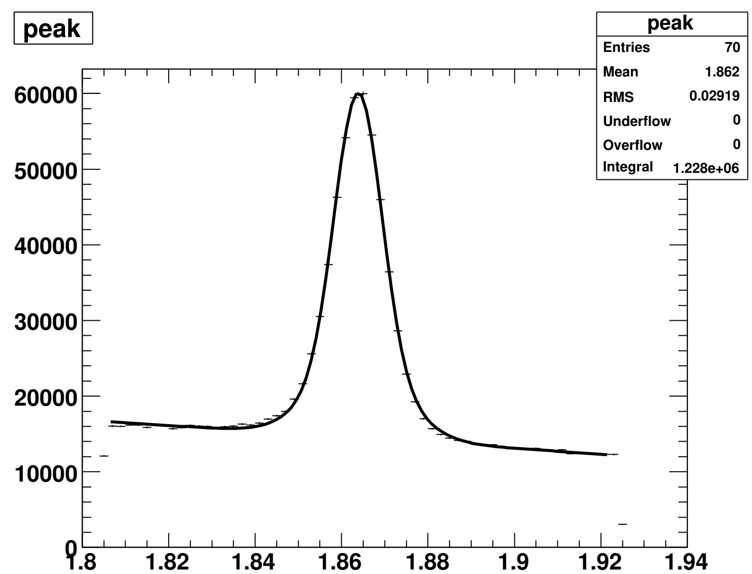

Figure 17: [D^0 **mass fit**] D^0 mass fit with linear function (top) and quadratic function (bottom).

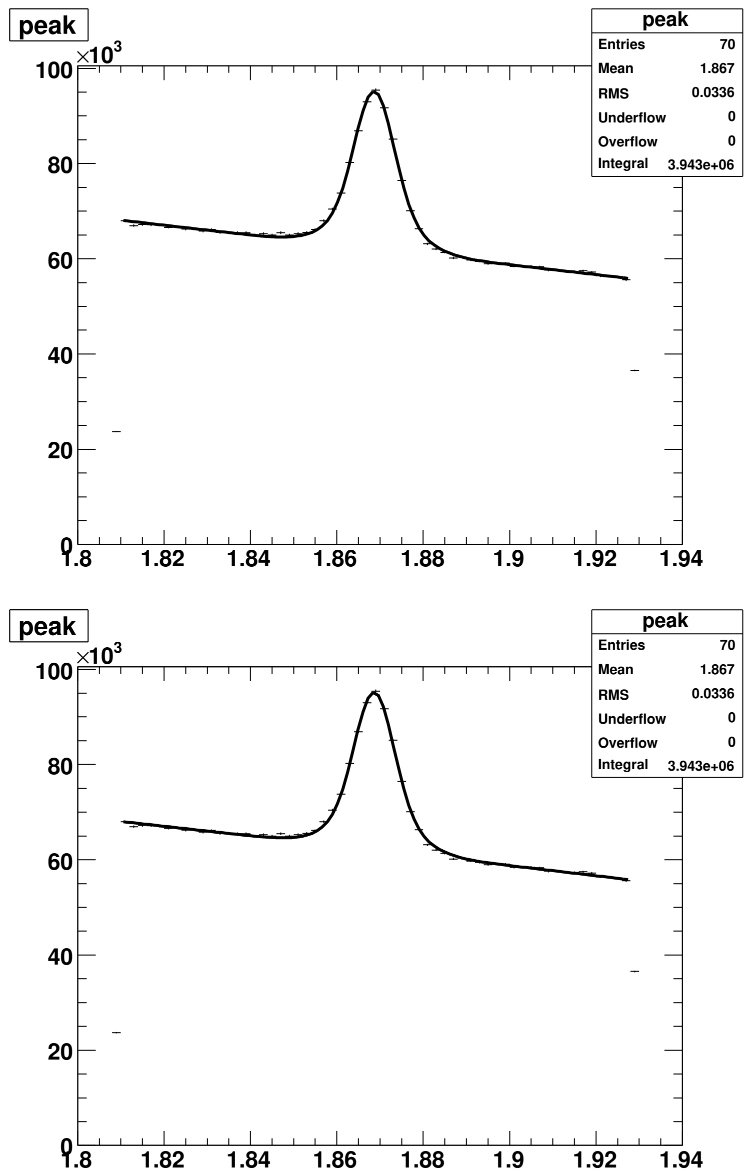

Figure 18: [D^+ **mass fit**] D^+ mass fit with linear function (top) and quadratic function (bottom).

8.3 Lepton momentum, D momentum and $\cos\theta_{B-Dl}$

Figures 19 - 27 show the lepton momentum, D momentum and $\cos\theta_{B-Dl}$ after tracking efficiency and PID correction with all leptons (= electrons + muons), electrons only, and muons only, respectively. These are the projections of 3D histograms.
Figure 28 - 33 show all bins of the 3D histograms after efficiency correction. Binning are described in section 3.

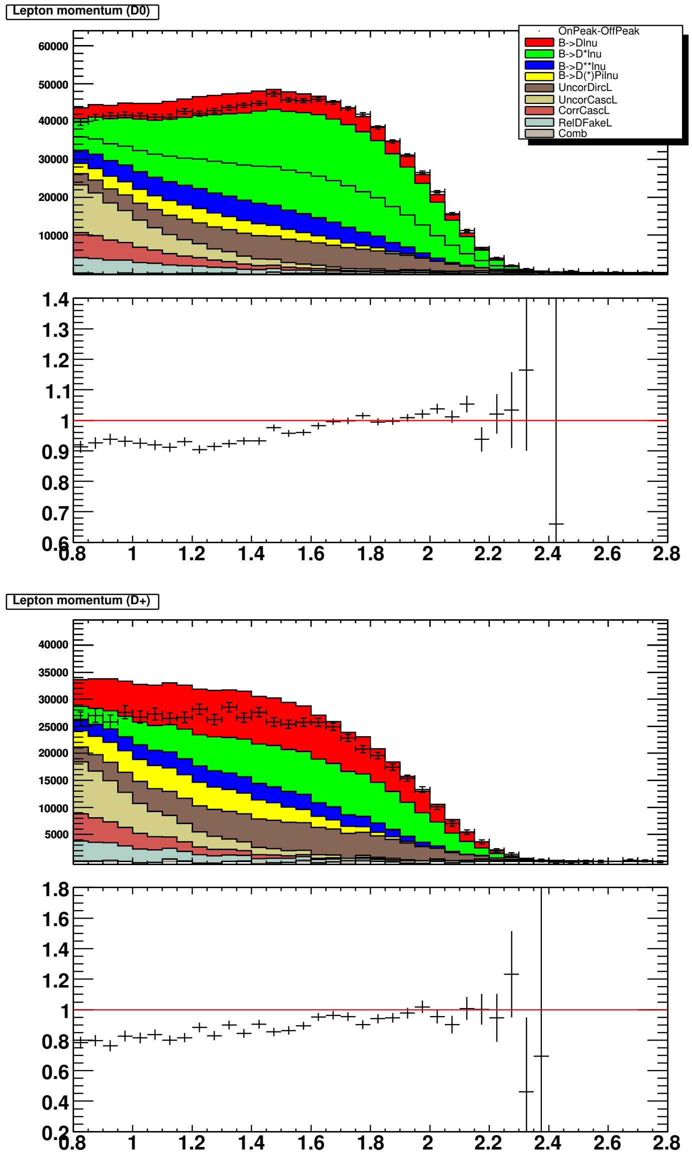

Figure 19: [p_ℓ **after Trk PID**] Lepton momentum plot after PID and tracking corrected and D mass sideband subtracted. The top is D^0 and the bottom is D^+. Black is OnPeak - OffPeak data. Red is $B \to D\ell\nu$, green is $B \to D^*\ell\nu$, blue is $B \to D^{**}\ell\nu$, yellow is non-resonant $B \to D^{(*)}\pi\ell\nu$, and the rest is background. Dark brown is UncorrDL, light brown is UncorrCL, dark red is CascL, blue gray is FakeL, and light gray is Comb. Comb is almost disappeared after D mass sideband subtraction.

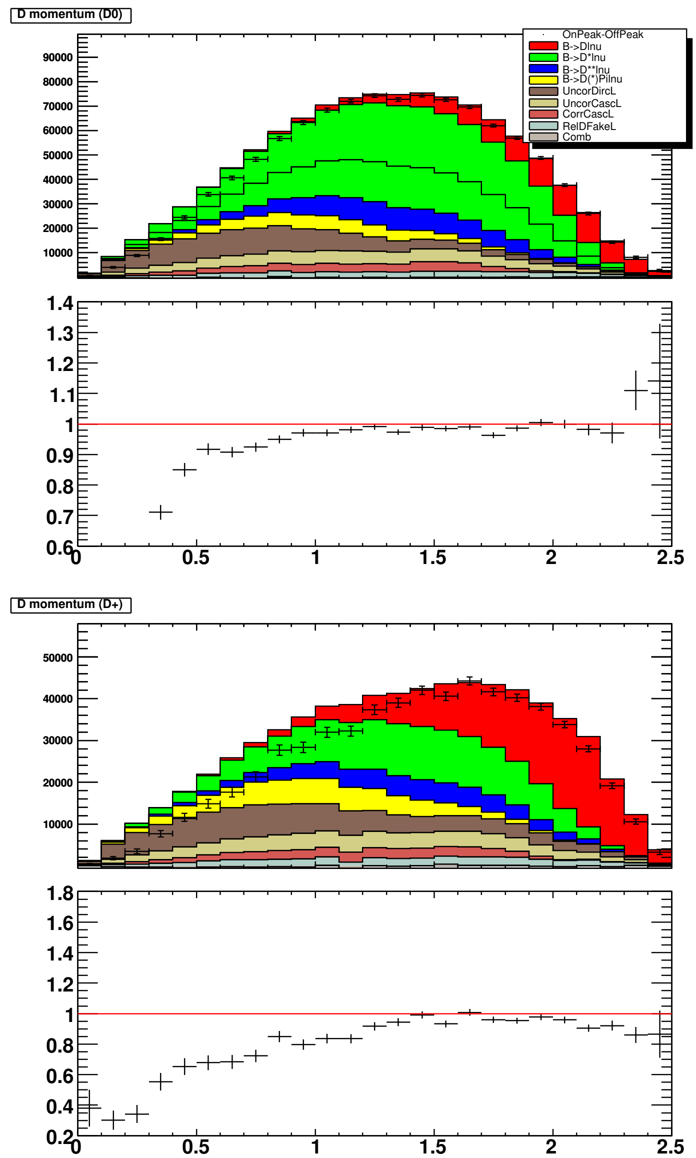

Figure 20: [p_D **after Trk PID**] D momentum plot after PID and tracking corrected and D mass sideband subtracted. The top is D^0 and the bottom is D^+. Black is OnPeak - OffPeak data. Red is $B \to D\ell\nu$, green is $B \to D^*\ell\nu$, blue is $B \to D^{**}\ell\nu$, yellow is non-resonant $B \to D^{(*)}\pi\ell\nu$, and the rest is background. Dark brown is UncorrDL, light brown is UncorrCL, dark red is CascL, blue gray is FakeL, and light gray is Comb. Comb is almost disappeared after D mass sideband subtraction.

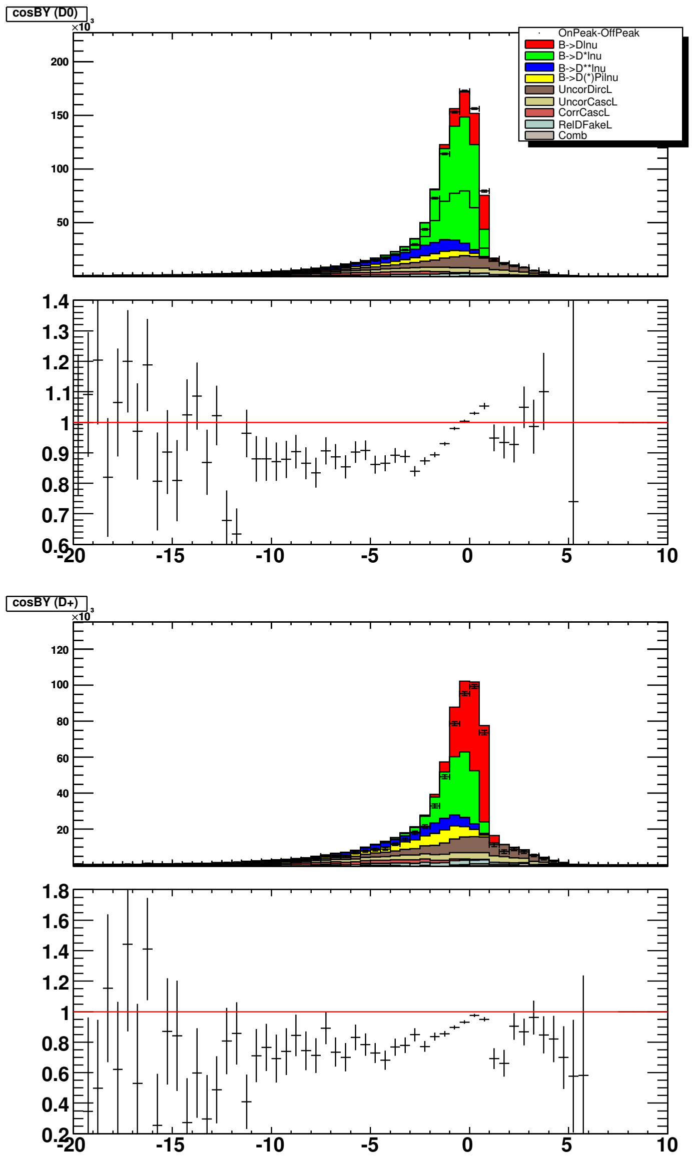

Figure 21: [$\cos\theta_{B-Dl}$ **after Trk PID**] $\cos\theta_{B-Dl}$ plot after PID and tracking corrected and D mass sideband subtracted. The top is D^0 and the bottom is D^+. Black is OnPeak - OffPeak data. Red is $B \to D\ell\nu$, green is $B \to D^*\ell\nu$, blue is $B \to D^{**}\ell\nu$, yellow is non-resonant $B \to D^{(*)}\pi\ell\nu$, and the rest is background. Dark brown is UncorrDL, light brown is UncorrCL, dark red is CascL, blue gray is FakeL, and light gray is Comb. Comb is almost disappeared after D mass sideband subtraction.

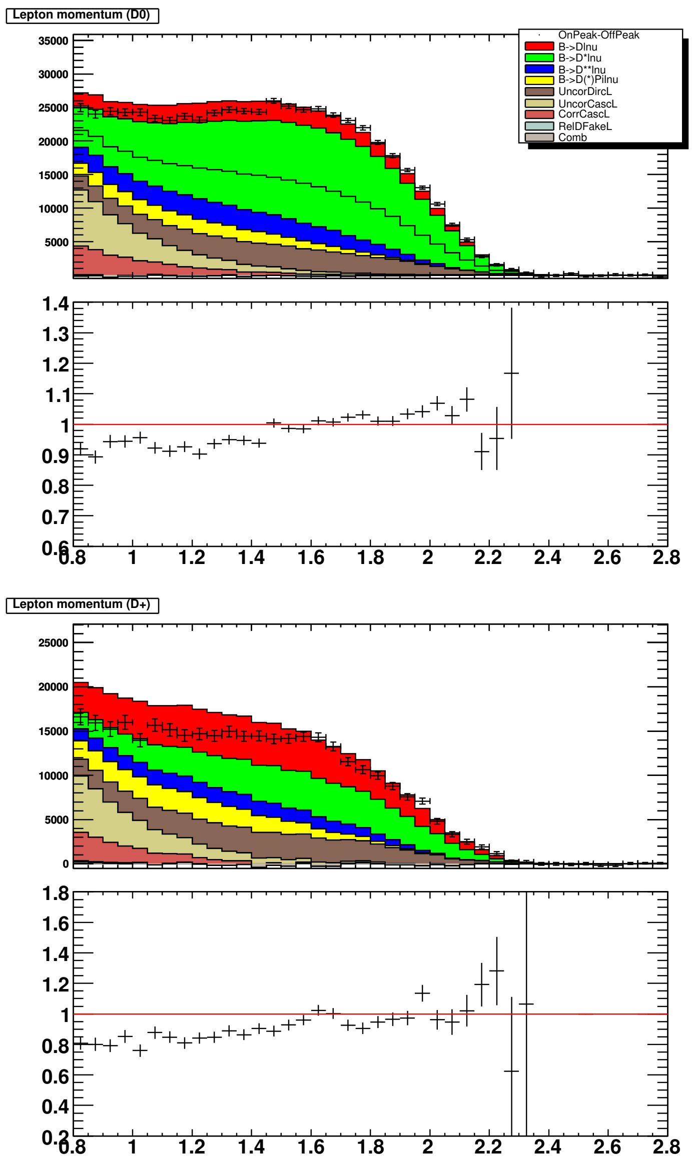

Figure 22: [p_ℓ **after Trk PID, Electron**] Lepton momentum plot after PID and tracking corrected and D mass sideband subtracted in the case $\ell = e$ (Electron only). The top is D^0 and the bottom is D^+. Black is OnPeak - OffPeak data. Red is $B \to D\ell\nu$, green is $B \to D^*\ell\nu$, blue is $B \to D^{**}\ell\nu$, yellow is non-resonant $B \to D^{(*)}\pi\ell\nu$, and the rest is background. Dark brown is UncorrDL, light brown is UncorrCL, dark red is CascL, blue gray is FakeL, and light gray is Comb. Comb is almost disappeared after D mass sideband subtraction.

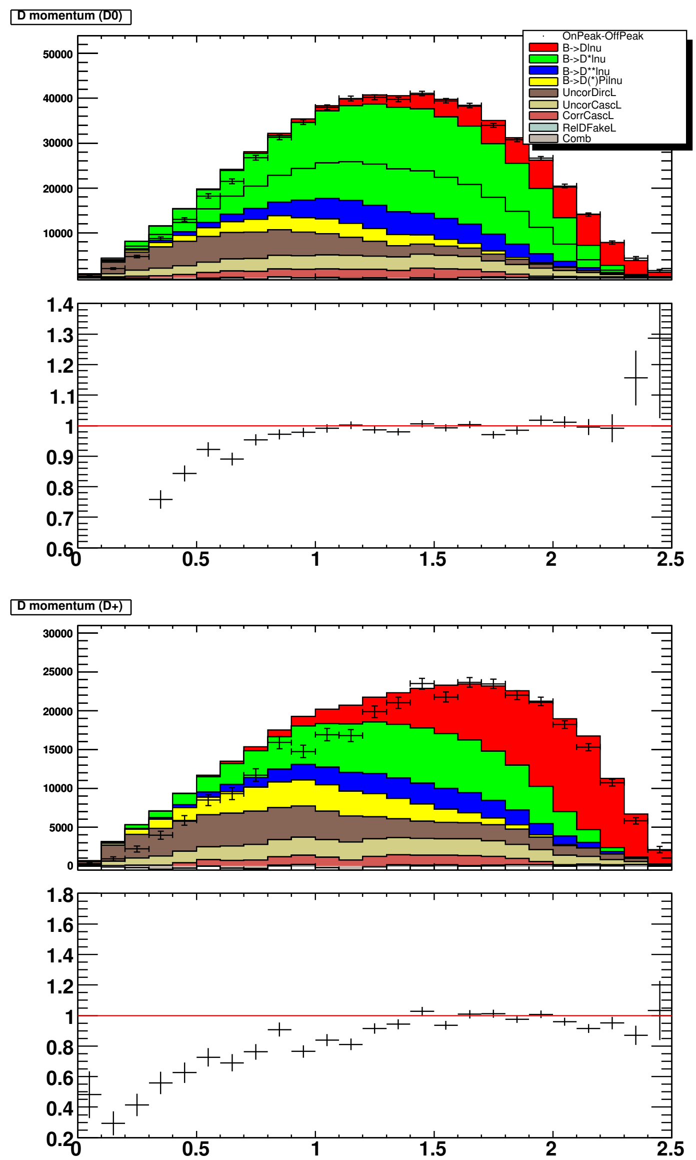

Figure 23: [p_D **after Trk PID, Electron**] D momentum plot after PID and tracking corrected and D mass sideband subtracted in the case $\ell = e$ (Electron only). The top is D^0 and the bottom is D^+. Black is OnPeak - OffPeak data. Red is $B \to D\ell\nu$, green is $B \to D^*\ell\nu$, blue is $B \to D^{**}\ell\nu$, yellow is non-resonant $B \to D^{(*)}\pi\ell\nu$, and the rest is background. Dark brown is UncorrDL, light brown is UncorrCL, dark red is CascL, blue gray is FakeL, and light gray is Comb. Comb is almost disappeared after D mass sideband subtraction.

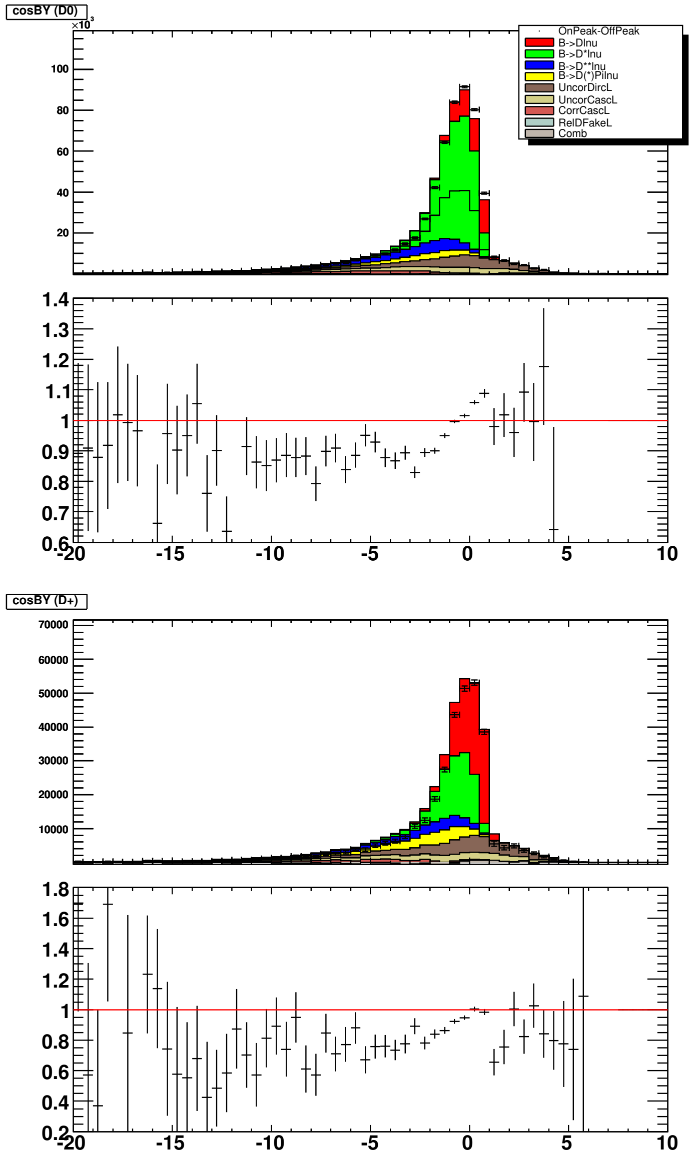

Figure 24: [$\cos\theta_{B-Dl}$ **after Trk PID, Electron**] $\cos\theta_{B-Dl}$ plot after PID and tracking corrected and D mass sideband subtracted in the case $\ell = e$ (Electron only). The top is D^0 and the bottom is D^+. Black is OnPeak - OffPeak data. Red is $B \to D\ell\nu$, green is $B \to D^*\ell\nu$, blue is $B \to D^{**}\ell\nu$, yellow is non-resonant $B \to D^{(*)}\pi\ell\nu$, and the rest is background. Dark brown is UncorrDL, light brown is UncorrCL, dark red is CascL, blue gray is FakeL, and light gray is Comb. Comb is almost disappeared after D mass sideband subtraction.

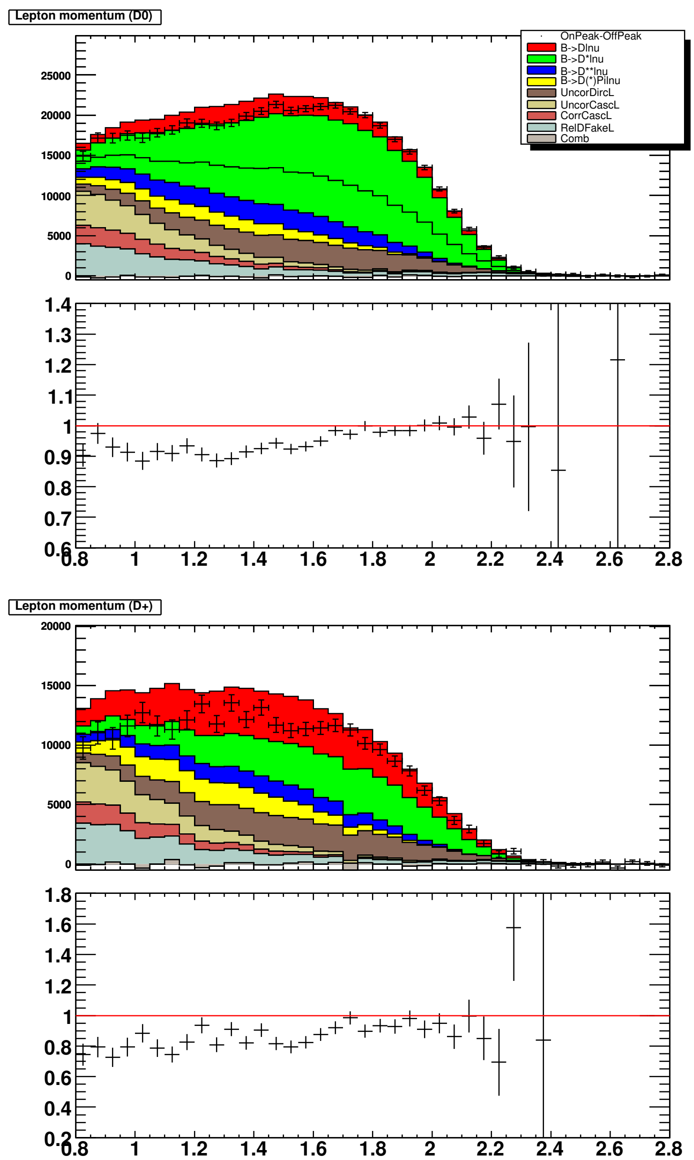

Figure 25: [p_ℓ **after Trk PID, Muon**] Lepton momentum plot after PID and tracking corrected and D mass sideband subtracted in the case $\ell = \mu$ (Muon only). The top is D^0 and the bottom is D^+. Black is OnPeak - OffPeak data. Red is $B \to D\ell\nu$, green is $B \to D^*\ell\nu$, blue is $B \to D^{**}\ell\nu$, yellow is non-resonant $B \to D^{(*)}\pi\ell\nu$, and the rest is background. Dark brown is UncorrDL, light brown is UncorrCL, dark red is CascL, blue gray is FakeL, and light gray is Comb. Comb is almost disappeared after D mass sideband subtraction.

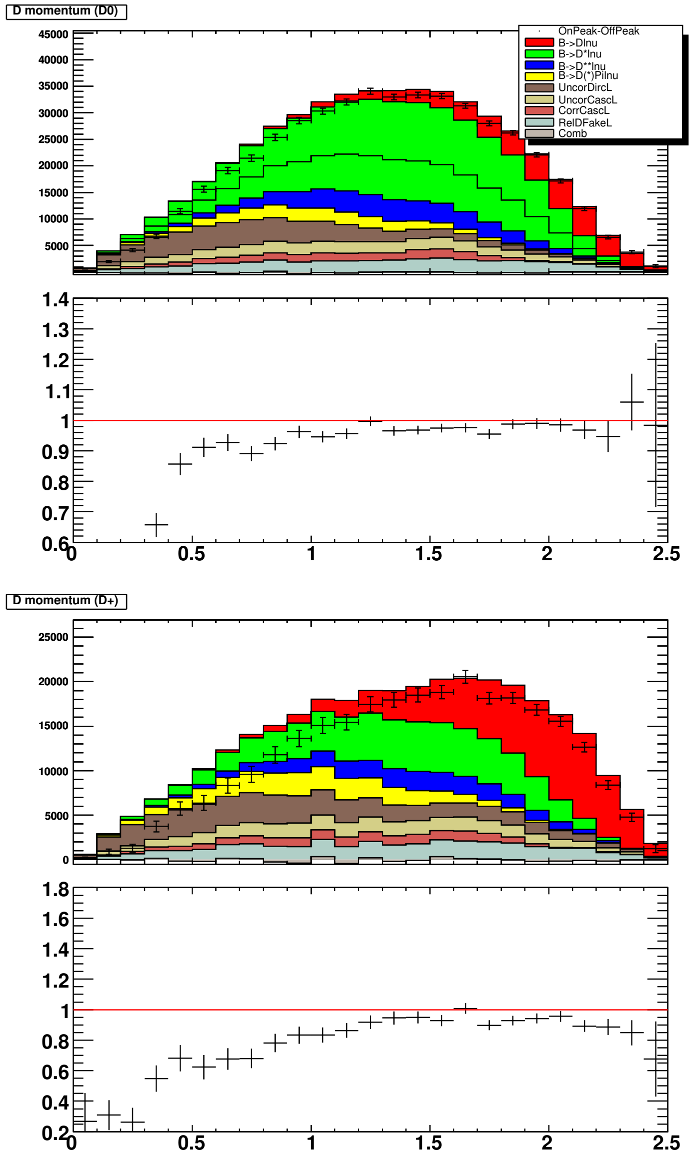

Figure 26: [p_D **after Trk PID, Muon**] D momentum plot after PID and tracking corrected and D mass sideband subtracted in the case $\ell = \mu$ (Muon only). The top is D^0 and the bottom is D^+. Black is OnPeak - OffPeak data. Red is $B \to D\ell\nu$, green is $B \to D^*\ell\nu$, blue is $B \to D^{**}\ell\nu$, yellow is non-resonant $B \to D^{(*)}\pi\ell\nu$, and the rest is background. Dark brown is UncorrDL, light brown is UncorrCL, dark red is CascL, blue gray is FakeL, and light gray is Comb. Comb is almost disappeared after D mass sideband subtraction.

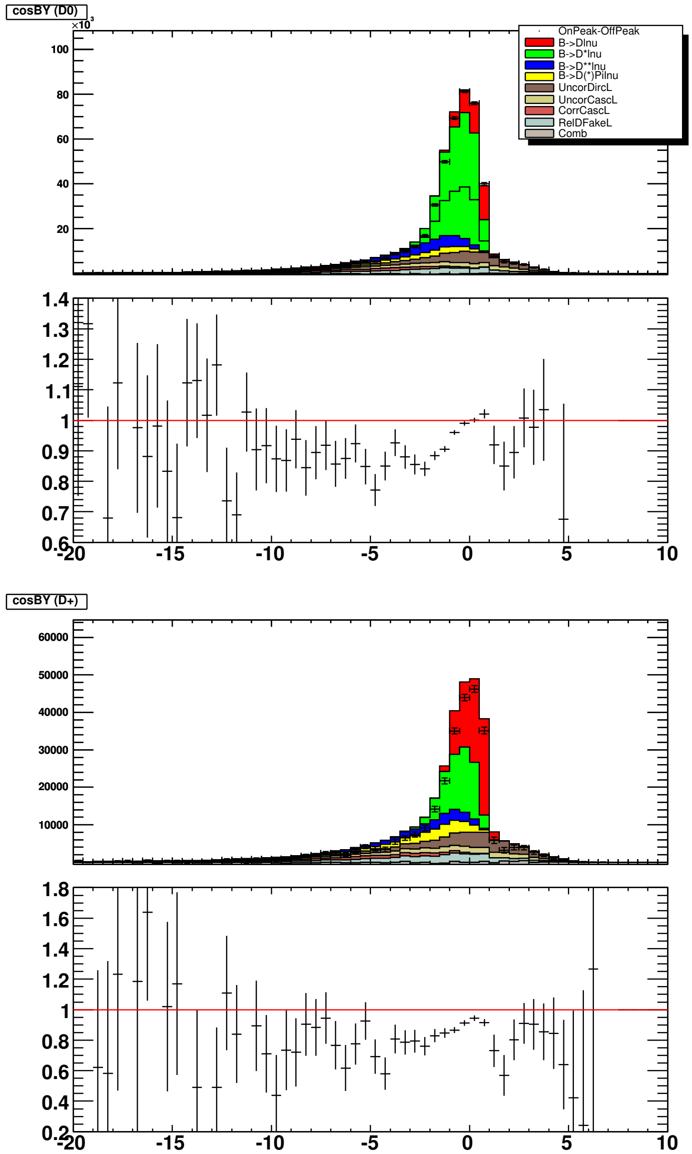

Figure 27: [$\cos\theta_{B-Dl}$ **after Trk PID, Muon**] $\cos\theta_{B-Dl}$ plot after PID and tracking corrected and D mass sideband subtracted in the case $\ell = \mu$ (Muon only). The top is D^0 and the bottom is D^+. Black is OnPeak - OffPeak data. Red is $B \to D\ell\nu$, green is $B \to D^*\ell\nu$, blue is $B \to D^{**}\ell\nu$, yellow is non-resonant $B \to D^{(*)}\pi\ell\nu$, and the rest is background. Dark brown is UncorrDL, light brown is UncorrCL, dark red is CascL, blue gray is FakeL, and light gray is Comb. Comb is almost disappeared after D mass sideband subtraction.

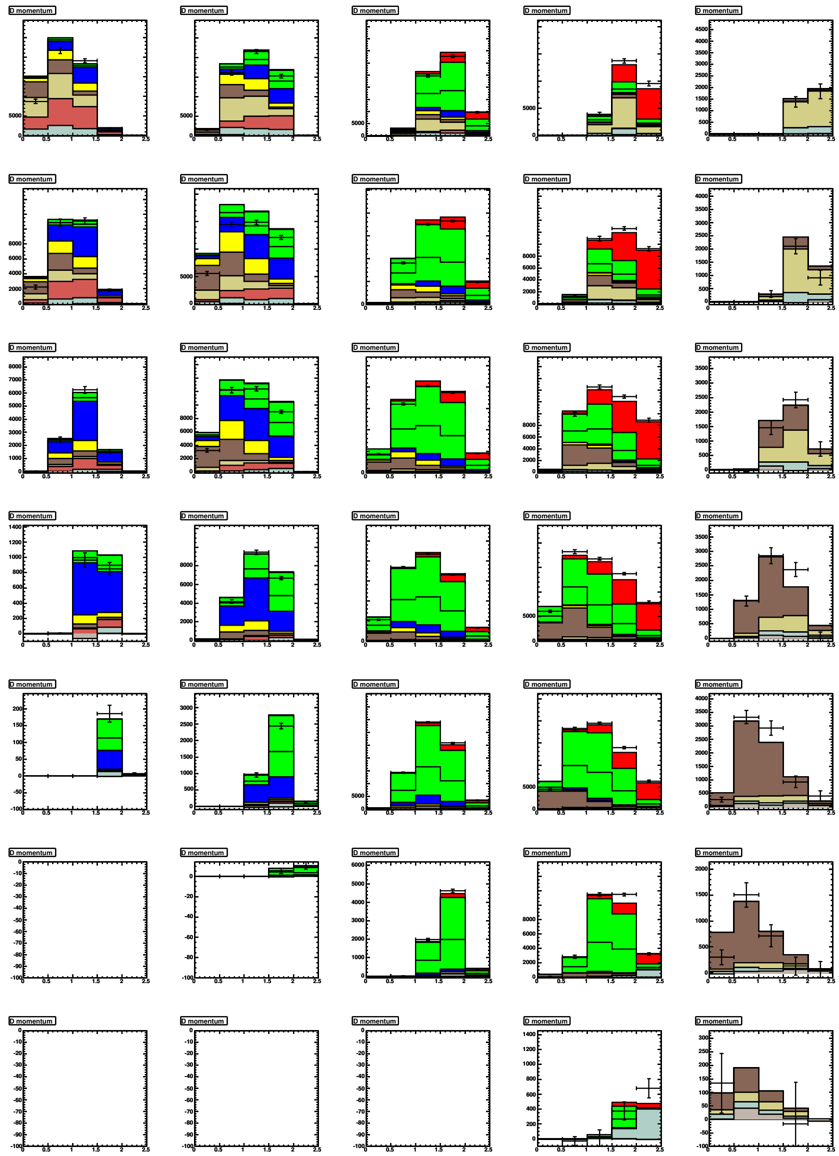

Figure 28: [**Bin by bin plot (D^0) after Trk PID**] D^0 momentum plots showing all bins after tracking efficiency and PID correction and D mass sideband subtraction. From top to bottom, lepton momentum bin changes from the lowest to the highest, and from left to right, cosBY bin changes from negative to positive. In each plots, colors are the same as other plots. Black is OnPeak - OffPeak data. Red is $B \to D\ell\nu$, green is $B \to D^*\ell\nu$, blue is $B \to D^{**}\ell\nu$, yellow is non-resonant $B \to D^{(*)}\pi\ell\nu$, and the rest is background. Dark brown is UncorrDL, light brown is UncorrCL, dark red is CascL, blue gray is FakeL, and light gray is Comb. Comb is almost disappeared after D mass sideband subtraction.

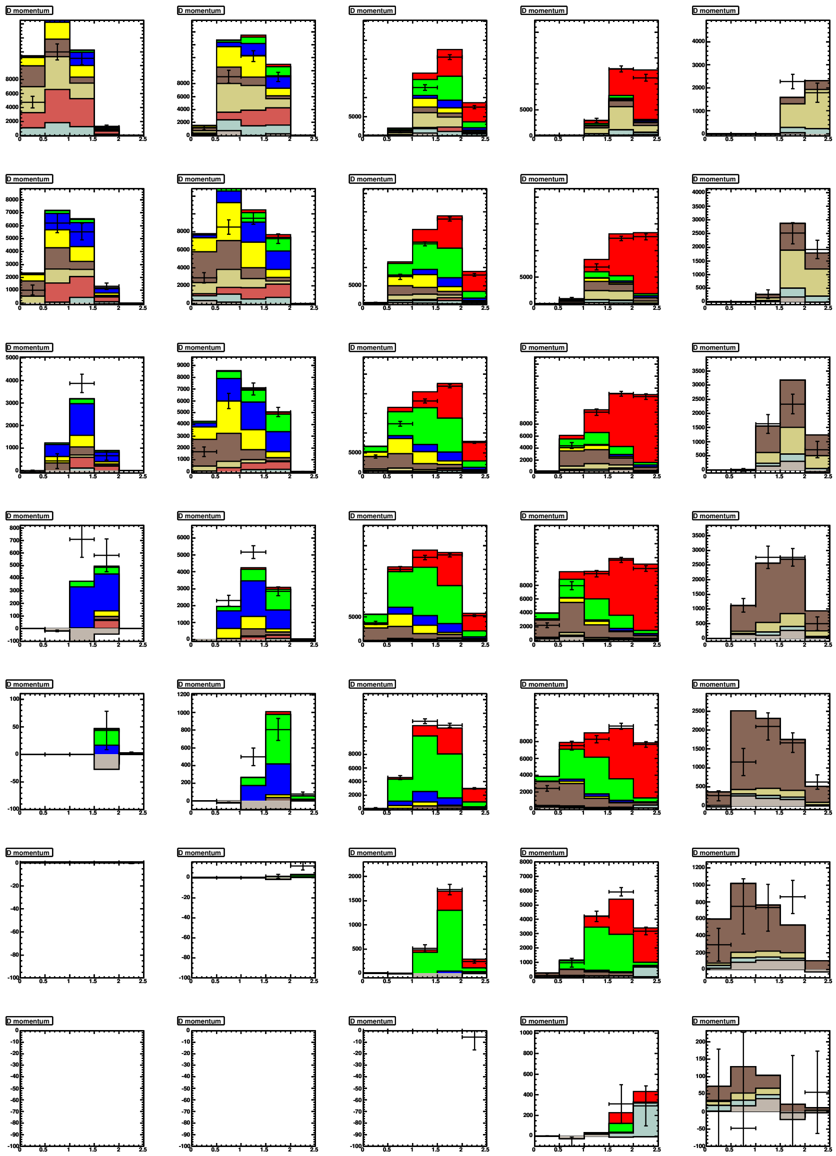

Figure 29: [**Bin by bin plot (D^+) after Trk PID**] D^+ momentum plots showing all bins after tracking efficiency and PID correction and D mass sideband subtraction. From top to bottom, lepton momentum bin changes from the lowest to the highest, and from left to right, cosBY bin changes from negative to positive. In each plots, colors are the same as other plots. Black is OnPeak - OffPeak data. Red is $B \to D\ell\nu$, green is $B \to D^*\ell\nu$, blue is $B \to D^{**}\ell\nu$, yellow is non-resonant $B \to D^{(*)}\pi\ell\nu$, and the rest is background. Dark brown is UncorrDL, light brown is UncorrCL, dark red is CascL, blue gray is FakeL, and light gray is Comb. Comb is almost disappeared after D mass sideband subtraction.

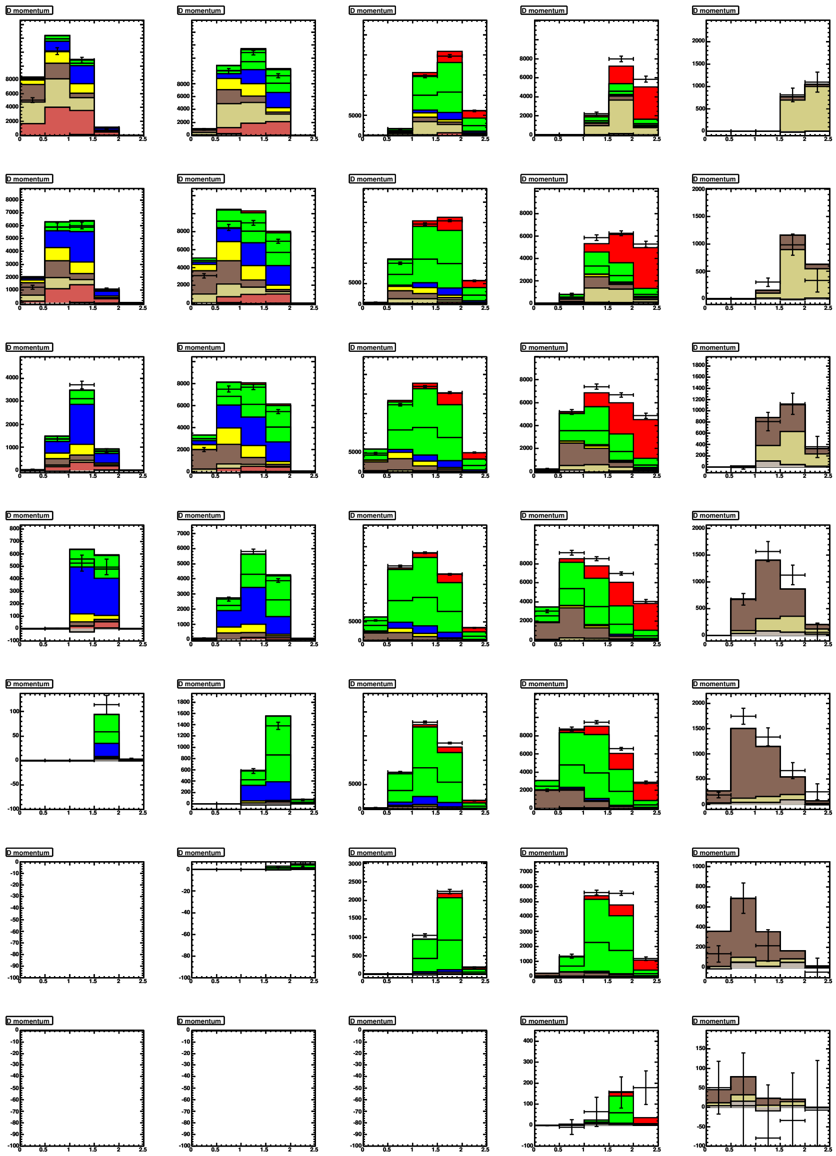

Figure 30: [**Bin by bin plot (D^0) after Trk PID, Electron**] D^0 momentum plots showing all bins after tracking efficiency and PID correction and D mass sideband subtraction in the case $\ell = e$ (Electron only). From top to bottom, lepton momentum bin changes from the lowest to the highest, and from left to right, cosBY bin changes from negative to positive. In each plots, colors are the same as other plots. Black is OnPeak - OffPeak data. Red is $B \to D\ell\nu$, green is $B \to D^*\ell\nu$, blue is $B \to D^{**}\ell\nu$, yellow is non-resonant $B \to D^{(*)}\pi\ell\nu$, and the rest is background. Dark brown is UncorrDL, light brown is UncorrCL, dark red is CascL, blue gray is FakeL, and light gray is Comb. Comb is almost disappeared after D mass sideband subtraction.

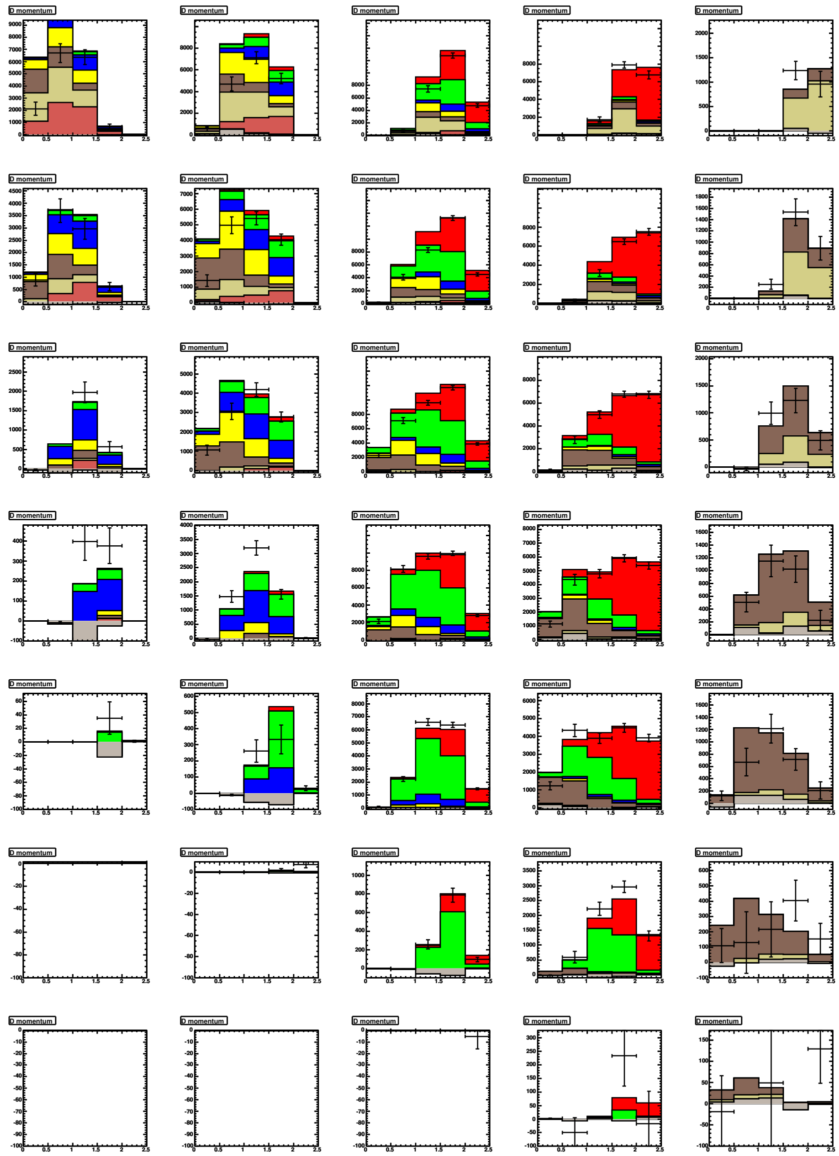

Figure 31: [**Bin by bin plot (D^+) after Trk PID, Electron**] D^+ momentum plots showing all bins after tracking efficiency and PID correction and D mass sideband subtraction in the case $\ell = e$ (Electron only). From top to bottom, lepton momentum bin changes from the lowest to the highest, and from left to right, cosBY bin changes from negative to positive. In each plots, colors are the same as other plots. Black is OnPeak - OffPeak data. Red is $B \to D\ell\nu$, green is $B \to D^*\ell\nu$, blue is $B \to D^{**}\ell\nu$, yellow is non-resonant $B \to D^{(*)}\pi\ell\nu$, and the rest is background. Dark brown is UncorrDL, light brown is UncorrCL, dark red is CascL, blue gray is FakeL, and light gray is Comb. Comb is almost disappeared after D mass sideband subtraction.

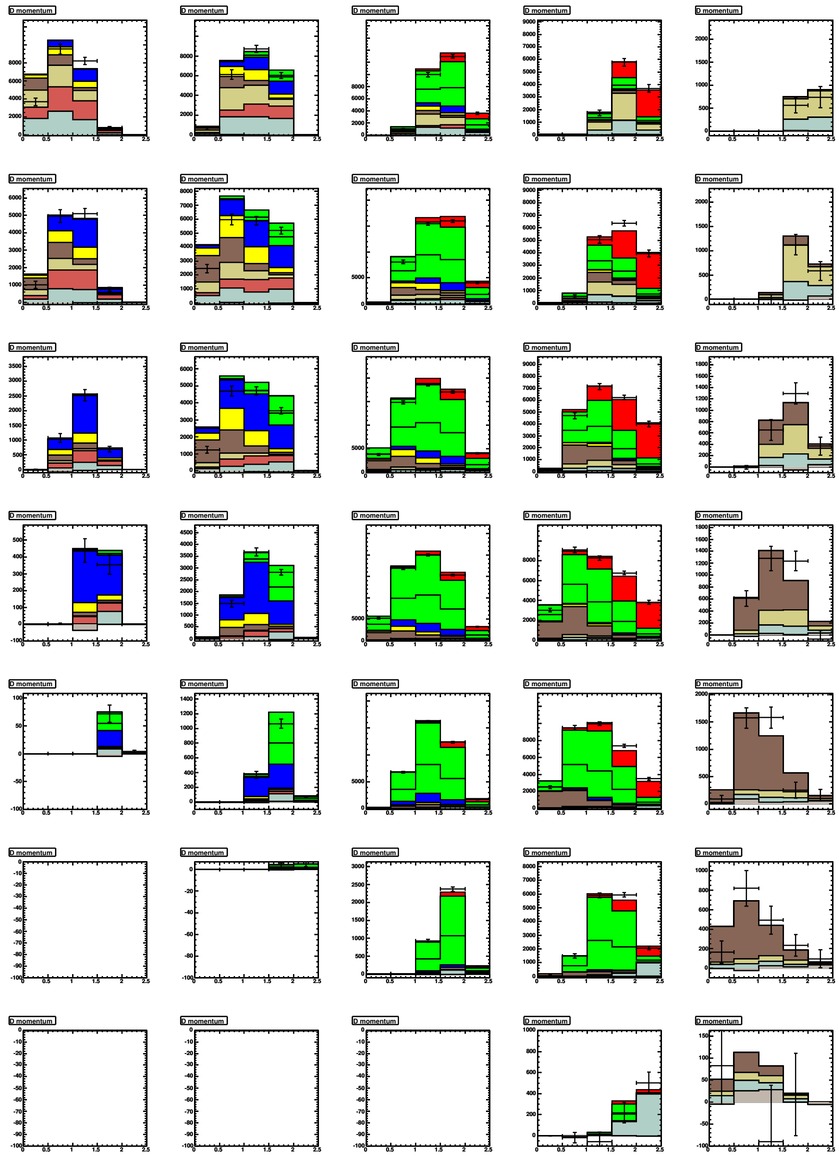

Figure 32: [**Bin by bin plot (D^0) after Trk PID, Muon**] D^0 momentum plots showing all bins after tracking efficiency and PID correction and D mass sideband subtraction in the case $\ell = \mu$ (Muon only). From top to bottom, lepton momentum bin changes from the lowest to the highest, and from left to right, cosBY bin changes from negative to positive. In each plots, colors are the same as other plots. Black is OnPeak - OffPeak data. Red is $B \to D\ell\nu$, green is $B \to D^*\ell\nu$, blue is $B \to D^{**}\ell\nu$, yellow is non-resonant $B \to D^{(*)}\pi\ell\nu$, and the rest is background. Dark brown is UncorrDL, light brown is UncorrCL, dark red is CascL, blue gray is FakeL, and light gray is Comb. Comb is almost disappeared after D mass sideband subtraction.

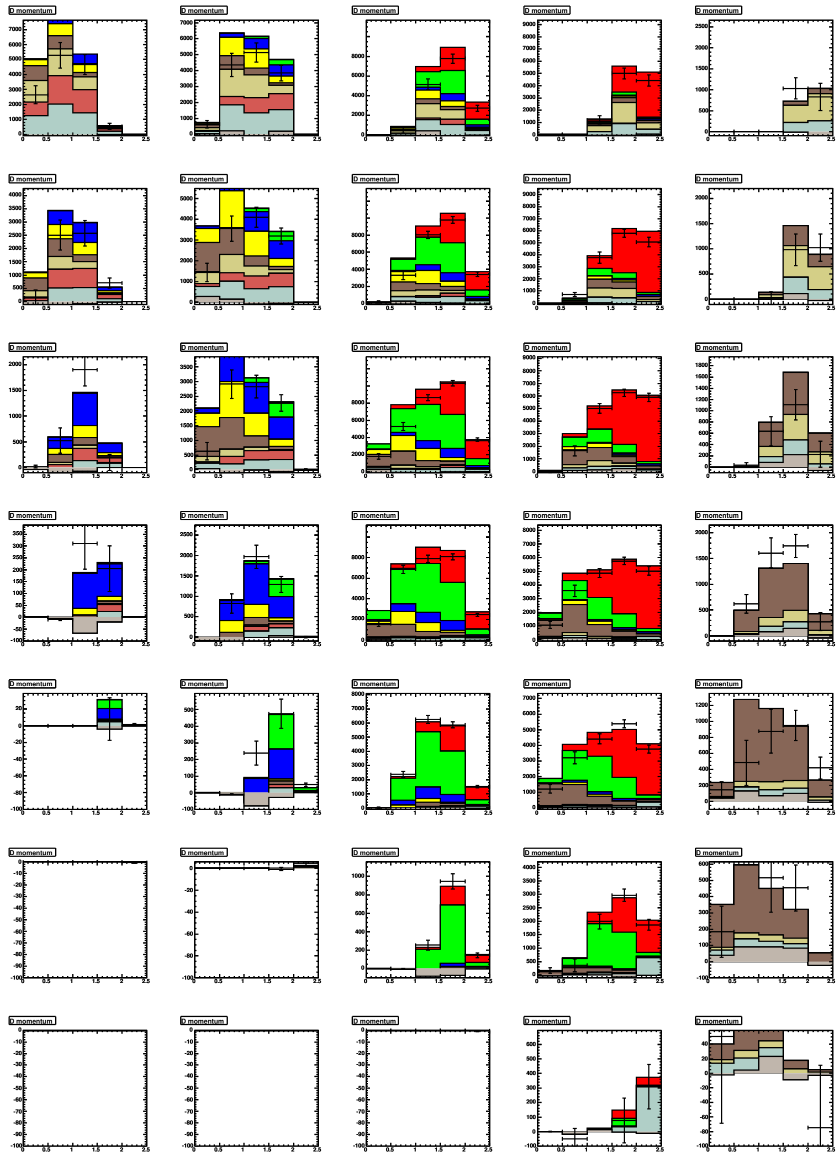

Figure 33: [**Bin by bin plot (D^+) after Trk PID, Muon**] D^+ momentum plots showing all bins after tracking efficiency and PID correction and D mass sideband subtraction in the case $\ell = \mu$ (Muon only). From top to bottom, lepton momentum bin changes from the lowest to the highest, and from left to right, cosBY bin changes from negative to positive. In each plots, colors are the same as other plots. Black is OnPeak - OffPeak data. Red is $B \to D\ell\nu$, green is $B \to D^*\ell\nu$, blue is $B \to D^{**}\ell\nu$, yellow is non-resonant $B \to D^{(*)}\pi\ell\nu$, and the rest is background. Dark brown is UncorrDL, light brown is UncorrCL, dark red is CascL, blue gray is FakeL, and light gray is Comb. Comb is almost disappeared after D mass sideband subtraction.

9 Monte Carlo Re-weighting (W_{jk}^{MC})

Because of theoretical and experimental improvements, some of numbers and formulas used in our MC are obsolete. In order to take new results into account, we need to re-wight MC. In this analysis, we re-weight decay branching fractions and form factors. In this section, details of branching fraction re-weighting is presented. Form factor re-weighting is described in section 10

9.1 Background components

As described in section 2, a few specific decay modes dominate the backgrounds. We need to update some of decay branching fraction to get better description of data.

9.1.1 Semileptonic $D(D_s)$ decay branching fractions

In case of CascL, UncrorrCL and CombRL backgrounds, the lepton we reconstruc is mainly come from semileptonic $D(D_s)$ decays. Thus, we correct the branching fractions of semileptonic $D(D_s)$ decays. The values used in SP5/SP6 MC and in PDG [12] are listed in Table 14 along with the weights. The weight is given by the ratio of new and old branching fractions. See section 9.4 for an example.

9.1.2 $B \to D^{(*)}\tau\nu$ decay branching fractions

In case of UncrorrCL and CascL backgrounds, we correct $B \to D^{(*)}\tau\nu$ decay branching fractions. Especially, approximately a half of CascL events are the case where the lepton comes from τ. For the decays $B^+ \to \bar{D}^0\tau^+\nu$, $B^+ \to \bar{D}^{*0}\tau^+\nu$ and $B^0 \to D^-\tau^+\nu$ we use Babar results [24]. For the decay $B^0 \to D^{*-}\tau^+\nu$ we take an average of Babar [24]

$$B^0 \to D^{*-}\tau^+\nu = 0.0162 \pm 0.0031 \pm 0.0010 \pm 0.005 \tag{180}$$

and Belle [25] results.

$$B^0 \to D^{*-}\tau^+\nu = 0.0202 \pm 0.004 \pm 0.0037 \pm 0.005 \tag{181}$$

Averaged BF and weights are given in Table 15

9.1.3 Inclusive $B \to X\ell\nu$ decay branching fractions

In case of UncorrDL and CombRL backgrounds, we correct the branching fraction of inclusive $B \to X\ell\nu$ decays. In SP5/SP6 MC, the following values are used :

$$\begin{aligned} \mathcal{B}(B^+ \to X_c\ell\nu) &= \mathcal{B}(B^0 \to X_c\ell\nu) = 0.104 \\ \mathcal{B}(B^+ \to X_u\ell\nu) &= 0.002088 \\ \mathcal{B}(B^0 \to X_u\ell\nu) &= 0.002100 \end{aligned} \tag{182}$$

Decay mode	SP5/SP6	PDG [12]	Weight
$D^0 \to K^{*-} e\nu$	0.0202	0.0216 ± 0.0016	1.0693 ± 0.0792
$D^0 \to K^- e\nu$	0.0364	0.0350 ± 0.0009	0.9315 ± 0.0247
$D^0 \to \pi^- e\nu$	0.0037	0.0028 ± 0.0002	0.7568 ± 0.0459
$D^0 \to \rho^- e\nu$	0.0029	0.0019 ± 0.0004	0.6552 ± 0.1379
$D^0 \to K^{*-} \mu\nu$	0.0198	0.0194 ± 0.0025	0.9798 ± 0.1263
$D^0 \to K^- \mu\nu$	0.0322	0.0327 ± 0.0013	1.0155 ± 0.0404
$D^0 \to \pi^- \mu\nu$	0.0037	0.0024 ± 0.0002	0.6378 ± 0.0649
$D^0 \to \rho^- \mu\nu$	0.0029	0.0019 ± 0.0004	0.6552 ± 0.1379
$D^+ \to K^{*0} e\nu$	0.0480	0.0556 ± 0.0032	1.1583 ± 0.0667
$D^+ \to K^0 e\nu$	0.0670	0.0860 ± 0.0050	1.2836 ± 0.0667
$D^+ \to \pi^0 e\nu$	0.0031	0.0044 ± 0.0007	1.4194 ± 0.2258
$D^+ \to \rho^0 e\nu$	0.0022	0.0022 ± 0.0004	1.000 ± 0.1818
$D^+ \to \omega e\nu$	0.0029	0.0016 ± 0.0007	0.5517 ± 0.2414
$D^+ \to K^{*0} \mu\nu$	0.0430	0.0550 ± 0.0050	1.2791 ± 0.1163
$D^+ \to K^0 \mu\nu$	0.0700	0.0960 ± 0.0080	1.3714 ± 0.1143
$D^+ \to \pi^0 \mu\nu$	0.0064	0.0044 ± 0.0007	0.6875 ± 0.1094
$D^+ \to \rho^0 \mu\nu$	0.0027	0.0025 ± 0.0005	0.9259 ± 0.1852
$D^+ \to \omega \mu\nu$	0.0029	0.0016 ± 0.0007	0.5517 ± 0.2222
$D_s^+ \to \phi \ell\nu$	0.0200	0.0249 ± 0.0028	1.2450 ± 0.2400
$D_s^+ \to \eta \ell\nu$	0.0260	0.0320 ± 0.0060	1.2308 ± 0.2308
$D_s^+ \to \eta' \ell\nu$	0.0089	0.0111 ± 0.0034	1.2472 ± 0.3820

Table 14: [**Semileptonic** D **decay BF weight**] D semileptonic decay branching fractions and weights.

Decay mode	SP5/SP6	Measured [24][25]	Weight
$B^+ \to \bar{D}^0 \tau^+ \nu$	0.0070	$0.0092 \pm 0.0026 \pm 0.0011 \pm 0.006$	1.3142 ± 0.4123
$B^+ \to \bar{D}^{*0} \tau^+ \nu$	0.0160	$0.0174 \pm 0.0033 \pm 0.0010 \pm 0.006$	1.0875 ± 0.2188
$B^0 \to D^- \tau^+ \nu$	0.0070	$0.0086 \pm 0.0024 \pm 0.0011 \pm 0.006$	1.2286 ± 0.3868
$B^0 \to D^{*-} \tau^+ \nu$	0.0160	0.0173 ± 0.0028	1.0795 ± 0.1762

Table 15: [$B \to D^{(*)} \tau\nu$ **decay BF weight**] $B \to D^{(*)} \tau\nu$ decay branching fractions and weights.

Decay mode	SP5/SP6	isospin averaged BF	Weight
$B^+ \to \bar{X}^0\ell^+\nu$	0.106088	0.1112 ± 0.0019	1.0480 ± 0.0179
$B^0 \to X^-\ell^+\nu$	0.106100	0.1038 ± 0.0018	0.9785 ± 0.0167

Table 16: [$B \to \ell$ **decay BF weight**] Inclusive $B \to x\ell\nu$ branching fractions.

Thus

$$\begin{aligned} \mathcal{B}(B^+ \to X\ell\nu) &= 0.106088 \\ \mathcal{B}(B^0 \to X\ell\nu) &= 0.106100 \end{aligned} \tag{183}$$

From PDG [12] and HFAG [26]

$$\mathcal{B}(B \to X\ell\nu) = 0.1075 \pm 0.0016 \tag{184}$$

We impose isospin constrain, then

$$\begin{aligned} \mathcal{B}(B^+ \to X\ell\nu) &= t_{+0}\mathcal{B}(B^0 \to X\ell\nu) \\ \mathcal{B}(B^+ \to X\ell\nu) + \mathcal{B}(B^0 \to X\ell\nu) &= \mathcal{B}(B \to X\ell\nu) \end{aligned} \tag{185}$$

Thus, we get

$$\mathcal{B}(B^+ \to X\ell\nu) = \frac{2t_{+0}}{1+t_{+0}}\mathcal{B}(B \to X\ell\nu) = 0.1112 \pm 0.0019 \tag{186}$$

and

$$\mathcal{B}(B^+ \to X\ell\nu) = \frac{1}{1+t_{+0}}\mathcal{B}(B \to X\ell\nu) = 0.1038 \pm 0.0018 \tag{187}$$

Weights are given by the ratios of new and old branching fractions as summarized in Table 16. These weights are applied to lepton side of each candidate.

9.1.4 Inclusive $B \to D(D_s)$ decay branching fractions

In UncorrDL, UncorrCL, CascL, FakeL and CombRL backgrounds, we correct the branching fraction of inclusive $B \to D(D_s)$ decays using measured branching fractions from [27][28]. We apply weights to D of $D\ell$ candidates, and for cascade lepton backgrounds such as $B \to D(D_s)X$ and $D(D_s) \to X'\ell\nu$, we also apply weights to the $B \to D(D_s)X$ part. $B \to D_s$ weights come in only the cascade case.
The $D(D_s)$ momentum dependent weights are given in Tables 17 - 22. If we apply these weights to, for example, UncorrDL ($B^+(B^-) \to D^0$), we get a distribution shown in Figure 34. The corrected histogram is fluctuated because of the statistical fluctuation of the weights. To smooth up the fluctuation, we use a 4th order polynomial to approximate the $B \to D$ weights as a function of D momentum and 3rd order polynomial to approximate the $B \to D_s$ weights as a function of D_s momentum. The

p_D (GeV)	$B^- \to D^0$	$\bar{B}^0 \to D^0$
0.00 - 0.15	0.0600 ± 0.1217	0.0275 ± 0.3010
0.15 - 0.30	0.4667 ± 0.1217	0.6083 ± 0.2374
0.30 - 0.45	0.9800 ± 0.1241	0.7300 ± 0.2080
0.45 - 0.60	0.8600 ± 0.1040	0.9036 ± 0.1863
0.60 - 0.75	1.1022 ± 0.1014	1.0000 ± 0.1779
0.75 - 0.90	1.2491 ± 0.1005	1.0125 ± 0.1677
0.90 - 1.05	1.1431 ± 0.0904	1.1791 ± 0.1516
1.05 - 1.20	1.1770 ± 0.0879	1.2500 ± 0.1519
1.20 - 1.35	1.1306 ± 0.0839	1.1738 ± 0.1451
1.35 - 1.50	1.1324 ± 0.0760	1.3902 ± 0.1516
1.50 - 1.65	1.0128 ± 0.0680	1.1245 ± 0.1214
1.65 - 1.80	1.1371 ± 0.0788	0.9500 ± 0.1538
1.80 - 1.95	0.9544 ± 0.0676	1.0423 ± 0.1600
1.95 - 2.10	0.9673 ± 0.0708	1.0850 ± 0.1789
2.10 - 2.25	0.8850 ± 0.0765	1.4500 ± 0.5274
2.25 - 2.40	0.8154 ± 0.1101	

Table 17: [p_D **dependent** $B \to D^0$ **weight (Correlated)**] D^0 momentum dependent, inclusive $B \to D^0$ branching fraction weights (Correlated). These are based on the branching fractions given in [27][28].

distributions of weights and fit results are given in Figures 35 - 46. Using the fitted coefficients, the weight w of $B \to D$ is given by

$$\begin{aligned} w = &(\text{Coefficient0}) + (\text{Coefficient1})p_D + (\text{Coefficient2})p_D^2 \\ &+(\text{Coefficient3})p_D^3 + (\text{Coefficient4})p_D^4 \end{aligned} \tag{188}$$

where p_D is the D momentum. In Figure 47, the same UncorrDL ($B^+(B^-) \to D^0$) using this fit resut is given. The corrected distribution is much smoother and retains similar character as the original distribution.

p_D (GeV)	$B^+ \to D^0$	$B^0 \to D^0$
0.00 - 0.15	0.1333 ± 0.1374	0.0938 ± 0.2519
0.15 - 0.30	0.4500 ± 0.1521	0.5114 ± 0.2636
0.30 - 0.45	0.7143 ± 0.1738	0.5172 ± 0.2695
0.45 - 0.60	0.9391 ± 0.1962	1.2000 ± 0.3265
0.60 - 0.75	1.2833 ± 0.2083	1.2214 ± 0.3465
0.75 - 0.90	1.4182 ± 0.2186	1.2424 ± 0.3601
0.90 - 1.05	2.3733 ± 0.3206	0.8182 ± 0.3961
1.05 - 1.20	1.1077 ± 0.2837	0.5647 ± 0.4759
1.20 - 1.35	0.8571 ± 0.4247	1.6000 ± 0.8412
1.35 - 1.50	2.9000 ± 1.1180	-3.5333 ± 1.9887
1.50 - 1.65	0.0833 ± 0.8580	3.4615 ± 2.6315
1.65 - 1.80	6.6667 ± 3.0732	6.3333 ± 8.3333

Table 18: [p_D **dependent** $B \to D^0$ **weight (Uncorrelated)**] D^0 momentum dependent, inclusive $B \to D^0$ branching fraction weights (Uncorrelated). These are based on the branching fractions given in [27][28].

p_D (GeV)	$B^- \to D^+$	$\bar{B}^0 \to D^+$
0.00 - 0.20	0.5588 ± 0.2712	0.1333 ± 0.2007
0.02 - 0.40	0.6484 ± 0.2190	0.6790 ± 0.2351
0.40 - 0.60	1.0438 ± 0.2285	0.3702 ± 0.1820
0.60 - 0.80	1.0402 ± 0.2032	0.6823 ± 0.1581
0.80 - 1.00	0.6615 ± 0.1655	0.6279 ± 0.1347
1.00 - 1.20	0.7929 ± 0.1585	0.7489 ± 0.1286
1.20 - 1.40	0.7056 ± 0.1557	1.0468 ± 0.1417
1.40 - 1.60	0.5414 ± 0.1762	1.0208 ± 0.1027
1.60 - 1.80	0.8313 ± 0.2642	1.0036 ± 0.1241
1.80 - 2.00	0.7500 ± 0.4413	1.0453 ± 0.1255
2.00 - 2.20	0.3333 ± 0.5429	0.8105 ± 0.1175
2.20 - 2.40		0.8490 ± 0.1514

Table 19: [p_D **dependent** $B \to D^+$ **weight (Correlated)**] D^+ momentum dependent, inclusive $B \to D^+$ branching fraction weights (Correlated). These are based on the branching fractions given in [27][28].

p_D (GeV)	$B^+ \to D^+$	$B^0 \to D^+$
0.00 - 0.20	0.1935 ± 0.1962	0.1613 ± 0.1962
0.20 - 0.40	0.2273 ± 0.2293	0.6462 ± 0.4440
0.40 - 0.60	1.0400 ± 0.3078	0.9315 ± 0.5156
0.60 - 0.80	0.0789 ± 0.2654	0.1143 ± 0.5157
0.80 - 1.00	0.8088 ± 0.3175	-0.0984 ± 0.5590
1.00 - 1.20	1.3400 ± 0.3795	1.7674 ± 0.9047
1.20 - 1.40	0.0800 ± 0.4948	-0.6667 ± 1.4414
1.40 - 1.60	0.5000 ± 1.3463	2.0000 ± 5.2100
1.60 - 1.80	2.1429 ± 1.4070	5.5000 ± 5.2633
1.80 - 2.00	2.0000 ± 2.2361	-8.0000 ± 6.4275

Table 20: [p_D **dependent** $B \to D^+$ **weight (Uncorrelated)**] D^+ momentum dependent, inclusive $B \to D^+$ branching fraction weights (Uncorrelated). These are based on the branching fractions given in [27][28].

p_D (GeV)	$B^- \to D_s^+$	$B^+ \to D_s^+$
0.00 - 0.34	-0.3810 ± 0.8624	1.3529 ± 0.5153
0.34 - 0.68	0.0938 ± 0.5703	0.0800 ± 0.2335
0.68 - 1.02	1.9167 ± 0.9904	0.7037 ± 0.2253
1.02 - 1.36	4.3333 ± 1.8295	0.4167 ± 0.1179
1.36 - 1.70	2.0000 ± 2.2804	0.9397 ± 0.1682
1.70 - 2.04	2.3333 ± 2.4267	1.2171 ± 0.2320

Table 21: [p_{D_s} **dependent** $B^\pm \to D_s^+$ **weight**] D_s^+ momentum dependent, inclusive $B^\pm \to D_s^+$ branching fraction weights. These are based on the branching fractions given in [27][28].

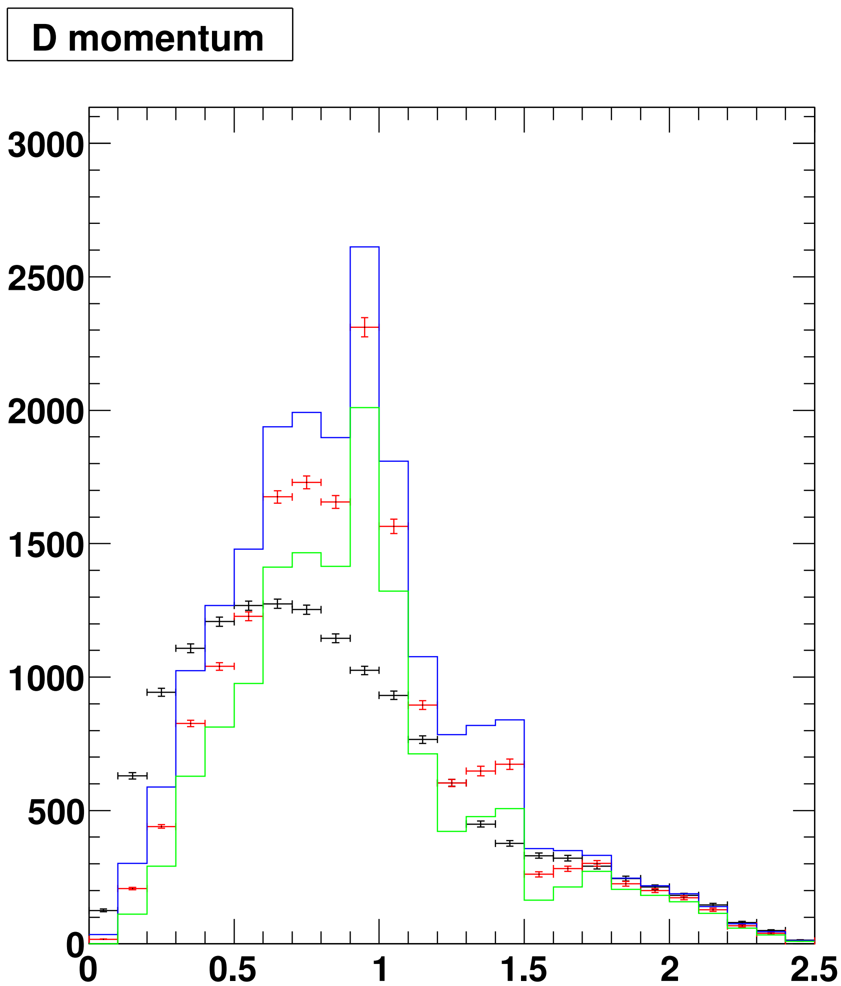

Figure 34: [**UncorrDL BF correction by Table**] Effect of BpBm UncorrDL background BF correction using weights given in tables. The black lines with error bars are before correction, and the red lines with error bars are after correction. Blue and green histograms show the range of uncertainty on the red histogram due to the uncertainties on inclusive $B \to D$ weights.

p_D (GeV)	$\bar{B}^0 \to D_s^+$	$B^0 \to D_s^+$
0.00 - 0.34	-1.0000 ± 0.6353	0.1579 ± 0.4243
0.34 - 0.68	1.8000 ± 1.2272	1.1800 ± 0.4847
0.68 - 1.02	0.1111 ± 1.4449	1.3714 ± 0.4006
1.02 - 1.36	5.8750 ± 2.8264	0.6917 ± 0.2072
1.36 - 1.70	-1.1250 ± 3.6443	1.1164 ± 0.2357
1.70 - 2.04	4.0000 ± 4.6690	1.2800 ± 0.3134

Table 22: [p_{D_s} **dependent** $B^0(\bar{B}^0) \to D_s^+$ **weight**] D_s^+ momentum dependent, inclusive $B^0(\bar{B}^0) \to D_s^+$ branching fraction weights. These are based on the branching fractions given in [27][28].

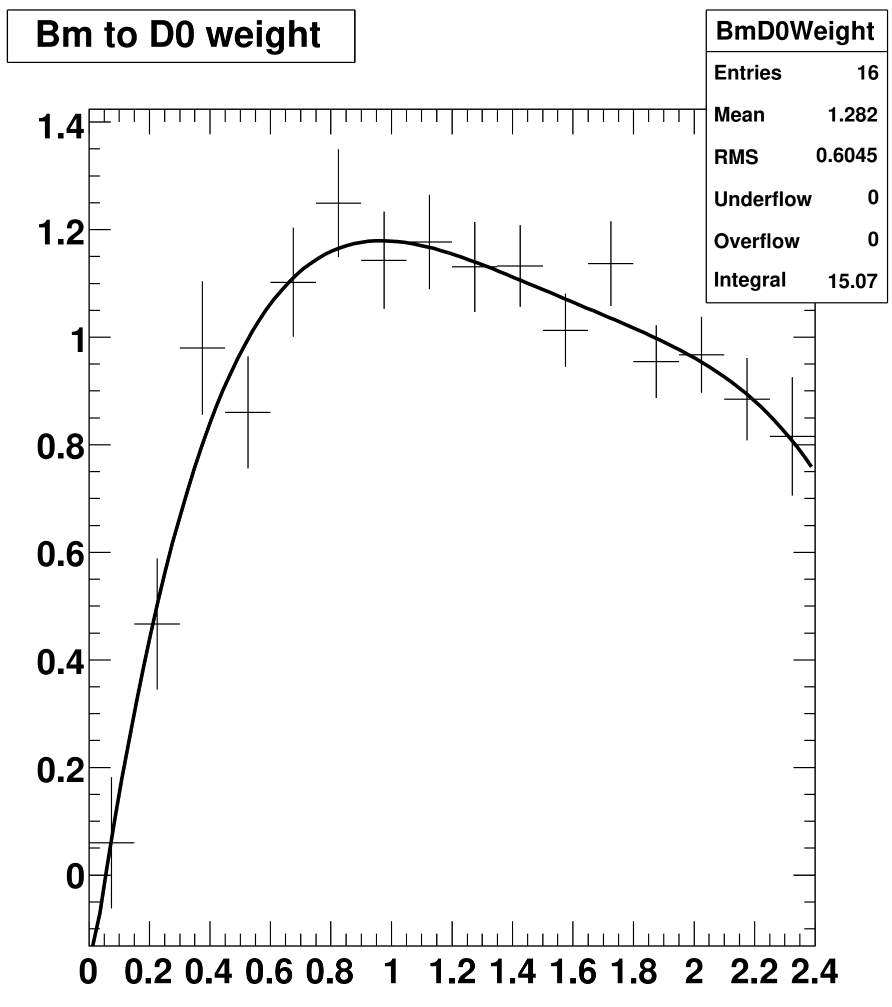

Figure 35: [**Fit for** $B^- \to D^0$ **weight**] 4th order polynomial fit for $B^- \to D^0$ weight.

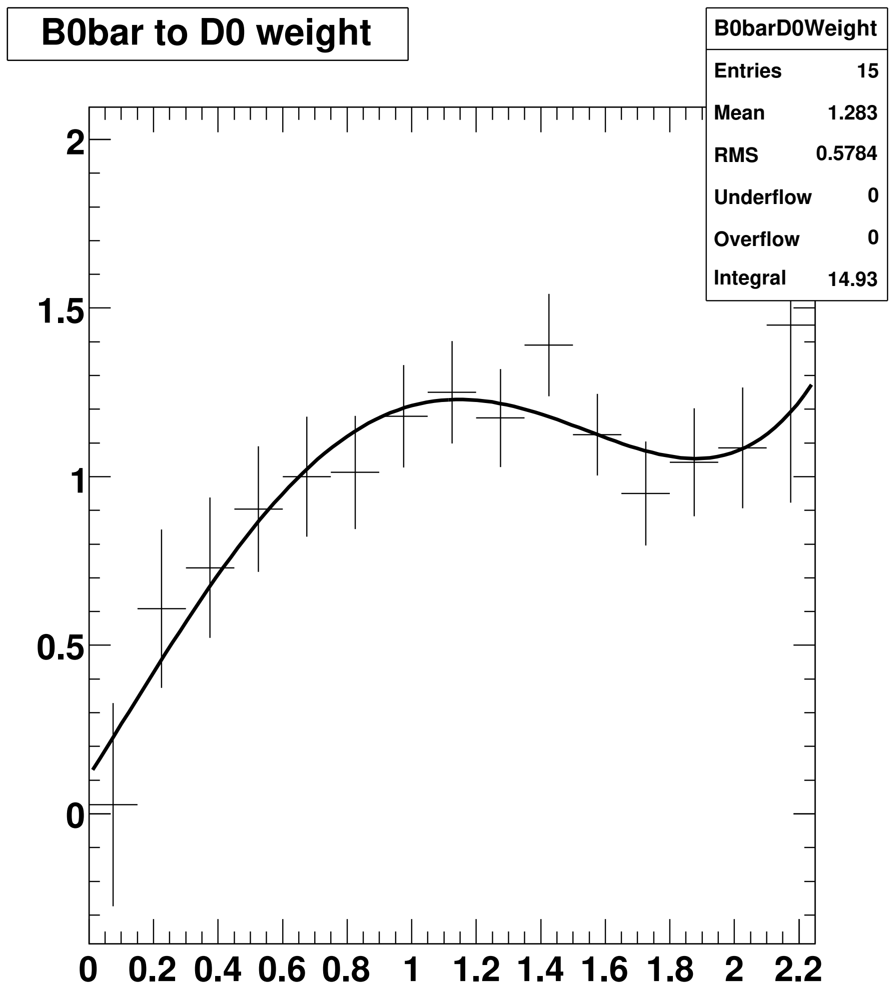

Figure 36: [**Fit for $\bar{B}^0 \to D^0$ weight**] 4th order polynomial fit for $\bar{B}^0 \to D^0$ weight.

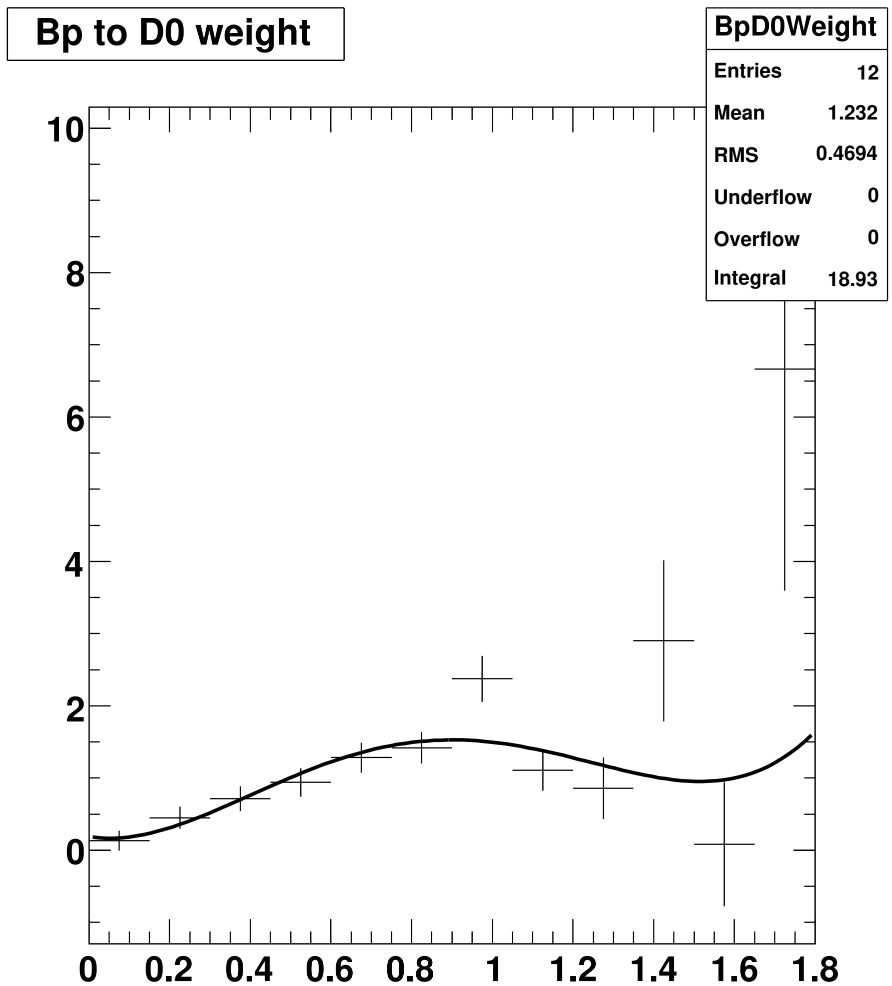

Figure 37: [**Fit for** $B^+ \to D^0$ **weight**] 4th order polynomial fit for $B^+ \to D^0$ weight.

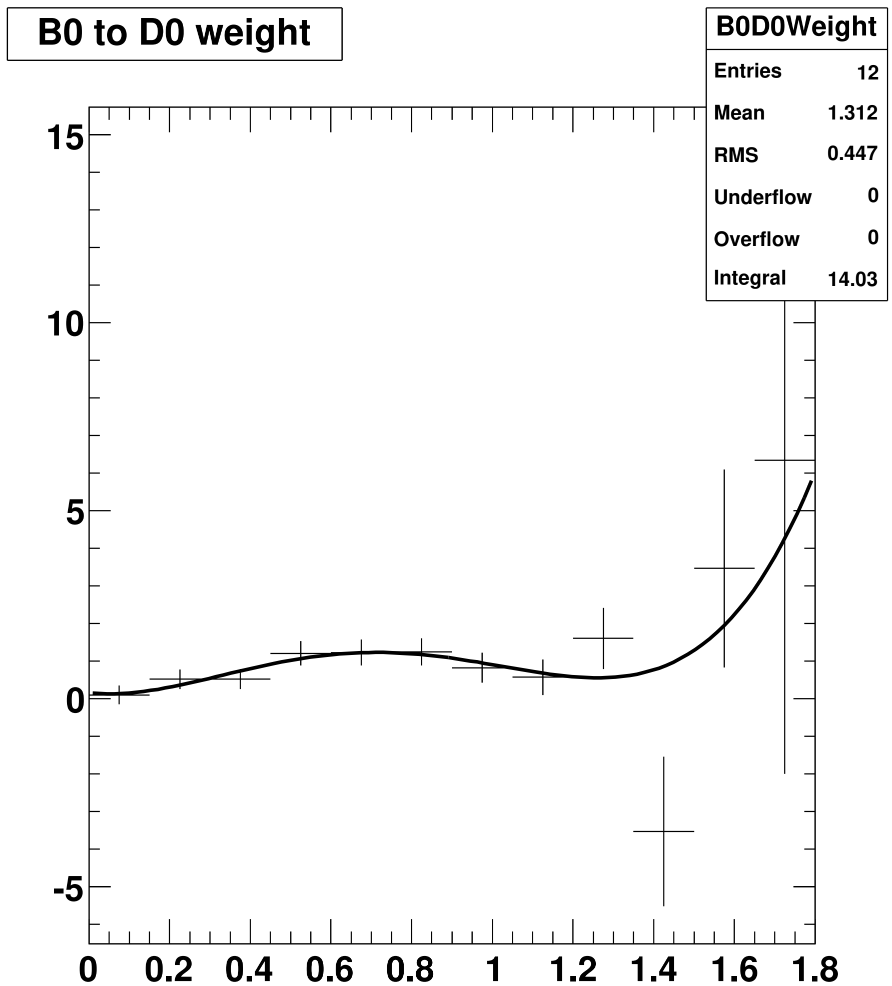

Figure 38: [**Fit for** $B^0 \rightarrow D^0$ **weight**] 4th order polynomial fit for $B^0 \rightarrow D^0$ weight.

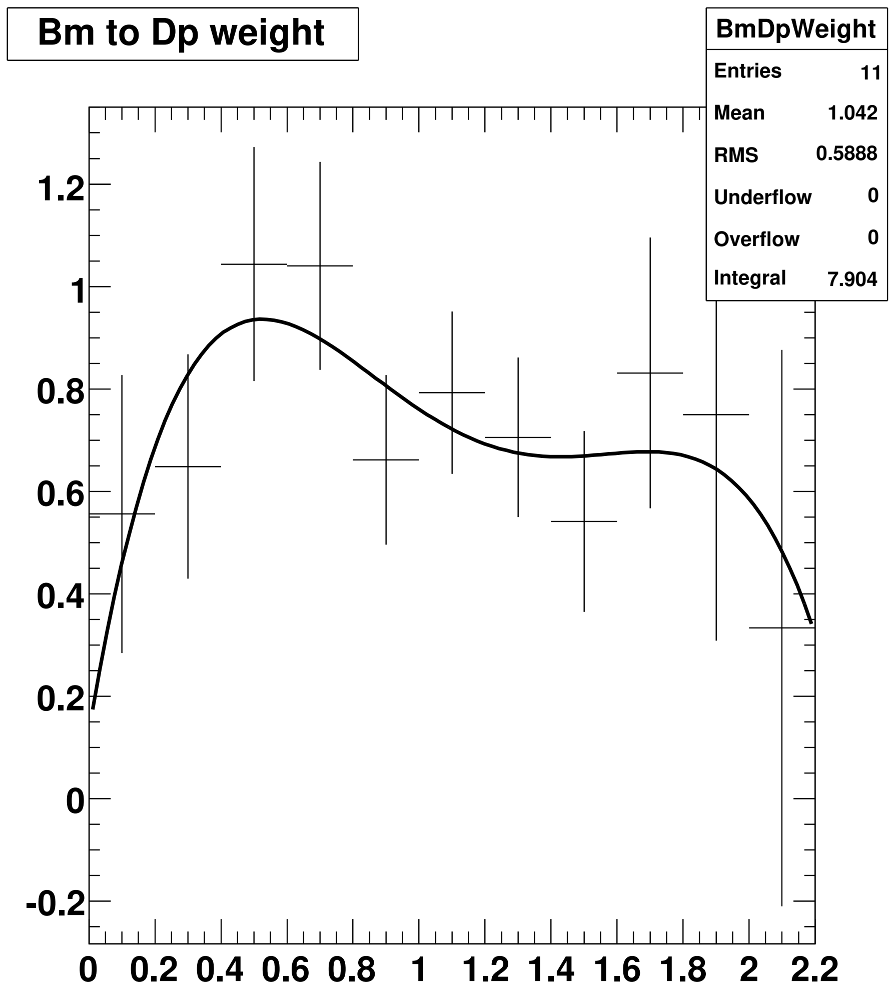

Figure 39: [**Fit for** $B^- \rightarrow D^+$ **weight**] 4th order polynomial fit for $B^- \rightarrow D^+$ weight.

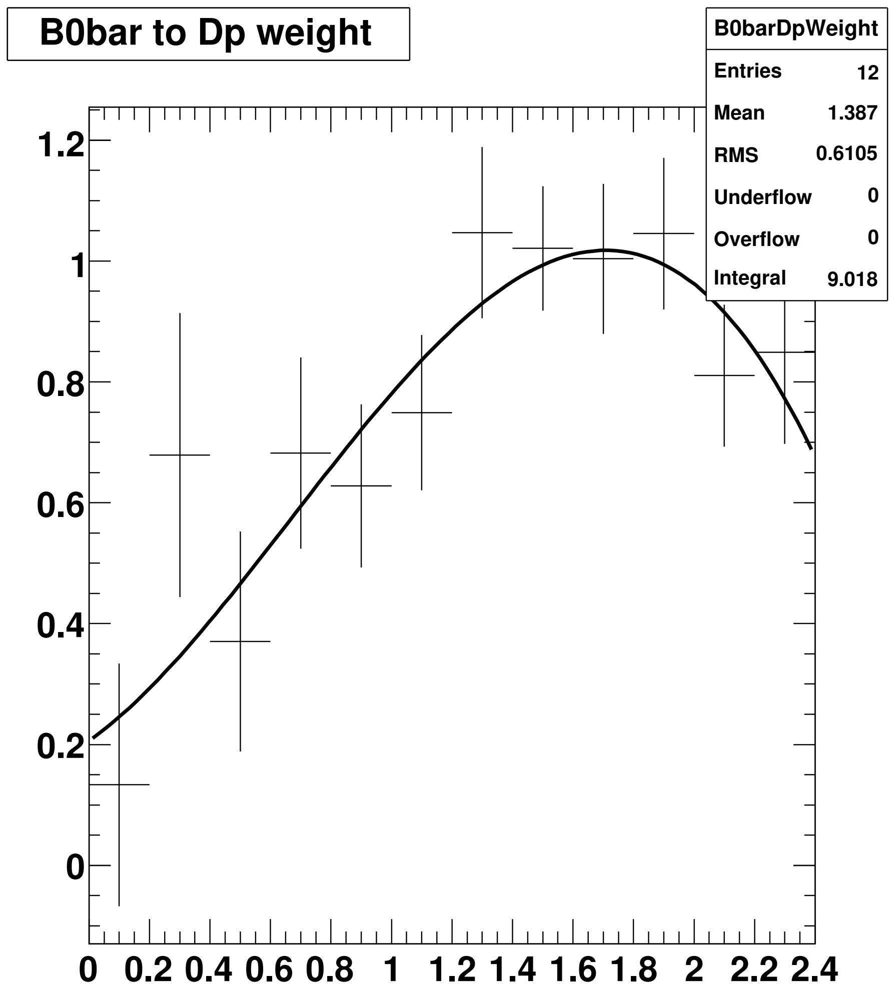

Figure 40: [**Fit for $\bar{B}^0 \to D^+$ weight**] 4th order polynomial fit for $\bar{B}^0 \to D^+$ weight.

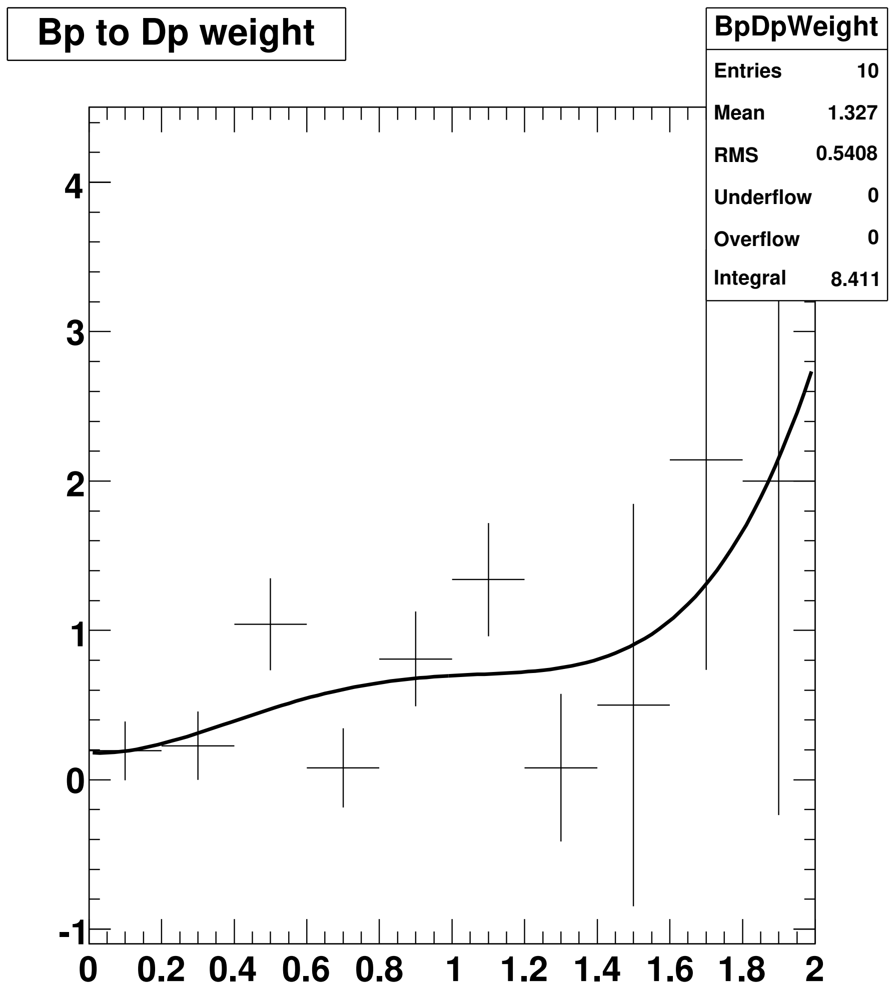

Figure 41: [**Fit for** $B^+ \to D^+$ **weight**] 4th order polynomial fit for $B^+ \to D^+$ weight.

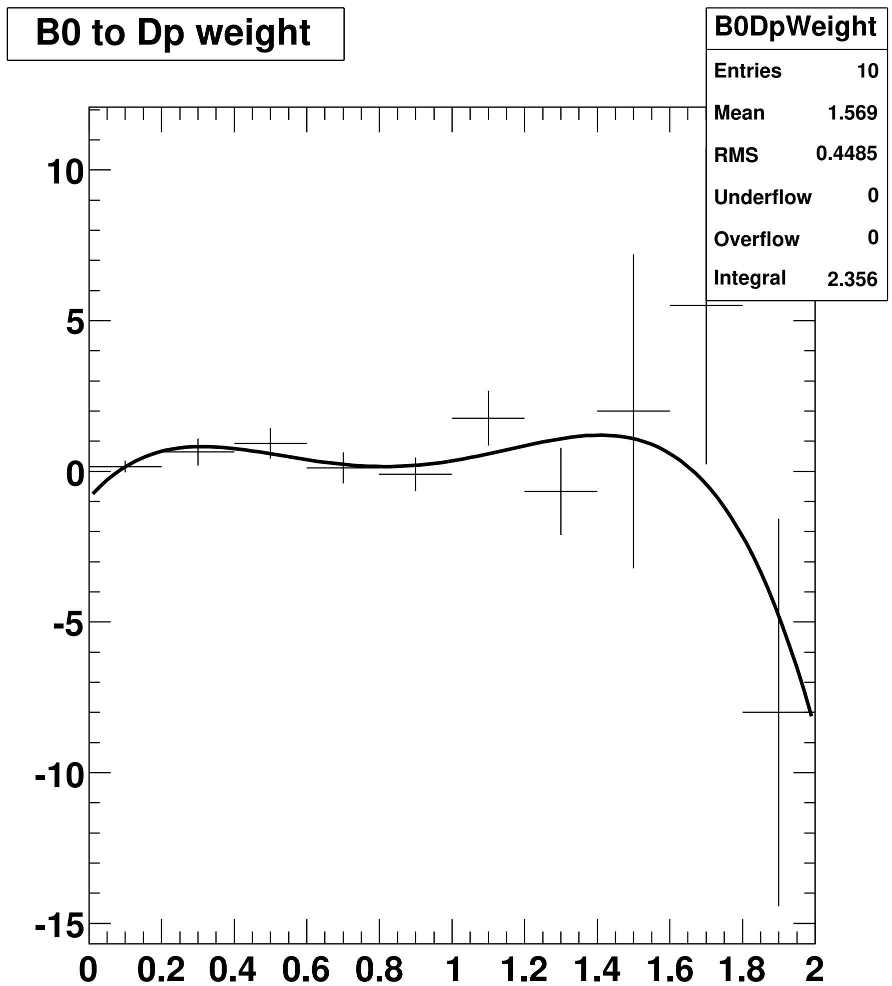

Figure 42: [**Fit for $B^0 \to D^+$ weight**] 4th order polynomial fit for $B^0 \to D^+$ weight.

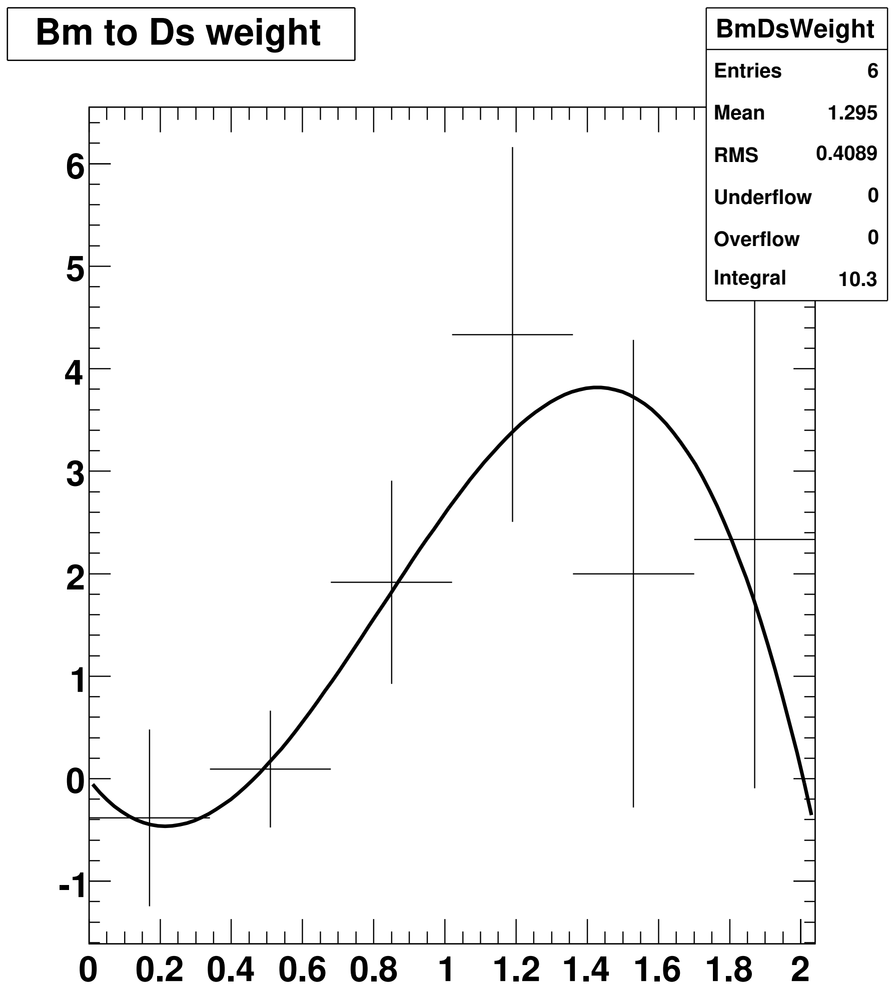

Figure 43: [**Fit for $B^- \to D_s^+$ weight**] 3rd order polynomial fit for $B^- \to D_s^+$ weight.

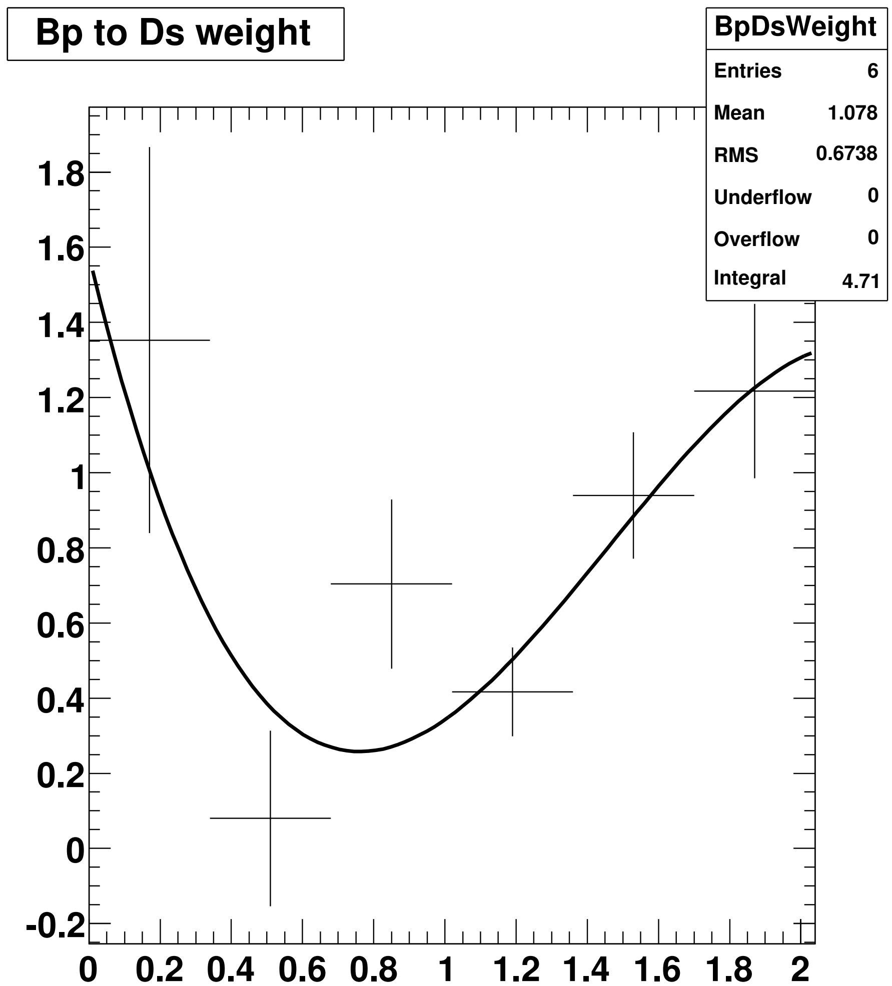

Figure 44: [**Fit for** $B^+ \to D_s^+$ **weight**] 3rd order polynomial fit for $B^+ \to D_s^+$ weight.

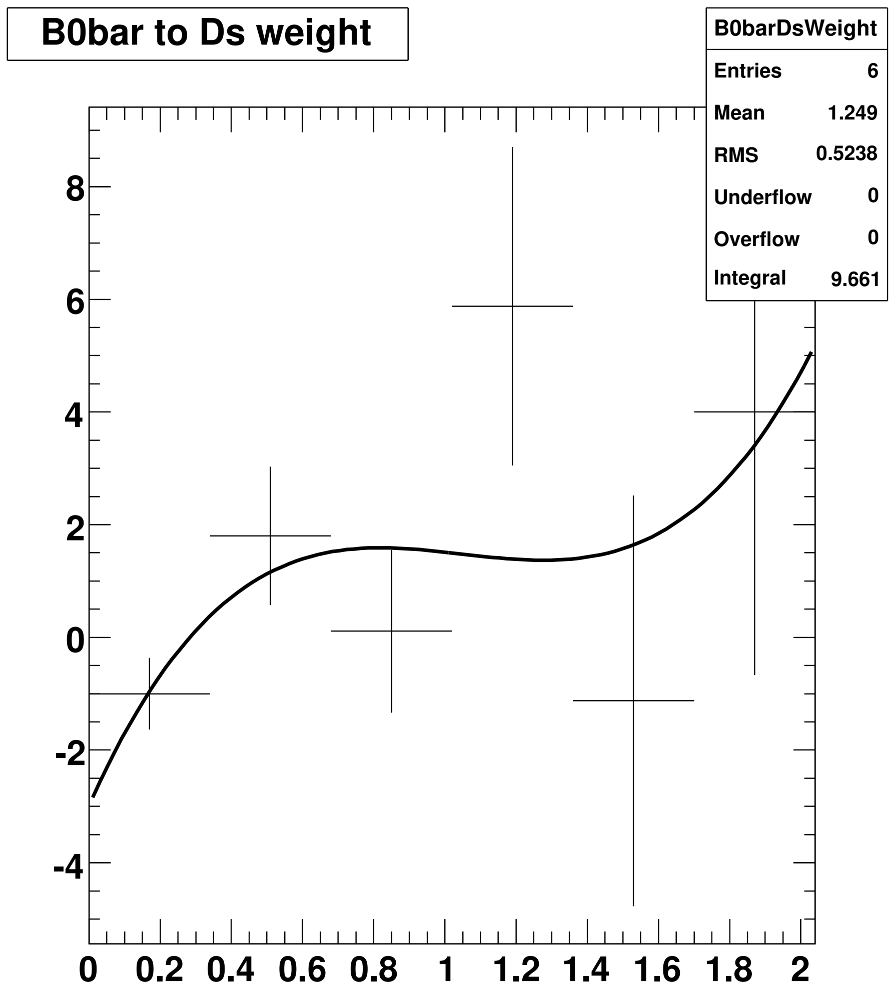

Figure 45: [**Fit for $\bar{B}^0 \rightarrow D_s^+$ weight**] 3rd order polynomial fit for $\bar{B}^0 \rightarrow D_s^+$ weight.

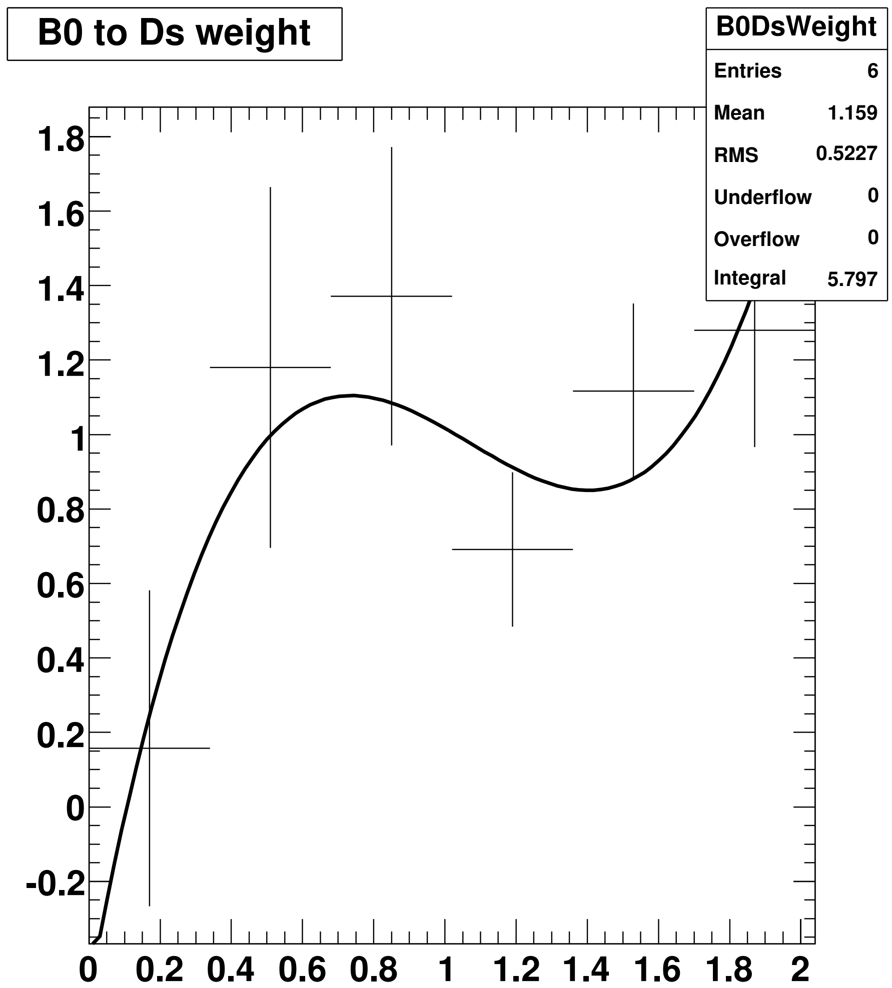

Figure 46: [**Fit for** $B^0 \to D_s^+$ **weight**] 3rd order polynomial fit for $B^0 \to D_s^+$ weight.

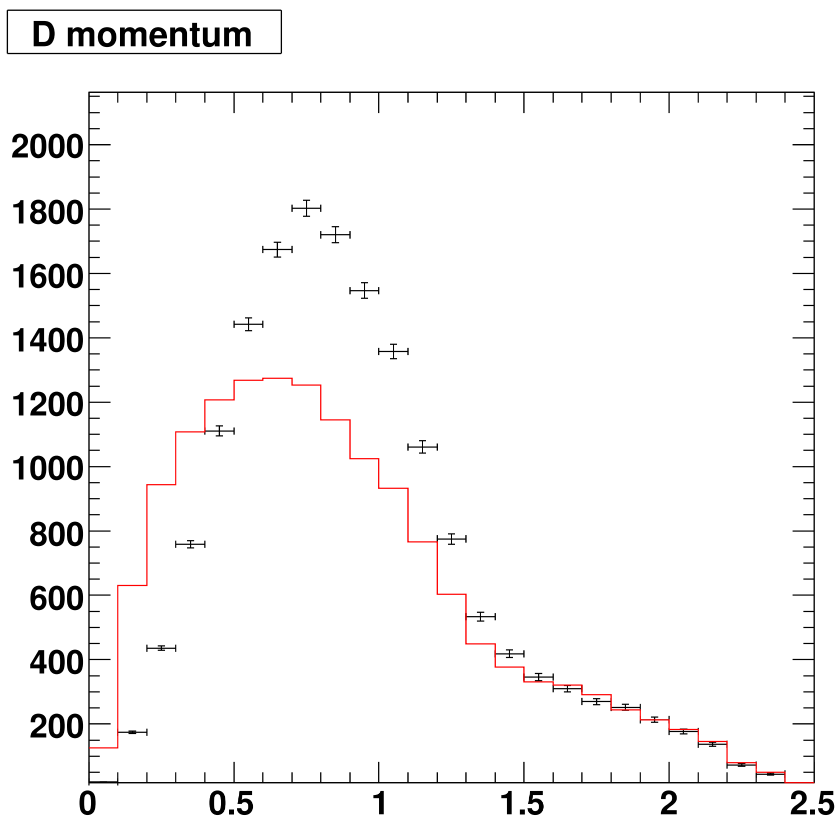

Figure 47: [**UncorrDL BF correction by Fitting**] Effect of BpBm UncorrDL background BF correction using a 3rd order polynomial. The red histogram is before correction, and the black lines with error bars are after correction.

9.2 D^{**} decay branching fractions

The values used in SP5/SP6 MC are summarized in Appendix D. We adopt the following new values in our fit. These are not applied in candidate level. Thus, these values goes into the coefficients in the fit. See details in section 4. For D_0^*, D_1 and D_1', based on isospin symmetry

$$\begin{aligned}
\mathcal{B}(D_0^{*+} \to D^0\pi^+) &= 2\mathcal{B}(D_0^{*+} \to D^+\pi^0) \\
\mathcal{B}(D_0^{*0} \to D^+\pi^-) &= 2\mathcal{B}(D_0^{*0} \to D^0\pi^0) \\
\mathcal{B}(D_1^+ \to D^{*0}\pi^+) &= 2\mathcal{B}(D_1^+ \to D^{*+}\pi^0) \\
\mathcal{B}(D_1^0 \to D^{*+}\pi^-) &= 2\mathcal{B}(D_1^0 \to D^{*0}\pi^0) \\
\mathcal{B}(D_1'^+ \to D^{*0}\pi^+) &= 2\mathcal{B}(D_1'^+ \to D^{*+}\pi^0) \\
\mathcal{B}(D_1'^0 \to D^{*+}\pi^-) &= 2\mathcal{B}(D_1'^0 \to D^{*0}\pi^0)
\end{aligned} \tag{189}$$

Thus, we use

$$\begin{aligned}
&\mathcal{B}(D_0^{*+} \to D^0\pi^+) = \mathcal{B}(D_0^{*0} \to D^+\pi^-) = \mathcal{B}(D_1^+ \to D^{*0}\pi^+) = \mathcal{B}(D_1^0 \to D^{*+}\pi^-) \\
&= \mathcal{B}(D_1'^+ \to D^{*0}\pi^+) = \mathcal{B}(D_1'^0 \to D^{*+}\pi^-) = 0.6667
\end{aligned} \tag{190}$$

and

$$\begin{aligned}
&\mathcal{B}(D_0^{*+} \to D^+\pi^0) = \mathcal{B}(D_0^{*0} \to D^0\pi^0) = \mathcal{B}(D_1^+ \to D^{*+}\pi^0) = \mathcal{B}(D_1^0 \to D^{*0}\pi^0) \\
&= \mathcal{B}(D_1'^+ \to D^{*+}\pi^0) = \mathcal{B}(D_1'^0 \to D^{*0}\pi^0) = 0.3333
\end{aligned} \tag{191}$$

Here we asuumed that D^{**} decays 100 % into $D^{(*)}\pi$. However there is an observation of $D_1 \to D\pi^+\pi^-$ decays [29]. We consider this in systematic study.
For D_2^*, from isospin symmetry

$$\begin{aligned}
\mathcal{B}(D_2^{*+} \to D^0\pi^+) &= 2\mathcal{B}(D_2^{*+} \to D^+\pi^0) \\
\mathcal{B}(D_2^{*+} \to D^{*0}\pi^+) &= 2\mathcal{B}(D_2^{*+} \to D^{*+}\pi^0) \\
\mathcal{B}(D_2^{*0} \to D^+\pi^-) &= 2\mathcal{B}(D_2^{*0} \to D^0\pi^0) \\
\mathcal{B}(D_2^{*0} \to D^{*+}\pi^-) &= 2\mathcal{B}(D_2^{*0} \to D^{*0}\pi^0)
\end{aligned} \tag{192}$$

From PDG [12]

$$\frac{\mathcal{B}(D_2^{*+} \to D^0\pi^+)}{\mathcal{B}(D_2^{*+} \to D^{*0}\pi^+)} = 1.9 \pm 1.1 \pm 0.3 \tag{193}$$

$$\frac{\mathcal{B}(D_2^{*0} \to D^+\pi^-)}{\mathcal{B}(D_2^{*0} \to D^{*+}\pi^-)} = 2.3 \pm 0.6 \tag{194}$$

By isospin symmetry, these two numbers are supposed to be same. Thus, we take an average and get

$$\begin{aligned}
f_{D_2^*} \equiv \frac{\mathcal{B}(D_2^{*+} \to D^0\pi^+)}{\mathcal{B}(D_2^{*+} \to D^{*0}\pi^+)} &= \frac{\mathcal{B}(D_2^{*0} \to D^+\pi^-)}{\mathcal{B}(D_2^{*0} \to D^{*+}\pi^-)} \\
&= 2.1 \pm 0.644
\end{aligned} \tag{195}$$

Hence, branching fractions are

$$\mathcal{B}(D_2^{*+} \to D^0\pi^+) = \mathcal{B}(D_2^{*0} \to D^+\pi^-) = \frac{2f_{D_2^*}}{3(1+f_{D_2^*})} = 0.452 \pm 0.167 \quad (196)$$

$$\mathcal{B}(D_2^{*+} \to D^+\pi^0) = \mathcal{B}(D_2^{*0} \to D^0\pi^0) = \frac{f_{D_2^*}}{3(1+f_{D_2^*})} = 0.226 \pm 0.084 \quad (197)$$

$$\mathcal{B}(D_2^{*+} \to D^{*0}\pi^+) = \mathcal{B}(D_2^{*0} \to D^{*+}\pi^-) = \frac{2}{3(1+f_{D_2^*})} = 0.215 \pm 0.045 \quad (198)$$

$$\mathcal{B}(D_2^{*+} \to D^{*+}\pi^0) = \mathcal{B}(D_2^{*0} \to D^{*0}\pi^0) = \frac{1}{3(1+f_{D_2^*})} = 0.107 \pm 0.022 \quad (199)$$

$$(200)$$

9.3 $D^{(*)}$ decay branching fractions

The values used in SP5/SP6 MC are summarized in Appendix D. We adopt the following new values in our fit. These are not applied in candidate level. Thus, these values goes into the coefficients in the fit. See details in section 4.

9.3.1 $\mathcal{B}(D^0 \to K^-\pi^+)$

PDG uses five measurements to make an average [12]. One of them is a CLEO-c result. Since we use updated CLEO-c result, we remove the CLEO-c result from PDG average. The rests used in PDG are

$$\begin{aligned}
\mathcal{B}(D^0 \to K^-\pi^+) &= 0.0382 \pm 0.0007 \pm 0.0012 \\
\mathcal{B}(D^0 \to K^-\pi^+) &= 0.039 \pm 0.0009 \pm 0.0012 \\
\mathcal{B}(D^0 \to K^-\pi^+) &= 0.0341 \pm 0.0012 \pm 0.0028 \\
\mathcal{B}(D^0 \to K^-\pi^+) &= 0.0362 \pm 0.0034 \pm 0.0044
\end{aligned} \quad (201)$$

We take an average of these four measurements and get

$$\mathcal{B}(D^0 \to K^-\pi^+) = 0.03806 \pm 0.00095 \quad (202)$$

Babar measured [30]

$$\mathcal{B}(D^0 \to K^-\pi^+) = 0.04007 \pm 0.00037 \pm 0.00070 \quad (203)$$

CLEO-c also measured [31]

$$\mathcal{B}(D^0 \to K^-\pi^+) = 0.03891 \pm 0.00035 \pm 0.00059 \pm 0.00035 \quad (204)$$

We take an average of these three numbers. The error of the average of these is given by

$$\frac{1}{\sigma^2} = \frac{1}{0.00095^2} + \frac{1}{0.00037^2 + 0.00070^2} + \frac{1}{0.00035^2 + 0.00059^2 + 0.00035^2} \quad (205)$$

Thus

$$\sigma = 0.00048 \tag{206}$$

The average value is given by

$$\left(\frac{0.03806}{0.00095^2} + \frac{0.04007}{0.00037^2 + 0.00070^2} + \frac{0.03891}{0.00035^2 + 0.00059^2 + 0.00035^2}\right)\sigma^2 = 0.03912 \tag{207}$$

Thus, the averaged BF is

$$\mathcal{B}(D^0 \to K^-\pi^+) = 0.03912 \pm 0.00048 \tag{208}$$

9.3.2 $\mathcal{B}(D^+ \to K^-\pi^+\pi^+)$

PDG uses three measurements to make an average [12]. One of them is a CLEO-c result. Since we use updated CLEO-c result, we remove the CLEO-c result from PDG average. The rests used in PDG are

$$\begin{aligned} \mathcal{B}(D^+ \to K^-\pi^+\pi^+) &= 0.093 \pm 0.006 \pm 0.008 \\ \mathcal{B}(D^+ \to K^-\pi^+\pi^+) &= 0.091 \pm 0.013 \pm 0.004 \end{aligned} \tag{209}$$

We take an average of these four measurements and get

$$\mathcal{B}(D^+ \to K^-\pi^+\pi^+) = 0.09230 \pm 0.00806 \tag{210}$$

CLEO-c measured [31]

$$\mathcal{B}(D^+ \to K^-\pi^+\pi^+) = 0.0915 \pm 0.0010 \pm 0.0016 \pm 0.0007 \tag{211}$$

We take an average of these numbers. The error of the average of these is given by

$$\frac{1}{\sigma^2} = \frac{1}{0.00806^2} + \frac{1}{0.0010^2 + 0.0016^2 + 0.0007^2} \tag{212}$$

Thus

$$\sigma = 0.0020 \tag{213}$$

The average value is given by

$$\left(\frac{0.09230}{0.00806^2} + \frac{0.0915}{0.0019^2 + 0.0016^2 + 0.0007^2}\right)\sigma^2 = 0.0915 \tag{214}$$

Thus, the averaged BF is

$$\mathcal{B}(D^+ \to K^-\pi^+\pi^+) = 0.0915 \pm 0.0020 \tag{215}$$

9.3.3 D^{*+} decay BF

From PDG [12]

$$\begin{aligned}\mathcal{B}(D^{*+} \to D^0\pi^+) &= 0.677 \pm 0.005 \\ \mathcal{B}(D^{*+} \to D^+\pi^0) &= 0.307 \pm 0.005 \\ \mathcal{B}(D^{*+} \to D^+\gamma) &= 0.016 \pm 0.004\end{aligned} \tag{216}$$

We use

$$\begin{aligned}&\mathcal{B}(D^{*+} \to D^0\pi^+) = 0.677 \pm 0.005 \\ &\mathcal{B}(D^{*+} \to D^+\pi^0) + \mathcal{B}(D^{*+} \to D^+\gamma) = 1 - \mathcal{B}(D^{*+} \to D^0\pi^+)\end{aligned} \tag{217}$$

9.4 An example

Here we give a specific example to illustrate BF re-weighting. In the case of

- $B^+ \to D^{*-}D^+K^+$
  with $D^{*-} \to \bar{D}^0\pi^-$ and $D^+ \to \bar{K}^0 e^+\nu$
  and these $\bar{D}^0$ and e^+ form a Dl candidate as if $B^+ \to \bar{D}^0 e^+\nu$

The number of this background is given by

$$
\begin{aligned}
&N = (\text{number of produced } B^+B^- \text{ pairs})\times \\
&\mathcal{B}(B^+ \to D^{*-}D^+K^+)\mathcal{B}(D^{*-} \to \bar{D}^0\pi^-)\mathcal{B}(D^+ \to \bar{K}^0e^+\nu)\mathcal{B}(D^0 \to K^-\pi^+)
\end{aligned}
\tag{218}
$$

Thus, it is proportional to all branching fractions. This means that the weight is given by the ratio of new and old branching fractions. This also means that even if you do not know the details of the decay chain, if you know, for example, $D^+ \to \bar{K}^0e^+\nu$ is included in the chain, you can still apply a weight only for the known part.
In above example, for the lepton side, we apply

- Inclusive $B^+ \to D^+$ BF weight (section 9.1.4)
- Semileptonic $D^+ \to \bar{K}^0e^+\nu$ BF weight (section 9.1.1)

and for the D side, we apply

- $D^{*-} \to \bar{D}^0\pi^-$ decay BF weight (section 9.3.3)
- $D^0 \to K^-\pi^+$ decay BF weight (section 9.3.1)

Total weight is given by the product of these 4 weights. The formar two weights are applied in the histogram making process and the latter two weights are applied in a part of fitting program before going into the actual fitting process.

9.5 Effect of branching fraction re-weighting

Figure 48 - 56 show the lepton momentum, D momentum and $\cos\theta_{B-Dl}$ after branching fraction re-weighting. These are the projections of 3D histograms. If you compare these with figure 19 - 27, you can see improvements of data-MC agreement.

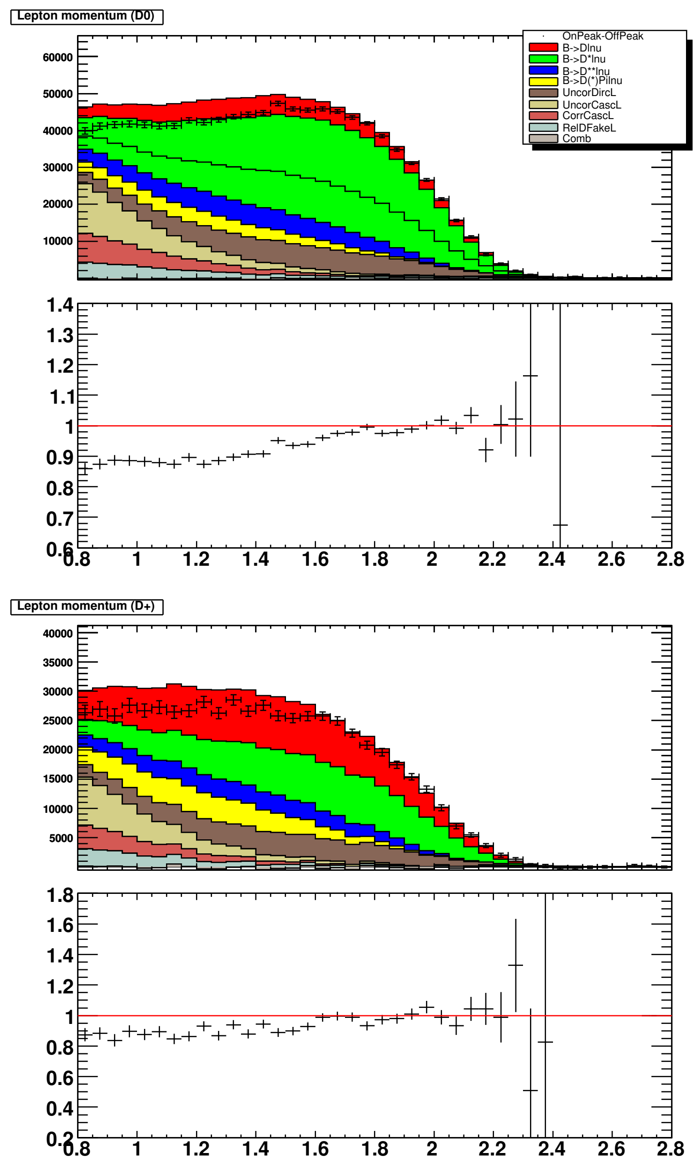

Figure 48: [p_ℓ **after MC re-weighting**] Lepton momentum plot after branching fraction re-weighting and D mass sideband subtraction. The top is D^0 and the bottom is D^+. Black is OnPeak - OffPeak data. Red is $B \to D\ell\nu$, green is $B \to D^*\ell\nu$, blue is $B \to D^{**}\ell\nu$, yellow is non-resonant $B \to D^{(*)}\pi\ell\nu$, and the rest is background. Dark brown is UncorrDL, light brown is UncorrCL, dark red is CascL, blue gray is FakeL, and light gray is Comb. Comb is almost disappeared after D mass sideband subtraction.

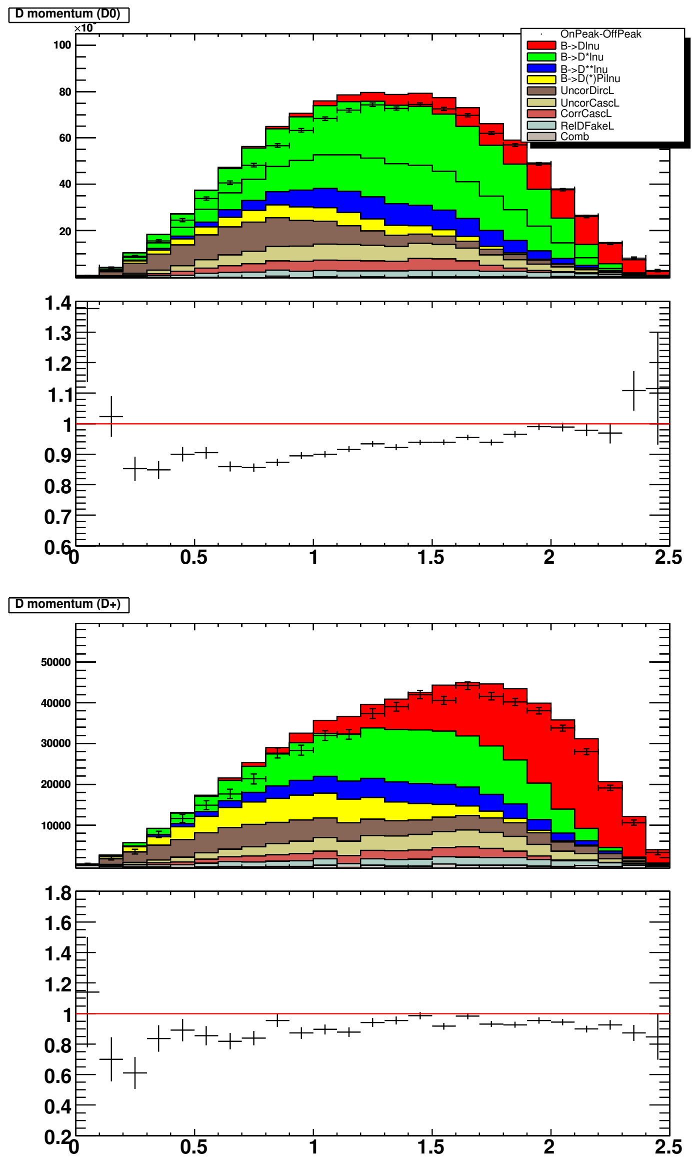

Figure 49: [p_D **after MC re-weighting**] D momentum plot after branching fraction re-weighting and D mass sideband subtraction. The top is D^0 and the bottom is D^+. Black is OnPeak - OffPeak data. Red is $B \to D\ell\nu$, green is $B \to D^*\ell\nu$, blue is $B \to D^{**}\ell\nu$, yellow is non-resonant $B \to D^{(*)}\pi\ell\nu$, and the rest is background. Dark brown is UncorrDL, light brown is UncorrCL, dark red is CascL, blue gray is FakeL, and light gray is Comb. Comb is almost disappeared after D mass sideband subtraction.

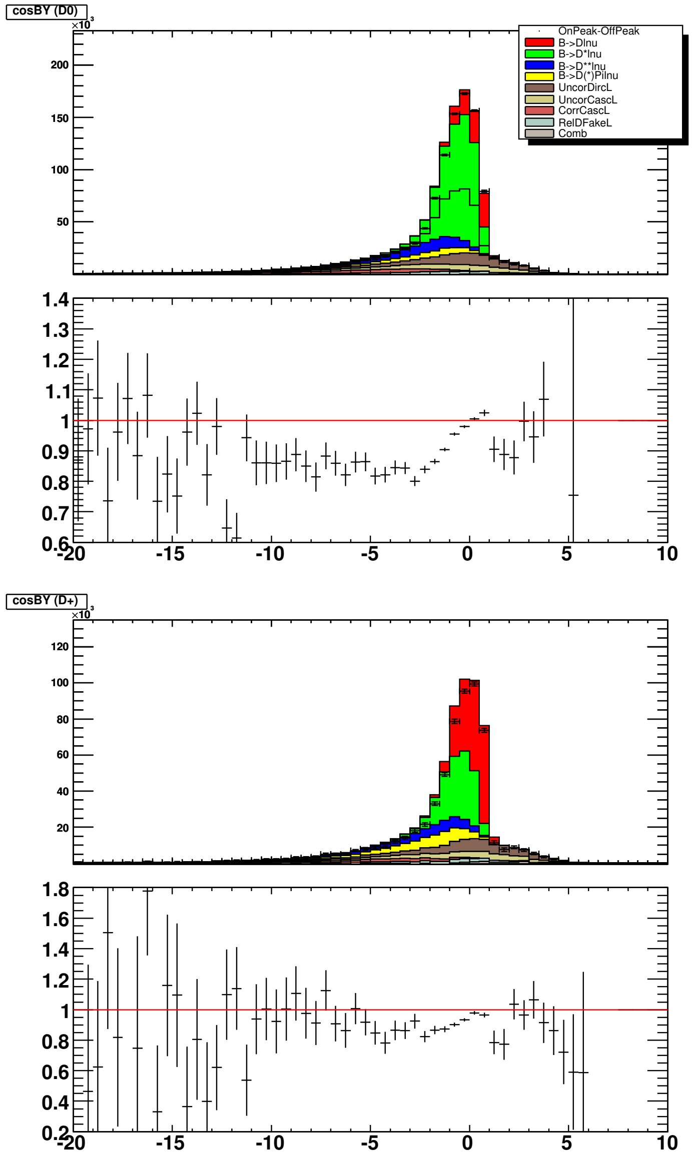

Figure 50: [$\cos\theta_{B-Dl}$ **after MC re-weighting**] $\cos\theta_{B-Dl}$ plot after branching fraction re-weighting and D mass sideband subtraction. The top is D^0 and the bottom is D^+. Black is OnPeak - OffPeak data. Red is $B \to D\ell\nu$, green is $B \to D^*\ell\nu$, blue is $B \to D^{**}\ell\nu$, yellow is non-resonant $B \to D^{(*)}\pi\ell\nu$, and the rest is background. Dark brown is UncorrDL, light brown is UncorrCL, dark red is CascL, blue gray is FakeL, and light gray is Comb. Comb is almost disappeared after D mass sideband subtraction.

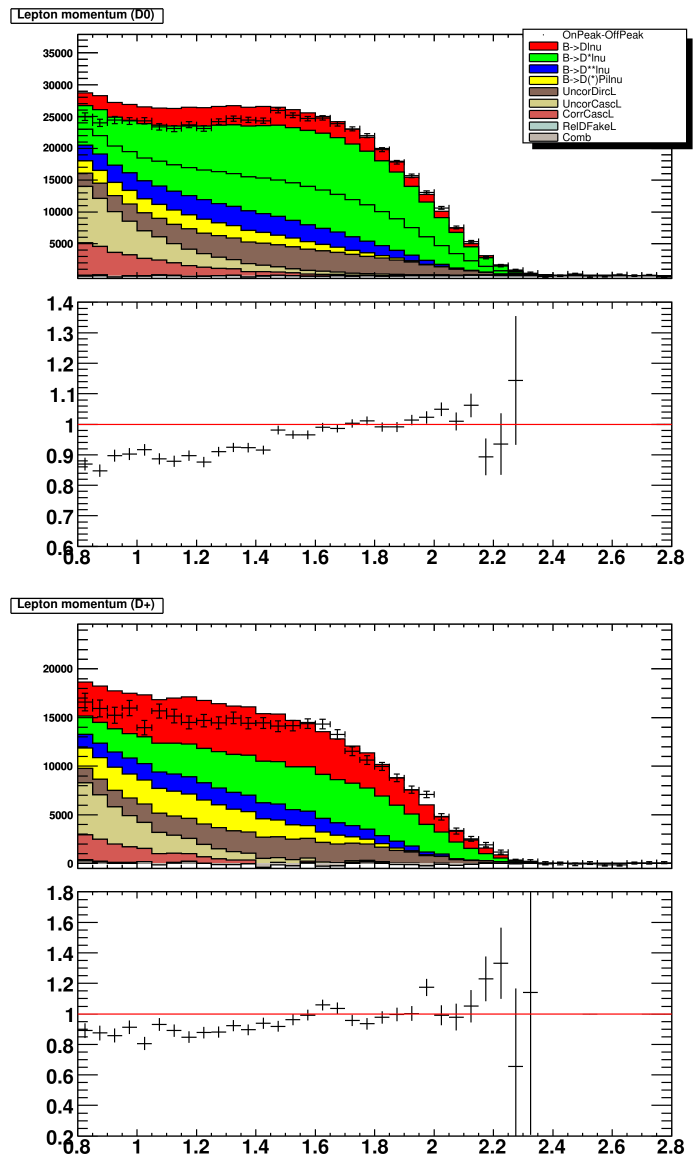

Figure 51: [p_ℓ **after MC re-weighting (Electron)**] Lepton momentum plot after branching fraction re-weighting and D mass sideband subtraction in the case $\ell = e$ (Electron only). The top is D^0 and the bottom is D^+. Black is OnPeak - OffPeak data. Red is $B \to D\ell\nu$, green is $B \to D^*\ell\nu$, blue is $B \to D^{**}\ell\nu$, yellow is non-resonant $B \to D^{(*)}\pi\ell\nu$, and the rest is background. Dark brown is UncorrDL, light brown is UncorrCL, dark red is CascL, blue gray is FakeL, and light gray is Comb. Comb is almost disappeared after D mass sideband subtraction.

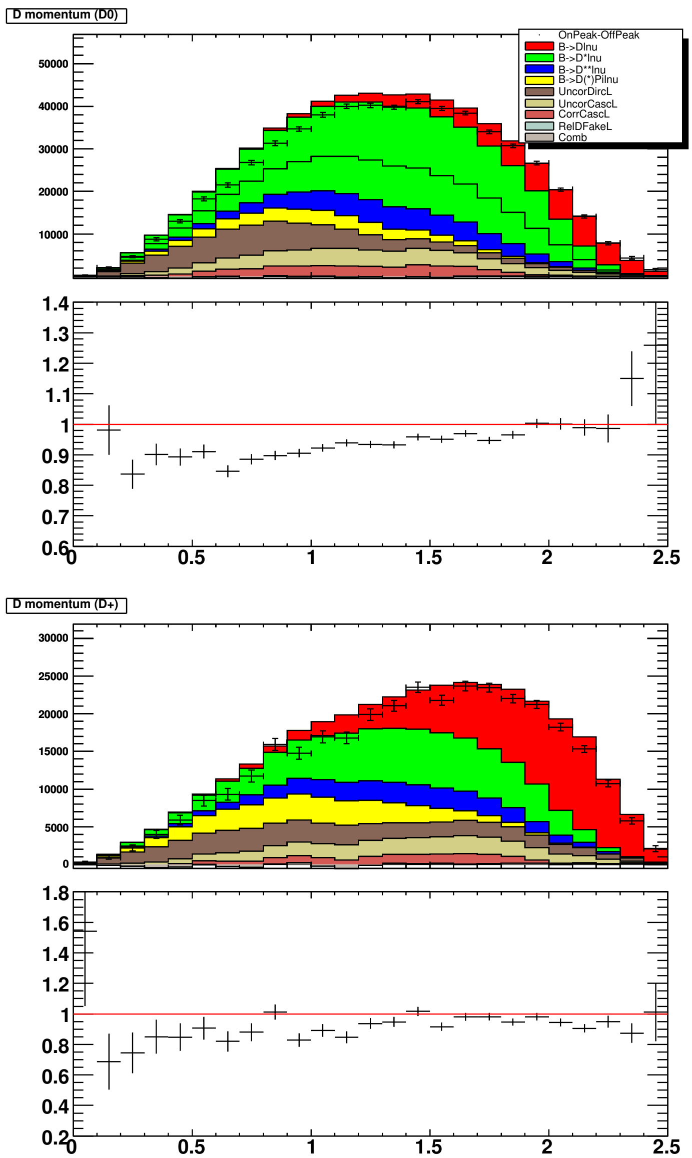

Figure 52: [p_D **after MC re-weighting (Electron)**] D momentum plot after branching fraction re-weighting and D mass sideband subtraction in the case $\ell = e$ (Electron only). The top is D^0 and the bottom is D^+. Black is OnPeak - OffPeak data. Red is $B \to D\ell\nu$, green is $B \to D^*\ell\nu$, blue is $B \to D^{**}\ell\nu$, yellow is non-resonant $B \to D^{(*)}\pi\ell\nu$, and the rest is background. Dark brown is UncorrDL, light brown is UncorrCL, dark red is CascL, blue gray is FakeL, and light gray is Comb. Comb is almost disappeared after D mass sideband subtraction.

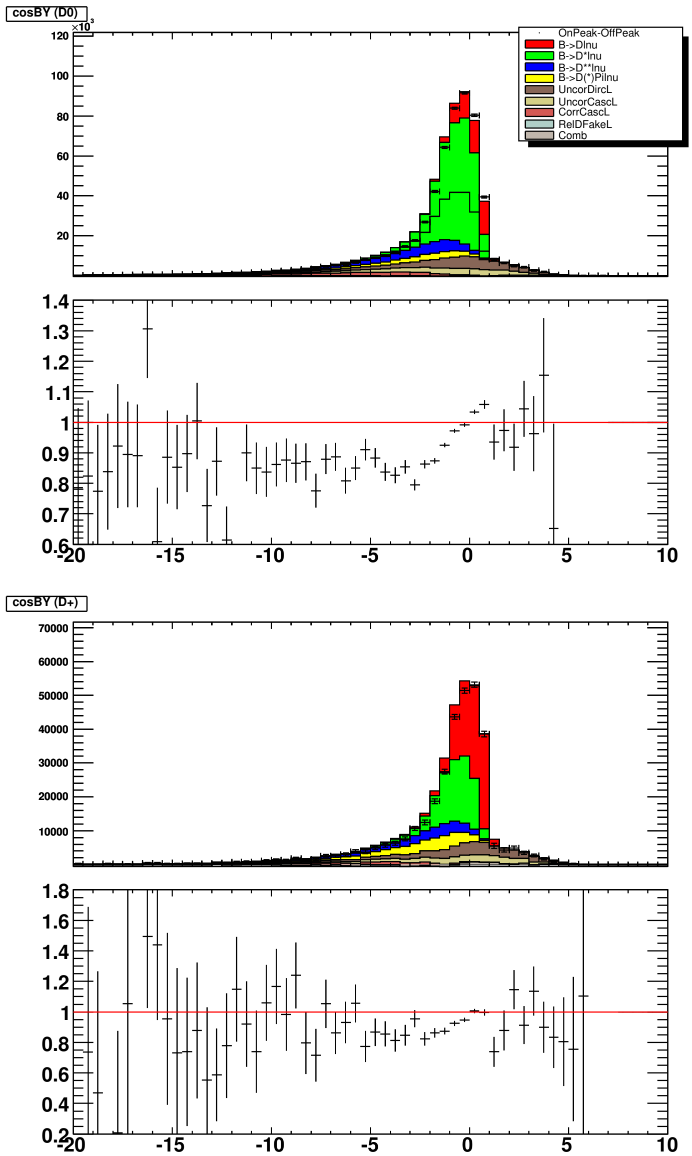

Figure 53: [$\cos\theta_{B-Dl}$ **after MC re-weighting (Electron)**] $\cos\theta_{B-Dl}$ plot after branching fraction re-weighting and D mass sideband subtraction in the case $\ell = e$ (Electron only). The top is D^0 and the bottom is D^+. Black is OnPeak - OffPeak data. Red is $B \to D\ell\nu$, green is $B \to D^*\ell\nu$, blue is $B \to D^{**}\ell\nu$, yellow is non-resonant $B \to D^{(*)}\pi\ell\nu$, and the rest is background. Dark brown is UncorrDL, light brown is UncorrCL, dark red is CascL, blue gray is FakeL, and light gray is Comb. Comb is almost disappeared after D mass sideband subtraction.

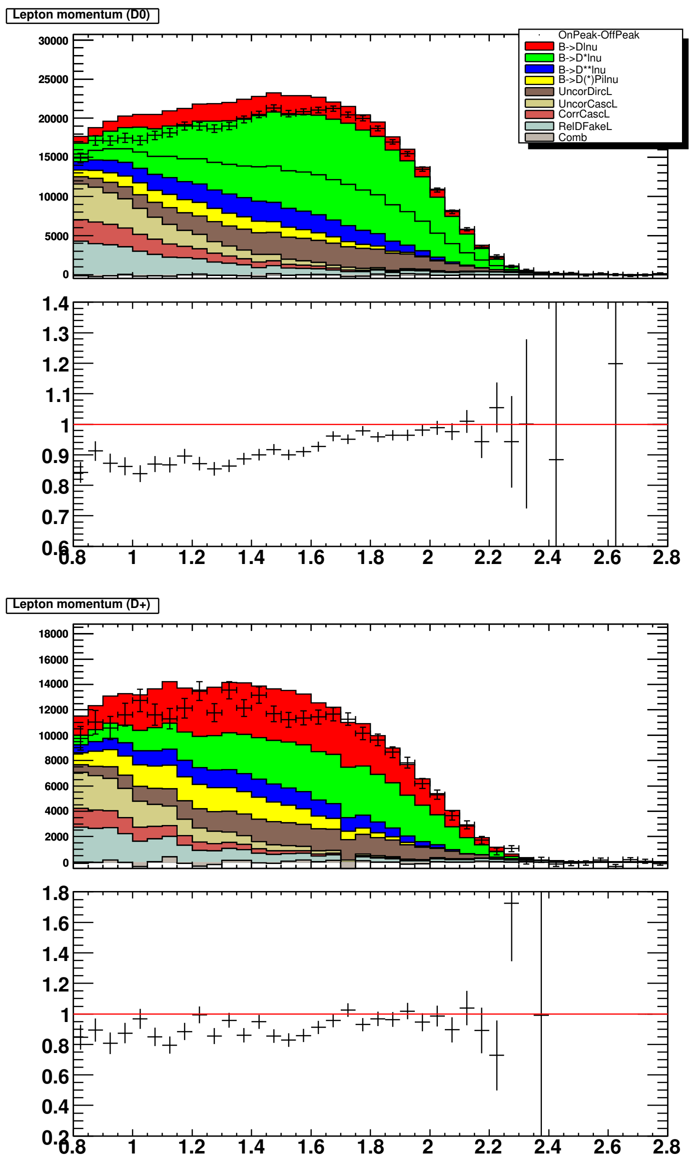

Figure 54: [p_ℓ **after MC re-weighting (Muon)**] Lepton momentum plot after branching fraction re-weighting and D mass sideband subtraction in the case $\ell = \mu$ (Muon only). The top is D^0 and the bottom is D^+. Black is OnPeak - OffPeak data. Red is $B \to D\ell\nu$, green is $B \to D^*\ell\nu$, blue is $B \to D^{**}\ell\nu$, yellow is non-resonant $B \to D^{(*)}\pi\ell\nu$, and the rest is background. Dark brown is UncorrDL, light brown is UncorrCL, dark red is CascL, blue gray is FakeL, and light gray is Comb. Comb is almost disappeared after D mass sideband subtraction.

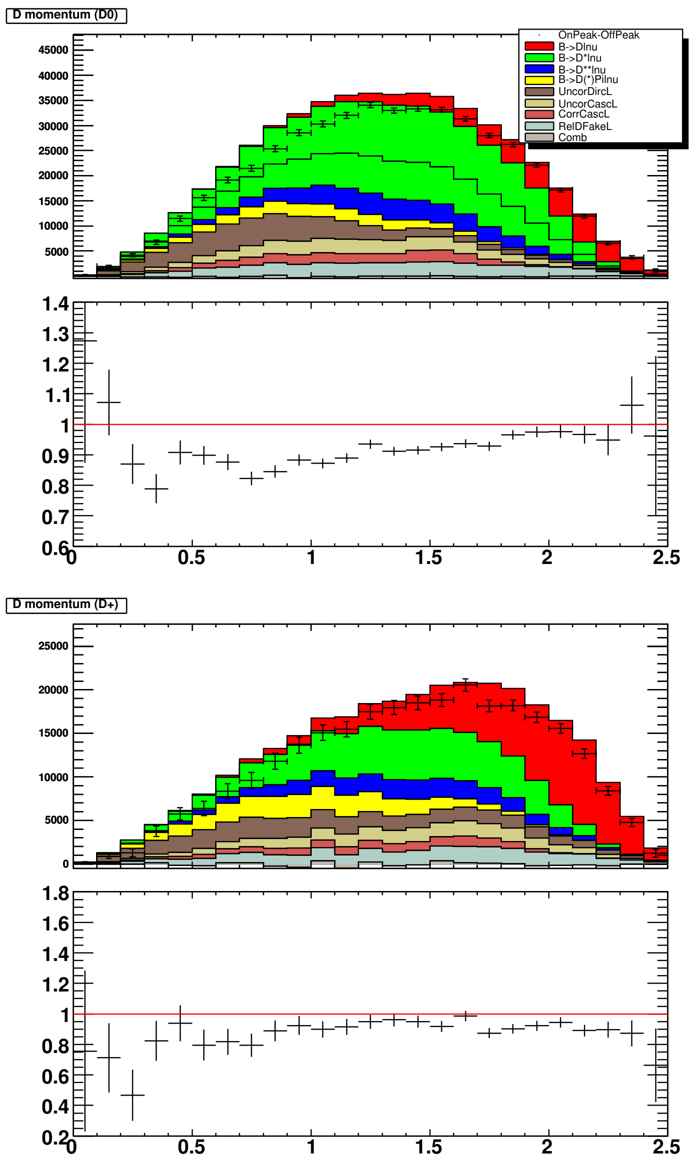

Figure 55: [p_D **after MC re-weighting (Muon)**] D momentum plot after branching fraction re-weighting and D mass sideband subtraction in the case $\ell = \mu$ (Muon only). The top is D^0 and the bottom is D^+. Black is OnPeak - OffPeak data. Red is $B \to D\ell\nu$, green is $B \to D^*\ell\nu$, blue is $B \to D^{**}\ell\nu$, yellow is non-resonant $B \to D^{(*)}\pi\ell\nu$, and the rest is background. Dark brown is UncorrDL, light brown is UncorrCL, dark red is CascL, blue gray is FakeL, and light gray is Comb. Comb is almost disappeared after D mass sideband subtraction.

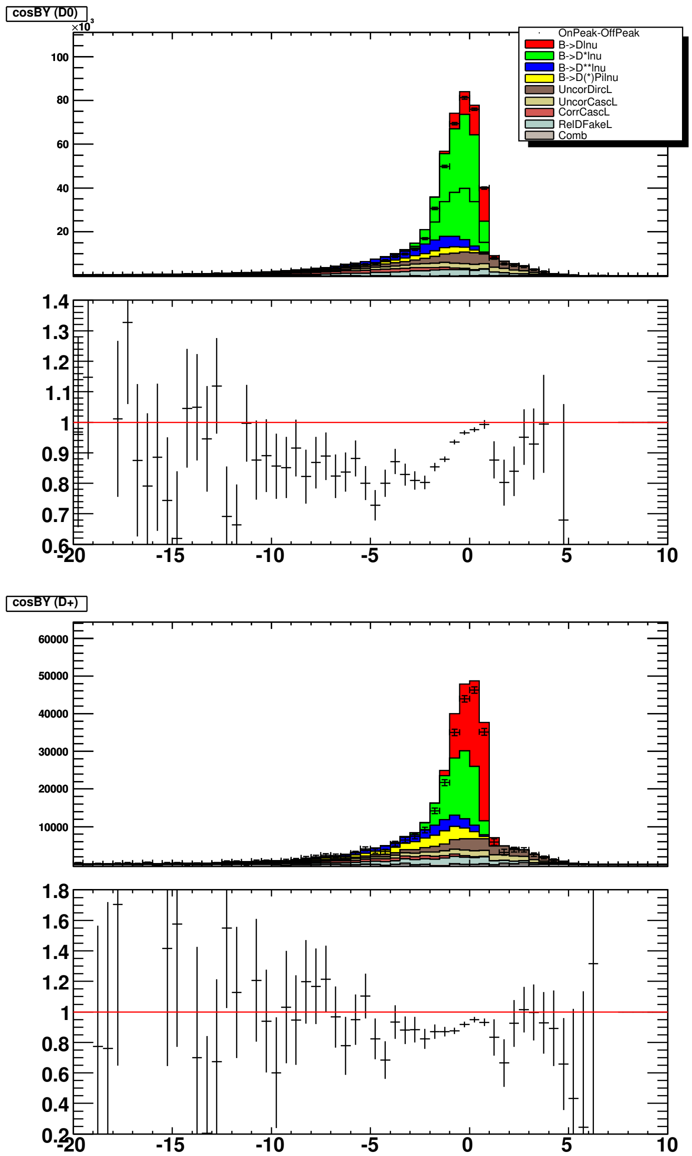

Figure 56: [$\cos\theta_{B-Dl}$ **after MC re-weighting (Muon)**] $\cos\theta_{B-Dl}$ plot after branching fraction re-weighting and D mass sideband subtraction in the case $\ell = \mu$ (Muon only). The top is D^0 and the bottom is D^+. Black is OnPeak - OffPeak data. Red is $B \to D\ell\nu$, green is $B \to D^*\ell\nu$, blue is $B \to D^{**}\ell\nu$, yellow is non-resonant $B \to D^{(*)}\pi\ell\nu$, and the rest is background. Dark brown is UncorrDL, light brown is UncorrCL, dark red is CascL, blue gray is FakeL, and light gray is Comb. Comb is almost disappeared after D mass sideband subtraction.

9.6 Beam energy re-weighting

The beam energy of data is not well simulated by MC. There is a dedicated study of data beam energy using fully reconstructed B tags [reference]. We can use the result to make MC beam energy distribution similar to data beam energy distribution. Table 23 show the mean and width of beam energy distributions of data and MC averaged over each Runs.
Beam energies of data and MC, as a fuction of energy E, are given by Gaussians

$$\exp\left[-\frac{(E_{\rm data}-E)^2}{2\sigma_{\rm data}^2}\right], \quad \exp\left[-\frac{(E_{\rm MC}-E)^2}{2\sigma_{\rm MC}^2}\right] \tag{219}$$

We take ratios og these two Gaussinas to get weight

$$W^{\rm beam}(E) = \xi \exp\left[-\frac{(E_{\rm data}-E)^2}{2\sigma_{\rm data}^2}\right] \Big/ \exp\left[-\frac{(E_{\rm MC}-E)^2}{2\sigma_{\rm MC}^2}\right] \tag{220}$$

where ξ is the normalization factor to make the integrals of original and weighted distributions equal.
The weight $W^{\rm beam}(E)$ can be read as the ratio of numbers of data and MC events at beam energy E. Thus, for example, if the weight is larger than 1 which means we need to increase the number of MC events by the factor $W^{\rm beam}(E)$. This is exactly what we did above. This $W^{\rm beam}(E)$ needs to be multiplied by other weights to be integrated into total weight W_{jk}^{MC}. $W^{\rm beam}(E)$ does not depend on MC mode (j) but depends on the event (k) because beam enrgy E differ event by event.
This re-weigting modify lepton memontum, D momentum and $\cos\theta_{B-Dl}$ distributions. These variables are plotted in Figures....

9.6.1 OffPeak data beam energy re-weighting

OffPeak data is taken at the energy 39MeV below the OnPeak data energy. Thus, we need to scale lepton enrgy and D energy by a factor $r_{\rm beam}$ to match OnPeak data. The factor is given by

$$r_{\rm beam} = \frac{E_{\rm data}^{OnPeak}}{E_{\rm data}^{OffPeak}} = \frac{E_{\rm data}}{E_{\rm data} - 0.039\,{\rm GeV}} \tag{221}$$

where $E_{\rm data}$ is given in Table 23.

Run	data [32]		SP5/SP6 MC		Normalization
	mean (E_{data})	width (σ_{data})	mean (E_{MC})	width (σ_{MC})	factor (ξ)
Run1	10.577618	0.00499	10.5778	0.00481	0.963934
Run2	10.578668	0.00501	10.5778	0.00481	0.960076
Run3	10.578393	0.00487	10.5778	0.00481	0.987636
Run4	10.577699	0.00492	10.5778	0.00481	0.977638

Table 23: [**Beam energy**] Average beam energy and width of each Run. Normalization factor ξ is also shown.

10 Form Factor (FF) Re-weighting (W_{jk}^{MC})

We use SP5/SP6 MC for our analysis. However, there have been some improvements of form factors (FF) since SP5/SP6 MC were generated. To take those improvements into account, form factor re-weighting is necessary. See also Appendix H for details of form factors.

10.1 Normalization

When we change parameters of form factors, we need to make sure that total rates stay same. Thus, we need a normalization factor, R_N, such that

$$\Gamma = \int \frac{d\Gamma(\text{old FF})}{dw} dw = R_N \int \frac{d\Gamma(\text{new FF})}{dw} dw \tag{222}$$

In actual integration the Gaussian quadrature method is used.

10.2 $B \to D\ell\nu$

In this mode, ISGW2 model [33][34] is used in MC. ISGW2 is a type of constituent quark models. We need to change it to HQET (Heavy Quark Effective Theory) model [35][36]. The ISGW2 model gives form factors $f_+(q^2)$ and $f_-(q^2)$, and the HQET model gives $h_+(w)$ and $h_-(w)$, where w is the velocity transfer (see Appendix G). These form factors are related by

$$h_+ = \frac{1}{R}\left(f_+ + \frac{1-r}{1+r} f_-\right) \tag{223}$$

$$h_- = \frac{1}{R}\left(\frac{1-r}{1+r} f_+ + f_-\right) \tag{224}$$

where

$$R = \frac{2\sqrt{m_B m_D}}{m_B + m_D} \tag{225}$$

and

$$r = \frac{m_D}{m_B} \tag{226}$$

q^2 is related to w by

$$w = \frac{m_B^2 + m_D^2 - q^2}{2m_B m_D} \quad \text{or} \quad q^2 = m_B^2 + m_D^2 - 2m_B m_D w \tag{227}$$

The differential decay rate is given by

$$\frac{d\Gamma(B \to D\ell\nu)}{dw} = \frac{G_F^2 |V_{cb}|^2 m_B^5}{48\pi^3} r^3 (w^2-1)^{3/2}\, \mathcal{J}_D(w) \tag{228}$$

where

$$\mathcal{J}_D(w) = [(1+r)h_+(w) - (1-r)h_-(w)]^2 \tag{229}$$

In the ISGW2 model,

$$
\begin{aligned}
&(1+r)h_+ - (1-r)h_- \\
&\quad = (1+r)\frac{1}{R}\left(f_+ + \frac{1-r}{1+r}f_-\right) - (1-r)\frac{1}{R}\left(\frac{1-r}{1+r}f_+ + f_-\right) \\
&\quad = \frac{1+r}{R}\frac{(1+r)^2-(1-r)^2}{(1+r)^2}f_+ = \frac{1+r}{R}\frac{4r}{(1+r)^2}f_+ = \frac{1+r}{R}R^2 f_+ \\
&\quad = (1+r)Rf_+
\end{aligned}
\tag{230}
$$

Thus

$$\mathcal{J}_D^{ISGW2} = [(1+r)Rf_+]^2 \tag{231}$$

In HQET model, we can set

$$
\begin{aligned}
h_+(w) &= h_+(1)[1-\rho_D^2(w-1)] \\
h_-(w) &= 0
\end{aligned}
\tag{232}
$$

where ρ_D^2 is the slope. $h_+(1)$ can be given by a Lattice QCD calculation [37]

$$h_+(1) = 1.074 \pm 0.018 \pm 0.016 = 1.074 \pm 0.024 \tag{233}$$

Thus

$$\mathcal{J}_D^{HQET} = (1+r)^2[h_+(1)]^2[1-\rho_D^2(w-1)]^2 \tag{234}$$

By using Equation (227), we can express f_+ as a function of w. Then, the weight is given by

$$W_{jk}^{MC}(w_k) = \frac{\mathcal{J}_D^{HQET}}{\mathcal{J}_D^{ISGW2}}R_N = \frac{[h_+(1)]^2[1-\rho_D^2(w-1)]^2}{[Rf_+]^2}R_N \tag{235}$$

where, the normalization factor, R_N, is given by

$$
\begin{aligned}
&\int_0^{1.590}(w^2-1)^{3/2}\,[Rf_+]^2\,dw \\
&\qquad = R_N\int_1^{1.590}(w^2-1)^{3/2}[h_+(1)]^2[1-\rho_D^2(w-1)]^2 dw
\end{aligned}
\tag{236}
$$

Or, we can use the CLN parametrization proposed by Caprini, Lellouch and Neubert [38]

$$h_+(w) = h_+(1)[1-8\rho_D^2 z + (51\rho_D^2-10)z^2 - (252\rho_D^2-84)z^3] \tag{237}$$

where

$$z = \frac{\sqrt{w+1}-\sqrt{2}}{\sqrt{w+1}+\sqrt{2}} \tag{238}$$

In this case, the weight is given by

$$W_{jk}^{MC}(w_k) = \frac{[h_+(1)]^2[1-8\rho_D^2 z + (51\rho_D^2-10)z^2 - (252\rho_D^2-84)z^3]^2}{[Rf_+]^2}R_N \tag{239}$$

where, the normalization factor, R_N, is given by

$$\begin{aligned}
&\int_0^{1.590} dw\ \ (w^2-1)^{3/2}\,[Rf_+]^2 \\
&= R_N \int_1^{1.590} dw\ \ (w^2-1)^{3/2}[h_+(1)]^2 \times \\
&\qquad \left[1 - 8\rho_D^2 z + (51\rho_D^2 - 10)z^2 - (252\rho_D^2 - 84)z^3\right]^2 \qquad (240)
\end{aligned}$$

Figure 57 shows the differential decay rate $d\Gamma(B \to D\ell\nu)/dw$ as a function of w. The black line shows the ISGW2 model, the red dashed line shows the HQET model with the standard slope in case of $\rho_D^2 = 0.8$, and the blue dotted line shows the HQET model with the CLN slope in case of $\rho_D^2 = 1.17$ [26]. Figure 58 shows the distribution of weight W_{jk}^{MC} in the case of the CLN slope of $\rho_D^2 = 1.17$, corresponding to the normalization factor $R_N = 1.363$. BpBm MC is used to create the plot. The change in the spectrum of lepton momentum, D momentum and $\cos\theta_{B-Dl}$ is given in Figure 59 - 61.

10.3 $B \to D^*\ell\nu$

We need three kinematic variables to describe this decay. We usually chose $\cos\theta_\ell$, $\cos\theta_V$ and χ as shown in the figure 62. The definition of these variables are

- $\cos\theta_\ell$: the cosine of the angle between the directions of "the ℓ in the W rest frame" and "the W in the B rest frame".
- $\cos\theta_V$: the cosine of the angle between the directions of "the D in the D^* rest frame" and "the D^* in the B rest frame".
- χ : the azimuthal angle between the planes formed by "W-ℓ system' ' and "$D^* - D$ system".

HQET model is used and the differential decay rate is given by [35][36]

$$\begin{aligned}
\frac{d\Gamma(B\to D^*\ell\nu)}{dw d\cos\theta_V d\cos\theta_\ell d\chi} \;=\; & \frac{3G_F^2}{4(4\pi)^4}|V_{cb}|^2 m_B m_{D^*}^2 \sqrt{w^2-1}(1-2wr+r^2)\times \\
& [(1-\cos\theta_\ell)^2\sin^2\theta_V|H_+(w)|^2 \\
& +(1+\cos\theta_\ell)^2\sin^2\theta_V|H_-(w)|^2 \\
& +4\sin^2\theta_\ell\cos^2\theta_V|H_0(w)|^2 \qquad (241)\\
& -4\sin\theta_\ell(1-\cos\theta_\ell)\sin\theta_V\cos\theta_V\cos\chi H_+(w)H_0(w) \\
& +4\sin\theta_\ell(1+\cos\theta_\ell)\sin\theta_V\cos\theta_V\cos\chi H_-(w)H_0(w) \\
& -2\sin^2\theta_\ell\sin^2\theta_V\cos 2\chi H_+(w)H_-(w)]
\end{aligned}$$

where r is the mass ratio

$$r = \frac{m_{D^*}}{m_B} \qquad (242)$$

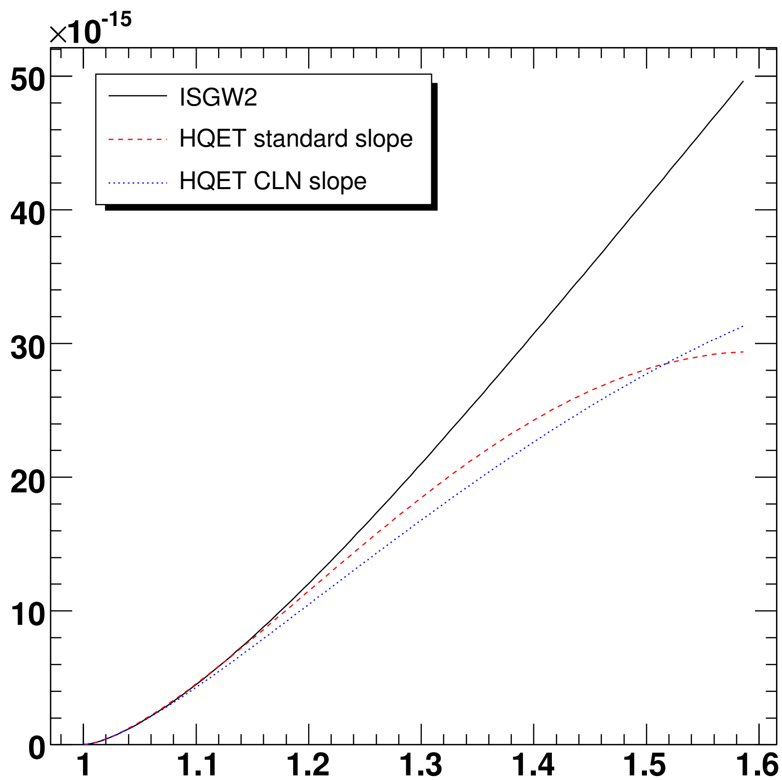

Figure 57: [$B \to D\ell\nu$ **FF**] The differential decay rate $d\Gamma(B \to D\ell\nu)/dw$ as a function of w. This is in case that the standard slope is $\rho_D^2 = 0.8$ and the CLN slope is $\rho_D^2 = 1.17$

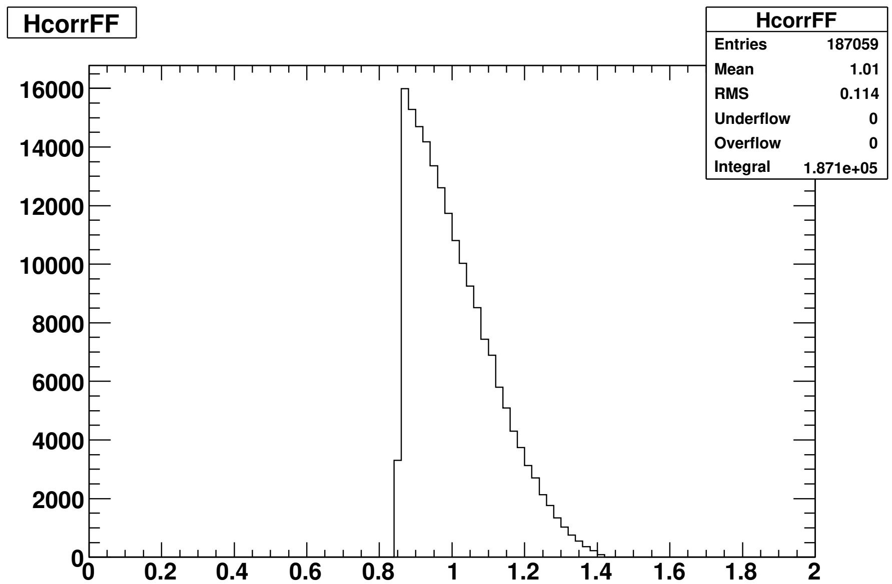

Figure 58: [$B \to D\ell\nu$ **FF weight**] The distribution of weight W_{jk}^{MC} for $B \to D\ell\nu$ decays This is made from BpBm MC.

$H_i(w)$ are

$$H_i = -m_B \frac{R^*(1-r^2)(w+1)}{2\sqrt{1-2wr+r^2}} h_{A_1}(w)\widetilde{H}_i(w) \tag{243}$$

where R^* is

$$R^* = \frac{2\sqrt{m_B m_{D^*}}}{m_B + m_{D^*}} \tag{244}$$

and $\widetilde{H}_i(w)$ are

$$\begin{aligned} \widetilde{H}_\pm(w) &= \tfrac{\sqrt{1-2wr+r^2}}{1-r}\left(1 \mp \sqrt{\tfrac{w-1}{w+1}}R_1(w)\right) \\ \widetilde{H}_0(w) &= 1 + \tfrac{w-1}{1-r}\left(1 - R_2(w)\right) \end{aligned} \tag{245}$$

were R_1 and R_2 are the form factor ratios. To make the notation simple, we define

$$\begin{aligned} &c_L \equiv \cos\theta_\ell \\ &c_V \equiv \cos\theta_V \\ &c_\chi \equiv \cos\chi \\ &\tilde{h}_\pm(w) \equiv (1-r)\widetilde{H}_\pm(w) = \sqrt{1-2wr+r^2}\left(1 \mp \sqrt{\tfrac{w-1}{w+1}}R_1(w)\right) \\ &\tilde{h}_0(w) \equiv (1-r)\widetilde{H}_0(w) = (1-r) + (w-1)\left(1 - R_2(w)\right) = (w-r) - (w-1)R_2(w) \end{aligned} \tag{246}$$

then (see Appendix H.4)

$$\frac{d\Gamma(B \to D^*\ell\nu)}{dw\,dc_V\,dc_L\,d\chi} = \frac{G_F^2|V_{cb}|^2 m_B^5}{48\pi^3} r^3 (w^2-1)^{1/2} \times \frac{9}{64\pi}(w+1)^2 \;\; \mathcal{J}_{FF} \tag{247}$$

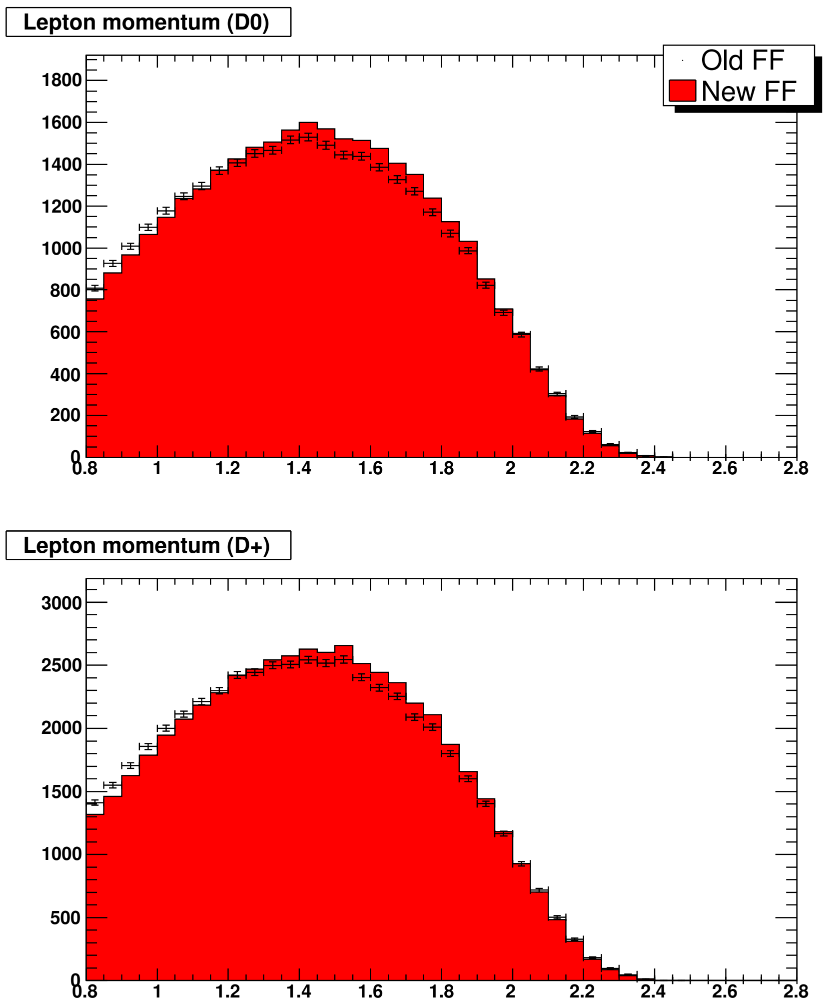

Figure 59: [p_ℓ **after** $B \to D\ell\nu$ **re-weighting**] Lepton momentum spectrum of $B^+ \to \bar{D}^0\ell\nu$ decays (top) and $B^0 \to D^-\ell\nu$ decays (bottom). Black line is ISGW2 model and red histogram is HQET model with CLN slope $\rho_D^2 = 1.17$

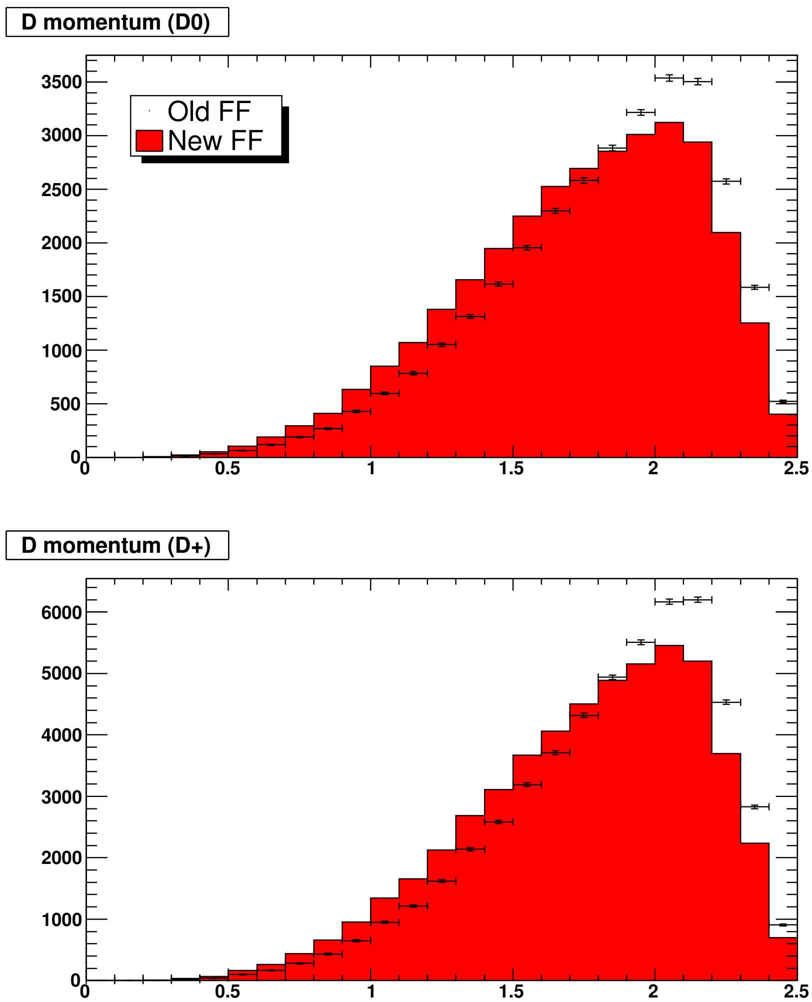

Figure 60: [p_D **after** $B \to D\ell\nu$ **re-weighting**] D momentum spectrum of $B^+ \to \bar{D}^0\ell\nu$ decays (top) and $B^0 \to D^-\ell\nu$ decays (bottom). Black line is ISGW2 model and red histogram is HQET model with CLN slope $\rho_D^2 = 1.17$

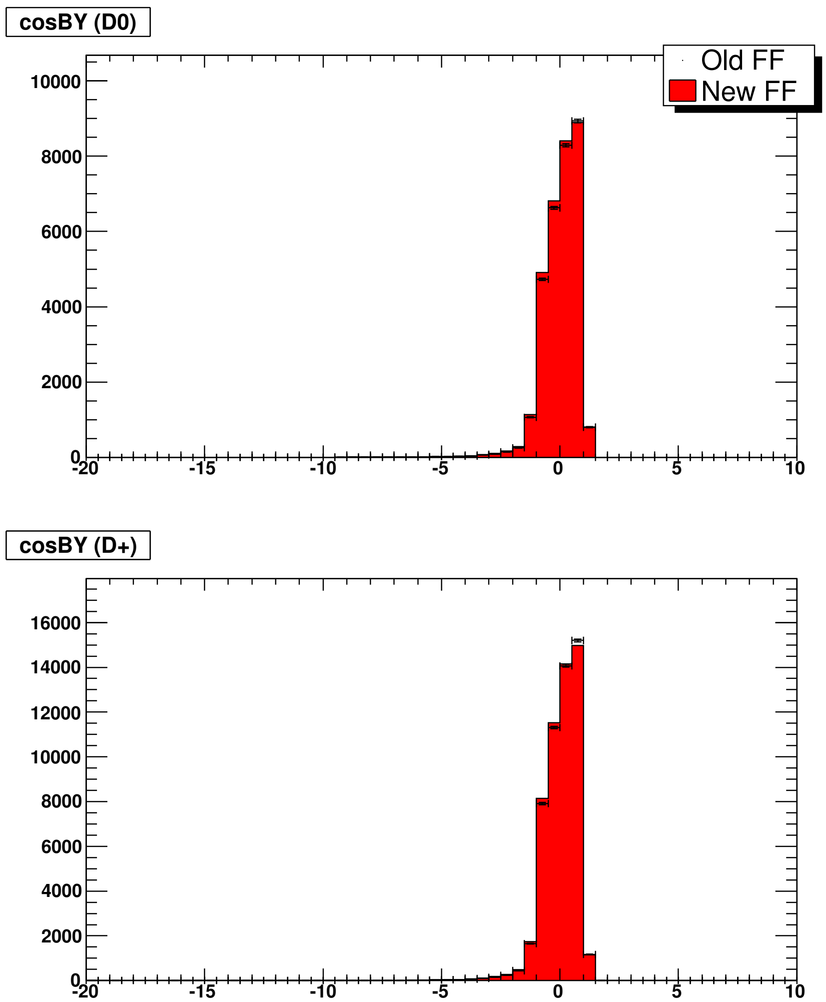

Figure 61: [$\cos\theta_{B-Dl}$ **after** $B \rightarrow D\ell\nu$ **re-weighting**] $\cos\theta_{B-Dl}$ of $B^+ \rightarrow \bar{D}^0\ell\nu$ decays (top) and $B^0 \rightarrow D^-\ell\nu$ decays (bottom). Black line is ISGW2 model and red histogram is HQET model with CLN slope $\rho^2_D = 1.17$

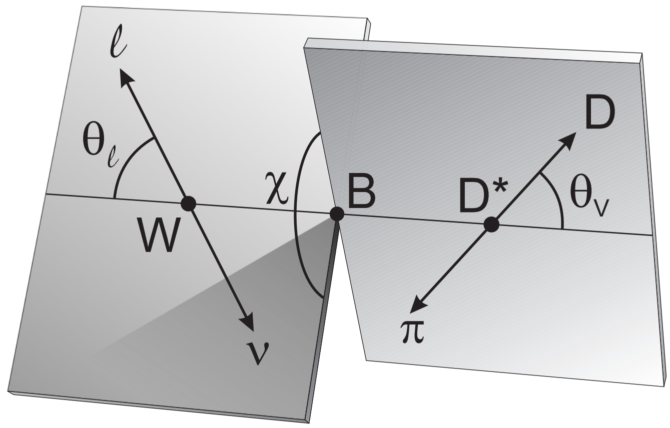

Figure 62: [$B \to D^*\ell\nu$ **decay geometry**] Geometry of $B \to D^*\ell\nu$ decays.

where

$$\begin{aligned}\mathcal{J}_{FF}(R_1, R_2, \rho^2) &= [h_{A_1}(w)]^2 \times \\ &[(1-c_L)^2(1-c_V^2)\tilde{h}_+^2 + (1+c_L)^2(1-c_V^2)\tilde{h}_-^2 \\ &+4(1-c_L^2)c_V^2\tilde{h}_0^2 - 2(1-c_L^2)(1-c_V^2)(2c_\chi^2-1)\tilde{h}_+\tilde{h}_- \\ &-4\sqrt{1-c_L^2}(1-c_L)\sqrt{1-c_V^2}c_V c_\chi \tilde{h}_+\tilde{h}_0 \\ &+4\sqrt{1-c_L^2}(1+c_L)\sqrt{1-c_V^2}c_V c_\chi \tilde{h}_-\tilde{h}_0]\end{aligned} \tag{248}$$

In SP5/SP6 MC, the values of parameters are

$$\begin{aligned}R_1^{MC} &= 1.18 \\ R_2^{MC} &= 0.72 \\ (\rho^2)^{MC} &= 0.92\end{aligned} \tag{249}$$

with

$$\begin{aligned}R_1(w) &= R_1^{MC} \\ R_2(w) &= R_2^{MC} \\ h_{A_1}(w) &= h_{A_1}(1)\left[1-(\rho^2)^{MC}(w-1)\right]\end{aligned} \tag{250}$$

where $h_{A_1}(1)$ can be givn by a Lattice calculation [39]. The values from a recent Babar measurement [40][41] are

$$\begin{aligned}R_1 &= 1.417 \pm 0.061 \pm 0.044 \\ R_2 &= 0.836 \pm 0.037 \pm 0.022 \\ \rho^2 &= 1.179 \pm 0.048 \pm 0.028\end{aligned} \tag{251}$$

where the CLN parametrization [38] is used

$$\begin{aligned} R_1(w) &= R_1 - 0.12(w-1) + 0.05(w-1)^2 \\ R_2(w) &= R_2 + 0.11(w-1) - 0.06(w-1)^2 \\ h_{A_1}(w) &= h_{A_1}(1)\,[1 - 8\rho^2 z + (53\rho^2 - 15)z^2 - (231\rho^2 - 91)z^3] \end{aligned} \tag{252}$$

where

$$z = \frac{\sqrt{w+1} - \sqrt{2}}{\sqrt{w+1} + \sqrt{2}} \tag{253}$$

We also use the CLN parametrization in our fit. The weight is given by

$$W_{jk}^{MC}(w_k) = \frac{\mathcal{J}_{FF}(R_1, R_2, \rho^2)}{\mathcal{J}_{FF}(R_1^0, R_2^0, \rho_0^2)} \tag{254}$$

To calculate the normalization factor R_N, we need to integrate over c_V, c_L and χ. Thus, it is easier to use $d\Gamma/dw$ (see Appendix H.4)

$$\frac{d\Gamma(B \to D^*\ell\nu)}{dw} = \frac{G_F^2 |V_{cb}|^2 m_B^5}{48\pi^3} r^3 (w^2-1)^{1/2} \mathcal{J}_{WD}(R_1, R_2, \rho^2) \tag{255}$$

where

$$\mathcal{J}_{WD}(R_1, R_2, \rho^2) = (w+1)^2 [h_{A_1}]^2 (\tilde{h}_+^2 + \tilde{h}_-^2 + \tilde{h}_0^2) \tag{256}$$

Thus, the normalization factor is given by

$$\begin{aligned} &\int_1^{1.504} dw\;\; (w^2-1)^{1/2} \mathcal{J}_{WD}(R_1^0, R_2^0, \rho_0^2) \\ &= R_N \int_1^{1.504} dw\;\; (w^2-1)^{1/2} \mathcal{J}_{WD}(R_1, R_2, \rho^2) \end{aligned} \tag{257}$$

Figure 63 shows the differential decay rate $d\Gamma(B \to D^*\ell\nu)/dw$ as a function of w. The red dashed line shows the HQET model with the old parameters of R_1, R_2 and ρ^2, and the blue dotted line shows the HQET model with new parameters. Figure 64 shows the distribution of weight W_{jk}^{MC} for BpBm MC corresponding to the normalization factor $R_N = 1.044$. The change in the spectrum of lepton momentum, D momentum and $\cos\theta_{B-Dl}$ is given in Figure 65 - 67.

10.4 $B \to D^{**}\ell\nu$

In SP5/SP6 MC, ISGW2 model is used. We would like to use HQET based LLSW model [42][43]. Details of LLSW model is given in Appendix H. We use the Approximation B1 to calculate the form factors and the Approximation B2 to estimate systematic uncertainties. The differential decay rates are given as functions of w and θ. This θ is the angle between the charged lepton and the charmed meson in the rest frame of the virtual W boson. Thus $\theta = \pi - \theta_\ell$, e.g.,

$$\cos\theta = \cos(\pi - \theta_\ell) = -\cos\theta_\ell \tag{258}$$

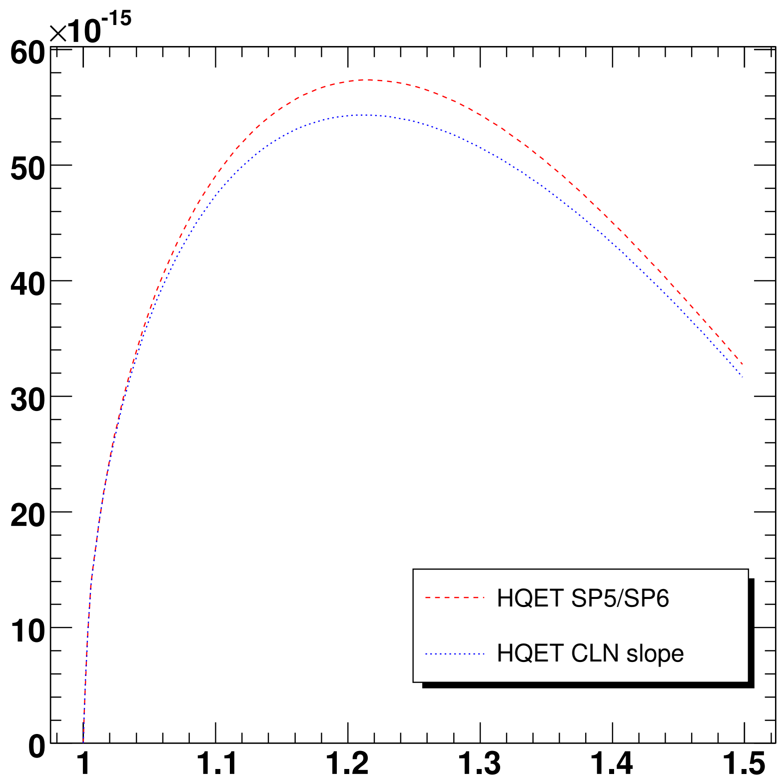

Figure 63: [$B \to D^*\ell\nu$ **FF**] The differential decay rate $d\Gamma(B \to D^*\ell\nu)/dw$ as a function of w.

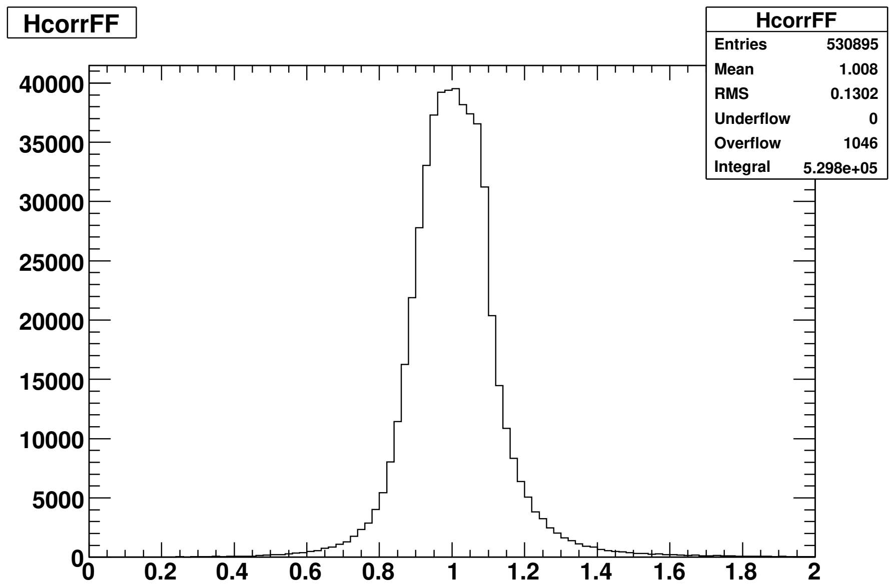

Figure 64: [$B \to D^*\ell\nu$ **FF weight**] The distribution of weight W^{MC}_{jk} for $B \to D^*\ell\nu$ decays This is made from BpBm MC.

10.4.1 $B \to D_0^*\ell\nu$

The ISGW2 form factors $u_+(q^2)$ and $u_-(q^2)$ are related to the LLSW form factors $g_+(w)$ and $g_-(w)$

$$g_+ = \frac{1}{R}\left(u_+ + \frac{1-r}{1+r}u_-\right), \quad g_- = \frac{1}{R}\left(\frac{1-r}{1+r}u_+ + u_-\right) \tag{259}$$

where

$$R = \frac{2\sqrt{m_B m_{D_0^*}}}{m_B + m_{D_0^*}}, \quad r = \frac{m_{D_0^*}}{m_B} \tag{260}$$

The differential decay rate is given by

$$\frac{d^2\Gamma_{D_0^*}}{dw d\cos\theta} = \frac{G_F^2|V_{cb}|^2 m_B^5}{64\pi^3} r^3(w^2-1)^{3/2}\,\mathcal{I}_{D_0^*}(w,\theta) \tag{261}$$

where

$$\mathcal{I}_{D_0^*}(w,\theta) = (1-\cos^2\theta)[(1+r)g_+ - (1-r)g_-]^2 \tag{262}$$

The weight is given by the ratio of $\mathcal{I}_{D_0^*}$ part.

$$W^{MC}_{jk}(w_k) = \frac{\mathcal{I}^{LLSW}_{D_0^*}}{\mathcal{I}^{ISGW2}_{D_0^*}} R_N \tag{263}$$

Integrated by θ, the differential decay rate is

$$\frac{d\Gamma(B \to D_0^*\ell\nu)}{dw} = \frac{G_F^2|V_{cb}|^2 m_B^5}{48\pi^3} r^3(w^2-1)^{3/2}\,\mathcal{J}_{D_0^*}(w) \tag{264}$$

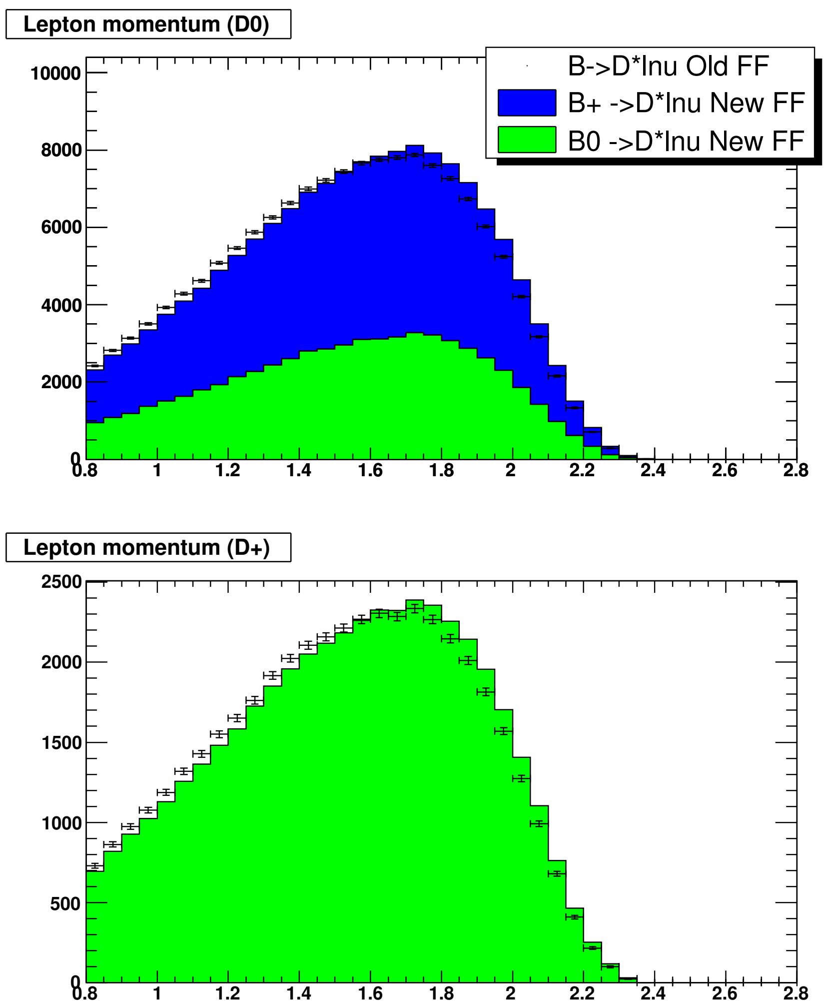

Figure 65: [p_ℓ **after** $B \to D^*\ell\nu$ **re-weighting**] Lepton momentum spectrum of $B \to D^*\ell\nu$ decays. The top is D^0 and the bottom is D^+. Black line is with old FF parameters and histogram is with new FF parameters. Green is the contribution from B^+ and blue is from B^0.

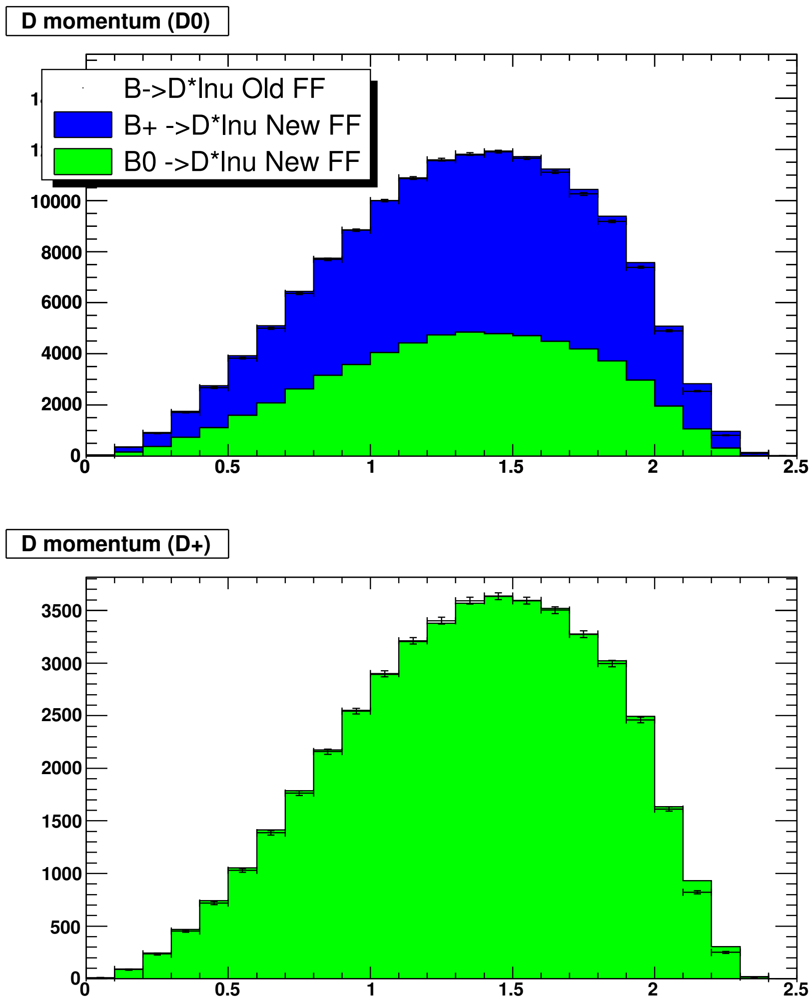

Figure 66: [p_D **after** $B \to D^* \ell \nu$ **re-weighting**] D momentum spectrum of $B \to D^* \ell \nu$ decays. The top is D^0 and the bottom is D^+. Black line is with old FF parameters and histogram is with new FF parameters. Green is the contribution from B^+ and blue is from B^0.

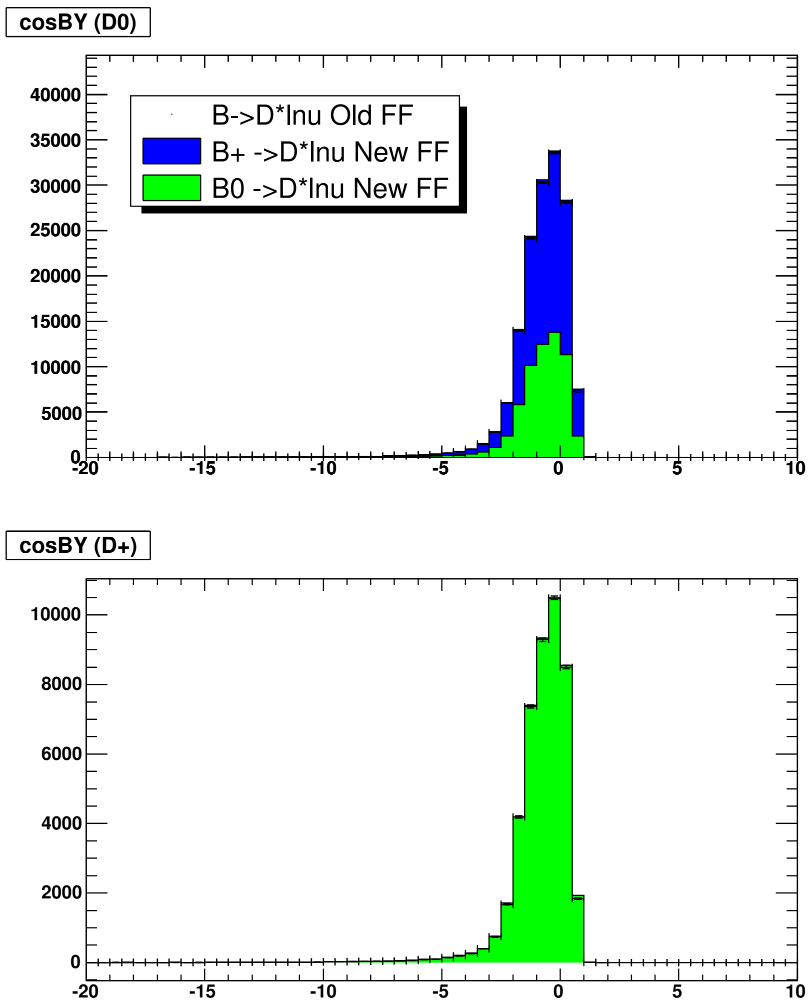

Figure 67: [$\cos\theta_{B-Dl}$ **after** $B \to D^*\ell\nu$ **re-weighting**] $\cos\theta_{B-Dl}$ of $B \to D^*\ell\nu$ decays. The top is D^0 and the bottom is D^+. Black line is with old FF parameters and histogram is with new FF parameters. Green is the contribution from B^+ and blue is from B^0.

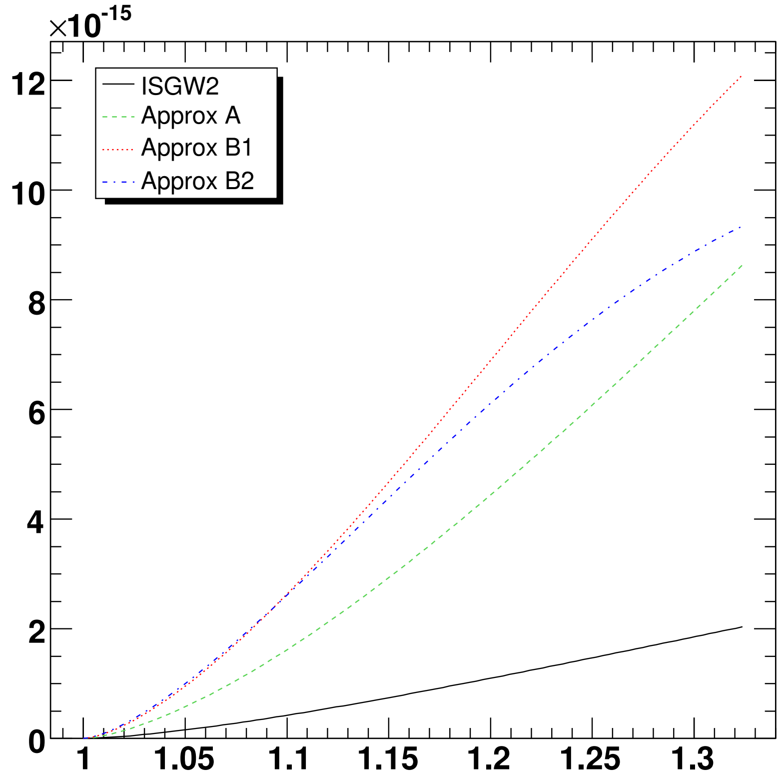

Figure 68: [$B \to D_0^* \ell \nu$ **FF**] The differential decay rate $d\Gamma(B \to D_0^* \ell \nu)/dw$ as a function of w.

where

$$\mathcal{J}_{D_0^*}(w) = [(1+r)g_+ - (1-r)g_-]^2 \tag{265}$$

Thus, the normalization factor, R_N, is given by

$$\int_0^{1.327} (w^2-1)^{3/2} \mathcal{J}_{D_0^*}^{ISGW2} dw = R_N \int_1^{1.327} (w^2-1)^{3/2} \mathcal{J}_{D_0^*}^{LLSW} dw \tag{266}$$

Figure 68 shows the differential decay rate $d\Gamma(B \to D_0^* \ell \nu)/dw$ as a function of w. The black line shows the ISGW2 model, the other lines show the LLSW model; the green dashed line is the Approximation A, the red dotted line is the Approximation B1 and the blue dot-dashed line is the Approximation B2. We use the Approximation B1 in our fit. Figure 69 shows the distribution of weight W_{jk}^{MC} in the case of the Approximation B1, corresponding to the normalization factor $R_N = 0.1624$. BpBm MC is used to create the plot.

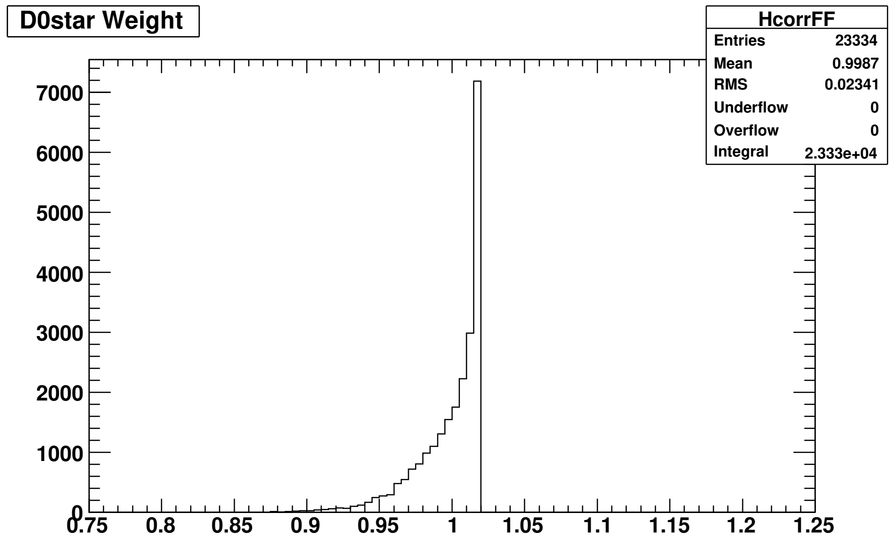

Figure 69: [$B \to D_0^* \ell\nu$ **FF weight**] The distribution of weight W_{jk}^{MC} for $B \to D_0^* \ell\nu$ decays This is made from BpBm MC.

10.4.2 $B \to D_1' \ell\nu$

The ISGW2 form factors q, l and c_+ are related to the LLSW form factors g_A, g_{V_1}, g_{V_2} and g_{V_3}.

$$g_A = Rm_B(1+r)q \tag{267}$$

$$g_{V_1} = \frac{2}{Rm_B(1+r)} l \tag{268}$$

$$g_{V_3} + r g_{V_2} = Rm_B(1+r)c_+ \tag{269}$$

where

$$R = \frac{2\sqrt{m_B m_{D_1'}}}{m_B + m_{D_1'}}, \quad r = \frac{m_{D_1'}}{m_B} \tag{270}$$

The differential decay rate is given by

$$\frac{d^2\Gamma_{D_1'}}{dw d\cos\theta} = \frac{G_F^2 |V_{cb}|^2 m_B^5}{64\pi^3} r^3 (w^2-1)^{1/2}\, \mathcal{I}_{D_1'}(w,\theta) \tag{271}$$

where

$$\begin{aligned}\mathcal{I}_{D_1'}(w,\theta) &= (1-\cos^2\theta)[(w-r)g_{V_1} + (w^2-1)(g_{V_3} + r g_{V_2})]^2 \\ &+(1-2rw+r^2)[(1+\cos^2\theta)(g_{V_1}^2 + (w^2-1)g_A^2) - 4\cos\theta\sqrt{w^2-1} g_{V_1} g_A]\end{aligned} \tag{272}$$

The weight is given by the ratio of $\mathcal{I}_{D_1'}$ part.

$$W_{jk}^{MC}(w_k) = \frac{\mathcal{I}_{D_1'}^{LLSW}}{\mathcal{I}_{D_1'}^{ISGW2}} R_N \tag{273}$$

Integrated by θ, the differential decay rate is

$$\frac{d\Gamma(B \to D_1 \ell\nu)}{dw} = \frac{G_F^2 |V_{cb}|^2 m_B^5}{48\pi^3} r^3 (w^2-1)^{1/2} \, \mathcal{J}_{D_1'}(w) \tag{274}$$

where

$$\begin{aligned} \mathcal{J}_{D_1'}(w) = & \left[(w-r)g_{V_1} + (w^2-1)(g_{V_3} + r g_{V_2})\right]^2 \\ & + 2(1-2rw+r^2)[g_{V_1}^2 + (w^2-1)g_A^2] \end{aligned} \tag{275}$$

Thus, the normalization factor, R_N, is given by

$$\int_0^{1.316} dw (w^2-1)^{1/2} \mathcal{J}_{D_1'}^{ISGW2} = R_N \int_1^{1.316} dw (w^2-1)^{1/2} \mathcal{J}_{D_1'}^{LLSW} \tag{276}$$

Figure 70 shows the differential decay rate $d\Gamma(B \to D_1' \ell\nu)/dw$ as a function of w. The black line shows the ISGW2 model, the other lines show the LLSW model; the green dashed line is the Approximation A, the red dotted line is the Approximation B1 and the blue dot-dashed line is the Approximation B2. We use the Approximation B1 in our fit. Figure 71 shows the distribution of weight W_{jk}^{MC} in the case of the Approximation B1, corresponding to the normalization factor $R_N = 0.5488$. BpBm MC is used to create the plot.

10.4.3 $B \to D_1 \ell\nu$

The ISGW2 form factors v, r and s_+ are related to the LLSW form factor f_A, f_{V_1}, f_{V_2} and f_{V_3}.

$$f_A = R m_B (1+r) v \tag{277}$$

$$f_{V_1} = \frac{2}{R m_B (1+r)} r \tag{278}$$

$$f_{V_3} + r f_{V_2} = R m_B (1+r) s_+ \tag{279}$$

where

$$R = \frac{2\sqrt{m_B m_{D_1}}}{m_B + m_{D_1}}, \quad r = \frac{m_{D_1}}{m_B} \tag{280}$$

The differential decay rate is given by

$$\frac{d^2\Gamma_{D_1}}{dw d\cos\theta} = \frac{G_F^2 |V_{cb}|^2 m_B^5}{64\pi^3} r^3 (w^2-1)^{1/2} \, \mathcal{I}_{D_1}(w,\theta) \tag{281}$$

where

$$\begin{aligned} \mathcal{I}_{D_1}(w,\theta) = & (1-\cos^2\theta)[(w-r)f_{V_1} + (w^2-1)(f_{V_3} + r f_{V_2})]^2 \\ & + (1-2rw+r^2)[(1+\cos^2\theta)(f_{V_1}^2 + (w^2-1)f_A^2) - 4\cos\theta\sqrt{w^2-1} f_{V_1} f_A] \end{aligned} \tag{282}$$

The weight is given by the ratio of $\mathcal{I}_{D_1}$ part.

$$W_{jk}^{MC}(w_k) = \frac{\mathcal{I}_{D_1}^{LLSW}}{\mathcal{I}_{D_1}^{ISGW2}} R_N \tag{283}$$

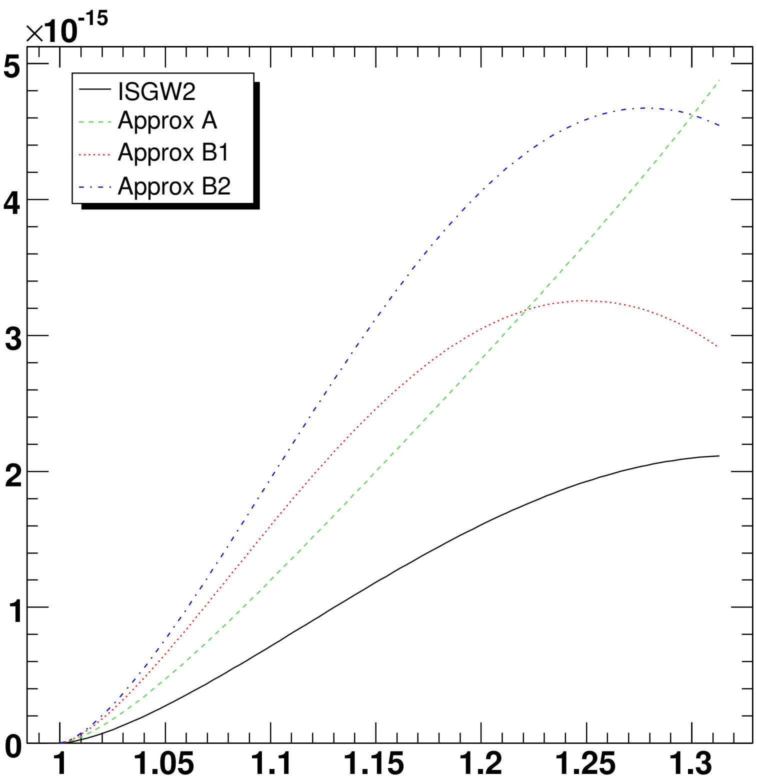

Figure 70: [$B \to D_1' \ell \nu$ **FF**] The differential decay rate $d\Gamma(B \to D_1'\ell\nu)/dw$ as a function of w.

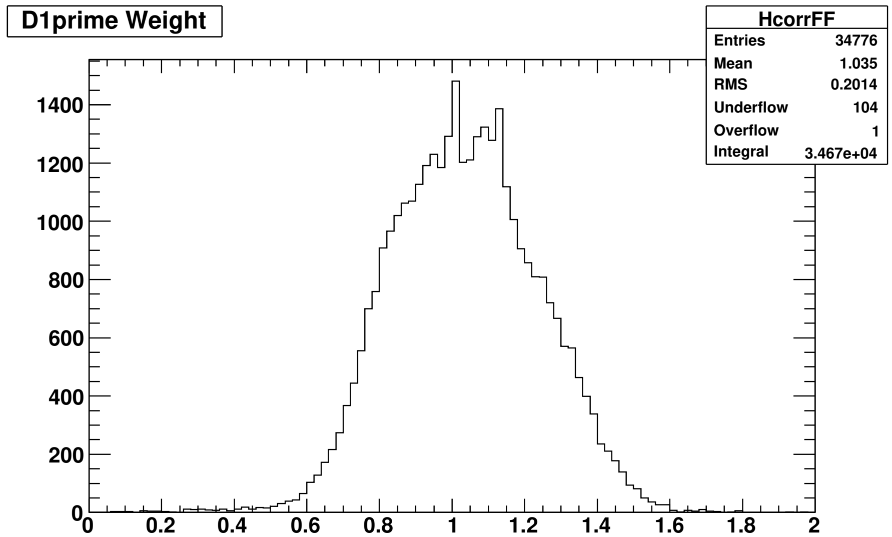

Figure 71: [$B \to D_1'\ell\nu$ **FF weight**] The distribution of weight W_{jk}^{MC} for $B \to D_1'\ell\nu$ decays This is made from BpBm MC.

Integrated by θ, the differential decay rate is

$$\frac{d\Gamma(B \to D_1\ell\nu)}{dw} = \frac{G_F^2|V_{cb}|^2 m_B^5}{48\pi^3} r^3(w^2-1)^{1/2}\, \mathcal{J}_{D_1}(w) \tag{284}$$

where

$$\begin{aligned}\mathcal{J}_{D_1}(w) = &\left[(w-r)f_{V_1} + (w^2-1)(f_{V_3} + r f_{V_2})\right]^2 \\ &+2(1-2rw+r^2)[f_{V_1}^2 + (w^2-1)f_A^2]\end{aligned} \tag{285}$$

Thus, the normalization factor, R_N, is given by

$$\int_0^{1.320} dw(w^2-1)^{1/2}\mathcal{J}_{D_1}^{ISGW2} = R_N \int_1^{1.320} dw(w^2-1)^{1/2}\mathcal{J}_{D_1}^{LLSW} \tag{286}$$

Figure 72 shows the differential decay rate $d\Gamma(B \to D_1\ell\nu)/dw$ as a function of w. The black line shows the ISGW2 model, the other lines show the LLSW model; the green dashed line is the Approximation A, the red dotted line is the Approximation B1 and the blue dot-dashed line is the Approximation B2. We use the Approximation B1 in our fit. Figure 73 shows the distribution of weight W_{jk}^{MC} in the case of the Approximation B1, corresponding to the normalization factor $R_N = 0.7330$. BpBm MC is used to create the plot.

10.4.4 $B \to D_2^*\ell\nu$

The ISGW2 form factors h, k and b_+ are related to the LLSW form factor k_V, k_{A_1}, k_{A_2} and k_{A_3}.

$$k_V = Rm_B^2(1-r)h \tag{287}$$

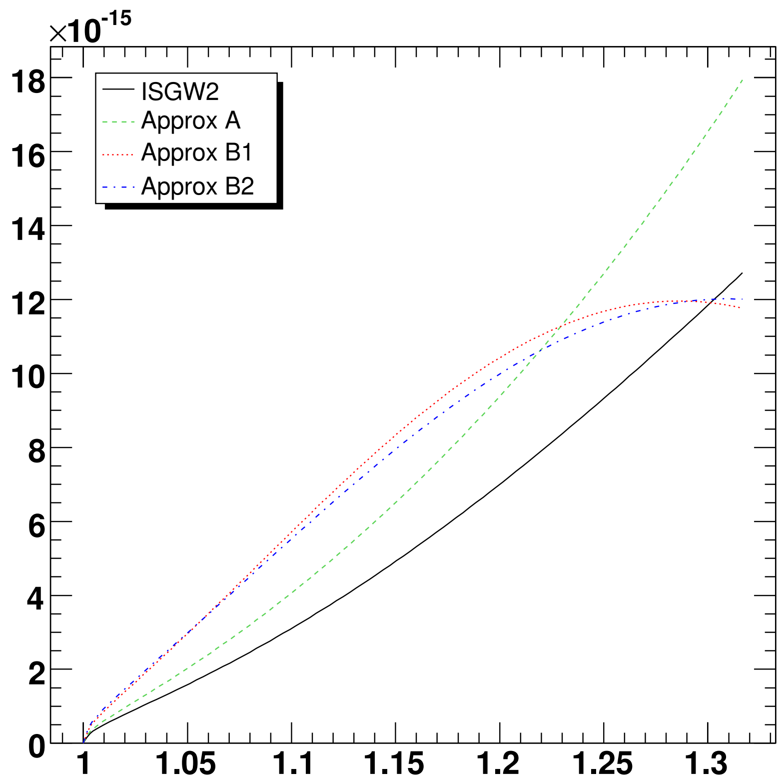

Figure 72: [$B \to D_1 \ell \nu$ **FF**] The differential decay rate $d\Gamma(B \to D_1 \ell \nu)/dw$ as a function of w.

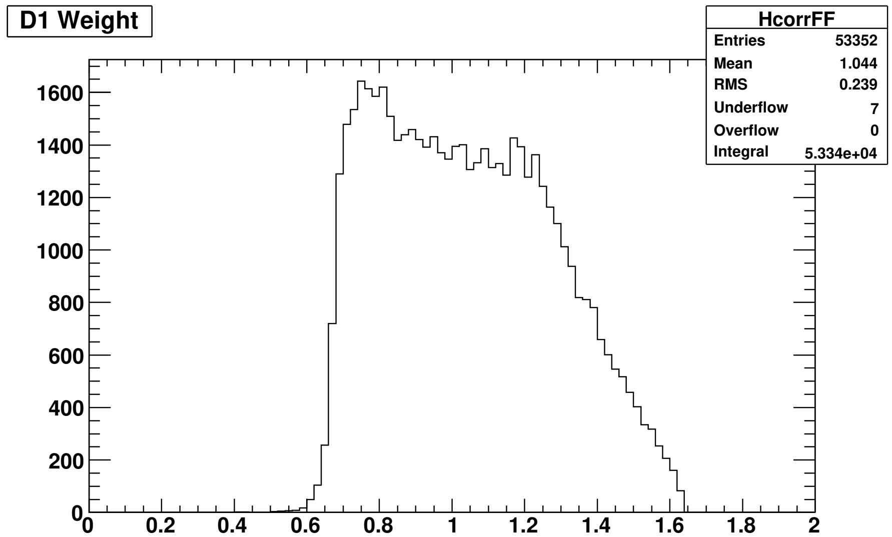

Figure 73: [$B \to D_1 \ell\nu$ **FF weight**] The distribution of weight W^{MC}_{jk} for $B \to D_1\ell\nu$ decays This is made from BpBm MC.

$$k_{A_1} = \frac{2}{R(1-r)} k \tag{288}$$

$$k_{A_3} + r k_{A_2} = R m_B^2 (1-r) b_+ \tag{289}$$

where

$$R = \frac{2\sqrt{m_B m_{D_2^*}}}{m_B + m_{D_2^*}}, \quad r = \frac{m_{D_2^*}}{m_B} \tag{290}$$

The differential decay rate is given by

$$\frac{d^2\Gamma_{D_2^*}}{dw d\cos\theta} = \frac{G_F^2 |V_{cb}|^2 m_B^5}{64\pi^3} r^3 (w^2-1)^{3/2} \, \frac{1}{2} \, \mathcal{I}_{D_2^*}(w,\theta) \tag{291}$$

where

$$\begin{aligned}\mathcal{I}_{D_2^*}(w,\theta) = {} & \frac{4}{3}(1-\cos^2\theta)[(w-r)k_{A_1} + (w^2-1)(k_{A_3} + r k_{A_2})]^2 \\ & +(1-2rw+r^2)[(1+\cos^2\theta)(k_{A_1}^2 + (w^2-1)k_V^2) - 4\cos\theta\sqrt{w^2-1}k_{A_1}k_V]\end{aligned} \tag{292}$$

The weight is given by the ratio of $\mathcal{I}_{D_2^*}$ part

$$W^{MC}_{jk}(w_k) = \frac{\mathcal{I}^{LLSW}_{D_2^*}}{\mathcal{I}^{ISGW2}_{D_2^*}} R_N \tag{293}$$

Integrated by θ, decay rate is

$$\frac{d\Gamma(B \to D_2^* \ell\nu)}{dw} = \frac{G_F^2 |V_{cb}|^2 m_B^5}{48\pi^3} r^3 (w^2-1)^{3/2} \, \mathcal{J}_{D_2^*}(w) \tag{294}$$

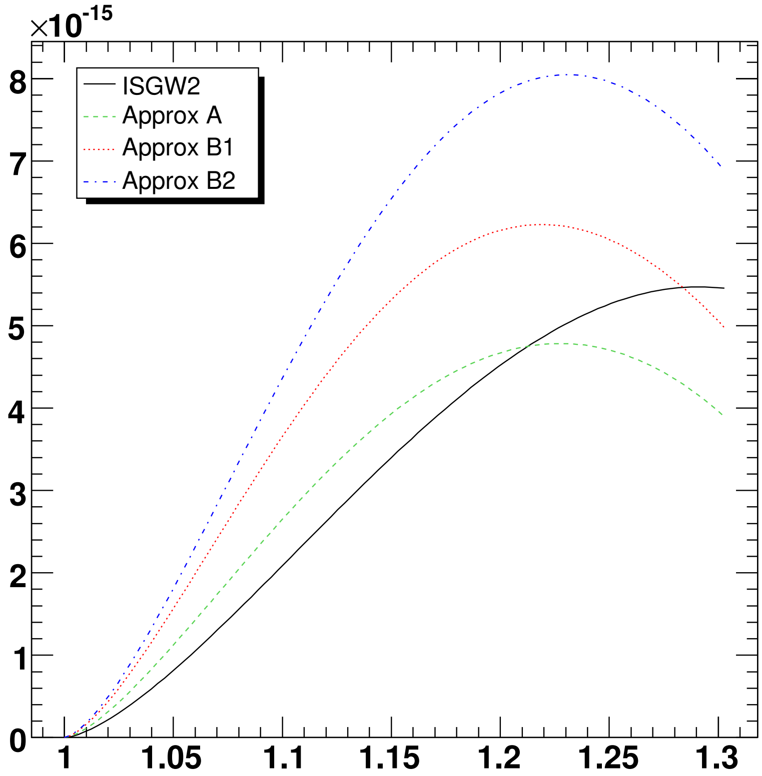

Figure 74: [$B \to D_2^* \ell \nu$ **FF**] The differential decay rate $d\Gamma(B \to D_2^* \ell\nu)/dw$ as a function of w.

where

$$\mathcal{J}_{D_2^*}(w) = \frac{2}{3}\left[(w-r)k_{A_1} + (w^2-1)(k_{A_3}+rk_{A_2})\right]^2 \\ +2(1-2rw+r^2)[k_{A_1}^2 + (w^2-1)k_V^2] \tag{295}$$

Thus, the normalization factor, R_N, is given by

$$\int_0^{1.306} dw(w^2-1)^{3/2}\mathcal{J}_{D_2^*}^{ISGW2} = R_N \int_1^{1.306} dw(w^2-1)^{3/2}\mathcal{J}_{D_2^*}^{LLSW} \tag{296}$$

Figure 74 shows the differential decay rate $d\Gamma(B \to D_2^*\ell\nu)/dw$ as a function of w. The black line shows the ISGW2 model, the other lines show the LLSW model; the green dashed line is the Approximation A, the red dotted line is the Approximation B1 and the blue dot-dashed line is the Approximation B2. We use the Approximation B1 in our fit. Figure 75 shows the distribution of weight W_{jk}^{MC} in the case of the Approximation B1, corresponding to the normalization factor $R_N = 0.7490$. BpBm MC is used to create the plot.

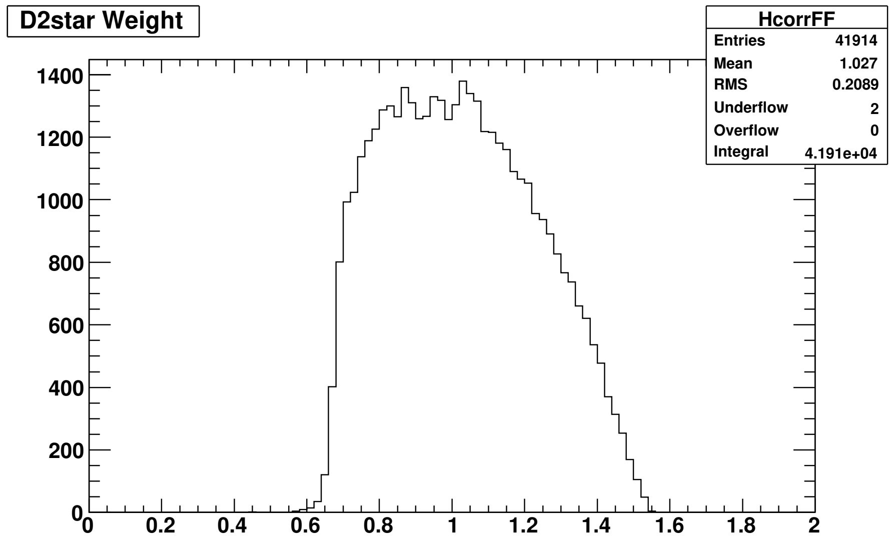

Figure 75: [$B \to D_2^* \ell \nu$ **FF weight**] The distribution of weight W_{jk}^{MC} for $B \to D_2^* \ell \nu$ decays This is made from BpBm MC.

10.4.5 Effect on kinematic variables

The change in the spectrum of lepton momentum, D momentum and $\cos \theta_{B-Dl}$ is given in Figure 76 - 78.

10.5 $B \to D^{(*)} \pi \ell \nu$ (non-resonant)

In SP5/SP6 Goiry-Roberts model [44][45] is used. We keep this model because these is no better alternative.

10.5.1 $B \to D \pi \ell \nu$

$$W_{jk}^{Sig}(w_k) = 1 \tag{297}$$

10.5.2 $B \to D^* \pi \ell \nu$

$$W_{jk}^{Sig}(w_k) = 1 \tag{298}$$

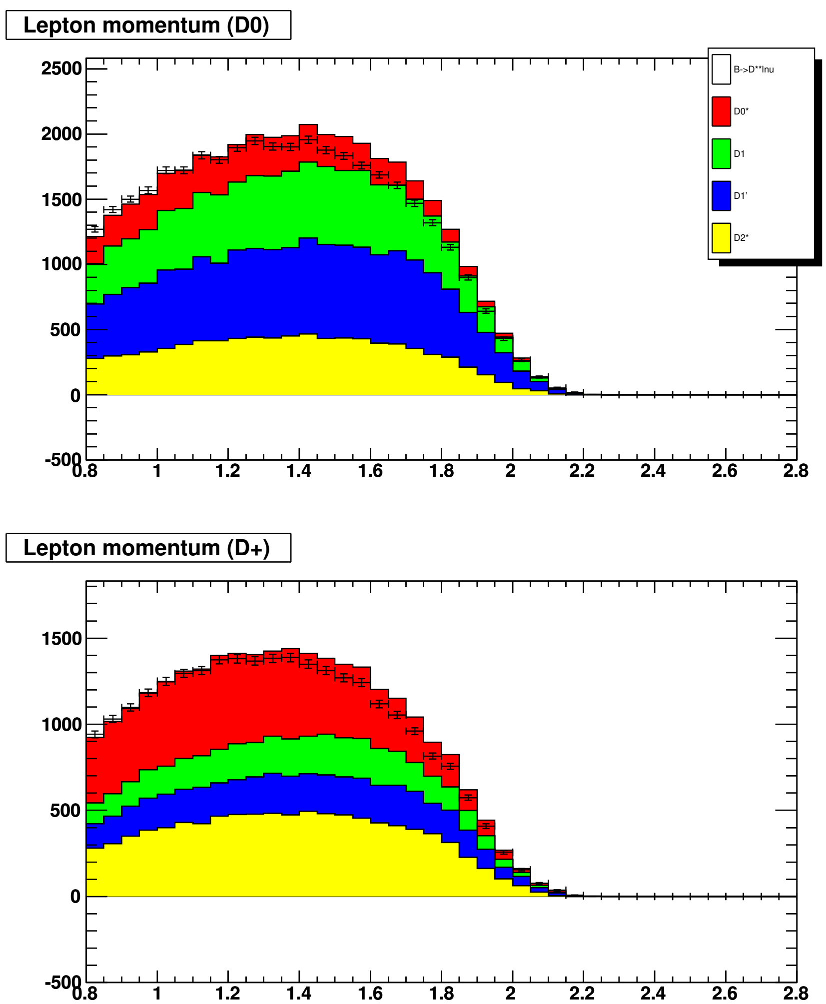

Figure 76: [p_ℓ **after** $B \to D^{**}\ell\nu$ **re-weighting**] Lepton momentum spectrum of $B \to D^{**}\ell\nu$ decays. Black line is ISGW2 model and colored histogram is HQET model. Red is D_0^*, green is D_1, blue is D_1' and yellow is D_2^*.

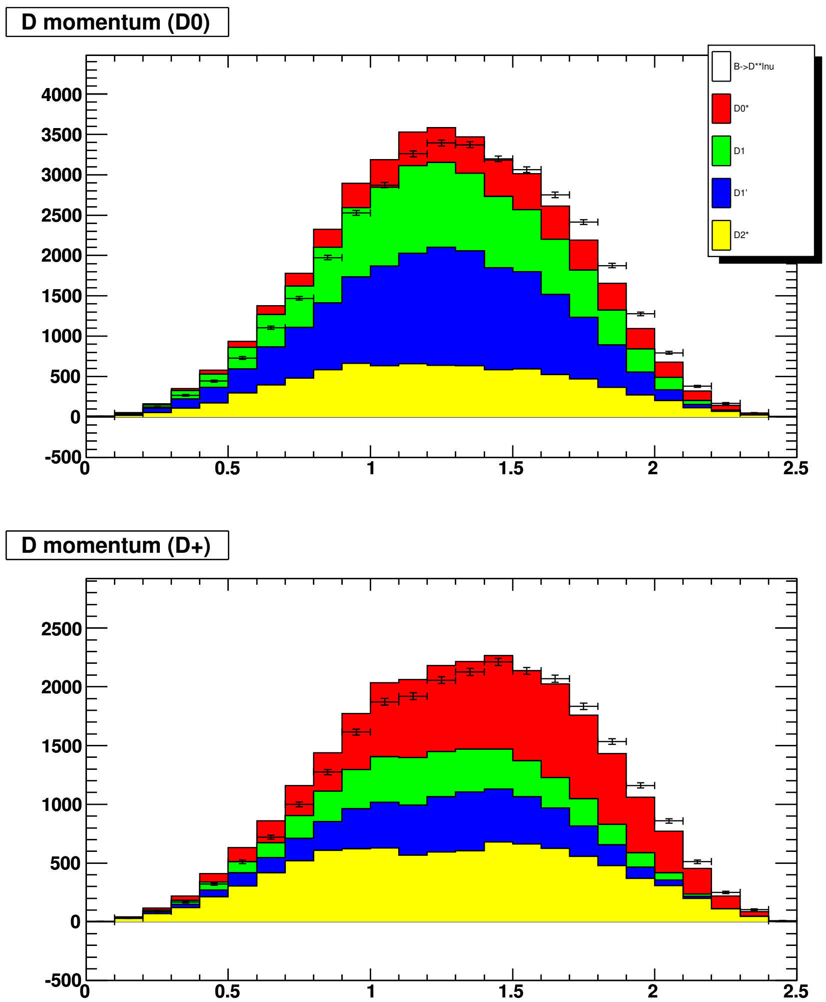

Figure 77: [p_D **after** $B \to D^{**}\ell\nu$ **re-weighting**] D momentum spectrum of $B \to D^{**}\ell\nu$ decays. Black line is ISGW2 model and colored histogram is HQET model. Red is D_0^*, green is D_1, blue is D_1' and yellow is D_2^*.

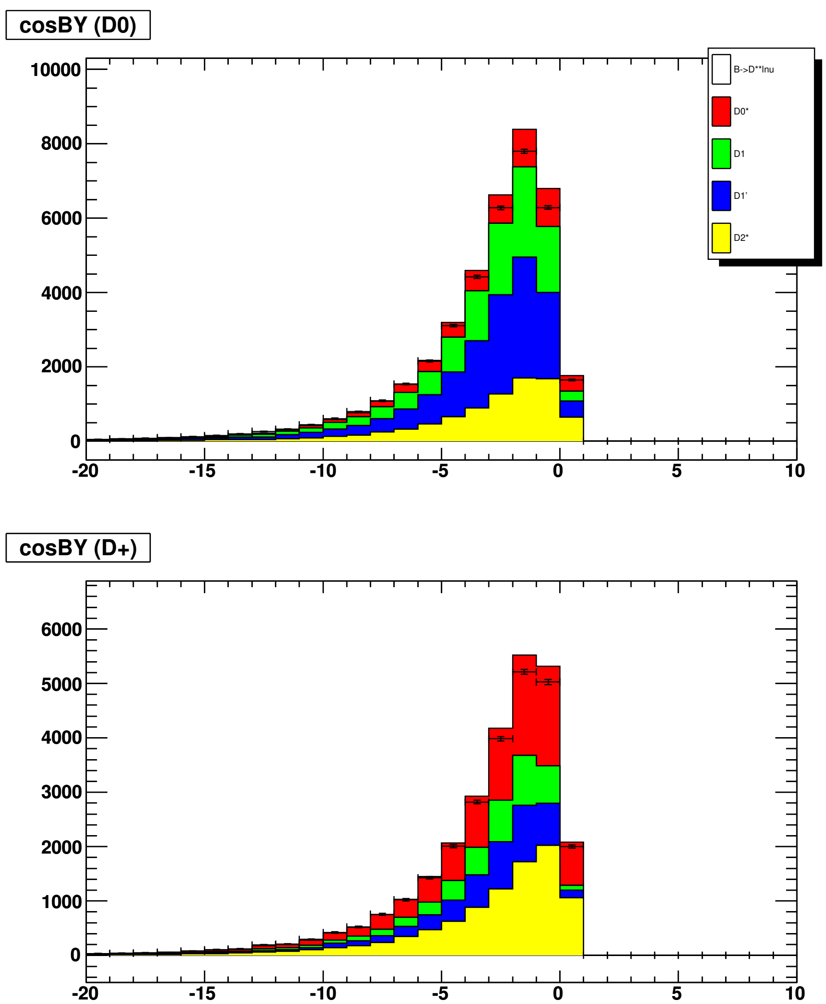

Figure 78: [$\cos\theta_{B-Dl}$ **after** $B \rightarrow D^{**}\ell\nu$ **re-weighting**] $\cos\theta_{B-Dl}$ of $B \rightarrow D^{**}\ell\nu$ decays. Black line is ISGW2 model and colored histogram is HQET model. Red is D_0^*, green is D_1, blue is D_1' and yellow is D_2^*.

10.6 Effect of FF re-weighting

Figure 79 - 87 show the lepton momentum, D momentum and $\cos\theta_{B-Dl}$ after FF re-weighting. To make these plots, we used

$$\begin{aligned} \rho_D^2 &= 1.17 \\ R_1 &= 1.417 \\ R_2 &= 0.836 \\ \rho^2 &= 1.179 \end{aligned} \tag{299}$$

with CLN parametrization and Approximation B1 as described above. We also used the B decay branching fraction given in section 5.2. These are the projections of 3D histograms. If you compare these with figure 48 - 56, you can see improvements of data-MC agreement.

We also show bin by bin plots in Figure 88 - 93.

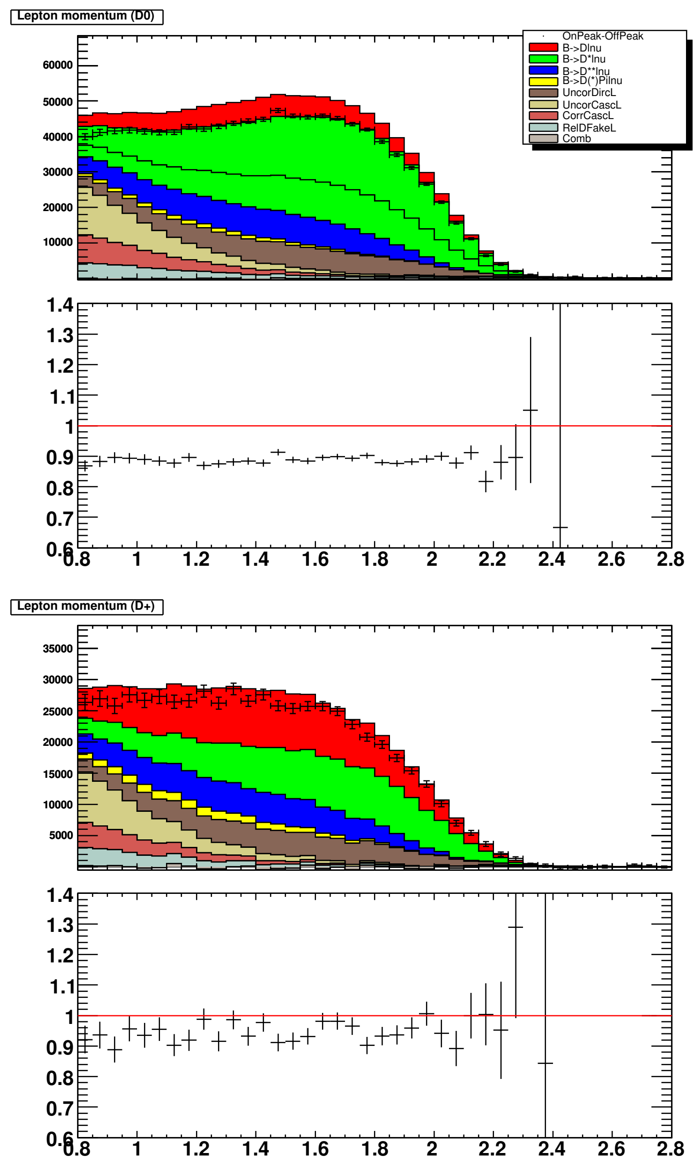

Figure 79: [p_ℓ **after FF re-weighting**] Lepton momentum plot after form factor re-weighting and D mass sideband subtraction. The top is D^0 and the bottom is D^+. Black is OnPeak - OffPeak data. Red is $B \to D\ell\nu$, green is $B \to D^*\ell\nu$, blue is $B \to D^{**}\ell\nu$, yellow is non-resonant $B \to D^{(*)}\pi\ell\nu$, and the rest is background. Dark brown is UncorrDL, light brown is UncorrCL, dark red is CascL, blue gray is FakeL, and light gray is Comb. Comb is almost disappeared after D mass sideband subtraction.

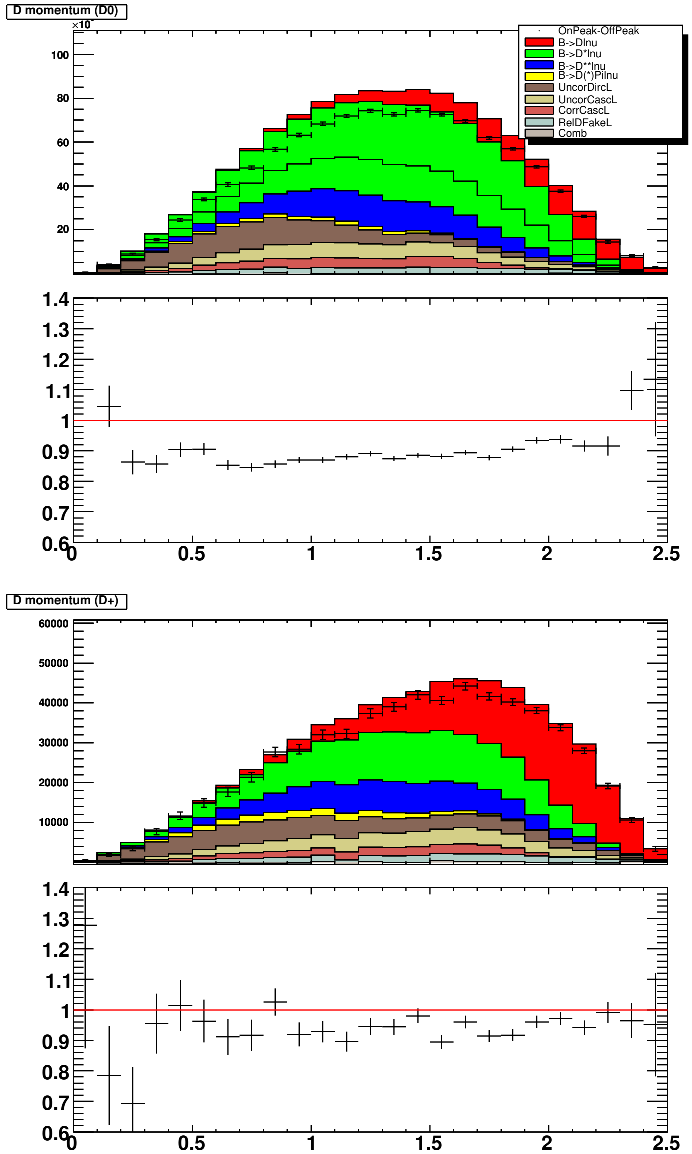

Figure 80: [p_D **after FF re-weighting**] D momentum plot after form factor re-weighting and D mass sideband subtraction. The top is D^0 and the bottom is D^+. Black is OnPeak - OffPeak data. Red is $B \to D\ell\nu$, green is $B \to D^*\ell\nu$, blue is $B \to D^{**}\ell\nu$, yellow is non-resonant $B \to D^{(*)}\pi\ell\nu$, and the rest is background. Dark brown is UncorrDL, light brown is UncorrCL, dark red is CascL, blue gray is FakeL, and light gray is Comb. Comb is almost disappeared after D mass sideband subtraction.

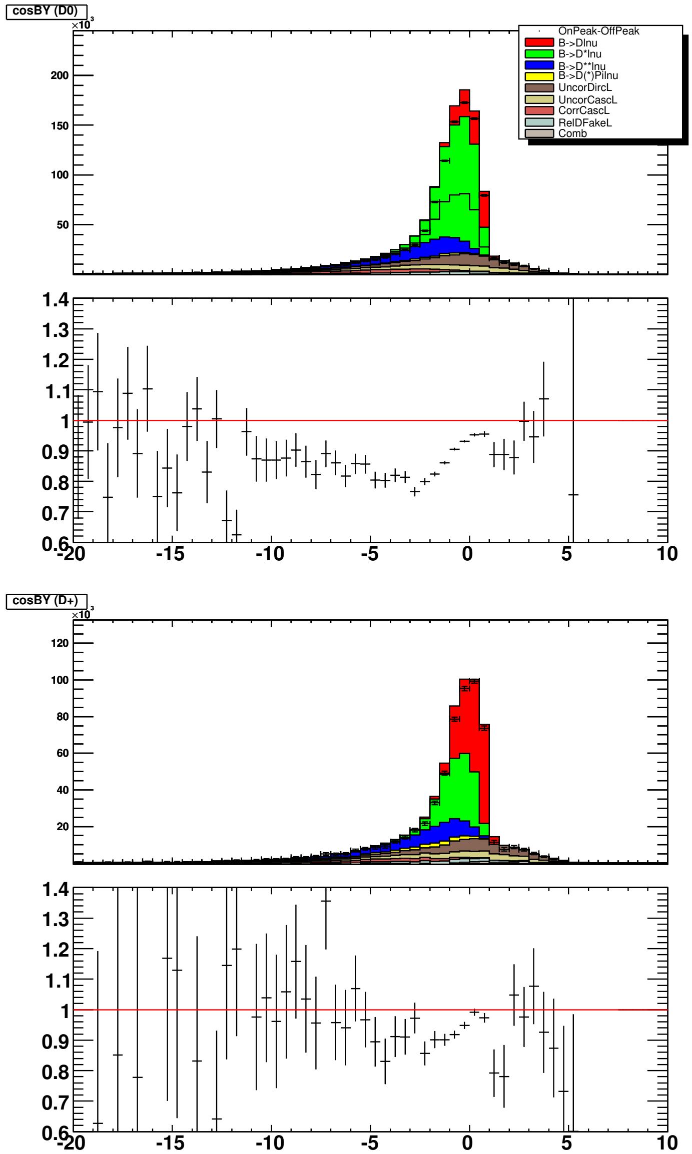

Figure 81: [$\cos\theta_{B-Dl}$ **after FF re-weighting**] $\cos\theta_{B-Dl}$ plot after form factor re-weighting and D mass sideband subtraction. The top is D^0 and the bottom is D^+. Black is OnPeak - OffPeak data. Red is $B \to D\ell\nu$, green is $B \to D^*\ell\nu$, blue is $B \to D^{**}\ell\nu$, yellow is non-resonant $B \to D^{(*)}\pi\ell\nu$, and the rest is background. Dark brown is UncorrDL, light brown is UncorrCL, dark red is CascL, blue gray is FakeL, and light gray is Comb. Comb is almost disappeared after D mass sideband subtraction.

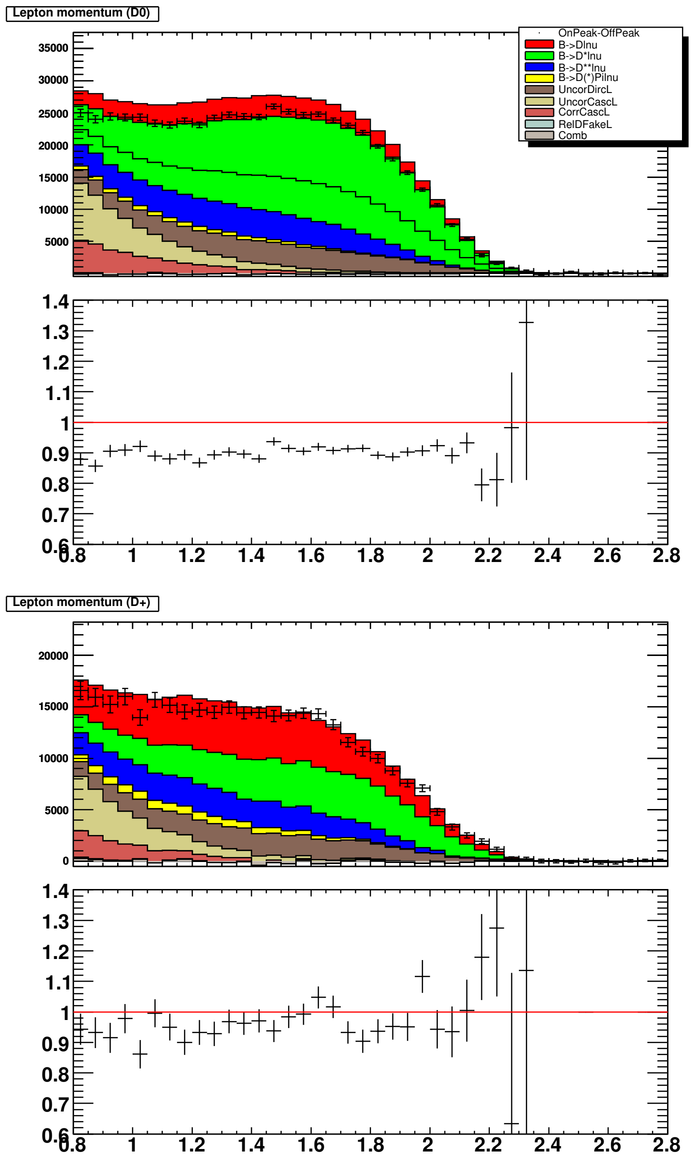

Figure 82: [p_ℓ **after FF re-weighting (Electron)**] Lepton momentum plot after form factor re-weighting and D mass sideband subtraction in the case $\ell = e$ (Electron only). The top is D^0 and the bottom is D^+. Black is OnPeak - OffPeak data. Red is $B \to D\ell\nu$, green is $B \to D^*\ell\nu$, blue is $B \to D^{**}\ell\nu$, yellow is non-resonant $B \to D^{(*)}\pi\ell\nu$, and the rest is background. Dark brown is UncorrDL, light brown is UncorrCL, dark red is CascL, blue gray is FakeL, and light gray is Comb. Comb is almost disappeared after D mass sideband subtraction.

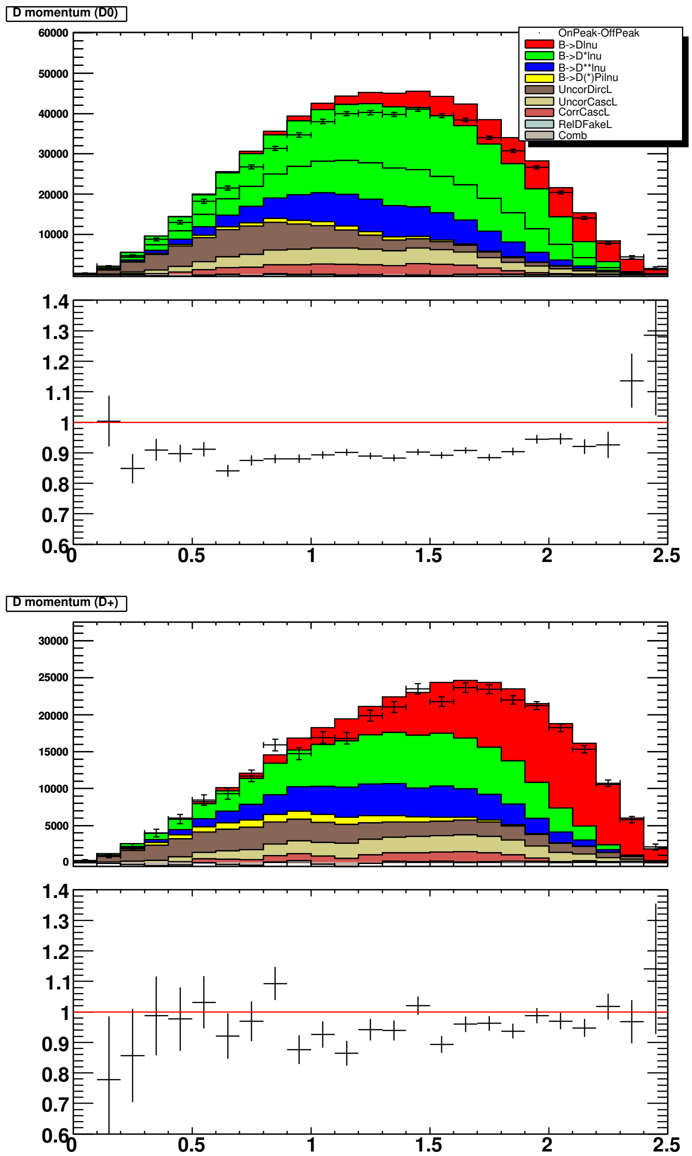

Figure 83: [p_D **after FF re-weighting (Electron)**] D momentum plot after form factor re-weighting and D mass sideband subtraction in the case $\ell = e$ (Electron only). The top is D^0 and the bottom is D^+. Black is OnPeak - OffPeak data. Red is $B \to D\ell\nu$, green is $B \to D^*\ell\nu$, blue is $B \to D^{**}\ell\nu$, yellow is non-resonant $B \to D^{(*)}\pi\ell\nu$, and the rest is background. Dark brown is UncorrDL, light brown is UncorrCL, dark red is CascL, blue gray is FakeL, and light gray is Comb. Comb is almost disappeared after D mass sideband subtraction.

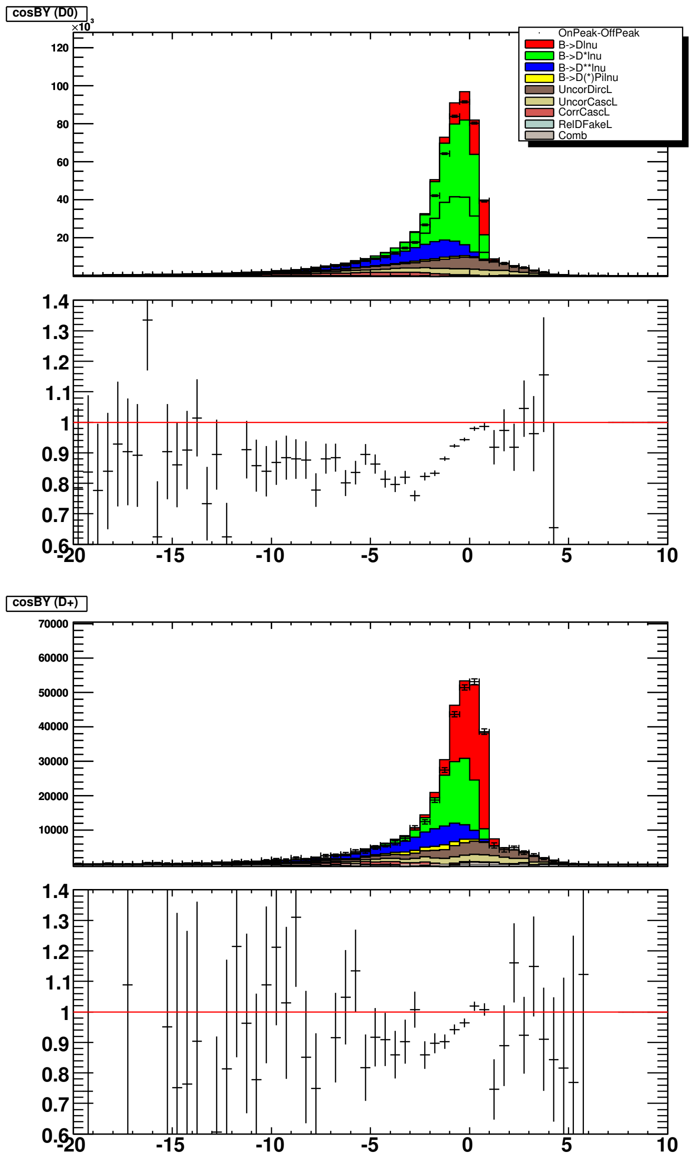

Figure 84: [$\cos\theta_{B-Dl}$ **after FF re-weighting (Electron)**] $\cos\theta_{B-Dl}$ plot after form factor re-weighting and D mass sideband subtraction in the case $\ell = e$ (Electron only). The top is D^0 and the bottom is D^+. Black is OnPeak - OffPeak data. Red is $B \to D\ell\nu$, green is $B \to D^*\ell\nu$, blue is $B \to D^{**}\ell\nu$, yellow is non-resonant $B \to D^{(*)}\pi\ell\nu$, and the rest is background. Dark brown is UncorrDL, light brown is UncorrCL, dark red is CascL, blue gray is FakeL, and light gray is Comb. Comb is almost disappeared after D mass sideband subtraction.

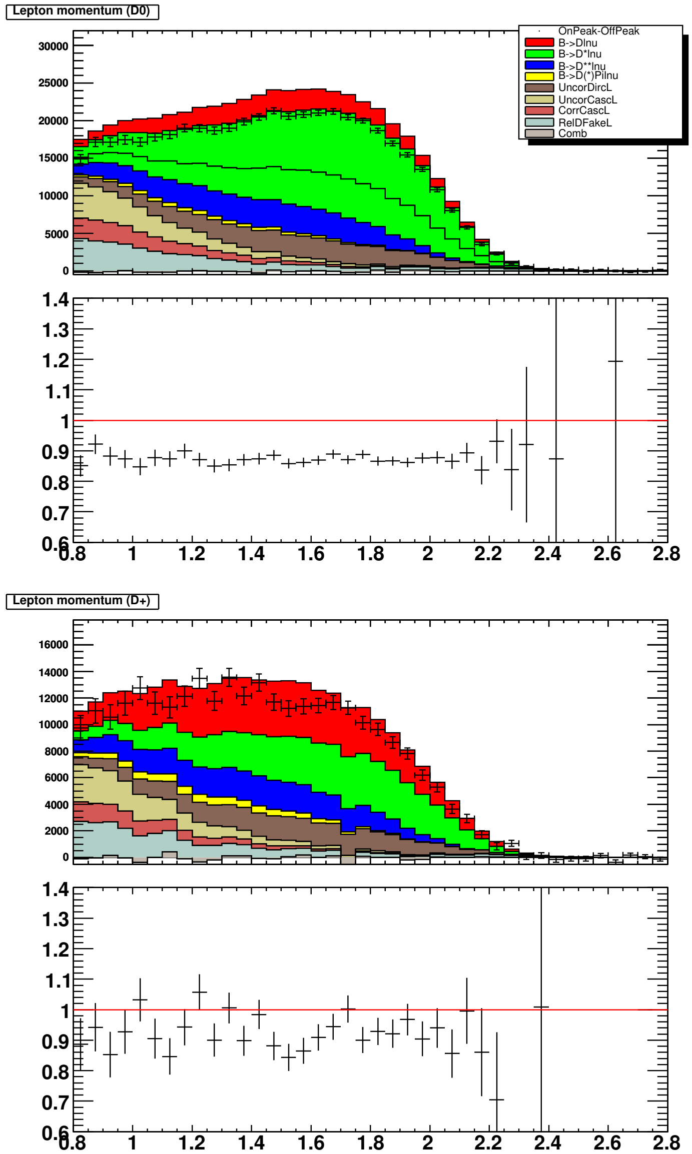

Figure 85: [p_ℓ **after FF re-weighting (Muon)**] Lepton momentum plot after form factor re-weighting and D mass sideband subtraction in the case $\ell = \mu$ (Muon only). The top is D^0 and the bottom is D^+. Black is OnPeak - OffPeak data. Red is $B \to D\ell\nu$, green is $B \to D^*\ell\nu$, blue is $B \to D^{**}\ell\nu$, yellow is non-resonant $B \to D^{(*)}\pi\ell\nu$, and the rest is background. Dark brown is UncorrDL, light brown is UncorrCL, dark red is CascL, blue gray is FakeL, and light gray is Comb. Comb is almost disappeared after D mass sideband subtraction.

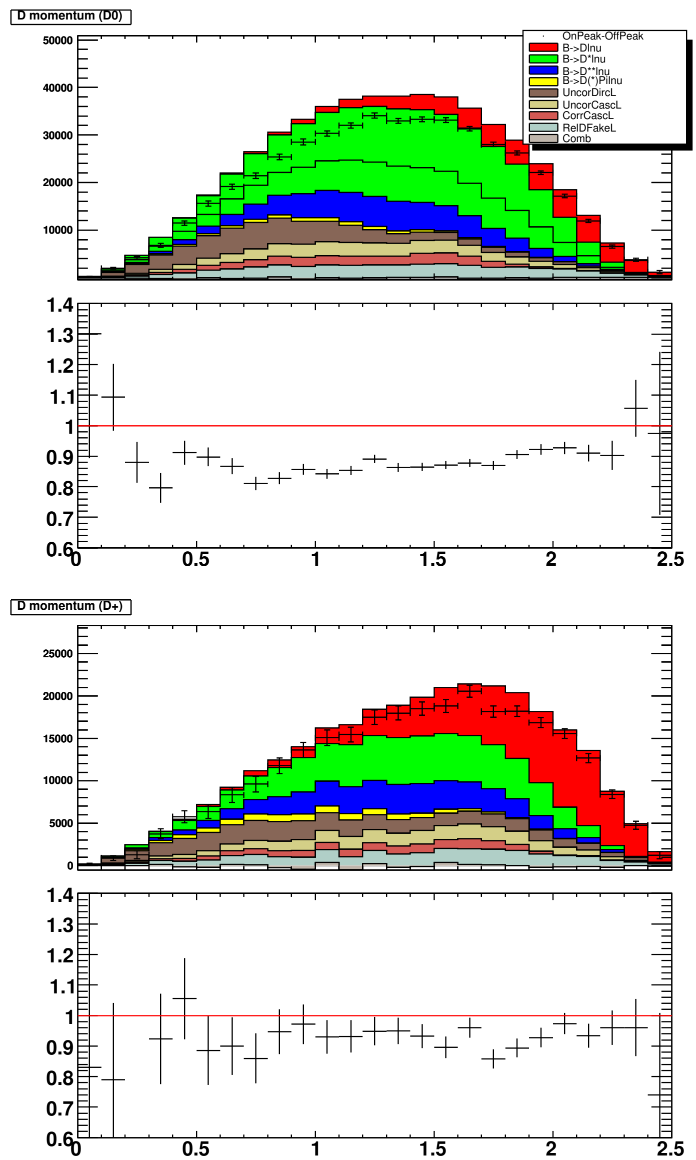

Figure 86: [p_D **after FF re-weighting (Muon)**] D momentum plot after form factor re-weighting and D mass sideband subtraction in the case $\ell = \mu$ (Muon only). The top is D^0 and the bottom is D^+. Black is OnPeak - OffPeak data. Red is $B \to D\ell\nu$, green is $B \to D^*\ell\nu$, blue is $B \to D^{**}\ell\nu$, yellow is non-resonant $B \to D^{(*)}\pi\ell\nu$, and the rest is background. Dark brown is UncorrDL, light brown is UncorrCL, dark red is CascL, blue gray is FakeL, and light gray is Comb. Comb is almost disappeared after D mass sideband subtraction.

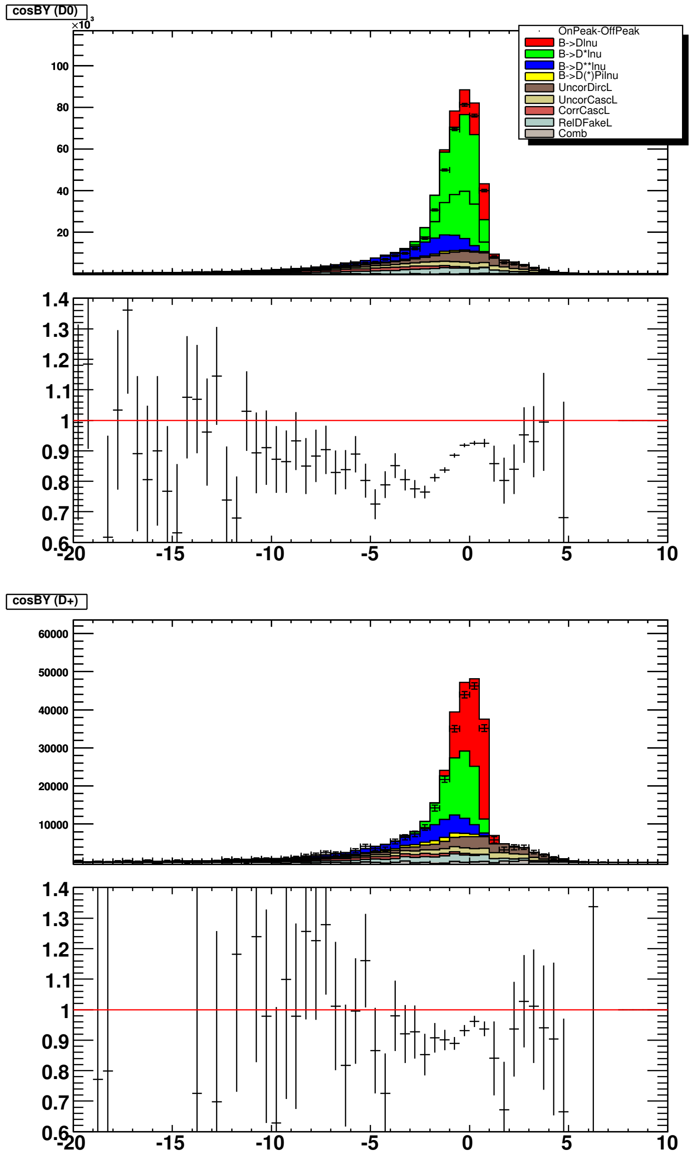

Figure 87: [$\cos\theta_{B-Dl}$ **after FF re-weighting (Muon)**] $\cos\theta_{B-Dl}$ plot after form factor re-weighting and D mass sideband subtraction in the case $\ell = \mu$ (Muon only). The top is D^0 and the bottom is D^+. Black is OnPeak - OffPeak data. Red is $B \to D\ell\nu$, green is $B \to D^*\ell\nu$, blue is $B \to D^{**}\ell\nu$, yellow is non-resonant $B \to D^{(*)}\pi\ell\nu$, and the rest is background. Dark brown is UncorrDL, light brown is UncorrCL, dark red is CascL, blue gray is FakeL, and light gray is Comb. Comb is almost disappeared after D mass sideband subtraction.

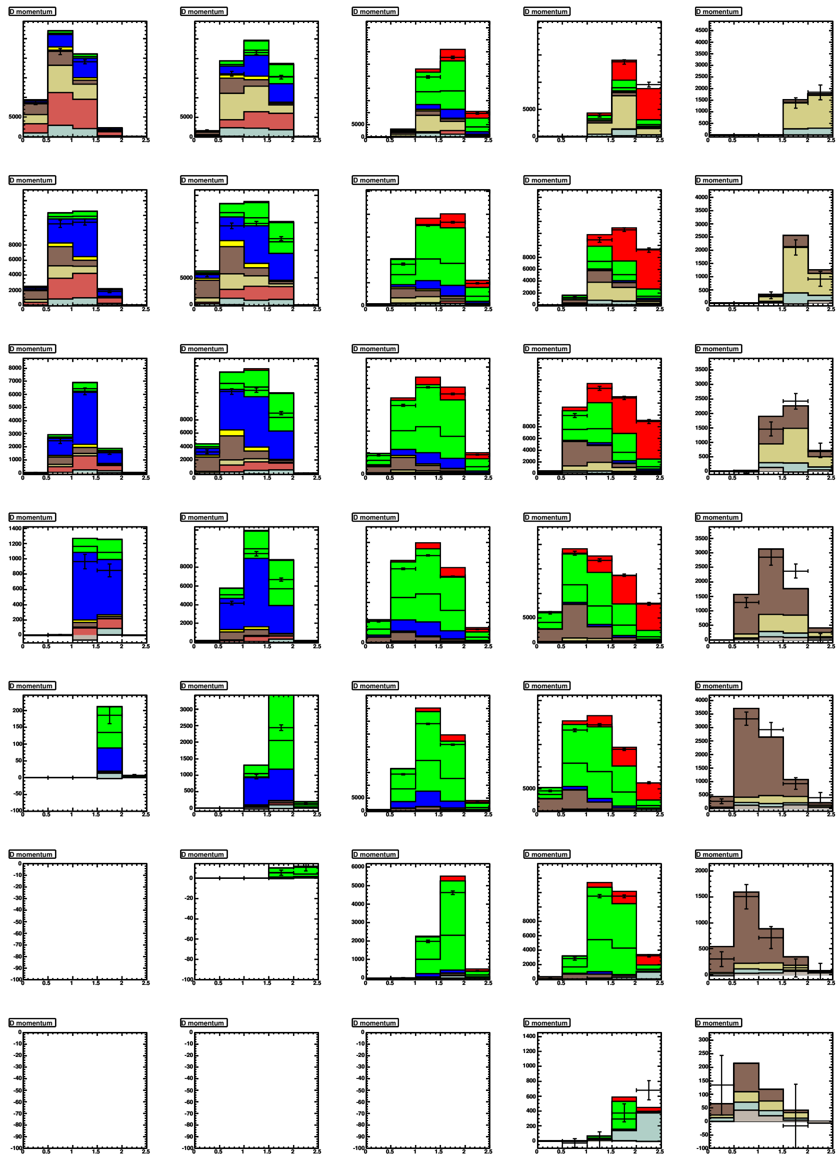

Figure 88: [**Bin by bin plot (D^0) aafter FF re-weighting**] D^0 momentum plots showing all bins after form factor re-weighting and D mass sideband subtraction. From top to bottom, lepton momentum bin changes from the lowest to the highest, and from left to right, cosBY bin changes from negative to positive. In each plots, colors are the same as other plots. Black is OnPeak - OffPeak data. Red is $B \to D\ell\nu$, green is $B \to D^*\ell\nu$, blue is $B \to D^{**}\ell\nu$, yellow is non-resonant $B \to D^{(*)}\pi\ell\nu$, and the rest is background. Dark brown is UncorrDL, light brown is UncorrCL, dark red is CascL, blue gray is FakeL, and light gray is Comb. Comb is almost disappeared after D mass sideband subtraction.

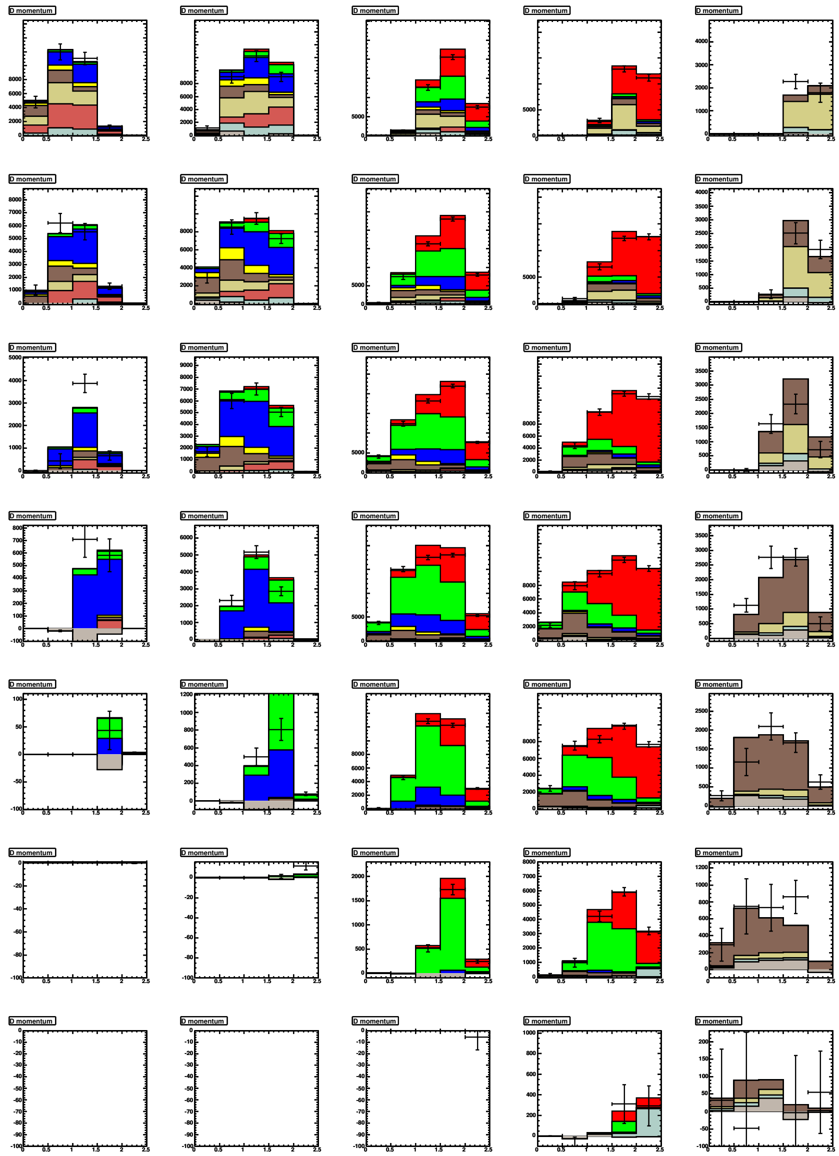

Figure 89: [**Bin by bin plot (D^+) aafter FF re-weighting**] D^+ momentum plots showing all bins after form factor re-weighting and D mass sideband subtraction. From top to bottom, lepton momentum bin changes from the lowest to the highest, and from left to right, cosBY bin changes from negative to positive. In each plots, colors are the same as other plots. Black is OnPeak - OffPeak data. Red is $B \to D\ell\nu$, green is $B \to D^*\ell\nu$, blue is $B \to D^{**}\ell\nu$, yellow is non-resonant $B \to D^{(*)}\pi\ell\nu$, and the rest is background. Dark brown is UncorrDL, light brown is UncorrCL, dark red is CascL, blue gray is FakeL, and light gray is Comb. Comb is almost disappeared after D mass sideband subtraction.

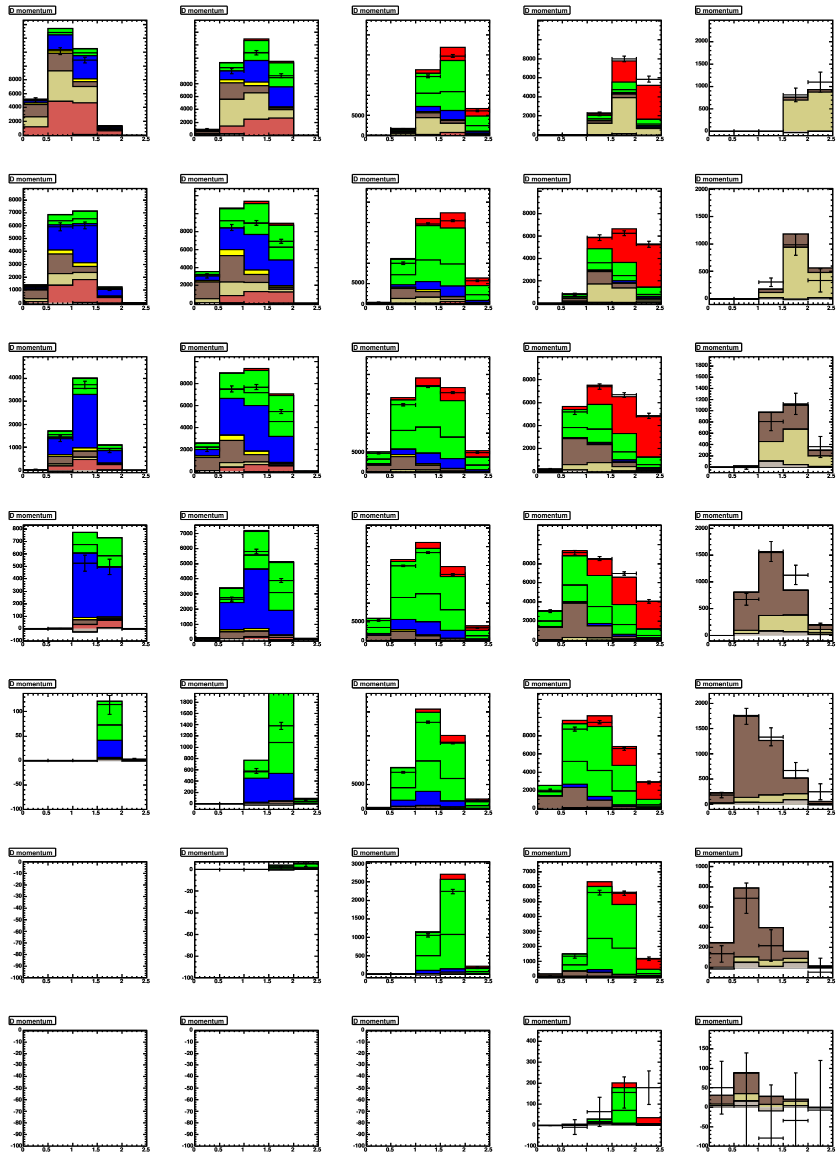

Figure 90: [**Bin by bin plot (D^0) aafter FF re-weighting, Electron**] D^0 momentum plots showing all bins after form factor re-weighting and D mass sideband subtraction in the case $\ell = e$ (Electron only). From top to bottom, lepton momentum bin changes from the lowest to the highest, and from left to right, cosBY bin changes from negative to positive. In each plots, colors are the same as other plots. Black is OnPeak - OffPeak data. Red is $B \to D\ell\nu$, green is $B \to D^*\ell\nu$, blue is $B \to D^{**}\ell\nu$, yellow is non-resonant $B \to D^{(*)}\pi\ell\nu$, and the rest is background. Dark brown is UncorrDL, light brown is UncorrCL, dark red is CascL, blue gray is FakeL, and light gray is Comb. Comb is almost disappeared after D mass sideband subtraction.

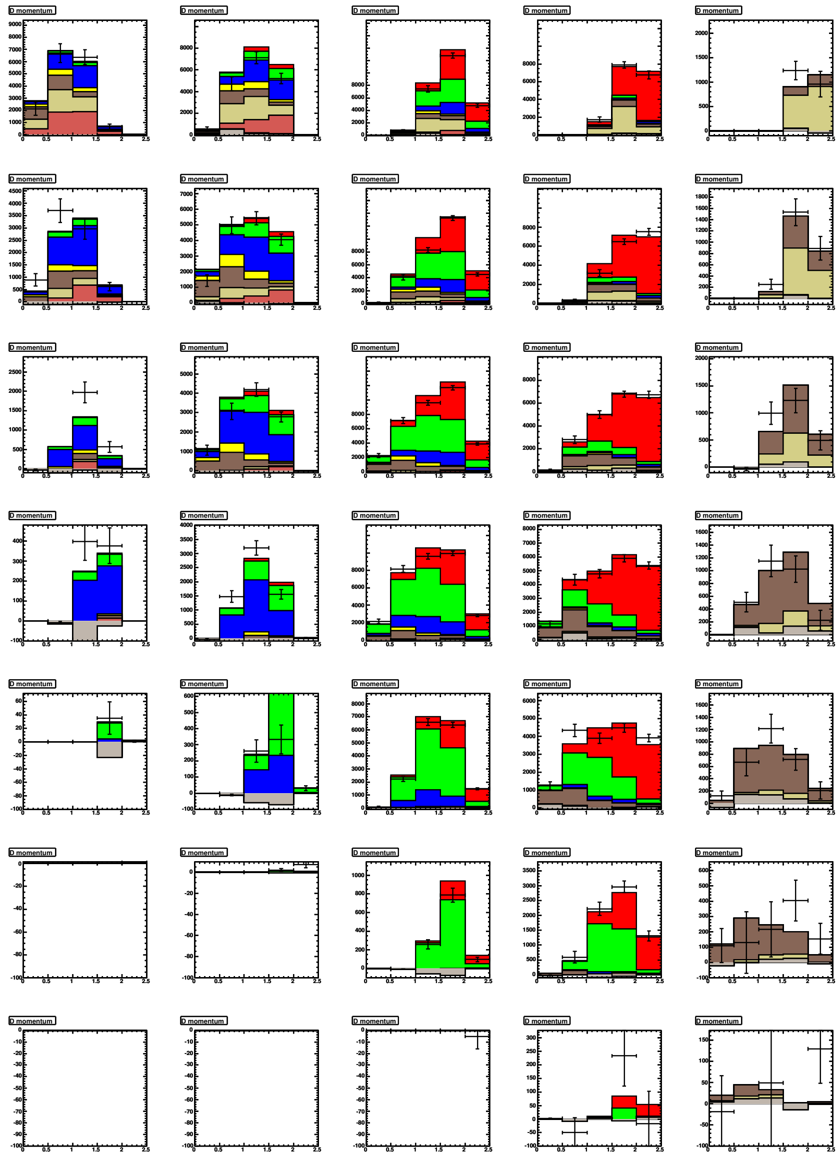

Figure 91: [**Bin by bin plot (D^+) aafter FF re-weighting, Electron**] D^+ momentum plots showing all bins after form factor re-weighting and D mass sideband subtraction in the case $\ell = e$ (Electron only). From top to bottom, lepton momentum bin changes from the lowest to the highest, and from left to right, cosBY bin changes from negative to positive. In each plots, colors are the same as other plots. Black is OnPeak - OffPeak data. Red is $B \to D\ell\nu$, green is $B \to D^*\ell\nu$, blue is $B \to D^{**}\ell\nu$, yellow is non-resonant $B \to D^{(*)}\pi\ell\nu$, and the rest is background. Dark brown is UncorrDL, light brown is UncorrCL, dark red is CascL, blue gray is FakeL, and light gray is Comb. Comb is almost disappeared after D mass sideband subtraction.

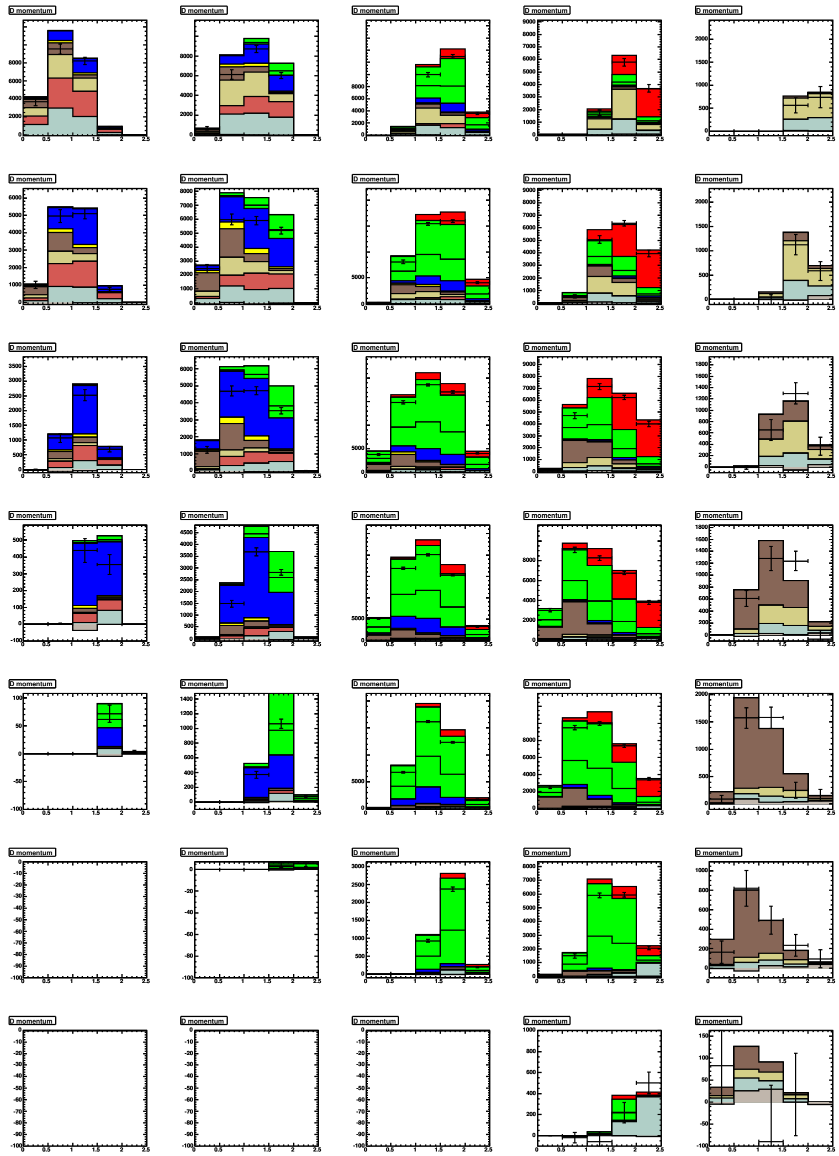

Figure 92: [**Bin by bin plot (D^0) aafter FF re-weighting, Muon**] D^0 momentum plots showing all bins after form factor re-weighting and D mass sideband subtraction in the case $\ell = \mu$ (Muon only). From top to bottom, lepton momentum bin changes from the lowest to the highest, and from left to right, cosBY bin changes from negative to positive. In each plots, colors are the same as other plots. Black is OnPeak - OffPeak data. Red is $B \to D\ell\nu$, green is $B \to D^*\ell\nu$, blue is $B \to D^{**}\ell\nu$, yellow is non-resonant $B \to D^{(*)}\pi\ell\nu$, and the rest is background. Dark brown is UncorrDL, light brown is UncorrCL, dark red is CascL, blue gray is FakeL, and light gray is Comb. Comb is almost disappeared after D mass sideband subtraction.

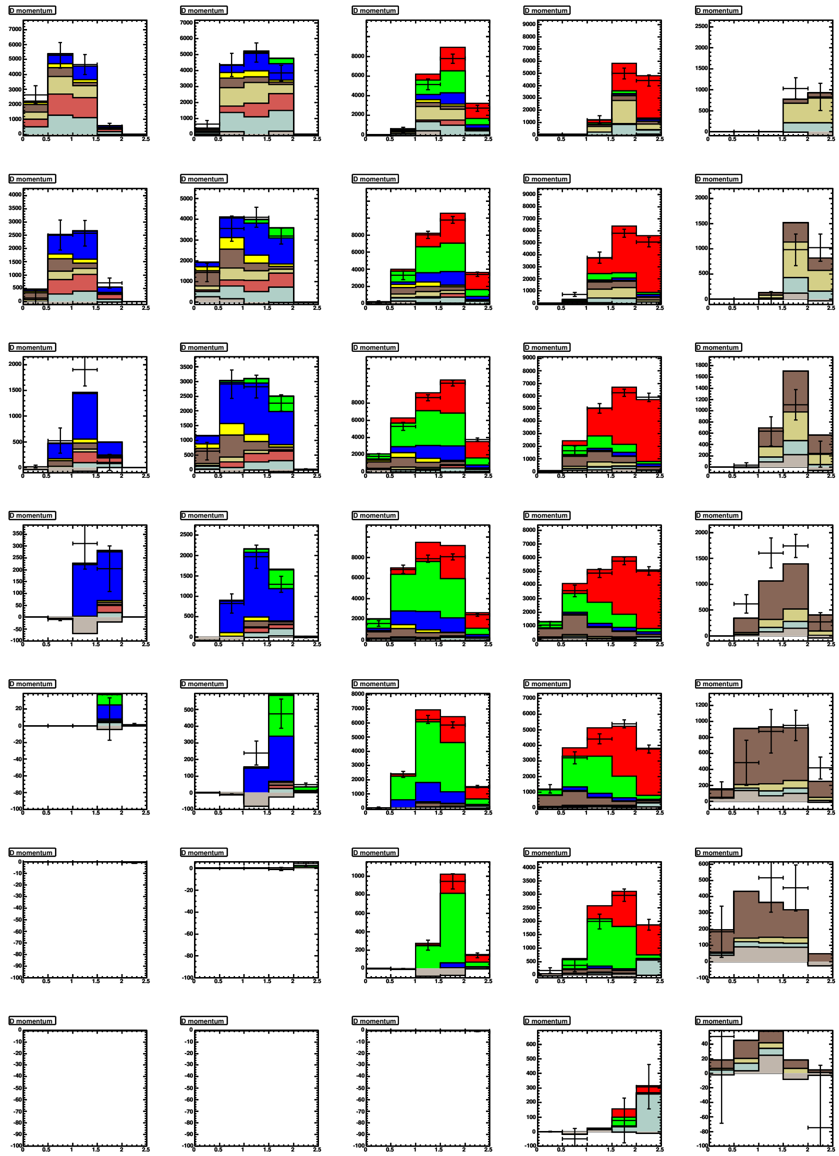

Figure 93: [**Bin by bin plot (D^+) aafter FF re-weighting, Muon**] D^+ momentum plots showing all bins after form factor re-weighting and D mass sideband subtraction in the case $\ell = \mu$ (Muon only). From top to bottom, lepton momentum bin changes from the lowest to the highest, and from left to right, cosBY bin changes from negative to positive. In each plots, colors are the same as other plots. Black is OnPeak - OffPeak data. Red is $B \to D\ell\nu$, green is $B \to D^*\ell\nu$, blue is $B \to D^{**}\ell\nu$, yellow is non-resonant $B \to D^{(*)}\pi\ell\nu$, and the rest is background. Dark brown is UncorrDL, light brown is UncorrCL, dark red is CascL, blue gray is FakeL, and light gray is Comb. Comb is almost disappeared after D mass sideband subtraction.

11 FF parameter fitting technique

11.1 $B \to D\ell\nu$ slope fitting

To fit for $B \to D\ell\nu$ slope, it is not computationally efficient to go through the calculation of the weight event by event. The following is a better way to do fitting.

11.1.1 Number of events

We may rewrite the weight (Equation (235))

$$W_{jk}^{MC}(w_k) = \left[\frac{[h_+(1)]^2}{[Rf_+]^2} - \frac{2(w-1)[h_+(1)]^2}{[Rf_+]^2}\rho_D^2 + \frac{(w-1)^2[h_+(1)]^2}{[Rf_+]^2}\left(\rho_D^2\right)^2\right] R_N \quad (300)$$

Hence, we define

$$W_{jk}^{MC}(w_k) \equiv \left[W_{jk}^0(w_k) - W_{jk}^1(w_k)\rho_D^2 + W_{jk}^2(w_k)\left(\rho_D^2\right)^2\right] R_N \quad (301)$$

Then, the number of events is

$$\begin{aligned} N_{ij}^{MC} = &\left[\sum_l \left(r_l^{Lumi} \sum_{k\in i,j,l} r_k^{Trk} r_k^{KPID} r_k^{LPID} W_{jk}^0\right)\right. \\ &- \sum_l \left(r_l^{Lumi} \sum_{k\in i,j,l} r_k^{Trk} r_k^{KPID} r_k^{LPID} W_{jk}^1\right)\rho_D^2 \\ &\left. + \sum_l \left(r_l^{Lumi} \sum_{k\in i,j,l} r_k^{Trk} r_k^{KPID} r_k^{LPID} W_{jk}^2\right)\left(\rho_D^2\right)^2\right] R_N \end{aligned} \quad (302)$$

Hence

$$N_{ij}^{MC} \equiv \left[N_{ij}^{MC0} - N_{ij}^{MC1}\rho_D^2 + N_{ij}^{MC2}\left(\rho_D^2\right)^2\right] R_N \quad (303)$$

Instead of going through event by event in fitting, first we create these three histograms (N_{ij}^{MC0}, N_{ij}^{MC1} and N_{ij}^{MC2}), and then use those histograms in fitting.
In another parametrization (Equation (237)).

$$\begin{aligned} &1 - 8\rho_D^2 z + (51\rho_D^2 - 10)z^2 - (252\rho_D^2 - 84)z^3 \\ &= (1 - 10z^2 + 84z^3) - (8z - 51z^2 + 252z^3)\rho_D^2 \end{aligned} \quad (304)$$

Thus, by replacing

$$\begin{aligned} &1 \to (1 - 10z^2 + 84z^3) \\ &(w-1) \to (8z - 51z^2 + 252z^3) \end{aligned} \quad (305)$$

we can use the same method

11.1.2 Weighted events and statistical uncertainty

Sine our events are weighted, calculation of statistical uncertainty is a little bit tricky. Suppose the weight of the k-th event or candidate is W_k and it is given by

$$W_k = F_{1k} - F_{2k}\rho_D^2 + F_{3k}\left(\rho_D^2\right)^2 \tag{306}$$

The number of events after D mass sideband subtraction is given by

$$\begin{aligned}\sum_k^{peak} W_k - \sum_k^{sideband} W_k = &\left(\sum_k^{peak} F_{1k} - \sum_k^{sideband} F_{1k}\right) \\ &- \left(\sum_k^{peak} F_{2k} - \sum_k^{sideband} F_{2k}\right)\rho_D^2 + \left(\sum_k^{peak} F_{3k} - \sum_k^{sideband} F_{3k}\right)\left(\rho_D^2\right)^2\end{aligned} \tag{307}$$

Thus, the number of events is still given by

$$N = \left[N_1 - N_2\rho_D^2 + N_3\left(\rho_D^2\right)^2\right] R_N \tag{308}$$

The square of statistical uncertainty is calculated by

$$\begin{aligned}\sum_k^{peak} W_k^2 + \sum_k^{sideband} W_k^2 = &\sum_k^{peak}\left(F_{1k} - F_{2k}\rho_D^2 + F_{3k}\left(\rho_D^2\right)^2\right)^2 \\ &+ \sum_k^{sideband}\left(F_{1k} - F_{2k}\rho_D^2 + F_{3k}\left(\rho_D^2\right)^2\right)^2\end{aligned} \tag{309}$$

Thus, no need to sum peak and sideband separately

$$\begin{aligned}\sum_k W_k^2 &= \sum_k \left(F_{1k} - F_{2k}\rho_D^2 + F_{3k}\left(\rho_D^2\right)^2\right)^2 \\ &= \sum_k F_{1k}^2 - \sum_k 2F_{1k}F_{2k}\rho_D^2 + \sum_k\left(2F_{1k}F_{3k} + F_{2k}^2\right)\left(\rho_D^2\right)^2 \\ &\quad - \sum_k 2F_{2k}F_{3k}\left(\rho_D^2\right)^3 + \sum_k F_{3k}^2\left(\rho_D^2\right)^4\end{aligned} \tag{310}$$

Hence, we need 5 histograms to calculate the square of statistical uncertainty

$$\sigma^2 = \left[N_1 - N_2\rho_D^2 + N_3\left(\rho_D^2\right)^2 - N_4\left(\rho_D^2\right)^3 + N_5\left(\rho_D^2\right)^4\right] R_N^2 \tag{311}$$

Note that in the above argumant, the sideband scale factor introduced in section 6 Equation (171), is included in the weight W_k (F_{nk}).

11.2 $B \to D^*\ell\nu$ parameter fitting

We may rewrite the $\mathcal{J}_{FF}(R_1, R_2, \rho^2)$. From equation (248),

$$\begin{aligned}
&\mathcal{J}_{FF}(R_1, R_2, \rho^2) \\
&= [F_1 - F_2\rho^2 + F_3(\rho^2)^2]\,[G_1 + G_2R_1 + G_3R_2 + G_4R_1^2 + G_5R_2^2 + G_6R_1R_2] \\
&= F_1G_1 - F_2G_1\rho^2 + F_3G_1(\rho^2)^2 \\
&\quad +F_1G_2R_1 - F_2G_2R_1\rho^2 + F_3G_2R_1(\rho^2)^2 \\
&\quad +F_1G_3R_2 - F_2G_3R_2\rho^2 + F_3G_3R_2(\rho^2)^2 \\
&\quad +F_1G_4R_1^2 - F_2G_4R_1^2\rho^2 + F_3G_4R_1^2(\rho^2)^2 \\
&\quad +F_1G_5R_2^2 - F_2G_5R_2^2\rho^2 + F_3G_5R_2^2(\rho^2)^2 \\
&\quad +F_1G_6R_1R_2 - F_2G_6R_1R_2\rho^2 + F_3G_6R_1R_2(\rho^2)^2
\end{aligned} \tag{312}$$

where, using the CLN parametrization of the slope,

$$
\begin{aligned}
F_1 &= (1 - 15z^2 + 91z^3)^2 \\
F_2 &= 2(1 - 15z^2 + 91z^3)(8z - 53z^2 + 231z^3) \\
F_3 &= (8z - 53z^2 + 231z^3)^2 \\
G_6 &= (-4)\sqrt{1-c_L^2}(1-c_L)\sqrt{1-c_V^2}c_V c_\chi\sqrt{1-2wr+r^2}(w-1)\sqrt{\tfrac{w-1}{w+1}} \\
&\quad +4\sqrt{1-c_L^2}(1+c_L)\sqrt{1-c_V^2}c_V c_\chi\sqrt{1-2wr+r^2}(-1)(w-1)\sqrt{\tfrac{w-1}{w+1}} \\
G_4 &= (1-c_L)^2(1-c_V^2)(1-2wr+r^2)\tfrac{w-1}{w+1} \\
&\quad +(1+c_L)^2(1-c_V^2)(1-2wr+r^2)\tfrac{w-1}{w+1} \\
&\quad +(-2)(1-c_L^2)(1-c_V^2)(2c_\chi^2-1)(1-2wr+r^2)(-1)\tfrac{w-1}{w+1} \\
G_2 &= (1-c_L)^2(1-c_V^2)(1-2wr+r^2)(-2)\sqrt{\tfrac{w-1}{w+1}} \\
&\quad +(1+c_L)^2(1-c_V^2)(1-2wr+r^2)(+2)\sqrt{\tfrac{w-1}{w+1}} \\
&\quad +(-4)\sqrt{1-c_L^2}(1-c_L)\sqrt{1-c_V^2}c_V c_\chi\sqrt{1-2wr+r^2}(-1)(w-r)\sqrt{\tfrac{w-1}{w+1}} \\
&\quad +4\sqrt{1-c_L^2}(1+c_L)\sqrt{1-c_V^2}c_V c_\chi\sqrt{1-2wr+r^2}(w-r)\sqrt{\tfrac{w-1}{w+1}} \\
&\quad +2G_4A_1 + G_6A_2 \\
G_5 &= 4(1-c_L^2)c_V^2(w-1)^2 \\
G_3 &= 4(1-c_L^2)c_V^2(-2)(w-r)(w-1) \\
&\quad +(-4)\sqrt{1-c_L^2}(1-c_L)\sqrt{1-c_V^2}c_V c_\chi\sqrt{1-2wr+r^2}(-1)(w-1) \\
&\quad +4\sqrt{1-c_L^2}(1+c_L)\sqrt{1-c_V^2}c_V c_\chi\sqrt{1-2wr+r^2}(-1)(w-1) \\
&\quad +2G_5A_2 + G_6A_1 \\
G_1 &= (1-c_L)^2(1-c_V^2)(1-2wr+r^2) \\
&\quad +(1+c_L)^2(1-c_V^2)(1-2wr+r^2) \\
&\quad +4(1-c_L^2)c_V^2(w-r)^2 \\
&\quad +(-2)(1-c_L^2)(1-c_V^2)(2c_\chi^2-1)(1-2wr+r^2) \\
&\quad +(-4)\sqrt{1-c_L^2}(1-c_L)\sqrt{1-c_V^2}c_V c_\chi\sqrt{1-2wr+r^2}(w-r) \\
&\quad +4\sqrt{1-c_L^2}(1+c_L)\sqrt{1-c_V^2}c_V c_\chi\sqrt{1-2wr+r^2}(w-r) \\
&\quad +(G_2 - 2G_4A_1 - G_6A_2)A_1 - (G_3 - 2G_5A_2 - G_6A_1)A_2 + G_4A_1^2 + G_5A_2^2 + G_6A_1A_2
\end{aligned}
\tag{313}
$$

where

$$
\begin{aligned}
A_1 &= -0.12(w-1) + 0.05(w-1)^2 \\
A_2 &= 0.11(w-1) - 0.06(w-1)^2
\end{aligned}
\tag{314}
$$

Thus, same as previous section, we can, first, make 18 histograms corresponding to the 18 terms in the above $\mathcal{J}_{FF}(R_1, R_2, \rho^2)$. Then we can calculate the number of events N

$$\begin{aligned}
N = [&N_1 - N_2\rho^2 + N_3(\rho^2)^2 \\
&+N_4R_1 - N_5R_1\rho^2 + N_6R_1(\rho^2)^2 \\
&+N_7R_2 - N_8R_2\rho^2 + N_9R_2(\rho^2)^2 \\
&+N_{10}R_1^2 - N_{11}R_1^2\rho^2 + N_{12}R_1^2(\rho^2)^2 \\
&+N_{13}R_2^2 - N_{14}R_2^2\rho^2 + N_{15}R_2^2(\rho^2)^2 \\
&+N_{16}R_1R_2 - N_{17}R_1R_2\rho^2 + N_{18}R_1R_2(\rho^2)^2]\, R_N
\end{aligned} \tag{315}$$

The square of statistical uncertainty can also be calculated in the same way.

$$\begin{aligned}
&\left[F_1 - F_2\rho^2 + F_3(\rho^2)^2\right]^2 \left[G_1 + G_2R_1 + G_3R_2 + G_4R_1^2 + G_5R_2^2 + G_6R_1R_2\right]^2 \\
&= [F_1^2 - 2F_1F_2\rho^2 + (2F_1F_3 + F_2^2)(\rho^2)^2 - 2F_2F_3(\rho^2)^3 + F_3^2(\rho^2)^4] \\
&\quad [G_1^2 + 2G_1G_2R_1 + 2G_1G_3R_2 \\
&\quad\; +(2G_1G_4 + G_2^2)R_1^2 + (2G_1G_5 + G_3^2)R_2^2 + 2(G_1G_6 + G_2G_3)R_1R_2 \\
&\quad\; +2G_2G_4R_1^3 + 2G_3G_5R_2^3 + 2(G_2G_6 + G_3G_4)R_1^2R_2 + 2(G_2G_5 + G_3G_6)R_1R_2^2 \\
&\quad\; +G_4^2R_1^4 + G_5^2R_2^4 + 2G_4G_6R_1^3R_2 + 2G_5G_6R_1R_2^3 + (2G_4G_5 + G_6^2)R_1^2R_2^2]
\end{aligned} \tag{316}$$

Thus, we need $5 \times 15 = 75$ histograms to calculate the statistical uncertainty.

12 Test Fit

12.1 Binning

We use the following binning :

- lepton momentum in the CM frame p^*_ℓ
  (6 bins (GeV)) : 0.8, 1.05, 1.3, 1.55, 1.8, 2.05, 2.3
- D momentum in the CM frame p^*_D
  (5 bins (GeV)) : 0, 0.5, 1, 1.5, 2.0, 2.5
- $\cos\theta_{B-Dl}$ (see below)
  (5 bins) : -20, -5.5, -2, 0, 2, 10

The binning is decided in the valance of two opposing requirements :

- It needs to be as fine as possible to preserve the shape of original distribution.
- It needs to be as coarse as necessary to have a good statistics per bin.

The binning of p^*_ℓ is finer to get finer lepton spectrum because lepton moentum spectrum is well modeled in MC.

12.2 Summary of the fitting configuration

In this fit, we are trying to fit for three branching fractions and $\Upsilon(4S)$ decay BF ratio

- $\mathcal{B}(B^+ \to \bar{D}^0\ell^+\nu)$
- $\mathcal{B}(B^+ \to \bar{D}^{*0}\ell^+\nu)$
- $\mathcal{BT}(B^+ \to \bar{D}^{**0}/(D\pi)^0\ell^+\nu)$
- f_{+0}

with isospin constraints

- $\mathcal{B}(B^+ \to \bar{D}^0\ell^+\nu) = t_{+0}\mathcal{B}(B^0 \to D^-\ell^+\nu)$
- $\mathcal{B}(B^+ \to \bar{D}^{*0}\ell^+\nu) = t_{+0}\mathcal{B}(B^0 \to D^{*-}\ell^+\nu)$
- $\mathcal{B}(B^+ \to \bar{D}^{*0}_0\ell^+\nu) = t_{+0}\mathcal{B}(B^0 \to D^{*-}_0\ell^+\nu)$
- $\mathcal{B}(B^+ \to \bar{D}^0_1\ell^+\nu) = t_{+0}\mathcal{B}(B^0 \to D^-_1\ell^+\nu)$
- $\mathcal{B}(B^+ \to \bar{D}^{*0}_1\ell^+\nu) = t_{+0}\mathcal{B}(B^0 \to D'^-_1\ell^+\nu)$
- $\mathcal{B}(B^+ \to \bar{D}^{*0}_2\ell^+\nu) = t_{+0}\mathcal{B}(B^0 \to D^{*-}_2\ell^+\nu)$
- $\mathcal{B}(B^+ \to D^-\pi^+\ell^+\nu) = 2\mathcal{B}(B^+ \to \bar{D}^0\pi^0\ell^+\nu)$
  $= t_{+0}\mathcal{B}(B^0 \to \bar{D}^0\pi^-\ell^+\nu) = 2t_{+0}\mathcal{B}(B^0 \to D^-\pi^0\ell^+\nu)$

- $\mathcal{B}(B^+ \to D^{*-}\pi^+\ell^+\nu) = 2\mathcal{B}(B^+ \to \bar{D}^{*0}\pi^0\ell^+\nu)$
  $= t_{+0}\mathcal{B}(B^0 \to \bar{D}^{*0}\pi^-\ell^+\nu) = 2t_{+0}\mathcal{B}(B^0 \to D^{*-}\pi^0\ell^+\nu)$

and constraints on relative branching fractions

- $f_{D_2^*/D_1} \equiv \frac{\mathcal{B}(B^+\to\bar{D}_2^{*0}\ell^+\nu)}{\mathcal{B}(B^+\to\bar{D}_1^0\ell^+\nu)} = 0.78 \pm 0.17$
- $f_{D_0^*D\pi T/D_1D_2^*T} \equiv \frac{\mathcal{BT}(B^+\to\bar{D}_0^{*0}/(D\pi)^0\ell^+\nu)}{\mathcal{BT}(B^+\to\bar{D}_1^0/\bar{D}_2^{*0}\ell^+\nu)} = 0.77 \pm 0.19$
- $f_{D_1'D^*\pi T/D_1D_2^*T} \equiv \frac{\mathcal{BT}(B^+\to\bar{D}_1^{*0}/(D^*\pi)^0\ell^+\nu)}{\mathcal{BT}(B^+\to\bar{D}_1^0/\bar{D}_2^{*0}\ell^+\nu)} = 0.98 \pm 0.24$
- $f_{D\pi/D_0^*} \equiv \frac{\mathcal{B}(B^+\to D^-\pi^+\ell^+\nu)}{\mathcal{B}(B^+\to\bar{D}_0^{*0}\ell^+\nu)} = 0.42 \pm 0.28$
- $f_{D^*\pi/D_1'} \equiv \frac{\mathcal{B}(B^+\to D^{*-}\pi^+\ell^+\nu)}{\mathcal{B}(B^+\to\bar{D}_1^{*0}\ell^+\nu)} = 0.071 \pm 0.050$

and by floating background components

- $C^{D^0}_{UncorDL}$
- $C^{D^0}_{UncorCL}$
- $C^{D^0}_{CascL}$
- $C^{D^+}_{UncorDL}$
- $C^{D^+}_{UncorCL}$
- $C^{D^+}_{CascL}$

but fixing background components

- $C^{D^0}_{FakeL} = 1$
- $C^{D^+}_{FakeL} = 1$

In addition, we are fitting for form factor parameters

- $B \to D\ell\nu$ decay FF slope : ρ_D^2
- $B \to D^*\ell\nu$ decay FF slope : ρ^2
- $B \to D^*\ell\nu$ decay FF ratio : R_1
- $B \to D^*\ell\nu$ decay FF ratio : R_2

by fixing

- $B \to D^{**}\ell\nu$ decay FF slope : $\hat{\tau}' = -1.5 \pm 0.5$
- Approximation B1 : $\tau_1 = 0, \tau_2 = 0$
  for systematics, Approximation B2 : $\tau_1 = \bar{\Lambda}\tau, \tau_2 = -\bar{\Lambda}'\tau$
  (see details of $B \to D^{**}\ell\nu$ decay FF in Appendix H)

Parameters	f_{+0} floated	f_{+0} fixed
ρ_D^2	1.239 ± 0.042 (3.3 %)	1.225 ± 0.042 (3.4 %)
ρ^2	1.316 ± 0.038 (2.9 %)	1.311 ± 0.039 (2.9 %)
R_1	1.408 ± 0.055 (3.9 %)	1.402 ± 0.055 (3.9 %)
R_2	0.764 ± 0.048 (6.3 %)	0.763 ± 0.049 (6.4 %)
$\mathcal{B}(B^+ \to \bar{D}^0 \ell^+ \nu)$	0.02383 ± 0.00033 (1.4 %)	0.02360 ± 0.00029 (1.2 %)
$\mathcal{B}(B^+ \to \bar{D}^{*0} \ell^+ \nu)$	0.05246 ± 0.00045 (0.87 %)	0.05284 ± 0.00037 (0.70 %)
$\mathcal{BT}(B^+ \to \bar{D}^{**0}/(D\pi)^0 \ell^+ \nu)$	0.02039 ± 0.00043 (2.1 %)	0.02025 ± 0.00043 (2.1 %)
f_{+0}	1.060 ± 0.016 (1.5 %)	1.037 (Fixed)
$C_{UncorDL}^{D^0}$	0.763 ± 0.034 (4.4 %)	0.762 ± 0.034 (4.5 %)
$C_{UncorCL}^{D^0}$	0.830 ± 0.035 (4.2 %)	0.838 ± 0.035 (4.2 %)
$C_{CascL}^{D^0}$	0.950 ± 0.081 (8.5 %)	0.952 ± 0.051 (8.5 %)
$C_{UncorDL}^{D^+}$	0.802 ± 0.105 (13.1 %)	0.786 ± 0.111 (14.1 %)
$C_{UncorCL}^{D^+}$	0.756 ± 0.072 (9.6 %)	0.740 ± 0.071 (9.7 %)
$C_{CascL}^{D^+}$	0.939 ± 0.130 (13.8 %)	0.928 ± 0.148 (16.0 %)
χ^2/ndof (P-value)	407/223 (5.0×10^{-14})	409/224 (4.2×10^{-14})

Table 24: [**Test fit results**] Test fit results.

12.3 Fit results

Fit results are shown in Table 24. Though we did a lot of corrections and re-weightings, χ^2 (P-value) is terrybly bad. We think this is still due to poor MC description of $B \to D^{**}\ell\nu$ and $B \to D^{(*)}\pi\ell\nu$ decays and backgrounds. Projected plots after fitting is shown in Figures 94-96. Significant amount of those components can be seen in these plots. In order to reduce data-MC disagreement, we try to reduce these components. Details are explained in the next section.

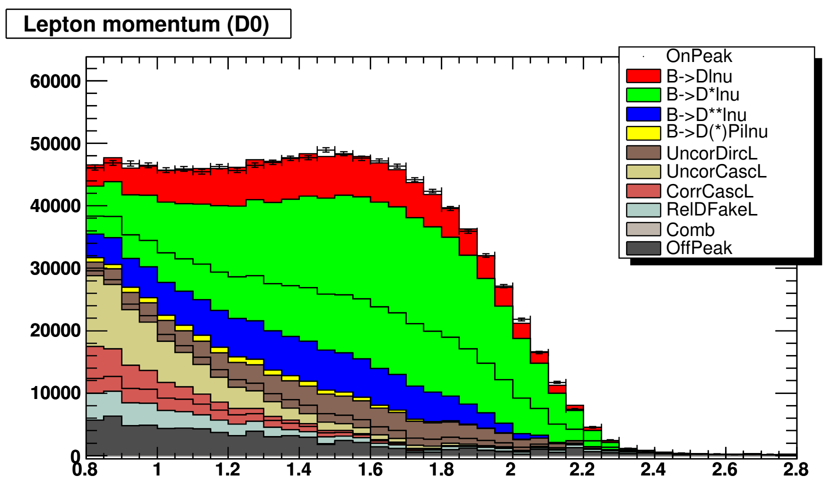

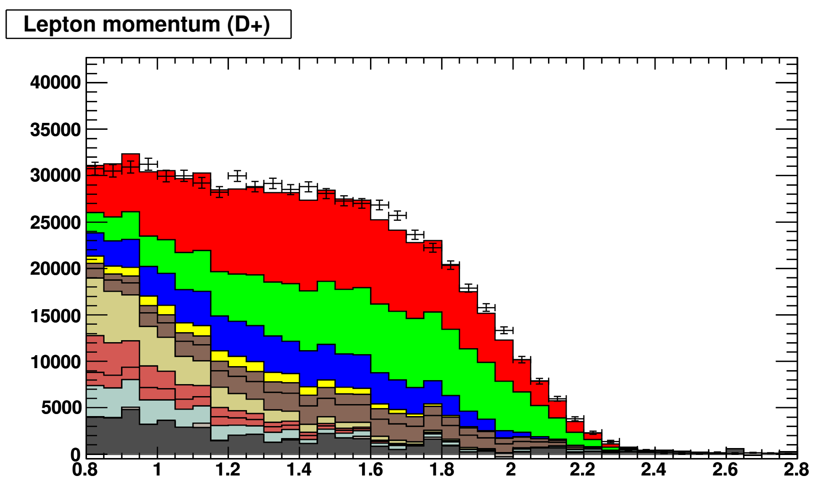

Figure 94: [p_ℓ **after fitting**] Lepton momentum plot after fitting. The top is D^0 and the bottom is D^+. Black is OnPeak data. Red is $B \to D\ell\nu$, green is $B \to D^*\ell\nu$, blue is $B \to D^{**}\ell\nu$, yellow is non-resonant $B \to D^{(*)}\pi\ell\nu$, and the rest is background. Dark brown is UncorrDL, light brown is UncorrCL, dark red is CascL, blue gray is FakeL, light gray is Comb and dark gray is OffPeak. Comb is almost disappeared after D mass sideband subtraction.

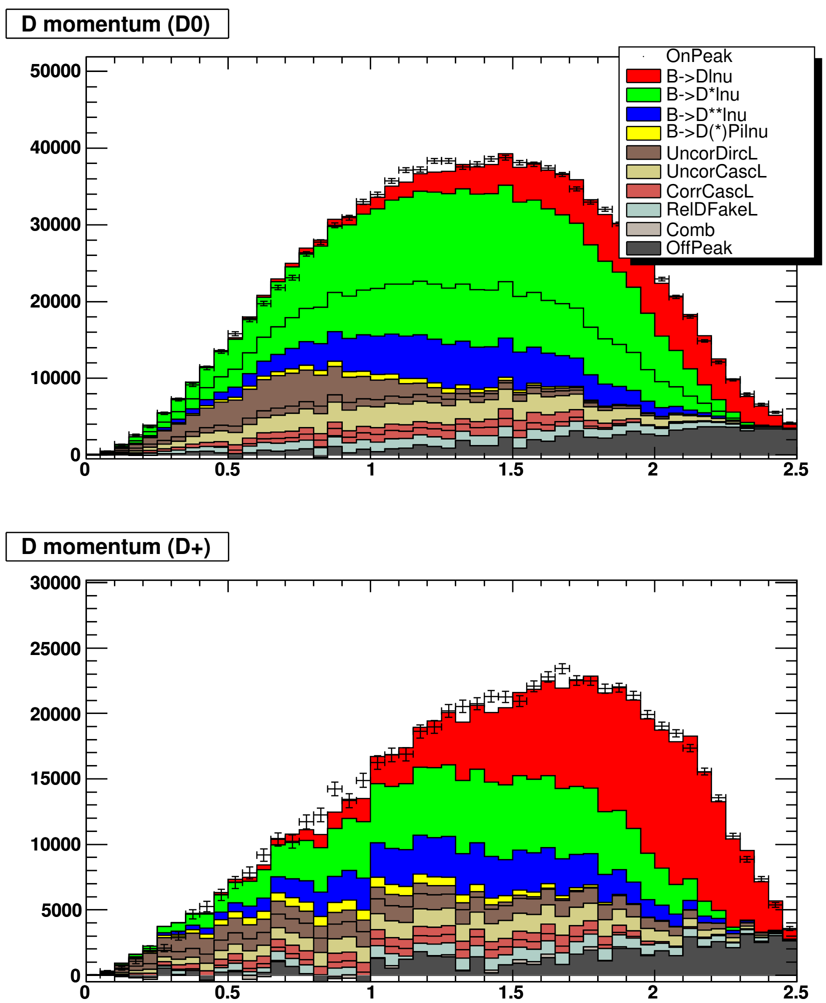

Figure 95: [p_D **after fitting**] D momentum plot after fitting. The top is D^0 and the bottom is D^+. Black is OnPeak data. Red is $B \to D\ell\nu$, green is $B \to D^*\ell\nu$, blue is $B \to D^{**}\ell\nu$, yellow is non-resonant $B \to D^{(*)}\pi\ell\nu$, and the rest is background. Dark brown is UncorrDL, light brown is UncorrCL, dark red is CascL, blue gray is FakeL, light gray is Comb and dark gray is OffPeak. Comb is almost disappeared after D mass sideband subtraction.

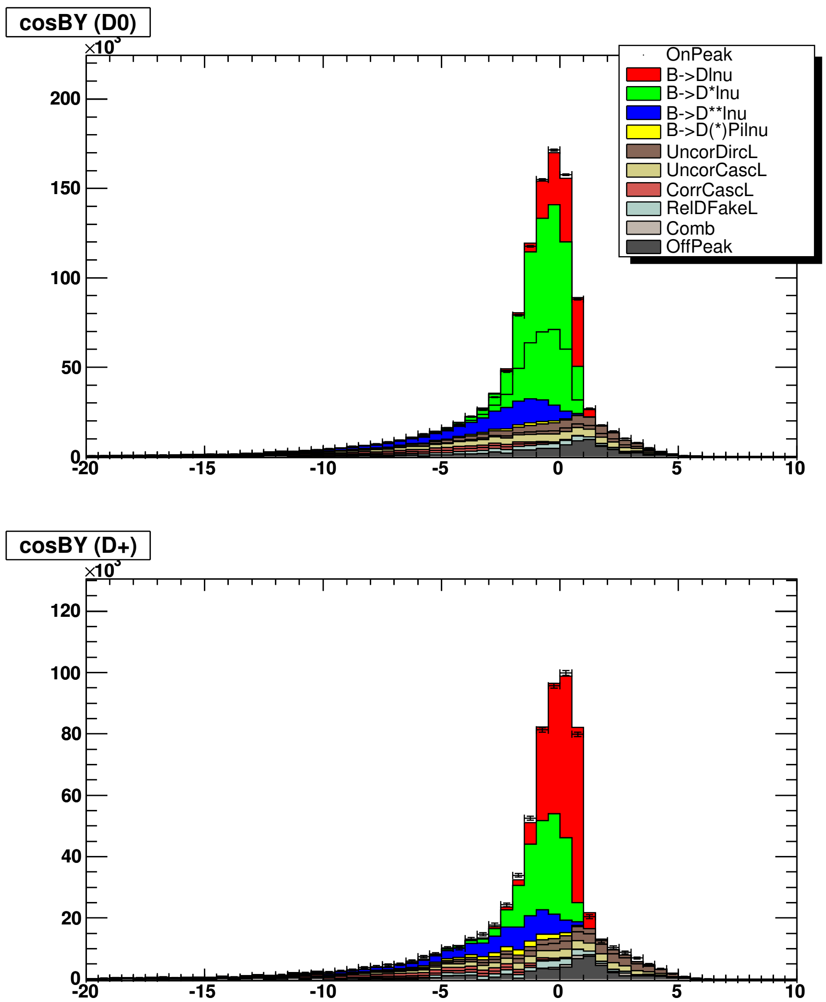

Figure 96: [$\cos\theta_{B-Dl}$ **after fitting**] $\cos\theta_{B-Dl}$ plot after fitting. The top is D^0 and the bottom is D^+. Black is OnPeak data. Red is $B \to D\ell\nu$, green is $B \to D^*\ell\nu$, blue is $B \to D^{**}\ell\nu$, yellow is non-resonant $B \to D^{(*)}\pi\ell\nu$, and the rest is background. Dark brown is UncorrDL, light brown is UncorrCL, dark red is CascL, blue gray is FakeL, light gray is Com and dark gray is OffPeakb. Comb is almost disappeared after D mass sideband subtraction.

13 Reduction of backgrounds and new fitting configuration

13.1 lepton momentum, D momentum and $\cos\theta_{B-Dl}$ cuts

To improve χ^2, we apply lepton momentum, D momentum and $\cos\theta_{B-Dl}$ cuts. Regardnig $\cos\theta_{B-Dl}$, it is clear from Figure 96 that the regions $\cos\theta_{B-Dl} < -2$ and $\cos\theta_{B-Dl} > 1$ are dominated by background. Thus, we select only

- $-2 < \cos\theta_{B-Dl} < 1$

As a trial, we use the following binning :

- lepton momentum in the CM frame p^*_ℓ
  (6 bins (GeV)) : 1.5, 1.6, 1.7, 1.8, 1.9, 2.0, 2.1
- D momentum in the CM frame p^*_D
  (6 bins (GeV)) : 1.0, 1.2, 1.4, 1.6, 1.8, 2.0, 2.2
- $\cos\theta_{B-Dl}$
  (2 bins) : -2, 0, 1

This binning gives an acceptable P-value 0.087. We then change low momentum cuts by adding lower bin to the above binning. When we change lower lepton momentum cuts

Lepton momentum cuts	P-value (χ^2/n.d.f.)
1.5 GeV	0.087 (160/137)
1.4 GeV	0.017 (210/161)
1.3 GeV	0.008 (234/185)
1.2 GeV	0.005 (266/209)

When we change lower D momentum cuts

Lepton momentum cuts	P-value (χ^2/n.d.f.)
1.0 GeV	0.087 (160/137)
0.8 GeV	0.090 (184/160)
0.6 GeV	0.049 (214/182)

Thus,

- $p_\ell > 1.5$ GeV
- $p_D > 0.8$ GeV

may be the best choice. But, since this remove large portion of full kinematic range, we need to try something else. Moreover, it is not a good idea to let P-value drive our choice of kinematic cuts becaue it might bias P-value. We need other reasoning to chose cuts.

Background ratio cuts	P-value (χ^2/n.d.f.)
30 %	0.00070 (447/357)
25 %	0.017 (408/350)
20 %	0.030 (390/339)

Table 25: [**New fit results with background ratio cuts**] Fit results.

13.2 Bckground ratio and (p_ℓ, p_D) cuts

Instead of looking at lepton momentum and D momentum separately, we can look at (p_ℓ, p_D) plane. Instead of P-value, we can look at the ratio of background in each bin of the plane. First we need to study hom many percent of backgrounds are included in each bin. In this section, by background, we mean

- Signal : $B \to D\ell\nu$ and $B \to D^*\ell\nu$ decays
- Background : $B \to D^{**}\ell\nu$ and $B \to D^{(*)}\pi\ell\nu$ decays, $B\bar{B}$ backgrounds and OffPeak

because we are interested in only $B \to D\ell\nu$ and $B \to D^*\ell\nu$ decay FF and BF.
The background ratio (= background / total) in 2D plane of (p_ℓ, p_D) is given in Figure 97. x-axis is p_ℓ and y-axis is p_D (GeV). This plot is made with 40 bins in p_ℓ and 50 bins in p_D. If we select only background ratio $<$ 0.25 bins, it looks like Figure 98. We can see significant reduction of kinematic region. To make the 2D plots, we use 40 bins for lepton momentum and 50 bins for D momentum. So, total of 2000 bins are plotted in the Figure. To select the colored region in the Figure, we print out the binns with background less than 25 % and decid a borderline between rejecting bins and keeping bins. Out of these 2000 bins, we selecte the following bins :
(p_ℓ, p_D) = (5, 33-44), (6, 28-44), (7, 26-44), (8, 24-44), (9, 23-44), (10, 20-44), (11, 20-44), (12, 20-46), (13, 18-46), (14, 17-46), (15, 16-46), (16, 16-46), (17, 12-46), (18, 11-46), (19, 11-46), (20, 7-46), (21, 7-46), (22, 7-46), (23, 7-46), (24, 8-46), (25, 14-44), (26, 17-44), (27, 18-40), (28, 21-39), (29, 21-38), (30, 32-37)
We apply the same cuts on D^+ as well.
We compare 30 %, 25 % and 20 % cuts. details are given in the following sections. Results are given in Table 25. The 25 % cuts may be the best choice because

- Regarding P-value, there is a significant difference between 30 % and 25 %, butnot much difference between 25 % and 20 %.
- With more than 25 % cuts, n.d.f. start to reduce significantly. This mean we loose more and more kinematic regions.

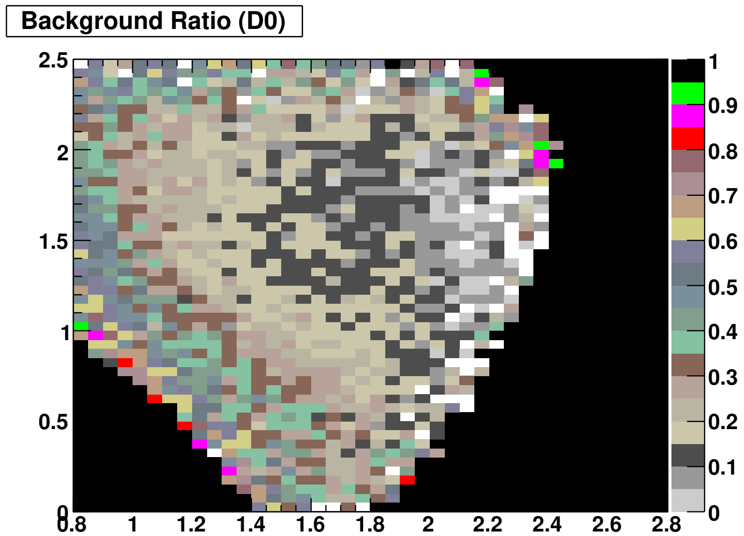

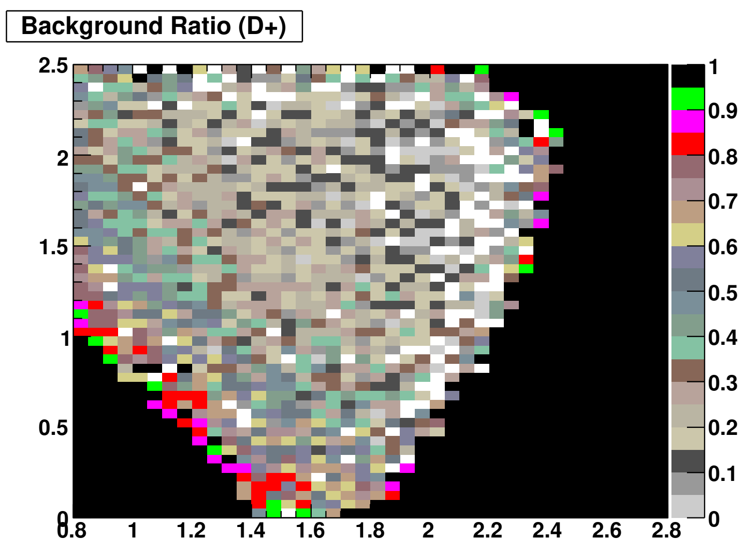

Figure 97: [**Background ratio**] Background ratio plot. x-axis is p_ℓ and y-axis is p_D (GeV).

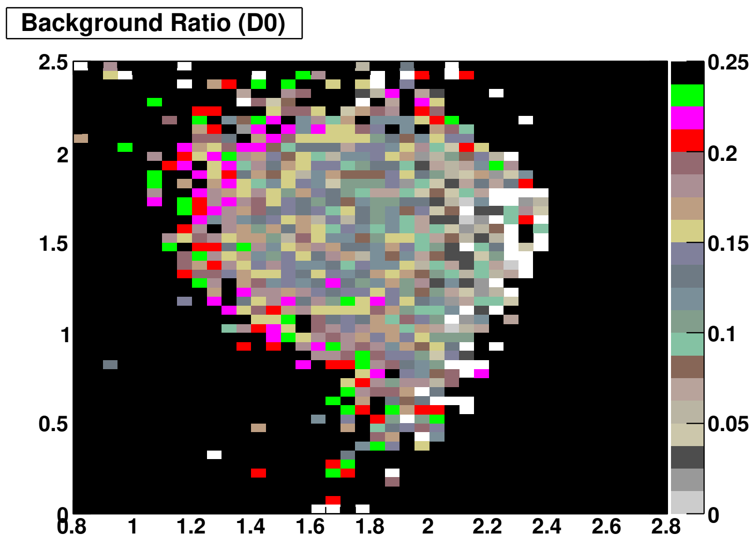

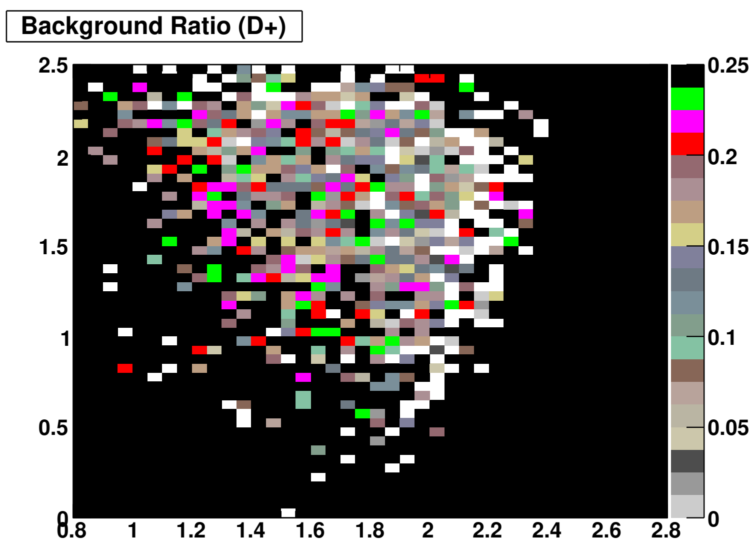

Figure 98: [**Background ratio** $<$ **0.25**] Background ratio < 0.25 plot. x-axis is p_ℓ and y-axis is p_D (GeV).

13.2.1 Background ratio < 30 % cuts

We apply the background ratio cuts to 30% to see the effect. With this selection, lepton momentum, D momentum and $\cos\theta_{B-Dl}$ looks like Figures 99-101. From these plots we decide a new binning for this fit :

- lepton momentum in the CM frame p^*_ℓ
  (9 bins (GeV)) : 1.0, 1.2, 1.4, 1.5, 1.6, 1.7, 1.8, 1.9, 2.0, 2.35
- D momentum in the CM frame p^*_D
  (7 bins (GeV)) : 0.6, 0.9, 1.2, 1.4, 1.6, 1.8, 2.0, 2.45
- $\cos\theta_{B-Dl}$ (see below)
  (3 bins) : -2, -1, 0, 1

Results are given in Table 25 along with other cuts.

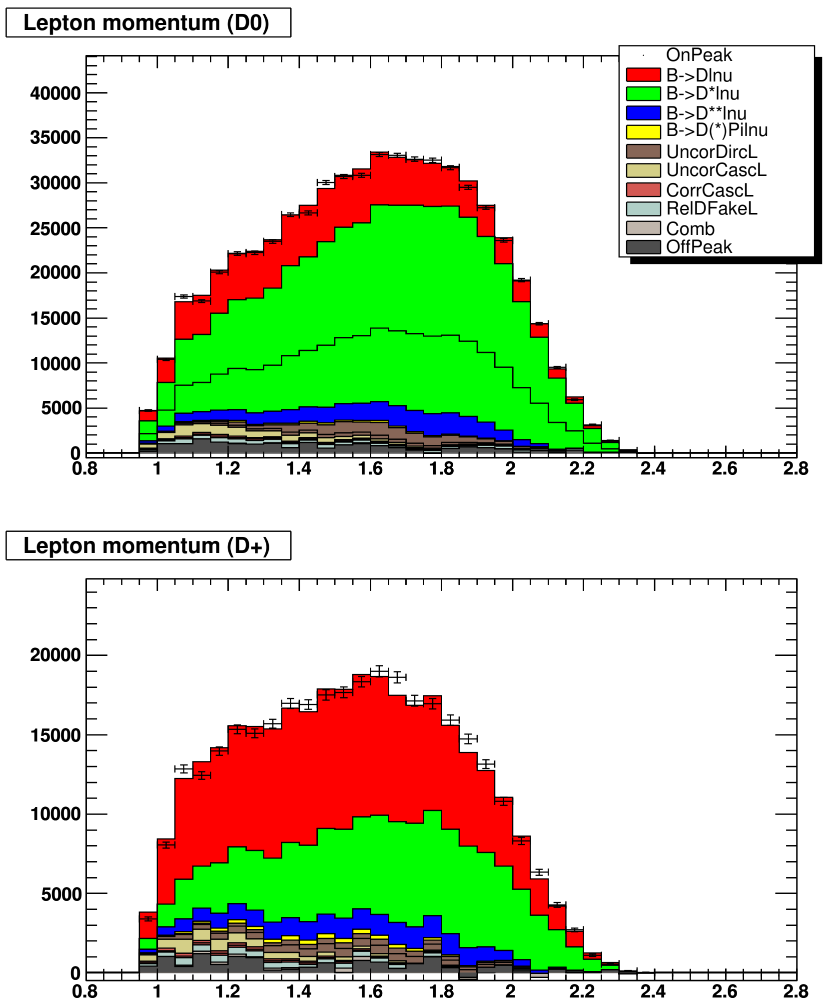

Figure 99: [p_ℓ **after background cuts** $<$ **30%**] Lepton momentum plot after background cuts. The top is D^0 and the bottom is D^+. Black is OnPeak - OffPeak data. Red is $B \to D\ell\nu$, green is $B \to D^*\ell\nu$, blue is $B \to D^{**}\ell\nu$, yellow is non-resonant $B \to D^{(*)}\pi\ell\nu$, and the rest is background. Dark brown is UncorrDL, light brown is UncorrCL, dark red is CascL, blue gray is FakeL, and light gray is Comb. Comb is almost disappeared after D mass sideband subtraction.

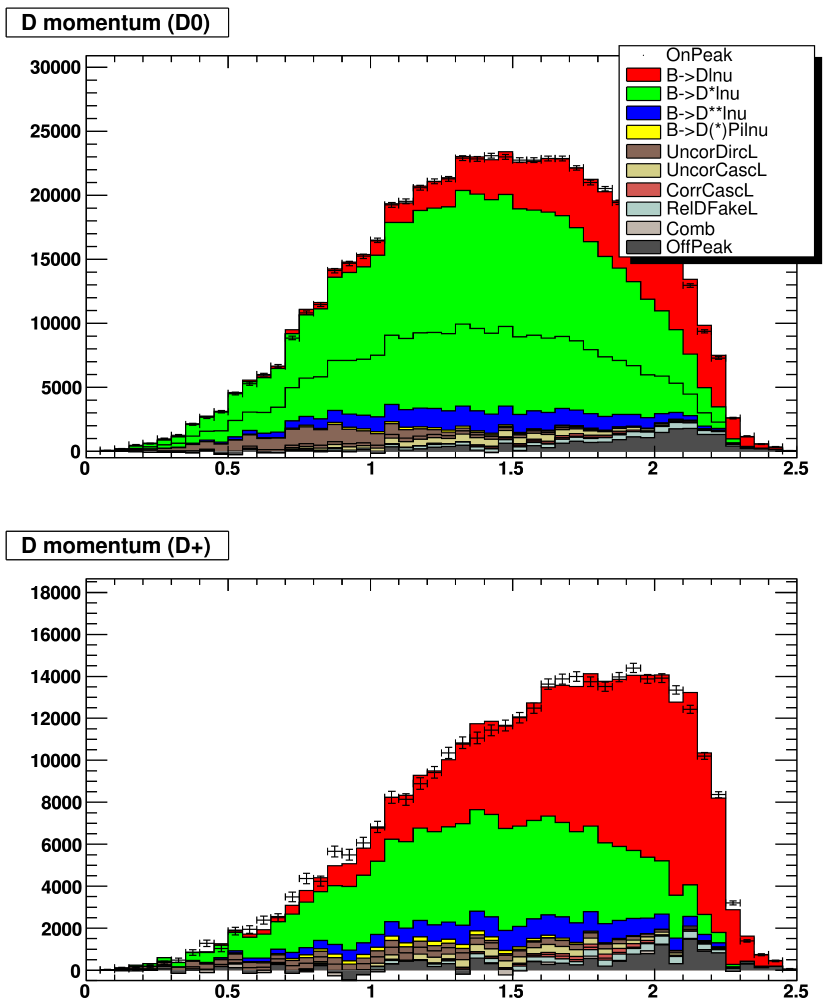

Figure 100: [p_D **after background cuts** $<$ **30%**] D momentum plot after background cuts. The top is D^0 and the bottom is D^+. Black is OnPeak - OffPeak data. Red is $B \to D\ell\nu$, green is $B \to D^*\ell\nu$, blue is $B \to D^{**}\ell\nu$, yellow is non-resonant $B \to D^{(*)}\pi\ell\nu$, and the rest is background. Dark brown is UncorrDL, light brown is UncorrCL, dark red is CascL, blue gray is FakeL, and light gray is Comb. Comb is almost disappeared after D mass sideband subtraction.

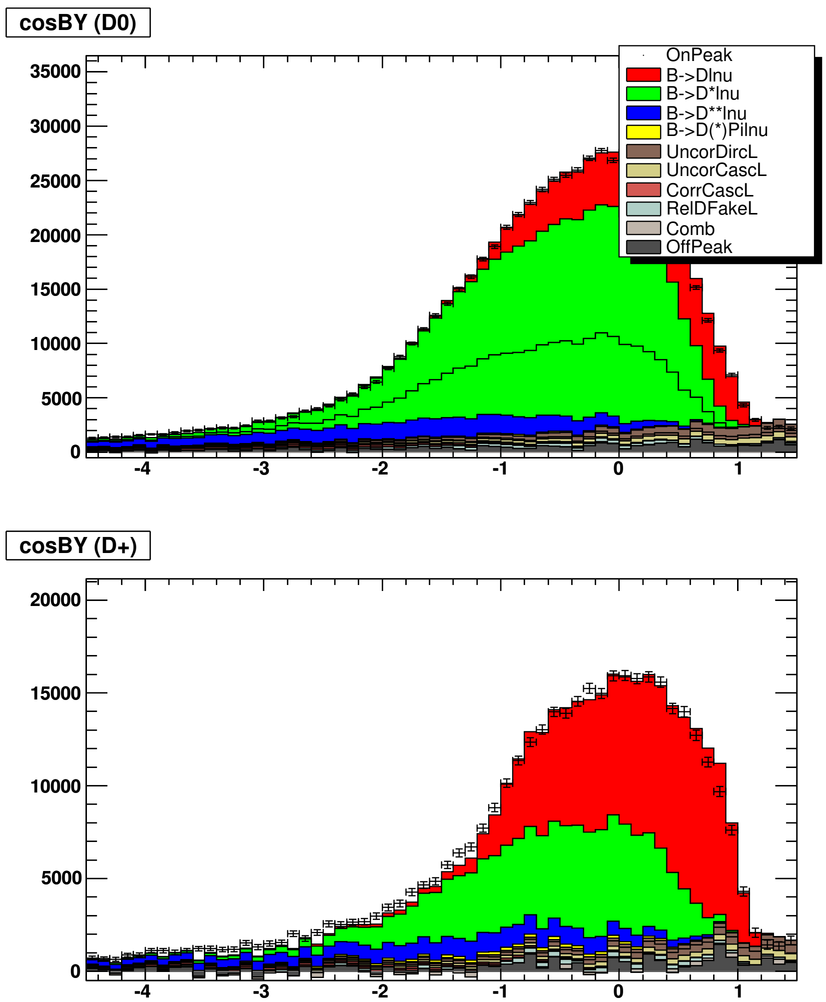

Figure 101: [$\cos\theta_{B-Dl}$ **after background cuts** $<$ **30%**] $\cos\theta_{B-Dl}$ plot after background cuts. The top is D^0 and the bottom is D^+. Black is OnPeak - OffPeak data. Red is $B \to D\ell\nu$, green is $B \to D^*\ell\nu$, blue is $B \to D^{**}\ell\nu$, yellow is non-resonant $B \to D^{(*)}\pi\ell\nu$, and the rest is background. Dark brown is UncorrDL, light brown is UncorrCL, dark red is CascL, blue gray is FakeL, and light gray is Comb. Comb is almost disappeared after D mass sideband subtraction.

13.2.2 Background ratio < 25 % cuts

With background ratio < 25 % cuts lepton momentum, D momentum and $\cos\theta_{B-Dl}$ changes to Figure 102 - 104. From these plots we decide a new binning to perform a fit.

- lepton momentum in the CM frame p^*_ℓ
  (9 bins (GeV)) : 1.05, 1.3, 1.4, 1.5, 1.6, 1.7, 1.8, 1.9, 2.0, 2.35
- D momentum in the CM frame p^*_D
  (7 bins (GeV)) : 0.35, 1.0, 1.2, 1.4, 1.6, 1.8, 2.0, 2.45
- $\cos\theta_{B-Dl}$ (see below)
  (3 bins) : -2, -1, 0, 1

Results are given in Table 25 along with other cuts.

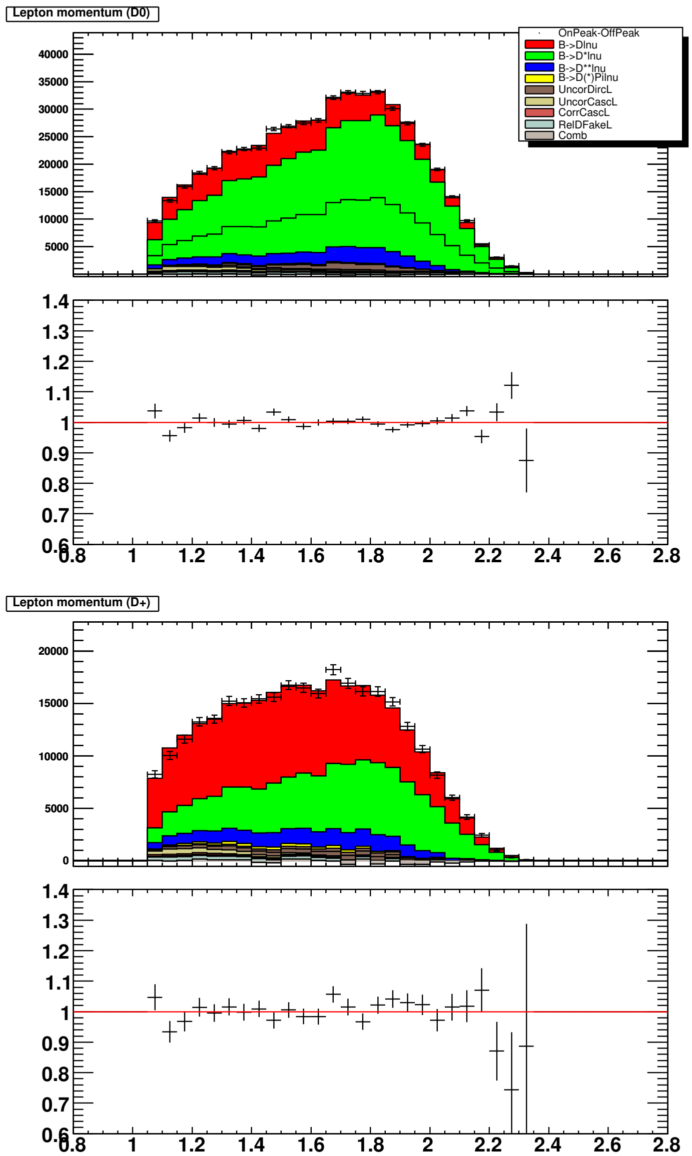

Figure 102: [p_ℓ **after background cuts** $<$ **25%**] Lepton momentum plot after background cuts. The top is D^0 and the bottom is D^+. Black is OnPeak - OffPeak data. Red is $B \to D\ell\nu$, green is $B \to D^*\ell\nu$, blue is $B \to D^{**}\ell\nu$, yellow is non-resonant $B \to D^{(*)}\pi\ell\nu$, and the rest is background. Dark brown is UncorrDL, light brown is UncorrCL, dark red is CascL, blue gray is FakeL, and light gray is Comb. Comb is almost disappeared after D mass sideband subtraction.

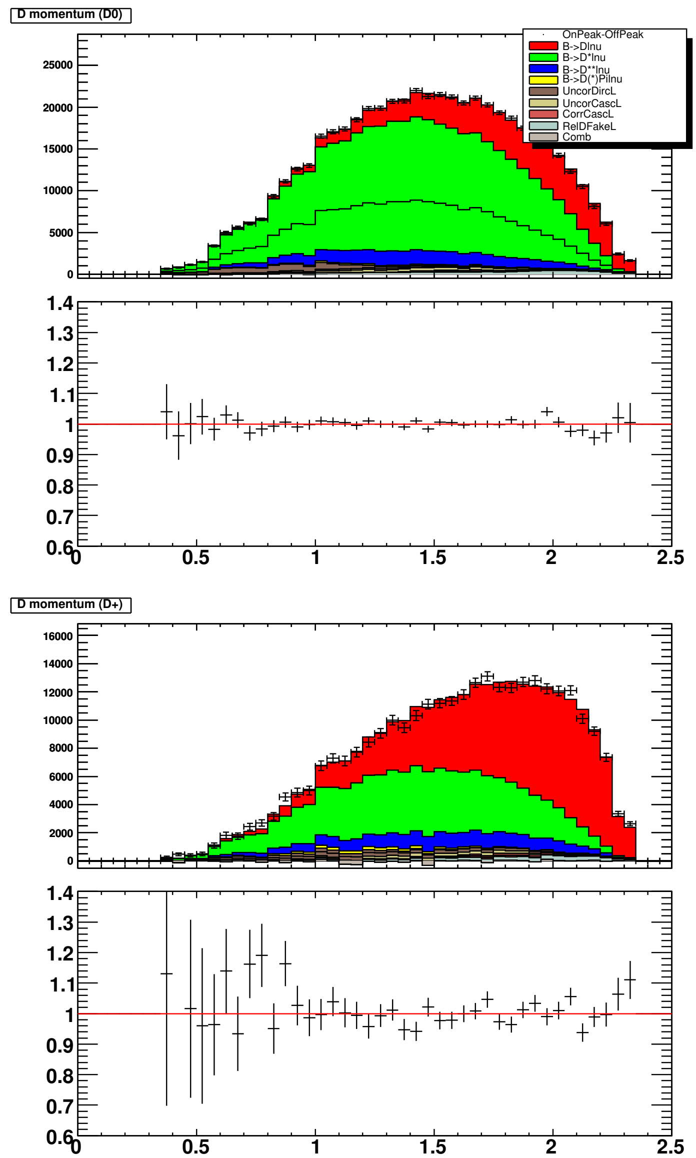

Figure 103: [p_D **after background cuts** $<$ **25%**] D momentum plot after background cuts. The top is D^0 and the bottom is D^+. Black is OnPeak - OffPeak data. Red is $B \to D\ell\nu$, green is $B \to D^*\ell\nu$, blue is $B \to D^{**}\ell\nu$, yellow is non-resonant $B \to D^{(*)}\pi\ell\nu$, and the rest is background. Dark brown is UncorrDL, light brown is UncorrCL, dark red is CascL, blue gray is FakeL, and light gray is Comb. Comb is almost disappeared after D mass sideband subtraction.

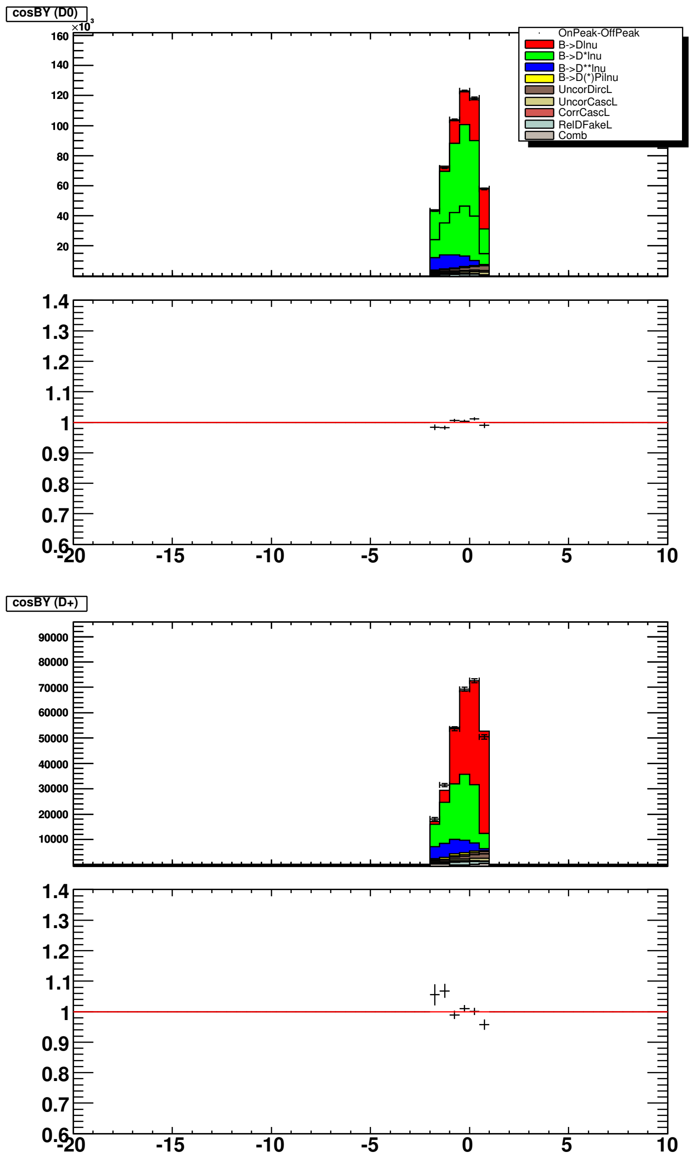

Figure 104: [$\cos\theta_{B-Dl}$ **after background cuts < 25%**] $\cos\theta_{B-Dl}$ plot after background cuts. The top is D^0 and the bottom is D^+. Black is OnPeak - OffPeak data. Red is $B \to D\ell\nu$, green is $B \to D^*\ell\nu$, blue is $B \to D^{**}\ell\nu$, yellow is non-resonant $B \to D^{(*)}\pi\ell\nu$, and the rest is background. Dark brown is UncorrDL, light brown is UncorrCL, dark red is CascL, blue gray is FakeL, and light gray is Comb. Comb is almost disappeared after D mass sideband subtraction.

13.2.3 Background ratio < 20 % cuts

With 20 % cuts, lepton momentum, D momentum and $\cos\theta_{B-Dl}$ looks like Figures 105-107. From these plots we decide new binning for this fit

- lepton momentum in the CM frame p^*_ℓ
  (9 bins (GeV)) : 1.25, 1.3, 1.4, 1.5, 1.6, 1.7, 1.8, 1.9, 2.0, 2.3
- D momentum in the CM frame p^*_D
  (7 bins (GeV)) : 0.8, 1.0, 1.2, 1.4, 1.6, 1.8, 2.0, 2.35
- $\cos\theta_{B-Dl}$ (see below)
  (3 bins) : -2, -1, 0, 1

Results are given in Table 25 along with other cuts.

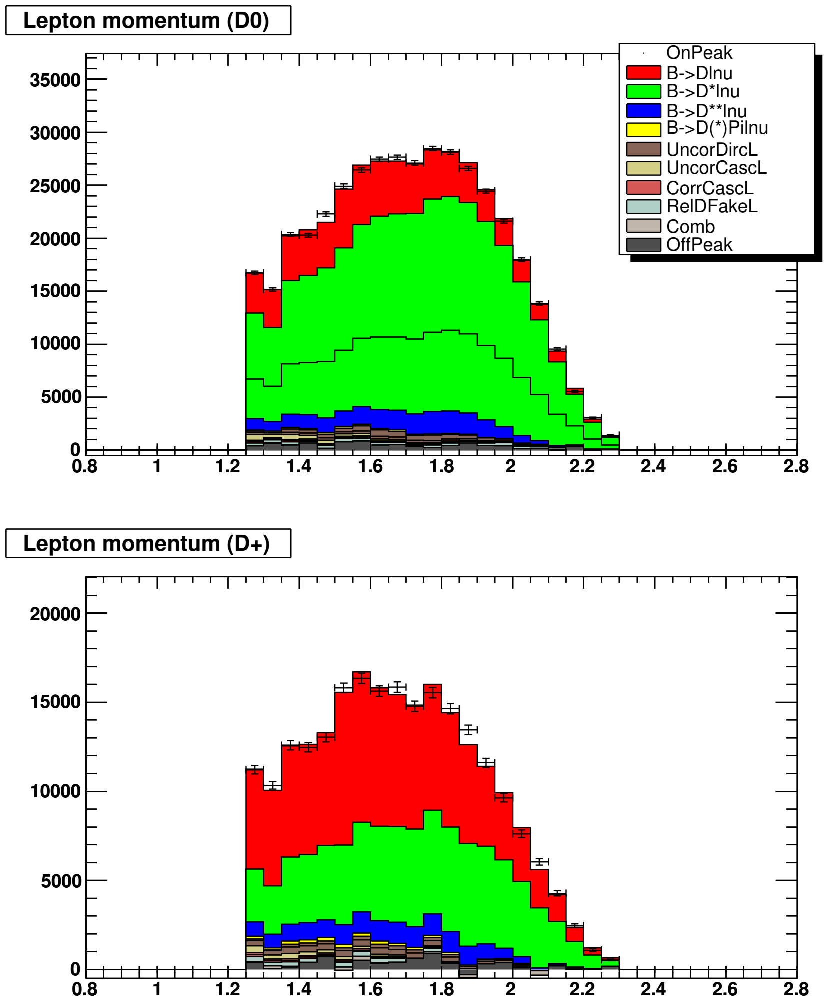

Figure 105: [p_ℓ **after background cuts $<$ 20%**] Lepton momentum plot after background cuts. The top is D^0 and the bottom is D^+. Black is OnPeak - OffPeak data. Red is $B \to D\ell\nu$, green is $B \to D^*\ell\nu$, blue is $B \to D^{**}\ell\nu$, yellow is non-resonant $B \to D^{(*)}\pi\ell\nu$, and the rest is background. Dark brown is UncorrDL, light brown is UncorrCL, dark red is CascL, blue gray is FakeL, and light gray is Comb. Comb is almost disappeared after D mass sideband subtraction.

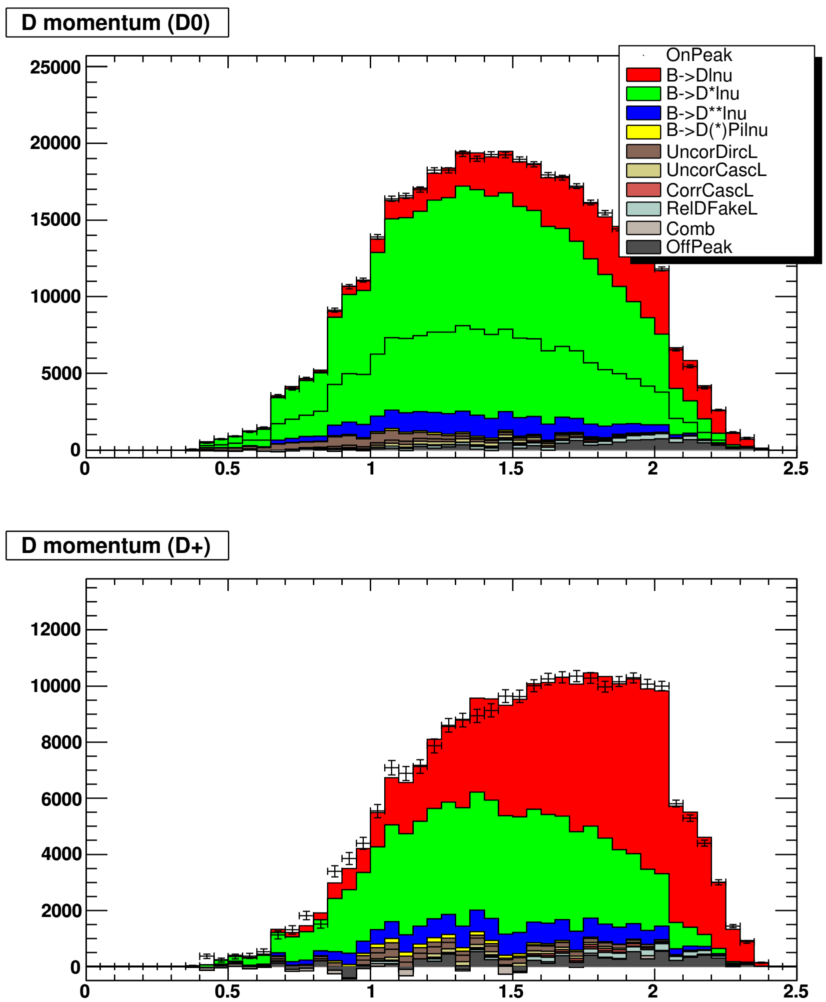

Figure 106: [p_D **after background cuts** $<$ **20%**] D momentum plot after background cuts. The top is D^0 and the bottom is D^+. Black is OnPeak - OffPeak data. Red is $B \to D\ell\nu$, green is $B \to D^*\ell\nu$, blue is $B \to D^{**}\ell\nu$, yellow is non-resonant $B \to D^{(*)}\pi\ell\nu$, and the rest is background. Dark brown is UncorrDL, light brown is UncorrCL, dark red is CascL, blue gray is FakeL, and light gray is Comb. Comb is almost disappeared after D mass sideband subtraction.

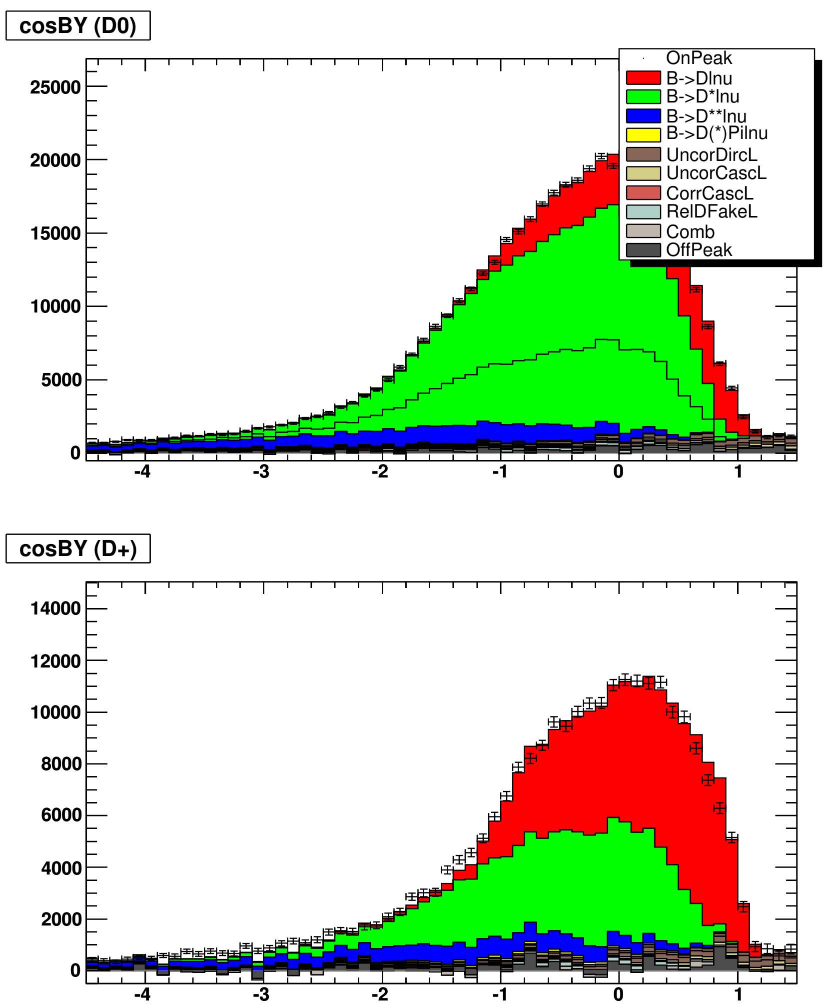

Figure 107: [$\cos\theta_{B-Dl}$ **after background cuts** $<$ **20%**] $\cos\theta_{B-Dl}$ plot after background cuts. The top is D^0 and the bottom is D^+. Black is OnPeak - OffPeak data. Red is $B \to D\ell\nu$, green is $B \to D^*\ell\nu$, blue is $B \to D^{**}\ell\nu$, yellow is non-resonant $B \to D^{(*)}\pi\ell\nu$, and the rest is background. Dark brown is UncorrDL, light brown is UncorrCL, dark red is CascL, blue gray is FakeL, and light gray is Comb. Comb is almost disappeared after D mass sideband subtraction.

13.3 Combination cuts

With background ratio 25 % cuts, we can achieve an acceptable χ^2. However, if we further apply low lepton momentum and D momentum cuts, we can get a better χ^2. Low momentum cust such as

- $p_\ell^* > 1.2$ GeV
- $p_D^* > 0.8$ GeV

can be a reasonable cuts because these cuts are ofte applied in $B \to X_c \ell \nu$ type of analysis in Babar. Thus, we deecide to **employ background ratio 25 % cuts with the following new binning** for our nominal fit

- lepton momentum in the CM frame p_ℓ^*
  (9 bins (GeV)) : 1.2, 1.3, 1.4, 1.5, 1.6, 1.7, 1.8, 1.9, 2.0, 2.35
- D momentum in the CM frame p_D^*
  (7 bins (GeV)) : 0.8, 1.0, 1.2, 1.4, 1.6, 1.8, 2.0, 2.45
- $\cos\theta_{B-Dl}$
  (3 bins) : -2, -1, 0, 1

13.4 New fit results

Since backgrounds are significantly reduced, we fix all background coefficients. Fit results are shown in Table 26 and correlations between parameters are given in Table 27 and 28. In case of f_{+0} floated, plots of lepton momentum, D momentum and $\cos\theta_{B-Dl}$ after fitting are given in Figure 108 - 110. Figure 111 - 113 show the same variables with fitted binning. Bin by bin plots after fitting are also shown in Figure 114 and 115.

Parameters	f_{+0} floated	f_{+0} fixed
ρ_D^2	1.164 ± 0.042 (3.6 %)	1.166 ± 0.039 (3.4 %)
ρ^2	1.278 ± 0.044 (3.5 %)	1.278 ± 0.044 (3.5 %)
R_1	1.402 ± 0.065 (4.6 %)	1.403 ± 0.064 (4.6 %)
R_2	0.752 ± 0.055 (7.3 %)	0.753 ± 0.055 (7.3 %)
$\mathcal{B}(B^+ \to \bar{D}^0\ell^+\nu)$	0.02328 ± 0.00031 (1.3 %)	0.02331 ± 0.00025 (1.1 %)
$\mathcal{B}(B^+ \to \bar{D}^{*0}\ell^+\nu)$	0.05443 ± 0.00073 (1.4 %)	0.05437 ± 0.00052 (0.96 %)
$\mathcal{BT}(B^+ \to \bar{D}^{**0}/(D\pi)^0\ell^+\nu)$	0.01630 ± 0.00111 (6.8 %)	0.01637 ± 0.00097 (5.9 %)
f_{+0}	1.035 ± 0.017 (1.6 %)	1.037 (Fixed)
χ^2/ndof (P-value)	379/350 (0.135)	379/351 (0.143)

Table 26: [**New fit results with background ratio 25 % cuts**] Fit results.

	ρ_D^2	ρ^2	R_1	R_2	$\mathcal{B}(D\ell\nu)$	$\mathcal{B}(D^*\ell\nu)$	$\mathcal{B}$(Oter)	f_{+0}
ρ_D^2	1							
ρ^2	-0.229	1						
R_1	+0.027	+0.837	1					
R_2	+0.134	-0.912	-0.901	1				
$\mathcal{B}(D\ell\nu)$	+0.411	+0.181	+0.332	-0.094	1			
$\mathcal{B}(D^*\ell\nu)$	-0.514	+0.326	+0.042	-0.355	-0.605	1		
$\mathcal{B}$(Oter)	+0.322	-0.362	-0.190	+0.354	+0.296	-0.813	1	
f_{+0}	+0.349	+0.016	+0.161	+0.044	+0.576	-0.695	+0.486	1

Table 27: [**Correlation coefficients : f_{+0} floated**] Correlations between parameters in case of f_{+0} floated.

	ρ_D^2	ρ^2	R_1	R_2	$\mathcal{B}(D\ell\nu)$	$\mathcal{B}(D^*\ell\nu)$	$\mathcal{B}$(Oter)
ρ_D^2	1						
ρ^2	-0.251	1					
R_1	-0.031	+0.845	1				
R_2	+0.127	-0.913	-0.921	1			
$\mathcal{B}(D\ell\nu)$	+0.274	+0.210	+0.296	-0.145	1		
$\mathcal{B}(D^*\ell\nu)$	-0.403	+0.468	+0.216	-0.451	-0.350	1	
$\mathcal{B}$(Oter)	+0.186	-0.423	-0.310	+0.380	-0.015	-0.756	1

Table 28: [**Correlation coefficients : f_{+0} fixed**] Correlations between parameters in case of f_{+0} fixed.

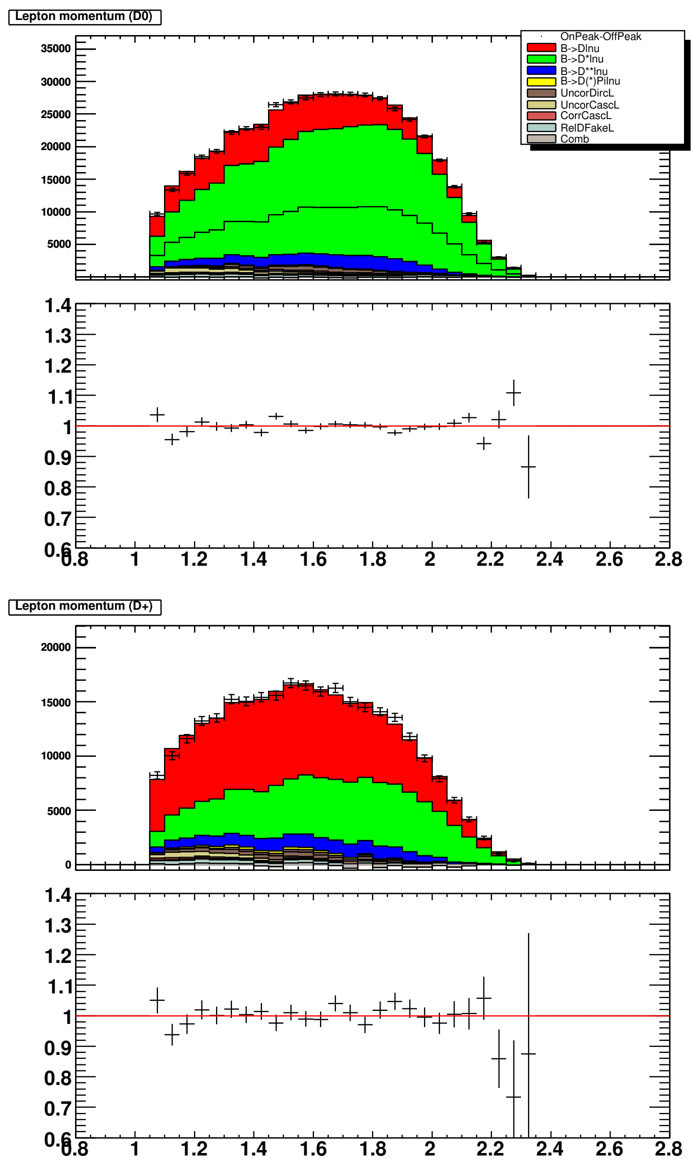

Figure 108: [p_ℓ **after fitting**] Lepton momentum plot after fitting. The top is D^0 and the bottom is D^+. Black is OnPeak - OffPeak data. Red is $B \to D\ell\nu$, green is $B \to D^*\ell\nu$, blue is $B \to D^{**}\ell\nu$, yellow is non-resonant $B \to D^{(*)}\pi\ell\nu$, and the rest is background. Dark brown is UncorrDL, light brown is UncorrCL, dark red is CascL, blue gray is FakeL, and light gray is Comb. Comb is almost disappeared after D mass sideband subtraction.

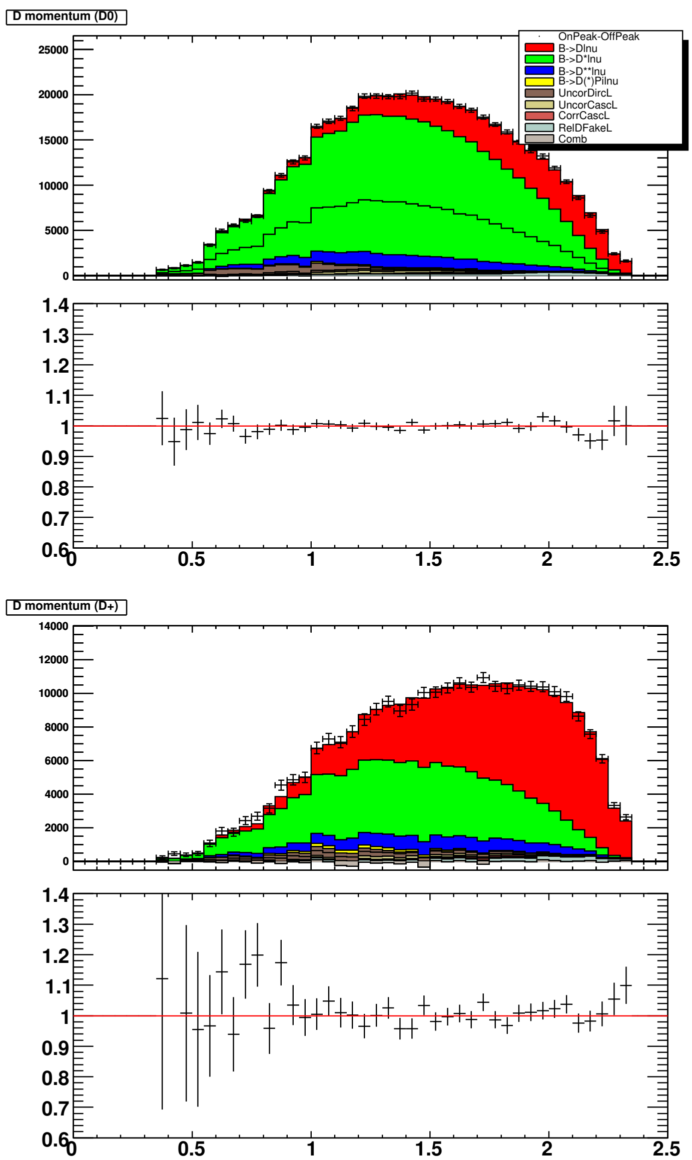

Figure 109: [p_D **after fitting**] D momentum plot after fitting. The top is D^0 and the bottom is D^+. Black is OnPeak - OffPeak data. Red is $B \to D\ell\nu$, green is $B \to D^*\ell\nu$, blue is $B \to D^{**}\ell\nu$, yellow is non-resonant $B \to D^{(*)}\pi\ell\nu$, and the rest is background. Dark brown is UncorrDL, light brown is UncorrCL, dark red is CascL, blue gray is FakeL, and light gray is Comb. Comb is almost disappeared after D mass sideband subtraction.

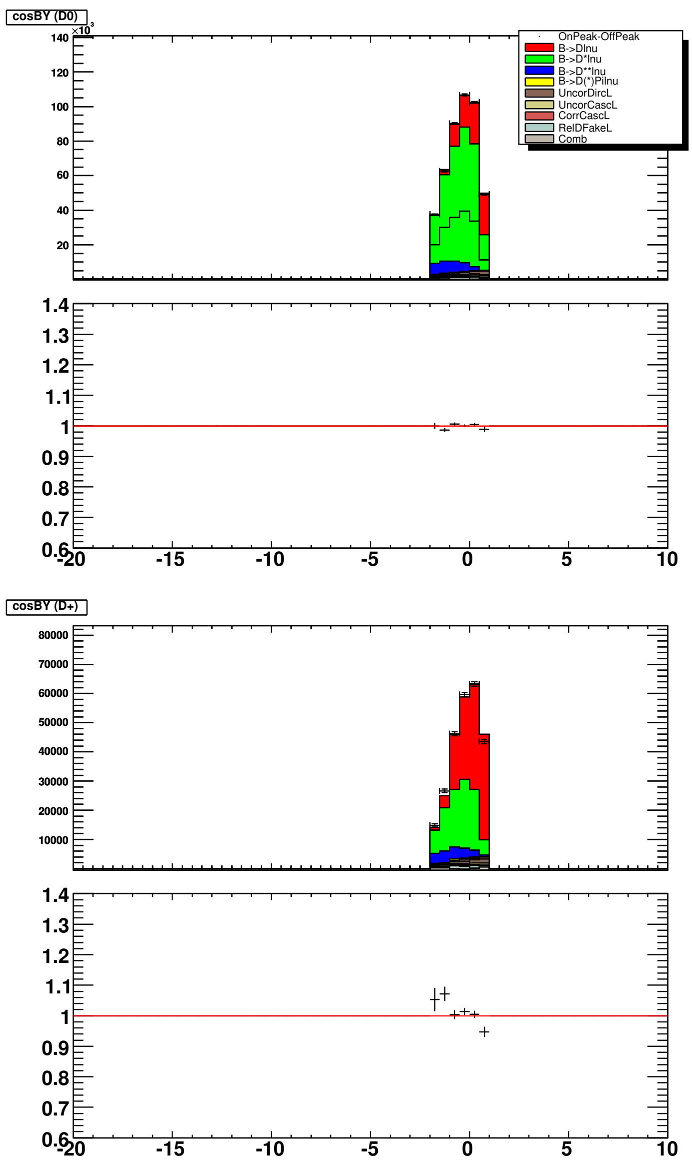

Figure 110: [$\cos\theta_{B-Dl}$ **after fitting**] $\cos\theta_{B-Dl}$ plot after fitting. The top is D^0 and the bottom is D^+. Black is OnPeak - OffPeak data. Red is $B \to D\ell\nu$, green is $B \to D^*\ell\nu$, blue is $B \to D^{**}\ell\nu$, yellow is non-resonant $B \to D^{(*)}\pi\ell\nu$, and the rest is background. Dark brown is UncorrDL, light brown is UncorrCL, dark red is CascL, blue gray is FakeL, and light gray is Comb. Comb is almost disappeared after D mass sideband subtraction.

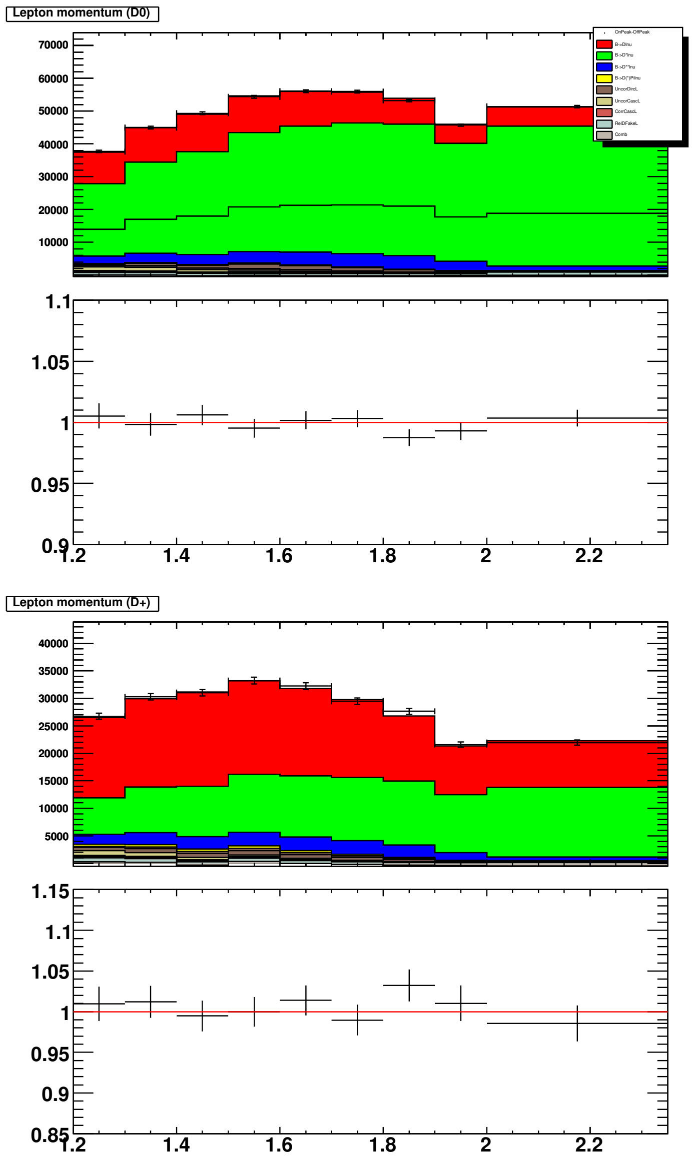

Figure 111: [p_ℓ **with fitted binning**] Lepton momentum plot with fitted binning after fitting. The top is D^0 and the bottom is D^+. Black is OnPeak - OffPeak data. Red is $B \to D\ell\nu$, green is $B \to D^*\ell\nu$, blue is $B \to D^{**}\ell\nu$, yellow is non-resonant $B \to D^{(*)}\pi\ell\nu$, and the rest is background. Dark brown is UncorrDL, light brown is UncorrCL, dark red is CascL, blue gray is FakeL, and light gray is Comb. Comb is almost disappeared after D mass sideband subtraction.

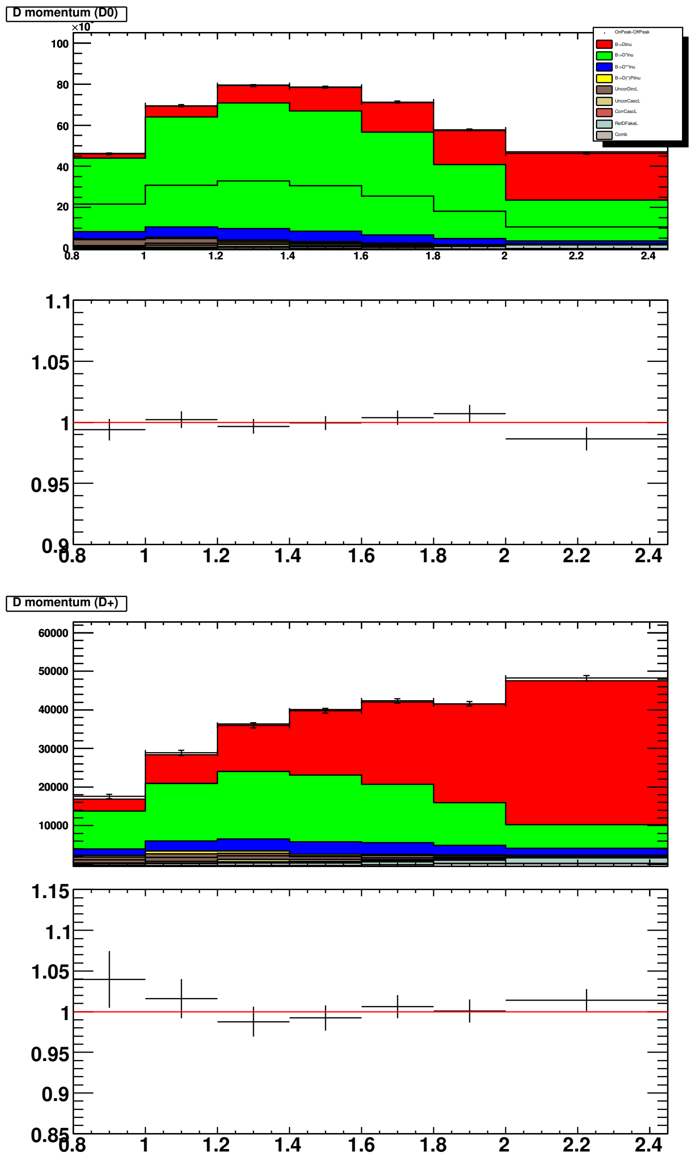

Figure 112: [p_D **with fitted binning**] D momentum plot with fitted binning after fitting. The top is D^0 and the bottom is D^+. Black is OnPeak - OffPeak data. Red is $B \to D\ell\nu$, green is $B \to D^*\ell\nu$, blue is $B \to D^{**}\ell\nu$, yellow is non-resonant $B \to D^{(*)}\pi\ell\nu$, and the rest is background. Dark brown is UncorrDL, light brown is UncorrCL, dark red is CascL, blue gray is FakeL, and light gray is Comb. Comb is almost disappeared after D mass sideband subtraction.

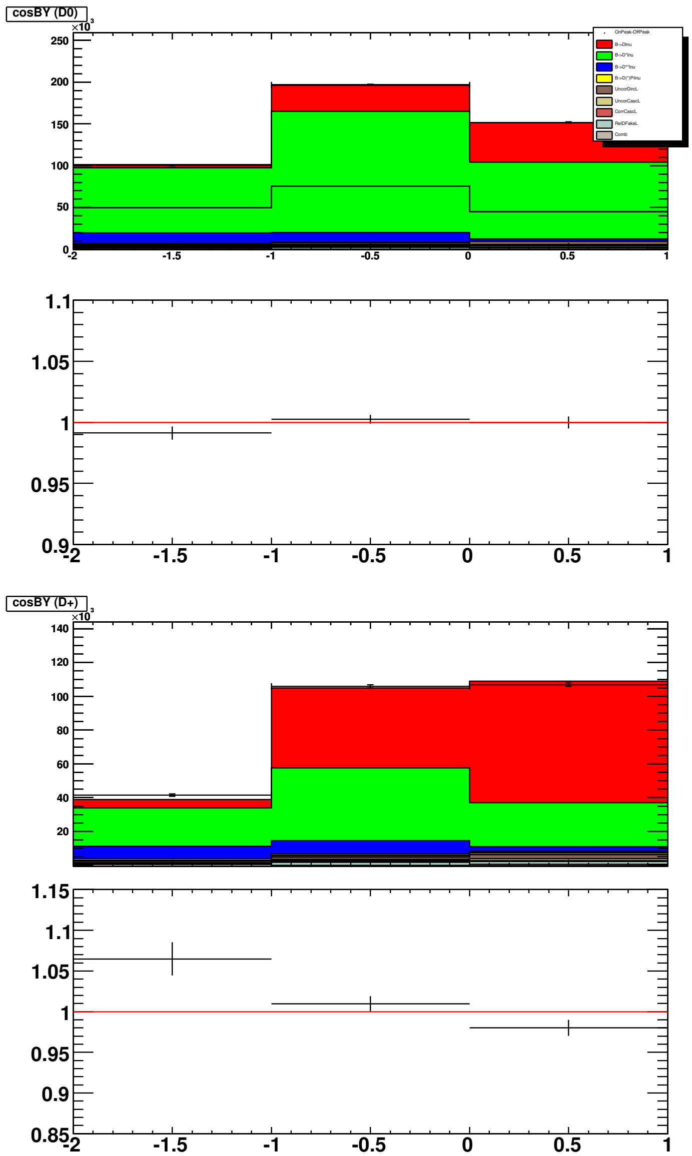

Figure 113: [$\cos\theta_{B-Dl}$ **with fitted binning**] $\cos\theta_{B-Dl}$ plot with fitted binning after fitting. The top is D^0 and the bottom is D^+. Black is OnPeak - OffPeak data. Red is $B \to D\ell\nu$, green is $B \to D^*\ell\nu$, blue is $B \to D^{**}\ell\nu$, yellow is non-resonant $B \to D^{(*)}\pi\ell\nu$, and the rest is background. Dark brown is UncorrDL, light brown is UncorrCL, dark red is CascL, blue gray is FakeL, and light gray is Comb. Comb is almost disappeared after D mass sideband subtraction.

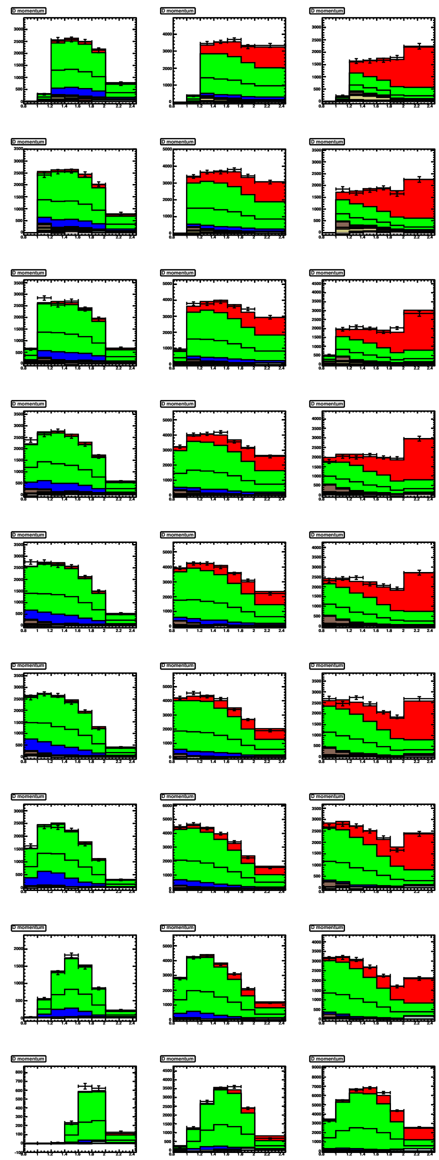

Figure 114: [D^0 **bin by bin after fitting**] D^0 momentum plots showing all bins after fitting. From top to bottom, lepton momentum bin changes from the lowest to the highest, and from left to right, cosBY bin changes from negative to positive. In each plots, colors are the same as other plots. Black is OnPeak - OffPeak data. Red is $B \to D\ell\nu$, green is $B \to D^*\ell\nu$, blue is $B \to D^{**}\ell\nu$, yellow is non-resonant $B \to D^{(*)}\pi\ell\nu$, and the rest is background. Dark brown is UncorrDL, light brown is UncorrCL, dark red is CascL, blue gray is FakeL, and light gray is Comb. Comb is almost disappeared after D mass sideband subtraction.

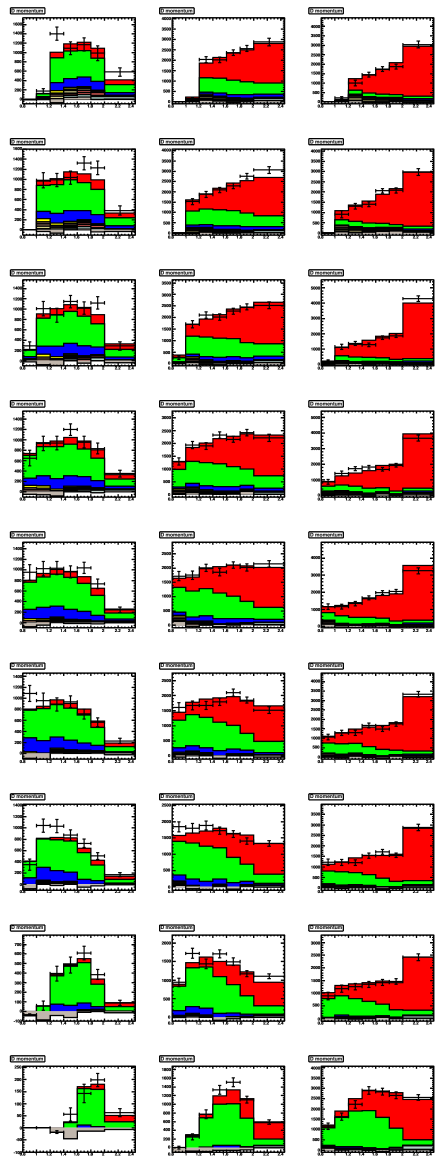

Figure 115: [D^+ **bin by bin after fitting**] D^+ momentum plots showing all bins after fitting. From top to bottom, lepton momentum bin changes from the lowest to the highest, and from left to right, cosBY bin charger's from negative to positive. In each plots, colors are the same as other plots. Black is OnPeak - OffPeak data. Red is $B \to D\ell\nu$, green is $B \to D^*\ell\nu$, blue is $B \to D^{**}\ell\nu$, yellow is non-resonant $B \to D^{(*)}\pi\ell\nu$, and the rest is background. Dark brown is UncorrDL, light brown is UncorrCL, dark red is CascL, blue gray is FakeL, and light gray is Comb. Comb is almost disappeared after D mass sideband subtraction.

14 D mass sideband subtraction revisited

We assume D mass sideband is flat when we do sideand subtraction. Here we check this assumption bin by bin.

14.1 Bin by bin D mass plots

The linearlity of the sideband region may depend on kinematic variables : lepton momentum, D momentum and $\cos\Theta_{B-D\ell}$. We plot OnPeak data D mass distribution with bin by bin of these kinematic variables. Binning are descibed in section 13.3. Plots are shown in Figures 116-118 for D^0 mass and in Figures 119-121 for D^+ mass. Thse Figures are in order of $\cos\Theta_{B-D\ell}$ bins. In one figure, plots are arranged in order of lepton momentum bins from top to bottom, and in oder of D momentum bins from left to right. No significant non-linearlity is obsedved from these plots.

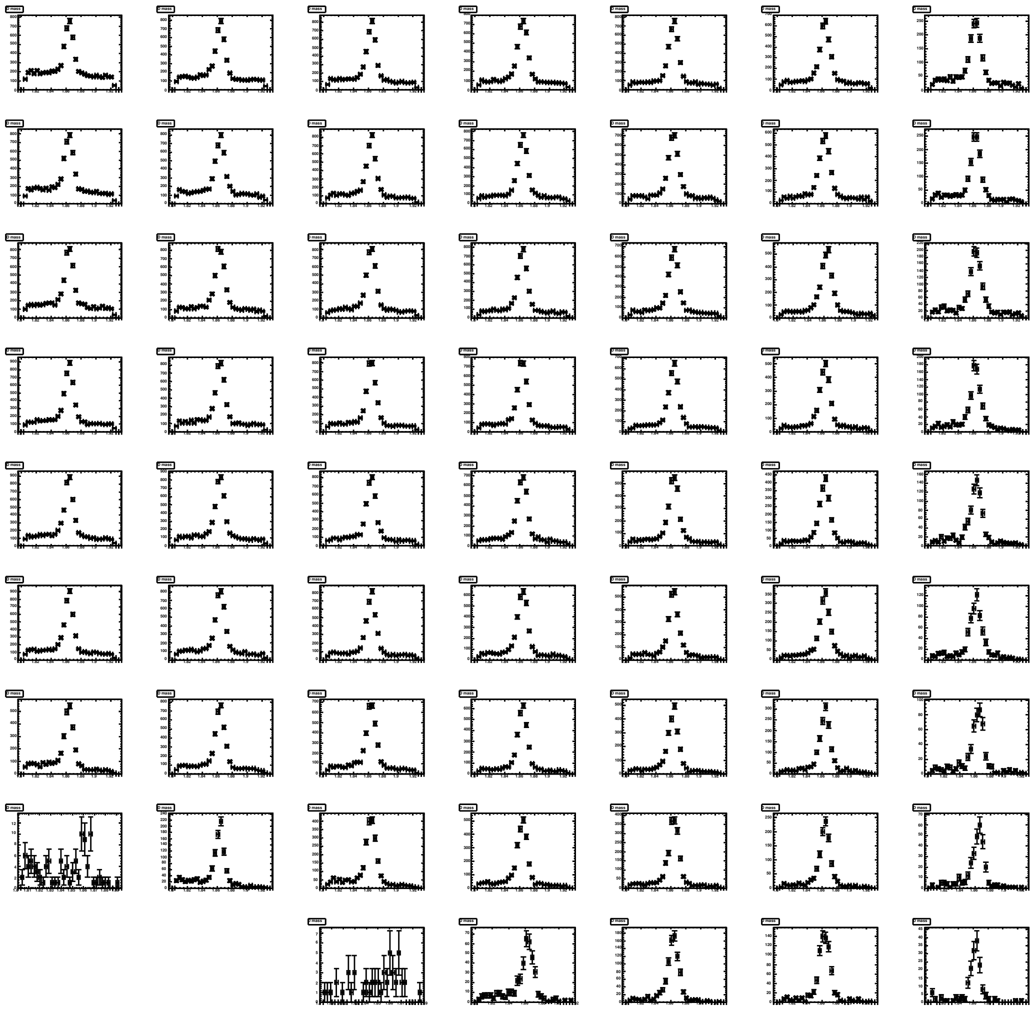

Figure 116: [**Bin by bin D^0 mass plots : OnPeak 1**] OnPeak D^0 mass plots of 1st $\cos\Theta_{B-D\ell}$ bin. From top to botton : in order of lepton momentum bins. From left to right : in order of D momentum bins. Plots are not shown for the bins whre there is no entry.

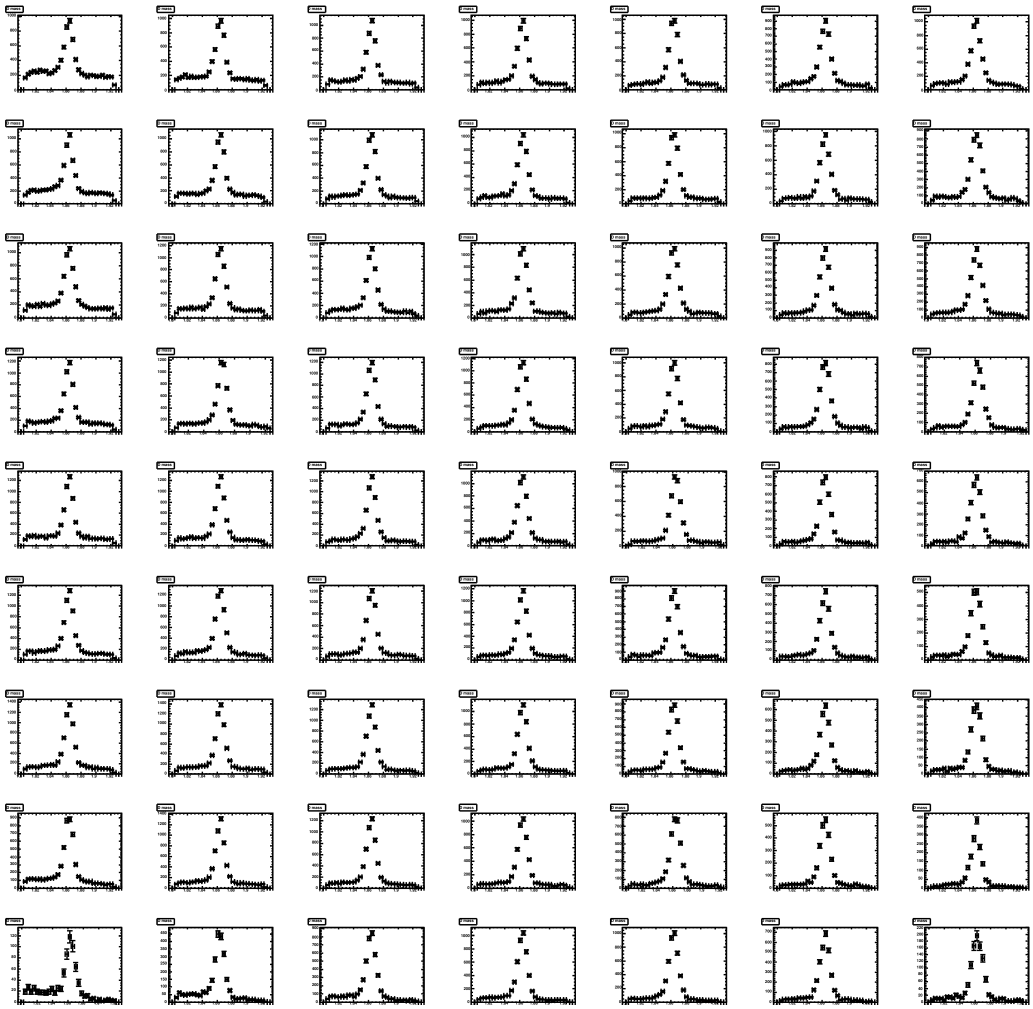

Figure 117: [**Bin by bin D^0 mass plots : OnPeak 2**] OnPeak D^0 mass plots of 2nd $\cos\Theta_{B-D\ell}$ bin. From top to botton : in order of lepton momentum bins. From left to right : in order of D momentum bins. Plots are not shown for the bins whre there is no entry.

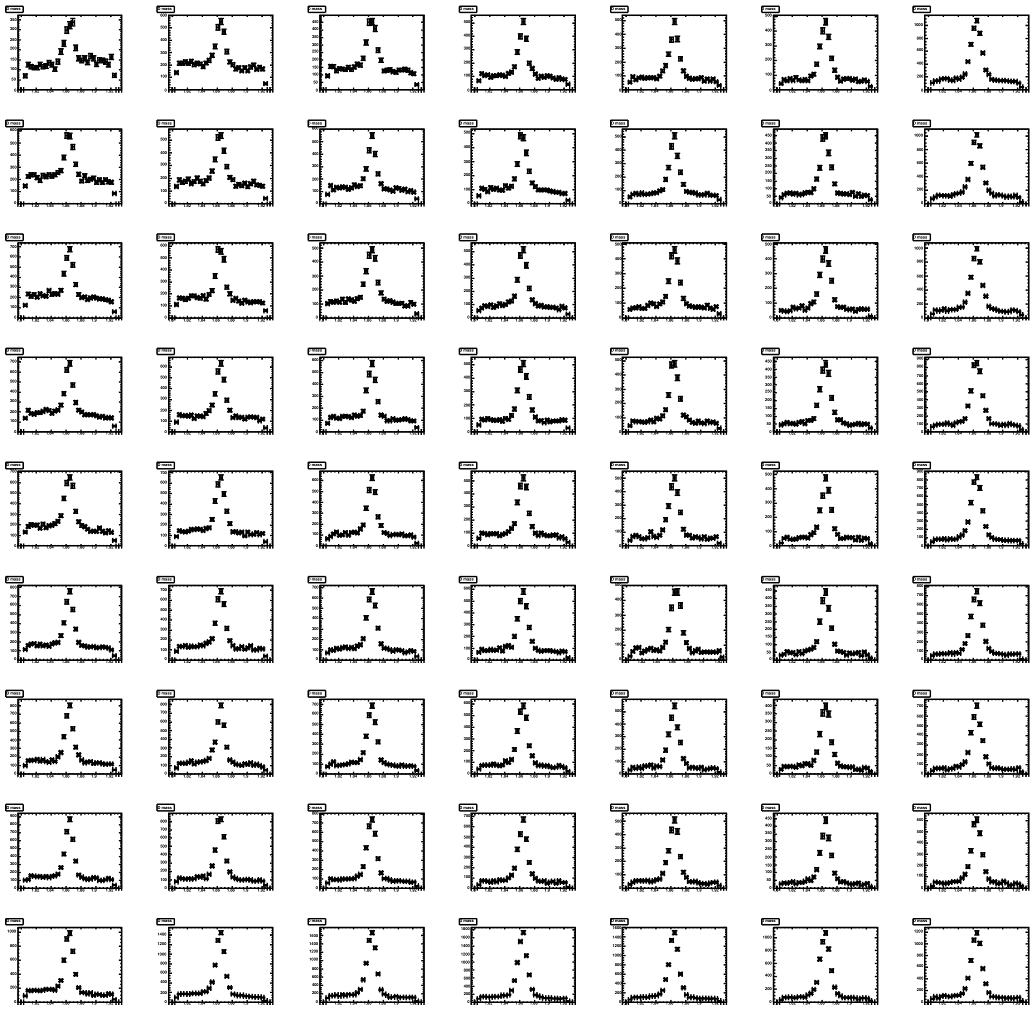

Figure 118: [**Bin by bin D^0 mass plots : OnPeak 3**] OnPeak D^0 mass plots of 3rd $\cos\Theta_{B-D\ell}$ bin. From top to botton : in order of lepton momentum bins. From left to right : in order of D momentum bins. Plots are not shown for the bins whre there is no entry.

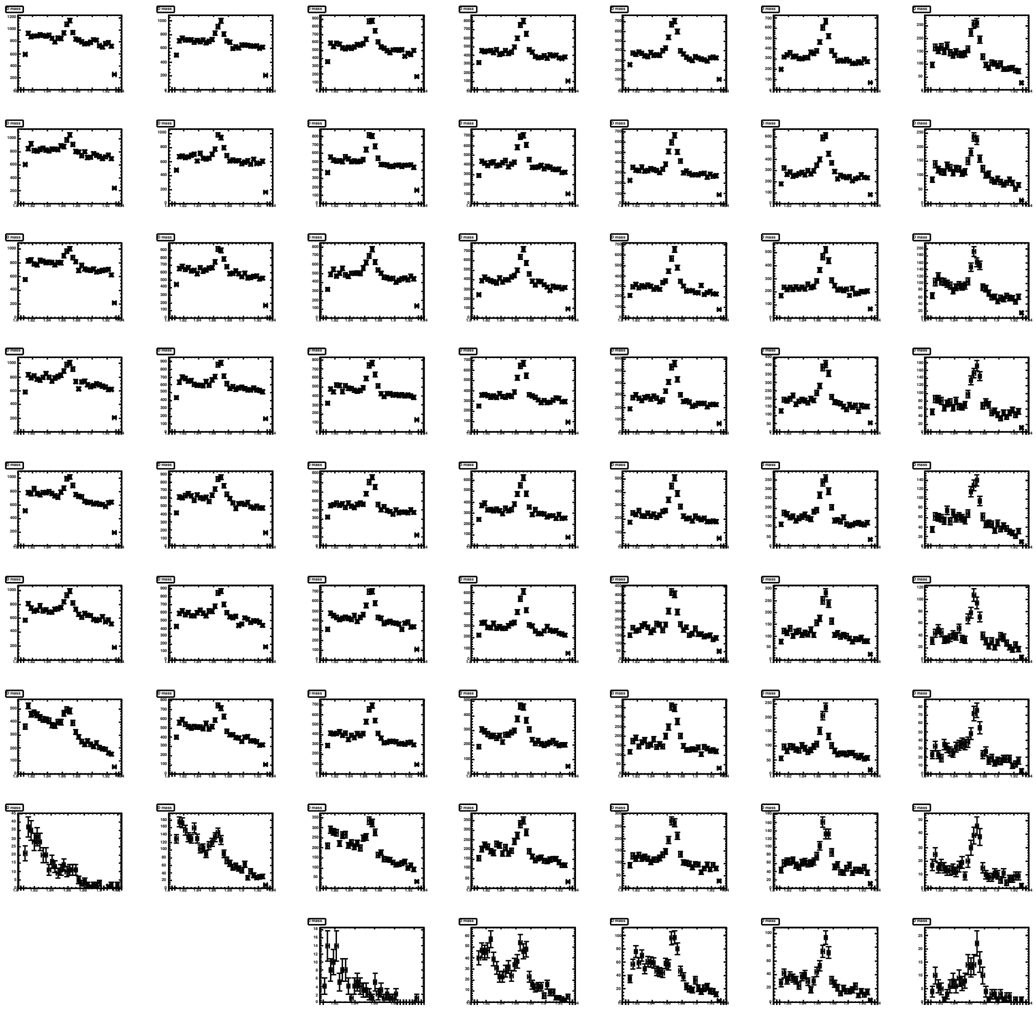

Figure 119: [**Bin by bin D^+ mass plots : OnPeak 1**] OnPeak D^+ mass plots of 1st $\cos\Theta_{B-D\ell}$ bin. From top to botton : in order of lepton momentum bins. From left to right : in order of D momentum bins. Plots are not shown for the bins whre there is no entry.

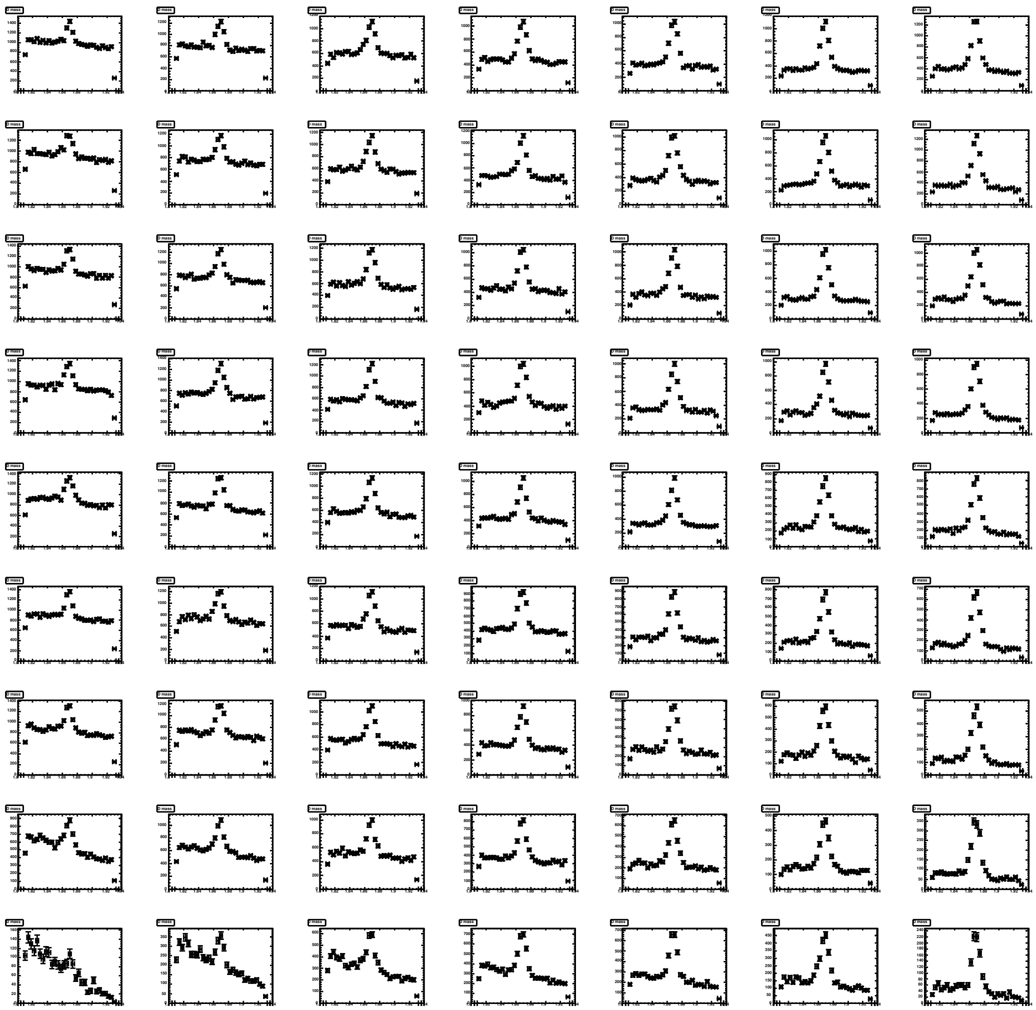

Figure 120: [**Bin by bin D^+ mass plots : OnPeak 2**] OnPeak D^+ mass plots of 2nd $\cos\Theta_{B-D\ell}$ bin. From top to botton : in order of lepton momentum bins. From left to right : in order of D momentum bins. Plots are not shown for the bins whre there is no entry.

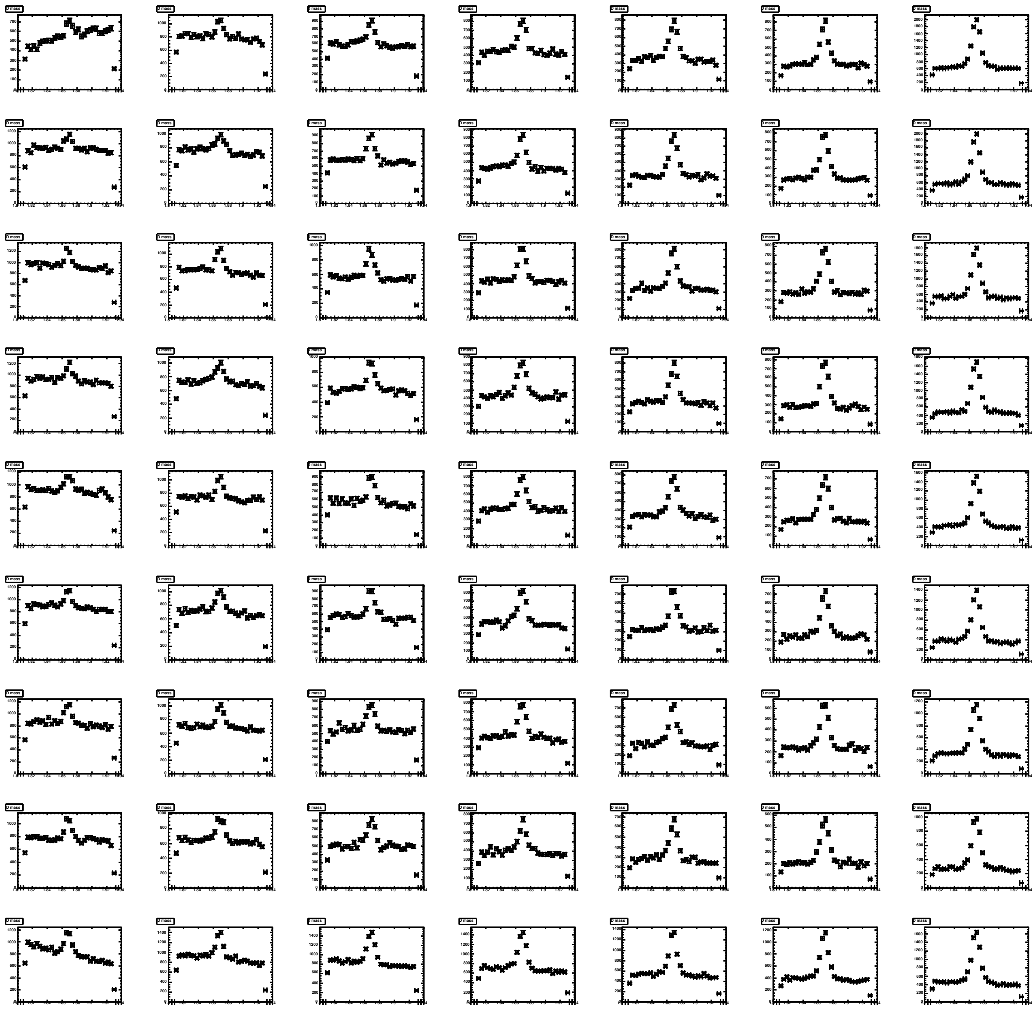

Figure 121: [**Bin by bin D^+ mass plots : OnPeak 3**] OnPeak D^+ mass plots of 3rd $\cos\Theta_{B-D\ell}$ bin. From top to botton : in order of lepton momentum bins. From left to right : in order of D momentum bins. Plots are not shown for the bins whre there is no entry.

15 Fit validation and Selectionn of nominal fit

We validate our fit as described in the following subsections.

15.1 Summary of validation fit configuration

As described in previous sections, we are trying to fit for two branching fractions and four form factors

- $\mathcal{B}(B^+ \to \bar{D}^0 \ell^+ \nu)$
- $\mathcal{B}(B^+ \to \bar{D}^{*0} \ell^+ \nu)$
- $B \to D\ell\nu$ decay FF slope : ρ_D^2
- $B \to D^*\ell\nu$ decay FF slope : ρ^2
- $B \to D^*\ell\nu$ decay FF ratio : R_1
- $B \to D^*\ell\nu$ decay FF ratio : R_2

by floating or fixing

- $\mathcal{BT}(B^+ \to \bar{D}^{**0}/(D\pi)^0 \ell^+ \nu)$

by imposing isospin constraints

- $\mathcal{B}(B^+ \to \bar{D}^0 \ell^+ \nu) = t_{+0}\mathcal{B}(B^0 \to D^- \ell^+ \nu)$
- $\mathcal{B}(B^+ \to \bar{D}^{*0} \ell^+ \nu) = t_{+0}\mathcal{B}(B^0 \to D^{*-} \ell^+ \nu)$
- $\mathcal{B}(B^+ \to \bar{D}_0^{*0} \ell^+ \nu) = t_{+0}\mathcal{B}(B^0 \to D_0^{*-} \ell^+ \nu)$
- $\mathcal{B}(B^+ \to \bar{D}_1^{0} \ell^+ \nu) = t_{+0}\mathcal{B}(B^0 \to D_1^{-} \ell^+ \nu)$
- $\mathcal{B}(B^+ \to \bar{D}_1^{*0} \ell^+ \nu) = t_{+0}\mathcal{B}(B^0 \to D_1^{\prime -} \ell^+ \nu)$
- $\mathcal{B}(B^+ \to \bar{D}_2^{*0} \ell^+ \nu) = t_{+0}\mathcal{B}(B^0 \to D_2^{*-} \ell^+ \nu)$
- $\mathcal{B}(B^+ \to D^- \pi^+ \ell^+ \nu) = 2\mathcal{B}(B^+ \to \bar{D}^0 \pi^0 \ell^+ \nu)$
  $= t_{+0}\mathcal{B}(B^0 \to \bar{D}^0 \pi^- \ell^+ \nu) = 2t_{+0}\mathcal{B}(B^0 \to D^- \pi^0 \ell^+ \nu)$
- $\mathcal{B}(B^+ \to D^{*-} \pi^+ \ell^+ \nu) = 2\mathcal{B}(B^+ \to \bar{D}^{*0} \pi^0 \ell^+ \nu)$
  $= t_{+0}\mathcal{B}(B^0 \to \bar{D}^{*0} \pi^- \ell^+ \nu) = 2t_{+0}\mathcal{B}(B^0 \to D^{*-} \pi^0 \ell^+ \nu)$

We put constraints on relative branching fractions

- $f_{D_2^*/D_1} \equiv \frac{\mathcal{B}(B^+ \to \bar{D}_2^{*0} \ell^+ \nu)}{\mathcal{B}(B^+ \to \bar{D}_1^{0} \ell^+ \nu)} = 0.78 \pm 0.17$
- $f_{D_0^* D\pi\mathcal{T}/D_1 D_2^* \mathcal{T}} \equiv \frac{\mathcal{BT}(B^+ \to \bar{D}_0^{*0}/(D\pi)^0 \ell^+ \nu)}{\mathcal{BT}(B^+ \to \bar{D}_1^{0}/\bar{D}_2^{*0} \ell^+ \nu)} = 0.77 \pm 0.19$

- $f_{D_1' D^* \pi T / D_1 D_2^* T} \equiv \frac{\mathcal{BT}(B^+ \to \bar{D}_1^{*0}/(D^*\pi)^0 \ell^+ \nu)}{\mathcal{BT}(B^+ \to \bar{D}_1^0/\bar{D}_2^{*0} \ell^+ \nu)} = 0.98 \pm 0.24$
- $f_{D\pi/D_0^*} \equiv \frac{\mathcal{B}(B^+ \to D^- \pi^+ \ell^+ \nu)}{\mathcal{B}(B^+ \to \bar{D}_0^{*0} \ell^+ \nu)} = 0.42 \pm 0.28$
- $f_{D^*\pi/D_1'} \equiv \frac{\mathcal{B}(B^+ \to D^{*-} \pi^+ \ell^+ \nu)}{\mathcal{B}(B^+ \to \bar{D}_1^{*0} \ell^+ \nu)} = 0.071 \pm 0.050$

We fix all background coefficients to 1.
We may float $\Upsilon(4S)$ decay BF ratio

- f_{+0}

and/or D^{*+} decay BF

- $\mathcal{B}(D^{*+} \to D^0 \pi^+)$
  with constraint : $\mathcal{B}(D^{*+} \to D^0 \pi^+) + \mathcal{B}(D^{*+} \to D^+ \pi^0/\gamma) = 1$

15.2 Toy MC study

15.2.1 Method of toy MC study

To validate our fitting method, we perform toy MC study. The procedure of toy MC study is the following

1. We create fake (OnPeak - OffPeak) data from $B\bar{B}$ MC, wth input values shown in Table 29.
2. Fluctuate the entry of each bin of the fake data using a Gaussian random number based on the uncertainty of each bin.
3. Fit for the fluctuated fake OnPeak data.
4. Iterate 2 and 3 for approximately 1,000 times.
5. Plot pull distributions and get the mean and the standard deviation of each distribution.

In Tablee 29, Set b has different FF slopes than Set a, Set c has different B decay BF values, Set d has different f_{+0} and Set e has different D^* decay BF.

15.2.2 Pull results.

Pulls are calculated by

$$\text{pull} = \frac{\text{fitted value} - \text{true value}}{\text{fitted uncertainty}} \tag{317}$$

We test the following four different configurations :

- Configuration 1

Parameters	Set a	Set b	Set c	Set d	Set e
ρ_D^2	1.17	1.3	1.17	1.17	1.17
ρ^2	1.179	1.23	1.179	1.179	1.179
R_1	1.417	1.417	1.417	1.417	1.417
R_2	0.836	0.836	0.836	0.836	0.836
$\mathcal{B}(B^+ \to \bar{D}^0\ell^+\nu)$	0.0233	0.0233	0.025	0.0233	0.0233
$\mathcal{B}(B^+ \to \bar{D}^{*0}\ell^+\nu)$	0.0583	0.0583	0.054	0.0583	0.0583
$\mathcal{BT}(B^+ \to \bar{D}^{**0}/(D\pi)^0\ell^+\nu)$	0.0152	0.0152	0.0152	0.0152	0.0152
$\mathcal{B}(D^{*+} \to D^0\pi^+)$	0.677	0.677	0.677	0.677	0.667
f_{+0}	1.037	1.037	1.037	1.06	1.037

Table 29: [**Parameters of fake data**] The parameter values used to create fake data. Set b has different FF slopes than Set a, Set c has different BF values, Set d has different f_{+0} and Set e has different D^* decay BF.

- Float $\mathcal{BT}(B^+ \to \bar{D}^{**0}/(D\pi)^0\ell^+\nu)$
- Fix $\mathcal{B}(D^{*+} \to D^0\pi^+)$
- Fix f_{+0}

- Configuration 2
  - Float $\mathcal{BT}(B^+ \to \bar{D}^{**0}/(D\pi)^0\ell^+\nu)$
  - Float $\mathcal{B}(D^{*+} \to D^0\pi^+)$
  - Fix f_{+0}
- Configuration 3
  - Float $\mathcal{BT}(B^+ \to \bar{D}^{**0}/(D\pi)^0\ell^+\nu)$
  - Fix $\mathcal{B}(D^{*+} \to D^0\pi^+)$
  - Float f_{+0}
- Configuration 4
  - Fix $\mathcal{BT}(B^+ \to \bar{D}^{**0}/(D\pi)^0\ell^+\nu)$
  - Fix $\mathcal{B}(D^{*+} \to D^0\pi^+)$
  - Float f_{+0}
- Configuration 5
  - Fix $\mathcal{BT}(B^+ \to \bar{D}^{**0}/(D\pi)^0\ell^+\nu)$

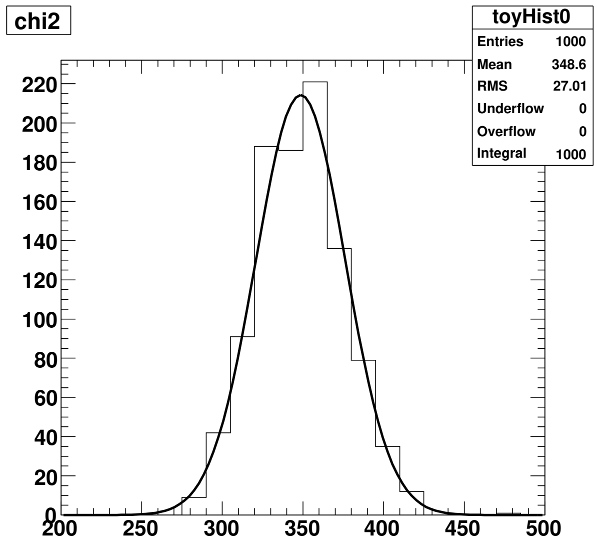

Figure 122: [**Toy MC χ^2 (Set a)**] Toy MC χ^2 plot for Configuration 2 and parameter Set a.

- Fix $\mathcal{B}(D^{*+} \to D^0\pi^+)$
- Fix f_{+0}

The mean and standard deviation (r.m.s.) of these pull distributions are listed in Table 30-34. In the bottom line of each Table, the uncertainty on mean and standard deviation are listed. We did 1000 toy fits for each parameter sets. Thus, assuming the standard deviation is $\sigma = 1$, the uncertainty on mean is

$$\frac{\sigma}{\sqrt{N}} = \frac{1}{\sqrt{1000}} = 0.0316 \tag{318}$$

and the uncertainty on standard deviation is

$$\frac{\sigma}{\sqrt{2N}} = \frac{1}{\sqrt{2 \times 1000}} = 0.0224 \tag{319}$$

The χ^2 and the pull plots are shown in Figure 122 - 124 only for Configuration 2 and parameter Set a.

Config. 1	Set a		Set b		Set c		Set d	
Parameters	Mean	r.m.s.	Mean	r.m.s.	Mean	r.m.s.	Mean	r.m.s.
ρ_D^2	+0.0168	0.939	+0.0344	0.950	+0.0226	0.938	+0.0158	0.936
ρ^2	-0.0717	0.956	-0.0766	0.952	-0.0626	0.959	-0.0699	0.955
R_1	+0.0064	0.946	-0.0008	0.974	+0.0086	0.972	+0.0036	0.973
R_2	+0.0469	0.990	+0.0498	0.990	+0.0526	0.989	+0.0471	0.989
$\mathcal{B}(B^+ \to \bar{D}^0 \ell^+ \nu)$	+0.0748	0.963	+0.0751	0.966	+0.0714	0.954	+0.0757	0.958
$\mathcal{B}(B^+ \to \bar{D}^{*0} \ell^+ \nu)$	-0.0525	0.977	-0.0527	0.977	-0.0664	0.976	-0.0515	0.977
$\mathcal{BT}(B^+ \to \bar{D}^{**0}/(D\pi)^0 \ell^+ \nu)$	+0.0051	1.012	+0.0087	1.010	+0.0162	1.011	+0.0019	1.011
Uncertainty	0.0317	0.0224	0.0317	0.0224	0.0317	0.0224	0.0317	0.0224

Table 30: [**Toy MC : Mean and Standard Deviation (Config. 1)**] Mean and standard deviation (r.m.s.) of pull distributions of toy MC. The uncertainty on mean and standard deviation are also listed in the bottom line. Pulls are calculated from the difference to nominal fit results.

Config. 2	Set a		Set b		Set c		Set e	
Parameters	Mean	r.m.s.	Mean	r.m.s.	Mean	r.m.s.	Mean	r.m.s.
ρ_D^2	+0.0329	0.964	+0.0347	0.969	+0.0446	0.967	+0.0266	0.967
ρ^2	-0.0652	0.965	-0.0659	0.964	-0.0597	0.974	-0.0667	0.966
R_1	-0.0043	0.975	-0.0048	0.977	-0.0052	0.974	-0.0008	0.977
R_2	+0.0446	0.979	+0.0480	0.979	+0.0573	0.981	+0.0430	0.977
$\mathcal{B}(B^+ \to \bar{D}^0 \ell^+ \nu)$	+0.0808	0.986	+0.0852	0.989	+0.0993	0.993	+0.0819	0.983
$\mathcal{B}(B^+ \to \bar{D}^{*0} \ell^+ \nu)$	-0.0498	0.983	-0.0541	0.980	-0.0699	0.980	-0.0487	0.982
$\mathcal{BT}(B^+ \to \bar{D}^{**0}/(D\pi)^0 \ell^+ \nu)$	+0.0303	0.951	+0.0295	0.952	+0.0441	0.949	+0.0299	0.952
$\mathcal{B}(D^{*+} \to D^0 \pi^+)$	+0.0059	0.998	+0.0145	1.000	+0.0238	1.005	+0.0090	0.999
Uncertainty	0.0316	0.0224	0.0316	0.0224	0.0316	0.0224	0.0316	0.0224

Table 31: [**Toy MC : Mean and Standard Deviation (Config. 2)**] Mean and standard deviation (r.m.s.) of pull distributions of toy MC fits. The uncertainty on mean and standard deviation are also listed in the bottom line. Pulls are calculated from the difference to nominal fit results.

Config. 3	Set a		Set b		Set c		Set d	
Parameters	Mean	r.m.s.	Mean	r.m.s.	Mean	r.m.s.	Mean	r.m.s.
ρ_D^2	+0.1118	1.008						
ρ^2	-0.0949	0.960						
R_1	-0.0372	0.979						
R_2	+0.1057	0.985						
$\mathcal{B}(B^+ \to \bar{D}^0\ell^+\nu)$	+0.0589	0.971						
$\mathcal{B}(B^+ \to \bar{D}^{*0}\ell^+\nu)$	-0.1116	0.983						
$\mathcal{BT}(B^+ \to \bar{D}^{**0}/(D\pi)^0\ell^+\nu)$	+0.1302	0.977						
f_{+0}	+0.0601	0.994						
Uncertainty	0.0316	0.0224	0.0316	0.0224	0.0316	0.0224	0.0316	0.0224

Table 32: [**Toy MC : Mean and Standard Deviation (Config. 3)**] Mean and standard deviation (r.m.s.) of pull distributions of toy MC fits. The uncertainty on mean and standard deviation are also listed in the bottom line. Pulls are calculated from the difference to nominal fit results.

Config. 4	Set a		Set b		Set c		Set d	
Parameters	Mean	r.m.s.	Mean	r.m.s.	Mean	r.m.s.	Mean	r.m.s.
ρ_D^2	+0.0647	0.992	+0.0334	0.983	+0.0180	0.933	+0.0172	0.933
ρ^2	-0.0190	1.014	-0.0467	0.961	-0.0439	0.964	-0.0550	0.956
R_1	-0.0506	1.001	-0.0235	0.993	+0.0362	0.971	+0.0350	0.968
R_2	+0.0343	1.036	+0.1045	0.968	+0.0580	0.974	+0.0643	0.976
$\mathcal{B}(B^+ \to \bar{D}^0\ell^+\nu)$	+0.1319	1.013	+0.0407	0.988	+0.0934	0.942	-0.0861	0.962
$\mathcal{B}(B^+ \to \bar{D}^{*0}\ell^+\nu)$	-0.0635	0.988	-0.0339	0.999	-0.0376	0.974	-0.0374	0.992
f_{+0}	+0.0895	0.961	-0.0837	0.991	+0.0332	0.996	+0.0118	0.999
Uncertainty	0.0316	0.0224	0.0316	0.0224	0.0316	0.0224	0.0316	0.0224

Table 33: [**Toy MC : Mean and Standard Deviation (Config. 4)**] Mean and standard deviation (r.m.s.) of pull distributions of toy MC fits. The uncertainty on mean and standard deviation are also listed in the bottom line. Pulls are calculated from the difference to nominal fit results.

Config. 5	Set a		Set b		Set c		Set d	
Parameters	Mean	r.m.s.	Mean	r.m.s.	Mean	r.m.s.	Mean	r.m.s.
ρ_D^2	+0.0009	0.939	+0.0123	0.942	+0.0112	0.937	+0.0149	0.941
ρ^2	-0.0670	0.944	-0.0663	0.942	-0.0595	0.944	-0.0658	0.945
R_1	+0.0174	0.946	+0.0280	0.954	-0.0232	0.950	-0.0107	0.939
R_2	+0.0621	0.970	+0.0632	0.976	+0.0603	0.970	+0.0657	0.967
$\mathcal{B}(B^+ \to \bar{D}^0\ell^+\nu)$	+0.0750	0.960	-0.0742	0.966	+0.0742	0.949	-0.0763	0.958
$\mathcal{B}(B^+ \to \bar{D}^{*0}\ell^+\nu)$	-0.0612	1.008	-0.0653	1.016	-0.0565	1.020	-0.0639	1.009
Uncertainty	0.0317	0.0224	0.0317	0.0224	0.0317	0.0224	0.0317	0.0224

Table 34: [**Toy MC : Mean and Standard Deviation (Config. 5)**] Mean and standard deviation (r.m.s.) of pull distributions of toy MC by fixing $f_{+0} = 1.037$. The uncertainty on mean and standard deviation are also listed in the bottom line. Pulls are calculated from the difference to nominal fit results.

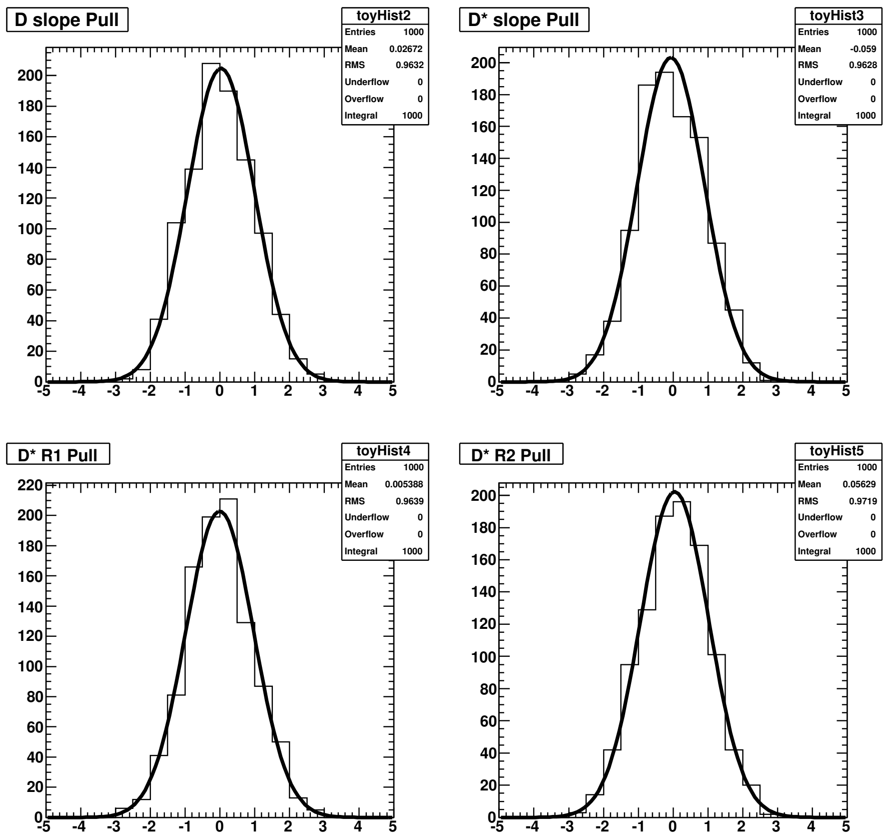

Figure 123: [**Toy MC Pull FF (Set a)**] Toy MC pull plots of FF parameters for Configuration 2 and parameter Set a.

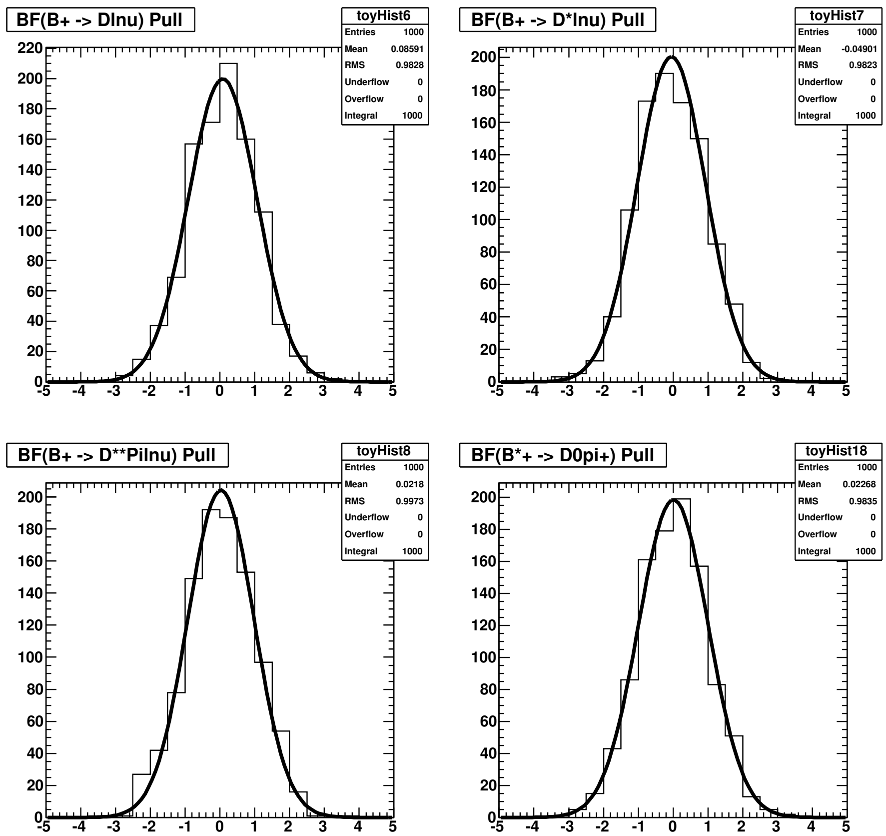

Figure 124: [**Toy MC Pull BF (Set a)**] Toy MC pull plots of BF for Configuration 2 and parameter Set a.

15.3 Rough estimate of systematic uncertainties

We make a rough estimate of major systematic uncertainty for Configurations 1 - 3 in previous subsection.

1. $D^{**}\ell\nu$ FF parameters
   We vary FF slope and we also use Approximation B to estimate systematic uncertainty.

2. $D^{**}\ell\nu/D^{(*)}\pi\ell\nu$ BF ratios
   We vary 5 BF ratios ($f_{D_2^*/D_1}$ etc.) to estimate uncertainty.

3. Effect of $D^{(*)}\pi\pi\ell\nu$ component
   We include $D^{(*)}\pi\pi\ell\nu$ component in our fit to estimate systematic uncertainty.

4. Effect of background re-weighting
   We use original non-wighted backgrounds to estimate systematic uncertainty.

5. Effect of f_{+0} We vary f_{+0} to estimate systematic uncertainty.

Results are shown in Table 35 - 37. Numbers are in %. chi^2/n.d.f and P-values are

	chi^2/n.d.f	P-values
Config. 1	371/351	0.225
Config. 2	364/350	0.286
Config. 3	370/350	0.220

Config. 1	ρ_D^2	ρ^2	R_1	R_2.	$\mathcal{B}(D\ell\nu)$	$\mathcal{B}(D^*\ell\nu)$	$\mathcal{B}(D^{(*)}\pi\ell\nu)$
Stat. Error	3.36	3.52	4.63	7.56	1.09	0.98	6.05
D^{**} FF	1.08	1.61	2.75	2.89	0.20	0.25	3.16
D^{**} BF	1.38	0.93	1.96	2.20	0.83	0.20	4.32
$D^{(*)}\pi^+\pi^-\ell\nu$	0.18	1.74	4.37	6.42	0.71	1.51	33.91
Background	0.03	0.26	5.55	5.20	0.21	1.18	3.17
f_{+0}	2.17	0.06	1.21	0.81	1.33	1.65	5.95
Sys. Error	2.80	2.56	7.93	9.06	1.74	2.54	34.98

Table 35: [**Major systematic error (Config. 1)**] Rough estimation of major systematic uncertainties (%).

Config. 2	ρ_D^2	ρ^2	R_1	R_2.	$\mathcal{B}(D\ell\nu)$	$\mathcal{B}(D^*\ell\nu)$	$\mathcal{B}(D^{(*)}\pi\ell\nu)$	$\mathcal{B}(D^0\pi^+)$
Stat. Error	4.12	3.53	4.67	8.04	1.31	1.29	7.38	0.84
D^{**} FF	1.31	1.41	2.49	2.89	0.19	0.29	3.66	0.24
D^{**} BF	0.96	0.54	1.86	2.23	0.26	0.51	5.52	0.68
$D^{(*)}\pi^+\pi^-\ell\nu$	0.92	1.07	3.69	4.99	1.04	0.75	29.83	0.51
Background	1.04	0.17	5.62	6.15	0.18	0.65	1.49	0.50
f_{+0}	0.52	0.76	1.39	0.82	0.62	0.67	2.78	0.94
Sys. Error	2.20	2.10	7.54	8.76	1.27	1.33	30.72	1.39

Table 36: [**Major systematic error (Config. 2)**] Rough estimation of major systematic uncertainties (%).

Config. 3	ρ_D^2	ρ^2	R_1	R_2.	$\mathcal{B}(D\ell\nu)$	$\mathcal{B}(D^*\ell\nu)$	$\mathcal{B}(D^{(*)}\pi\ell\nu)$	f_{+0}
Stat. Error	3.66	3.52	4.67	7.58	1.34	1.35	7.13	1.62
D^{**} FF	1.30	1.60	2.46	2.84	0.27	0.45	4.39	0.64
D^{**} BF	0.95	0.93	2.20	2.17	0.31	0.54	5.83	1.16
$D^{(*)}\pi^+\pi^-\ell\nu$	0.32	1.76	4.33	6.50	0.63	1.61	35.35	0.15
Background	0.59	0.26	5.25	5.38	0.14	0.74	1.65	0.74
Sys. Error	1.74	2.57	7.56	9.16	0.77	1.90	36.13	1.52

Table 37: [**Major systematic error (Config. 3)**] Rough estimation of major systematic uncertainties (%).

15.4 D^+ $\cos\theta_{B-Dl}$ problem

After background and lower momentum cuts, there is one major problem in our fit :

- D^+ $\cos\theta_{B-Dl}$ problem
  D^+ $\cos\theta_{B-Dl}$ plots aftre fitting with Configuration 1 are shown in Figures 125 and 126. There is a data-MC disagreement in D^+ D^+ $\cos\theta_{B-Dl} < 0$ bin. Configuration 3 also shows the similar difference.

This can be caused by a tension between D^0 and D^+ yeilds. We try to float D^+ decay BF, D^0 decay BF and D^{*+} decay BF to see what values our fit prefer. As a reasult, our fit gave the most different value for D^{*+} decay BF. In fact, if we float $\mathcal{B}(D^{*+} \to D^0\pi^+)$ (Configuratin 2) with constraint

$$\mathcal{B}(D^{*+} \to D^0\pi^+) + \mathcal{B}(D^{*+} \to D^+\pi^0/\gamma) = 1 \tag{320}$$

data-MC difference in D^+ D^+ $\cos\theta_{B-Dl} < 0$ reduced as seen in Figures 127 and 128.

15.5 Selection of nominal fit configuration

Considering baises from toy fits, possible systematic uncertainty and isospin and $\cos\theta_{B-Dl}$ problems, **Configuration 2 can be the best chioce for our nominal fit**.

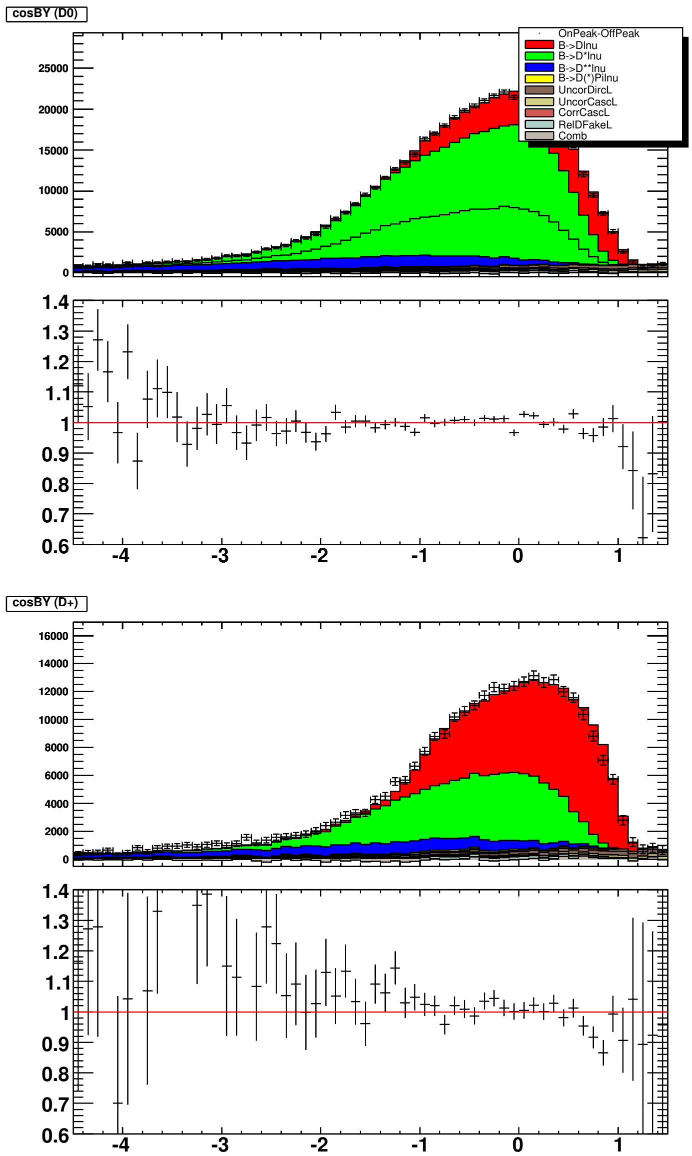

Figure 125: [$\cos\theta_{B-Dl}$ **(Config. 1)**] $\cos\theta_{B-Dl}$ plot with fitted binning after fitting. The top is D^0 and the bottom is D^+. Black is OnPeak - OffPeak data. Red is $B \to D\ell\nu$, green is $B \to D^*\ell\nu$, blue is $B \to D^{**}\ell\nu$, yellow is non-resonant $B \to D^{(*)}\pi\ell\nu$, and the rest is background. Dark brown is UncorrDL, light brown is UncorrCL, dark red is CascL, blue gray is FakeL, and light gray is Comb. Comb is almost disappeared after D mass sideband subtraction.

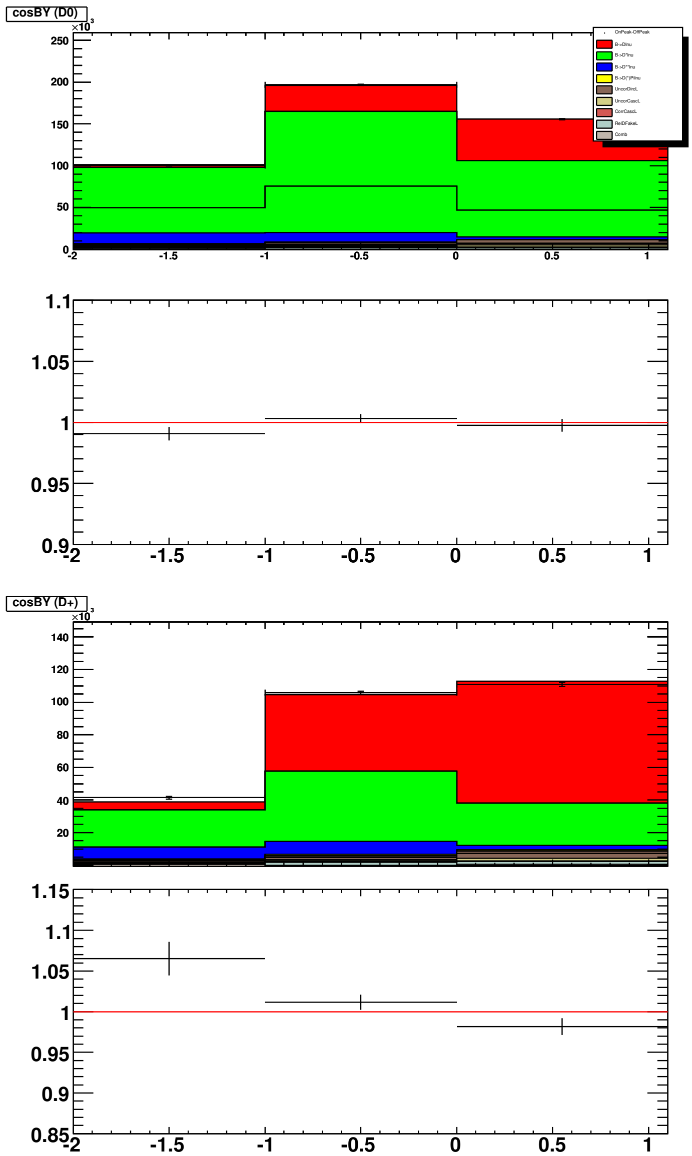

Figure 126: [$\cos\theta_{B-Dl}$ **with fitted binning (Config. 1)**] $\cos\theta_{B-Dl}$ plot with fitted binning after fitting. The top is D^0 and the bottom is D^+. Black is OnPeak - OffPeak data. Red is $B \to D\ell\nu$, green is $B \to D^*\ell\nu$, blue is $B \to D^{**}\ell\nu$, yellow is non-resonant $B \to D^{(*)}\pi\ell\nu$, and the rest is background. Dark brown is UncorrDL, light brown is UncorrCL, dark red is CascL, blue gray is FakeL, and light gray is Comb. Comb is almost disappeared after D mass sideband subtraction.

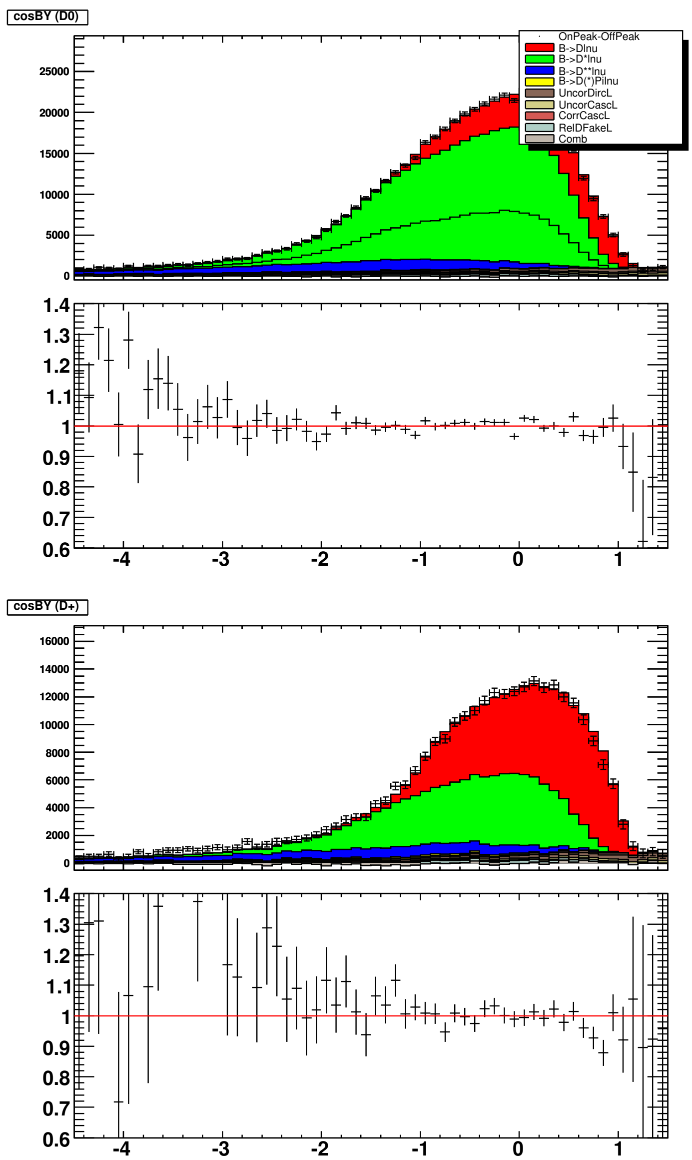

Figure 127: [$\cos\theta_{B-Dl}$ **(Config. 2)**] $\cos\theta_{B-Dl}$ plot with fitted binning after fitting. The top is D^0 and the bottom is D^+. Black is OnPeak - OffPeak data. Red is $B \to D\ell\nu$, green is $B \to D^*\ell\nu$, blue is $B \to D^{**}\ell\nu$, yellow is non-resonant $B \to D^{(*)}\pi\ell\nu$, and the rest is background. Dark brown is UncorrDL, light brown is UncorrCL, dark red is CascL, blue gray is FakeL, and light gray is Comb. Comb is almost disappeared after D mass sideband subtraction.

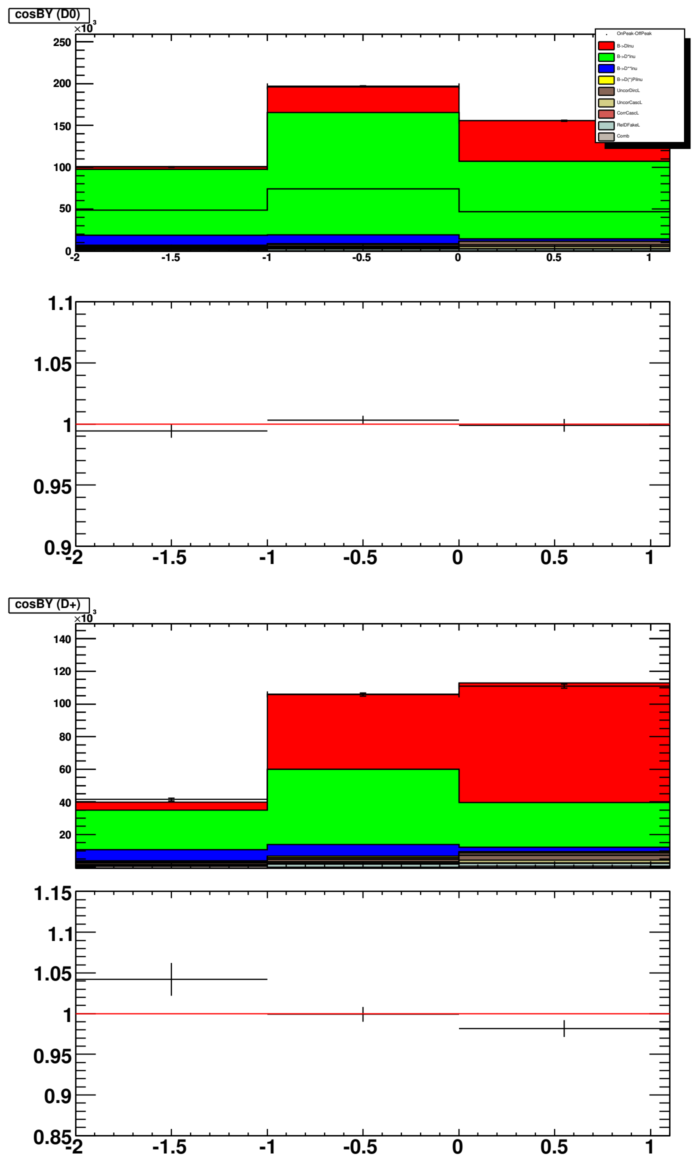

Figure 128: [$\cos\theta_{B-Dl}$ **with fitted binning (Config. 2)**] $\cos\theta_{B-Dl}$ plot with fitted binning after fitting. The top is D^0 and the bottom is D^+. Black is OnPeak - OffPeak data. Red is $B \to D\ell\nu$, green is $B \to D^*\ell\nu$, blue is $B \to D^{**}\ell\nu$, yellow is non-resonant $B \to D^{(*)}\pi\ell\nu$, and the rest is background. Dark brown is UncorrDL, light brown is UncorrCL, dark red is CascL, blue gray is FakeL, and light gray is Comb. Comb is almost disappeared after D mass sideband subtraction.

15.6 Validation fits by splitted MC

15.6.1 Validation fit method

To validate our fitting method, we construct fake (OnPeak - OffPeak) data from $B\bar{B}$ MC. We split MC into two halves. We use one half to construct fake data. We, then, create component histograms from the other half, and fit the fake data by the histograms. We can construct fake data with any branching fractions and form factor parameters we want. We then perform fitting to see if our method produce reasonable fitting results.
We use four different parameter sets to create fake data which are shown in Tables 29. The same values are listed as input values in the following tables. We split MC by four different ways

- Split A : Separate even number events and odd number events.
- Split B : Separate events using a set of random nombers.
- Split C : Separate events using another set of random nombers.
- Split D : Separate events using a different set of random nombers.

Thus, there are 16 different validation fittings need to be done.

15.6.2 Validation fit results

We perform this validation only for Configuration 2 :

- Float $\mathcal{BT}(B^+ \to \bar{D}^{**0}/(D\pi)^0\ell^+\nu)$
- Float $\mathcal{B}(D^{*+} \to D^0\pi^+)$
- Fix f_{+0}

Fit results are given in Tables 38 - 41. As an index of agreement, we calculate pulls as defined in the above Equation (317). We also caluculate overall χ^2 between input and fitted parameter values, namely

$$\chi^2_{Val} = (\Delta_1, \Delta_2, ..., \Delta_k) \begin{pmatrix} \text{Invers} \\ \text{covariance} \\ \text{matrix} \end{pmatrix} \begin{pmatrix} \Delta_1 \\ \Delta_2 \\ . \\ . \\ . \\ \Delta_k \end{pmatrix} \tag{321}$$

where Δ_i is the differnce between fitted and input values of i-th parameter :

$$\Delta_i = \text{fitted value} - \text{true value} \tag{322}$$

For example, we expect the r.m.s. of a χ^2 distribution with 218 dof to be about 21.

Config. 2	Input (Set a)	Split A		Split B		Split C		Split D	
		fit result	pulls	fit result	pulls	fit result	pulls	fit result	pulls
ρ_D^2	1.17	$\pm$0.027	-1.38	$\pm$0.025	+0.94	$\pm$0.026	-0.33	$\pm$0.026	+0.13
ρ^2	1.23	$\pm$0.021	+1.24	$\pm$0.021	+0.46	$\pm$0.021	-1.27	$\pm$0.021	+1.23
R_1	1.417	$\pm$0.029	+1.32	$\pm$0.028	-0.23	$\pm$0.026	-1.55	$\pm$0.029	+1.23
R_2	0836	$\pm$0.025	-1.69	$\pm$0.025	-0.27	$\pm$0.023	+1.23	$\pm$0.025	-1.28
$\mathcal{B}(B^+ \to \bar{D}^0 \ell^+ \nu)$	0.0233	$\pm$0.00019	-0.65	$\pm$0.00019	+1.61	$\pm$0.00019	+0.29	$\pm$0.00019	+0.52
$\mathcal{B}(B^+ \to \bar{D}^{*0} \ell^+ \nu)$	0.0583	$\pm$0.00027	+0.92	$\pm$0.00027	-1.46	$\pm$0.00027	+0.23	$\pm$0.00027	-1.15
$\mathcal{BT}(B^+ \to \bar{D}^{**0}/(D\pi)^0 \ell^+ \nu)$	0.0583	$\pm$0.00027	+0.92	$\pm$0.00027	-1.46	$\pm$0.00027	+0.23	$\pm$0.00027	-1.15
$\mathcal{B}(D^{*+} \to D^0 \pi^+)$	0.0583	$\pm$0.00027	+0.92	$\pm$0.00027	-1.46	$\pm$0.00027	+0.23	$\pm$0.00027	-1.15
χ^2/ndof (P-value)		204/220 (0.77)		250/219 (0.07)		192/221 (0.92)		218/220 (0.53)	
χ^2_{Val}			18.4		11.7		12.1		14.5

Table 38: [**MC vs MC (Parameter set a)**] Validation fit results using parameter set a.

Config. 2	Input (Set b)	Split A		Split B		Split C		Split D	
		fit result	pulls	fit result	pulls	fit result	pulls	fit result	pulls
ρ_D^2	1.17	1.126 ± 0.027	-1.65	1.198 ± 0.027	+1.03	1.160 ± 0.028	-0.38	1.174 ± 0.026	+0.17
ρ^2	1.23	1.258 ± 0.020	+1.40	1.237 ± 0.020	+0.34	1.207 ± 0.019	-1.22	1.254 ± 0.019	+1.21
R_1	1.417	1.455 ± 0.027	+1.40	1.408 ± 0.026	-0.34	1.380 ± 0.025	-1.50	1.450 ± 0.027	+1.20
R_2	0.836	0.793 ± 0.024	-1.83	0.831 ± 0.023	-0.20	0.862 ± 0.022	+1.20	0.806 ± 0.024	-1.28
$\mathcal{B}(B^+ \to \bar{D}^0 \ell^+ \nu)$	0.0215	0.02136 ± 0.00017	-0.83	0.02156 ± 0.00018	+0.30	0.02180 ± 0.00019	+1.58	0.02160 ± 0.00017	+0.60
$\mathcal{B}(B^+ \to \bar{D}^{*0} \ell^+ \nu)$	0.065	0.06530 ± 0.00028	+1.08	0.06462 ± 0.00028	-1.35	0.06506 ± 0.00028	+0.23	0.06467 ± 0.00028	-1.18
$\mathcal{B}\mathcal{T}(B^+ \to \bar{D}^{**0}/(D\pi)^0 \ell^+ \nu)$	0.0583	± 0.00027	+0.92	± 0.00027	-1.46	± 0.00027	+0.23	± 0.00027	-1.15
$\mathcal{B}(D^{*+} \to D^0 \pi^+)$	0.0583	± 0.00027	+0.92	± 0.00027	-1.46	± 0.00027	+0.23	± 0.00027	-1.15
χ^2/ndof (P-value)		203/220 (0.79)		245/219 (0.08)		195/222 (0.91)		220/220 (0.48)	
χ^2_{Val}			19.2		11.1		12.5		17.5

Table 39: [**MC vs MC (Parameter set b)**] Validation fit results using parameter set b.

Config. 2	Input (Set c)	Split A		Split B		Split C		Split D	
		fit result	pulls	fit result	pulls	fit result	pulls	fit result	pulls
ρ^2_D	1.17	1.133 ± 0.027	-1.38	1.194 ± 0.024	+1.00	1.160 ± 0.026	-0.37	1.173 ± 0.026	+0.11
ρ^2	1.23	1.258 ± 0.021	+1.33	1.238 ± 0.021	+0.40	1.204 ± 0.021	-1.27	1.255 ± 0.021	+1.21
R_1	1.417	1.457 ± 0.029	+1.40	1.408 ± 0.028	-0.30	1.375 ± 0.026	-1.59	1.453 ± 0.029	+1.25
R_2	0.836	0.792 ± 0.025	-1.77	0.831 ± 0.024	-0.21	0.865 ± 0.023	+1.26	0.805 ± 0.025	-1.24
$\mathcal{B}(B^+ \to \bar{D}^0 \ell^+ \nu)$	0.0233	0.02319 ± 0.00019	-0.61	0.02361 ± 0.00018	+1.67	0.02335 ± 0.00019	+0.25	0.02340 ± 0.00019	+0.52
$\mathcal{B}(B^+ \to \bar{D}^{*0} \ell^+ \nu)$	0.0583	0.05855 ± 0.00026	+0.94	0.05791 ± 0.00026	-1.49	0.05837 ± 0.00027	+0.25	0.05797 ± 0.00026	-1.26
$\mathcal{BT}(B^+ \to \bar{D}^{**0}/(D\pi)^0 \ell^+ \nu)$	0.0583	± 0.00027	+0.92	± 0.00027	-1.46	± 0.00027	+0.23	± 0.00027	-1.15
$\mathcal{B}(D^{*+} \to D^0 \pi^+)$	0.0583	± 0.00027	+0.92	± 0.00027	-1.46	± 0.00027	+0.23	± 0.00027	-1.15
χ^2/ndof (P-value)		207/219 (0.72)		249/219 (0.08)		192/221 (0.92)		217/220 (0.54)	
χ^2_{Val}			18.5		13.5		12.1		14.2

Table 40: [**MC vs MC (Parameter set c)**] Validation fit results using parameter set c.

Config. 2	Input (Set d)	Split A		Split B		Split C		Split D	
		fit result	pulls	fit result	pulls	fit result	pulls	fit result	pulls
ρ_D^2	1.3	1.267 ± 0.023	-1.43	1.321 ± 0.021	+0.97	1.290 ± 0.023	-0.43	1.301 ± 0.023	+0.04
ρ^2	1.3	1.330 ± 0.023	+1.27	1.313 ± 0.024	+0.56	1.275 ± 0.023	-1.06	1.333 ± 0.024	+1.38
R_1	1.5	1.543 ± 0.034	+1.28	1.494 ± 0.033	-0.17	1.455 ± 0.031	-1.42	1.550 ± 0.036	+1.40
R_2	0.6	0.553 ± 0.030	-1.54	0.588 ± 0.030	-0.40	0.631 ± 0.029	+1.08	0.555 ± 0.032	-1.42
$\mathcal{B}(B^+ \to \bar{D}^0 \ell^+ \nu)$	0.0233	0.02342 ± 0.00019	-0.51	0.02362 ± 0.00019	+1.73	0.02333 ± 0.00019	+0.19	0.02341 ± 0.00019	+0.60
$\mathcal{B}(B^+ \to \bar{D}^{*0} \ell^+ \nu)$	0.0583	0.05850 ± 0.00025	+0.77	0.05787 ± 0.00025	-1.72	0.05838 ± 0.00026	+0.32	0.05798 ± 0.00026	-1.26
$\mathcal{BT}(B^+ \to \bar{D}^{**0}/(D\pi)^0 \ell^+ \nu)$	0.0583	± 0.00027	+0.92	± 0.00027	-1.46	± 0.00027	+0.23	± 0.00027	-1.15
$\mathcal{B}(D^{*+} \to D^0 \pi^+)$	0.0583	± 0.00027	+0.92	± 0.00027	-1.46	± 0.00027	+0.23	± 0.00027	-1.15
χ^2/ndof (P-value)		208/219 (0.69)		249/219 (0.08)		194/221 (0.91)		217/220 (0.54)	
χ^2_{Val}			19.2		13.4		11.7		14.1

Table 41: [**MC vs MC (Parameter set e)**] Validation fit results using parameter set e.

16 Fit Results

From this section we rename $\mathcal{BT}(B^+ \to \bar{D}^{**0}/(D\pi)^0\ell^+\nu)$ to $\mathcal{B}(B^+ \to \bar{D}^{(*)}\pi\ell^+\nu)$

16.1 New AWG recomended BF

- B^+ decays
  - $\mathcal{B}(B^+ \to \bar{D}_0^{*0}\ell^+\nu) = 0.0045 \pm 0.0009$
  - $\mathcal{B}(B^+ \to \bar{D}_1^0\ell^+\nu) = 0.0054 \pm 0.0006$
  - $\mathcal{B}(B^+ \to \bar{D}_1^{\prime 0}\ell^+\nu) = 0.0085 \pm 0.0020$
  - $\mathcal{B}(B^+ \to \bar{D}_2^{*0}\ell^+\nu) = 0.0042 \pm 0.0008$
  - $\mathcal{B}(B^+ \to D^-\pi^+\ell^+\nu) = 0.0019 \pm 0.0012$
  - $\mathcal{B}(B^+ \to \bar{D}^0\pi^0\ell^+\nu) = 0.0010 \pm 0.0006$
  - $\mathcal{B}(B^+ \to D^{*-}\pi^+\ell^+\nu) = 0.0006 \pm 0.0004$
  - $\mathcal{B}(B^+ \to \bar{D}^{*0}\pi^0\ell^+\nu) = 0.0003 \pm 0.0002$
- B^0 decays
  - $\mathcal{B}(B^0 \to D_0^{*-}\ell^+\nu) = 0.0043 \pm 0.0009$
  - $\mathcal{B}(B^0 \to D_1^-\ell^+\nu) = 0.0050 \pm 0.0008$
  - $\mathcal{B}(B^0 \to D_1^{\prime -}\ell^+\nu) = 0.0080 \pm 0.0020$
  - $\mathcal{B}(B^0 \to D_2^{*-}\ell^+\nu) = 0.0039 \pm 0.0007$
  - $\mathcal{B}(B^0 \to \bar{D}^0\pi^-\ell^+\nu) = 0.0019 \pm 0.0012$
  - $\mathcal{B}(B^0 \to D^-\pi^0\ell^+\nu) = 0.0009 \pm 0.0006$
  - $\mathcal{B}(B^0 \to \bar{D}^{*0}\pi^-\ell^+\nu) = 0.0006 \pm 0.0004$
  - $\mathcal{B}(B^0 \to D^{*-}\pi^0\ell^+\nu) = 0.0003 \pm 0.0004$

We calculate the branching fraction ratios by assuming the above branching fractions are independent.

$$\begin{aligned}
&f_{D_2^*/D_1} \equiv \frac{\mathcal{B}(B^+\to\bar{D}_2^{*0}\ell^+\nu)}{\mathcal{B}(B^+\to\bar{D}_1^0\ell^+\nu)} = 0.78 \pm 0.17 \\
&f_{D_0^*D\pi T/D_1D_2^*T} \equiv \frac{\mathcal{BT}(B^+\to\bar{D}_0^{*0}/(D\pi)^0\ell^+\nu)}{\mathcal{BT}(B^+\to\bar{D}_1^0/\bar{D}_2^{*0}\ell^+\nu)} = 0.77 \pm 0.19 \\
&f_{D_1'D^*\pi T/D_1D_2^*T} \equiv \frac{\mathcal{BT}(B^+\to\bar{D}_1^{*0}/(\bar{D}^*\pi)^0\ell^+\nu)}{\mathcal{BT}(B^+\to\bar{D}_1^0/\bar{D}_2^{*0}\ell^+\nu)} = 0.98 \pm 0.24 \\
&f_{D\pi/D_0^*} \equiv \frac{\mathcal{B}(B^+\to D^-\pi^+\ell^+\nu)}{\mathcal{B}(B^+\to\bar{D}_0^{*0}\ell^+\nu)} = 0.42 \pm 0.28 \\
&f_{D^*\pi/D_1'} \equiv \frac{\mathcal{B}(B^+\to D^{*-}\pi^+\ell^+\nu)}{\mathcal{B}(B^+\to\bar{D}_1^{*0}\ell^+\nu)} = 0.071 \pm 0.050
\end{aligned} \tag{323}$$

16.2 Summary of nominal fit configuration

We are trying to fit for two branching fractions and four form factor parameters

- $\mathcal{B}(B^+ \to \bar{D}^0 \ell^+ \nu)$
- $\mathcal{B}(B^+ \to \bar{D}^{*0} \ell^+ \nu)$
- $B \to D\ell\nu$ decay FF slope : ρ_D^2
- $B \to D^*\ell\nu$ decay FF slope : ρ^2
- $B \to D^*\ell\nu$ decay FF ratio : R_1
- $B \to D^*\ell\nu$ decay FF ratio : R_2

by floating two branching fractions

- $\mathcal{B}(B^+ \to \bar{D}^{(*)} \pi \ell^+ \nu)$
- $\mathcal{B}(D^{*+} \to D^0 \pi^+)$
  with constraint : $\mathcal{B}(D^{*+} \to D^0 \pi^+) + \mathcal{B}(D^{*+} \to D^+ \pi^0/\gamma) = 1$

by imposing isospin constraints

- $\mathcal{B}(B^+ \to \bar{D}^0 \ell^+ \nu) = t_{+0} \mathcal{B}(B^0 \to D^- \ell^+ \nu)$
- $\mathcal{B}(B^+ \to \bar{D}^{*0} \ell^+ \nu) = t_{+0} \mathcal{B}(B^0 \to D^{*-} \ell^+ \nu)$
- $\mathcal{B}(B^+ \to \bar{D}_0^{*0} \ell^+ \nu) = t_{+0} \mathcal{B}(B^0 \to D_0^{*-} \ell^+ \nu)$
- $\mathcal{B}(B^+ \to \bar{D}_1^0 \ell^+ \nu) = t_{+0} \mathcal{B}(B^0 \to D_1^- \ell^+ \nu)$
- $\mathcal{B}(B^+ \to \bar{D}_1^{*0} \ell^+ \nu) = t_{+0} \mathcal{B}(B^0 \to D_1^{\prime -} \ell^+ \nu)$
- $\mathcal{B}(B^+ \to \bar{D}_2^{*0} \ell^+ \nu) = t_{+0} \mathcal{B}(B^0 \to D_2^{*-} \ell^+ \nu)$
- $\mathcal{B}(B^+ \to D^- \pi^+ \ell^+ \nu) = 2\mathcal{B}(B^+ \to \bar{D}^0 \pi^0 \ell^+ \nu)$
  $= t_{+0} \mathcal{B}(B^0 \to \bar{D}^0 \pi^- \ell^+ \nu) = 2t_{+0} \mathcal{B}(B^0 \to D^- \pi^0 \ell^+ \nu)$
- $\mathcal{B}(B^+ \to D^{*-} \pi^+ \ell^+ \nu) = 2\mathcal{B}(B^+ \to \bar{D}^{*0} \pi^0 \ell^+ \nu)$
  $= t_{+0} \mathcal{B}(B^0 \to \bar{D}^{*0} \pi^- \ell^+ \nu) = 2t_{+0} \mathcal{B}(B^0 \to D^{*-} \pi^0 \ell^+ \nu)$

We fix relative branching fractions

- $f_{D_2^*/D_1}$
- $f_{D_0^* D\pi T/D_1 D_2^* T}$
- $f_{D_1' D^*\pi T/D_1 D_2^* T}$
- $f_{D\pi/D_0^*}$
- $f_{D^*\pi/D_1'}$

and also fix all background coefficients.

ρ_D^2	1.157 ± 0.039 (3.4 %)
ρ^2	1.300 ± 0.040 (3.1 %)
R_1	1.428 ± 0.062 (4.4 %)
R_2	0.727 ± 0.052 (7.2 %)
$\mathcal{B}(B^+ \to \bar{D}^0 \ell^+ \nu)$	0.02331 ± 0.00025 (1.1 %)
$\mathcal{B}(B^+ \to \bar{D}^{*0} \ell^+ \nu)$	0.05485 ± 0.00034 (0.62 %)
$\mathcal{B}(D^{(*)} \pi \ell \nu)$	1.027 ± 0.014 (1.4 %)
$\mathcal{B}(D^{*+} \to D^0 \pi^+)$	1.027 ± 0.014 (1.4 %)
χ^2/ndof (P-value)	381/351 (0.132)

Table 42: [**Nominal fit results**] Fit results.

16.3 Fit results

Fit results are shown in Table 42 and correlations between parameters are given in Table 43. Plots of lepton momentum, D momentum and $\cos\theta_{B-Dl}$ after fitting are given in Figure 129 - 131 with fitted binning. Bin by bin plots after fitting are also shown in Figure 132 and 133.

	ρ_D^2	ρ^2	R_1	R_2	$\mathcal{B}(D\ell\nu)$	$\mathcal{B}(D^*\ell\nu)$	$\mathcal{B}(D\pi\ell\nu)$	D^{*+} BF
ρ_D^2	1							
ρ^2	-0.125	1						
R_1	+0.095	+0.843	1					
R_2	+0.022	-0.903	-0.910	1				
$\mathcal{B}(D\ell\nu)$	+0.358	+0.311	+0.405	-0.215	1			
$\mathcal{B}(D^*\ell\nu)$	-0.459	+0.056	-0.197	-0.117	-0.689	1		
$\mathcal{B}(D\pi\ell\nu)$	+0.233	+0.236	+0.296	-0.161	+0.531	-0.590	1	
D^{*+} BF	+0.233	+0.236	+0.296	-0.161	+0.531	-0.590		1

Table 43: [**Correlation coefficients (Nominal fit)**] Correlations between parameters.

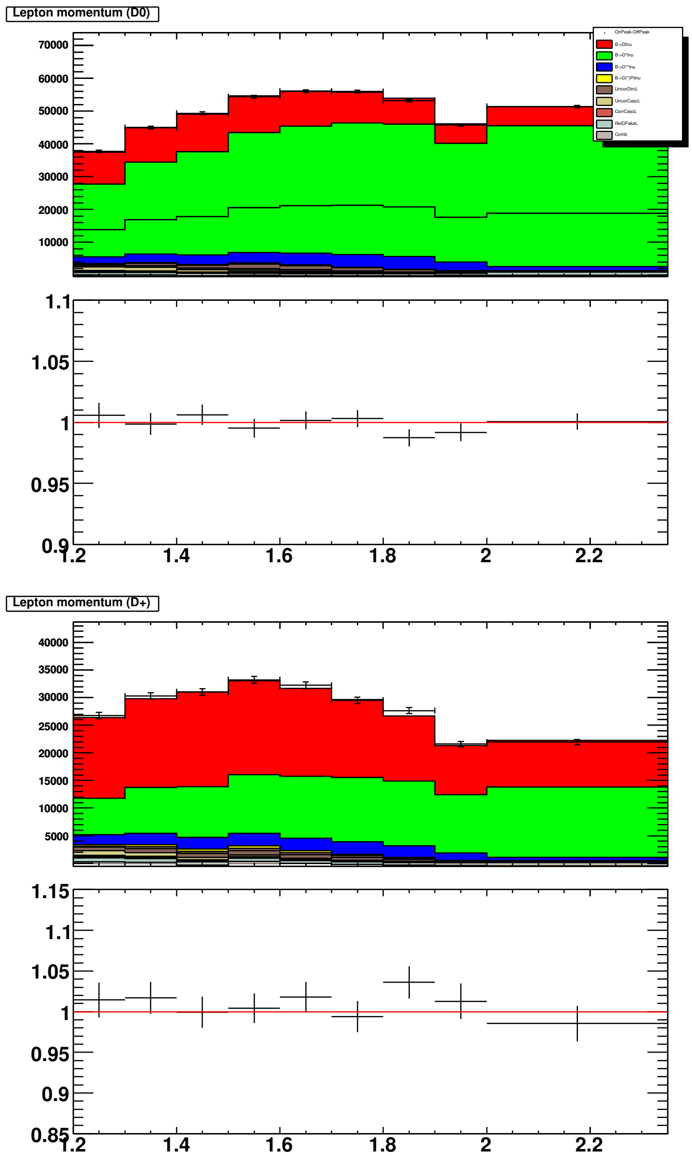

Figure 129: [p_ℓ **with fitted binning**] Lepton momentum plot with fitted binning after fitting. The top is D^0 and the bottom is D^+. Black is OnPeak - OffPeak data. Red is $B \to D\ell\nu$, green is $B \to D^*\ell\nu$, blue is $B \to D^{**}\ell\nu$, yellow is non-resonant $B \to D^{(*)}\pi\ell\nu$, and the rest is background. Dark brown is UncorrDL, light brown is UncorrCL, dark red is CascL, blue gray is FakeL, and light gray is Comb. Comb is almost disappeared after D mass sideband subtraction.

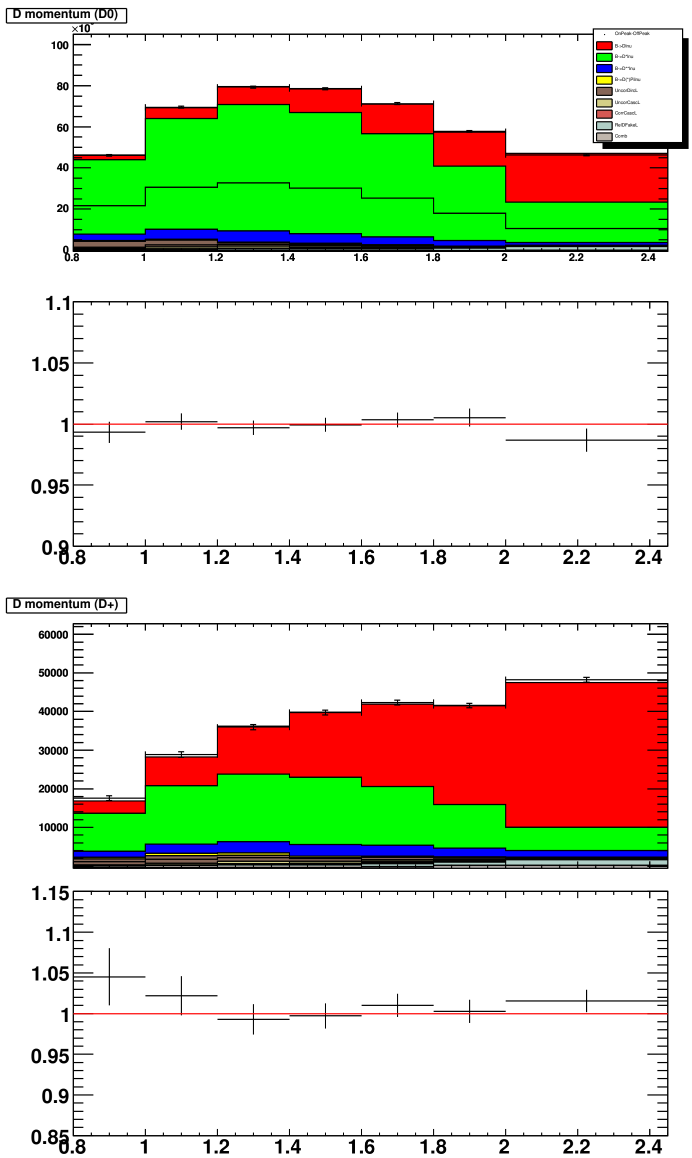

Figure 130: [p_D **with fitted binning**] D momentum plot with fitted binning after fitting. The top is D^0 and the bottom is D^+. Black is OnPeak - OffPeak data. Red is $B \to D\ell\nu$, green is $B \to D^*\ell\nu$, blue is $B \to D^{**}\ell\nu$, yellow is non-resonant $B \to D^{(*)}\pi\ell\nu$, and the rest is background. Dark brown is UncorrDL, light brown is UncorrCL, dark red is CascL, blue gray is FakeL, and light gray is Comb. Comb is almost disappeared after D mass sideband subtraction.

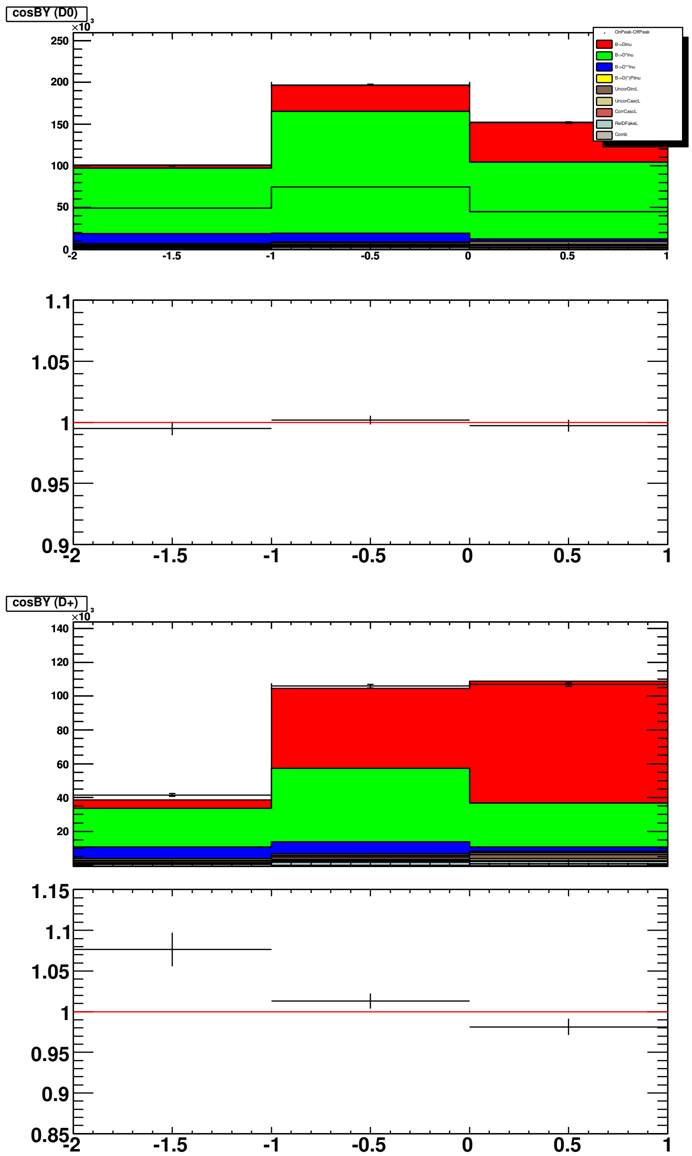

Figure 131: [$\cos\theta_{B-Dl}$ **with fitted binning**] $\cos\theta_{B-Dl}$ plot with fitted binning after fitting. The top is D^0 and the bottom is D^+. Black is OnPeak - OffPeak data. Red is $B \to D\ell\nu$, green is $B \to D^*\ell\nu$, blue is $B \to D^{**}\ell\nu$, yellow is non-resonant $B \to D^{(*)}\pi\ell\nu$, and the rest is background. Dark brown is UncorrDL, light brown is UncorrCL, dark red is CascL, blue gray is FakeL, and light gray is Comb. Comb is almost disappeared after D mass sideband subtraction.

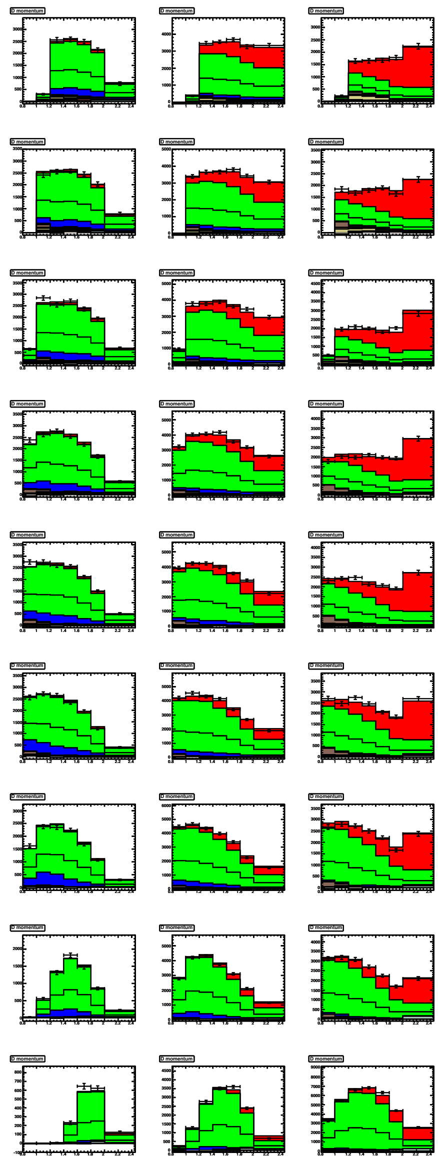

Figure 132: [D^0 **bin by bin after fitting**] D^0 momentum plots showing all bins after fitting. From top to bottom, lepton momentum bin changes from the lowest to the highest, and from left to right, cosBY bin changes from negative to positive. In each plots, colors are the same as other plots. Black is OnPeak - OffPeak data. Red is $B \to D\ell\nu$, green is $B \to D^{*}\ell\nu$, blue is $B \to D^{**}\ell\nu$, yellow is non-resonant $B \to D^{(*)}\pi\ell\nu$, and the rest is background. Dark brown is UncorrDL, light brown is UncorrCL, dark red is CascL, blue gray is FakeL, and light gray is Comb. Comb is almost disappeared after D mass sideband subtraction.

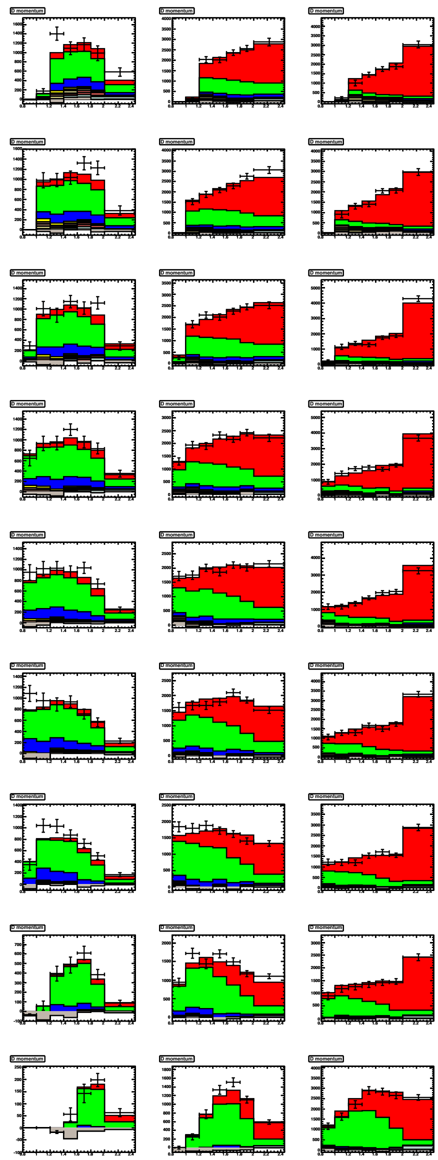

Figure 133: [D^+ **bin by bin after fitting**] D^+ momentum plots showing all bins after fitting. From top to bottom, lepton momentum bin changes from the lowest to the highest, and from left to right, cosBY bin charger's from negative to positive. In each plots, colors are the same as other plots. Black is OnPeak - OffPeak data. Red is $B \to D\ell\nu$, green is $B \to D^*\ell\nu$, blue is $B \to D^{**}\ell\nu$, yellow is non-resonant $B \to D^{(*)}\pi\ell\nu$, and the rest is background. Dark brown is UncorrDL, light brown is UncorrCL, dark red is CascL, blue gray is FakeL, and light gray is Comb. Comb is almost disappeared after D mass sideband subtraction.

17 Cross Checks

In the following fitting, we fix f_{+0}.

17.1 Electron vs muon

We compare the two cases of leptons, namely electrons and muons. We separate the $D\ell$ candidate into two by selecting $\ell = e$ and $\ell = \mu$. Then we perform fitting separately. The results are give in Table 44. The normalized residuals (NR) in the Table is defined by

$$\mathrm{NR} = \frac{\text{(Muon fitted value)} - \text{(Elctron fitted value)}}{\sqrt{\sigma_e^2 + \sigma_\mu^2}} \tag{324}$$

Plots from fit results are also shown in Figures 134-139. No systematic uncertainty is assigned based on this.

Parameters	Electron result	Muon result	NR
ρ_D^2	1.216 ± 0.047	1.088 ± 0.064	-1.60
ρ^2	1.350 ± 0.053	1.239 ± 0.062	-1.36
R_1	1.512 ± 0.089	1.350 ± 0.088	-1.29
R_2	0.668 ± 0.074	0.788 ± 0.075	+1.14
$\mathcal{B}(B \to D\ell\nu)$	0.02396 ± 0.00033	0.02271 ± 0.00038	-2.47
$\mathcal{B}(B \to D^*\ell\nu)$	0.05584 ± 0.00046	0.05370 ± 0.00051	-3.11
χ^2/ndof (P-value)	332/351 (0.761)	368/350 (0.248)	

Table 44: [**Electron only and muon only fits**] Electrons and muons separated fit results and normaliaed residuals (NR).

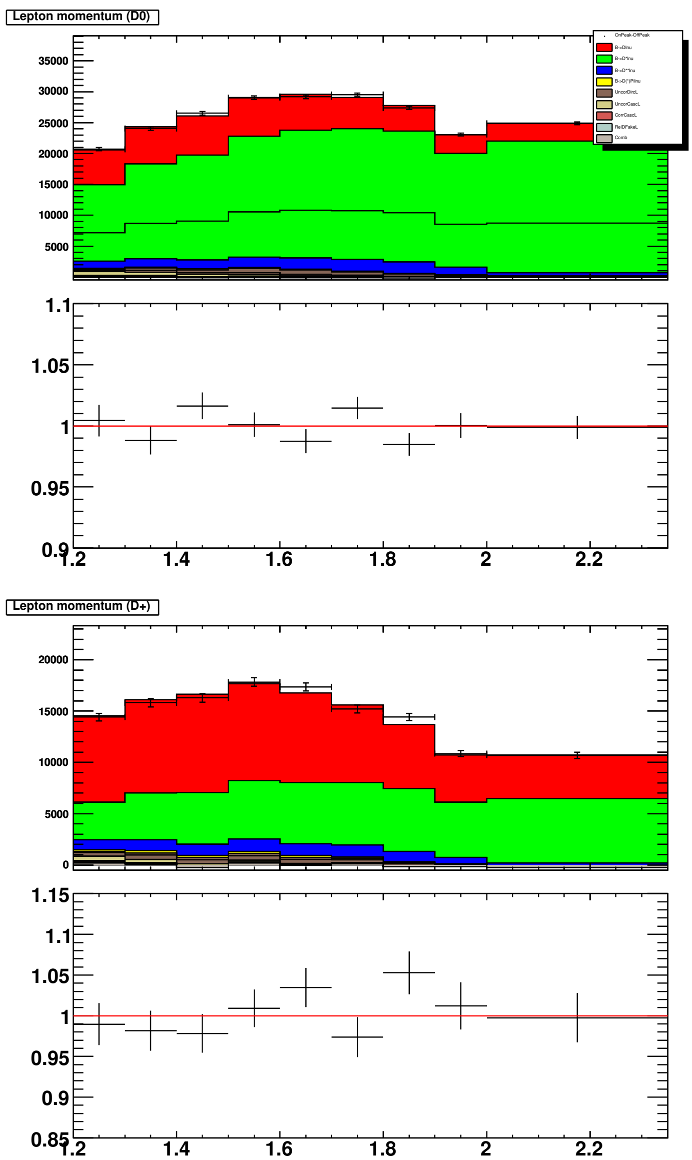

Figure 134: [**Electron** p_ℓ] $\ell = e$. Lepton momentum plot after fitting. The top is D^0 and the bottom is D^+. Black is OnPeak - OffPeak data. Red is $B \to D\ell\nu$, green is $B \to D^*\ell\nu$, blue is $B \to D^{**}\ell\nu$, yellow is non-resonant $B \to D^{(*)}\pi\ell\nu$, and the rest is background. Dark brown is UncorrDL, light brown is UncorrCL, dark red is CascL, blue gray is FakeL, and light gray is Comb. Comb is almost disappeared after D mass sideband subtraction.

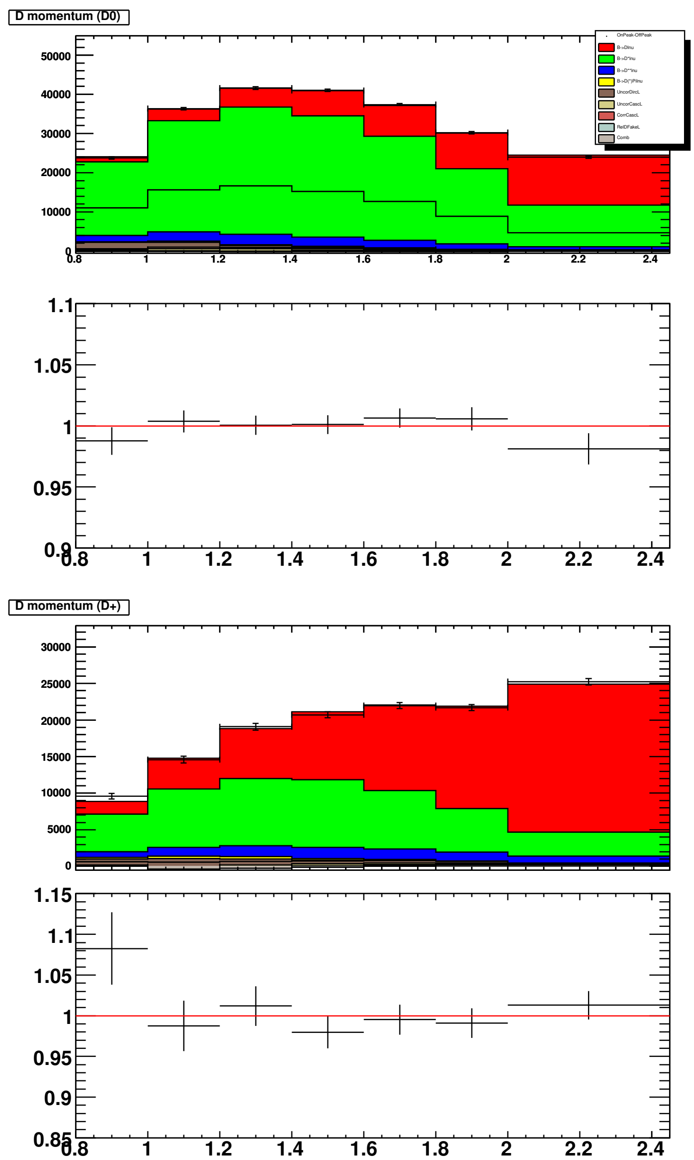

Figure 135: [**Electron** p_D] $\ell = e$. D momentum plot after fitting. The top is D^0 and the bottom is D^+. Black is OnPeak - OffPeak data. Red is $B \to D\ell\nu$, green is $B \to D^*\ell\nu$, blue is $B \to D^{**}\ell\nu$, yellow is non-resonant $B \to D^{(*)}\pi\ell\nu$, and the rest is background. Dark brown is UncorrDL, light brown is UncorrCL, dark red is CascL, blue gray is FakeL, and light gray is Comb. Comb is almost disappeared after D mass sideband subtraction.

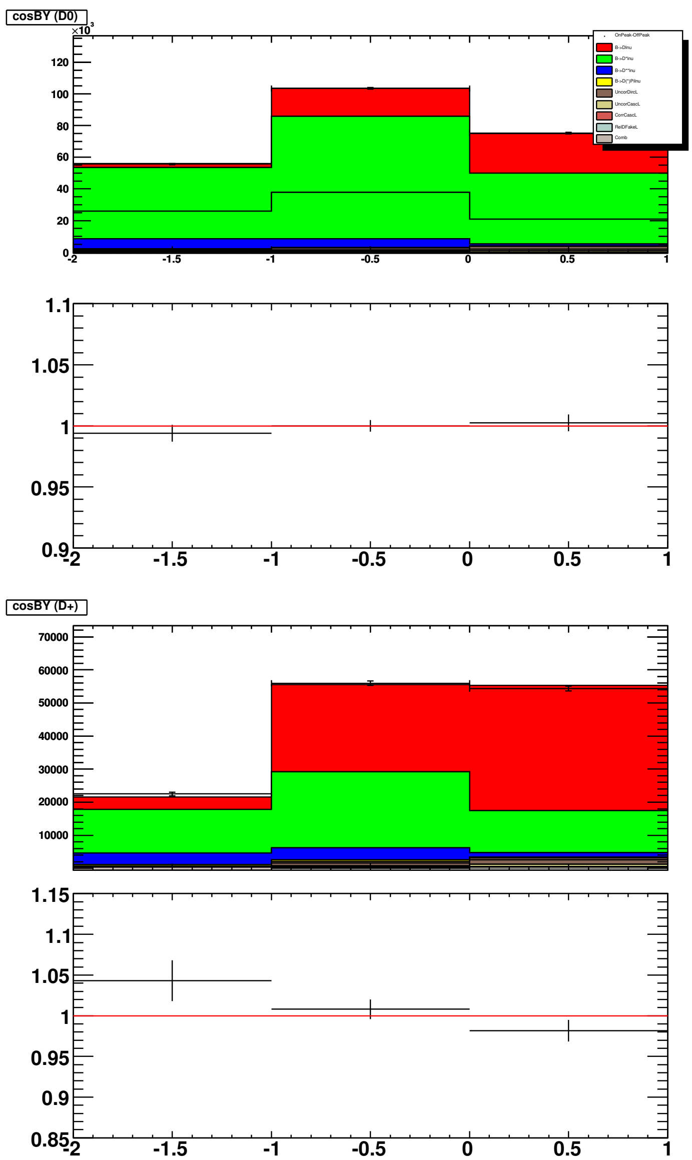

Figure 136: [**Electron** $\cos\theta_{B-Dl}$] $\ell = e$. $\cos\theta_{B-Dl}$ plot after fitting. The top is D^0 and the bottom is D^+. Black is OnPeak - OffPeak data. Red is $B \to D\ell\nu$, green is $B \to D^*\ell\nu$, blue is $B \to D^{**}\ell\nu$, yellow is non-resonant $B \to D^{(*)}\pi\ell\nu$, and the rest is background. Dark brown is UncorrDL, light brown is UncorrCL, dark red is CascL, blue gray is FakeL, and light gray is Comb. Comb is almost disappeared after D mass sideband subtraction.

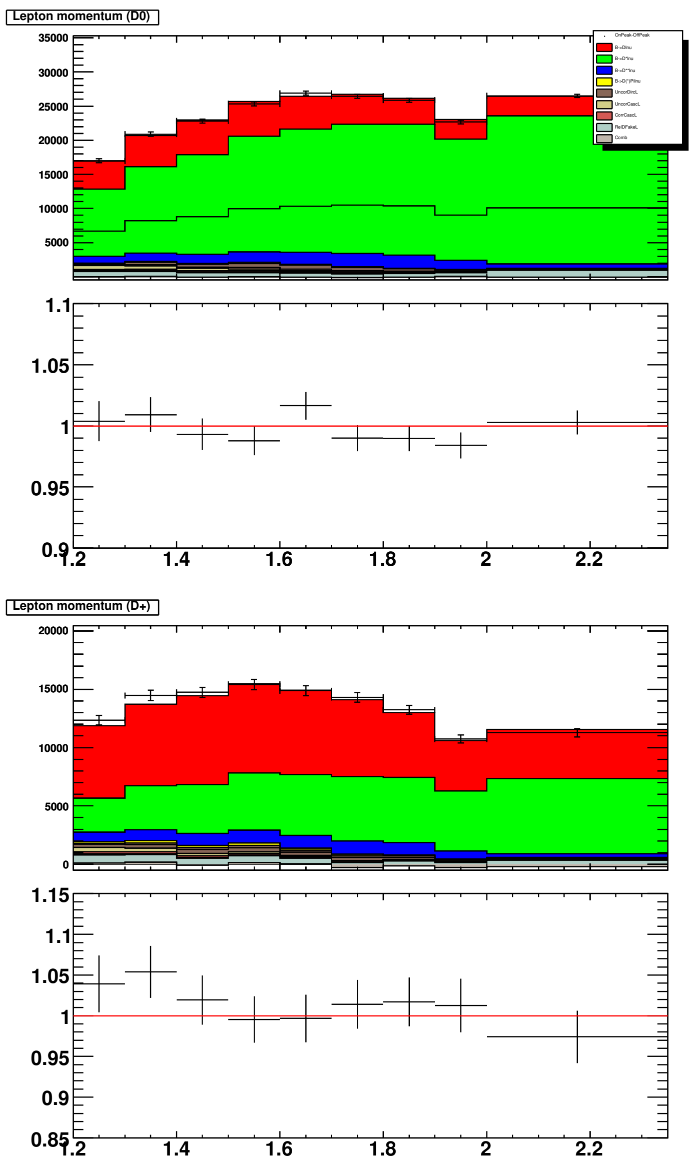

Figure 137: [**Muon** p_ℓ] $\ell = \mu$. Lepton momentum plot after fitting. The top is D^0 and the bottom is D^+. Black is OnPeak - OffPeak data. Red is $B \to D\ell\nu$, green is $B \to D^*\ell\nu$, blue is $B \to D^{**}\ell\nu$, yellow is non-resonant $B \to D^{(*)}\pi\ell\nu$, and the rest is background. Dark brown is UncorrDL, light brown is UncorrCL, dark red is CascL, blue gray is FakeL, and light gray is Comb. Comb is almost disappeared after D mass sideband subtraction.

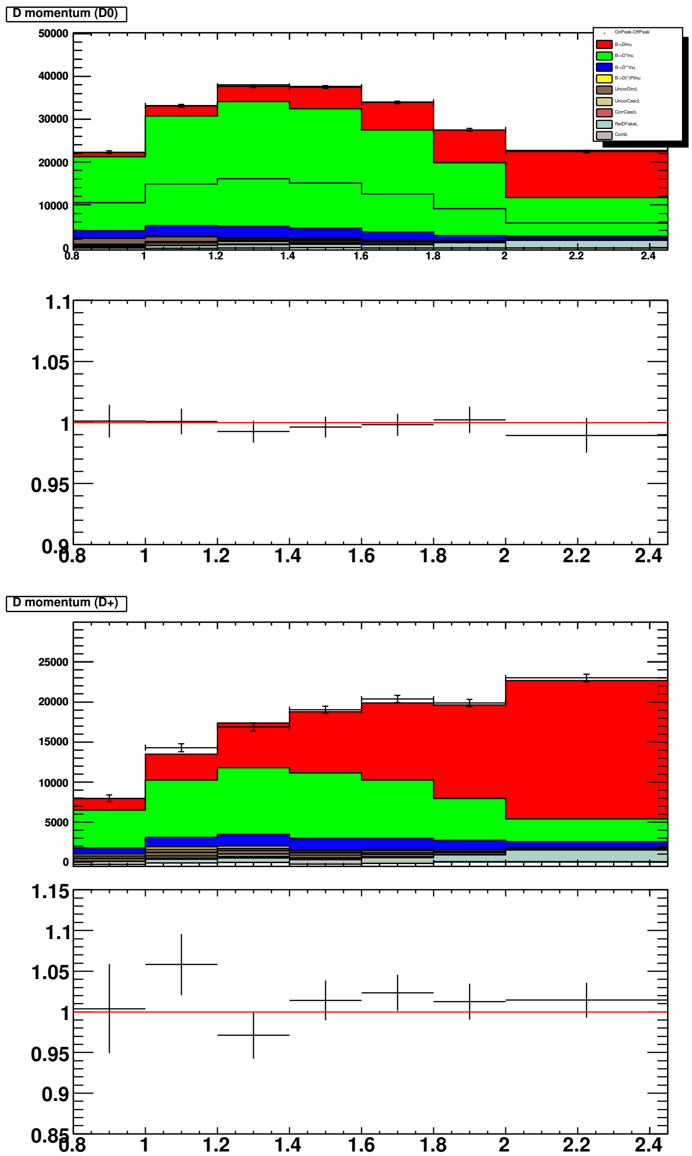

Figure 138: [**Muon** p_D] $\ell = \mu$. D momentum plot after fitting. The top is D^0 and the bottom is D^+. Black is OnPeak - OffPeak data. Red is $B \to D\ell\nu$, green is $B \to D^*\ell\nu$, blue is $B \to D^{**}\ell\nu$, yellow is non-resonant $B \to D^{(*)}\pi\ell\nu$, and the rest is background. Dark brown is UncorrDL, light brown is UncorrCL, dark red is CascL, blue gray is FakeL, and light gray is Comb. Comb is almost disappeared after D mass sideband subtraction.

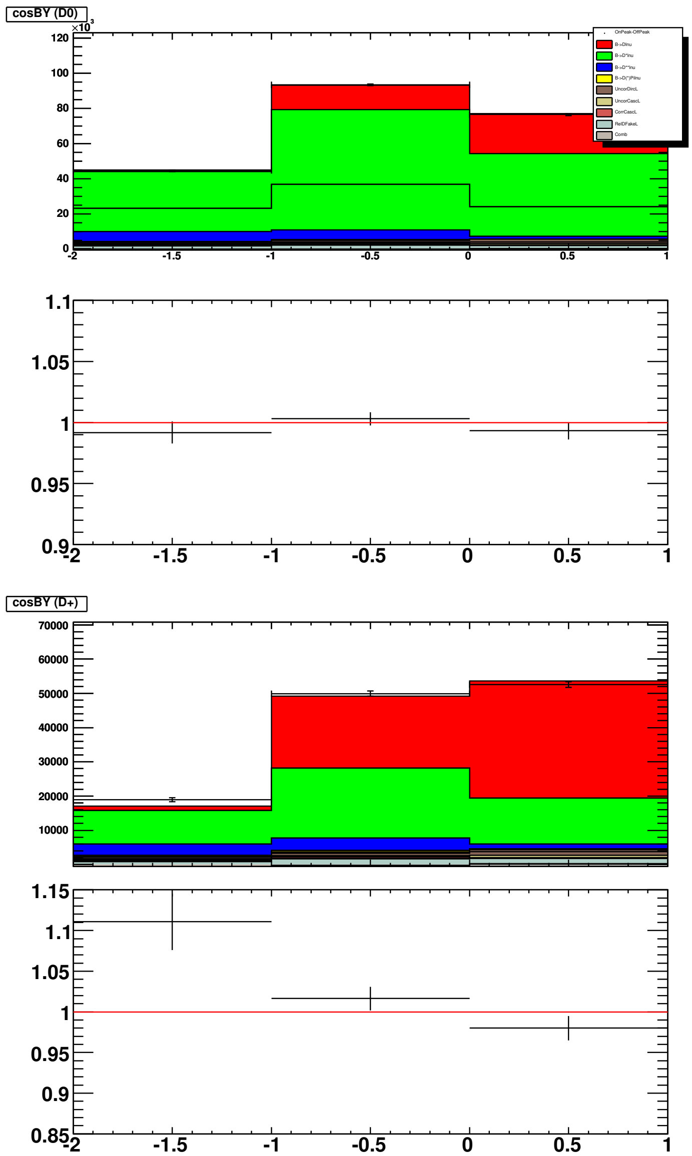

Figure 139: [**Muon** $\cos\theta_{B-Dl}$] $\ell = \mu$. $\cos\theta_{B-Dl}$ plot after fitting. The top is D^0 and the bottom is D^+. Black is OnPeak - OffPeak data. Red is $B \to D\ell\nu$, green is $B \to D^*\ell\nu$, blue is $B \to D^{**}\ell\nu$, yellow is non-resonant $B \to D^{(*)}\pi\ell\nu$, and the rest is background. Dark brown is UncorrDL, light brown is UncorrCL, dark red is CascL, blue gray is FakeL, and light gray is Comb. Comb is almost disappeared after D mass sideband subtraction.

17.2 Run1-3 vs Run4

We fit separately only for D^0 and only for D^+. In this fit we fixed $f_{+0} = 1.037$ because otherwise f_{+0} results in far from 1.037 and we get unreasonable fit results. The results are give in Table 45. The normalized residuals (NR) in the Table is defined by

$$\mathrm{NR} = \frac{(\text{Run4 fitted value}) - (\text{Run1-3 fitted value})}{\sqrt{\sigma^2_{\text{Run4}} + \sigma^2_{\text{Run1-3}}}} \tag{325}$$

Plots from fit results are also shown in Figures 140-145. No systematic uncertainty is assigned based on this.

Parameters	Run1-3 result	Run4 result	NR
ρ_D^2	1.191 ± 0.053	1.117 ± 0.057	-0.95
ρ^2	1.253 ± 0.056	1.359 ± 0.057	+1.33
R_1	1.376 ± 0.081	1.496 ± 0.095	+0.96
R_2	0.766 ± 0.069	0.671 ± 0.079	-0.91
$\mathcal{B}(B \to D\ell\nu)$	0.02289 ± 0.00035	0.02386 ± 0.00036	+1.94
$\mathcal{B}(B \to D^*\ell\nu)$	0.05462 ± 0.00047	0.05512 ± 0.00049	+0.73
χ^2/ndof (P-value)	338/351 (0.677)	391/351 (0.068)	

Table 45: [**Run1-3 and Run4 fits**] Run1-3 and Run4 fit results and normaliaed residuals (NR).

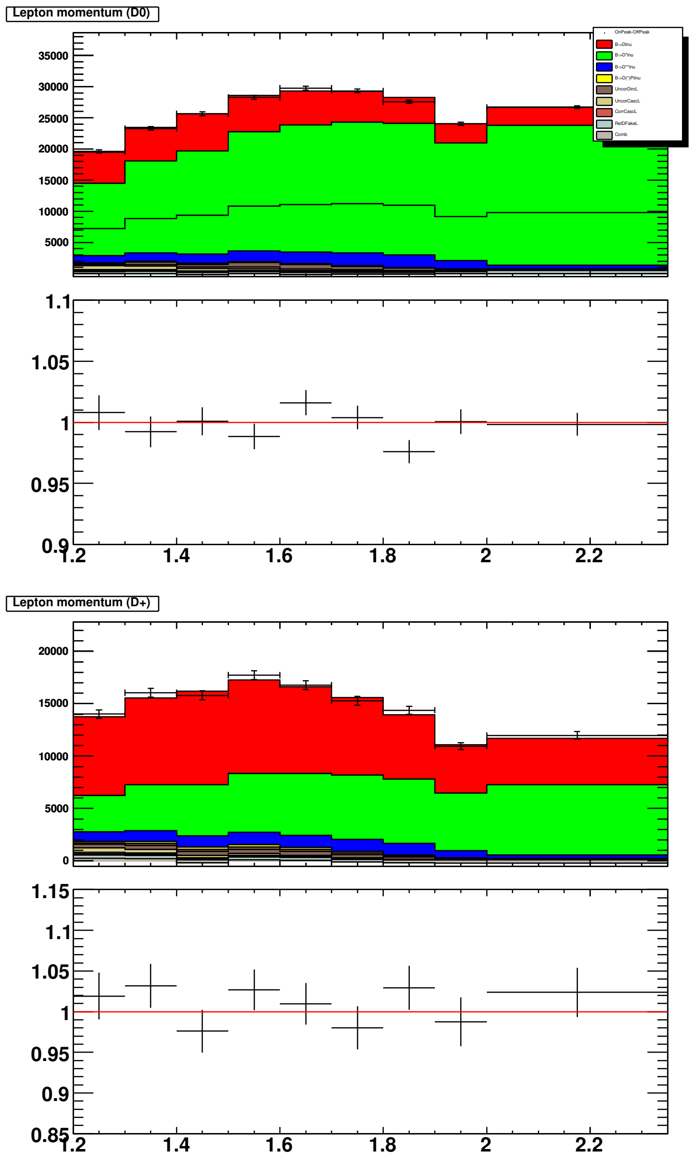

Figure 140: [**Run1-3** p_ℓ] Lepton momentum plot of Run1-3 fitting. The top is D^0 and the bottom is D^+. The bottom plot has no contribution to fitting. Black is OnPeak - OffPeak data. Red is $B \to D\ell\nu$, green is $B \to D^*\ell\nu$, blue is $B \to D^{**}\ell\nu$, yellow is non-resonant $B \to D^{(*)}\pi\ell\nu$, and the rest is background. Dark brown is UncorrDL, light brown is UncorrCL, dark red is CascL, blue gray is FakeL, and light gray is Comb. Comb is almost disappeared after D mass sideband subtraction.

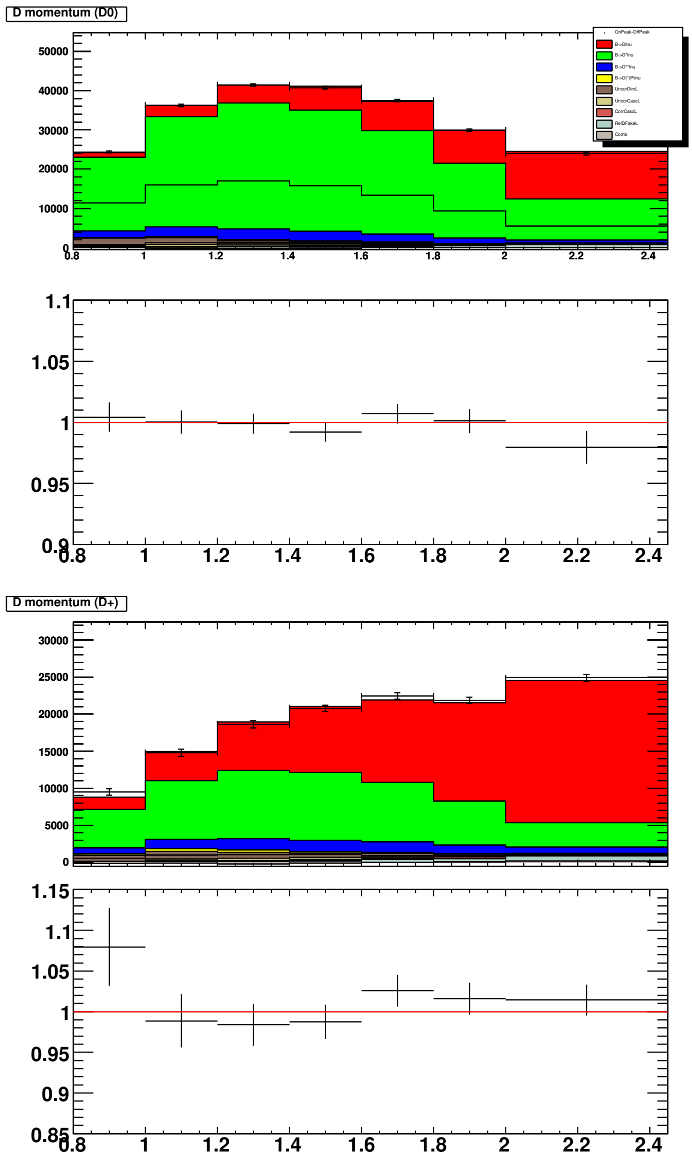

Figure 141: [**Run1-3** p_D] D momentum plot of Run1-3 fitting. The top is D^0 and the bottom is D^+. The bottom plot has no contribution to fitting. Black is OnPeak - OffPeak data. Red is $B \to D\ell\nu$, green is $B \to D^*\ell\nu$, blue is $B \to D^{**}\ell\nu$, yellow is non-resonant $B \to D^{(*)}\pi\ell\nu$, and the rest is background. Dark brown is UncorrDL, light brown is UncorrCL, dark red is CascL, blue gray is FakeL, and light gray is Comb. Comb is almost disappeared after D mass sideband subtraction.

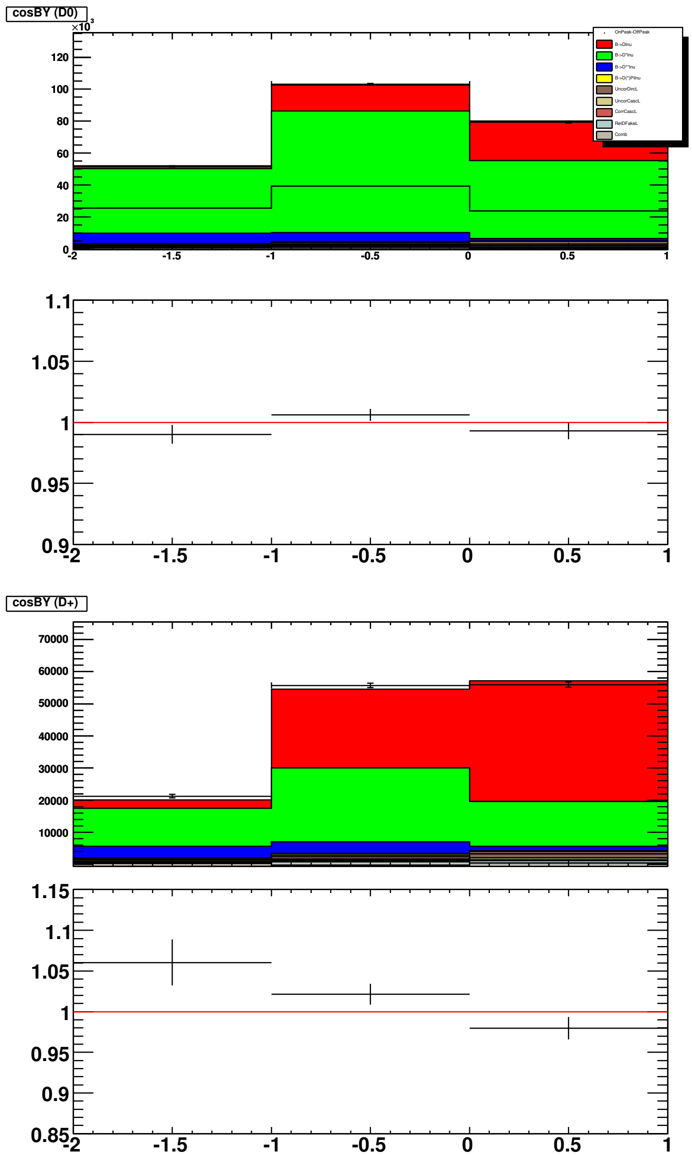

Figure 142: [**Run1-3** $\cos\theta_{B-Dl}$] $\cos\theta_{B-Dl}$ plot of Run1-3 fitting. The top is D^0 and the bottom is D^+. The bottom plot has no contribution to fitting. Black is OnPeak - OffPeak data. Red is $B \to D\ell\nu$, green is $B \to D^*\ell\nu$, blue is $B \to D^{**}\ell\nu$, yellow is non-resonant $B \to D^{(*)}\pi\ell\nu$, and the rest is background. Dark brown is UncorrDL, light brown is UncorrCL, dark red is CascL, blue gray is FakeL, and light gray is Comb. Comb is almost disappeared after D mass sideband subtraction.

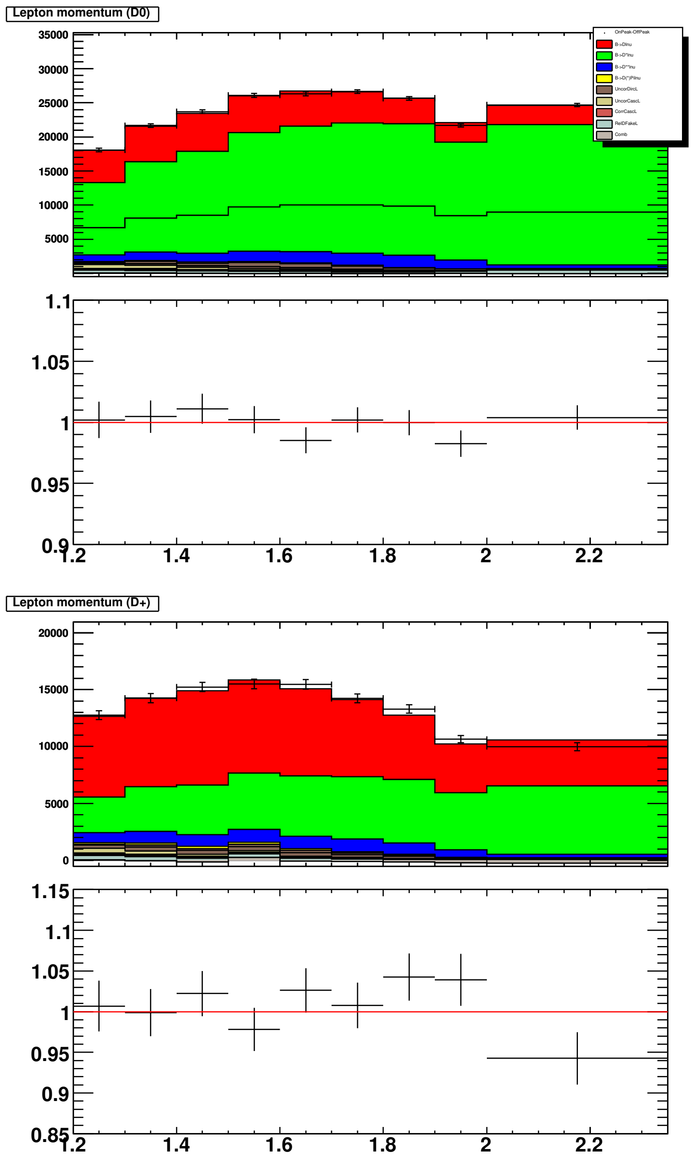

Figure 143: [**Run4** p_ℓ] Lepton momentum plot of Run4 fitting. The top is D^0 and the bottom is D^+. The top plot has no contribution to fitting. Black is OnPeak - OffPeak data. Red is $B \to D\ell\nu$, green is $B \to D^*\ell\nu$, blue is $B \to D^{**}\ell\nu$, yellow is non-resonant $B \to D^{(*)}\pi\ell\nu$, and the rest is background. Dark brown is UncorrDL, light brown is UncorrCL, dark red is CascL, blue gray is FakeL, and light gray is Comb. Comb is almost disappeared after D mass sideband subtraction.

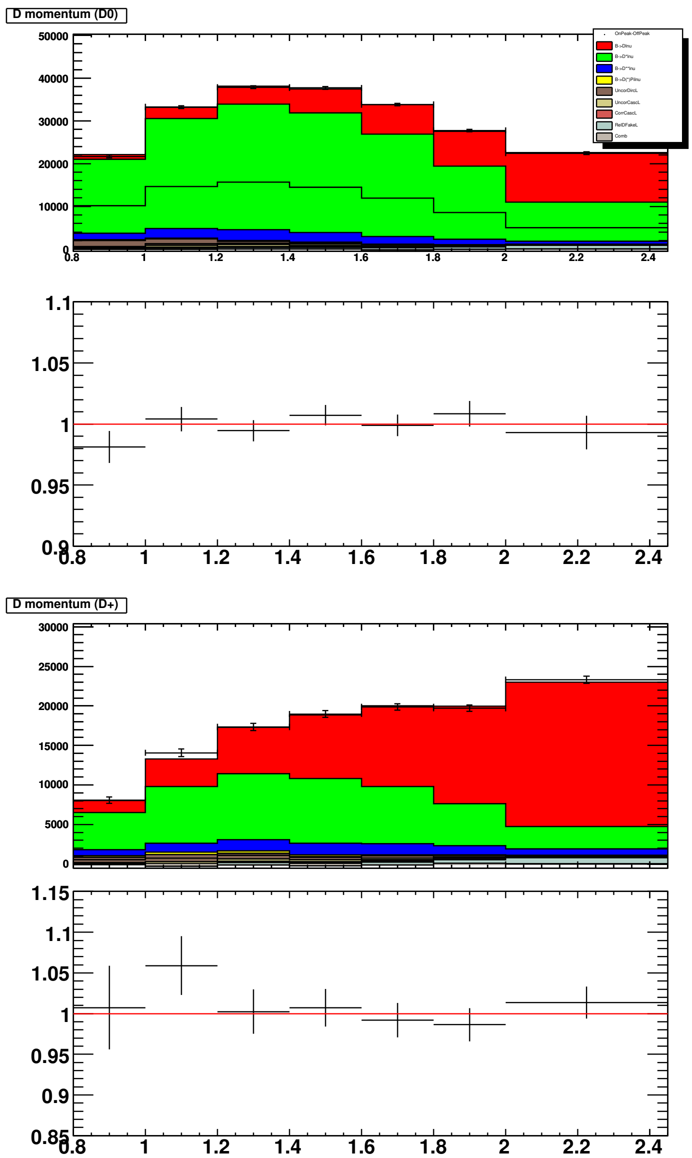

Figure 144: [**Run4** p_D] D momentum plot of Run4 fitting. The top is D^0 and the bottom is D^+. The top plot has no contribution to fitting. Black is OnPeak - OffPeak data. Red is $B \to D\ell\nu$, green is $B \to D^*\ell\nu$, blue is $B \to D^{**}\ell\nu$, yellow is non-resonant $B \to D^{(*)}\pi\ell\nu$, and the rest is background. Dark brown is UncorrDL, light brown is UncorrCL, dark red is CascL, blue gray is FakeL, and light gray is Comb. Comb is almost disappeared after D mass sideband subtraction.

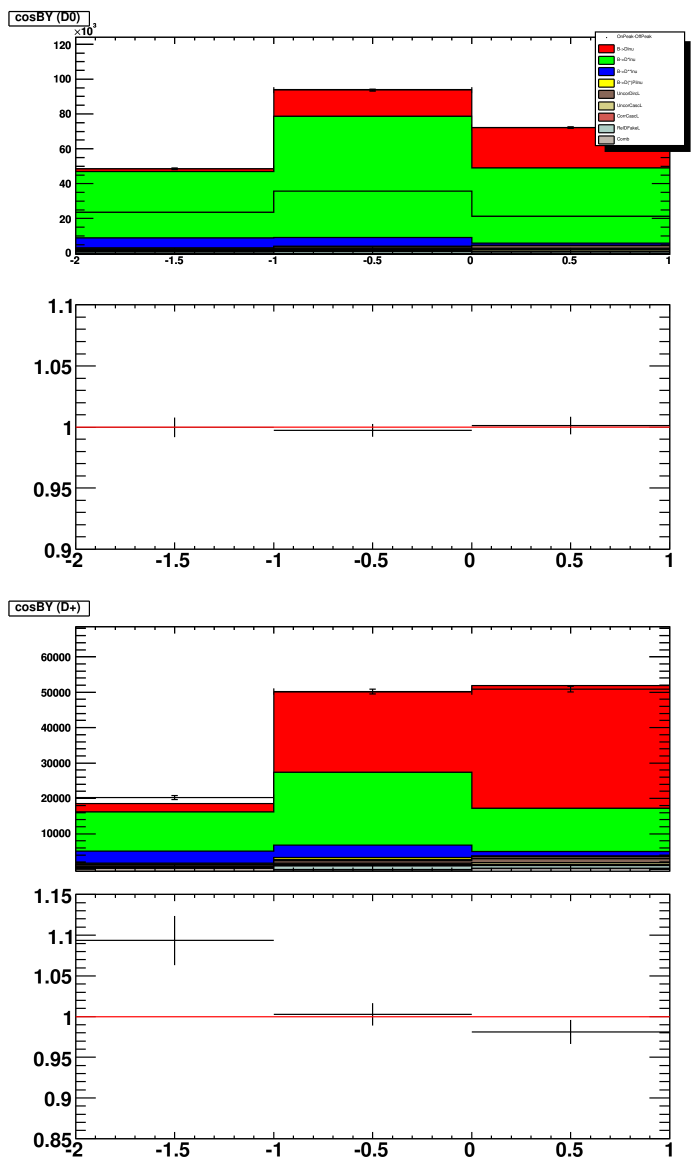

Figure 145: [**Run4** $\cos\theta_{B-Dl}$] $\cos\theta_{B-Dl}$ plot of Run4 fitting. The top is D^0 and the bottom is D^+. The top plot has no contribution to fitting. Black is OnPeak - OffPeak data. Red is $B \to D\ell\nu$, green is $B \to D^*\ell\nu$, blue is $B \to D^{**}\ell\nu$, yellow is non-resonant $B \to D^{(*)}\pi\ell\nu$, and the rest is background. Dark brown is UncorrDL, light brown is UncorrCL, dark red is CascL, blue gray is FakeL, and light gray is Comb. Comb is almost disappeared after D mass sideband subtraction.

$\mathcal{B}(B \to D^{(*)}\pi\pi\ell\nu)$ floated	Fit result	NR
ρ_D^2	1.169 ± 0.039	+0.058
ρ^2	1.295 ± 0.045	+0.384
R_1	1.458 ± 0.071	+0.778
R_2	0.712 ± 0.059	-0.679
$\mathcal{B}(B^+ \to \bar{D}^0\ell^+\nu)$	0.02349 ± 0.00026	+0.708
$\mathcal{B}(B^+ \to \bar{D}^{*0}\ell^+\nu)$	0.05501 ± 0.00057	+1.115
$\mathcal{BT}(B^+ \to \bar{D}^{(*)}\pi\pi\ell^+\nu)$	0.01138 ± 0.00204	-2.446
$\mathcal{B}(B \to D^{(*)}\pi\pi\ell\nu)$	0.02290 ± 0.00823	n/a
χ^2/ndof (P-value)	372/350 (0.205)	

Table 46: [$\mathcal{B}(B \to D^{(*)}\pi\pi\ell\nu)$ **floated**] Fit results.

17.3 Effect of $B \to D^{(*)}\pi\pi\ell\nu$ decays

We included $B \to D^{(*)}\pi\pi\ell\nu$ decay component (sum of X, X*, Y and Y*) in our fit. Plots are for $\mathcal{B}(B \to D^{(*)}\pi\pi\ell\nu)$ floated fit.

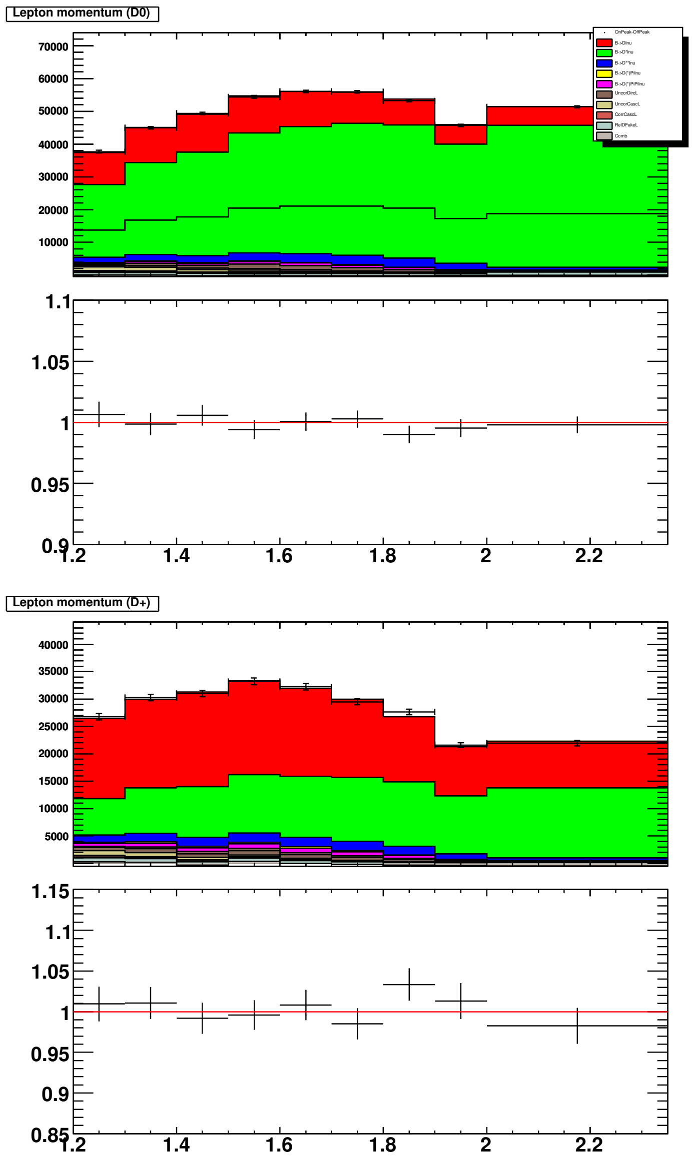

Figure 146: [**Fit with** $D\pi\pi\ell\nu$ **:** p_ℓ] Fit with $D\pi\pi\ell\nu$. Lepton momentum plot after fitting. The top is D^0 and the bottom is D^+. Black is OnPeak - OffPeak data. Red is $B \to D\ell\nu$, green is $B \to D^*\ell\nu$, blue is $B \to D^{**}\ell\nu$, yellow is non-resonant $B \to D^{(*)}\pi\ell\nu$, and the rest is background. Dark brown is UncorrDL, light brown is UncorrCL, dark red is CascL, blue gray is FakeL, and light gray is Comb. Comb is almost disappeared after D mass sideband subtraction.

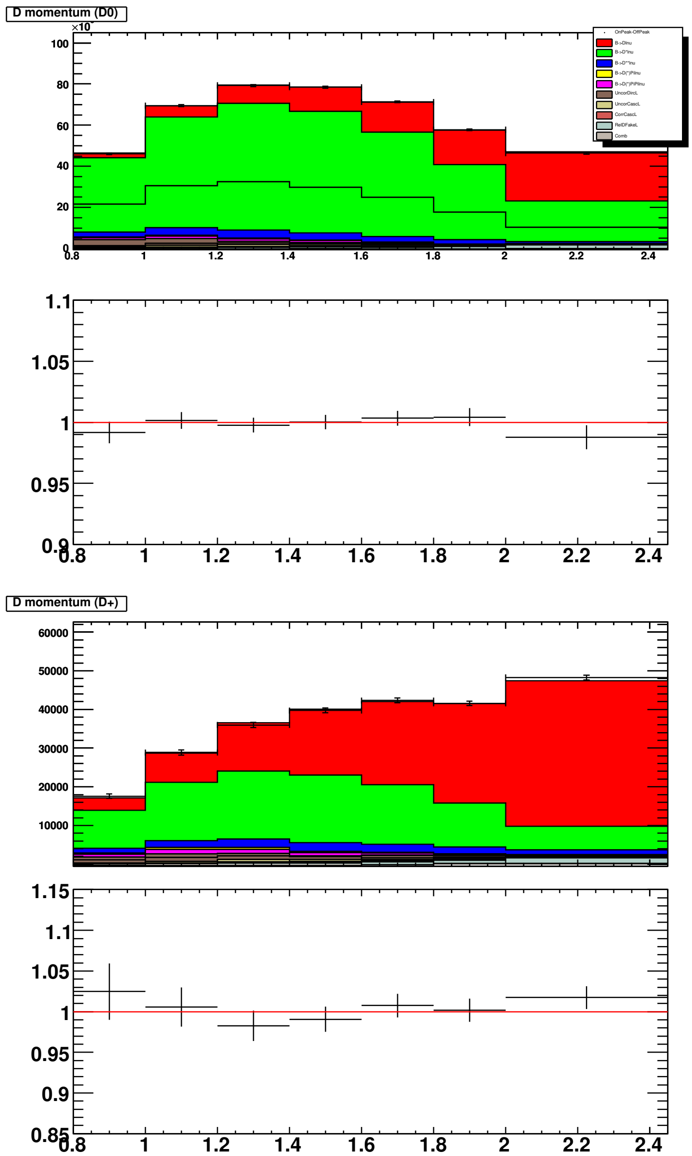

Figure 147: [**Fit with** $D\pi\pi\ell\nu$ **:** p_D] Fit with $D\pi\pi\ell\nu$. D momentum plot after fitting. The top is D^0 and the bottom is D^+. Black is OnPeak - OffPeak data. Red is $B \to D\ell\nu$, green is $B \to D^*\ell\nu$, blue is $B \to D^{**}\ell\nu$, yellow is non-resonant $B \to D^{(*)}\pi\ell\nu$, and the rest is background. Dark brown is UncorrDL, light brown is UncorrCL, dark red is CascL, blue gray is FakeL, and light gray is Comb. Comb is almost disappeared after D mass sideband subtraction.

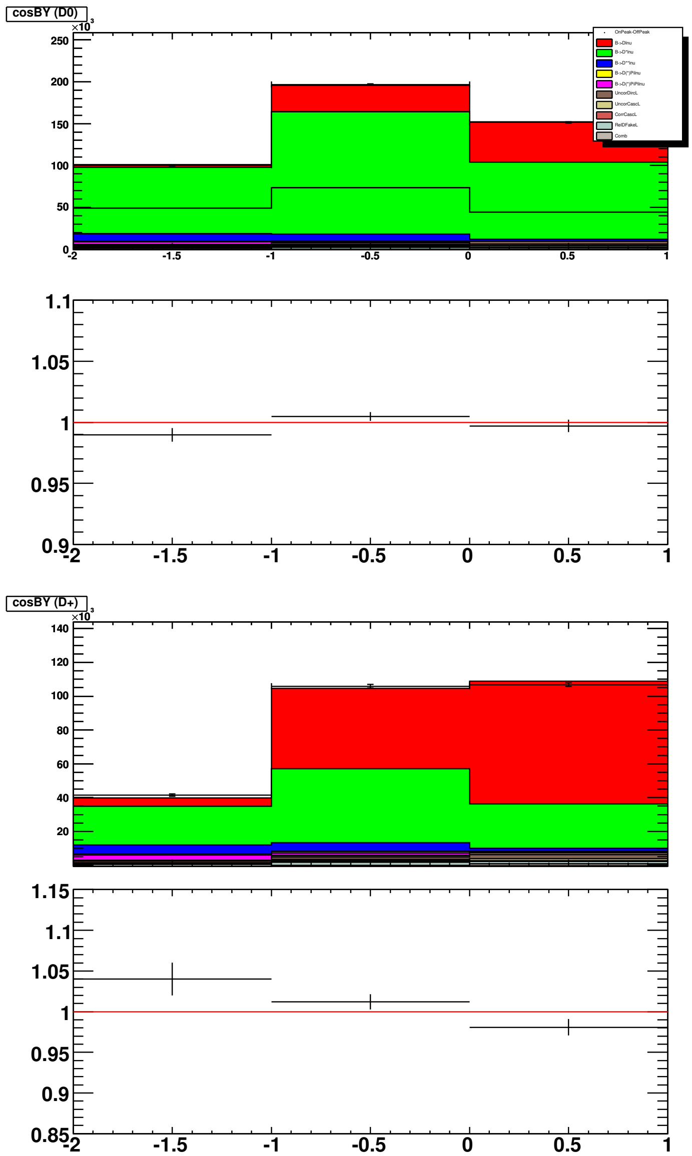

Figure 148: [**Fit with** $D\pi\pi\ell\nu$ **:**$\cos\theta_{B-Dl}$] Fit with $D\pi\pi\ell\nu$. $\cos\theta_{B-Dl}$ plot after fitting. The top is D^0 and the bottom is D^+. Black is OnPeak - OffPeak data. Red is $B \to D\ell\nu$, green is $B \to D^*\ell\nu$, blue is $B \to D^{**}\ell\nu$, yellow is non-resonant $B \to D^{(*)}\pi\ell\nu$, and the rest is background. Dark brown is UncorrDL, light brown is UncorrCL, dark red is CascL, blue gray is FakeL, and light gray is Comb. Comb is almost disappeared after D mass sideband subtraction.

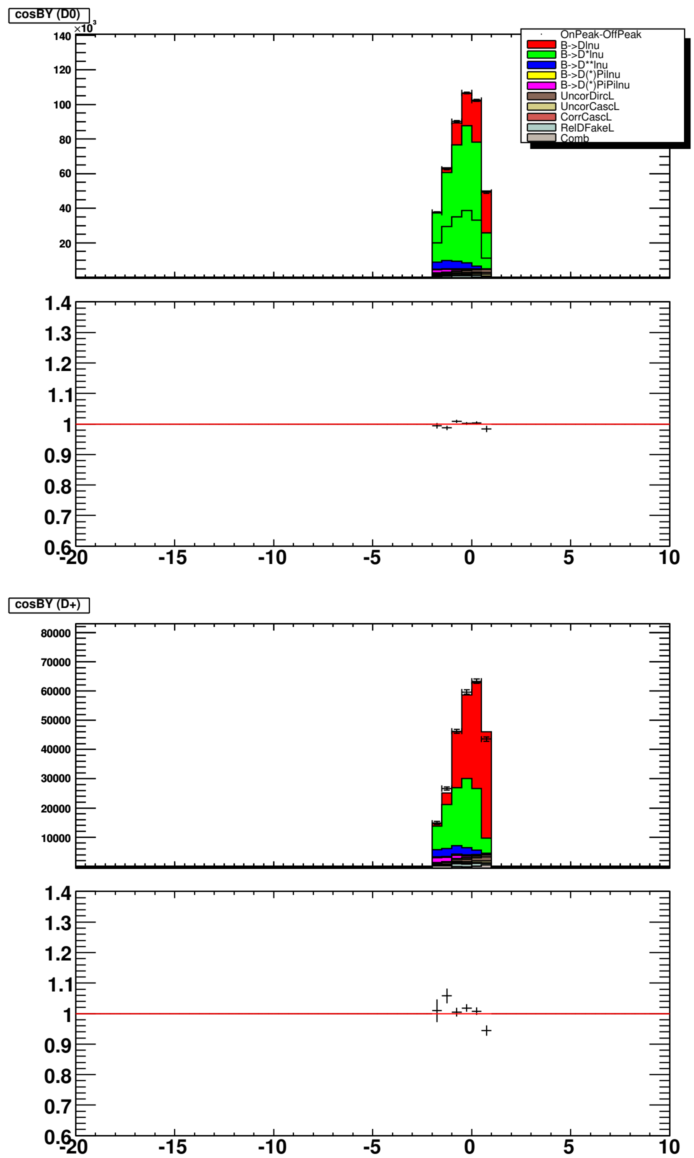

Figure 149: [**Fit with** $D\pi\pi\ell\nu$ **:**$\cos\theta_{B-Dl}$] Fit with $D\pi\pi\ell\nu$. $\cos\theta_{B-Dl}$ plot after fitting. The top is D^0 and the bottom is D^+. Black is OnPeak - OffPeak data. Red is $B \to D\ell\nu$, green is $B \to D^*\ell\nu$, blue is $B \to D^{**}\ell\nu$, yellow is non-resonant $B \to D^{(*)}\pi\ell\nu$, and the rest is background. Dark brown is UncorrDL, light brown is UncorrCL, dark red is CascL, blue gray is FakeL, and light gray is Comb. Comb is almost disappeared after D mass sideband subtraction.

	Fit result	NR
ρ_D^2	1.130 ± 0.042	-0.645
ρ^2	1.312 ± 0.042	+0.279
R_1	1.434 ± 0.065	+0.099
R_2	0.721 ± 0.053	-0.122
$\mathcal{B}(B^+ \to \bar{D}^0 \ell^+ \nu)$	0.02356 ± 0.00044	+0.563
$\mathcal{B}(B^0 \to D^- \ell^+ \nu)$	0.02128 ± 0.00031	-1.567
$\mathcal{B}(B^+ \to \bar{D}^{*0} \ell^+ \nu)$	0.05287 ± 0.00084	-2.341
$\mathcal{B}(B^0 \to D^{*-} \ell^+ \nu)$	0.05393 ± 0.00115	+2.366
χ^2/ndof (P-value)	374/349 (0.170)	

Table 47: [**No ispspin constraints on $B \to D^{(*)} \ell \nu$ decays**] Fit results.

17.4 No ispspin constraints on $B \to D^{(*)} \ell \nu$ decays

We remobed ispspin constraints on $B \to D^{(*)} \ell \nu$ decays.

17.5 Float $\mathcal{B}(B \to D^{(*)} \pi\pi \ell \nu)$ and $\mathcal{B}(D^{*+} \to D^0 \pi^+)$

We changed the upper cut of $\cos\theta_{B-Dl}$ to 1.1 to avoid the sharpe edge at $\cos\theta_{B-Dl} = 1$

17.6 Float $\mathcal{B}(B \to D^{(*)} \pi\pi \ell \nu)$ and no ispspin constraints on $B \to D^{(*)} \ell \nu$

We changed the upper cut of $\cos\theta_{B-Dl}$ to 1.1 to avoid the sharpe edge at $\cos\theta_{B-Dl} = 1$

	Fit result	NR
ρ_D^2	1.144 ± 0.046	-0.496
ρ^2	1.317 ± 0.047	-0.842
R_1	1.469 ± 0.073	+0.901
R_2	0.686 ± 0.062	-1.078
$\mathcal{B}(B^+ \to \bar{D}^0\ell^+\nu)$	0.02305 ± 0.00031	-0.823
$\mathcal{B}(B^+ \to \bar{D}^{*0}\ell^+\nu)$	0.05602 ± 0.00074	+2.228
$\mathcal{BT}(B^+ \to \bar{D}^{(*)}\pi\pi\ell^+\nu)$	0.01061 ± 0.00205	-2.809
$\mathcal{B}(B \to D^{(*)}\pi\pi\ell\nu)$	0.01996 ± 0.00760	n/a
$\mathcal{B}(D^{*+} \to D^0\pi^+)$	0.06664 ± 0.0058	-1.820
χ^2/ndof (P-value)	358/349 (0.364)	

Table 48: [**Float** $\mathcal{B}(B \to D^{(*)}\pi\pi\ell\nu)$ **and** $\mathcal{B}(D^{*+} \to D^0\pi^+)$] Fit results.

	Fit result	NR
ρ_D^2	1.148 ± 0.045	+0.355
ρ^2	1.321 ± 0.047	+0.096
R_1	1.477 ± 0.074	+0.124
R_2	0.684 ± 0.062	-0.147
$\mathcal{B}(B^+ \to \bar{D}^0\ell^+\nu)$	0.02333 ± 0.00046	-0.434
$\mathcal{B}(B^0 \to D^-\ell^+\nu)$	0.02146 ± 0.00033	-0.434
$\mathcal{B}(B^+ \to \bar{D}^{*0}\ell^+\nu)$	0.05402 ± 0.00100	+0.085
$\mathcal{B}(B^0 \to D^{*-}\ell^+\nu)$	0.05405 ± 0.00155	+0.085
$\mathcal{BT}(B^+ \to \bar{D}^{(*)}\pi\pi\ell^+\nu)$	0.01069 ± 0.00212	-0.011
$\mathcal{B}(B \to D^{(*)}\pi\pi\ell\nu)$	0.01996 ± 0.00763	n/a
χ^2/ndof (P-value)	358/348 (0.348)	

Table 49: [**Float** $\mathcal{B}(B \to D^{(*)}\pi\pi\ell\nu)$ **and no ispspin constraints**] Fit results.

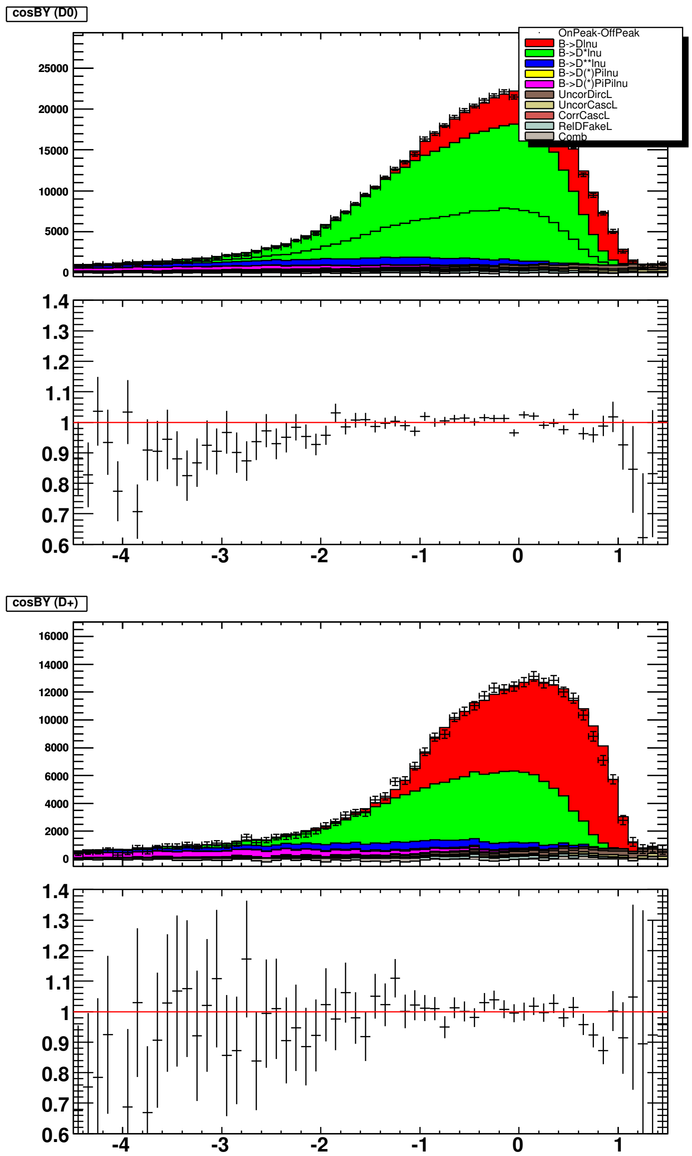

Figure 150: [**Float** $\mathcal{B}(B \to D^{(*)}\pi\pi\ell\nu)$ **and** $\mathcal{B}(D^{*+} \to D^0\pi^+)$] $\cos\theta_{B-Dl}$ plot after fitting. The top is D^0 and the bottom is D^+. Black is OnPeak - OffPeak data. Red is $B \to D\ell\nu$, green is $B \to D^*\ell\nu$, blue is $B \to D^{**}\ell\nu$, yellow is non-resonant $B \to D^{(*)}\pi\ell\nu$, and the rest is background. Dark brown is UncorrDL, light brown is UncorrCL, dark red is CascL, blue gray is FakeL, and light gray is Comb. Comb is almost disappeared after D mass sideband subtraction.

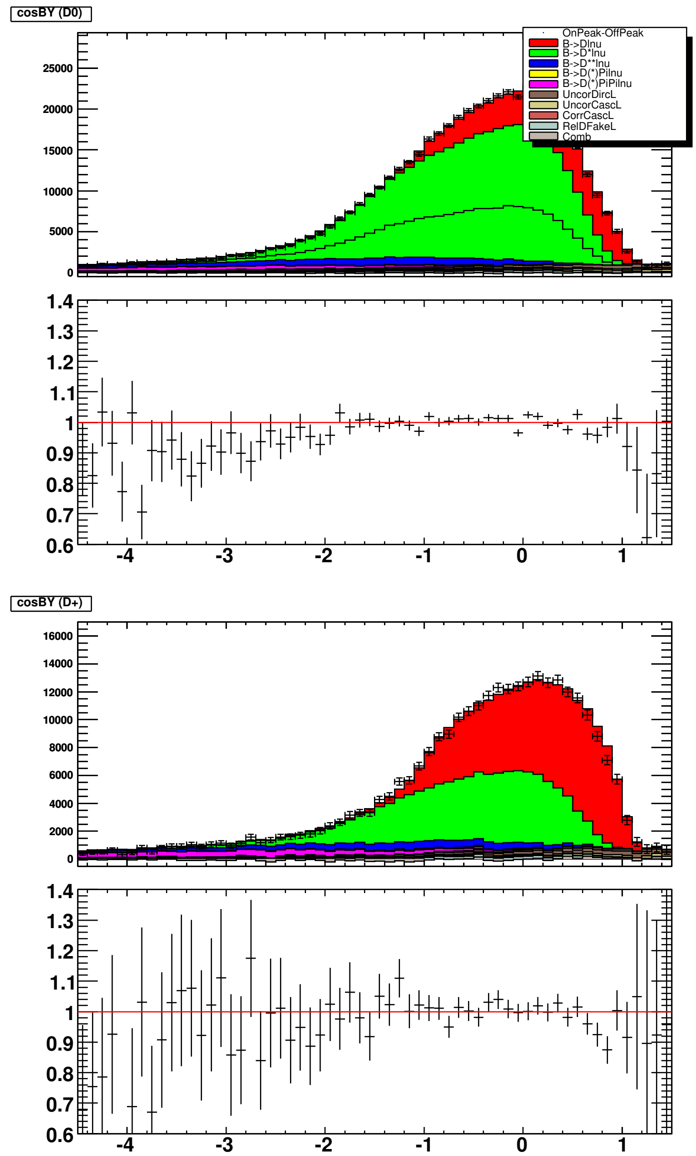

Figure 151: [**Float $\mathcal{B}(B \to D^{(*)}\pi\pi\ell\nu)$ and no ispspin constraints**] $\cos\theta_{B-Dl}$ plot after fitting. The top is D^0 and the bottom is D^+. Black is OnPeak - OffPeak data. Red is $B \to D\ell\nu$, green is $B \to D^*\ell\nu$, blue is $B \to D^{**}\ell\nu$, yellow is non-resonant $B \to D^{(*)}\pi\ell\nu$, and the rest is background. Dark brown is UncorrDL, light brown is UncorrCL, dark red is CascL, blue gray is FakeL, and light gray is Comb. Comb is almost disappeared after D mass sideband subtraction.

	Fit result
ρ_D^2	1.196 ± 0.036
ρ^2	1.231 ± 0.040
$\mathcal{B}(B^+ \to \bar{D}^0 \ell^+ \nu)$	0.02371 ± 0.00023
$\mathcal{B}(B^+ \to \bar{D}^{*0} \ell^+ \nu)$	0.05355 ± 0.00023
χ^2/ndof (P-value)	405/353 (0.028)

Table 50: [**Fix R_1 and R_2**] Fit results.

	Fit result
ρ_D^2	1.230 ± 0.033
$\mathcal{B}(B^+ \to \bar{D}^0 \ell^+ \nu)$	0.02358 ± 0.00022
$\mathcal{B}(B^+ \to \bar{D}^{*0} \ell^+ \nu)$	0.05348 ± 0.00023
χ^2/ndof (P-value)	413/354 (0.016)

Table 51: [**Fix R_1, R_2 and ρ^2**] Fit results.

17.7 Fix R_1 and R_2

We fixed $R_1 = 1.471$ and $R_2 = 0.836$.

17.8 Fix R_1, R_2 and ρ^2

We fixed $R_1 = 1.471$, $R_2 = 0.836$ and $\rho^2 = 1.179$.

17.9 ISGW2 FF for $B \to D\ell\nu$ decays

We use ISGW2 FF for $B \to D\ell\nu$ decays.

	Fit result
ρ^2	1.355 ± 0.039
R_1	1.399 ± 0.061
R_2	0.706 ± 0.053
$\mathcal{B}(B^+ \to \bar{D}^0 \ell^+ \nu)$	0.02255 ± 0.00023
$\mathcal{B}(B^+ \to \bar{D}^{*0} \ell^+ \nu)$	0.05611 ± 0.00030
χ^2/ndof (P-value)	448/352 (0.00040)

Table 52: [**ISGW2 FF for** $B \to D\ell\nu$ **decays**] Fit results.

	Fit result	NR
ρ^2_D	1.143 ± 0.043	-0.326
ρ^2	1.301 ± 0.040	+0.018
R_1	1.414 ± 0.071	-0.191
R_2	0.733 ± 0.056	-0.112
$\mathcal{B}(B^+ \to \bar{D}^0\ell^+\nu)$	0.02324 ± 0.00026	-0.284
$\mathcal{B}(B^+ \to \bar{D}^{*0}\ell^+\nu)$	0.05499 ± 0.00041	+0.338
$C^{D^0}_{UncorDL}$	0.926 ± 0.181	-0.407
$C^{D^+}_{UncorDL}$	1.401 ± 0.523	+0.767
χ^2/ndof (P-value)	380/349 (0.123)	

Table 53: [**Floating** $C^{D^0}_{UncorDL}$ **and** $C^{D^+}_{UncorDL}$] Fit results.

17.10 Floating $C^{D^0}_{UncorDL}$ and $C^{D^+}_{UncorDL}$

We floated $C^{D^0}_{UncorDL}$ and $C^{D^+}_{UncorDL}$.

17.11 Floating total background coefficients

We floated $C^{D^0}_{background}$ and $C^{D^+}_{background}$.

17.12 Fix all background coefficient to 0.9

We fixed all background coefficiencts to 0.9.

	Fit result	NR
ρ_D^2	1.133 ± 0.044	-0.757
ρ^2	1.274 ± 0.048	-0.082
R_1	1.361 ± 0.077	-0.551
R_2	0.764 ± 0.061	+0.192
$\mathcal{B}(B^+ \to \bar{D}^0 \ell^+ \nu)$	0.02291 ± 0.00031	-1.276
$\mathcal{B}(B^+ \to \bar{D}^{*0} \ell^+ \nu)$	0.05531 ± 0.00068	+1.385
$\mathcal{BT}(B^+ \to \bar{D}^{**0}/(D\pi)^0 \ell^+ \nu)$	0.01540 ± 0.00110	-0.888
$C^{D^0}_{background}$	0.887 ± 0.112	-1.008
$C^{D^+}_{background}$	1.357 ± 0.197	+1.816
χ^2/ndof (P-value)	374/349 (0.172)	

Table 54: [**Floating total background coefficients**] Fit results.

	Fit result	NR
ρ_D^2	1.169 ± 0.039	+0.065
ρ^2	1.261 ± 0.044	-0.390
R_1	1.360 ± 0.060	-0.723
R_2	0.780 ± 0.053	+0.519
$\mathcal{B}(B^+ \to \bar{D}^0 \ell^+ \nu)$	0.02335 ± 0.00025	+0.174
$\mathcal{B}(B^+ \to \bar{D}^{*0} \ell^+ \nu)$	0.05456 ± 0.00052	+0.370
$\mathcal{BT}(B^+ \to \bar{D}^{**0}/(D\pi)^0 \ell^+ \nu)$	0.01661 ± 0.00097	+0.241
χ^2/ndof (P-value)	379/351 (0.140)	

Table 55: [**Fix all background coefficient to 0.9**] Fit results.

	Fit result	NR
ρ^2_D	1.157 ± 0.039	-0.004
ρ^2	1.300 ± 0.040	+0.004
R_1	1.427 ± 0.062	-0.002
R_2	0.727 ± 0.052	-0.002
$\mathcal{B}(B^+ \to \bar{D}^0\ell^+\nu)$	0.02331 ± 0.00025	-0.001
$\mathcal{B}(B^+ \to \bar{D}^{*0}\ell^+\nu)$	0.05485 ± 0.00034	+0.004
χ^2/ndof (P-value)	380/349 (0.126)	

Table 56: [**Effect of minimum candidates per bin > 25**] Fit results.

	Fit result	NR
ρ^2_D	1.157 ± 0.039	-0.004
ρ^2	1.300 ± 0.040	+0.004
R_1	1.427 ± 0.062	-0.002
R_2	0.727 ± 0.052	-0.002
$\mathcal{B}(B^+ \to \bar{D}^0\ell^+\nu)$	0.02331 ± 0.00025	-0.001
$\mathcal{B}(B^+ \to \bar{D}^{*0}\ell^+\nu)$	0.05485 ± 0.00034	+0.004
χ^2/ndof (P-value)	380/349 (0.126)	

Table 57: [**Effect of minimum candidates per bin > 50**] Fit results.

17.13 Minimum entry per bin

We change the requirement of minimum entries per bin to 25, 50, 75 and 100. In nominal fit it is set to 10. Results are shown in Table 56-59. No systematic uncertainty is assigned based on this.
When we change thie requirement, the number of bins goes into χ^2 changes as follows

- Minimum entry ber bin > 10 : number of bins goes into $\chi^2 = 358$
- Minimum entry ber bin > 25 : number of bins goes into $\chi^2 = 356$
- Minimum entry ber bin > 50 : number of bins goes into $\chi^2 = 356$
- Minimum entry ber bin > 75 : number of bins goes into $\chi^2 = 354$
- Minimum entry ber bin > 100 : number of bins goes into $\chi^2 = 353$

	Fit result	NR
ρ_D^2	1.158 ± 0.039	+0.003
ρ^2	1.301 ± 0.040	+0.018
R_1	1.428 ± 0.062	+0.009
R_2	0.726 ± 0.052	-0.018
$\mathcal{B}(B^+ \to \bar{D}^0 \ell^+ \nu)$	0.02331 ± 0.00025	-0.005
$\mathcal{B}(B^+ \to \bar{D}^{*0} \ell^+ \nu)$	0.05485 ± 0.00034	+0.011
χ^2/ndof (P-value)	379/347 (0.114)	

Table 58: [**Effect of minimum candidates per bin** $>$ **75**] Fit results.

	Fit result	NR
ρ_D^2	1.158 ± 0.039	+0.003
ρ^2	1.301 ± 0.040	+0.018
R_1	1.428 ± 0.062	+0.009
R_2	0.726 ± 0.052	-0.017
$\mathcal{B}(B^+ \to \bar{D}^0 \ell^+ \nu)$	0.02331 ± 0.00025	-0.006
$\mathcal{B}(B^+ \to \bar{D}^{*0} \ell^+ \nu)$	0.05485 ± 0.00034	+0.011
χ^2/ndof (P-value)	379/346 (0.107)	

Table 59: [**Effect of minimum candidates per bin** $>$ **100**] Fit results.

17.14 Binning

We change binning and see how fit results change. Nominal binnings are (section 13.3).

- lepton momentum in the CM frame p^*_ℓ
  (9 bins (GeV)) : 1.2, 1.3, 1.4, 1.5, 1.6, 1.7, 1.8, 1.9, 2.0, 2.35

- D momentum in the CM frame p^*_D
  (7 bins (GeV)) : 0.8, 1.0, 1.2, 1.4, 1.6, 1.8, 2.0, 2.45

- $\cos\theta_{B-Dl}$ (see below)
  (3 bins) : -2, -1, 0, 1

First, we chcnage lepton momentum binning

- p^*_ℓ Binning 1
  (9 bins (GeV)) : 1.2, 1.35, 1.45, 1.55, 1.65, 1.75, 1.85, 1.95, 2.05, 2.35)

- p^*_ℓ Binning 2
  (5 bins (GeV)) : 1.2, 1.4, 1.6, 1.8, 2.0, 2.35)

Results are given in Table 60 and 61. No systematic uncertainty is assigned based on this.
Next, we change D momentum binning

- p^*_D Binning 1
  (7 bins (GeV)) : 0.8, 1.1, 1.3, 1.5, 1.7, 1.9, 2.1, 2.45

- p^*_D Binning 2
  (4 bins (GeV)) : 0.8, 1.2, 1.6, 2.0, 2.45

Results are given in Table 62 and 63. No systematic uncertainty is assigned based on this.
Finally, we change $\cos\theta_{B-Dl}$ bining

- $\cos\theta_{B-Dl}$ Binning 1
  (2 bins) : -2, 0, 1

- $\cos\theta_{B-Dl}$ Binning 2
  (1 bins) : -2, 1

Results are given in Table 64 and 65. No systematic uncertainty is assigned based on this.

	Fit result	NR
ρ_D^2	1.156 ± 0.039	-0.020
ρ^2	1.296 ± 0.040	-0.096
R_1	1.424 ± 0.061	-0.063
R_2	0.729 ± 0.052	+0.040
$\mathcal{B}(B^+ \to \bar{D}^0\ell^+\nu)$	0.02326 ± 0.00025	-0.226
$\mathcal{B}(B^+ \to \bar{D}^{*0}\ell^+\nu)$	0.05488 ± 0.00034	+0.109
χ^2/ndof (P-value)	396/341 (0.022)	

Table 60: [**Effect of** p_ℓ **binning 1**] Fit results.

	Fit result	NR
ρ_D^2	1.158 ± 0.039	+0.007
ρ^2	1.299 ± 0.041	-0.023
R_1	1.427 ± 0.064	-0.015
R_2	0.730 ± 0.053	+0.051
$\mathcal{B}(B^+ \to \bar{D}^0\ell^+\nu)$	0.02328 ± 0.00025	-0.118
$\mathcal{B}(B^+ \to \bar{D}^{*0}\ell^+\nu)$	0.05483 ± 0.00034	-0.038
χ^2/ndof (P-value)	225/190 (0.042)	

Table 61: [**Effect of** p_ℓ **binning 2**] Fit results.

	Fit result	NR
ρ_D^2	1.144 ± 0.039	-0.347
ρ^2	1.344 ± 0.039	+1.125
R_1	1.490 ± 0.063	+0.993
R_2	0.663 ± 0.052	-1.227
$\mathcal{B}(B^+ \to \bar{D}^0\ell^+\nu)$	0.02331 ± 0.00025	-0.022
$\mathcal{B}(B^+ \to \bar{D}^{*0}\ell^+\nu)$	0.05501 ± 0.00034	+0.491
χ^2/ndof (P-value)	366/356 (0.344)	

Table 62: [**Effect of** p_D **binning 1**] Fit results.

	Fit result	NR
ρ_D^2	1.153 ± 0.040	-0.122
ρ^2	1.310 ± 0.042	+0.235
R_1	1.432 ± 0.065	+0.067
R_2	0.717 ± 0.056	-0.174
$\mathcal{B}(B^+ \to \bar{D}^0 \ell^+ \nu)$	0.02333 ± 0.00025	+0.061
$\mathcal{B}(B^+ \to \bar{D}^{*0} \ell^+ \nu)$	0.05467 ± 0.00035	+0.069
χ^2/ndof (P-value)	228/206 (0.137)	

Table 63: [**Effect of** p_D **binning 2**] Fit results.

	Fit result	NR
ρ_D^2	1.164 ± 0.040	+0.159
ρ^2	1.302 ± 0.042	+0.054
R_1	1.437 ± 0.066	+0.151
R_2	0.726 ± 0.055	-0.013
$\mathcal{B}(B^+ \to \bar{D}^0 \ell^+ \nu)$	0.02341 ± 0.00026	+0.384
$\mathcal{B}(B^+ \to \bar{D}^{*0} \ell^+ \nu)$	0.05471 ± 0.00035	-0.381
χ^2/ndof (P-value)	283/236 (0.019)	

Table 64: [**Effect of** $\cos\theta_{B-Dl}$ **binning 1**] Fit results.

	Fit result	NR
ρ_D^2	1.225 ± 0.046	+1.459
ρ^2	1.228 ± 0.049	-1.467
R_1	1.356 ± 0.068	-1.049
R_2	0.801 ± 0.059	+1.268
$\mathcal{B}(B^+ \to \bar{D}^0 \ell^+ \nu)$	0.02353 ± 0.00037	+0.601
$\mathcal{B}(B^+ \to \bar{D}^{*0} \ell^+ \nu)$	0.05434 ± 0.00047	-1.089
χ^2/ndof (P-value)	122/115 (0.300)	

Table 65: [**Effect of** $\cos\theta_{B-Dl}$ **binning 2**] Fit results.

ρ_D^2	1.222 ± 0.049 (4.0 %)
ρ^2	1.345 ± 0.060 (4.4 %)
R_1	1.503 ± 0.094 (6.3 %)
R_2	0.671 ± 0.080 (11.9 %)
$\mathcal{B}(B^+ \to \bar{D}^0 \ell^+ \nu)$	0.02387 ± 0.00033 (1.4 %)
$\mathcal{B}(B^+ \to \bar{D}^{*0} \ell^+ \nu)$	0.05606 ± 0.00072 (1.3 %)
$\mathcal{B}(D^{(*)} \pi \ell \nu)$	0.01477 ± 0.00139 (9.4 %)
$\mathcal{B}(D^{(*)} \pi \pi \ell \nu)$	not included
χ^2/ndof (P-value)	344/351 (0.59)

Table 66: [**With background cuts**] Fit results.

18 Electron Only Fit Results

From this section we rename $\mathcal{BT}(B^+ \to \bar{D}^{**0}/(D\pi)^0 \ell^+ \nu)$ to $\mathcal{B}(B^+ \to \bar{D}^{(*)} \pi \ell^+ \nu)$
We use following binning for lepton momentum and D momentum

- lepton momentum in the CM frame p_ℓ^*
  (9 bins (GeV)) : 1.2, 1.3, 1.4, 1.5, 1.6, 1.7, 1.8, 1.9, 2.0, 2.35
- D momentum in the CM frame p_D^*
  (7 bins (GeV)) : 0.8, 1.0, 1.2, 1.4, 1.6, 1.8, 2.0, 2.45

18.1 $\cos\theta_{B-Dl}$ bin (-2, -1, 0, 1.1) (3 bins)

18.1.1 With background cuts same as 25 % cuts

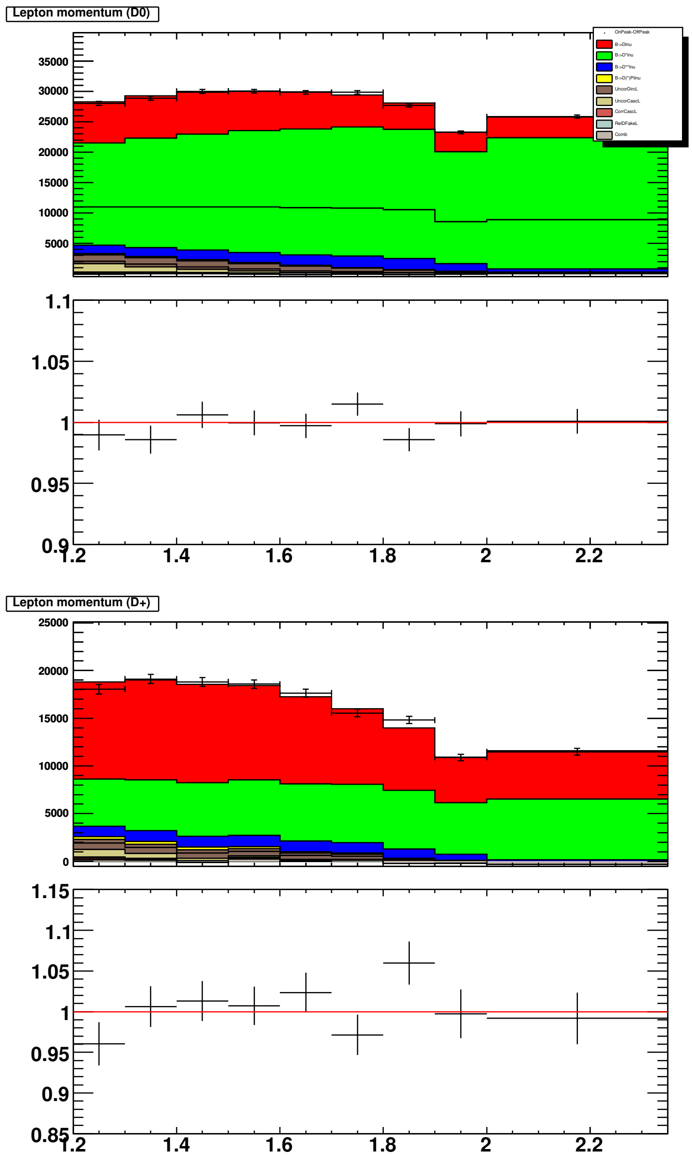

Figure 152: [p_ℓ **with fitted binning**] Lepton momentum plot with fitted binning after fitting. The top is D^0 and the bottom is D^+. Black is OnPeak - OffPeak data. Red is $B \to D\ell\nu$, green is $B \to D^*\ell\nu$, blue is $B \to D^{**}\ell\nu$, yellow is non-resonant $B \to D^{(*)}\pi\ell\nu$, and the rest is background. Dark brown is UncorrDL, light brown is UncorrCL, dark red is CascL, blue gray is FakeL, and light gray is Comb. Comb is almost disappeared after D mass sideband subtraction.

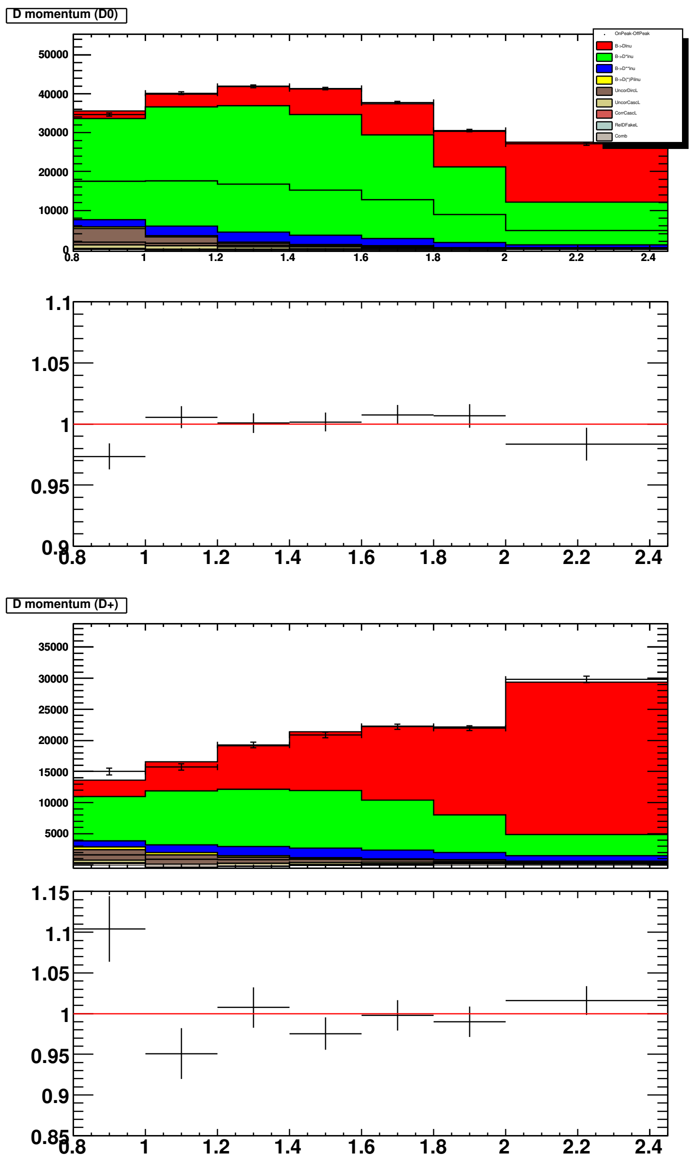

Figure 153: [p_D **with fitted binning**] D momentum plot with fitted binning after fitting. The top is D^0 and the bottom is D^+. Black is OnPeak - OffPeak data. Red is $B \to D\ell\nu$, green is $B \to D^*\ell\nu$, blue is $B \to D^{**}\ell\nu$, yellow is non-resonant $B \to D^{(*)}\pi\ell\nu$, and the rest is background. Dark brown is UncorrDL, light brown is UncorrCL, dark red is CascL, blue gray is FakeL, and light gray is Comb. Comb is almost disappeared after D mass sideband subtraction.

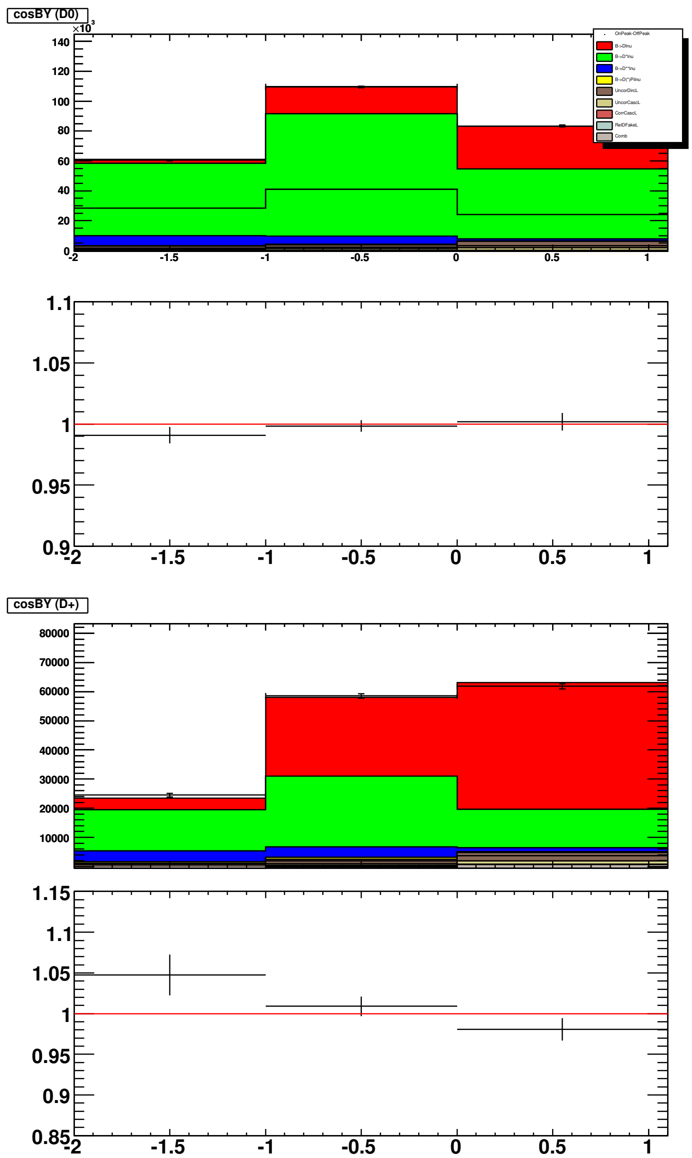

Figure 154: [$\cos\theta_{B-Dl}$ **with fitted binning**] $\cos\theta_{B-Dl}$ plot with fitted binning after fitting. The top is D^0 and the bottom is D^+. Black is OnPeak - OffPeak data. Red is $B \to D\ell\nu$, green is $B \to D^*\ell\nu$, blue is $B \to D^{**}\ell\nu$, yellow is non-resonant $B \to D^{(*)}\pi\ell\nu$, and the rest is background. Dark brown is UncorrDL, light brown is UncorrCL, dark red is CascL, blue gray is FakeL, and light gray is Comb. Comb is almost disappeared after D mass sideband subtraction.

ρ_D^2	1.224 ± 0.045 (3.7 %)
ρ^2	1.372 ± 0.059 (4.3 %)
R_1	1.569 ± 0.093 (5.9 %)
R_2	0.625 ± 0.080 (12.8 %)
$\mathcal{B}(B^+ \to \bar{D}^0 \ell^+ \nu)$	0.02399 ± 0.00033 (1.4 %)
$\mathcal{B}(B^+ \to \bar{D}^{*0} \ell^+ \nu)$	0.05601 ± 0.00071 (1.3 %)
$\mathcal{B}(D^{(*)} \pi \ell \nu)$	0.01454 ± 0.00138 (9.5 %)
$\mathcal{B}(D^{(*)} \pi\pi \ell \nu)$	not included
χ^2/ndof (P-value)	375/363 (0.32)

Table 67: [**No background cuts**] Fit results.

18.1.2 No background cuts

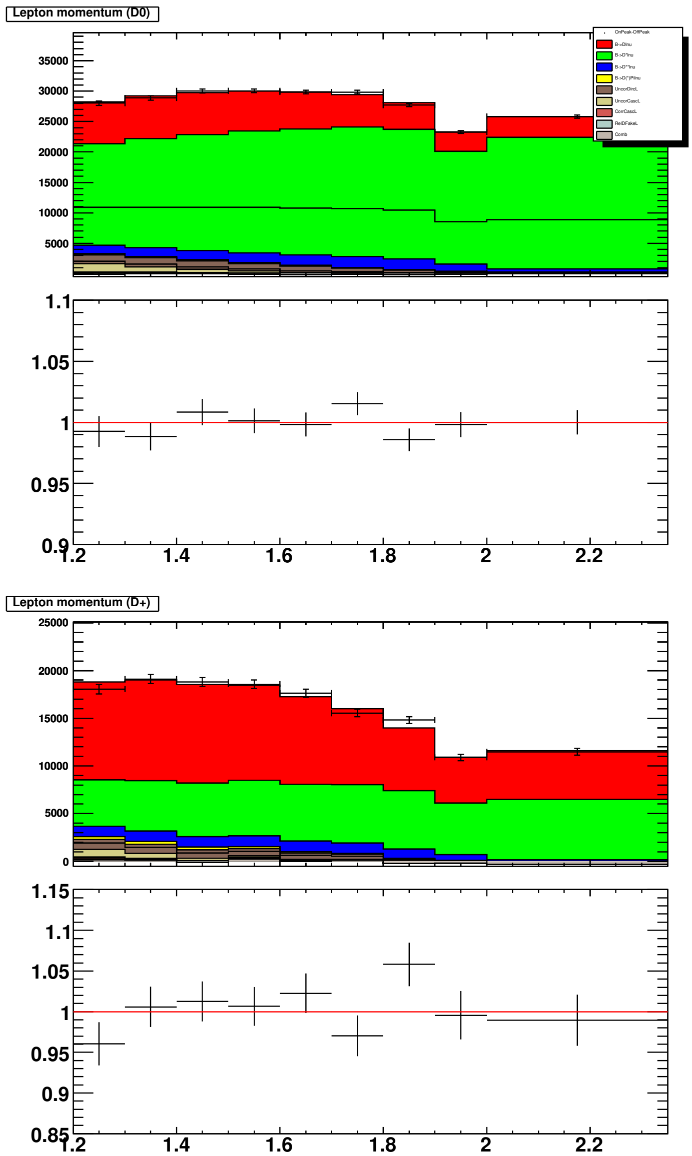

Figure 155: [p_ℓ **with fitted binning**] Lepton momentum plot with fitted binning after fitting. The top is D^0 and the bottom is D^+. Black is OnPeak - OffPeak data. Red is $B \to D\ell\nu$, green is $B \to D^*\ell\nu$, blue is $B \to D^{**}\ell\nu$, yellow is non-resonant $B \to D^{(*)}\pi\ell\nu$, and the rest is background. Dark brown is UncorrDL, light brown is UncorrCL, dark red is CascL, blue gray is FakeL, and light gray is Comb. Comb is almost disappeared after D mass sideband subtraction.

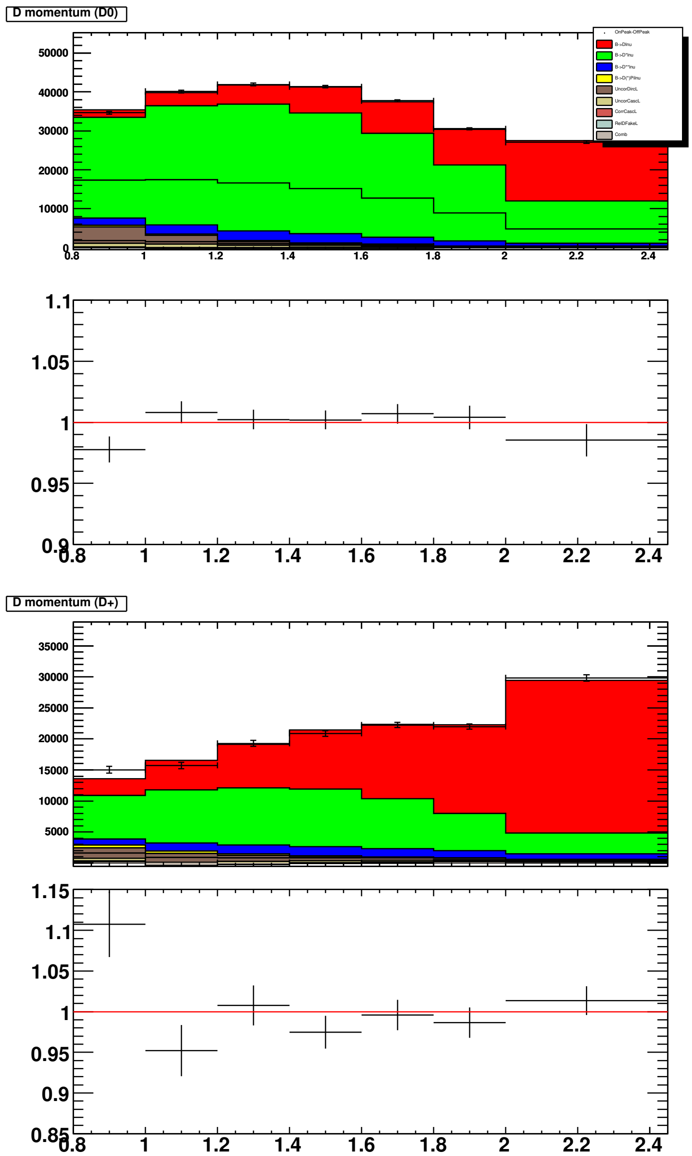

Figure 156: [p_D **with fitted binning**] D momentum plot with fitted binning after fitting. The top is D^0 and the bottom is D^+. Black is OnPeak - OffPeak data. Red is $B \to D\ell\nu$, green is $B \to D^*\ell\nu$, blue is $B \to D^{**}\ell\nu$, yellow is non-resonant $B \to D^{(*)}\pi\ell\nu$, and the rest is background. Dark brown is UncorrDL, light brown is UncorrCL, dark red is CascL, blue gray is FakeL, and light gray is Comb. Comb is almost disappeared after D mass sideband subtraction.

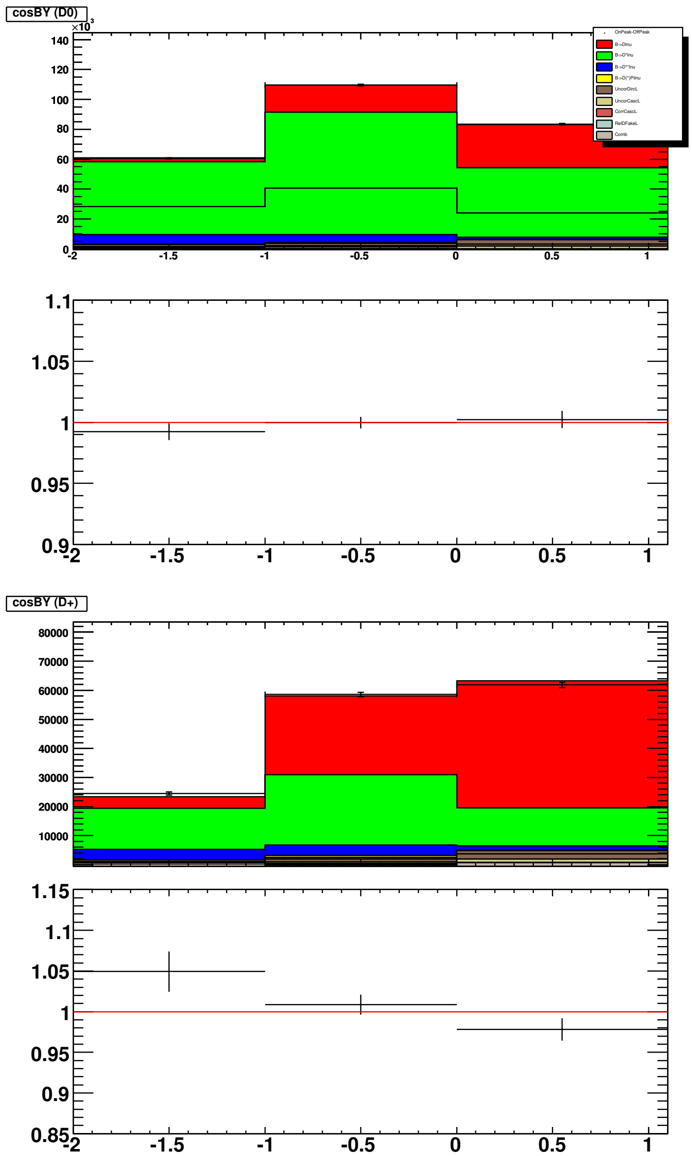

Figure 157: [$\cos\theta_{B-Dl}$ **with fitted binning**] $\cos\theta_{B-Dl}$ plot with fitted binning after fitting. The top is D^0 and the bottom is D^+. Black is OnPeak - OffPeak data. Red is $B \to D\ell\nu$, green is $B \to D^*\ell\nu$, blue is $B \to D^{**}\ell\nu$, yellow is non-resonant $B \to D^{(*)}\pi\ell\nu$, and the rest is background. Dark brown is UncorrDL, light brown is UncorrCL, dark red is CascL, blue gray is FakeL, and light gray is Comb. Comb is almost disappeared after D mass sideband subtraction.

ρ_D^2	1.212 ± 0.046 (3.8 %)
ρ^2	1.375 ± 0.058 (4.2 %)
R_1	1.586 ± 0.092 (5.8 %)
R_2	0.613 ± 0.080 (13.1 %)
$\mathcal{B}(B^+ \to \bar{D}^0\ell^+\nu)$	0.02384 ± 0.00032 (1.4 %)
$\mathcal{B}(B^+ \to \bar{D}^{*0}\ell^+\nu)$	0.05610 ± 0.00071 (1.3 %)
$\mathcal{B}(D^{(*)}\pi\ell\nu)$	0.01491 ± 0.00146 (9.8 %)
$\mathcal{B}(D^{(*)}\pi\pi\ell\nu)$	not included
χ^2/ndof (P-value)	376/365 (0.34)

Table 68: [**Nominal fit**] Fit results.

	ρ_D^2	ρ^2	R_1	R_2	$\mathcal{B}(D\ell\nu)$	$\mathcal{B}(D^*\ell\nu)$	$\mathcal{B}(D^{(*)}\pi\ell\nu)$
ρ_D^2	1						
ρ^2	-0.239	1					
R_1	-0.058	+0.865	1				
R_2	+0.144	-0.930	-0.928	1			
$\mathcal{B}(D\ell\nu)$	+0.324	+0.172	+0.242	-0.111	1		
$\mathcal{B}(D^*\ell\nu)$	-0.364	+0.496	+0.283	-0.486	-0.291	1	
$\mathcal{B}(D^{(*)}\pi\ell\nu)$	+0.150	-0.430	-0.332	+0.388	-0.065	-0.782	1

Table 69: [**Correlation coefficients (Nominal fit)**] Correlations between parameters.

18.2 $\cos\theta_{B-Dl}$ bin (-1.9, -0.9, 0.1, 1.1) (3 bins), No background cuts

18.2.1 Nominal fit

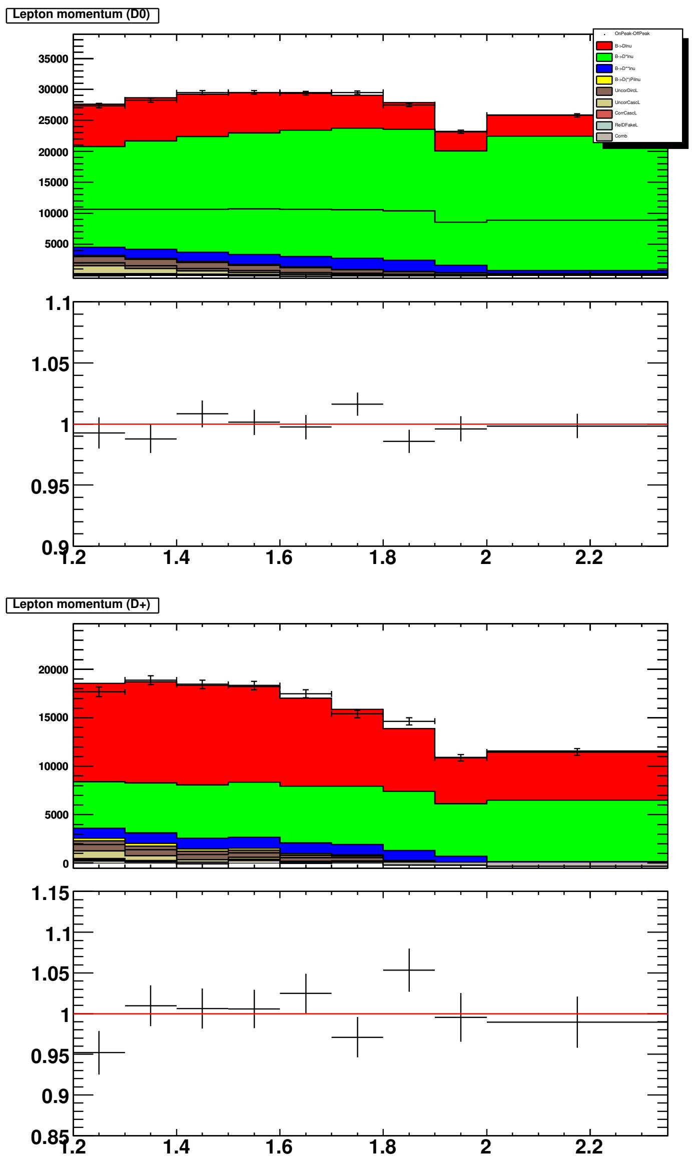

Figure 158: [p_ℓ **with fitted binning**] Lepton momentum plot with fitted binning after fitting. The top is D^0 and the bottom is D^+. Black is OnPeak - OffPeak data. Red is $B \to D\ell\nu$, green is $B \to D^*\ell\nu$, blue is $B \to D^{**}\ell\nu$, yellow is non-resonant $B \to D^{(*)}\pi\ell\nu$, and the rest is background. Dark brown is UncorrDL, light brown is UncorrCL, dark red is CascL, blue gray is FakeL, and light gray is Comb. Comb is almost disappeared after D mass sideband subtraction.

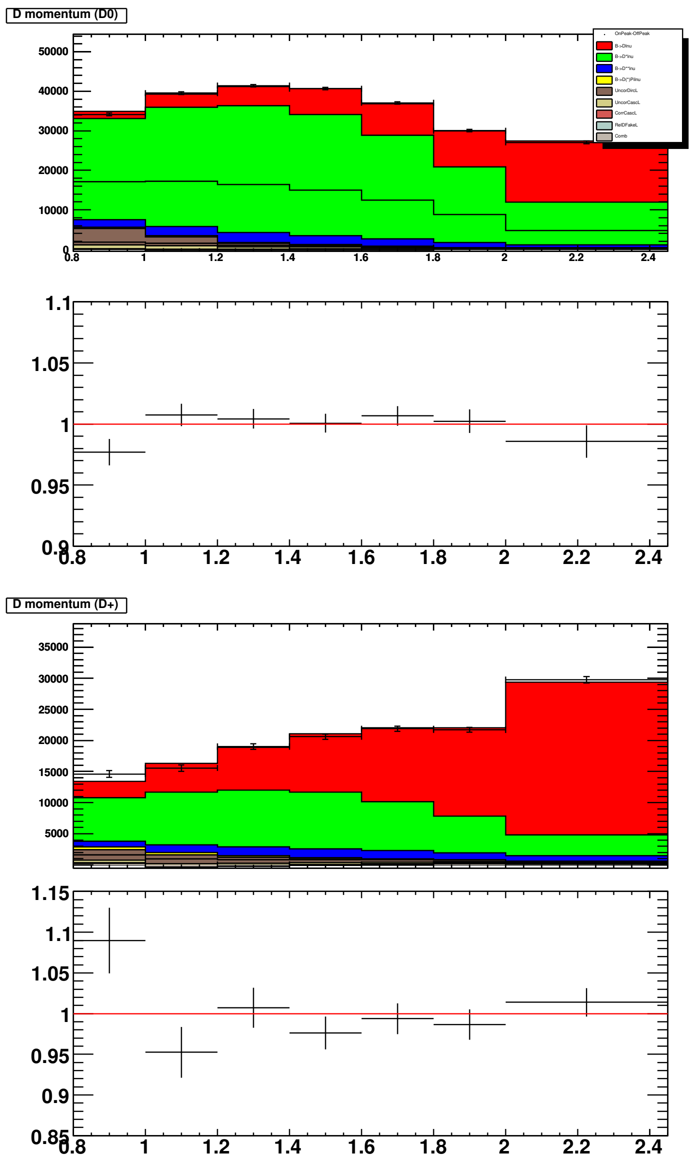

Figure 159: [p_D **with fitted binning**] D momentum plot with fitted binning after fitting. The top is D^0 and the bottom is D^+. Black is OnPeak - OffPeak data. Red is $B \to D\ell\nu$, green is $B \to D^*\ell\nu$, blue is $B \to D^{**}\ell\nu$, yellow is non-resonant $B \to D^{(*)}\pi\ell\nu$, and the rest is background. Dark brown is UncorrDL, light brown is UncorrCL, dark red is CascL, blue gray is FakeL, and light gray is Comb. Comb is almost disappeared after D mass sideband subtraction.

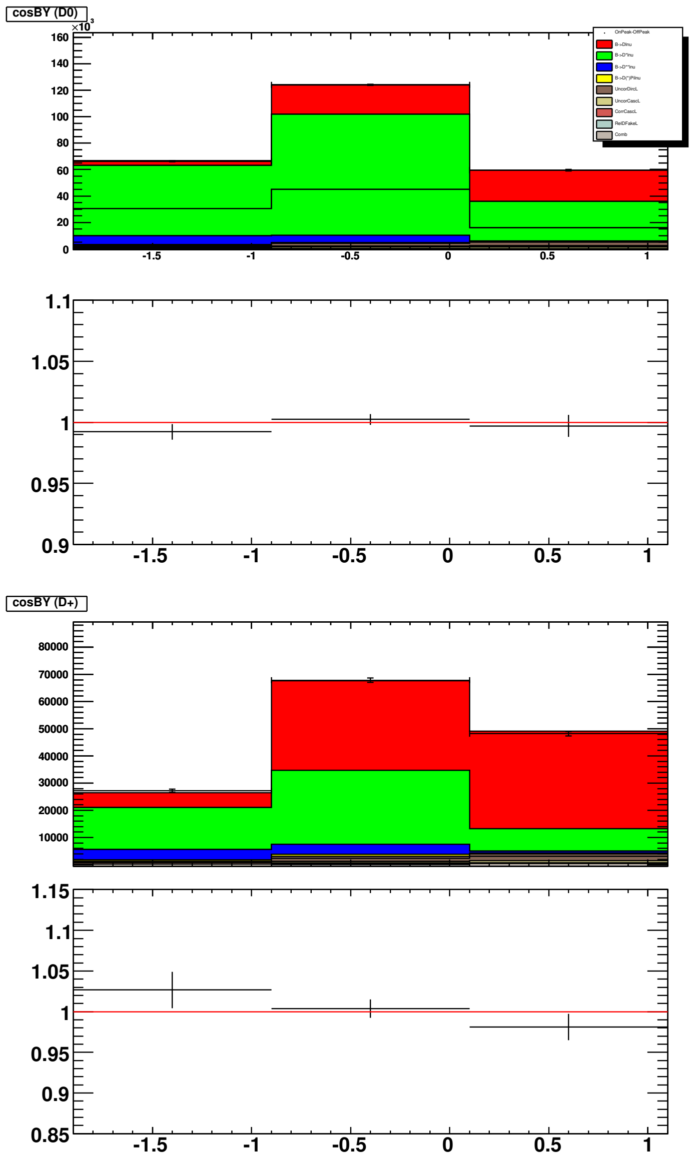

Figure 160: [$\cos\theta_{B-Dl}$ **with fitted binning**] $\cos\theta_{B-Dl}$ plot with fitted binning after fitting. The top is D^0 and the bottom is D^+. Black is OnPeak - OffPeak data. Red is $B \to D\ell\nu$, green is $B \to D^*\ell\nu$, blue is $B \to D^{**}\ell\nu$, yellow is non-resonant $B \to D^{(*)}\pi\ell\nu$, and the rest is background. Dark brown is UncorrDL, light brown is UncorrCL, dark red is CascL, blue gray is FakeL, and light gray is Comb. Comb is almost disappeared after D mass sideband subtraction.

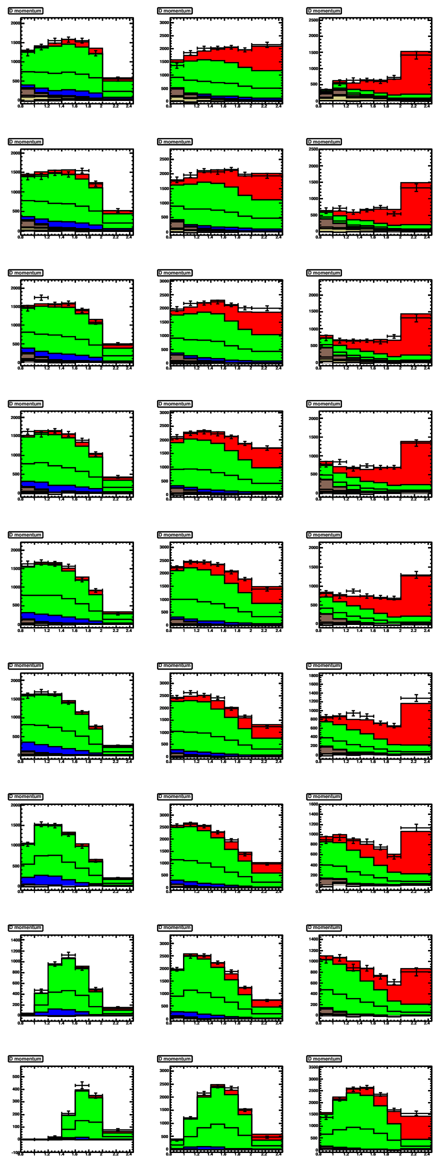

Figure 161: [D^0 **bin by bin after fitting**] D^0 momentum plots showing all bins after fitting. From top to bottom, lepton momentum bin changes from the lowest to the highest, and from left to right, cosBY bin changes from negative to positive. In each plots, colors are the same as other plots. Black is OnPeak - OffPeak data. Red is $B \to D\ell\nu$, green is $B \to D^{*}\ell\nu$, blue is $B \to D^{**}\ell\nu$, yellow is non-resonant $B \to D^{(*)}\pi\ell\nu$, and the rest is background. Dark brown is UncorrDL, light brown is UncorrCL, dark red is CascL, blue gray is FakeL, and light gray is Comb. Comb is almost disappeared after D mass sideband subtraction.

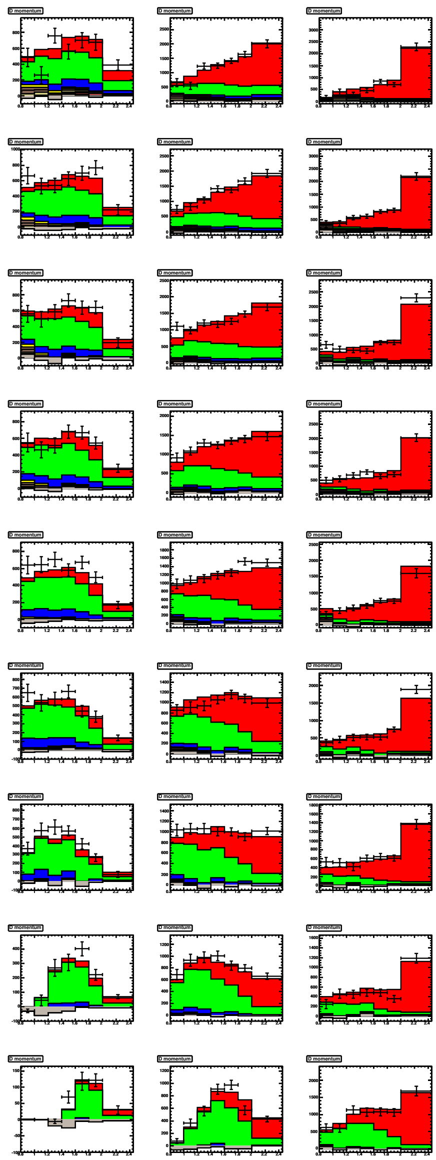

Figure 162: [D^+ **bin by bin after fitting**] D^+ momentum plots showing all bins after fitting. From top to bottom, lepton momentum bin changes from the lowest to the highest, and from left to right, cosBY bin charger's from negative to positive. In each plots, colors are the same as other plots. Black is OnPeak - OffPeak data. Red is $B \to D\ell\nu$, green is $B \to D^*\ell\nu$, blue is $B \to D^{**}\ell\nu$, yellow is non-resonant $B \to D^{(*)}\pi\ell\nu$, and the rest is background. Dark brown is UncorrDL, light brown is UncorrCL, dark red is CascL, blue gray is FakeL, and light gray is Comb. Comb is almost disappeared after D mass sideband subtraction.

ρ_D^2	1.224 ± 0.046 (3.7 %)
ρ^2	1.378 ± 0.058 (4.2 %)
R_1	1.593 ± 0.093 (5.8 %)
R_2	0.613 ± 0.080 (13.1 %)
$\mathcal{B}(B^+ \to \bar{D}^0 \ell^+ \nu)$	0.02414 ± 0.00032 (1.3 %)
$\mathcal{B}(B^+ \to \bar{D}^{*0} \ell^+ \nu)$	0.05625 ± 0.00071 (1.3 %)
$\mathcal{B}(D^{(*)} \pi \ell \nu)$	0.01508 ± 0.00146 (9.7 %)
$\mathcal{B}(D^{(*)} \pi\pi \ell \nu)$	not included
χ^2/ndof (P-value)	376/365 (0.34)

Table 70: [**No beam energy correction**] Fit results.

18.2.2 No beam energy correction

Almost no difference.

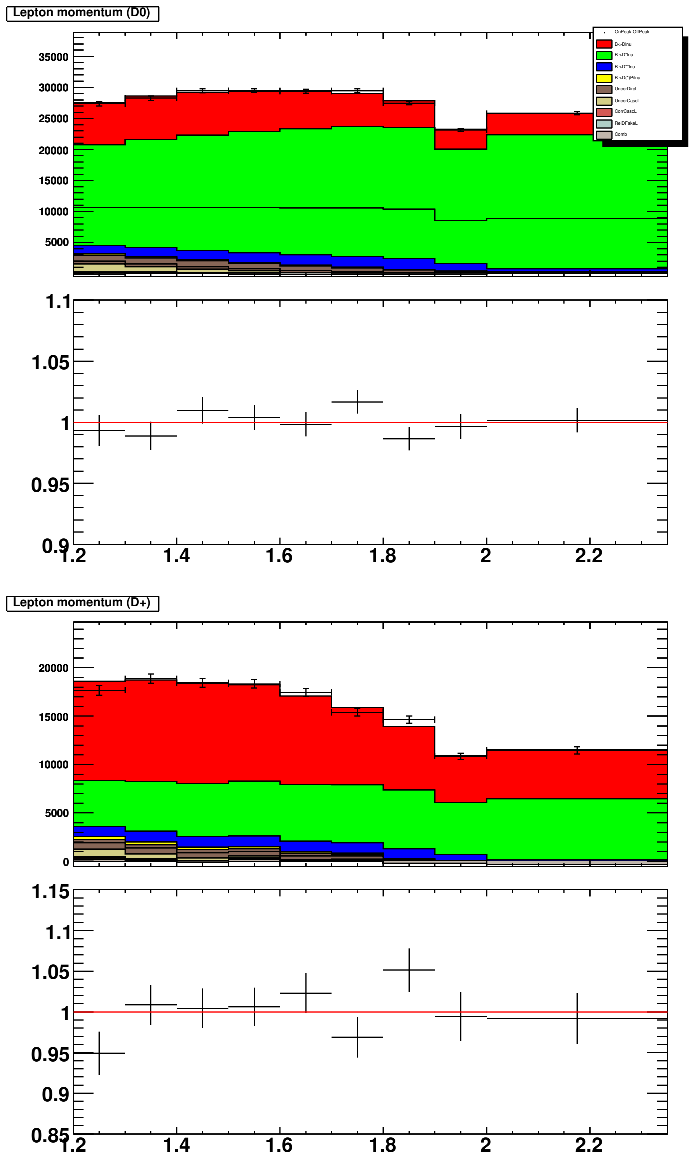

Figure 163: [p_ℓ **with fitted binning**] Lepton momentum plot with fitted binning after fitting. The top is D^0 and the bottom is D^+. Black is OnPeak - OffPeak data. Red is $B \to D\ell\nu$, green is $B \to D^*\ell\nu$, blue is $B \to D^{**}\ell\nu$, yellow is non-resonant $B \to D^{(*)}\pi\ell\nu$, and the rest is background. Dark brown is UncorrDL, light brown is UncorrCL, dark red is CascL, blue gray is FakeL, and light gray is Comb. Comb is almost disappeared after D mass sideband subtraction.

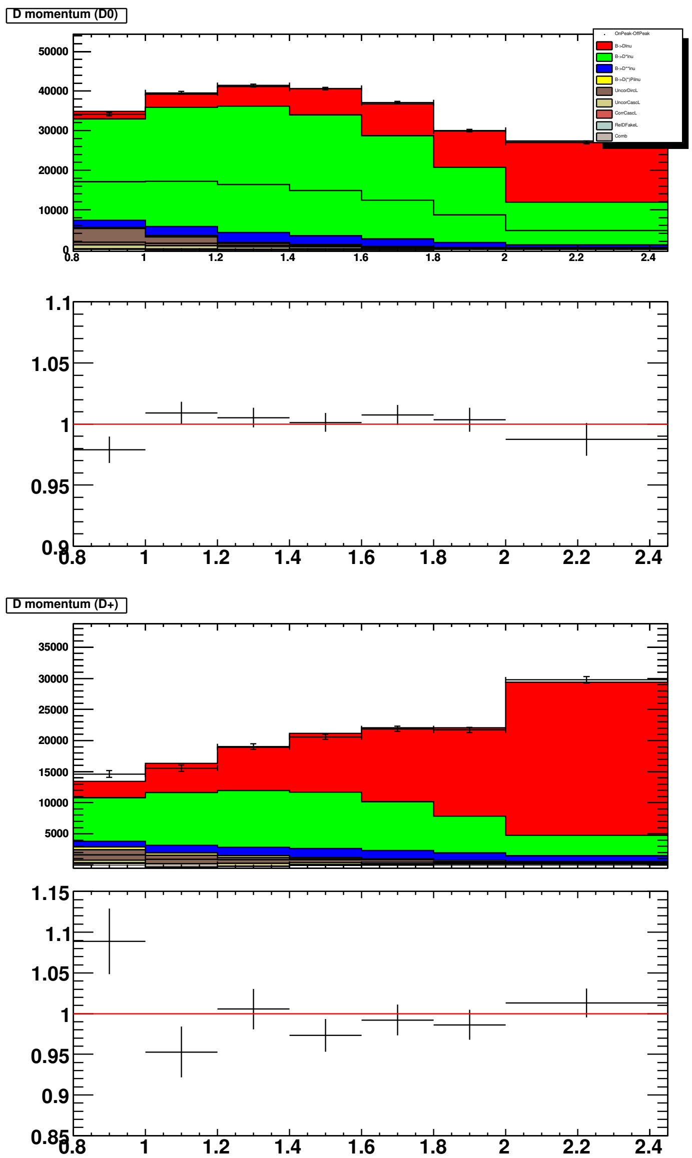

Figure 164: [p_D **with fitted binning**] D momentum plot with fitted binning after fitting. The top is D^0 and the bottom is D^+. Black is OnPeak - OffPeak data. Red is $B \rightarrow D\ell\nu$, green is $B \rightarrow D^*\ell\nu$, blue is $B \rightarrow D^{**}\ell\nu$, yellow is non-resonant $B \rightarrow D^{(*)}\pi\ell\nu$, and the rest is background. Dark brown is UncorrDL, light brown is UncorrCL, dark red is CascL, blue gray is FakeL, and light gray is Comb. Comb is almost disappeared after D mass sideband subtraction.

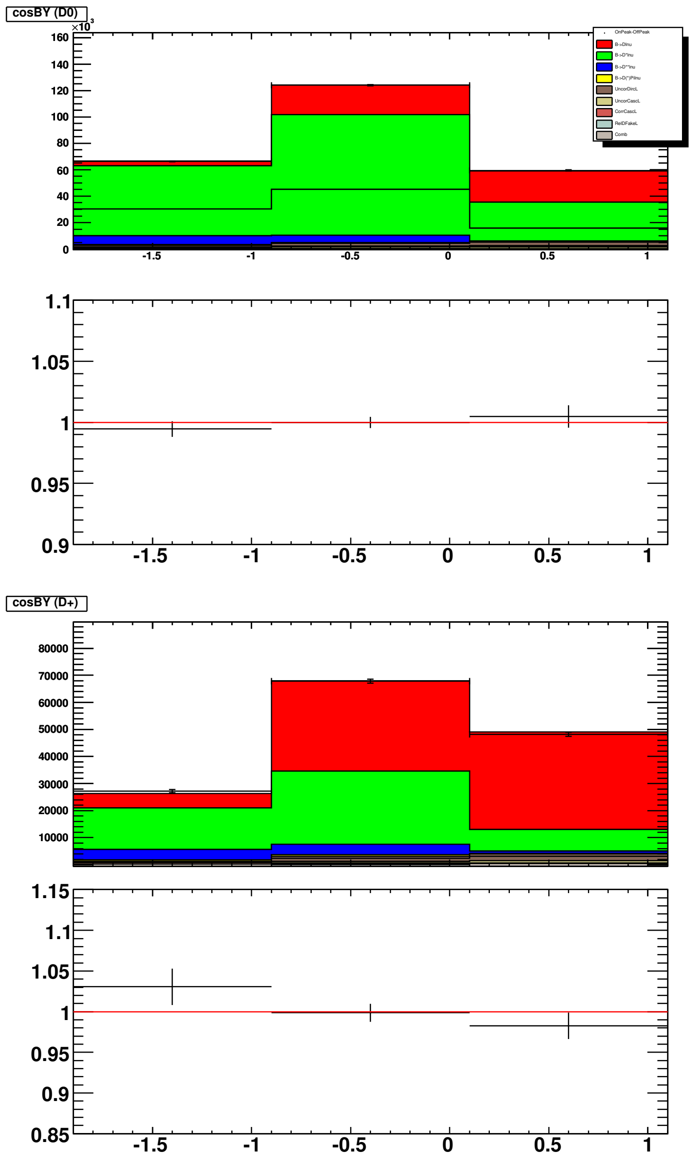

Figure 165: [$\cos\theta_{B-Dl}$ **with fitted binning**] $\cos\theta_{B-Dl}$ plot with fitted binning after fitting. The top is D^0 and the bottom is D^+. Black is OnPeak - OffPeak data. Red is $B \rightarrow D\ell\nu$, green is $B \rightarrow D^*\ell\nu$, blue is $B \rightarrow D^{**}\ell\nu$, yellow is non-resonant $B \rightarrow D^{(*)}\pi\ell\nu$, and the rest is background. Dark brown is UncorrDL, light brown is UncorrCL, dark red is CascL, blue gray is FakeL, and light gray is Comb. Comb is almost disappeared after D mass sideband subtraction.

Parameters	Run1-3 result	Run4 result	NR
ρ_D^2	1.227 ± 0.063	1.119 ± 0.066	-0.31
ρ^2	1.321 ± 0.080	1.411 ± 0.082	+0.79
R_1	1.515 ± 0.118	1.628 ± 0.134	+0.63
R_2	0.682 ± 0.104	0.566 ± 0.117	-0.74
$\mathcal{B}(B \to D\ell\nu)$	0.02381 ± 0.00045	0.02400 ± 0.00046	+0.29
$\mathcal{B}(B \to D^*\ell\nu)$	0.05567 ± 0.00100	0.05635 ± 0.00101	+0.47
$\mathcal{B}(B \to D^{(*)}\pi\ell\nu)$	0.01652 ± 0.00202	0.01359 ± 0.00209	-1.01
$\mathcal{B}(B \to D^{(*)}\pi\pi\ell\nu)$	not included	not included	n/a
χ^2/ndof (P-value)	365/364 (0.47)	365/365 (0.49)	

Table 71: [**Run1-3 and Run4 fits**] Run1-3 and Run4 fit results and normaliaed residuals (NR).

18.3 Cross checks

18.3.1 Run1-3 vs Run4

18.3.2 D^0 vs D^+

Parameters	D^0 result	D^+ result	NR
ρ_D^2	1.353 ± 0.065	1.034 ± 0.093	-2.81
ρ^2	1.350 ± 0.065	1.497 ± 0.213	+0.66
R_1	1.589 ± 0.097	1.756 ± 0.358	+0.45
R_2	0.634 ± 0.085	0.530 ± 0.325	-0.31
$\mathcal{B}(B \to D\ell\nu)$	0.02479 ± 0.00060	0.02296 ± 0.00054	-2.27
$\mathcal{B}(B \to D^*\ell\nu)$	0.05506 ± 0.00102	0.05841 ± 0.00528	+0.62
$\mathcal{B}(B \to D^{(*)}\pi\ell\nu)$	0.01551 ± 0.00194	0.01689 ± 0.00496	+0.26
$\mathcal{B}(B \to D^{(*)}\pi\pi\ell\nu)$	not included	not included	n/a
χ^2/ndof (P-value)	177/180 (0.56)	184/178 (0.37)	

Table 72: [D^0 **and** D^+ **fits**] Run1-3 and Run4 fit results and normaliaed residuals (NR).

ρ_D^2	1.209 ± 0.046
ρ^2	1.388 ± 0.060
R_1	1.623 ± 0.102
R_2	0.584 ± 0.087
$\mathcal{B}(B^+ \to \bar{D}^0 \ell^+ \nu)$	0.02392 ± 0.00033
$\mathcal{B}(B^+ \to \bar{D}^{*0} \ell^+ \nu)$	0.05654 ± 0.00082
$\mathcal{B}(D^{(*)} \pi \ell \nu)$	0.01206 ± 0.00294
$\mathcal{B}(D^{(*)} \pi\pi \ell \nu)$	0.01051 ± 0.00939
χ^2/ndof (P-value)	374/364 (0.34)

Table 73: [**Include** $D^{(*)}\pi\pi\ell\nu$] Fit results.

18.4 Isospin and $\cos\theta_{B-Dl}$ problems

We use $\cos\theta_{B-Dl}$ bin (-1.9, -0.9, 0.1, 1.1) (3 bins), No background cuts configuration. By using this new $\cos\theta_{B-Dl}$, data - MC agrement of D^+ $\cos\theta_{B-Dl}$ has already improved (Figure 160).

18.4.1 Include $D^{(*)}\pi\pi\ell\nu$

By including $D^{(*)}\pi\pi\ell\nu$ component (Figure 166), D^+ $\cos\theta_{B-Dl}$ problem is solved. However, $D^*\ell\nu$ isospin problem is not really solved (Table 74). This is because $D^{(*)}\pi\pi\ell\nu$ is compensated. If we fix $D^{(*)}\pi\ell\nu$ and $D^{(*)}\pi\pi\ell\nu$ BF, isospin symmetry holds (Table 75).

ρ_D^2	1.193 ± 0.051
ρ^2	1.405 ± 0.061
R_1	1.637 ± 0.103
R_2	0.575 ± 0.088
$\mathcal{B}(B^+ \to \bar{D}^0 \ell^+ \nu)$	0.02435 ± 0.00056
$\mathcal{B}(B^0 \to D^- \ell^+ \nu)$	0.02185 ± 0.00042
$\mathcal{B}(B^+ \to \bar{D}^{*0} \ell^+ \nu)$	0.05485 ± 0.00132
$\mathcal{B}(B^0 \to D^{*-} \ell^+ \nu)$	0.05473 ± 0.00200
$\mathcal{B}(D^{(*)} \pi \ell \nu)$	0.01288 ± 0.00307
$\mathcal{B}(D^{(*)} \pi\pi \ell \nu)$	0.00587 ± 0.00988
χ^2/ndof (P-value)	372/362 (0.35)

Table 74: [**Include $D^{(*)}\pi\pi\ell\nu$, no isospin constraints**] Fit results.

ρ_D^2	1.227 ± 0.046
ρ^2	1.353 ± 0.054
R_1	1.592 ± 0.090
R_2	0.637 ± 0.074
$\mathcal{B}(B^+ \to \bar{D}^0 \ell^+ \nu)$	0.02463 ± 0.00055
$\mathcal{B}(B^0 \to D^- \ell^+ \nu)$	0.02198 ± 0.00040
$\mathcal{B}(B^+ \to \bar{D}^{*0} \ell^+ \nu)$	0.05456 ± 0.00109
$\mathcal{B}(B^0 \to D^{*-} \ell^+ \nu)$	0.05195 ± 0.00146
$\mathcal{B}(D^{(*)} \pi \ell \nu)$	0.0152 (Fixed)
$\mathcal{B}(D^{(*)} \pi\pi \ell \nu)$	0.0105 (Fixed)
χ^2/ndof (P-value)	376/363 (0.31)

Table 75: [**Include $D^{(*)}\pi\pi\ell\nu$, no isospin constraints, Fix BF**] Fit results.

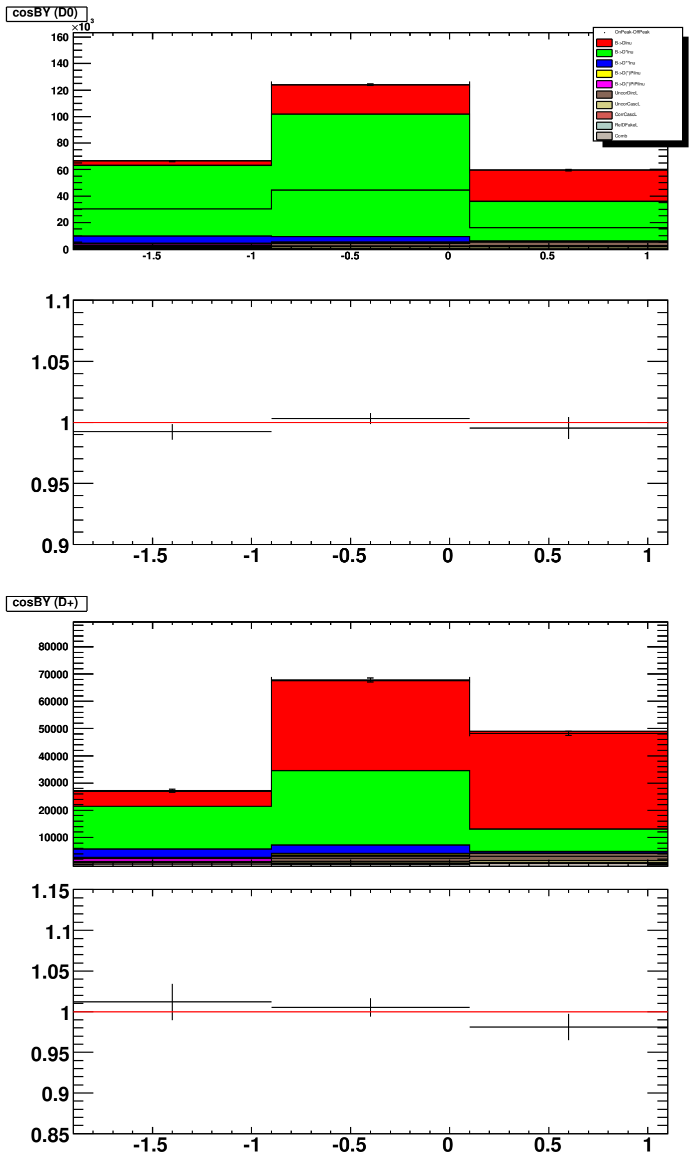

Figure 166: [$\cos\theta_{B-Dl}$ **with fitted binning**] $\cos\theta_{B-Dl}$ plot with fitted binning after fitting. The top is D^0 and the bottom is D^+. Black is OnPeak - OffPeak data. Red is $B \to D\ell\nu$, green is $B \to D^*\ell\nu$, blue is $B \to D^{**}\ell\nu$, yellow is non-resonant $B \to D^{(*)}\pi\ell\nu$, and the rest is background. Dark brown is UncorrDL, light brown is UncorrCL, dark red is CascL, blue gray is FakeL, and light gray is Comb. Comb is almost disappeared after D mass sideband subtraction.

Parameters	Electron result	Muon result	NR
ρ_D^2	1.212 ± 0.046	1.082 ± 0.064	-1.65
ρ^2	1.375 ± 0.058	1.258 ± 0.069	-1.30
R_1	1.586 ± 0.092	1.413 ± 0.093	-1.32
R_2	0.613 ± 0.081	0.741 ± 0.083	+1.10
$\mathcal{B}(B \to D\ell\nu)$	0.02384 ± 0.00032	0.02243 ± 0.00037	-2.88
$\mathcal{B}(B \to D^*\ell\nu)$	0.05610 ± 0.00032	0.05314 ± 0.00079	-3.49
$\mathcal{B}(B \to D^{(*)}\pi\ell\nu)$	0.01491 ± 0.00146	0.01744 ± 0.00150	+1.21
χ^2/ndof (P-value)	376/365 (0.34)	357/365 (0.60)	29.3/7 (0.00013)

Table 76: [**Electron vs Muon**] Fit results and normaliaed residuals (NR).

19 Electron vs Muon

19.1 Electron vs Muon

There is a significant difference between electron and muon.

Parameters	Run1-3 result	Run4 result	NR
ρ_D^2	1.227 ± 0.063	1.199 ± 0.066	-0.31
ρ^2	1.321 ± 0.080	1.411 ± 0.082	+0.79
R_1	1.515 ± 0.118	1.628 ± 0.134	+0.63
R_2	0.682 ± 0.104	0.566 ± 0.117	-0.74
$\mathcal{B}(B \to D\ell\nu)$	0.02381 ± 0.00045	0.02400 ± 0.00046	+0.29
$\mathcal{B}(B \to D^*\ell\nu)$	0.05567 ± 0.00100	0.05635 ± 0.00101	+0.47
$\mathcal{B}(B \to D^{(*)}\pi\ell\nu)$	0.01652 ± 0.00202	0.01359 ± 0.00209	-1.01
χ^2/ndof (P-value)	365/364 (0.47)	365/365 (0.49)	3.0/7 (0.885)

Table 77: [**Run1-3 vs Run4 (Electron)**] Fit results and normaliaed residuals (NR).

19.2 Electron

There is no significant internal inconsistency in electron

19.2.1 Electron : Run123 vs Run4

19.2.2 Electron : D^0 vs D^+

Parameters	D^0 result	D^+ result	NR
ρ_D^2	1.353 ± 0.065	1.034 ± 0.093	-2.81
ρ^2	1.350 ± 0.065	1.497 ± 0.213	+0.66
R_1	1.589 ± 0.097	1.756 ± 0.358	+0.45
R_2	0.634 ± 0.085	0.530 ± 0.325	-0.31
$\mathcal{B}(B \to D\ell\nu)$	0.02479 ± 0.00060	0.02296 ± 0.00054	-2.27
$\mathcal{B}(B \to D^*\ell\nu)$	0.05506 ± 0.00102	0.05841 ± 0.00528	+0.62
$\mathcal{B}(B \to D^{(*)}\pi\ell\nu)$	0.01551 ± 0.00194	0.01689 ± 0.00496	+0.26
χ^2/ndof (P-value)	177/180 (0.56)	184/178 (0.37)	14.2/7 (0.047)

Table 78: [D^0 **vs** D^+ **(Electron)**] Fit results and normaliaed residuals (NR).

Parameters	Run1-3 result	Run4 result	NR
ρ_D^2	1.178 ± 0.082	0.973 ± 0.099	-1.60
ρ^2	1.236 ± 0.092	1.302 ± 0.103	+0.48
R_1	1.349 ± 0.116	1.514 ± 0.156	+0.85
R_2	0.773 ± 0.107	0.667 ± 0.132	-0.62
$\mathcal{B}(B \to D\ell\nu)$	0.02194 ± 0.00051	0.02311 ± 0.00054	+1.58
$\mathcal{B}(B \to D^*\ell\nu)$	0.05334 ± 0.00108	0.05310 ± 0.00112	-0.16
$\mathcal{B}(B \to D^{(*)}\pi\ell\nu)$	0.01481 ± 0.00202	0.02028 ± 0.00220	+1.83
χ^2/ndof (P-value)	358/364 (0.58)	390/365 (0.18)	9.7/7 (0.204)

Table 79: [**Run1-3 vs Run4 (Muon)**] Fit results and normaliaed residuals (NR).

19.3 Muon

There is no significant internal inconsistency in muon.

19.3.1 Muon : Run123 vs Run4

19.3.2 Muon : D^0 vs D^+

Parameters	D^0 result	D^+ result	NR
ρ_D^2	1.026 ± 0.115	1.063 ± 0.111	+0.23
ρ^2	1.326 ± 0.077	0.703 ± 0.364	-1.67
R_1	1.470 ± 0.107	1.019 ± 0.266	-1.58
R_2	0.665 ± 0.097	1.111 ± 0.280	+1.51
$\mathcal{B}(B \to D\ell\nu)$	0.02187 ± 0.00066	0.02172 ± 0.00063	-0.16
$\mathcal{B}(B \to D^*\ell\nu)$	0.05466 ± 0.00107	0.05047 ± 0.00582	-0.71
$\mathcal{B}(B \to D^{(*)}\pi\ell\nu)$	0.01411 ± 0.00195	0.02463 ± 0.00514	+1.91
χ^2/ndof (P-value)	185/180 (0.39)	160/178 (0.83)	11.8/7 (0.108)

Table 80: [D^0 **vs** D^+ **(Muon)**] Fit results and normaliaed residuals (NR).

Parameters	Electron result	Muon result	NR
ρ_D^2	1.208 ± 0.046	1.084 ± 0.063	-1.58
ρ^2	1.378 ± 0.058	1.242 ± 0.068	-1.51
R_1	1.601 ± 0.094	1.380 ± 0.090	-1.70
R_2	0.604 ± 0.081	0.763 ± 0.081	+1.38
$\mathcal{B}(B \to D\ell\nu)$	0.02336 ± 0.00032	0.02343 ± 0.00039	+0.14
$\mathcal{B}(B \to D^*\ell\nu)$	0.05498 ± 0.00070	0.05544 ± 0.00082	+0.43
$\mathcal{B}(B \to D^{(*)}\pi\ell\nu)$	0.01457 ± 0.00144	0.01839 ± 0.00156	+1.80
χ^2/ndof (P-value)	376/365 (0.34)	355/365 (0.64)	13.1/7 (0.071)

Table 81: [**Electron vs Muon : Lepton PID efficiency**] Fit results and normaliaed residuals (NR).

19.4 Lepton PID efficiency

We

- Increase electron efficiency by 2 %
- Decrease muon efficiency by 4 %

19.5 New sideband

Old D mass peak and sideband

- D^0
  - Lower sideband : 1.806 - 1.840 GeV
  - D mass peak : 1.840 - 1.888 GeV
  - Lower sideband : 1.888 - 1.922 GeV
- D^+
  - Lower sideband : 1.810 - 1.848 GeV
  - D mass peak : 1.848 - 1.890 GeV
  - Lower sideband : 1.890 - 1.928 GeV

This is too close to D mass edge?
New D mass peak and sideband

- D^0
  - Lower sideband : 1.816 - 1.840 GeV
  - D mass peak : 1.840 - 1.888 GeV
  - Lower sideband : 1.888 - 1.912 GeV
- D^+
  - Lower sideband : 1.821 - 1.845 GeV
  - D mass peak : 1.845 - 1.893 GeV
  - Lower sideband : 1.893 - 1.917 GeV

Same width of D mass peak.

Parameters	Electron result	Muon result	NR
ρ_D^2	1.211 ± 0.051	1.119 ± 0.070	-1.06
ρ^2	1.363 ± 0.063	1.262 ± 0.072	-1.05
R_1	1.573 ± 0.098	1.416 ± 0.098	-1.14
R_2	0.630 ± 0.085	0.757 ± 0.088	+1.04
$\mathcal{B}(B \to D\ell\nu)$	0.02411 ± 0.00037	0.02234 ± 0.00042	-3.20
$\mathcal{B}(B \to D^*\ell\nu)$	0.05557 ± 0.00078	0.05316 ± 0.00087	-2.07
$\mathcal{B}(B \to D^{(*)}\pi\ell\nu)$	0.01567 ± 0.00160	0.01633 ± 0.00165	+0.29
χ^2/ndof (P-value)	376/365 (0.34)	357/365 (0.60)	19.2/7 (0.0076)

Table 82: [**Electron vs Muon : New sideband**] Fit results and normaliaed residuals (NR).

20 Calculation of $\mathcal{G}(1)|V_{cb}|$ and $\mathcal{F}(1)|V_{cb}|$

20.1 $\mathcal{G}(1)|V_{cb}|$

Differential decay rate of $B \to D\ell\nu$ decays are given by

$$\frac{d\Gamma(B \to D\ell\nu)}{dw} = \frac{G_F^2|V_{cb}|^2 m_B^5}{48\pi^3} r^3(w^2-1)^{3/2}\,\mathcal{J}_D(w) \tag{326}$$

where

$$\mathcal{J}_D(w) = [(1+r)h_+(w) - (1-r)h_-(w)]^2 \tag{327}$$

and

$$r = \frac{m_D}{m_B} \tag{328}$$

In HQET model, we can set

$$\begin{aligned} h_+(w) &= h_+(1)[1 - 8\rho_D^2 z + (51\rho_D^2 - 10)z^2 - (252\rho_D^2 - 84)z^3] \\ h_-(w) &= 0 \end{aligned} \tag{329}$$

where

$$z = \frac{\sqrt{w+1}-\sqrt{2}}{\sqrt{w+1}+\sqrt{2}} \tag{330}$$

Thus, differential decay rate is

$$\begin{aligned} &\frac{d\Gamma(B \to D\ell\nu)}{dw} \\ &= \frac{G_F^2 m_B^5}{48\pi^3} r^3(w^2-1)^{3/2}\,(1+r)^2[1 - 8\rho_D^2 z + (51\rho_D^2 - 10)z^2 - (252\rho_D^2 - 84)z^3]^2 \\ &\quad \times (\mathcal{G}(1)|V_{cb}|)^2 \end{aligned} \tag{331}$$

Note that $\mathcal{G}(1) = h_+(1)$. By integrating over w, we get

$$\begin{aligned} &\frac{\mathcal{B}(B \to D\ell\nu)}{\tau_B} \\ &= \frac{G_F^2 m_B^5}{48\pi^3} r^3(1+r)^2 \int (w^2-1)^{3/2}[1 - 8\rho_D^2 z + (51\rho_D^2 - 10)z^2 - (252\rho_D^2 - 84)z^3]^2 dw \\ &\quad \times (\mathcal{G}(1)|V_{cb}|)^2 \end{aligned} \tag{332}$$

where τ_B the lifetime of the B meson. If we define

$$C^D \equiv \sqrt{\frac{48\pi^3}{G_F^2 m_B^5 \tau_B r^3(1+r)^2}} \tag{333}$$

$$I_1^D \equiv \int (w^2-1)^{3/2}(1 - 10z^2 + 84z^3)^2 dw \tag{334}$$

$$I_2^D \equiv 2\int (w^2-1)^{3/2}(1 - 10z^2 + 84z^3)(8z - 51z^2 + 252z^3) dw \tag{335}$$

$$I_3^D \equiv \int (w^2-1)^{3/2}(8z - 51z^2 + 252z^3)^2 dw \tag{336}$$

then

$$\mathcal{G}(1)|V_{cb}| = C^D \mathcal{B}(B \to D\ell\nu)^{1/2}[I_1^D - \rho_D^2 I_2^D + (\rho_D^2)^2 I_3^D]^{-1/2} \quad (337)$$

Thus, using fit results $\mathcal{B}(B \to D\ell\nu)$ and ρ_D^2, we can calculate $\mathcal{G}(1)|V_{cb}|$. We use the following numerical values

$$\begin{aligned} \tau_{B^+} &= 1.638 \times 10^{-12}/6.58211915 \times 10^{-25} \;\; \text{GeV}^{-1} \\ m_{B^+} &= 5.2790 \;\; \text{GeV} \\ m_{D^0} &= 1.8645 \;\; \text{GeV} \\ G_F &= 1.166371 \times 10^{-5} \;\; \text{GeV}^{-2} \end{aligned} \quad (338)$$

20.2 $\mathcal{F}(1)|V_{cb}|$

Differential decay rate of $B \to D^*\ell\nu$ decays are given by

$$\frac{d\Gamma(B \to D^*\ell\nu)}{dw} = \frac{G_F^2|V_{cb}|^2 m_B^5}{48\pi^3} r^3 (w^2-1)^{1/2} \mathcal{J}_{WD}(R_1, R_2, \rho^2) \quad (339)$$

where

$$\mathcal{J}_{WD}(R_1, R_2, \rho^2) = (w+1)^2 [h_{A_1}]^2 (\tilde{h}_+^2 + \tilde{h}_-^2 + \tilde{h}_0^2) \quad (340)$$

Here, the form factors are given by

$$\begin{aligned} &\tilde{h}_\pm(w) \equiv (1-r)\widetilde{H}_\pm(w) = \sqrt{1-2wr+r^2}\left(1 \mp \sqrt{\tfrac{w-1}{w+1}} R_1(w)\right) \\ &\tilde{h}_0(w) \equiv (1-r)\widetilde{H}_0(w) = (1-r) + (w-1)(1-R_2(w)) = (w-r) - (w-1)R_2(w) \\ &h_{A_1}(w) = h_{A_1}(1)\left[1 - 8\rho^2 z + (53\rho^2 - 15)z^2 - (231\rho^2 - 91)z^3\right] \end{aligned} \quad (341)$$

where

$$\begin{aligned} R_1(w) &= R_1 - 0.12(w-1) + 0.05(w-1)^2 \\ R_2(w) &= R_2 + 0.11(w-1) - 0.06(w-1)^2 \\ r &= \tfrac{m_{D^*}}{m_B} \\ z &= \tfrac{\sqrt{w+1}-\sqrt{2}}{\sqrt{w+1}+\sqrt{2}} \end{aligned} \quad (342)$$

Thus, the differential decay rate is

$$\begin{aligned} &\frac{d\Gamma(B \to D^*\ell\nu)}{dw} \\ &= \frac{G_F^2|V_{cb}|^2 m_B^5}{48\pi^3} r^3 (w^2-1)^{1/2}(w+1)^2 \\ &\quad \times [\mathcal{F}(1)]^2 [1 - 8\rho^2 z + (53\rho^2-15)z^2 - (231\rho^2-91)z^3]^2 (\tilde{h}_+^2 + \tilde{h}_-^2 + \tilde{h}_0^2) \end{aligned} \quad (343)$$

Note that $\mathcal{F}(1) = h_{A_1}(1)$. By integrating over w, we get

$$\begin{aligned} \frac{\mathcal{B}(B \to D^*\ell\nu)}{\tau_B} &= \frac{G_F^2 m_B^5}{48\pi^3} r^3 (\mathcal{F}(1)|V_{cb}|)^2 \\ &\int (w^2-1)^{1/2}(w+1)^2(\tilde{h}_+^2 + \tilde{h}_-^2 + \tilde{h}_0^2) \\ &\quad \times [1 - 8\rho^2 z + (53\rho^2-15)z^2 - (231\rho^2-91)z^3]^2 dw \end{aligned} \quad (344)$$

where τ_B the lifetime of the B meson. Let us simplify this equation. By defining

$$\begin{aligned} k_1 &\equiv -0.12(w-1) + 0.05(w-1)^2 \\ k_2 &\equiv 0.11(w-1) - 0.06(w-1)^2 \end{aligned} \tag{345}$$

we get

$$\begin{aligned} &\tilde{h}_+^2 + \tilde{h}_-^2 + \tilde{h}_0^2 \\ &= (1-2wr+r^2)\left[1 - 2\sqrt{\frac{w-1}{w+1}}(R_1+k_1) + \frac{w-1}{w+1}(R_1+k_1)^2\right] \\ &\quad +(1-2wr+r^2)\left[1 + 2\sqrt{\frac{w-1}{w+1}}(R_1+k_1) + \frac{w-1}{w+1}(R_1+k_1)^2\right] \\ &\quad +(w-r)^2 - 2(w-r)(w-1)(R_2+k_2) + (w-1)^2(R_2+k_2)^2 \\ &= (2+w^2-6wr+3r^2) + 2(1-2wr+r^2)\frac{w-1}{w+1}(R_1^2+2k_1R_1+k_1^2) \\ &\quad -2(w-r)(w-1)(R_2+k_2) + (w-1)^2(R_2^2+2k_2R_2+k_2^2) \end{aligned} \tag{346}$$

Thus, if we define

$$\begin{aligned} A \equiv{} & (2+w^2-6wr+3r^2) + 2(1-2wr+r^2)\frac{w-1}{w+1}k_1^2 \\ & -2(w-r)(w-1)k_2 + (w-1)^2k_2^2 \end{aligned} \tag{347}$$

$$B_1 \equiv 4(1-2wr+r^2)\frac{w-1}{w+1}k_1 \tag{348}$$

$$D_1 \equiv 2(1-2wr+r^2)\frac{w-1}{w+1} \tag{349}$$

$$B_2 \equiv -2(w-r)(w-1) + 2k_2(w-1)^2 \tag{350}$$

$$D_2 \equiv (w-1)^2 \tag{351}$$

then

$$\tilde{h}_+^2 + \tilde{h}_-^2 + \tilde{h}_0^2 = A + B_1R_1 + D_1R_1^2 + B_2R_2 + D_2R_2^2 \tag{352}$$

If we further define

$$\begin{aligned} E_1 &\equiv (w^2-1)^{1/2}(w+1)^2(1-15z^2+91z^3)^2 \\ E_2 &\equiv 2(w^2-1)^{1/2}(w+1)^2(1-15z^2+91z^3)(8z-53z^2+231z^3) \\ E_3 &\equiv (w^2-1)^{1/2}(w+1)^2(8z-53z^2+231z^3)^2 \end{aligned} \tag{353}$$

and

$$I_1 \equiv \int AE_1dw \tag{354}$$

$$I_2 \equiv \int AE_2dw \tag{355}$$

$$I_3 \equiv \int AE_3 dw \tag{356}$$

$$I_4 \equiv \int B_1 E_1 dw \tag{357}$$

$$I_5 \equiv \int B_1 E_2 dw \tag{358}$$

$$I_6 \equiv \int B_1 E_3 dw \tag{359}$$

$$I_7 \equiv \int C_1 E_1 dw \tag{360}$$

$$I_8 \equiv \int C_1 E_2 dw \tag{361}$$

$$I_9 \equiv \int C_1 E_3 dw \tag{362}$$

$$I_{10} \equiv \int B_2 E_1 dw \tag{363}$$

$$I_{11} \equiv \int B_2 E_2 dw \tag{364}$$

$$I_{12} \equiv \int B_2 E_3 dw \tag{365}$$

$$I_{13} \equiv \int C_2 E_1 dw \tag{366}$$

$$I_{14} \equiv \int C_2 E_2 dw \tag{367}$$

$$I_{15} \equiv \int C_2 E_3 dw \tag{368}$$

and also

$$C \equiv \sqrt{\frac{48\pi^3}{G_F^2 m_B^5 \tau_B r^3}} \tag{369}$$

$$\begin{aligned} \mathcal{F}(1)|V_{cb}| = C\mathcal{B}(B \to D^*\ell\nu)^{1/2}[&I_1 - I_2\rho^2 + I_3(\rho^2)^2 \\ &+ I_4 R_1 - I_5 R_1 \rho^2 + I_6 R_1 (\rho^2)^2 \\ &+ I_7 R_1^2 - I_8 R_1^2 \rho^2 + I_9 R_1^2 (\rho^2)^2 \\ &+ I_{10} R_2 - I_{11} R_2 \rho^2 + I_{12} R_2 (\rho^2)^2 \\ &+ I_{13} R_2^2 - I_{14} R_2^2 \rho^2 + I_{15} R_2^2 (\rho^2)^2]^{-1/2} \end{aligned} \tag{370}$$

Thus, using fit results $\mathcal{B}(B \to D^* \ell \nu)$, R_1, R_2 and ρ^2, we can calculate $\mathcal{F}(1)|V_{cb}|$. We use the following numerical values

$$\begin{aligned}
\tau_{B^+} &= 1.638 \times 10^{-12}/6.58211915 \times 10^{-25} \quad \mathrm{GeV}^{-1} \\
m_{B^+} &= 5.2790 \quad \mathrm{GeV} \\
m_{D^{*0}} &= 2.0067 \quad \mathrm{GeV} \\
G_F &= 1.166371 \times 10^{-5} \quad \mathrm{GeV}^{-2}
\end{aligned} \tag{371}$$

20.3 Statistical uncertainties

To calculate statistical uncertainties and correlation, for simplicity, we define

$$\begin{aligned}
y_1 &\equiv \mathcal{G}(1)|V_{cb}| \\
y_2 &\equiv \mathcal{F}(1)|V_{cb}| \\
y_3 &\equiv \rho^2 \\
y_4 &\equiv \rho_D^2 \\
y_5 &\equiv R_1 \\
y_6 &\equiv R_2 \\
x_1 &\equiv \rho_D^2 \\
x_2 &\equiv \rho^2 \\
x_3 &\equiv R_1 \\
x_4 &\equiv R_2 \\
x_5 &\equiv \mathcal{B}(B \to D \ell \nu) \\
x_6 &\equiv \mathcal{B}(B \to D^* \ell \nu)
\end{aligned} \tag{372}$$

then, Equation (337) becomes

$$y_1 = C^D x_5^{1/2} (I_1^D - I_2^D x_1 + I_3^D x_1^2)^{-1/2} \tag{373}$$

and Equation (370) becomes

$$\begin{aligned}
y_2 = C x_6^{1/2} [& I_1 - I_2 x_2 + I_3 x_2^2 \\
& + I_4 x_3 - I_5 x_3 x_2 + I_6 x_3 x_2^2 \\
& + I_7 x_3^2 - I_8 x_3^2 x_2 + I_9 x_3^2 x_2^2 \\
& + I_{10} x_4 - I_{11} x_4 x_2 + I_{12} x_4 x_2^2 \\
& + I_{13} x_4^2 - I_{14} x_4^2 x_2 + I_{15} x_4^2 x_2^2]^{-1/2}
\end{aligned} \tag{374}$$

The error matrix M(y) of y_1 - y_6 is determined by

$$M(y) = \left(\frac{\partial y_i}{\partial x_j} \right) M(x) \left(\frac{\partial y_i}{\partial x_j} \right) \tag{375}$$

where $M(x)$ the error matrix of x_1 - x_6

$$M(x) = \begin{pmatrix} 4.379\times10^{-3} & -1.559\times10^{-3} & -1.617\times10^{-3} & 1.789\times10^{-3} & 2.015\times10^{-5} & -2.288\times10^{-5} \\ -1.559\times10^{-3} & 5.841\times10^{-3} & 7.817\times10^{-3} & -7.167\times10^{-3} & 4.054\times10^{-6} & 1.244\times10^{-5} \\ -1.617\times10^{-3} & 7.817\times10^{-3} & 1.534\times10^{-2} & -1.183\times10^{-2} & 4.659\times10^{-6} & -2.025\times10^{-6} \\ 1.789\times10^{-3} & -7.167\times10^{-3} & -1.183\times10^{-2} & 1.067\times10^{-2} & 1.559\times10^{-6} & -1.887\times10^{-5} \\ 2.015\times10^{-5} & 4.054\times10^{-6} & 4.659\times10^{-6} & 1.559\times10^{-6} & 6.755\times10^{-7} & -3.001\times10^{-9} \\ -2.288\times10^{-5} & 1.244\times10^{-5} & -2.025\times10^{-6} & -1.887\times10^{-5} & -3.001\times10^{-9} & 1.498\times10^{-6} \end{pmatrix} \tag{376}$$

and

$$\frac{\partial y_1}{\partial x_1} = \frac{C}{2}x_5^{1/2}(I_2^D - 2I_3^D x_1)(I_1^D - I_2^D x_1 + I_3^D x_1^2)^{-3/2} \tag{377}$$

$$\frac{\partial y_1}{\partial x_5} = \frac{C}{2}x_5^{-1/2}(I_1^D - I_2^D x_1 + I_3^D x_1^2)^{-1/2} \tag{378}$$

$$\begin{aligned}\frac{\partial y_2}{\partial x_2} = -\frac{C}{2}x_6^{1/2}(&-I_2 + 2I_3x_2 - I_5x_3 + 2I_6x_3x_2 - I_8x_3^2 + 2I_9x_3^2x_2 \\ &-I_{11}x_6 + 2I_{12}x_6x_2 - I_{14}x_6^2 + 2I_{15}x_6^2x_2)F^{-3/2}\end{aligned} \tag{379}$$

$$\frac{\partial y_2}{\partial x_3} = -\frac{C}{2}x_6^{1/2}(I_4 - I_5x_2 + I_6x_2^2 + 2I_7x_3 - 2I_8x_3x_2 + 2I_9x_3x_2^2)F^{-3/2} \tag{380}$$

$$\frac{\partial y_2}{\partial x_4} = -\frac{C}{2}x_6^{1/2}(I_{10} - I_{11}x_2 + I_{12}x_2^2 + 2I_{13}x_4 - 2I_{14}x_4x_2 + 2I_{15}x_4x_2^2)F^{-3/2} \tag{381}$$

$$\frac{\partial y_2}{\partial x_6} = \frac{C}{2}x_6^{-1/2}F^{-1/2} \tag{382}$$

$$\frac{\partial y_3}{\partial x_1} = 1 \tag{383}$$

$$\frac{\partial y_4}{\partial x_2} = 1 \tag{384}$$

$$\frac{\partial y_5}{\partial x_3} = 1 \tag{385}$$

$$\frac{\partial y_6}{\partial x_4} = 1 \tag{386}$$

where

$$\begin{aligned}F = I_1 - I_2x_2 + I_3x_2^2 + I_4x_3 - I_5x_3x_2 + I_6x_3x_2^2 + I_7x_3^2 - I_8x_3^2x_2 + I_9x_3^2x_2^2 \\ +I_{10}x_4 - I_{11}x_4x_2 + I_{12}x_4x_2^2 + I_{13}x_4^2 - I_{14}x_4^2x_2 + I_{15}x_4^2x_2^2\end{aligned} \tag{387}$$

and all other partial derivatives are zero.
Using the fit results presented in the section 16, $\mathcal{G}(1)|V_{cb}|$ and $\mathcal{F}(1)|V_{cb}|$ are calculated to be

$$\begin{aligned}\mathcal{G}(1)|V_{cb}| = 0.04818 \pm 0.00185 \\ \mathcal{F}(1)|V_{cb}| = 0.03505 \pm 0.00049\end{aligned} \tag{388}$$

The correlation coefficient between these can be calculated to be

$$\frac{\mathrm{cov}(y_1, y_2)}{\sigma_{y_1}\sigma_{y_2}} = -0.228. \tag{389}$$

21 Systematic Uncertainties

Systematic uncertainties are shown in Tables 83-85. Numbers are negative when the corresponding fitted values decrease as a input parameter increases. Details are given in the following subsections. Note that the break down of background BF correction systematics are given in separate tables : Tables 86-88.

21.1 Form factors

21.1.1 w dependence of R_1 and R_2

We use the CLN parametrization of $B \to D^{(*)}\ell\nu$ decay form factors [38] (see section 10). Thus, we use

$$\begin{aligned} R_1(w) &= R_1 - 0.12(w-1) + 0.05(w-1)^2 \\ R_2(w) &= R_2 + 0.11(w-1) - 0.06(w-1)^2 \end{aligned} \tag{390}$$

Since there are different parametrization [40][41] and we cannot decide which is the best, we remove w dependence from R_1 and R_2 and consider the deviation as a systematic uncertainty.

21.1.2 $B \to D^{**}\ell\nu$ decay form factors

There are two sources of systematic uncertainty of D^{**} form factors :

- One is the FF slope $\tilde{\tau}' = -1.5$
- The other is the Approximation B$_1$ ($\tau_1 = 0$ and $\tau_2 = 0$).

To estimate systematic uncertainties,

- We change slope to -2.0 and -1.0, and take larger deviation.
- We use the Approximation B$_2$ ($\tau_1 \neq 0$ and $\tau_2 \neq 0$).

21.2 $B \to D^{**}/D^{(*)}\pi\ell\nu$ decay branching fractions

21.2.1 BF ratios

We have five BF ratios as input :

- $f_{D_2^*/D_1} \equiv \frac{\mathcal{B}(B^+\to\bar{D}_2^{*0}\ell^+\nu)}{\mathcal{B}(B^+\to\bar{D}_1^0\ell^+\nu)} = 0.78 \pm 0.17$
- $f_{D_0^*D\pi T/D_1D_2^*T} \equiv \frac{\mathcal{BT}(B^+\to\bar{D}_0^{*0}/(D\pi)^0\ell^+\nu)}{\mathcal{BT}(B^+\to\bar{D}_1^0/\bar{D}_2^{*0}\ell^+\nu)} = 0.77 \pm 0.19$
- $f_{D_1'D^*\pi T/D_1D_2^*T} \equiv \frac{\mathcal{BT}(B^+\to\bar{D}_1^{*0}/(D^*\pi)^0\ell^+\nu)}{\mathcal{BT}(B^+\to\bar{D}_1^0/\bar{D}_2^{*0}\ell^+\nu)} = 0.98 \pm 0.24$

item	ρ_D^2	ρ^2	R_1	R_2	f_{+0}
$R_1(w)$ and $R_2(w)$	0.11	1.42	-1.38	3.18	0.12
D^{**} slope	-0.58	-2.77	1.67	-1.54	-0.56
D^{**} B$_2$	-0.62	1.21	1.15	-0.19	0.09
FF total	**0.85**	**3.34**	**2.45**	**3.54**	**0.58**
$f_{D_2^*/D_1}$	-0.02	0.03	0.09	0.10	0.26
$f_{D_0^* D\pi/D_1 D_2^*}$	-0.37	0.86	2.15	-1.49	0.77
$f_{D_1^* D^*\pi/D_1 D_2^*}$	0.16	-0.53	-1.56	0.12	-0.75
$f_{D\pi/D_0^*}$	-0.60	0.25	2.32	-4.21	-0.61
$f_{D^*\pi/D_1^*}$	-0.02	0.00	0.56	-0.70	0.04
BF ratios total	**0.72**	**1.04**	**3.58**	**4.53**	**1.26**
$f_{D_2^*}$	-0.12	0.13	0.17	-0.34	0.31
D^{*+} BF	0.49	-0.37	-0.39	0.73	-0.83
D^0 BF	-0.32	0.33	0.39	-0.75	2.71
D^+ BF	0.24	-0.11	-0.16	0.30	-1.54
t_{+0}	-0.00	-0.03	-0.06	0.10	-0.82
Luminosity	0.05	0.07	0.06	-0.12	-0.01
Input parms total	**0.64**	**0.53**	**0.61**	**1.15**	**3.34**
Bkg BF total	**2.58**	**1.34**	**2.51**	**4.37**	**1.27**
Lepton PID	-0.45	-0.26	4.02	0.86	0.32
Kaon PID	0.01	0.91	0.41	-0.91	-0.31
Tracking eff.	-0.05	0.37	0.26	-0.52	1.14
PHOTOS	not yet	not yet	not yet	not yet	not yet
Corrections total	**0.46**	**1.01**	**4.05**	**1.35**	**1.23**
$D^{(*)}\pi\pi\ell\nu$	**1.12**	**1.50**	**0.99**	**5.37**	**1.76**
Grand total	**3.12**	**4.20**	**6.55**	**9.16**	**4.40**

Table 83: **(Run2 only)** [**Systematics : FF parms**] Systematic uncertainties on form factor parameters. Numbers are given in %. Numbers are negative when fitted value decrease as input parameter increase.

item	$\mathcal{B}(B \to D\ell\nu)$	$\mathcal{B}(B \to D^*\ell\nu)$	$\mathcal{B}(B \to D^{**}/D^{(*)}\pi\ell\nu)$
$R_1(w)$ and $R_2(w)$	0.16	-1.54	0.05
D^{**} slope	0.04	0.33	-3.69
D^{**} B_2	0.07	-0.12	1.09
FF total	**0.17**	**1.58**	**3.84**
$f_{D_2^*/D_1}$	-0.20	-0.07	0.38
$f_{D_0^* D\pi/D_1 D_2^*}$	-0.19	-0.34	3.47
$f_{D_1^* D^*\pi/D_1 D_2^*}$	0.35	0.27	-3.37
$f_{D\pi/D_0^*}$	0.62	0.07	1.67
$f_{D^*\pi/D_1^*}$	-0.08	0.11	1.32
BF ratios total	**0.77**	**0.46**	**5.30**
$f_{D_2^*}$	-0.08	-0.01	0.41
D^{*+} BF	0.22	-0.17	0.05
D^0 BF	-1.28	-0.28	-0.43
D^+ BF	-0.54	-1.10	-0.97
t_{+0}	0.39	0.40	0.43
Luminosity	-1.12	-1.12	-1.08
Input parms total	**1.85**	**1.65**	**1.63**
Bkg BF total	**0.93**	**0.42**	**1.49**
Lepton PID	-3.17	-3.91	-1.99
Kaon PID	-0.08	0.18	-0.31
Tracking eff.	-1.85	-1.50	-1.62
PHOTOS	not yet	not yet	not yet
Corrections total	**3.67**	**4.19**	**2.59**
$D^{(*)}\pi\pi\ell\nu$	**0.55**	**2.69**	**13.63**
Grand total	**4.33**	**5.52**	**15.50**

Table 84: **(Run2 only)** [**Systematics : BF**] Systematic uncertainties on branching fractions. Numbers are given in %. Numbers are negative when fitted value decrease as input parameter increase.

item	$\mathcal{G}(1)V_{cb}$	$\mathcal{F}(1)V_{cb}$
$R_1(w)$ and $R_2(w)$	0.15	0.34
D^{**} slope	-0.36	-1.22
D^{**} B$_2$	-0.36	0.29
FF total	**0.53**	**1.30**
$f_{D_2^*/D_1}$	-0.11	-0.02
$f_{D_0^* D\pi/D_1 D_2^*}$	-0.33	-0.22
$f_{D_1^* D^*\pi/D_1 D_2^*}$	0.27	0.06
$f_{D\pi/D_0^*}$	-0.07	-0.68
$f_{D^*\pi/D_1^*}$	-0.06	-0.09
BF ratios total	**0.45**	**0.72**
$f_{D_2^*}$	-0.11	-0.02
D^{*+} BF	0.42	-0.09
D^0 BF	-0.84	-0.15
D^+ BF	-0.13	-0.53
t_{+0}	0.19	0.21
Luminosity	-0.53	-0.56
Input parms total	**1.11**	**0.82**
Bkg BF total	**2.00**	**0.46**
Lepton PID	-1.88	-2.22
Kaon PID	-0.03	0.27
Tracking eff.	-0.96	-0.71
PHOTOS	not yet	not yet
Corrections total	**2.11**	**2.34**
$D^{(*)}\pi\pi\ell\nu$	**0.98**	**1.05**
Grand total	**3.34**	**3.11**

Table 85: **(Run2 only)** [**Systematics : $\mathcal{G}(1)V_{cb}$ and $\mathcal{F}(1)V_{cb}$**] Systematic uncertainties on $\mathcal{G}(1)V_{cb}$ and $\mathcal{F}(1)V_{cb}$. Numbers are given in %. Numbers are negative when fitted value decrease as input parameter increase.

- $f_{D\pi/D_0^*} \equiv \frac{\mathcal{B}(B^+\to D^-\pi^+\ell^+\nu)}{\mathcal{B}(B^+\to \bar{D}_0^{*0}\ell^+\nu)} = 0.42 \pm 0.28$
- $f_{D^*\pi/D_1'} \equiv \frac{\mathcal{B}(B^+\to D^{*-}\pi^+\ell^+\nu)}{\mathcal{B}(B^+\to \bar{D}_1^{*0}\ell^+\nu)} = 0.071 \pm 0.050$

We change these ratios to $\pm$ one standard deviation and take larger deviation as systematic uncertainties.

21.2.2 Non-resonant $B \to D^{(*)}\pi\ell\nu$ decay BF

Non-resonant $B \to D^{(*)}\pi\ell\nu$ decays are not well modeled. We estimate systematic uncertainties due to this component by the following two mehods :

- We set $\mathcal{B}(B^+ \to D^{*-}\pi^+\ell^+\nu) = \mathcal{B}(B^+ \to D^-\pi^+\ell^+\nu) = 0$
- We change the ratio

$$f_{D^*\pi/D\pi} \equiv \frac{\mathcal{B}(B^+ \to D^{*-}\pi^+\ell^+\nu)}{\mathcal{B}(B^+ \to D^-\pi^+\ell^+\nu)} \tag{391}$$

We add the two uncertainties by quadrature.

21.3 Input parameters

21.3.1 D_2^* decay branching fractions

As described in section 9.2, we have one parameter,

- $f_{D_2^*} = 2.1 \pm 0.644$

to calculate D_2^* decay branching fractions. We change $f_{D_2^*}$ to $\pm$ one standard deviation and take larger deviation as systematic uncertainties.

21.3.2 $D^{(*)}$ decay branching fractions

The $D^{(*)}$ decay branching fractions

- $\mathcal{B}(D^{*+} \to D^0\pi^+) = 0.677 \pm 0.005$
- $\mathcal{B}(D^0 \to K^-\pi^+) = 0.03912 \pm 0.00048$
- $\mathcal{B}(D^+ \to K^-\pi^+\pi^+) = 0.0915 \pm 0.0020$

are also input parameters of our fitting. We change these BFs to $\pm$ one standard deviation and take larger deviation as systematic uncertainties.

21.3.3 t_{+0}

Another input parameter of our fitting is lifetime ratio

- $t_{+0} \equiv \frac{\tau_{B^+}}{\tau_{B^0}} = 1.071 \pm 0.009$

We change t_{+0} to $\pm$ one standard deviation and take larger deviation as systematic uncertainties.

21.3.4 f_{+0}

Another input parameter of our fitting is lifetime ratio

- $f_{+0} \equiv \frac{f_{+-}}{f_{00}} = 1.037 \pm 0.029$

We change f_{+0} to $\pm$ one standard deviation and take larger deviation as systematic uncertainties.

21.3.5 Luminosity normalization

For $B\bar{B}$ MC

- There is 1.1 % uncertainty (statistical + systematic) on B counting.

For OffPeak data

- There is 0.25 % uncertainty.

Thus we change luminosity normalization factors by one standard deviation and take larger deviation as systematic uncertainties. .

21.4 Background BF re-weighting

As describe in section 9, we re-weight branching fractions of background components. We change those BF to $\pm$ one standard deviation and take larger deviation as systematic uncertainties. We use different method for inclusive $B \to D$ decays as explained in the following subsection.

21.4.1 D momentum dependent inclusive $B(B_s) \to D$ BF re-weighting

As described in section 9.1.4, we fit for D (D_s) momentum dependent weight by 4-th (3-rd) order polynomial, and we use the fitted function to re-weight MC. To estimate the systematic uncertainty due to the uncertainty on weights, we do the following procedure :

1. We deviate each weight using Gaussian random numbers.
2. We fit the distribution of weight vs. D momentum using 3rd order polynomial.
3. We re-weight MC by the fitted functions to create 3D histograms.
4. Using the histograms, we perform fitting.
5. We iterate the above 1 to 4 400 times.
6. We make distributions of the deviations from the 400 fit results.
7. We take the standard deviation of each distribution as a systematic uncertainty.

To estimate the systematic uncertainty due to fit function, we do the following

- Use 7-th (4-th) order polynomial for D (D_s) momentum dependent weight fitting.
- Use binned correction without fitting.

and add uncertainties by quadrature.

21.5 Various corrections

21.5.1 Lepton PID correction

We cam evaluate systematic uncertainty as follows :

- Effect on the shape of histograms
  We can evaluate this by fitting without PID correction.
- Overall scale
  We can take appropriate numbers from previous analysis. Then we multiply PID correction factors by the number and perform fitting.

We take

- 2 % for electron? [reference]?
- 4 % for muon? [reference]?

21.5.2 Kaon PID correction

For the D^0 channel the BToDlnu skim does not require Kaon PID. We can therefore check the PID efficiency, independently data and MC, by making the following ratio

$$r = \frac{\text{Number of } D^0 \text{ with } K \text{ PID}}{\text{Number of } D^0 \text{ without } K \text{ PID}} \tag{392}$$

We can calculate r_{data} and r_{MC} in bins of kaon momentum and $\cos\theta$. By conparing the ratio

$$f = \frac{r_{data}}{r_{MC}} \tag{393}$$

with kaon PID correction factors, we can validate kaon PID correction and we can also get a meaningful way of assigning an uncertainty to the PID corrections.

21.5.3 Tracking efficiency correction

We compare the fit results with and without tracking efficiency correction.

item	ρ_D^2	ρ^2	R_1	R_2	f_{+0}
$D^0 \to K^{*-}\ell\nu$	0.04	-0.01	0.00	-0.04	-0.02
$D^0 \to K^-\ell\nu$	-0.04	0.01	0.01	-0.05	-0.03
$D^0 \to \pi^-\ell\nu$	-0.03	0.01	-0.00	-0.01	-0.02
$D^0 \to \rho^-\ell\nu$	0.03	0.01	-0.00	-0.02	-0.02
$D^+ \to K^{*0}\ell\nu$	0.03	-0.01	-0.00	-0.02	0.03
$D^+ \to K^0\ell\nu$	-0.04	-0.05	-0.06	0.07	-0.02
$D^+ \to \pi^0\ell\nu$	-0.03	0.00	-0.01	-0.02	-0.02
$D^+ \to \rho^0\ell\nu$	-0.03	0.01	0.00	-0.01	0.02
$D^+ \to \omega\ell\nu$	0.03	0.01	-0.00	-0.01	0.02
$D_s^+ \to \phi\ell\nu$	-0.09	0.02	-0.04	0.05	0.03
$D_s^+ \to \eta\ell\nu$	-0.05	-0.14	-0.15	0.56	0.03
$D_s^+ \to \eta'\ell\nu$	-0.04	-0.03	0.01	0.02	-0.03
$B^+ \to \bar{D}^0\tau^+\nu$	0.03	-0.05	0.09	0.40	0.03
$B^+ \to \bar{D}^{*0}\tau^+\nu$	-0.04	0.09	0.13	-0.39	-0.03
$B^0 \to D^-\tau^+\nu$	-0.03	-0.00	-0.00	-0.01	-0.02
$B^0 \to D^{*-}\tau^+\nu$	-0.03	-0.00	-0.00	-0.01	-0.02
$B^+ \to \bar{X}^0\ell^+\nu$	-0.04	0.02	0.08	-0.12	0.02
$B^0 \to X^-\ell^+\nu$	-0.04	-0.06	-0.12	0.23	-0.03
$B^- \to D_s^+$	-0.03	0.01	-0.00	-0.01	0.02
$B^+ \to D_s^+$	0.03	0.01	-0.00	-0.02	0.02
$\bar{B}^0 \to D_s^+$	0.03	0.01	-0.00	-0.03	0.02
$B^0 \to D_s^+$	0.04	0.01	0.00	-0.02	-0.02
Sub total	**0.19**	**0.20**	**0.27**	**0.84**	**0.11**
$B \to D$	2.58	1.32	2.49	4.28	1.27
Grand total	**2.58**	**1.34**	**2.51**	**4.37**	**1.27**

Table 86: **(Run2 only)** [**Bkg BF Systematics : FF parms**] Systematic uncertainties on form factor parameters. Numbers are given in %. Numbers are negative when fitted value decrease as input parameter increase.

item	$\mathcal{B}(B \to D\ell\nu)$	$\mathcal{B}(B \to D^*\ell\nu)$	$\mathcal{B}(B \to D^{**}/D^{(*)}\pi\ell\nu)$
$D^0 \to K^{*-}\ell\nu$	0.02	-0.00	0.06
$D^0 \to K^-\ell\nu$	-0.03	0.00	0.07
$D^0 \to \pi^-\ell\nu$	-0.02	0.00	0.03
$D^0 \to \rho^-\ell\nu$	-0.02	0.00	0.03
$D^+ \to K^{*0}\ell\nu$	-0.02	-0.00	0.05
$D^+ \to K^0\ell\nu$	-0.04	0.00	0.14
$D^+ \to \pi^0\ell\nu$	-0.02	0.00	0.03
$D^+ \to \rho^0\ell\nu$	-0.02	-0.00	0.03
$D^+ \to \omega\ell\nu$	0.02	-0.00	0.03
$D_s^+ \to \phi\ell\nu$	-0.04	-0.01	-0.02
$D_s^+ \to \eta\ell\nu$	0.06	-0.05	0.09
$D_s^+ \to \eta'\ell\nu$	0.02	-0.02	0.16
$B^+ \to \bar{D}^0\tau^+\nu$	0.10	-0.08	-0.18
$B^+ \to \bar{D}^{*0}\tau^+\nu$	0.02	0.09	-0.45
$B^0 \to D^-\tau^+\nu$	-0.02	-0.00	-0.02
$B^0 \to D^{*-}\tau^+\nu$	-0.02	-0.00	-0.02
$B^+ \to \bar{X}^0\ell^+\nu$	0.02	-0.02	0.06
$B^0 \to X^-\ell^+\nu$	-0.05	0.02	0.08
$B^- \to D_s^+$	0.02	0.00	0.03
$B^+ \to D_s^+$	0.02	0.00	0.02
$\bar{B}^0 \to D_s^+$	0.02	0.00	0.04
$B^0 \to D_s^+$	0.03	0.00	-0.02
Sub total	**0.16**	**0.14**	**0.57**
$B \to D$	0.92	0.39	1.38
Grand total	**0.93**	**0.42**	**1.49**

Table 87: **(Run2 only)** [**Bkg BF Systematics : BF**] Systematic uncertainties on branching fractions. Numbers are given in %. Numbers are negative when fitted value decrease as input parameter increase.

item	$\mathcal{G}(1)V_{cb}$	$\mathcal{F}(1)V_{cb}$
$D^0 \to K^{*-}\ell\nu$	0.04	-0.01
$D^0 \to K^-\ell\nu$	-0.04	-0.00
$D^0 \to \pi^-\ell\nu$	-0.03	0.00
$D^0 \to \rho^-\ell\nu$	0.03	-0.00
$D^+ \to K^{*0}\ell\nu$	0.03	-0.00
$D^+ \to K^0\ell\nu$	-0.05	-0.00
$D^+ \to \pi^0\ell\nu$	-0.03	0.00
$D^+ \to \rho^0\ell\nu$	-0.03	0.00
$D^+ \to \omega\ell\nu$	0.03	-0.00
$D_s^+ \to \phi\ell\nu$	-0.08	0.01
$D_s^+ \to \eta\ell\nu$	0.03	0.02
$D_s^+ \to \eta'\ell\nu$	-0.04	-0.02
$B^+ \to \bar{D}^0\tau^+\nu$	0.07	-0.00
$B^+ \to \bar{D}^{*0}\tau^+\nu$	-0.04	0.01
$B^0 \to D^-\tau^+\nu$	-0.03	-0.00
$B^0 \to D^{*-}\tau^+\nu$	-0.03	-0.00
$B^+ \to \bar{X}^0\ell^+\nu$	-0.03	-0.03
$B^0 \to X^-\ell^+\nu$	-0.05	0.03
$B^- \to D_s^+$	-0.03	0.00
$B^+ \to D_s^+$	0.03	0.00
$\bar{B}^0 \to D_s^+$	0.03	0.00
$B^0 \to D_s^+$	0.04	0.00
Sub total	**0.19**	**0.05**
$B \to D$	1.99	0.46
Grand total	**2.00**	**0.46**

Table 88: **(Run2 only)** [**Bkg BF Systematics :** $\mathcal{G}(1)V_{cb}$ **and** $\mathcal{F}(1)V_{cb}$] Systematic uncertainties on $\mathcal{G}(1)V_{cb}$ and $\mathcal{F}(1)V_{cb}$. Numbers are given in %. Numbers are negative when fitted value decrease as input parameter increase.

21.5.4 Radiative corrections : PHOTOS

We study the effect of radiation correction in generator level by comparing MC generated with PHOTOS on and off and seeing how the fit results change. Since we do not have fully simulated MC with PHOTOS off, we need to consrruct efficiency matrices for D^0 and D^+ as explained below. Once we have the efficiency matrices, we can take the D^0 and D^+ 3D histograms from generator-level MC, multiply them by the efficiency matrices, and do fits with and without PHOTOS; we can take the difference between the fits as an estimate of the systematic uncertainty.
Now, we explain about the efficiency matrix. This is a 3D matrix which can be constructed by the following procedure

1. We generate full MC with PHOTOS on.
2. We produce 3D histograms using MC truth as we do in our analysis, but we do not apply any event selection cuts or corrections.
3. We devide the above histograms, bin by bin, by the corresponding histograms which we use for the nominal fitting. Normalization can be done by the genarated number of events.
4. Then, we get 3D efficiency matrices/histograms, one for each MC mode.

21.5.5 Bremssrtrahlung

Due to emission of bremsstrahlung photons, the electron loses energy when traveling through the detector material. Since the amount of detector material has uertainty, the effect due to Bremssrtrahlung also has uncertainty. This was studied in detail in [49]. We apply this method in our fitting.

21.6 D mass sideband

Change D mass sideband region ± 1 MeV.

21.7 Vertexing

The vertexing cut is described in the event selection section 6. Nonimal cuts are

$$\begin{aligned} P^D(\chi^2, dof) &> 0.001 \\ P^B(\chi^2, dof) &> 0.01 \end{aligned} \tag{394}$$

We change them to

$$\begin{aligned} P^D(\chi^2, dof) &> 0.0001 \\ P^B(\chi^2, dof) &> 0.0001 \end{aligned} \tag{395}$$

and take the deviation as systematic uncertainty.

21.8 Effect of $B \to D^{(*)}\pi\pi\ell\nu$ decays

21.8.1 Event generation

The generic $B\bar{B}$ samples do not contain decays of the type $B \to X_c\ell\nu$ where X_c is a charm system that produces a $D^{(*)}$ and two pions. These decays must be modeled separately using EVTGEN and their impact on the fitted parameters must be determined. To do this we proceed as follows.

- The X_c systems studied cover a range of spin states and decay mechanisms. They are listed in Table 89. The decay $B \to X_c\ell\nu$ is performed using the HQET matrix element, i.e. the X_c system is treated as a heavier D or D^* according to the spin. The mass and spin of the X_c state therefore determine the lepton momentum spectrum. The D momentum and the $\cos\theta_{D\ell}$ depend on the decay dynamics as well. The Xc states are decayed into D or D* (with equal branching fractions) and two pions according to phase space; the Xc* states are decayed the same way. The Yc and Yc* states, on the other hand, are decayed as two-body $D^{(*)}\rho$ states (the Yc(*) mass was chosen to be just above threshold for this decay). These various choices of spin, mass and decay mode serve as a reasonable sample of the potential $B \to D^{(*)}\pi\pi$ decay modes.

- Each sample is used in turn, with its yield fixed by the difference in branching fraction between the inclusive $b \to c\ell\nu$ branching fraction and the sum over the exclusive decays to $D\ell\nu$, $D^*\ell\nu$ and $D^{**}\ell\nu$. With this component fixed the fit is performed as usual, and differences with respect to the nominal fit are used to estimate systematic errors.

21.8.2 3D efficiency histogram

21.8.3 Estimation of systematic uncertainties

- Change X*/X and Y*/Y ratios

- Effect of $D_1 \to D\eta$ decays

name	mass	width	$\max_D m$	charge	spin
Xc0	2.61	0.3	0.3	0	0
anti-Xc0	2.61	0.3	0.3	0	0
Xc+	2.61	0.3	0.3	+1	0
Xc-	2.61	0.3	0.3	-1	0
Xc*0	2.61	0.3	0.3	0	1
anti-Xc*0	2.61	0.3	0.3	0	1
Xc*+	2.61	0.3	0.3	+1	1
Xc*-	2.61	0.3	0.3	-1	1
Yc0	2.87	0.1	0.1	0	0
anti-Yc0	2.87	0.1	0.1	0	0
Yc+	2.87	0.1	0.1	+1	0
Yc-	2.87	0.1	0.1	-1	0
Yc*0	2.87	0.1	0.1	0	1
anti-Yc*0	2.87	0.1	0.1	0	1
Yc*+	2.87	0.1	0.1	+1	1
Yc*-	2.87	0.1	0.1	-1	1

Table 89: [X_c **systems**] X_c systems studied for systematic study.

22 Full Covariance Matrix

We construct full covariance matrices to keep track of correlation. For statistical uncertainty, if the statistical uncertainty of the i-th parameter is Δ_i^{stat}, the ij element of a statistical error correlation matrix is given by

$$\mathrm{cov}_{ij}^{stat} = \Delta_i^{stat} \cdot \Delta_j^{stat} \tag{396}$$

When we estimate systematic uncertainty, we vary the value of a quantity (k-th source of systematic uncertainty) and take differences, Δ^{sys}, between fitted values and nominal values of parameters. For i-th parameter

$$\Delta_{ik}^{sys} = \text{(fitted value - nominal value) of } i\text{-th parameter} \tag{397}$$

Then, the ij element of a systematic error correlation matrix is given by

$$\mathrm{cov}_{ij}^{sys} = \sum_k \Delta_{ik}^{sys} \cdot \Delta_{jk}^{sys} \tag{398}$$

In cases where we do two fits (one with a + variation and the other with a - variation), we calculate the two covariances (one for each fit) and average them.
Total error is given by the sum of these two matrices : cov_{ij}^{stat} and cov_{ij}^{sys}

23 Discussions

23.1 $B \to D^*\ell\nu$ form factors

We compare our results with previous Babar measurements [41][46]. The [41] reconstruct the decays

- $B^0 \to D^{*-}\ell^+\nu$, $D^{*-} \to D^0\pi_s^-$

Thus,

- $D^{*-} \to D^-\pi^0$ and $D^{*-} \to D^-\gamma$

are not included. They also use the cuts

$$\begin{aligned} &p_T(\pi_s^-) > 50 \ \text{GeV} \\ &p_\ell^* > 1.2 \ \text{GeV} \end{aligned} \tag{399}$$

where p_ℓ^* is the lepton momentum in the CM frame ($\Upsilon(4S)$ rest frame). The results are

$$\begin{aligned} \rho^2 &= 1.179 \pm 0.048 \pm 0.028 \\ R_1 &= 1.417 \pm 0.061 \pm 0.044 \\ R_2 &= 0.836 \pm 0.037 \pm 0.022 \end{aligned} \tag{400}$$

The analysis in Ref.[46] use the decay mode

- $B^- \to D^{*0}\ell^-\bar{\nu}$, $D^{*0} \to D^0\pi_s^0$

Thus,

- $D^{*0} \to D^0\gamma$

is not included. They also apply the cuts

$$\begin{aligned} &E_\gamma(\text{from } \pi_s^0) > 30 \ \text{GeV} \\ &p_\ell^* > 1.2 \ \text{GeV} \end{aligned} \tag{401}$$

They use R_1 and R_2 from the above measurement. The result is

$$\rho^2 = 1.15 \pm 0.06 \pm 0.08 \tag{402}$$

Our results are

$$\begin{aligned} \rho^2 &= 1.303 \pm 0.047 \pm 0.057 \\ R_1 &= 1.417 \pm 0.066 \pm 0.108 \\ R_2 &= 0.722 \pm 0.058 \pm 0.064 \end{aligned} \tag{403}$$

Suppose all experiments are independent, normalized residuals (NR) compare to [41] are

$$\begin{aligned} NR_{\rho^2} &= +1.341 \\ NR_{R_1} &= 0 \\ NR_{R_2} &= -0.66 \end{aligned} \tag{404}$$

In [46] derivatives

$$\frac{\partial \rho^2}{\partial R_1} = 0.0303, \qquad \frac{\partial \rho^2}{\partial R_2} = -1.22 \tag{405}$$

are given. Thus, if [41] apply our R_2 result, they could have got

$$\rho^2 = 1.15 - 1.22 \times (0.772 - 0.836) = 1.228 \tag{406}$$

which agrees with our slope.
We requested the author of the paper [41] to perform a fit by fixing R_1 and R_2 to

$$\begin{aligned} R_1 &= 1.542 \\ R_2 &= 0.584 \end{aligned} \tag{407}$$

Then their slope came out to be

$$\rho^2 = 1.331 \pm 0.0033 \tag{408}$$

If we fix R_1 and R_2 to previous values, our fit results are the values shown in Table 90.

23.1.1 Soft pion reconstruction

We do not apply any cuts on soft pion since we do not explicitly reconstruct D^*. This is the biggest difference between other measurements and our method. Figure 167 shows the transverse momentum distribution of soft pion in our analysis. These plots are made using MC truth info. Three modes are plotted separately :

- $B^+ \to \bar{D}^{*0}\ell^+\nu$, $D^{*0} \to D^0\pi^0_s$
- $B^0 \to D^{*-}\ell^+\nu$, $D^{*+} \to D^0\pi^+_s$
- $B^0 \to D^{*-}\ell^+\nu$, $D^{*+} \to D^+\pi^0_s$

The lines with error bars are based on our nominal fit results and the green histograms are based on previous Babar FF parameters [41]. The bottom plot of each mode is the ratio ($p_T(\pi_s)$ of previous FF)/($p_T(\pi_s)$ of our FF). In our analysis, the transverse momentum is well populated under the cut of previous measurements.
The acceptance of soft pions in out analysis is larger and more uniform than previous measurements. Figure 168 shows the population of soft pion as a function of their transverse momentum and $\cos\theta$, where θ is the angle with respect to the beam axis. Soft pions are most populated in the low θ region where SVT and DCH does not cover.

Parameters	Fit results	Pull
ρ_D^2	1.399 ± 0.059	0.775
ρ^2	1.239 ± 0.036	-2.766
R_1	1.417 (Fixed)	n/a
R_2	0.836 (Fixed)	n/a
$\mathcal{B}(B^+ \to \bar{D}^0 \ell^+ \nu)$	0.02587 ± 0.00059	1.092
$\mathcal{B}(B^+ \to \bar{D}^{*0} \ell^+ \nu)$	0.04983 ± 0.00067	-2.568
$\mathcal{BT}(B^+ \to \bar{D}^{**0}/(D\pi)^0 \ell^+ \nu)$	0.02231 ± 0.00095	0.356
f_{+0}	1.119 ± 0.030	0.622
$C^{D^0}_{UncorDL}$	0.998 ± 0.048	0.039
$C^{D^0}_{UncorCL}$	0.833 ± 0.062	0.245
$C^{D^0}_{CascL}$	0.802 ± 0.091	0.046
$C^{D^+}_{UncorDL}$	1.089 ± 0.126	-0.079
$C^{D^+}_{UncorCL}$	0.818 ± 0.137	0.020
$C^{D^+}_{CascL}$	1.372 ± 0.225	0.093
χ^2/ndof (P-value)	248/215 (0.06)	

Table 90: **(Run2 only)** [R_1 **and** R_2 **fixed fit results**] Fit results with fixed R_1 and R_2. Pulls are calculated from the difference to nominal fit results.

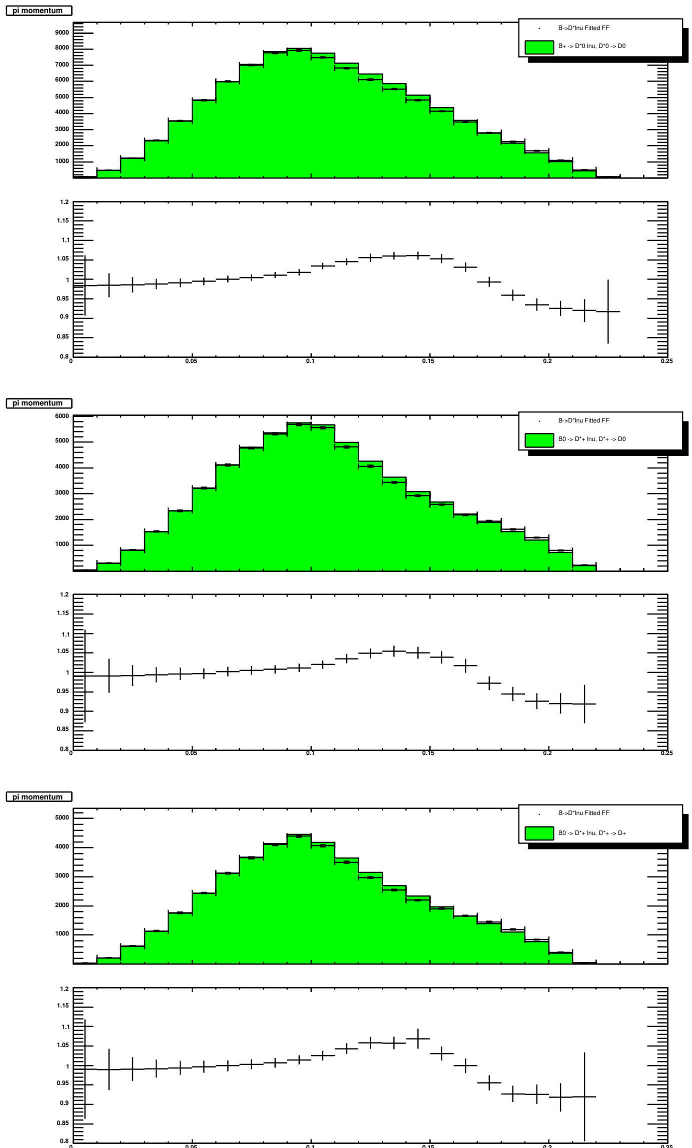

Figure 167: **(Run2 only)** [**Soft pi** p_T] The transverse momentum distribution of soft pion. From top to bottom : $B^+ \to \bar{D}^{*0}\ell^+\nu$ with $D^{*0} \to D^0\pi_s^0$, $B^0 \to D^{*-}\ell^+\nu$ with $D^{*+} \to D^0\pi_s^+$ and $B^0 \to D^{*-}\ell^+\nu$ with $D^{*+} \to D^+\pi_s^0$. The lines with error bars are based on our nominal fit results and the green histograms are based on previous Babar FF parameters [41]. The bottom plot of each mode is the ratio ($p_T(\pi_s)$ of our FF)/($p_T(\pi_s)$ of previous FF). These plots are made using MC truth info.

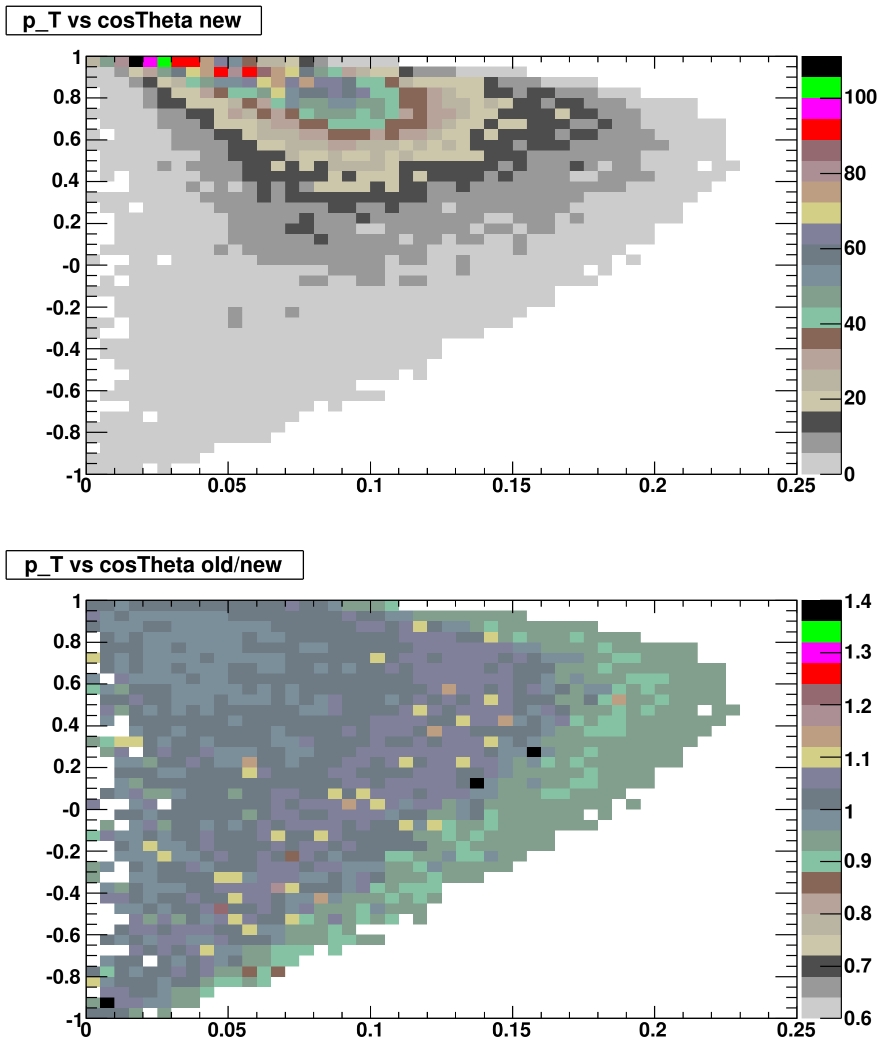

Figure 168: **(Run2 only)** [**Soft pi** p_T **vs** $\cos\theta$**;** $B^0 \to D^-$] The transverse momentum distribution vs $cos\theta$ of soft pion for the decay mode $B^0 \to D^{*-}\ell^+\nu$ with $D^{*+} \to D^+\pi_s^0$. The bottom plot is the ratio (based on our FF)/(based on previous FF). These plots are made using MC truth info.

23.2 Branching fractions

Babar recntly also measured [4]

$$\begin{aligned}
\mathcal{B}(B^+ \to \bar{D}^0\ell^+\nu) &= 0.0233 \pm 0.0009 \pm 0.0009 \\
\mathcal{B}(B^0 \to D^-\ell^+\nu) &= 0.0221 \pm 0.0011 \pm 0.0012 \\
\mathcal{B}(B^+ \to \bar{D}^{*0}\ell^+\nu) &= 0.0583 \pm 0.0015 \pm 0.0030 \\
\mathcal{B}(B^0 \to D^{*-}\ell^+\nu) &= 0.0549 \pm 0.0016 \pm 0.0025
\end{aligned} \tag{409}$$

If we take isospin average using $t_{+0} = 1.071 \pm 0.009$ and assuming these are independent, we get

$$\begin{aligned}
\mathcal{B}(B^+ \to \bar{D}^0\ell^+\nu) &= 0.0235 \pm 0.0010 \\
\mathcal{B}(B^+ \to \bar{D}^{*0}\ell^+\nu) &= 0.0585 \pm 0.0023
\end{aligned} \tag{410}$$

Our results are

$$\begin{aligned}
\mathcal{B}(D^{*+} \to D^0\pi^+) &= 0.0228 \pm 0.0003 \pm 0.0007 \\
\mathcal{B}(B^+ \to \bar{D}^{*0}\ell^+\nu) &= 0.0556 \pm 0.0007 \pm 0.0015
\end{aligned} \tag{411}$$

Thus, if we devide the above Babar results by our results, for $B^+ \to \bar{D}^0\ell^+\nu$, we get

$$1.03 \pm 0.19 \tag{412}$$

and, for $B^+ \to \bar{D}^{*0}\ell^+\nu$, we get

$$1.05 \pm 0.18 \tag{413}$$

Both $\mathcal{B}(B^+ \to \bar{D}^0\ell^+\nu)$ and $\mathcal{B}(B^+ \to \bar{D}^{*0}\ell^+\nu)$ agree well.

23.3 $B \to D^{(*)}\ell\nu$ isospin symmetry

We perform fitting by relaxing the isospin constraints on $B \to D\ell\nu$ and $B \to D^*\ell\nu$ decays. Fit results are shown in Table 91. We need to fix D^{*+} BF to get a reasonable fit results. Isospin symmetry does not hold for $B \to D^*\ell\nu$ decays. There are some couses we can think of such as

- Our fit result of D^{*+} BF is smaller than PDG value.
- There are missing signals such as $D\pi\pi\ell\nu$.

Thus we tried the similar fitting with by fixing D^{*+} BF to nominal fit value. The result is given in Table 92.

We tried the similar fitting with by fixing D^{*+} BF to nominal fit value. The result is given in Table 93.

Parameters	Fit results	Pull
ρ_D^2	1.354 ± 0.068	0.007
ρ^2	1.344 ± 0.078	0.076
R_1	1.453 ± 0.117	0.087
R_2	0.670 ± 0.102	-0.099
$\mathcal{B}(B^+ \to \bar{D}^0 \ell^+ \nu)$	0.0230 ± 0.0026	-0.849
$\mathcal{B}(B^0 \to D^- \ell^+ \nu)$	0.0264 ± 0.0040	0.699
$\mathcal{B}(B^+ \to \bar{D}^{*0} \ell^+ \nu)$	0.0474 ± 0.0046	-0.900
$\mathcal{B}(B^0 \to D^{*-} \ell^+ \nu)$	0.0532 ± 0.0068	0.739
$\mathcal{BT}(B^+ \to \bar{D}^{**0}/(D\pi)^0 \ell^+ \nu)$	0.0218 ± 0.0010	-0.161
f_{+0}	1.339 ± 0.320	0.747
$C_{UncorDL}^{D^0}$	1.012 ± 0.055	0.289
$C_{UncorCL}^{D^0}$	0.811 ± 0.062	-0.110
$C_{CascL}^{D^0}$	0.784 ± 0.092	-0.146
$C_{UncorDL}^{D^+}$	1.130 ± 0.141	0.223
$C_{UncorCL}^{D^+}$	0.906 ± 0.189	0.485
$C_{CascL}^{D^+}$	1.363 ± 0.241	0.052
χ^2/ndof (P-value)	236/215 (0.16)	

Table 91: **(Run2 only)** [**No isospin constraints**] Fit results without isospin constraints on $B \to D\ell\nu$ and $B \to D^*\ell\nu$, by floating f_{+0}. Pulls are calculated from the difference to nominal fit results.

Parameters	Fit results	Pull
ρ_D^2	1.385 ± 0.069 (5.1 %)	-0.073
ρ^2	1.338 ± 0.077 (5.7 %)	0.004
R_1	1.443 ± 0.114 (7.9 %)	-0.003
R_2	0.680 ± 0.099 (14.5 %)	0.004
$\mathcal{B}(B^+ \to \bar{D}^0\ell^+\nu)$	0.02592 ± 0.00096 (3.7 %)	0.733
$\mathcal{B}(B^0 \to D^-\ell^+\nu)$	0.02275 ± 0.00079 (3.5 %)	-1.010
$\mathcal{B}(B^+ \to \bar{D}^{*0}\ell^+\nu)$	0.05252 ± 0.00184 (3.5 %)	0.526
$\mathcal{B}(B^0 \to D^{*-}\ell^+\nu)$	0.04746 ± 0.00242 (5.1 %)	-0.280
$\mathcal{BT}(B^+ \to \bar{D}^{**0}/(D\pi)^0\ell^+\nu)$	0.02197 ± 0.00097 (4.4 %)	0.003
f_{+0}	1.040 ± 0.029 (2.8 %)	-2.083
$C_{UncorDL}^{D^0}$	0.994 ± 0.051 (5.1 %)	0.054
$C_{UncorCL}^{D^0}$	0.821 ± 0.063 (7.7 %)	0.038
$C_{CascL}^{D^0}$	0.804 ± 0.093 (11.5 %)	0.061
$C_{UncorDL}^{D^+}$	1.080 ± 0.126 (11.6 %)	-0.144
$C_{UncorCL}^{D^+}$	0.798 ± 0.137 (17.1 %)	-0.123
$C_{CascL}^{D^+}$	1.338 ± 0.222 (16.6 %)	-0.060
χ^2/ndof (P-value)	237/215 (0.14)	

Table 92: **(Run2 only)** [**No isospin constraints, Gaussian constraint on** f_{+0}] Fit results without isospin constraints on $B \to D\ell\nu$ and $B \to D^*\ell\nu$, by floating f_{+0} with Gaussian constraint to PDG. Pulls are calculated from the difference to nominal fit results.

Parameters	Fit results	Pull
ρ_D^2	1.349 ± 0.069	-0.074
ρ^2	1.338 ± 0.077	0.003
R_1	1.443 ± 0.114	-0.004
R_2	0.680 ± 0.099	0.005
$\mathcal{B}(B^+ \to \bar{D}^0 \ell^+ \nu)$	0.02597 ± 0.00090	0.835
$\mathcal{B}(B^0 \to D^- \ell^+ \nu)$	0.02271 ± 0.00071	-1.183
$\mathcal{B}(B^+ \to \bar{D}^{*0} \ell^+ \nu)$	0.05260 ± 0.00173	0.602
$\mathcal{B}(B^0 \to D^{*-} \ell^+ \nu)$	0.04740 ± 0.00236	-0.315
$\mathcal{BT}(B^+ \to \bar{D}^{**0}/(D\pi)^0 \ell^+ \nu)$	0.02198 ± 0.00097	0.005
f_{+0}	1.037 (Fixed)	n/a
$C^{D^0}_{UncorDL}$	0.993 ± 0.051	-0.059
$C^{D^0}_{UncorCL}$	0.821 ± 0.063	0.040
$C^{D^0}_{CascL}$	0.804 ± 0.093	0.063
$C^{D^+}_{UncorDL}$	1.080 ± 0.125	-0.149
$C^{D^+}_{UncorCL}$	0.797 ± 0.136	-0.132
$C^{D^+}_{CascL}$	1.337 ± 0.222	-0.062
χ^2/ndof (P-value)	237/215 (0.14)	

Table 93: **(Run2 only)** [**No isospin constraints, Fix** f_{+0}] Fit results without isospin constraints on $B \to D\ell\nu$ and $B \to D^*\ell\nu$, by fixing f_{+0} to PDG. Pulls are calculated from the difference to nominal fit results.

24 Conclusion

We measured form factor parameters

$$\begin{aligned}
\rho_D^2 &= 1.354 \pm 0.066(\text{stat.}, 4.9\%) \pm 0.040(\text{syst.}, 2.92\%) \\
\rho^2 &= 1.338 \pm 0.076(\text{stat.}, 5.7\%) \pm 0.052(\text{syst.}, 3.92\%) \\
R_1 &= 1.443 \pm 0.123(\text{stat.}, 7.8\%) \pm 0.093(\text{syst.}, 6.47\%) \\
R_2 &= 0.680 \pm 0.099(\text{stat.}, 14.5\%) \pm 0.051(\text{syst.}, 7.43\%)
\end{aligned} \tag{414}$$

production ratio

$$f_{+0} = 1.100 \pm 0.031(\text{stat.}, 2.8\%) \pm 0.044(\text{syst.}, 4.03\%) \tag{415}$$

branching fractions

$$\begin{aligned}
&\mathcal{B}(D^{*+} \to D^0\pi^+) = 0.02522 \pm 0.00063(\text{stat.}, 2.4\%) \pm 0.00108(\text{syst.}, 4.29\%) \\
&\mathcal{B}(B^+ \to \bar{D}^{*0}\ell^+\nu) = 0.05156 \pm 0.00083(\text{stat.}, 1.6\%) \pm 0.00249(\text{syst.}, 4.82\%) \\
&\mathcal{BT}(B^+ \to \bar{D}^{**0}/(D\pi)^0\ell^+\nu) = 0.02197 \pm 0.00096(\text{stat.}, 4.4\%) \pm 0.00162(\text{syst.}, 7.38\%)
\end{aligned} \tag{416}$$

and

$$\begin{aligned}
\mathcal{G}(1)|V_{cb}| &= 0.04818 \pm 0.00185(\text{stat.}, 3.8\%) \pm 0.00154(\text{syst.}, 3.19\%) \\
\mathcal{F}(1)|V_{cb}| &= 0.03505 \pm 0.00049(\text{stat.}, 1.4\%) \pm 0.00103(\text{syst.}, 2.93\%)
\end{aligned} \tag{417}$$

re-normalized branching fractions

$$\begin{aligned}
&\tilde{\mathcal{B}}(D^{*+} \to D^0\pi^+) = 0.02757 \pm 0.00068(\text{stat.}, 2.5\%) \pm 0.00073(\text{syst.}, 2.63\%) \\
&\tilde{\mathcal{B}}(B^+ \to \bar{D}^{*0}\ell^+\nu) = 0.05637 \pm 0.00091(\text{stat.}, 1.7\%) \pm 0.00145(\text{syst.}, 2.57\%) \\
&\tilde{\mathcal{BT}}(B^+ \to \bar{D}^{**0}/(D\pi)^0\ell^+\nu) = 0.02402 \pm 0.00105(\text{stat.}, 4.4\%) \pm 0.00160(\text{syst.}, 6.66\%)
\end{aligned} \tag{418}$$

with re-normalized branching fractions

$$\begin{aligned}
\mathcal{G}(1)|V_{cb}| &= 0.05038 \pm 0.00193(\text{stat.}, 3.8\%) \pm 0.00125(\text{syst.}, 2.48\%) \\
\mathcal{F}(1)|V_{cb}| &= 0.03665 \pm 0.00051(\text{stat.}, 1.4\%) \pm 0.00072(\text{syst.}, 1.96\%)
\end{aligned} \tag{419}$$

Run2 only. These are not final!!

25 Acknowledgements

A Decay modes to consider

A.1 Semileptonic $B \to D^{(*,**)}\ell\nu$ decays

A.1.1 Semileptonic B^+ decays

There are three types of decay modes (Figure 169).

- $B^+ \to \bar{D}^{(*,**)0}\ell^+\nu_\ell$
- $B^+ \to \bar{D}^{(*)0}\pi^0\ell^+\nu_\ell$
- $B^+ \to D^{(*)-}\pi^+\ell^+\nu_\ell$

A.1.2 Semileptonic B^0 decays

There are three types of decay modes (Figure 170).

- $B^0 \to D^{(*,**)-}\ell^+\nu_\ell$
- $B^0 \to D^{(*)-}\pi^0\ell^+\nu_\ell$
- $B^0 \to \bar{D}^{(*)0}\pi^-\ell^+\nu_\ell$

A.2 D^* and D^{**} decays

A.2.1 $D^{*,**+}$ decays

There are three types of decay modes (Figure 171).

- $D^{*,**+} \to D^{(*)0}\pi^+$
- $D^{*,**+} \to D^{(*)+}\pi^0$
- $D^{*,**+} \to D^{(*)+}\gamma$

Note that $D^{**+} \to D^{*+}\gamma$ is an electromagnetic process. Thus, it is negligible compared to strong processes. In case of $D^{*+} \to D^{*+}\gamma$, because strong processes are suppressed by phase space, the EM process amplitude has comparable size to strong processes.

A.2.2 $D^{*,**0}$ decays

There are three types of decay modes (Figure 172).

- $D^{*,**0} \to D^{(*)+}\pi^-$
- $D^{*,**0} \to D^{(*)0}\pi^0$
- $D^{*,**0} \to D^{(*)0}\gamma$

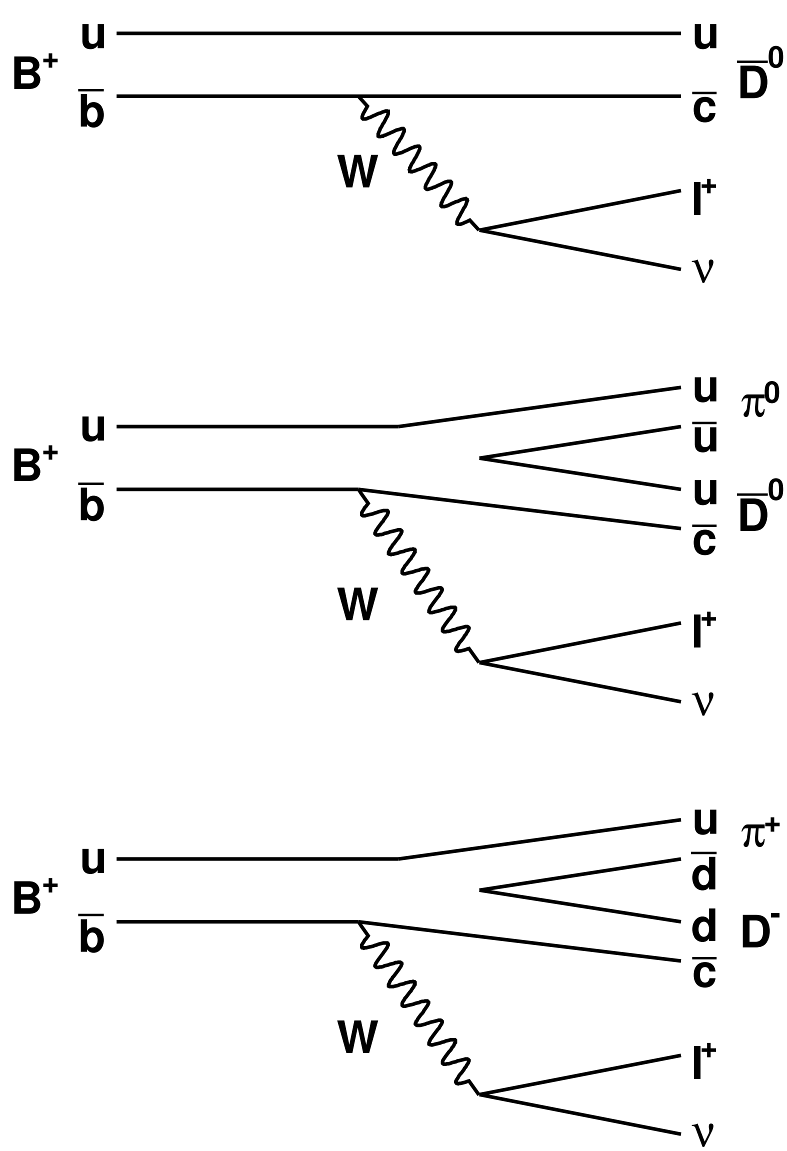

Figure 169: Feynman diagrams of semileptonic $B^+ \to D^{(*,**)}\ell\nu$ decays

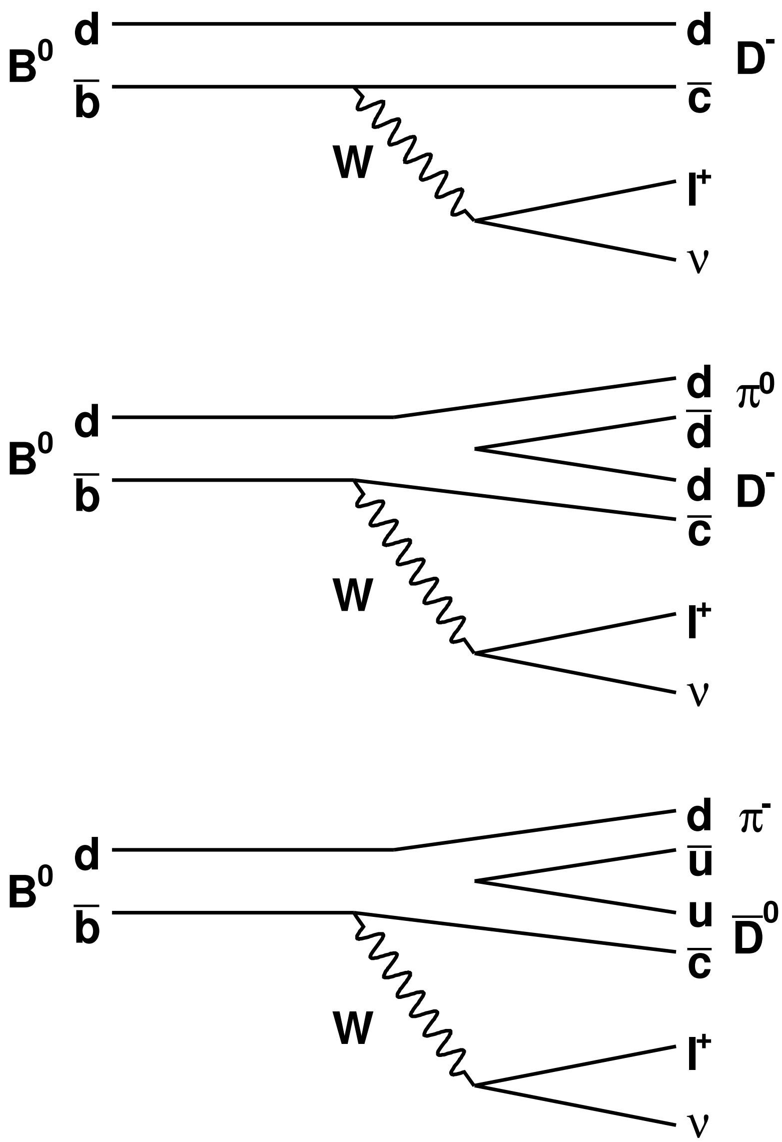

Figure 170: Feynman diagrams of semileptonic $B^0 \to D^{(*,**)}\ell\nu$ decays

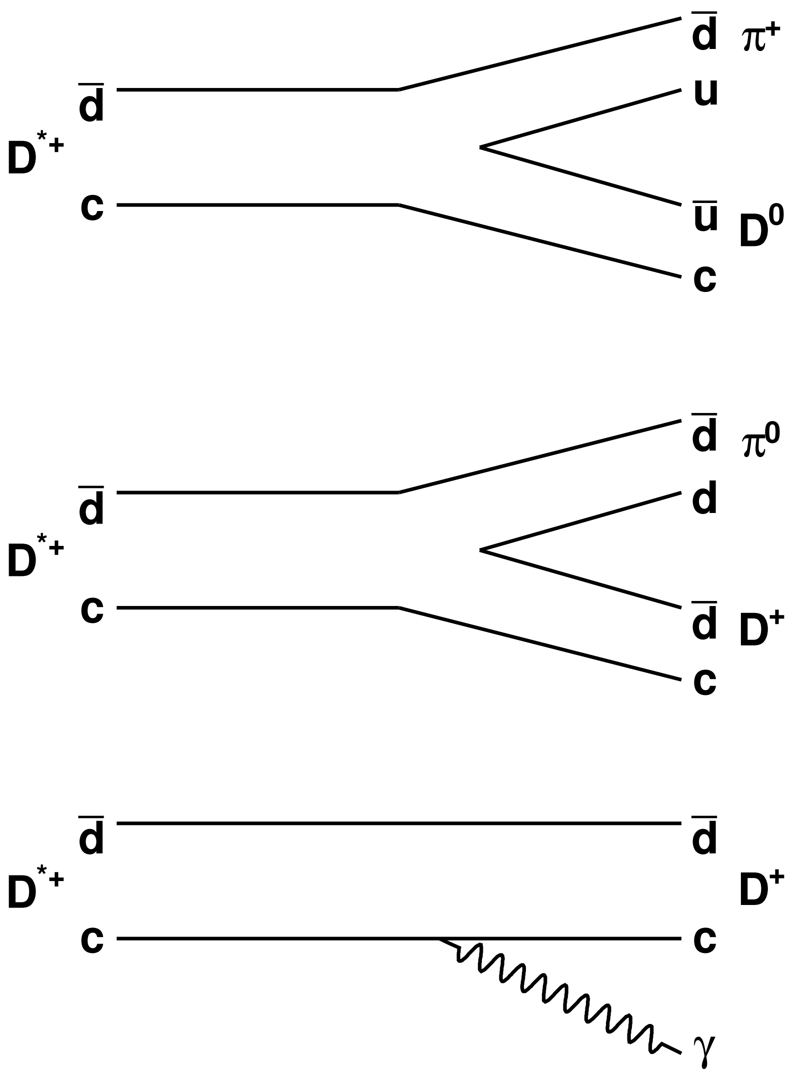

Figure 171: Feynman diagrams of $D^{*,**+}$ decays

Note that

- $D^{*0} \to D^+\pi^-$ is not allowed
  because $m_{D^{*0}} < m_{D^+} + m_{\pi^-}$
- $D^{**0} \to D^{*0}\gamma$ is negligible

A.3 D^0 and D^+ decays

A.3.1 D^0 decays

There are four decay modes used in the reconstruction of D^0 (Figure 173).

- $D^0 \to K^-\pi^+$
- $D^0 \to K^-\pi^+\pi^+\pi^-$
- $D^0 \to K^-\pi^+\pi^0$
- $D^0 \to K_s^0\pi^+\pi^-$

A.3.2 D^+ decays

There are two decay modes used in the reconstruction of D^+ (Figure 174).

- $D^+ \to K^-\pi^+\pi^+$
- $D^+ \to \bar{K}_s^0\pi^+$

A.3.3 π^0 and K_s^0

π^0 is reconstructed from 2γ.
K_s^0 is reconstructed from $\pi^0\pi^0$ or $\pi^+\pi^-$.

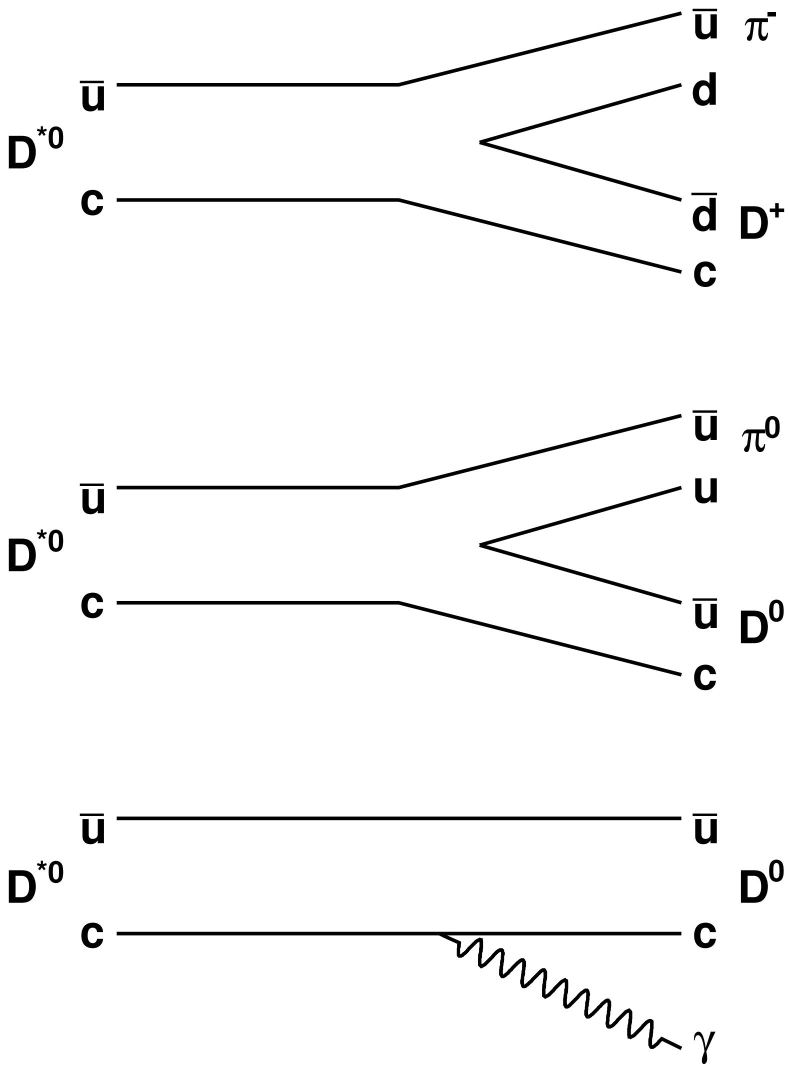

Figure 172: Feynman diagrams of $D^{*,**0}$ decays

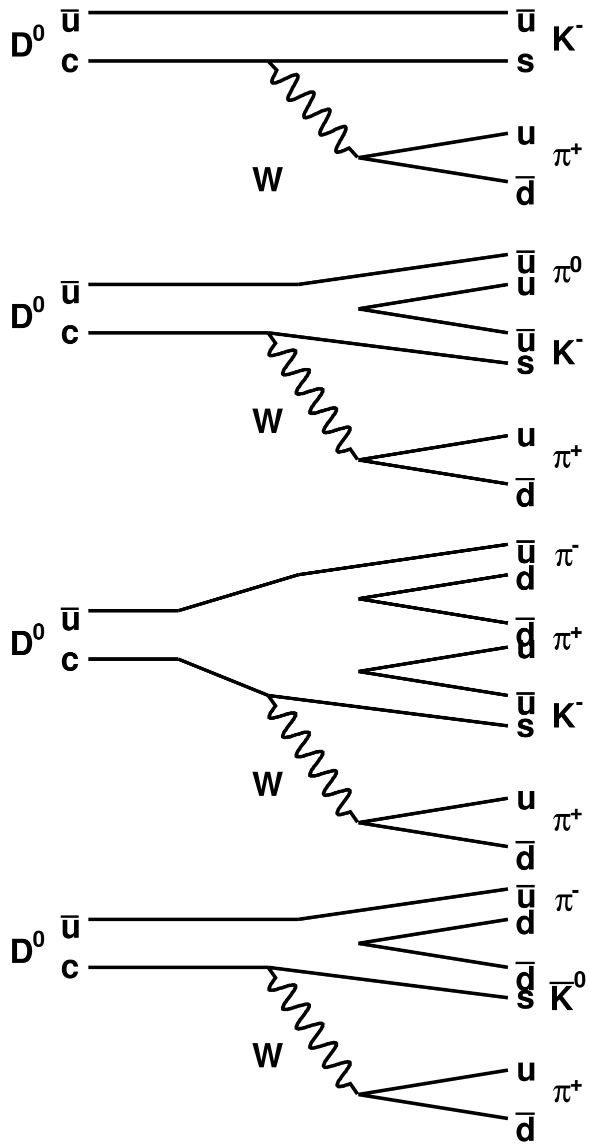

Figure 173: Feynman diagrams of D^0 decays

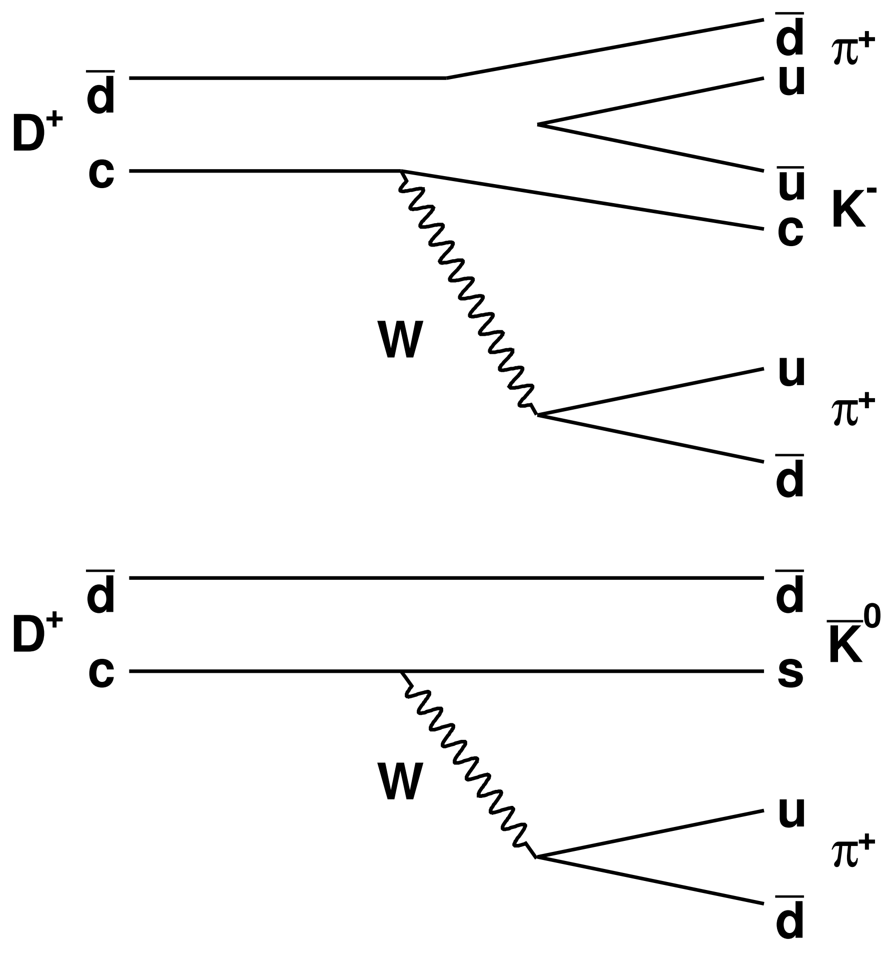

Figure 174: Feynman diagrams of D^+ decays

A.4 Decay chain

A.4.1 B^+ decay chain

1. $B^+ \to \bar{D}^0 \ell^+ \nu_\ell$ — (D^0)
2. $B^+ \to \bar{D}^{*0} \ell^+ \nu_\ell$
   - $\to D^- \pi^+$ — (not possible)
   - $\to \bar{D}^0 \pi^0$ — (D^0)
   - $\to \bar{D}^0 \gamma$ — (D^0)
3. $B^+ \to \bar{D}^{**0} \ell^+ \nu_\ell$
   - $\to D^- \pi^+$ — (D^+)
   - $\to \bar{D}^0 \pi^0$ — (D^0)
   - $\to \bar{D}^0 \gamma$ — (D^0)
   - $\to D^{*-} \pi^+$
     - $\to \bar{D}^0 \pi^-$ — (D^0)
     - $\to D^- \pi^0$ — (D^+)
     - $\to D^- \gamma$ — (D^+)
   - $\to \bar{D}^{*0} \pi^0$
     - $\to D^- \pi^+$ — (D^+)
     - $\to \bar{D}^0 \pi^0$ — (D^0)
     - $\to \bar{D}^0 \gamma$ — (D^0)
   - $\to \bar{D}^{*0} \gamma$ — (negligible)
4. $B^+ \to \bar{D}^0 \pi^0 \ell^+ \nu_\ell$ — (D^0)
5. $B^+ \to D^- \pi^+ \ell^+ \nu_\ell$ — (D^+)

6. $B^+ \to \bar{D}^{*0}\pi^0\ell^+\nu_\ell$
   - $\to D^-\pi^+$ (not possible)
   - $\to \bar{D}^0\pi^0$ (D^0)
   - $\to \bar{D}^0\gamma$ (D^0)
7. $B^+ \to D^{*-}\pi^+\ell^+\nu_\ell$
   - $\to \bar{D}^0\pi^-$ (D^0)
   - $\to D^-\pi^0$ (D^+)
   - $\to D^-\gamma$ (D^+)

A.4.2 B^0 decay chain

1. $B^0 \to D^-\ell^+\nu_\ell$ (D^0)
2. $B^0 \to D^{*-}\ell^+\nu_\ell$
   - $\to \bar{D}^0\pi^-$ (D^0)
   - $\to D^-\pi^0$ (D^+)
   - $\to D^-\gamma$ (D^+)

3. $B^0 \to D^{**-}\ell^+\nu_\ell$
   - $\to \bar{D}^0\pi^-$ (D^0)
   - $\to D^-\pi^0$ (D^+)
   - $\to D^-\gamma$ (D^+)
   - $\to D^{*-}\pi^0$
     - $\to \bar{D}^0\pi^-$ (D^0)
     - $\to D^-\pi^0$ (D^+)
     - $\to D^-\gamma$ (D^+)
   - $\to \bar{D}^{*0}\pi^-$
     - $\to D^-\pi^+$ (not possible)
     - $\to \bar{D}^0\pi^0$ (D^0)
     - $\to \bar{D}^0\gamma$ (D^0)
   - $\to \bar{D}^{*-}\gamma$ (negligible)
4. $B^0 \to D^-\pi^0\ell^+\nu_\ell$ (D^+)
5. $B^0 \to \bar{D}^0\pi^-\ell^+\nu_\ell$ (D^0)
6. $B^0 \to D^{*-}\pi^0\ell^+\nu_\ell$
   - $\to \bar{D}^0\pi^-$ (D^0)
   - $\to D^-\pi^0$ (D^+)
   - $\to D^-\gamma$ (D^+)
7. $B^0 \to \bar{D}^{*0}\pi^-\ell^+\nu_\ell$
   - $\to D^-\pi^+$ (not possible)
   - $\to \bar{D}^0\pi^0$ (D^0)
   - $\to \bar{D}^0\gamma$ (D^0)

B Classification of D^{**}

B.1 Angular momentum of a meson

In atomic spectroscopy, there are two useful schemes to add angular momentum: LS-coupling and jj-coupling.

- LS-coupling

$$\begin{aligned}\vec{S} &= \vec{s}_1 + \vec{s}_2 \\ \vec{J} &= \vec{L} + \vec{S}\end{aligned} \tag{420}$$

- jj-coupling

$$\begin{aligned}\vec{j}_1 &= \vec{L} + \vec{s}_1 \\ \vec{J} &= \vec{j}_1 + \vec{s}_2\end{aligned} \tag{421}$$

where s, l and j are the spin, orbital angular momentum and total angular momentum of individual particles, and S, L and J are the spin, orbital angular momentum and total angular momentum of the system.

B.2 Parity of a meson ($Q\bar{q}$-system) : $P = (-1)^{L+1}$

The parity of

- Quark [3] : $P_Q = +1$
- Anti-quark : $P_{\bar{q}} = -1$
- Orbital angular momentum L : $(-1)^L$

Thus, the parity of a $Q\bar{q}$-system is given by

$$P = (P_Q)(P_{\bar{q}})(-1)^L = (+1)(-1)(-1)^L = (-1)^{L+1} \tag{422}$$

Hence, $P = (-)$ for $L = 0$ and $P = (+)$ for $L = 1$.

B.3 Standard classification of mesons

For equal-mass meson system, it is traditional to couple the orbital angular momentum, $\vec{L}$, with the total spin of the quark and anti-quark, $\vec{S}$ (LS-coupling scheme).

$$\begin{aligned}\vec{S} &= \vec{s}_1 + \vec{s}_2 \\ \vec{J} &= \vec{L} + \vec{S}\end{aligned} \tag{423}$$

This is the standard practice for light mesons and heavy quarkonium ($c\bar{c}$ and $b\bar{b}$).
The good quantum numbers are then S, L and J.
There are spin-singlet and spin-triplet levels because S is always $S = 0$ or $S = 1$.

[3] One could define the parity of quark to be (-1). Then its of anti-quark is (+1). But, as far as P(quark) = - P(anti-quark), the final result won't change.

	Particle	J^P
$^1S_0$	D	0^-
$^3S_1$	D^*	1^-
$^1P_1$	D_1	1^+
$^3P_0$	D_0^*	0^+
$^3P_1$	D_1^*	1^+
$^3P_2$	D_2^*	2^+

Table 94: Traditional spectroscopic notation of D, D^* and D^{**} mesons.

- For $L = 0$ and $S = 0$, $J = 0$: $^1S_0$
- For $L = 0$ and $S = 1$, $J = 1$: $^3S_1$
- For $L = 1$ and $S = 0$, $J = 1$: $^1P_1$
- For $L = 1$ and $S = 1$, $J = 0, 1, 2$: $^3P_0$, $^3P_1$ or $^3P_2$

In general, for $S = 0$ and $S = 1$

$$^1L_L \quad \text{and} \quad ^3L_{L-1,L,L+1} \tag{424}$$

We may apply this classification to D, D^* and D^{**} mesons. It is summarized in Table 94. In this classification D^{**} consists of one singlet (D_1) and a triplet (D_0^*, D_1^* and D_2^*).

B.4 Heavy Quark Effective Theory (HQET) and D, D^* and D^{**} mesons

In HQET, the spin symmetry suggests that the spin of heavy quark is conserved. Thus, for the mesons consist of heavy and light quarks, we can apply jj coupling scheme. First, we can add the angular momentum (L) and the spin of the light quark (s_l) to get the angular momentum of light constituent (j_l). Then we can add the spin of the heavy quark (s_h) to j_l.

$$\begin{aligned} \vec{j}_l &= \vec{L} + \vec{s}_l \\ \vec{J} &= \vec{j}_l + \vec{s}_h \end{aligned} \tag{425}$$

For $L = 0$ and $s_l = 1/2$, $j_l = 1/2$ only, and for $L = 1$ and $s_l = 1/2$, $j_l = 1/2$ or $j_l = 3/2$. Hence,

- $L = 0$, $j_l = 1/2 \rightarrow J = 0$ (D) or 1 (D^*)
- $L = 1$, $j_l = 1/2 \rightarrow J = 0$ (D_0^*) or 1 (D_1')

j_l^P	Particles	J^P	mass (GeV)
$\frac{1}{2}^+$	$D,\ D^*$	$0^-,\ 1^-$	1.971
$\frac{1}{2}^+$	$D_0^*,\ D_1'$	$0^+,\ 1^+$	2.40
$\frac{3}{2}^+$	$D_1,\ D_2^*$	$1^+,\ 2^+$	2.445

Table 95: Spin parity of charmed meson doublets

Initial state	Final state	ΔL	description
D_0^*	$D\pi$	0	broad S-wave transition
	$D^*\pi$	1	parity violation
D_1'	$D\pi$	1	parity violation
	$D^*\pi$	0	broad S-wave transition
		2	heavy quark spin symmetry violation
D_1	$D\pi$	1	parity violation
	$D^*\pi$	0	heavy quark spin symmetry violation
		2	narrow D-wave transition
D_2^*	$D\pi$	2	narrow D-wave transition
	$D^*\pi$	2	narrow D-wave transition

Table 96: D^{**} decay modes.

- $L = 1,\ j_l = 3/2 \to J = 1\ (D_1)$ or $2\ (D_2^*)$

These are summarized in Table 95. In this classification, D^{**} consists of two doublets : $(D_0^*,\ D_1')$ and $(D_1,\ D_2^*)$.

B.5 Decay modes of D^{**}

The HQET based classification implies that the $j = 3/2$ states will decay only through the d-wave ($D_1 \to D^*$ and $D_2^* \to D$) and so will be narrow. The $j = 1/2$ states can decay through the s-wave ($D_0^* \to D$ and $D_1' \to D^*$) and, in general, will be broad. This is shown in Figure 175 and summarized in Table 96. We consider this in detail.

Spin-parity of $D\pi$ system is

- Since $D : S = 0, P = (-)$ and $\pi : S = 0, P = (-)$
- if $L = 0,\ J = 0$ and $P = (-)(-)(-)^0 = (+)$, then $J^P = 0^+$
- if $L = 1,\ J = 1$ and $P = (-)(-)(-)^1 = (-)$, then $J^P = 1^-$

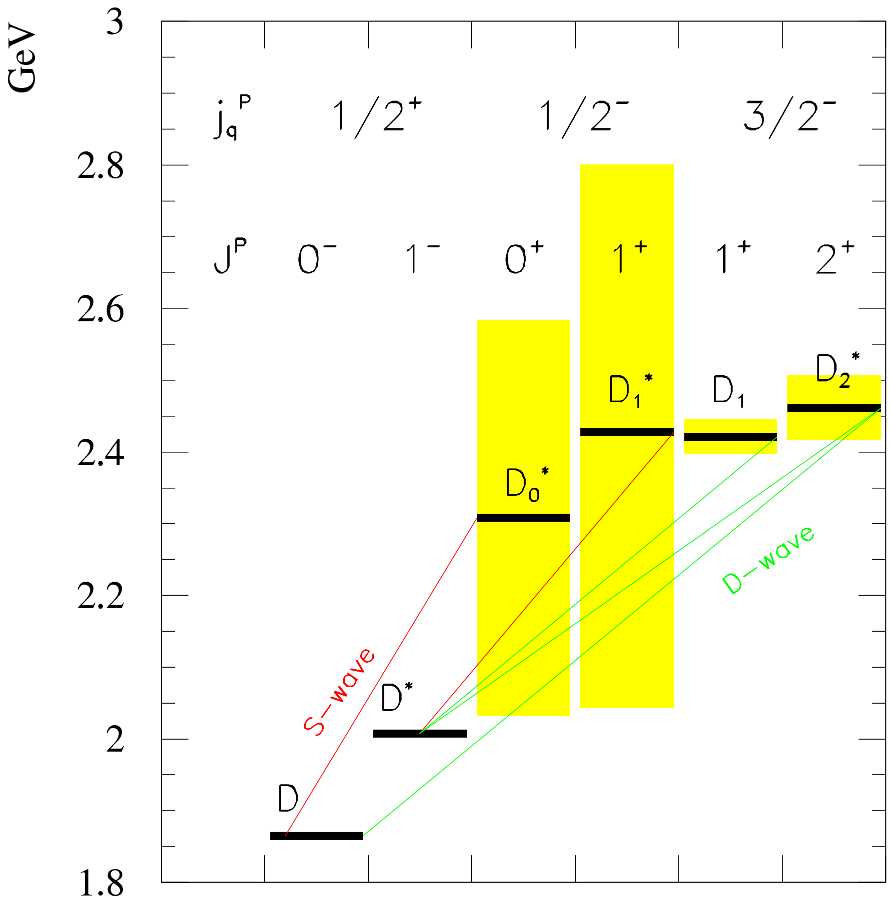

Figure 175: Charmed meson levels and transitions. $j_q = j_l$ in the text. The yellow bands show the width of each D^{**} state [15]

.

- if $L = 2,\ J = 2$ and $P = (-)(-)(-)^2 = (+)$, then $J^P = 2^+$

Note that $P = (-)^L$ for a orbital angular momentum L system. Spin-parity of $D^*\pi$ system is

- Since $D^* : S = 1, P = (-)$ and $\pi : S = 0, P = (-)$
- if $L = 0,\ J = 1$ and $P = (-)(-)(-)^0 = (+)$, then $J^P = 1^+$
- if $L = 1,\ J = 2, 1, 0$ and $P = (-)(-)(-)^1 = (-)$, then $J^P = 0^-, 1^-, 2^-$
- if $L = 2,\ J = 3, 2, 1$ and $P = (-)(-)(-)^2 = (+)$, then $J^P = 1^+, 2^+, 3^+$

Thus,

- $J^P = 0^+$ state (D_0^*) can decay only to $D\pi$ and $\Delta L = 0$
- $J^P = 1^+$ state (D_1 and D_1') can decay only to $D^*\pi$ and $\Delta L = 0, 2$
- $J^P = 2^+$ state (D_2^*) can decay both to $D\pi$ and to $D^*\pi$ and $\Delta L = 2$

Next, we consider angular momentum of D_1 and D_1' decays.

- $D_1(L = +1, s_l = +1/2, j_l = +3/2; s_h = -1/2, J = +1)$
  $\rightarrow D^*(s_l = +1/2, s_h = +1/2, j_D = +1) + \pi(j_\pi = 0) + (L = 0); J = +1$
  This violates heavy quark spin symmetry ($s_h = -1/2 \rightarrow s_h = +1/2$)
- $D_1(L = +1, s_l = +1/2, j_l = +3/2; s_h = -1/2, J = +1)$
  $\rightarrow D^*(s_l = -1/2, s_h = -1/2, j_D = -1) + \pi(j_\pi = 0) + (L = +2); J = +1$
  This conserves heavy quark spin symmetry ($s_h = -1/2 \rightarrow s_h = -1/2$)
- $D_1'(L = +1, s_l = -1/2, j_l = +1/2; s_h = +1/2, J = +1)$
  $\rightarrow D^*(s_l = +1/2, s_h = +1/2, j_D = +1) + \pi(j_\pi = 0) + (L = 0); J = +1$
  This conserves heavy quark spin symmetry ($s_h = +1/2 \rightarrow s_h = +1/2$)
- $D_1'(L = +1, s_l = -1/2, j_l = +1/2; s_h = +1/2, J = +1)$
  $\rightarrow D^*(s_l = -1/2, s_h = -1/2, j_D = -1) + \pi(j_\pi = 0) + (L = +2); J = +1$
  This violates heavy quark spin symmetry ($s_h = +1/2 \rightarrow s_h = -1/2$)

C Isospin Symmetry

C.1 Semileptonic B decays

From isospin symmetry, these B decay rates are identical

$$\begin{aligned}\Gamma(B^+ \to \bar{D}^0\ell^+\nu) &= \Gamma(B^0 \to D^-\ell^+\nu) \\ \Gamma(B^+ \to \bar{D}^{*0}\ell^+\nu) &= \Gamma(B^0 \to D^{*-}\ell^+\nu) \\ \Gamma(B^+ \to \bar{D}^{**0}\ell^+\nu) &= \Gamma(B^0 \to D^{**-}\ell^+\nu)\end{aligned} \tag{426}$$

Isospin symmetry may be applied to non-resonant $B \to D^{(*)}\pi\ell\nu$ decays.

$$\begin{aligned}\Gamma(B^+ \to D^-\pi^+\ell^+\nu) &= \Gamma(B^0 \to \bar{D}^0\pi^-\ell^+\nu) \\ \Gamma(B^+ \to D^{*-}\pi^+\ell^+\nu) &= \Gamma(B^0 \to \bar{D}^{*0}\pi^-\ell^+\nu)\end{aligned} \tag{427}$$

$$\begin{aligned}\Gamma(B^+ \to D^-\pi^+\ell^+\nu) &= 2\Gamma(B^+ \to \bar{D}^0\pi^0\ell^+\nu) \\ \Gamma(B^0 \to \bar{D}^0\pi^-\ell^+\nu) &= 2\Gamma(B^0 \to D^-\pi^0\ell^+\nu) \\ \Gamma(B^+ \to D^{*-}\pi^+\ell^+\nu) &= 2\Gamma(B^+ \to \bar{D}^{*0}\pi^0\ell^+\nu) \\ \Gamma(B^0 \to \bar{D}^{*0}\pi^-\ell^+\nu) &= 2\Gamma(B^0 \to D^{*-}\pi^0\ell^+\nu)\end{aligned} \tag{428}$$

The origin of the factor 2 is, for example,

$$\begin{aligned}&B^+(u\bar{b}) : |1/2, 1/2> \\ &D^-(d\bar{c}) : |1/2, -1/2> \\ &\pi^+(u\bar{d}) : |1, 1> \\ &D^-\pi^+ : |1, 1> \times |1/2, -1/2> = \sqrt{\tfrac{1}{3}}|3/2, 1/2> + \sqrt{\tfrac{2}{3}}|1/2, 1/2> \\ &\bar{D}^0(u\bar{c}) : |1/2, 1/2> \\ &\pi^0(u\bar{u} \text{ or } d\bar{d}) : |1, 0> \\ &\bar{D}^0\pi^0 : |1, 0> \times |1/2, 1/2> = \sqrt{\tfrac{2}{3}}|3/2, 1/2> - \sqrt{\tfrac{1}{3}}|1/2, 1/2>\end{aligned} \tag{429}$$

hence

$$\Gamma(B^+ \to D^-\pi^+\ell^+\nu) : \Gamma(B^+ \to \bar{D}^0\pi^0\ell^+\nu) = \frac{2}{3} : \frac{1}{3} = 2 : 1 \tag{430}$$

Branching fractions are not same because of the difference in total rate (Γ) or life time (τ) of B^+ and B^0. We define

$$t_{+0} \equiv \frac{\tau_{B^+}}{\tau_{B^0}} = \frac{\Gamma_{B^0}}{\Gamma_{B^+}} \tag{431}$$

and

$$t_{0+} \equiv \frac{\tau_{B^0}}{\tau_{B^+}} = \frac{\Gamma_{B^+}}{\Gamma_{B^0}} \tag{432}$$

So branching fractions are, for example,

$$\frac{\mathcal{B}(B^+ \to \bar{D}^{*0}\ell^+\nu)}{\mathcal{B}(B^0 \to D^{*-}\ell^+\nu)} = \frac{\Gamma(B^+ \to D^*\ell\nu)}{\Gamma(B^0 \to D^*\ell\nu)}\frac{\Gamma_{B^0}}{\Gamma_{B^+}} = t_{+0} \tag{433}$$

Thus, due to isospin symmetry, we have the following relations between branching fractions of semileptonic B decays.

$$\begin{aligned}
&\mathcal{B}(B^+ \to \bar{D}^0\ell^+\nu) = t_{+0}\mathcal{B}(B^0 \to D^-\ell^+\nu)\\
&\mathcal{B}(B^+ \to \bar{D}^{*0}\ell^+\nu) = t_{+0}\mathcal{B}(B^0 \to D^{*-}\ell^+\nu)\\
&\mathcal{B}(B^+ \to \bar{D}^{**0}\ell^+\nu) = t_{+0}\mathcal{B}(B^0 \to D^{**-}\ell^+\nu)\\
&\mathcal{B}(B^+ \to D^-\pi^+\ell^+\nu) = 2\mathcal{B}(B^+ \to \bar{D}^0\pi^0\ell^+\nu)\\
&= t_{+0}\mathcal{B}(B^0 \to \bar{D}^0\pi^-\ell^+\nu) = 2t_{+0}\mathcal{B}(B^0 \to D^-\pi^0\ell^+\nu)\\
&\mathcal{B}(B^+ \to D^{*-}\pi^+\ell^+\nu) = 2\mathcal{B}(B^+ \to \bar{D}^{*0}\pi^0\ell^+\nu)\\
&= t_{+0}\mathcal{B}(B^0 \to \bar{D}^{*0}\pi^-\ell^+\nu) = 2t_{+0}\mathcal{B}(B^0 \to D^{*-}\pi^0\ell^+\nu)
\end{aligned} \tag{434}$$

C.2 D^{**} decays

Isospin symmetry may be applied to D^{**} decays as well.

$$\begin{aligned}
\Gamma(D^{**0} \to D^+\pi^-) &= \Gamma(D^{**+} \to D^0\pi^+)\\
\Gamma(D^{**0} \to D^0\pi^0) &= \Gamma(D^{**+} \to D^+\pi^0)\\
\Gamma(D^{**0} \to D^{*+}\pi^-) &= \Gamma(D^{**+} \to D^{*0}\pi^+)\\
\Gamma(D^{**0} \to D^{*0}\pi^0) &= \Gamma(D^{**+} \to D^{*+}\pi^0)
\end{aligned} \tag{435}$$

And also

$$\begin{aligned}
\Gamma(D^{**0} \to D^+\pi^-) &= 2\Gamma(D^{**0} \to D^0\pi^0)\\
\Gamma(D^{**+} \to D^0\pi^+) &= 2\Gamma(D^{**+} \to D^+\pi^0)\\
\Gamma(D^{**0} \to D^{*+}\pi^-) &= 2\Gamma(D^{**0} \to D^{*0}\pi^0)\\
\Gamma(D^{**+} \to D^{*0}\pi^+) &= 2\Gamma(D^{**+} \to D^{*+}\pi^0)
\end{aligned} \tag{436}$$

This factor 2 has the same origin as B decay case. For example,

$$\begin{aligned}
&D^{**+} : |1/2, 1/2 >\\
&D^0 : |1/2, -1/2 >\\
&\pi^+ : |1, 1 >\\
&D^0\pi^+ : |1, 1 > \times|1/2, -1/2 >= \sqrt{\tfrac{1}{3}}|3/2, 1/2 > +\sqrt{\tfrac{2}{3}}|1/2, 1/2 >\\
&D^+ : |1/2, 1/2 >\\
&\pi^0 : |1, 0 >\\
&D^+\pi^0 : |1, 0 > \times|1/2, 1/2 >= \sqrt{\tfrac{2}{3}}|3/2, 1/2 > -\sqrt{\tfrac{1}{3}}|1/2, 1/2 >
\end{aligned} \tag{437}$$

hence

$$\Gamma(D^{**+} \to D^0\pi^+) : \Gamma(D^{**+} \to D^+\pi^0) = \frac{2}{3} : \frac{1}{3} = 2 : 1 \tag{438}$$

Supposing total rates or lifetimes of D^{**0} and D^{**+} are same, branching fractions for D^{**} decays are

$$\begin{aligned}
&\mathcal{B}(D^{**0} \to D^+\pi^-) = 2\mathcal{B}(D^{**0} \to D^0\pi^0) = \mathcal{B}(D^{**+} \to D^0\pi^+) = 2\mathcal{B}(D^{**+} \to D^+\pi^0) \\
&\mathcal{B}(D^{**0} \to D^{*+}\pi^-) = 2\mathcal{B}(D^{**0} \to D^{*0}\pi^0) = \mathcal{B}(D^{**+} \to D^{*0}\pi^+) = 2\mathcal{B}(D^{**+} \to D^{*+}\pi^0)
\end{aligned} \tag{439}$$

D Values used in SP5/SP6 MC and related to our fit

The values used in SP5/SP6 MC are given in Tables 97-104. Calculated and used values are given in relevant sections in the text.

D.1 Definition of total or summed branching fractions, and branching fraction ratios

In section 5, we define the following total or summed branching fractions.

1. $\mathcal{BT}(B^+ \to \bar{D}^{**0}\ell^+\nu)$
   $\equiv \mathcal{B}(B^+ \to \bar{D}_0^{*0}\ell^+\nu) + \mathcal{B}(B^+ \to \bar{D}_1^0\ell^+\nu) + \mathcal{B}(B^+ \to \bar{D}_1^{\prime 0}\ell^+\nu) + \mathcal{B}(B^+ \to \bar{D}_2^{*0}\ell^+\nu)$

2. $\mathcal{BT}(B^0 \to D^{**-}\ell^+\nu)$
   $\equiv \mathcal{B}(B^0 \to D_0^{*-}\ell^+\nu) + \mathcal{B}(B^0 \to D_1^-\ell^+\nu) + \mathcal{B}(B^0 \to D_1^{\prime -}\ell^+\nu) + \mathcal{B}(B^0 \to D_2^{*-}\ell^+\nu)$

3. $\mathcal{BT}(B^+ \to \bar{D}_1^0/\bar{D}_2^{*0}\ell^+\nu) \equiv \mathcal{B}(B^+ \to \bar{D}_1^0\ell^+\nu) + \mathcal{B}(B^+ \to \bar{D}_2^{*0}\ell^+\nu)$

4. $\mathcal{BT}(B^0 \to D_1^-/D_2^{*-}\ell^+\nu) \equiv \mathcal{B}(B^0 \to D_1^-\ell^+\nu) + \mathcal{B}(B^0 \to D_2^{*-}\ell^+\nu)$

5. $\mathcal{BT}(B^+ \to D^-\pi^+\ell^+\nu)$
   $\equiv \mathcal{B}(B^+ \to \bar{D}_2^{*0}\ell^+\nu)\mathcal{B}(\bar{D}_2^{*0} \to D^-\pi^+) + \mathcal{B}(B^+ \to \bar{D}_0^{*0}\ell^+\nu)\mathcal{B}(\bar{D}_0^{*0} \to D^-\pi^+)$
   $+\mathcal{B}(B^+ \to D^-\pi^+\ell^+\nu)$

6. $\mathcal{BT}(B^0 \to \bar{D}^0\pi^-\ell^+\nu)$
   $\equiv \mathcal{B}(B^0 \to D_2^{*-}\ell^+\nu)\mathcal{B}(D_2^{*-} \to \bar{D}^0\pi^-) + \mathcal{B}(B^0 \to D_0^{*-}\ell^+\nu)\mathcal{B}(D_0^{*-} \to \bar{D}^0\pi^-)$
   $+\mathcal{B}(B^0 \to \bar{D}^0\pi^-\ell^+\nu)$

7. $\mathcal{BT}(B^+ \to \bar{D}_0^{*0}/(D\pi)^0\ell^+\nu)$
   $\equiv \mathcal{B}(B^+ \to \bar{D}_0^{*0}\ell^+\nu) + \mathcal{B}(B^+ \to D^-\pi^+\ell^+\nu) + \mathcal{B}(B^+ \to \bar{D}^0\pi^0\ell^+\nu)$

8. $\mathcal{BT}(B^0 \to D_0^{*-}/(D\pi)^-\ell^+\nu)$
   $\equiv \mathcal{B}(B^0 \to D_0^{*-}\ell^+\nu) + \mathcal{B}(B^0 \to \bar{D}^0\pi^-\ell^+\nu) + \mathcal{B}(B^0 \to D^-\pi^0\ell^+\nu)$

9. $\mathcal{BT}(B^+ \to D^{*-}\pi^+\ell^+\nu)$
   $\equiv \mathcal{B}(B^+ \to \bar{D}_1^0\ell^+\nu)\mathcal{B}(\bar{D}_1^0 \to D^{*-}\pi^+) + \mathcal{B}(B^+ \to \bar{D}_2^{*0}\ell^+\nu)\mathcal{B}(\bar{D}_2^{*0} \to D^{*-}\pi^+)$
   $+\mathcal{B}(B^+ \to \bar{D}_1^{\prime 0}\ell^+\nu)\mathcal{B}(\bar{D}_1^{\prime 0} \to D^{*-}\pi^+) + \mathcal{B}(B^+ \to D^{*-}\pi^+\ell^+\nu)$

10. $\mathcal{BT}(B^0 \to \bar{D}^{*0}\pi^-\ell^+\nu)$
    $\equiv \mathcal{B}(B^0 \to D_1^-\ell^+\nu)\mathcal{B}(D_1^- \to \bar{D}^{*0}\pi^-) + \mathcal{B}(B^0 \to D_2^{*-}\ell^+\nu)\mathcal{B}(D_2^{*-} \to \bar{D}^{*0}\pi^-)$
    $+\mathcal{B}(B^0 \to D_1^{\prime -}\ell^+\nu)\mathcal{B}(D_1^{\prime -} \to \bar{D}^{*0}\pi^-) + \mathcal{B}(B^0 \to \bar{D}^{*0}\pi^-\ell^+\nu)$

11. $\mathcal{BT}(B^+ \to \bar{D}_1^{\prime 0}/(D^*\pi)^0\ell^+\nu)$
    $\equiv \mathcal{B}(B^+ \to \bar{D}_1^{\prime 0}\ell^+\nu) + \mathcal{B}(B^+ \to D^{*-}\pi^+\ell^+\nu) + \mathcal{B}(B^+ \to \bar{D}^{*0}\pi^0\ell^+\nu)$

12. $\mathcal{BT}(B^0 \to D_1^{\prime -}/(D^*\pi)^-\ell^+\nu)$
    $\equiv \mathcal{B}(B^0 \to D_1^{\prime -}\ell^+\nu) + \mathcal{B}(B^0 \to \bar{D}^{*0}\pi^-\ell^+\nu) + \mathcal{B}(B^0 \to D^{*-}\pi^0\ell^+\nu)$

13. $\mathcal{BT}(B^+ \to \bar{D}^{**0}/(D\pi)^0\ell^+\nu)$
$\equiv \mathcal{B}(B^+ \to \bar{D}_0^{*0}\ell^+\nu) + \mathcal{B}(B^+ \to \bar{D}_1^0\ell^+\nu) + \mathcal{B}(B^+ \to \bar{D}_1'^0\ell^+\nu) + \mathcal{B}(B^+ \to \bar{D}_2^{*0}\ell^+\nu)$
$+\mathcal{B}(B^+ \to D^-\pi^+\ell^+\nu) + \mathcal{B}(B^+ \to \bar{D}^0\pi^0\ell^+\nu)$
$+\mathcal{B}(B^+ \to D^{*-}\pi^+\ell^+\nu) + \mathcal{B}(B^+ \to \bar{D}^{*0}\pi^0\ell^+\nu)$

14. $\mathcal{BT}(B^0 \to D^{**-}/(D\pi)^-\ell^+\nu)$
$\equiv \mathcal{B}(B^0 \to D_0^{*-}\ell^+\nu) + \mathcal{B}(B^0 \to D_1^-\ell^+\nu) + \mathcal{B}(B^0 \to D_1'^-\ell^+\nu) + \mathcal{B}(B^0 \to D_2^{*-}\ell^+\nu)$
$+\mathcal{B}(B^0 \to \bar{D}^0\pi^-\ell^+\nu) + \mathcal{B}(B^0 \to D^-\pi^0\ell^+\nu)$
$+\mathcal{B}(B^0 \to \bar{D}^{*0}\pi^-\ell^+\nu) + \mathcal{B}(B^0 \to D^{*-}\pi^0\ell^+\nu)$

We also define the following branching fraction ratios :

1. $f_{D_2^*} \equiv \frac{\mathcal{B}(D_2^{*+} \to D^0\pi^+)}{\mathcal{B}(D_2^{*+} \to D^{*0}\pi^+)}$

2. $f_{D_2^*/D_1} \equiv \frac{\mathcal{B}(B^+ \to \bar{D}_2^{*0}\ell^+\nu)}{\mathcal{B}(B^+ \to \bar{D}_1^0\ell^+\nu)}$

3. $f_{D\pi/D_0^*} \equiv \frac{\mathcal{B}(B^+ \to D^-\pi^+\ell^+\nu)}{\mathcal{B}(B^+ \to \bar{D}_0^{*0}\ell^+\nu)}$

4. $f_{D^*\pi/D_1'} \equiv \frac{\mathcal{B}(B^+ \to D^{*-}\pi^+\ell^+\nu)}{\mathcal{B}(B^+ \to \bar{D}_1'^0\ell^+\nu)}$

5. $f_{D_0^*D\pi T/D_1D_2^*T} \equiv \frac{\mathcal{BT}(B^+ \to \bar{D}_0^{*0}/(D\pi)^0\ell^+\nu)}{\mathcal{BT}(B^+ \to \bar{D}_1^0/\bar{D}_2^{*0}\ell^+\nu)}$

6. $f_{D_1'D^*\pi T/D_1D_2^*T} \equiv \frac{\mathcal{BT}(B^+ \to \bar{D}_1'^0/(D^*\pi)^0\ell^+\nu)}{\mathcal{BT}(B^+ \to \bar{D}_1^0/\bar{D}_2^{*0}\ell^+\nu)}$

D.2 Measured $B \to D^{(*)}\pi^+\ell^+\nu$ branching fractions

$B \to D^{(*)}\pi^+\ell^+\nu$ branching fractions given in Table 97 and 98 includes not only non-resonant contribution but also $B \to D^{(*)}\pi^+\ell^+\nu$ contributions. Thus,

$$\mathcal{BT}(B^+ \to D^-\pi^+\ell^+\nu) = \mathcal{B}(B^+ \to \bar{D}_0^{*0}\ell^+\nu)\mathcal{B}(D_0^{*0} \to D^+\pi^-) + \mathcal{B}(B^+ \to \bar{D}_2^{*0}\ell^+\nu)\mathcal{B}(D_2^{*0} \to D^+\pi^-) + \mathcal{B}(B^+ \to D^-\pi^+\ell^+\nu) \tag{440}$$

$$\begin{aligned}\mathcal{BT}(B^+ \to D^{*-}\pi^+\ell^+\nu) = {} & \mathcal{B}(B^+ \to \bar{D}_1^0\ell^+\nu)\mathcal{B}(D_1^0 \to D^{*+}\pi^-) + \mathcal{B}(B^+ \to \bar{D}_1'^0\ell^+\nu)\mathcal{B}(D_1'^0 \to D^{*+}\pi^-) \\ & +\mathcal{B}(B^+ \to \bar{D}_2^{*0}\ell^+\nu)\mathcal{B}(D_2^{*0} \to D^{*+}\pi^-) + \mathcal{B}(B^+ \to D^{*-}\pi^+\ell^+\nu)\end{aligned} \tag{441}$$

$$\mathcal{BT}(B^0 \to \bar{D}^0\pi^-\ell^+\nu) = \mathcal{B}(B^0 \to D_0^{*-}\ell^+\nu)\mathcal{B}(D_0^{*+} \to D^0\pi^+) + \mathcal{B}(B^0 \to D_2^{*-}\ell^+\nu)\mathcal{B}(D_2^{*+} \to D^0\pi^+) + \mathcal{B}(B^0 \to \bar{D}^0\pi^-\ell^+\nu) \tag{442}$$

$$\begin{aligned}\mathcal{BT}(B^0 \to \bar{D}^{*0}\pi^-\ell^+\nu) = {} & \mathcal{B}(B^0 \to D_1^-\ell^+\nu)\mathcal{B}(D_1^+ \to D^{*0}\pi^+) + \mathcal{B}(B^0 \to D_1'^-\ell^+\nu)\mathcal{B}(D_1'^+ \to D^{*0}\pi^+) \\ & +\mathcal{B}(B^0 \to D_2^{*-}\ell^+\nu)\mathcal{B}(D_2^{*+} \to D^{*0}\pi^+) + \mathcal{B}(B^0 \to \bar{D}^{*0}\pi^-\ell^+\nu)\end{aligned} \tag{443}$$

Thus, using SP5/SP6 MC values

$$\begin{aligned}\mathcal{BT}(B^+ \to D^-\pi^+\ell^+\nu) &= 0.0020 \times 0.6667 + 0.0037 \times 0.459 + 0.0060 \\ &= 0.00903\end{aligned} \tag{444}$$

$$\begin{aligned}\mathcal{BT}(B^+ \to D^{*-}\pi^+\ell^+\nu) &= 0.0056 \times 0.6667 + 0.0037 \times 0.6667 \\ &\quad +0.0037 \times 0.209 + 0.0020 \\ &= 0.00897\end{aligned} \tag{445}$$

$$\begin{aligned}\mathcal{BT}(B^0 \to \bar{D}^0\pi^-\ell^+\nu) &= 0.0020 \times 0.6667 + 0.0037 \times 0.459 + 0.0060 \\ &= 0.00903\end{aligned} \tag{446}$$

$$\begin{aligned}\mathcal{BT}(B^0 \to \bar{D}^{*0}\pi^-\ell^+\nu) &= 0.0056 \times 0.6667 + 0.0037 \times 0.6667 \\ &\quad +0.0037 \times 0.209 + 0.0020 \\ &= 0.00897\end{aligned} \tag{447}$$

D.3 Inclusive $\mathcal{B}(B \to X_c\ell\nu)$

Inclusive branching fractions in SP5/SP6 MC are given by the sum of exclusive branching fractions :

$$\mathcal{B}(B^+ \to \bar{D}^0\ell^+\nu)+\mathcal{B}(B^+ \to \bar{D}^{*0}\ell^+\nu)+\mathcal{BT}(B^+ \to \bar{D}^{**0}/(D\pi)^0\ell^+\nu) = \mathcal{B}(B^+ \to X_c\ell^+\nu) \tag{448}$$

and

$$\mathcal{B}(B^0 \to D^-\ell^+\nu)+\mathcal{B}(B^0 \to D^{*-}\ell^+\nu)+\mathcal{BT}(B^0 \to D^{**-}/(D\pi)^-\ell^+\nu) = \mathcal{B}(B^0 \to X_c\ell^+\nu) \tag{449}$$

In SP5/SP6 the following value is used :

$$\mathcal{B}(B^+ \to X_c\ell\nu) = \mathcal{B}(B^0 \to X_c\ell\nu) = 0.104 \tag{450}$$

Measured values form PDG [12] are

$$\begin{aligned}\mathcal{B}(B \to X\ell\nu) &= 0.1081 \pm 0.0014 \\ \mathcal{B}(B \to X_u\ell\nu) &= 0.00233 \pm 0.00022\end{aligned} \tag{451}$$

Thus,

$$\begin{aligned}\mathcal{B}(B \to X_c\ell\nu) &= (0.1081 \pm 0.0014) - (0.00233 \pm 0.00022) \\ &= 0.10577 \pm 0.001417\end{aligned} \tag{452}$$

Combining this with lifetime ratio [12]

$$t_{+0} \equiv \frac{\tau_{B^+}}{\tau_{B^0}} = 1.071 \pm 0.009 \tag{453}$$

Branching fraction	SP5/SP6	Measurement [reference]
$\mathcal{B}(B^+ \to \bar{D}^0\ell^+\nu)$	0.0210	0.0215 ± 0.0022 [12]
		$0.0233 \pm 0.0009 \pm 0.0008$ [4]
$\mathcal{B}(B^+ \to \bar{D}^{*0}\ell^+\nu)$	0.0560	0.065 ± 0.005 [12]
		$0.0583 \pm 0.0015 \pm 0.0028$ [4]
$\mathcal{B}(B^+ \to \bar{D}_0^{*0}\ell^+\nu)$	0.0020	
$\mathcal{B}(B^+ \to \bar{D}_1^0\ell^+\nu)$	0.0056	0.0056 ± 0.0016 [12]
		$0.00448 \pm 0.00026 \pm 0.00035$ [15]
$\mathcal{B}(B^+ \to \bar{D}_1^{\prime 0}\ell^+\nu)$	0.0037	
$\mathcal{B}(B^+ \to \bar{D}_2^{*0}\ell^+\nu)$	0.0037	$0.00354 \pm 0.00032 \pm 0.00054$ [15]
$\mathcal{B}(B^+ \to D^-\pi^+\ell^+\nu)$	0.0060	
$\mathcal{B}(B^+ \to \bar{D}^0\pi^0\ell^+\nu)$	0.0030	
$\mathcal{B}(B^+ \to D^{*-}\pi^+\ell^+\nu)$	0.0020	
$\mathcal{B}(B^+ \to \bar{D}^{*0}\pi^0\ell^+\nu)$	0.0010	
$\mathcal{BT}(B^+ \to D^-\pi^+\ell^+\nu)$	0.00903	0.0052 ± 0.0010 [12]
		$0.0042 \pm 0.0006 \pm 0.0003$ [4]
$\mathcal{BT}(B^+ \to D^{*-}\pi^+\ell^+\nu)$	0.00897	0.0063 ± 0.0015 [12]
		$0.0059 \pm 0.0005 \pm 0.0004$ [4]

Table 97: B^+ decay branching fractions.

we can calculate B^+ and B^0 separately. By assuming B^+ and B^0 contributions are equal,

$$\mathcal{B}(B^+ \to \bar{X}_c^0\ell^+\nu) + \mathcal{B}(B^0 \to X_c^-\ell^+\nu) = 2\mathcal{B}(B \to X_c\ell\nu) \tag{454}$$

From isospin symmetry

$$\mathcal{B}(B^+ \to \bar{X}_c^0\ell^+\nu) = t_{+0}\mathcal{B}(B^0 \to X_c^-\ell^+\nu) \tag{455}$$

Thus

$$\mathcal{B}(B^+ \to \bar{X}_c^0\ell^+\nu) = \frac{2t_{+0}}{1+t_{+0}}\mathcal{B}(B \to X_c\ell\nu) = 0.1094 \pm 0.0014 \tag{456}$$

and

$$\mathcal{B}(B^+ \to \bar{X}_c^0\ell^+\nu) = \frac{2}{1+t_{+0}}\mathcal{B}(B \to X_c\ell\nu) = 0.1021 \pm 0.0014 \tag{457}$$

Branching fraction	SP5/SP6	Measurement [reference]
$\mathcal{B}(B^0 \to D^-\ell^+\nu)$	0.0210	0.0208 ± 0.0018 [12] $0.0221 \pm 0.0011 \pm 0.0009$ [4]
$\mathcal{B}(B^0 \to D^{*-}\ell^+\nu)$	0.0560	0.0529 ± 0.0019 [12] $0.0549 \pm 0.0016 \pm 0.0023$ [4]
$\mathcal{B}(B^0 \to D_0^{*-}\ell^+\nu)$	0.0020	$0.0042 \pm 0.0033 \pm 0.022$ [16]
$\mathcal{B}(B^0 \to D_1^-\ell^+\nu)$	0.0056	$0.00364 \pm 0.00032 \pm 0.00049$ [15]
$\mathcal{B}(B^0 \to D_1'^-\ell^+\nu)$	0.0037	$0.0124 \pm 0.0025 \pm 0.027$ [16]
$\mathcal{B}(B^0 \to D_2^{*-}\ell^+\nu)$	0.0037	$0.00270 \pm 0.00035 \pm 0.00043$ [15]
$\mathcal{BT}(B^0 \to D^{**-}\ell^+\nu)$	0.0150	$0.027 \pm 0.007 \pm 0.002$ [16]
$\mathcal{B}(B^0 \to \bar{D}^0\pi^-\ell^+\nu)$	0.0060	
$\mathcal{B}(B^0 \to D^-\pi^0\ell^+\nu)$	0.0030	
$\mathcal{B}(B^0 \to \bar{D}^{*0}\pi^-\ell^+\nu)$	0.0020	
$\mathcal{B}(B^0 \to \bar{D}^{*-}\pi^0\ell^+\nu)$	0.0010	
$\mathcal{BT}(B^0 \to \bar{D}^0\pi^-\ell^+\nu)$	0.00903	0.0032 ± 0.0010 [12] $0.0043 \pm 0.0008 \pm 0.0003$ [4]
$\mathcal{BT}(B^0 \to \bar{D}^{*0}\pi^-\ell^+\nu)$	0.00897	0.0065 ± 0.0015 [12] $0.0048 \pm 0.0008 \pm 0.0004$ [4]

Table 98: B^0 decay branching fractions.

Branching fraction	SP5/SP6	AWG average
$\mathcal{B}(B^+ \to \bar{D}_1^0 \ell^+ \nu)$	0.0056	0.0054 ± 0.0006
$\mathcal{B}(B^+ \to \bar{D}_2^{*0} \ell^+ \nu)$	0.0037	0.0042 ± 0.0008
$\mathcal{BT}(B^+ \to \bar{D}_1^0/\bar{D}_2^{*0} \ell^+ \nu)$	0.0093	
$\mathcal{B}(B^+ \to \bar{D}_0^{*0} \ell^+ \nu)$	0.0020	0.0085 ± 0.0020
$\mathcal{B}(B^+ \to D^- \pi^+ \ell^+ \nu)$	0.0060	0.0019 ± 0.0012
$\mathcal{B}(B^+ \to \bar{D}^0 \pi^0 \ell^+ \nu)$	0.0030	0.0010 ± 0.0006
$\mathcal{BT}(B^+ \to \bar{D}_0^{*0}/(D\pi)^0 \ell^+ \nu)$	0.0110	
$\mathcal{B}(B^+ \to \bar{D}_1'^0 \ell^+ \nu)$	0.0037	0.0045 ± 0.0009
$\mathcal{B}(B^+ \to D^{*-} \pi^+ \ell^+ \nu)$	0.0020	0.0006 ± 0.0004
$\mathcal{B}(B^+ \to \bar{D}^{*0} \pi^0 \ell^+ \nu)$	0.0010	0.0003 ± 0.0002
$\mathcal{BT}(B^+ \to \bar{D}_1^{*0}/(D^*\pi)^0 \ell^+ \nu)$	0.0067	
$\mathcal{BT}(B^+ \to \bar{D}^{**0}/(D\pi)^0 \ell^+ \nu)$	0.0270	
$f_{D_2^*/D_1}$	$37/56 = 0.66$	
$f_{D\pi/D_0^*}$	$60/20 = 3.0$	
$f_{D^*\pi/D_1^*}$	$20/37 = 0.54$	
$f_{D_0^* D\pi T/D_1 D_2^* T}$	$110/93 = 1.18$	
$f_{D_1^* D^*\pi T/D_1 D_2^* T}$	$67/93 = 0.72$	

Table 99: $B^+ \to D^{**}\ell\nu$ and $B^+ \to D^{(*)}\pi\ell\nu$ decay branching fractions and ratios defined in section 5.

Branching fraction	SP5/SP6	Measurement [reference]
$\mathcal{B}(B^+ \to X \ell^+ \nu)$		0.1099 ± 0.0028 [12]
$\mathcal{B}(B^+ \to \bar{X}_c^0 \ell^+ \nu)$	0.1040	0.108 ± 0.004 [12]
$\mathcal{B}(B^0 \to X \ell^+ \nu)$		0.1033 ± 0.0028 [12]
$\mathcal{B}(B^0 \to X_c^- \ell^+ \nu)$	0.1040	0.101 ± 0.004 [12]
$\mathcal{B}(B \to X \ell^+ \nu)$		0.1024 ± 0.0015 [12]
$\mathcal{B}(B \to X_c \ell \nu)$	0.1040	0.1057 ± 0.0015 [12]
$\mathcal{B}(B \to X_u \ell \nu)$		0.00233 ± 0.00022 [12]
$\mathcal{B}(B \to X_c e \nu(\gamma), E_e > 1.5\mathrm{GeV})$		$0.0454 \pm 0.0003 \pm 0.0008$ [47]

Table 100: Inclusive B decay branching fractions.

Branching fraction	SP5/SP6	Measurement [reference]
$\mathcal{B}(D_0^{*+} \to D^0\pi^+)$	0.6667	
$\mathcal{B}(D_0^{*+} \to D^+\pi^0)$	0.3333	
$\mathcal{B}(D_0^{*0} \to D^+\pi^-)$	0.6667	
$\mathcal{B}(D_0^{*0} \to D^0\pi^0)$	0.3333	
$\mathcal{B}(D_1^{+} \to D^{*0}\pi^+)$	0.6667	
$\mathcal{B}(D_1^{+} \to D^{*+}\pi^0)$	0.3333	
$\mathcal{B}(D_1^{0} \to D^{*+}\pi^-)$	0.6667	
$\mathcal{B}(D_1^{0} \to D^{*0}\pi^0)$	0.3333	
$\mathcal{B}(D_1^{\prime +} \to D^{*0}\pi^+)$	0.6667	
$\mathcal{B}(D_1^{\prime +} \to D^{*+}\pi^0)$	0.3333	
$\mathcal{B}(D_1^{\prime 0} \to D^{*+}\pi^-)$	0.6667	
$\mathcal{B}(D_1^{\prime 0} \to D^{*0}\pi^0)$	0.3333	
$f_{D_2^*}$	$459/209 = 2.2$	$\frac{\mathcal{B}(D_2^{*+}\to D^0\pi^+)}{\mathcal{B}(D_2^{*+}\to D^{*0}\pi^+)} = 1.9 \pm 1.1 \pm 0.3$ [12] $\frac{\mathcal{B}(D_2^{*0}\to D^+\pi^-)}{\mathcal{B}(D_2^{*0}\to D^{*+}\pi^-)} = 2.3 \pm 0.6$ [12]
$\mathcal{B}(D_2^{*+} \to D^0\pi^+)$	0.4590	
$\mathcal{B}(D_2^{*+} \to D^+\pi^0)$	0.2290	
$\mathcal{B}(D_2^{*+} \to D^{*0}\pi^+)$	0.2090	
$\mathcal{B}(D_2^{*+} \to D^{*+}\pi^0)$	0.1030	
$\mathcal{B}(D_2^{*0} \to D^+\pi^-)$	0.4590	
$\mathcal{B}(D_2^{*0} \to D^0\pi^0)$	0.2290	
$\mathcal{B}(D_2^{*0} \to D^{*+}\pi^-)$	0.2090	
$\mathcal{B}(D_2^{*0} \to D^{*0}\pi^0)$	0.1030	

Table 101: D^{**} decay branching fractions.

Branching fraction	SP5/SP6	Measurement [reference]
$\mathcal{B}(D^{*+} \to D^0\pi^+)$	0.6830	0.677 ± 0.005 [12]
$\mathcal{B}(D^{*+} \to D^+\pi^0)$	0.3060	0.307 ± 0.005 [12]
$\mathcal{B}(D^{*+} \to D^+\gamma)$	0.0110	0.016 ± 0.004 [12]
$\mathcal{B}(D^{*0} \to D^0\pi^0)$	0.6190	0.619 ± 0.029 [12]
$\mathcal{B}(D^{*0} \to D^0\gamma)$	0.3810	0.381 ± 0.029 [12]
$\mathcal{B}(D^0 \to K^-\pi^+)$	0.0383	0.0382 ± 0.0007 [12] $0.04007 \pm 0.00037 \pm 0.00070$ [30] $0.03891 \pm 0.00035 \pm 0.00059 \pm 0.00035$ [31]
$\mathcal{B}(D^+ \to K^-\pi^+\pi^+)$	0.0900	0.0951 ± 0.0034 [12] $0.0915 \pm 0.0010 \pm 0.0016 \pm 0.0007$ [31]

Table 102: $D^{(*)}$ decay branching fractions.

Constant	SP5/SP6	Measurement [reference]
t_{+0}	1	1.071 ± 0.009 [12]
f_{+0}	1	1.037 ± 0.029 [12]

Table 103: Constants.

Parameter	SP5/SP6	Measurement [reference]
ρ^2	0.92	$1.145 \pm 0.059 \pm 0.030 \pm 0.035$ [40]
R_1	1.18	$1.396 \pm 0.060 \pm 0.035 \pm 0.027$ [40]
R_2	0.72	$0.885 \pm 0.040 \pm 0.022 \pm 0.013$ [40]
ρ^2	0.92	$1.191 \pm 0.048 \pm 0.028$ [41]
R_1	1.18	$1.429 \pm 0.061 \pm 0.044$ [41]
R_2	0.72	$0.827 \pm 0.038 \pm 0.022$ [41]
$\mathcal{F}(1)\lvert V_{cb}\rvert$		$(34.4 \pm 0.3 \pm 1.1) \times 10^{-3}$ [41]
$\mathcal{B}(B^0 \to D^{*-}\ell^+\nu)$	0.0560	$0.0469 \pm 0.0004 \pm 0.0034$ [41]
ρ^2	0.92	$1.16 \pm 0.06 \pm 0.08$ [46]
$\mathcal{F}(1)\lvert V_{cb}\rvert$		$(35.9 \pm 0.6 \pm 1.4) \times 10^{-3}$ [46]
$\mathcal{B}(B^- \to D^{*0}e^-\bar{\nu}_e)$	0.0560	$0.0556 \pm 0.0008 \pm 0.0041$ [46]

Table 104: $B \to D^*\ell\nu$ FF parameters. "Measurement" is the most recent measured value from Babar. Definition of these parameters are given in Appendix H. Note that different parametrizations of ρ^2 was used in SP5/SP6 MC and [40]. See details in section 10

Decay mode	SP5/SP6	Measurement [4]
$\mathcal{B}(B^- \to D^0\ell^-\bar{\nu})$	0.0210	$0.0233 \pm 0.0009 \pm 0.0009$
$\mathcal{B}(B^- \to D^{*0}\ell^-\bar{\nu})$	0.0560	$0.0583 \pm 0.0015 \pm 0.0030$
$\mathcal{B}(B^- \to D^+\pi^-\ell^-\bar{\nu})$	0.00903	$0.0042 \pm 0.0006 \pm 0.0003$
$\mathcal{B}(B^- \to D^{*+}\pi^-\ell^-\bar{\nu})$	0.00897	$0.0059 \pm 0.0005 \pm 0.0004$
$\mathcal{B}(B^- \to D^{(*)}\pi\ell^-\bar{\nu})$	0.0270	$0.0152 \pm 0.0012 \pm 0.0010$
$\mathcal{B}(\bar{B}^0 \to D^+\ell^-\bar{\nu})$	0.0210	$0.0221 \pm 0.0011 \pm 0.0012$
$\mathcal{B}(\bar{B}^0 \to D^{*+}\ell^-\bar{\nu})$	0.0560	$0.0549 \pm 0.0016 \pm 0.0025$
$\mathcal{B}(\bar{B}^0 \to D^0\pi^+\ell^-\bar{\nu})$	0.00903	$0.0043 \pm 0.0008 \pm 0.0003$
$\mathcal{B}(\bar{B}^0 \to D^{*0}\pi^+\ell^-\bar{\nu})$	0.00897	$0.0048 \pm 0.0008 \pm 0.0004$
$\mathcal{B}(\bar{B}^0 \to D^{(*)}\pi\ell^-\bar{\nu})$	0.0270	$0.0137 \pm 0.0017 \pm 0.0010$

Table 105: $B \to D^{(*)}(\pi)\ell\nu$ branching fractions.

E BToDlnu skim rates and luminosities

The event selection rates and luminosities of R16b BToDlnu skims of data and MC is summarized in Table 107 and 108.
The luminosities of BpBm and B0B0bar MC are calculated by the generated number of events and B counting number in the OnPeak table 107. For example, in case of BpBm MC Run2, the generated number of events is 146536000. The B counting number for Run2 OnPeak is 65697538.1 ± 723956.4, which corresponds to the luminosity of 59.402357 fb^{-1}. We assume the half of the $B\bar{B}$ is B^+B^-. Thus, the luminosity is

$$\frac{146536000}{(65697538.1 \pm 723956.4)/2} \times 59.402357 = 264.99 \pm 2.92 \ \mathrm{fb}^{-1}$$

The luminosities of ccbar, uds and tautau MC are calculated by the generated number of events and their cross section. Cross sections are taken from the Babar Physics Book [52] and given in Table 106. The luminosities are calculated based on the cross sections and the number of events before skimming. For example, in case of ccbar Run4 MC, as the number of events before skimming is 188718626, its luminosity is

$$\frac{188718626}{1.30 \times 10^3} = 1.452 \times 10^5 \mathrm{pb}^{-1} = 145.2 \ \mathrm{fb}^{-1}$$

Type of MC	Cross section (nb)
$B\bar{B}$	1.05
$c\bar{c}$	1.30
uds	2.09
$\tau^+\tau^-$	0.94

Table 106: Cross sections used to calculate MC luminosities.

Data set	Selection rate	Luminosity (fb^{-1})	Number of BBbar
OnPeak Run1	8792976/245552690	17.807136	19411539.8 ± 214782.8
Run2	31374579/852649140	59.402357	65697538.1 ± 723956.4
Run3	17527801/438622047	30.630558	33754342.8 ± 372583.9
Run4	57952809/1448776065	99.405417	$109449337.9 \pm 1205214.0$
Total		207.245468	
OffPeak Run1	515760/28946433	2.330076	
Run2	1674989/90665305	6.833280	
Run3	659867/31451100	2.394734	
Run4	2878531/132941301	9.929434	
Total		21.487524	

Table 107: BToDlnu Data skims event selection rates and luminosities.

Data set	Selection rate	Luminosity (fb^{-1})
BpBm Run1	6920906/27176000	49.86 ± 0.55
Run2	39029539/146536000	264.99 ± 2.92
Run3	23854196/86492000	156.98 ± 1.73
Run4	89759580/323822000	588.21 ± 6.48
Total		1060.04 ± 7.34
B0B0bar Run1	7421839/28762000	52.77 ± 0.58
Run2	30164526/111924000	202.40 ± 2.23
Run3	17081965/61158000	111.00 ± 1.23
Run4	90093404/321150000	583.36 ± 6.42
Total		949.53 ± 6.93
ccbar Run1	1897239/21346000	16.420
Run2	9838664/99972000	76.708
Run3	6127861/57700000	44.385
Run4	25956105/246602000	189.69
Total		327.20
uds Run1	948025/30168000	14.434
Run2	6799899/176242000	84.326
Run3	5639210/124040000	59.349
Run4	15259514/346551000	165.81
Total		323.919
tautau Run1	135022/22098000	23.509
Run2	695973/99806000	106.18
Run3	544465/69852000	74.311
Run4	1472037/154900000	164.79
Total		368.79

Table 108: BToDlnu MC skims event selection rates and luminosities.

F $\cos\theta_{BY}$

F.1 $B \to D\ell\nu$ decays

In the decay of $B \to Dl + \nu$, 4-momentum conservation gives

$$p_B = p_{Dl} + p_\nu \tag{458}$$

As the mass of neutrino is equal to zero

$$0 = p_\nu^2 = (p_B - p_{Dl})^2 = p_B^2 + p_{Dl}^2 - 2p_B \cdot p_{Dl} = m_B^2 + m_{Dl}^2 - 2p_B \cdot p_{Dl} \tag{459}$$

Here,

$$p_B \cdot p_{Dl} = E_B E_{Dl} - \vec{p}_B \cdot \vec{p}_{Dl} = E_B E_{Dl} - |\vec{p}_B||\vec{p}_{Dl}| \cos\Theta_{B-Dl} \tag{460}$$

Hence

$$\begin{aligned} 0 &= m_B^2 + m_{Dl}^2 - 2(E_B E_{Dl} - |\vec{p}_B||\vec{p}_{Dl}| \cos\Theta_{B-Dl}) \\ \Rightarrow m_B^2 + m_{Dl}^2 &= 2E_B E_{Dl} - 2|\vec{p}_B||\vec{p}_{Dl}| \cos\Theta_{B-Dl} \end{aligned} \tag{461}$$

Therefore

$$\cos\Theta_{B-Dl} = \frac{2E_B E_{Dl} - m_B^2 - m_{Dl}^2}{2|\vec{p}_B||\vec{p}_{Dl}|} \tag{462}$$

In practice, E_B is given by the half of the beam energy in the CM frame. $|\vec{p}_B|$ is given by

$$|\vec{p}_B| = \sqrt{E_B^2 - m_B^2} \tag{463}$$

F.2 With an additional pion

If there are additional particles, $\cos\Theta_{B-Dl} < -1$ is possible. Let us consider an additional pion, for example, from D^*. Conservation of 4-momentum is

$$p_B = p_{Dl} + p_\pi + p_\nu \tag{464}$$

Then,

$$\begin{aligned} &(p_\nu + p_\pi)^2 = (p_B - p_{Dl})^2 \\ &\Rightarrow p_\nu^2 + p_\pi^2 + 2p_\nu \cdot p_\pi = p_B^2 + p_{Dl}^2 - 2p_B \cdot p_{Dl} \\ &\Rightarrow 0 + m_\pi^2 + 2p_\nu \cdot p_\pi = m_B^2 + m_{Dl}^2 - 2p_B \cdot p_{Dl} \end{aligned} \tag{465}$$

Since $m_\pi \ll m_B$,

$$0 + 0 + 2p_\nu \cdot p_\pi = m_B^2 + m_{Dl}^2 - 2p_B \cdot p_{Dl} \tag{466}$$

and also

$$\begin{aligned} p_\nu \cdot p_\pi &= E_\nu E_\pi - \vec{p}_\nu \cdot \vec{p}_\pi = E_\nu E_\pi - |\vec{p}_\nu||\vec{p}_\pi| \cos\Theta_{\nu-\pi} \\ &= E_\nu E_\pi - E_\nu E_\pi \cos\Theta_{\nu-\pi} = E_\nu E_\pi (1 - \cos\Theta_{\nu-\pi}) \geq 0 \end{aligned} \tag{467}$$

Let the angle between B and Dl be Θ'_{B-Dl}. Then,

$$p_B \cdot p_{Dl} = E_B E_{Dl} - \vec{p}_B \cdot \vec{p}_{Dl} = E_B E_{Dl} - |\vec{p}_B||\vec{p}_{Dl}| \cos\Theta'_{B-Dl} \tag{468}$$

Hence,

$$\begin{aligned}\cos\Theta'_{B-Dl} &= \tfrac{2E_B E_{Dl} - m_B^2 - m_{Dl}^2}{2|\vec{p}_B||\vec{p}_{Dl}|} + \tfrac{2p_\nu \cdot p_\pi}{2|\vec{p}_B||\vec{p}_{Dl}|} \\ &= \cos\Theta_{B-Dl} + \alpha\end{aligned} \tag{469}$$

where

$$\alpha = \frac{2p_\nu \cdot p_\pi}{2|\vec{p}_B||\vec{p}_{Dl}|} \geq 0 \tag{470}$$

Considering

$$-1 \leq \cos\Theta'_{B-Dl} \leq 1 \tag{471}$$

$\cos\Theta_{B-Dl} = \cos\Theta'_{B-Dl} - \alpha$ is

$$-1 - \alpha \leq \cos\Theta_{B-Dl} \leq 1 - \alpha \leq 1 \tag{472}$$

Since $\alpha \geq 0$, the lower end of $\cos\Theta_{B-Dl}$ can be smaller than -1, whereas the upper end remains to 1.

F.3 If D and l come from different B

In the case that D and l came from different B, $\cos\Theta_{B-Dl} > 1$ is possible. The p_{Dl} is

$$p_{Dl} = p_D + p_l = (E_D + E_l, -\vec{p}_D - \vec{p}_l) = (E_{Dl}, -\vec{p}_{Dl}) \tag{473}$$

Hence

$$\begin{aligned}&E_{Dl} = E_D + E_l = \sqrt{m_D^2 + |\vec{p}_D|^2} + \sqrt{m_l^2 + |\vec{p}_l|^2} = \sqrt{m_D^2 + |\vec{p}_D|^2} + |\vec{p}_l| \\ &|\vec{p}_{Dl}|^2 = |\vec{p}_D + \vec{p}_l|^2 = |\vec{p}_D|^2 + |\vec{p}_l|^2 + 2|\vec{p}_D||\vec{p}_l|\cos\theta\end{aligned} \tag{474}$$

and

$$\begin{aligned}m_{Dl}^2 &= p_{Dl}^2 = E_{Dl}^2 - |\vec{p}_{Dl}|^2 \\ &= m_D^2 + |\vec{p}_D|^2 + |\vec{p}_l|^2 + 2|\vec{p}_l|\sqrt{m_D^2 + |\vec{p}_D|^2} - |\vec{p}_D|^2 - |\vec{p}_l|^2 - 2|\vec{p}_D||\vec{p}_l|\cos\theta \\ &= m_D^2 + 2|\vec{p}_l|\sqrt{m_D^2 + |\vec{p}_D|^2} - 2|\vec{p}_D||\vec{p}_l|\cos\theta \\ &= m_D^2 + |\vec{p}_l|(2\sqrt{m_D^2 + |\vec{p}_D|^2} - 2|\vec{p}_D|\cos\theta)\end{aligned} \tag{475}$$

If D and l come from different B, p_D and p_l are not restricted by energy momentum conservation. The $|\vec{p}_D|$ and $|\vec{p}_l|$ can be any value. If $|\vec{p}_l|$ is very large, E_{Dl} is very large but m_{Dl}^2 can be as small as m_D^2 if

$$2\sqrt{m_D^2 + |\vec{p}_D|^2} \simeq 2|\vec{p}_D|\cos\theta \tag{476}$$

Hence

$$\cos\Theta_{B-Dl} = \frac{2E_B E_{Dl} - m_B^2 - m_{Dl}^2}{2|\vec{p}_B||\vec{p}_{Dl}|} \tag{477}$$

can be larger than 1.

G Velocity transfer w

G.1 w and q^2

In the framework of Heavy Quark Effective Theory (HQET) it is convenient to use the velocity transfer w instead of momentum transfer q^2. In semileptonic $B \to D^{(*)}\ell\nu$ decays, w is defined as the product of 4-velocities of B and $D^{(*)}$

$$w \equiv v_B \cdot v_{D^{(*)}} = \frac{p_B \cdot p_{D^{(*)}}}{m_B m_{D^{(*)}}} \tag{478}$$

The momentum transfer q from B to $D^{(*)}$ (or the invariant mass of the virtual W) is given by

$$q = p_\ell + p_\nu = p_B - p_{D^{(*)}} \tag{479}$$

Thus

$$\begin{aligned} &q^2 = (p_B - p_{D^{(*)}})^2 = p_B^2 + p_{D^{(*)}}^2 - 2p_B \cdot p_{D^{(*)}} = m_B^2 + m_{D^{(*)}}^2 - 2p_B \cdot p_{D^{(*)}} \\ &\Rightarrow p_B \cdot p_{D^{(*)}} = \tfrac{m_B^2 + m_{D^{(*)}}^2 - q^2}{2} \end{aligned} \tag{480}$$

Hence

$$w = \frac{m_B^2 + m_{D^{(*)}}^2 - q^2}{2m_B m_{D^{(*)}}} \tag{481}$$

w is a Lorentz invariant and linearly related to q^2.
w corresponds to the relativistic boost γ of the $D^{(*)}$ in the B rest frame.

$$\gamma_{D^{(*)}} = \frac{E_{D^{(*)}}}{m_{D^{(*)}}} \tag{482}$$

G.2 $1 \le w \lesssim 1.5$

The range of w and q^2 are restricted by kinematics of the decay. When $q^2 = 0$, w is maximum

$$w_{\rm max} = \frac{m_B^2 + m_{D^{(*)}}^2}{2m_B m_{D^{(*)}}} \tag{483}$$

Using $m_B = 5279$, $m_D = 1867$ and $m_{D^*} = 2008$ MeV,

$$\frac{m_B^2 + m_D^2}{2m_B m_D} = 1.590, \qquad \frac{m_B^2 + m_{D^*}^2}{2m_B m_{D^*}} = 1.504 \tag{484}$$

Using $m_{D_0^*} = 2400$, $m_{D_1'} = 2430$, $m_{D_1} = 2420$ and $m_{D_2^*} = 2460$ MeV,

$$\begin{aligned} &\frac{m_B^2 + m_{D_0^*}^2}{2m_B m_{D_0^*}} = 1.327, \qquad \frac{m_B^2 + m_{D_1'}^2}{2m_B m_{D_1'}} = 1.316, \\ &\frac{m_B^2 + m_{D_1}^2}{2m_B m_{D_1}} = 1.320, \qquad \frac{m_B^2 + m_{D_2^*}^2}{2m_B m_{D_2^*}} = 1.306 \end{aligned} \tag{485}$$

The minimum of the w is

$$w_{\text{min}} = 1 \tag{486}$$

which corresponds to

$$q^2_{\text{max}} = (m_B - m_{D^{(*)}})^2 \tag{487}$$

where

$$(m_B - m_D)^2 = 11.64, \quad (m_B - m_{D^*})^2 = 10.69 \ (\text{GeV}/c^2)^2 \tag{488}$$

and

$$(m_B - m_{D_0^*})^2 = 8.29, \quad (m_B - m_{D_1'})^2 = 8.12 \ (\text{GeV}/c^2)^2, \tag{489}$$

$$(m_B - m_{D_1})^2 = 8.17, \quad (m_B - m_{D_2^*})^2 = 7.95 \ (\text{GeV}/c^2)^2 \tag{490}$$

G.3 Practical calculation of w

We can calculate w by the following formula

$$w = \frac{p_B \cdot p_{D^{(*)}}}{m_B m_{D^{(*)}}} = \frac{E_B E_{D^{(*)}} - |\vec{P}_B||\vec{P}_{D^{(*)}}| \cos\theta_{B-D}}{m_B m_{D^{(*)}}} \tag{491}$$

In practice, E_B is the half of the beam energy, and $|\vec{P}_B|$ is given by

$$|\vec{P}_B| = \sqrt{E_B^2 - m_B^2} \tag{492}$$

$\cos\theta_{B-D}$ can be calculated from $\cos\theta_{B-Dl}$ (see Appendix F and Figure 62).

H Form Factors (FF) of $B \to D^{(*,**)}X\ell\nu$ decays

H.1 Matrix elements, form factors and decay rates

The amplitude of $B \to D^{(*,**)}\ell\nu$ decay is given by

$$\mathcal{M} = -i\frac{G_F}{\sqrt{2}}V_{cb}L^\mu H_\mu \tag{493}$$

where the leptonic current can be written in terms of Dirac spinors u_l and v_ν

$$L^\mu = \bar{u}_l\gamma^\mu(1-\gamma_5)v_\nu \tag{494}$$

The hadronic current H_μ can be written in terms of quark spinors b and c

$$H^\mu =< D|\bar{c}\gamma^\mu(1-\gamma_5)b|B >=< D|V^\mu|B > - < D|A^\mu|B > \tag{495}$$

where

$$\begin{aligned} V^\mu &= \bar{c}\gamma^\mu b \quad \text{(vector current)} \\ A^\mu &= \bar{c}\gamma^\mu\gamma_5 b \quad \text{(axial-vector current)} \end{aligned} \tag{496}$$

The matrix elements $< D|V^\mu|B >$ and $< D|A^\mu|B >$ can be expressed by form factors. In constituent quark models such as ISGW2 model [33][34], form factors are functions of momentum transfer q^2, whereas in HQET (Heavy Quark Effective Theory) models, it is more natural to express form factors as functions of the velocity transfer w

$$w = v \cdot v' = v_B \cdot v_D = \frac{p_B \cdot p_D}{m_B m_D} \tag{497}$$

We also use the following mass ratios

$$r = \frac{m_D}{m_B}, \quad R = \frac{2\sqrt{m_B m_D}}{m_B + m_D} \tag{498}$$

where D in the v_D, p_D and m_D may be D^*, D_0^*, D_1', D_1 or D_2^* depending on the final state.

H.1.1 $B \to D\ell\nu$

In the ISGW2 model, the matrix elements are given by

$$< D(p')|V^\mu|B(p) >= f_+(q^2)(p+p')^\mu + f_-(q^2)(p-p')^\mu \tag{499}$$

$$< D(p')|A^\mu|B(p) >= 0 \tag{500}$$

In HQET models,

$$\frac{< D(v')|V^\mu|B(v) >}{\sqrt{m_D m_B}} = h_+(v+v')^\mu + h_-(v-v')^\mu \tag{501}$$

$$\frac{< D(v')|A^\mu|B(v) >}{\sqrt{m_D m_B}} = 0 \tag{502}$$

We can relate ISGW2 form factors with HQET form factors using $p = m_B v$ and $p' = m_D v'$. By comparing the coefficients of v^μ and v'^μ,

$$f_+ m_B + f_- m_B = \sqrt{m_D m_B}(h_+ + h_-) \tag{503}$$
$$f_+ m_D - f_- m_D = \sqrt{m_D m_B}(h_+ - h_-) \tag{504}$$

Thus

$$h_+ = \frac{m_B + m_D}{2\sqrt{m_D m_B}}\left(f_+ + \frac{m_B - m_D}{m_B + m_D} f_-\right) \tag{505}$$
$$h_- = \frac{m_B + m_D}{2\sqrt{m_D m_B}}\left(\frac{m_B - m_D}{m_B + m_D} f_+ + f_-\right) \tag{506}$$

Hence,

$$h_+ = \frac{1}{R}\left(f_+ + \frac{1-r}{1+r} f_-\right) \tag{507}$$
$$h_- = \frac{1}{R}\left(\frac{1-r}{1+r} f_+ + f_-\right) \tag{508}$$

The differential decay rate is given by

$$\frac{d\Gamma(B \to D\ell\nu)}{dw} = \frac{G_F^2 |V_{cb}|^2 m_B^5}{48\pi^3} r^3 (w^2 - 1)^{3/2} \mathcal{J}_D(w) \tag{509}$$

where

$$\mathcal{J}_D(w) = [(1+r)h_+ - (1-r)h_-]^2 \tag{510}$$

H.1.2 $B \to D^*\ell\nu$

In the ISGW2 model, the matrix elements are given by

$$< D^*(p', \varepsilon)|V^\mu|B(p) >= -ig(q^2)\epsilon^{\mu\nu\alpha\beta}\varepsilon^*_\nu (p+p')_\alpha (p-p')_\beta \tag{511}$$

$$< D^*(p', \varepsilon)|A^\mu|B(p) >= f(q^2)\varepsilon^{*\mu} + a_+(q^2)(\varepsilon^* \cdot p)(p+p')^\mu + a_-(q^2)(\varepsilon^* \cdot p)(p-p')^\mu \tag{512}$$

In HQET models,

$$\frac{< D^*(v', \varepsilon)|V^\mu|B(v) >}{\sqrt{m_{D^*} m_B}} = i h_V \epsilon^{\mu\nu\alpha\beta}\varepsilon^*_\nu v'_\alpha v_\beta \tag{513}$$

$$\frac{< D^*(v', \varepsilon)|A^\mu|B(v) >}{\sqrt{m_{D^*} m_B}} = h_{A_1}(w+1)\varepsilon^{*\mu} - (h_{A_2} v^\mu + h_{A_3} v'^\mu)(\varepsilon^* \cdot v) \tag{514}$$

We can relate ISGW2 form factors with HQET form factors using $p = m_B v$ and $p' = m_D v'$. First, we use $< D^*(p',\varepsilon)|V^\mu|B(p) >$. We can simplify

$$\begin{aligned}&\epsilon^{\mu\nu\alpha\beta}\varepsilon^*_\nu(p+p')_\alpha(p-p')_\beta = \epsilon^{\mu\nu\alpha\beta}\varepsilon^*_\nu(m_B v + m_{D^*}v')_\alpha(m_B v - m_{D^*}v')_\beta \\ &= -2m_B m_{D^*}\epsilon^{\mu\nu\alpha\beta}\varepsilon^*_\nu v_\alpha v'_\beta\end{aligned} \tag{515}$$

where we used the fact that $\epsilon^{\mu\nu\alpha\beta}$ is antisymmetric but $v_\alpha v_\beta$ and $v'_\alpha v'_\beta$ are symmetric between α and β. Thus,

$$2m_B m_{D^*} g = \sqrt{m_{D^*}m_B}\, h_V \tag{516}$$

Hence

$$h_V = 2\sqrt{m_{D^*}m_B}\, g = m_B R(1+r)g \tag{517}$$

Next, we use $< D^*(p',\varepsilon)|A^\mu|B(p) >$. By comparing the coefficient of $\varepsilon^{*\mu}$,

$$f = \sqrt{m_{D^*}m_B} h_{A_1}(w+1) = \frac{m_B R(1+r)}{2}(w+1)h_{A_1} \tag{518}$$

Thus

$$h_{A_1} = \frac{2}{m_B R(1+r)(w+1)} f \tag{519}$$

By comparing the coefficients of v^μ and v'^μ,

$$m_B a_+ + m_B a_- = \sqrt{m_{D^*}m_B} h_{A_2} \tag{520}$$

$$m_{D^*}a_+ - m_{D^*}a_- = \sqrt{m_{D^*}m_B} h_{A_3} \tag{521}$$

Thus

$$h_{A_3} + r h_{A_2} = \frac{m_{D^*}m_B}{\sqrt{m_{D^*}m_B}} \cdot 2a_+ = m_B R(1+r)a_+ \tag{522}$$

The differential decay rate is given by

$$\frac{d\Gamma(B \to D^*\ell\nu)}{dw} = \frac{G_F^2|V_{cb}|^2 m_B^5}{48\pi^3} r^3(w^2-1)^{1/2}\mathcal{J}_{D^*}(w) \tag{523}$$

where

$$\begin{aligned}\mathcal{J}_{D^*}(w) = {}& 2(1-2wr+r^2)\left[(w+1)^2 h_{A_1}^2 + (w^2-1)h_V^2\right] \\ &+ \left[(w+1)(w-r)h_{A_1} - (w^2-1)(h_{A_3}+r h_{A_2})\right]^2\end{aligned} \tag{524}$$

H.1.3 $B \to D_0^*\ell\nu$

In the ISGW2 model, the matrix elements are given by

$$< D_0^*(p')|V^\mu|B(p) >= 0 \tag{525}$$

$$< D_0^*(p')|A^\mu|B(p) >= u_+(q^2)(p+p')^\mu + u_-(q^2)(p-p')^\mu \tag{526}$$

In HQET models,

$$\frac{< D_0^*(v')|V^\mu|B(v) >}{\sqrt{m_{D_0^*}m_B}} = 0 \tag{527}$$

$$\frac{< D_0^*(v')|A^\mu|B(v) >}{\sqrt{m_{D_0^*} m_B}} = g_+(v+v')^\mu + g_-(v-v')^\mu \tag{528}$$

We can relate the form factors as we did in the $B \to D\ell\nu$ case

$$g_+ = \frac{1}{R}\left(u_+ + \frac{1-r}{1+r}u_-\right) \tag{529}$$

$$g_- = \frac{1}{R}\left(\frac{1-r}{1+r}u_+ + u_-\right) \tag{530}$$

The differential decay rate is given by

$$\frac{d\Gamma(B \to D_0^*\ell\nu)}{dw} = \frac{G_F^2|V_{cb}|^2 m_B^5}{48\pi^3} r^3 (w^2-1)^{3/2}\, \mathcal{J}_{D_0^*}(w) \tag{531}$$

where

$$\mathcal{J}_{D_0^*}(w) = [(1+r)g_+ - (1-r)g_-]^2 \tag{532}$$

H.1.4 $B \to D_1'\ell\nu$

In the ISGW2 model, the matrix elements are given by

$$< D_1'(p',\varepsilon)|V^\mu|B(p) >= l(q^2)\varepsilon^{*\mu} + c_+(q^2)(\varepsilon^*\cdot p)(p+p')^\mu + c_-(q^2)(\varepsilon^*\cdot p)(p-p')^\mu \tag{533}$$

$$< D_1'(p',\varepsilon)|A^\mu|B(p) >= -iq(q^2)\epsilon^{\mu\nu\alpha\beta}\varepsilon_\nu^*(p+p')_\alpha(p-p')_\beta \tag{534}$$

In HQET models,

$$\frac{< D_1'(v',\varepsilon)|V^\mu|B(v) >}{\sqrt{m_{D_1'} m_B}} = g_{V_1}\varepsilon^{*\mu} + (g_{V_2}v^\mu + g_{V_3}v'^\mu)(\varepsilon^*\cdot v) \tag{535}$$

$$\frac{< D_1(v',\varepsilon)|A^\mu|B(v) >}{\sqrt{m_{D_1} m_B}} = i g_A \epsilon^{\mu\nu\alpha\beta}\varepsilon_\nu^* v_\alpha v'_\beta \tag{536}$$

We can relate the form factors as we did in the $B \to D^*\ell\nu$ case

$$g_A = m_B R(1+r)q \tag{537}$$

and

$$g_{V_1} = \frac{2}{m_B R(1+r)} l \tag{538}$$

$$g_{V_3} + r g_{V_2} = m_B R(1+r)c_+ \tag{539}$$

The differential decay rate is given by

$$\frac{d\Gamma(B \to D_1'\ell\nu)}{dw} = \frac{G_F^2|V_{cb}|^2 m_B^5}{48\pi^3} r^3 (w^2-1)^{1/2}\, \mathcal{J}_{D_1'}(w) \tag{540}$$

where

$$\begin{aligned}\mathcal{J}_{D_1'}(w) = {} & \left[(w-r)g_{V_1} + (w^2-1)(g_{V_3}+r g_{V_2})\right]^2 \\ & +2(1-2rw+r^2)[g_{V_1}^2 + (w^2-1)g_A^2]\end{aligned} \tag{541}$$

H.1.5 $B \to D_1 \ell\nu$

In the ISGW2 model, the matrix elements are given by

$$< D_1'(p',\varepsilon)|V^\mu|B(p) >= r(q^2)\varepsilon^{*\mu} + s_+(q^2)(\varepsilon^*\cdot p)(p+p')^\mu + s_-(q^2)(\varepsilon^*\cdot p)(p-p')^\mu \quad (542)$$

$$< D_1'(p',\varepsilon)|A^\mu|B(p) >= -iv(q^2)\epsilon^{\mu\nu\alpha\beta}\varepsilon^*_\nu(p+p')_\alpha(p-p')_\beta \quad (543)$$

In HQET models,

$$\frac{< D_1(v',\varepsilon)|V^\mu|B(v) >}{\sqrt{m_{D_1} m_B}} = f_{V_1}\varepsilon^{*\mu} + (f_{V_2}v^\mu + f_{V_3}v'^\mu)(\varepsilon^*\cdot v) \quad (544)$$

$$\frac{< D_1(v',\varepsilon)|A^\mu|B(v) >}{\sqrt{m_{D_1} m_B}} = i f_A \epsilon^{\mu\nu\alpha\beta}\varepsilon^*_\nu v_\alpha v'_\beta \quad (545)$$

We can relate the form factors as we did in the $B \to D^*\ell\nu$ case

$$f_A = m_B R(1+r)v \quad (546)$$

and

$$f_{V_1} = \frac{2}{m_B R(1+r)} r \quad (547)$$

$$f_{V_3} + r f_{V_2} = m_B R(1+r) s_+ \quad (548)$$

The differential decay rate is given by

$$\frac{d\Gamma(B \to D_1\ell\nu)}{dw} = \frac{G_F^2 |V_{cb}|^2 m_B^5}{48\pi^3} r^3 (w^2-1)^{1/2}\, \mathcal{J}_{D_1}(w) \quad (549)$$

where

$$\begin{aligned}\mathcal{J}_{D_1}(w) = &\left[(w-r)f_{V_1} + (w^2-1)(f_{V_3} + r f_{V_2})\right]^2 \\ &+2(1-2rw+r^2)[f_{V_1}^2 + (w^2-1)f_A^2]\end{aligned} \quad (550)$$

H.1.6 $B \to D_2^*\ell\nu$

In the ISGW2 model, the matrix elements are given by

$$< D_2^*(p',\varepsilon)|V^\mu|B(p) >= -ih(q^2)\epsilon^{\mu\nu\alpha\beta}\varepsilon^*_{\nu\sigma}p^\sigma(p+p')_\alpha(p-p')_\beta \quad (551)$$

$$\begin{aligned}&< D_2^*(p',\varepsilon)|A^\mu|B(p) > \\ &= k(q^2)\varepsilon^{*\mu\alpha}p_\alpha + b_+(q^2)\varepsilon^*_{\alpha\beta}p^\alpha p^\beta(p+p')^\mu + b_-(q^2)\varepsilon^*_{\alpha\beta}p^\alpha p^\beta(p-p')^\mu\end{aligned} \quad (552)$$

In HQET models,

$$\frac{< D_2^*(v',\varepsilon)|V^\mu|B(v) >}{\sqrt{m_{D_2^*} m_B}} = i k_V \epsilon^{\mu\nu\alpha\beta}\varepsilon^*_{\nu\sigma}v^\sigma v_\alpha v'_\beta \quad (553)$$

$$\frac{< D_2^*(v',\varepsilon)|A^\mu|B(v) >}{\sqrt{m_{D_2^*} m_B}} = k_{A_1}\varepsilon^{*\mu\alpha}v_\alpha + (k_{A_2}v^\mu + k_{A_3}v'^\mu)\varepsilon^{*\alpha\beta}v_\alpha v'_\beta \quad (554)$$

We can relate the form factors as we did in the $B \to D^*\ell\nu$ case. Notice that we pick up an extra m_B from $\varepsilon^{*\mu\alpha}p_\alpha$.

$$k_V = m_B^2 R(1+r)v \tag{555}$$

and

$$k_{A_1} = \frac{2}{R(1+r)}r \tag{556}$$

$$k_{A_3} + rk_{A_2} = m_B^2 R(1+r)s_+ \tag{557}$$

The differential decay rate is given by

$$\frac{d\Gamma(B \to D_2^*\ell\nu)}{dw} = \frac{G_F^2|V_{cb}|^2 m_B^5}{48\pi^3} r^3(w^2-1)^{3/2}\, \mathcal{J}_{D_2^*}(w) \tag{558}$$

where

$$\begin{aligned}\mathcal{J}_{D_2^*}(w) = \frac{2}{3}&\left[(w-r)k_{A_1} + (w^2-1)(k_{A_3}+rk_{A_2})\right]^2 \\ &+(1-2rw+r^2)[k_{A_1}^2 + (w^2-1)k_V^2]\end{aligned} \tag{559}$$

H.2 Traditional notation

We summarize a traditional notation of form factors and decay rates as a reference.

H.2.1 $B \to D\ell\nu$

Traditionally, the form factors $F_0(q^2)$ and $F_1(q^2)$ are used.

$$\begin{aligned}&< D(p')|V^\mu|B(p) > \\ &= F_1(q^2)\left[(p+p')^\mu - \tfrac{m_B^2-m_D^2}{q^2}q^\mu\right] + F_0(q^2)\tfrac{m_B^2-m_D^2}{q^2}q^\mu\end{aligned} \tag{560}$$

where

$$q^\mu = p^\mu - p'^\mu \tag{561}$$

We can relate these form factors with $f_+(q^2)$ and $f_-(q^2)$

$$\begin{aligned}F_1(q^2) &= f_+(q^2) \\ F_0(q^2) &= f_+(q^2) + \tfrac{q^2}{m_B^2-m_D^2}f_-(q^2)\end{aligned} \tag{562}$$

The form factors $F_1(q^2)$ and $F_0(q^2)$ can be associated with the exchange of particles with quantum numbers $J^P = 1^-$ and $J^P = 0^+$, respectively. There is no singular behavior at $q^2 = 0$ because $F_1(0) = F_0(0)$. In practice the terms proportional to q^μ are nearly always negligible. Thus

$$< D(p')|V^\mu|B(p) >= F_1(q^2)(p+p')^\mu \tag{563}$$

or

$$< D(p')|V^\mu|B(p) >= f_+(q^2)(p+p')^\mu \tag{564}$$

The differential decay rate is given by

$$\begin{aligned}\frac{d\Gamma(B\to D\ell\nu)}{dq^2} &= \frac{G_F^2|V_{cb}|^2}{24\pi^3}|\vec{P}_D|^3|f_+(q^2)|^2\\ &= \frac{G_F^2|V_{cb}|^2}{192\pi^3 m_B^3}\left[(q^2-m_B^2-m_D^2)^2-4m_B^2m_D^2\right]^{3/2}|f_+(q^2)|^2\end{aligned} \tag{565}$$

where we used the following calculation. In the B rest frame,

$$p=(m_B,\vec{0}), \quad p'=(\sqrt{m_D^2+|\vec{P}_D|^2},\vec{p}') \tag{566}$$

Thus

$$\begin{aligned}&q^2=(p-p')^2=p^2+p'^2-2p\cdot p'=m_B^2+m_D^2-2m_B\sqrt{m_D^2+|\vec{P}_D|^2}\\ &\Rightarrow 4m_B^2\left(m_D^2+|\vec{P}_D|^2\right)=(q^2-m_B^2-m_D^2)^2\\ &\Rightarrow |\vec{P}_D|=\tfrac{1}{2m_B}\left[(q^2-m_B^2-m_D^2)^2-4m_B^2m_D^2\right]^{1/2}\end{aligned} \tag{567}$$

We can derive $\frac{d\Gamma(B\to D\ell\nu)}{dq^2}$ from $\frac{d\Gamma(B\to D\ell\nu)}{dw}$ (Equation (509)). Since

$$w=\frac{m_B^2+m_D^2-q^2}{2m_Bm_D} \quad\Rightarrow\quad dw=-\frac{dq^2}{2m_Bm_D} \tag{568}$$

the left-hand side is

$$\frac{d\Gamma(B\to D\ell\nu)}{dw}=2m_Bm_D\frac{d\Gamma(B\to D\ell\nu)}{dq^2} \tag{569}$$

where we removed a negative sign because it is not relevant to the decay rate, which is positive. The right-hand side is

$$\begin{aligned}&\frac{G_F^2|V_{cb}|^2m_B^5}{48\pi^3}r^3(w^2-1)^{3/2}|(1+r)h_+-(1-r)h_-|^2\\ &\quad=\frac{G_F^2|V_{cb}|^2m_B^5}{48\pi^3}\left(\frac{m_D}{m_B}\right)^3\left[\left(\frac{m_B^2+m_D^2-q^2}{2m_Bm_D}\right)^2-1\right]^{3/2}\\ &\qquad\times\left|\left(1+\frac{m_D}{m_B}\right)h_+-\left(1-\frac{m_D}{m_B}\right)h_-\right|^2\\ &=\frac{G_F^2|V_{cb}|^2}{48\pi^3}\frac{m_B^5m_D^3(m_B+m_D)^2}{m_B^3(8m_B^3m_D^3)m_B^2}[(m_B^2+m_D^2-q^2)^2-4m_B^2m_D^2]^{3/2}\\ &\qquad\times\left|h_+-\frac{m_B-m_D}{m_B+m_D}h_-\right|^2\\ &=\frac{G_F^2|V_{cb}|^2}{192\pi^3m_B^3}\frac{(m_B+m_D)^2}{2}[(m_B^2+m_D^2-q^2)^2-4m_B^2m_D^2]^{3/2}\\ &\qquad\times\left|\frac{2\sqrt{m_Bm_D}}{m_B+m_D}f_+\right|^2\\ &=2m_Bm_D\frac{G_F^2|V_{cb}|^2}{192\pi^3m_B^3}[(m_B^2+m_D^2-q^2)^2-4m_B^2m_D^2]^{3/2}|f_+|^2\end{aligned} \tag{570}$$

Thus, we recover

$$\frac{d\Gamma(B \to D\ell\nu)}{dq^2} = \frac{G_F^2 |V_{cb}|^2}{192\pi^3 m_B^3} [(m_B^2 + m_D^2 - q^2)^2 - 4m_B^2 m_D^2]^{3/2} |f_+|^2 \tag{571}$$

H.2.2 $B \to D^* \ell\nu$

In this case

$$< D^*(p', \varepsilon)|V^\mu|B(p) >= \frac{2i\epsilon^{\mu\nu\alpha\beta}}{m_B + m_{D^*}} \varepsilon_\nu^* p'_\alpha p_\beta V(q^2) \tag{572}$$

and

$$\begin{aligned} < D^*(p', \varepsilon)|A^\mu|B(p) >= -(m_B + m_{D^*})\varepsilon^{*\mu} A_1(q^2) \\ + \frac{\varepsilon^* \cdot q}{m_B + m_{D^*}} (p + p')^\mu A_2(q^2) \\ +2m_{D^*} \frac{\varepsilon^* \cdot q}{q^2} q^\mu A_3(q^2) \\ -2m_{D^*} \frac{\varepsilon^* \cdot q}{q^2} q^\mu A_0(q^2) \end{aligned} \tag{573}$$

where

$$A_3(q^2) = \frac{m_B + m_{D^*}}{2m_{D^*}} A_1(q^2) - \frac{m_B - m_{D^*}}{2m_{D^*}} A_2(q^2) \tag{574}$$

with $A_0(0) = A_3(0)$. The form factors $A_1(q^2)$ and $A_2(q^2)$ can be associated with the exchange of particles with quantum numbers $J^P = 1^+$, whereas $V(q^2)$ is associated with $J^P = 1^-$.
We can relate these form factors with $g(q^2)$, $f(q^2)$, $a_+(q^2)$ and $a_-(q^2)$

$$\begin{aligned} V(q^2) &= (m_B + m_{D^*}) g(q^2) \\ A_1(q^2) &= \tfrac{1}{m_B + m_{D^*}} f(q^2) \\ A_2(q^2) &= (m_B + m_{D^*}) a_+(q^2) \\ A_3(q^2) - A_0(q^2) &= \tfrac{q^2}{2m_{D^*}} a_-(q^2) \end{aligned} \tag{575}$$

Here, we used

$$\begin{aligned} \epsilon^{\mu\nu\alpha\beta} p_\alpha p_\beta &= \epsilon^{\mu\nu\alpha\beta} p'_\alpha p'_\beta = 0 \\ \epsilon^{\mu\nu\alpha\beta} p_\alpha p'_\beta &= -\epsilon^{\mu\nu\alpha\beta} p'_\alpha p_\beta \end{aligned} \tag{576}$$

Again, terms proportional to q^μ only play an important role only for the case $l = \tau$. Thus those are negligible in our case

$$\begin{aligned} < D^*(p', \varepsilon)|A^\mu|B(p) >= -(m_B + m_{D^*})\varepsilon^{*\mu} A_1(q^2) \\ + \frac{\varepsilon^* \cdot q}{m_B + m_{D^*}} (p + p')^\mu A_2(q^2) \end{aligned} \tag{577}$$

or

$$< D^*(p', \varepsilon)|A^\mu|B(p) >= \varepsilon^{*\mu} f(q^2) + \varepsilon^* \cdot q (p + p')^\mu a_+(q^2) \tag{578}$$

H.3 ISGW2 model

ISGW2 model [33][34] is a quark model before the Heavy Quark Effective Theory (HQET) Form Factors (FF) are developed. It provides a method to calculate $B \to D^{(*,**)}\ell\nu$ decay FF. In this model, the quark-model B and D masses are defined as

$$\begin{aligned}\tilde{m}_B &= m_b + m_u = m_b + m_d \\ \tilde{m}_D &= m_c + m_u = m_c + m_d\end{aligned} \tag{579}$$

where m_u, m_d, m_c and m_b are u, d, c and b quark masses, respectively. In ISGW2 model,

$$\begin{aligned}m_d &= m_u = 0.33\text{GeV} \\ m_c &= 1.82\text{GeV} \\ m_b &= 5.20\text{GeV}\end{aligned} \tag{580}$$

are used. Using, these quark masses, ISGW2 define

$$\mu_\pm = \left(\frac{1}{m_c} \pm \frac{1}{m_b}\right)^{-1} \tag{581}$$

The hyperfine-averaged physical mass of a HQS multiplet with light degrees of freedom having angular momentum j_l is

$$\bar{m}_{j_l} = \frac{j_l+1}{2j_l+1} m_{J=j_l+\frac{1}{2}} + \frac{j_l}{2j_l+1} m_{J=j_l-\frac{1}{2}} \tag{582}$$

For example

$$\begin{aligned}\bar{m}_B &= \tfrac{3}{4}m_B + \tfrac{1}{4}m_{B^*} = 5.31 \\ \bar{m}_D &= \bar{m}_{D^*} = \tfrac{3}{4}m_D + \tfrac{1}{4}m_{D^*} \\ \bar{m}_{D_0^*} &= \bar{m}_{D_1'} = \tfrac{3}{4}m_{D_1'} + \tfrac{1}{4}m_{D_0^*} \\ \bar{m}_{D_1} &= \bar{m}_{D_2^*} = \tfrac{5}{8}m_{D_2^*} + \tfrac{3}{8}m_{D_1}\end{aligned} \tag{583}$$

where

$$\begin{aligned}m_B &= 5.27\text{GeV}, \quad m_{B^*} = 5.33\text{GeV} \\ m_D &= 1.87\text{GeV}, \quad m_{D^*} = 2.01\text{GeV} \\ m_{D_0^*} &= 2.40\text{GeV}, \quad m_{D_1'} = 2.49\text{GeV} \\ m_{D_1} &= 2.42\text{GeV}, \quad m_{D_2^*} = 2.46\text{GeV}\end{aligned} \tag{584}$$

There are also parameters β in the wave functions, and those values in the ISGW2 model are

$$\begin{aligned}\beta_B &= 0.431\text{GeV} \\ \beta_D &= 0.45\text{GeV} \\ \beta_{D^*} &= 0.38\text{GeV} \\ \beta_{D^{**}} &= 0.33\text{GeV}\end{aligned} \tag{585}$$

Also, β^2_{BX} ($X = D$, D^* or D^{**}) is defined as

$$\beta^2_{BX} \equiv \frac{1}{2}(\beta^2_B + \beta^2_X) \tag{586}$$

The momentum transfer is

$$t = (p_B - p_D)^2 = q^2 \tag{587}$$

and the maximum momentum transfer is

$$t_m = (m_B - m_D)^2 \tag{588}$$

where m_D can be m_{D^*} or $m_{D^{**}}$.
In ISGW2 model, the factor $F^{(\alpha)}_n$ is defined as

$$F^{(\alpha)}_n = \left(\frac{\bar{m}_B}{\tilde{m}_B}\right)^{n_B(\alpha)} \left(\frac{\bar{m}_D}{\tilde{m}_D}\right)^{n_X(\alpha)} \left(\frac{\tilde{m}_D}{\tilde{m}_B}\right)^{1/2} \left(\frac{\beta_B\beta_D}{\beta^2_{BD}}\right)^{n/2} \left[1 + \frac{1}{6N} r^2(t_m - t)\right]^{-N} \tag{589}$$

where $N = 2 + n + n'$. n and n' are the harmonic oscillator quantum numbers of the initial and final wave-functions. Therefore, $N = 2$ for S wave to S wave ($B \to D$ or D^*), and $N = 3$ for S wave to P wave ($B \to D^{**}$). $n_B(\alpha)$ and $n_X(\alpha)$ is given in the table

Form factors (α)	$n_B(\alpha)$	$n_X(\alpha)$
$f_+ + f_-$	-1/2	+1/2
$f_+ - f_-$	+1/2	-1/2
g	-1/2	-1/2
f	+1/2	+1/2
$a_+ + a_-$	-3/2	+1/2
$a_+ - a_-$	-1/2	-1/2
$u_+ + u_-$	-1/2	+1/2
$u_+ - u_-$	+1/2	-1/2
$l_{(3/2,1/2)}, r$	+1/2	+1/2
$c_{+(3/2,1/2)} + c_{-(3/2,1/2)}, s_+ + s_-$	-3/2	+1/2
$c_{+(3/2,1/2)} - c_{-(3/2,1/2)}, s_+ - s_-$	-1/2	-1/2
$q_{(3/2,1/2)}, v$	-1/2	-1/2
h	-3/2	-1/2
k	-1/2	+1/2
$b_+ + b_-$	-5/2	+1/2
$b_+ - b_-$	-3/2	-1/2

The form factors in this table are defined later. r^2 is

$$r^2 = \frac{3}{4m_b m_c} + \frac{3m^2_d}{2\bar{m}_B\bar{m}_D\beta^2_{BD}} + \frac{1}{\bar{m}_B\bar{m}_D}\left(\frac{16}{33 - 2N_f}\right) \ln\left[\frac{\alpha_s(\mu_{QM})}{\alpha_s(m_c)}\right] \tag{590}$$

where, if a scale $\mu < 0.6$ GeV,

$$\alpha_s(\mu) = 0.6 \tag{591}$$

and if $\mu > 0.6$ GeV,

$$\alpha_s(\mu) = \frac{12\pi}{33 - 2N_f}\left[\ln\left(\frac{\mu^2}{\Lambda^2_{QCD}}\right)\right]^{-1} \tag{592}$$

where N_f is the number of active flavors below the scale μ. For $\mu = m_c$, $N_f = 3$, and for $\mu = m_b$, $N_f = 4$. Thus, $N_f = 3$ for $b \to c$ decays. The constants in the above equations are

$$\begin{aligned} \mu_{QM} &= 0.1\text{GeV} \\ \Lambda^2_{QCD} &= 0.04\text{GeV}^2 \end{aligned} \tag{593}$$

The factor $R^{(\alpha)}$ is defined as

$$R^{(\alpha)} = C_{cb}\left[f^{(\alpha)} + \tilde{\beta}^{(\alpha)}_{cb}(w)\frac{\alpha_s\left(\sqrt{m_b m_c}\right)}{\pi}\right] \tag{594}$$

where $f^{(\alpha)} = 0$ for $a_+ + a_-$ and $f^{(\alpha)} = 1$ for others.
Here

$$C_{cb} = \left[\frac{\alpha_s(m_b)}{\alpha_s(m_c)}\right]^{a_I}\left[\frac{\alpha_s(m_c)}{\alpha_s(\mu_{QM})}\right]^{a_L(w)} \tag{595}$$

is independent of α and has

$$a_I = -\frac{6}{33 - 2N_f} \tag{596}$$

and

$$a_L(w) = -\frac{8}{33 - 2N'_f}[wr(w) - 1] \tag{597}$$

with

$$r(w) = \frac{1}{\sqrt{w^2 - 1}}\ln\left(w + \sqrt{w^2 - 1}\right) \tag{598}$$

and

$$w = 1 + \frac{t_m - t}{2m_B m_D} \tag{599}$$

where m_D may be m^*_D or m^{**}_D depending on the decay modes. N_f is the number of active flavors below the scale m_b and N'_f is the number of active flavors below the scale m_c. Thus, $N_f = 4$ and $N'_f = 3$. In ISGW2, $\tilde{w}$ is defined as

$$\tilde{w} = 1 + \frac{t_m - t}{2\bar{m}_B\bar{m}_D} \tag{600}$$

For w near 1

$$\left[\frac{\alpha_s(m_c)}{\alpha_s(\mu_{QM})}\right]^{a_L(w)} = 1 - \frac{2}{3}\left(\frac{8}{33 - 2N'_f}\right)\ln\left[\frac{\alpha_s(\mu_{QM})}{\alpha_s(m_c)}\right](w - 1) \tag{601}$$

In SP5/SP6, $\left[\frac{\alpha_s(m_c)}{\alpha_s(\mu_{QM})}\right]^{a_L(w)} = 1$ was used.

At $w = 1$, $\tilde{\beta}_{cb}$ are

$$\begin{array}{l}
\tilde{\beta}_{cb}^{(f_+ + f_-)}(1) = \gamma_{cb} - \frac{2}{3}\chi_{cb} \\
\tilde{\beta}_{cb}^{(f_+ - f_-)}(1) = \gamma_{cb} + \frac{2}{3}\chi_{cb} \\
\tilde{\beta}_{cb}^{(g)}(1) = \gamma_{cb} + \frac{2}{3} \\
\tilde{\beta}_{cb}^{(f)}(1) = \gamma_{cb} - \frac{2}{3} \\
\tilde{\beta}_{cb}^{(a_+ + a_-)}(1) = -1 - \chi_{cb} + \frac{4}{3}\frac{1}{(1-z_{cb})} + \frac{2}{3}\frac{1+z_{cb}}{(1-z_{cb})^2}\gamma_{cb} \\
\tilde{\beta}_{cb}^{(a_+ - a_-)}(1) = -\frac{1}{3} - \chi_{cb} + \frac{4}{3}\frac{1}{(1-z_{cb})} + \left[1 - \frac{2}{3}\frac{1+z_{cb}}{(1-z_{cb})^2}\right]\gamma_{cb}
\end{array} \tag{602}$$

where

$$\gamma_{cb} = \frac{2z_{cb}}{1-z_{cb}} \ln\left(\frac{1}{z_{cb}}\right) - 2 \tag{603}$$

and

$$\chi_{cb} = -1 - \frac{\gamma_{cb}}{1-z_{cb}} \tag{604}$$

with

$$z_{cb} = \frac{m_c}{m_b} \tag{605}$$

w dependence of $\tilde{\beta}$ is weak and negligible.

In ISGW [34], LL-coupling was used, and ISGW2 [33] also follows the convention. But, ISGW2 aware that jj-coupling is a better representation of heavy-light mesons. Thus, ISGW2 also gives jj-coupling type of form factors for D_1 and D_1'.

H.3.1 $B \to D\ell\nu$ (1^2S_0)

Matrix element is

$$< D(p')|V^\mu|B(p) >= f_+(q^2)(p+p')^\mu + f_-(q^2)(p-p')^\mu \tag{606}$$

where f_+ and f_- are the form factors. These are calculated as follows :

$$f_+ + f_- = \left[2 - \frac{\tilde{m}_D}{m_c}\left(1 - \frac{m_d m_c}{2\mu_+ \tilde{m}_D}\frac{\beta_B^2}{\beta_{BD}^2}\right)\right] F_3^{(f_+ + f_-)} R^{(f_+ + f_-)} \tag{607}$$

and

$$f_+ - f_- = \frac{\tilde{m}_B}{m_c}\left(1 - \frac{m_d m_c}{2\mu_+ \tilde{m}_D}\frac{\beta_B^2}{\beta_{BD}^2}\right) F_3^{(f_+ - f_-)} R^{(f_+ - f_-)} \tag{608}$$

Thus, we get f_+ and f_- from these two equations. For example,

$$f_+ = \frac{(f_+ + f_-) + (f_+ - f_-)}{2} \tag{609}$$

H.3.2 $B \to D^* \ell\nu$ (1^3S_0)

Matrix element is

$$< D^*(p', \varepsilon)|V^\mu|B(p) >= i\epsilon^{\mu\nu\alpha\beta}\varepsilon^*_\nu (p+p')_\alpha (p-p')_\beta g(q^2) \tag{610}$$

and

$$< D^*(p', \varepsilon)|A^\mu|B(p) >= \varepsilon^{*\mu} f(q^2) + \varepsilon^* \cdot p(p+p')^\mu a_+(q^2) + \varepsilon^* \cdot p(p-p')^\mu a_-(q^2) \tag{611}$$

Form factors g, f, a_+ and a_- are given by the following equations.

$$f = C_f \tilde{m}_B \left[(1+\tilde{w}) + \frac{m_d(\tilde{w}-1)}{2\mu_+}\right] F_3^{(f)} R^{(f)} \tag{612}$$

where $C_f = 0.989$ for $B \to D^*$.

$$g = \frac{1}{2}\left[\frac{1}{m_c} - \frac{m_d \beta_B^2}{2\mu_- \tilde{m}_D \beta_{BD}^2}\right] F_3^{(g)} R^{(g)} \tag{613}$$

$$\begin{aligned} &a_+ + a_- \\ &= C_{cb}\left[\frac{m_d}{(1+\tilde{w})m_c m_b}\frac{\beta_D^2}{\beta_{BD}^2}\left(1 - \frac{m_d}{2\tilde{m}_B}\frac{\beta_D^2}{\beta_{BD}^2}\right) + \tilde{\beta}^{(a_+ + a_-)}\frac{\alpha_s}{\pi}\tilde{m}_B\right] \\ &\qquad F_3^{(a_+ + a_-)} \end{aligned} \tag{614}$$

$$\begin{aligned} &a_+ - a_- \\ &= -\frac{1}{\tilde{m}_D}\left[\frac{\tilde{m}_B}{m_b} - \frac{m_d}{2\mu_+}\frac{\beta_D^2}{\beta_{BD}^2} + \frac{\tilde{w} m_d \tilde{m}_B}{(1+\tilde{w})m_c m_b}\frac{\beta_D^2}{\beta_{BD}^2}\left(1 - \frac{m_d}{2\tilde{m}_B}\frac{\beta_D^2}{\beta_{BD}^2}\right)\right] \\ &\qquad F_3^{(a_+ - a_-)} R^{(a_+ - a_-)} \end{aligned} \tag{615}$$

H.3.3 $B \to D_0^* \ell\nu$ (1^3P_0)

Matrix element is

$$< D_0^*(p')|V^\mu|B(p) >= 0 \tag{616}$$

and

$$< D_0^*(p')|A^\mu|B(p) >= u_+(q^2)(p+p')^\mu + u_-(q^2)(p-p')^\mu \tag{617}$$

Form factors u_+ and u_- are given by the following two equations.

$$u_+ + u_- = -\sqrt{\frac{2}{3}}\frac{m_d}{\beta_B} F_5^{(u_+ + u_-)} \tag{618}$$

$$u_+ - u_- = \sqrt{\frac{2}{3}}\frac{m_d \tilde{m}_B}{\beta_B \tilde{m}_D} F_5^{(u_+ - u_-)} \tag{619}$$

H.3.4 $B \to D_1' \ell \nu$ (1^3P_1)

Matrix element is

$$< D_1'(p', \varepsilon)|V^\mu|B(p) >= \varepsilon^{*\mu} l(q^2) + \varepsilon^* \cdot p(p+p')^\mu c_+(q^2) + \varepsilon^* \cdot p(p-p')^\mu c_-(q^2) \quad (620)$$

and

$$< D_1'(p', \varepsilon)|A^\mu|B(p) >= i\epsilon^{\mu\nu\alpha\beta} \varepsilon^*_\nu (p+p')_\alpha (p-p')_\beta q(q^2) \quad (621)$$

Form factors l, c_+, c_- and q are given by the following equations.

$$q = -\frac{m_d}{2\tilde{m}_D \beta_B} \left(\frac{5+\tilde{w}}{6} \right) F_5^{(q)} \quad (622)$$

$$l = -\tilde{m}_B \beta_B \left[\frac{1}{\mu_-} + \frac{m_d \tilde{m}_D (\tilde{w}-1)}{\beta_B^2} \left(\frac{5+\tilde{w}}{6m_c} - \frac{1}{2\mu_-} \frac{m_d}{\tilde{m}_D} \frac{\beta_B^2}{\beta_{BD}^2} \right) \right] F_5^{(l)} \quad (623)$$

$$c_+ + c_- = -\frac{m_d \tilde{m}_D}{2m_c \tilde{m}_B \beta_B} \left(1 - \frac{m_d m_c}{2\tilde{m}_D \mu_-} \frac{\beta_B^2}{\beta_{BD}^2} \right) F_5^{(c_+ + c_-)} \quad (624)$$

$$c_+ - c_- = -\frac{m_d \tilde{m}_D}{2m_c \tilde{m}_B \beta_B} \left(\frac{\tilde{w}+2}{3} - \frac{m_d m_c}{2\tilde{m}_D \mu_-} \frac{\beta_B^2}{\beta_{BD}^2} \right) F_5^{(c_+ - c_-)} \quad (625)$$

H.3.5 $B \to D_1 \ell \nu$ (1^1P_1)

Matrix element is

$$< D_1'(p', \varepsilon)|V^\mu|B(p) >= \varepsilon^{*\mu} r(q^2) + \varepsilon^* \cdot p(p+p')^\mu s_+(q^2) + \varepsilon^* \cdot p(p-p')^\mu s_-(q^2) \quad (626)$$

and

$$< D_1'(p', \varepsilon)|A^\mu|B(p) >= i\epsilon^{\mu\nu\alpha\beta} \varepsilon^*_\nu (p+p')_\alpha (p-p')_\beta v(q^2) \quad (627)$$

Form factors r, s_+, s_- and v are given by the following equations.

$$v = \left[\frac{\tilde{m}_B \beta_B}{4\sqrt{2} m_b m_c \tilde{m}_D} + \frac{(\tilde{w}-1)}{6\sqrt{2}} \frac{m_d}{\tilde{m}_D \beta_B} \right] F_5^{(v)} \quad (628)$$

$$r = \frac{\tilde{m}_B \beta_B}{\sqrt{2}} \left[\frac{1}{\mu_+} + \frac{m_d \tilde{m}_D}{3m_c \beta_B^2} (\tilde{w}-1)^2 \right] F_5^{(r)} \quad (629)$$

$$s_+ + s_- = \frac{m_d}{\sqrt{2} \tilde{m}_B \beta_B} \left(1 - \frac{m_d}{m_c} + \frac{m_d}{2\mu_+} \frac{\beta_B^2}{\beta_{BD}^2} \right) F_5^{(s_+ + s_-)} \quad (630)$$

$$s_+ - s_- = \frac{m_d}{\sqrt{2} m_c \beta_B} \left(\frac{4-\tilde{w}}{3} - \frac{m_d m_c}{2\tilde{m}_D \mu_+} \frac{\beta_B^2}{\beta_{BD}^2} \right) F_5^{(s_+ - s_-)} \quad (631)$$

H.3.6 $B \to D_2^* \ell \nu$ $(1^3 P_2)$

Matrix element is

$$< D_2^*(p', \varepsilon)|V^\mu|B(p) >= i\epsilon^{\mu\nu\alpha\beta}\varepsilon^*_{\nu\sigma}p^\sigma(p+p')_\alpha(p-p')_\beta h(q^2) \tag{632}$$

and

$$\begin{aligned} &< D_2^*(p', \varepsilon)|A^\mu|B(p) > \\ &= \varepsilon^{*\mu\sigma}p_\sigma k(q^2) + \varepsilon^*_{\alpha\beta}p^\alpha p^\beta (p+p')^\mu b_+(q^2) + \varepsilon^*_{\alpha\beta}p^\alpha p^\beta (p-p')^\mu b_-(q^2) \end{aligned} \tag{633}$$

Form factors h, b_+, b_- and k are given by the following equations.

$$h = \frac{m_d}{2\sqrt{2}\tilde{m}_B\beta_B}\left[\frac{1}{m_c} - \frac{m_d\beta_B^2}{2\mu_-\tilde{m}_D\beta_{BD}^2}\right]F_5^{(h)} \tag{634}$$

$$k = \frac{m_d}{\sqrt{2}\beta_B}(1+\tilde{w})F_5^{(k)} \tag{635}$$

$$b_+ + b_- = \frac{m_d^2}{4\sqrt{2}m_c m_b \tilde{m}_B\beta_B}\frac{\beta_D^2}{\beta_{BD}^2}\left(1 - \frac{m_d}{2\tilde{m}_B}\frac{\beta_D^2}{\beta_{BD}^2}\right)F_5^{(b_+ + b_-)} \tag{636}$$

$$\begin{aligned} &b_+ - b_- \\ &= -\frac{m_d}{\sqrt{2}m_b\tilde{m}_D\beta_B}\left[1 - \frac{m_d m_b}{2\mu_+\tilde{m}_B}\frac{\beta_D^2}{\beta_{BD}^2} + \frac{m_d}{4m_c}\frac{\beta_D^2}{\beta_{BD}^2}\left(1 - \frac{m_d}{2\tilde{m}_B}\frac{\beta_D^2}{\beta_{BD}^2}\right)\right] \\ &\qquad F_5^{(b_+ - b_-)} \end{aligned} \tag{637}$$

H.3.7 $B \to D_1^* \ell \nu$ $(\frac{1}{2}^+)$

Form factors are

$$q_{1/2} = \sqrt{\frac{1}{6}}\frac{m_d}{\tilde{m}_D\beta_B}\left(1 - \frac{\beta_B^2\tilde{m}_B}{4m_d m_c m_b}\right)F_5^{(q_{1/2})} \tag{638}$$

$$l_{1/2} = \sqrt{\frac{2}{3}}\tilde{m}_B\beta_B\left[\frac{1}{2m_c} - \frac{3}{2m_b} + \frac{m_d\tilde{m}_D(\tilde{w}-1)}{\beta_B^2}\left(\frac{1}{m_c} - \frac{1}{2\mu_-}\frac{m_d}{\tilde{m}_D}\frac{\beta_B^2}{\beta_{BD}^2}\right)\right]F_5^{(l_{1/2})} \tag{639}$$

$$c_{1/2+} + c_{1/2-} = \frac{m_d^2\beta_D^2}{\sqrt{6}m_c\tilde{m}_B\beta_B\beta_{BD}^2}F_5^{(c_{1/2+}+c_{1/2-})} \tag{640}$$

$$c_{1/2+} - c_{1/2-} = -\sqrt{\frac{2}{3}}\frac{m_d}{2\tilde{m}_D\beta_B}\left(1 + \frac{m_d}{2m_c}\frac{\beta_D^2}{\beta_{BD}^2}\right)F_5^{(c_{1/2+}-c_{1/2-})} \tag{641}$$

H.3.8 $B \to D_1\ell\nu$ ($\frac{3}{2}^+$)

Form factors are

$$q_{3/2} = -\frac{1}{2\sqrt{3}}\frac{m_d}{\tilde{m}_D\beta_B}\left(\frac{1+\tilde{w}}{2} + \frac{\beta_B^2\tilde{m}_B}{2m_d m_c m_b}\right) F_5^{(q_{3/2})} \tag{642}$$

$$l_{3/2} = -\frac{2}{\sqrt{3}}\tilde{m}_B\beta_B\left[\frac{1}{m_c} + \frac{m_d\tilde{m}_D(\tilde{w}-1)}{2\beta_B^2}\left(\frac{\tilde{w}+1}{2m_c} - \frac{1}{2\mu_-}\frac{m_d}{\tilde{m}_D}\frac{\beta_B^2}{\beta_{BD}^2}\right)\right] F_5^{(l_{3/2})} \tag{643}$$

$$c_{3/2+} + c_{3/2-} = -\frac{\sqrt{3}m_d}{2\tilde{m}_B\beta_B}\left[1 - \frac{m_d}{2m_c} - \frac{m_d}{3}\frac{\beta_B^2}{\beta_{BD}^2}\left(\frac{1}{2\mu_-} - \frac{1}{\mu_+}\right)\right] F_5^{(c_{3/2+}+c_{3/2-})} \tag{644}$$

$$c_{3/2+} - c_{3/2-} = -\frac{m_d}{2\sqrt{3}\tilde{m}_D\beta_B}\left[\frac{(2-\tilde{w})\tilde{m}_D}{m_c} + \frac{m_d\beta_B^2}{\beta_{BD}^2}\left(\frac{1}{2\mu_-} - \frac{1}{\mu_+}\right)\right] F_5^{(c_{3/2+}-c_{3/2-})} \tag{645}$$

H.4 HQET model

Details of HQET model is described in [35][36]. We will summarize the part which is related to our analysis.

H.4.1 $B \to D\ell\nu$

In heavy quark limit, the form factors $h_+(w)$ and $h_-(w)$ are

$$h_+(w) = \xi(w), \;\; h_-(w) = 0 \tag{646}$$

where $\xi(w)$ is the Isgur-Wise Function.

$$\xi(w) = \xi(1)[1 - \rho_D^2(w-1)] \tag{647}$$

where ρ_D^2 is the form factor slope. $h_+(1) = \xi(1)$ can be calculated by the Lattice QCD.

H.4.2 $B \to D^*\ell\nu$

The kinematic variables in $B \to D^*\ell\nu$ decays are shown in Figure 62.

- θ_ℓ : Angle between the directions of "the ℓ in the W rest frame" and "the W in the B rest frame".
- θ_V : Angle between the directions of "the D in the D^* rest frame" and "the D^* in the B rest frame".
- χ : Azimuthal angle between the planes formed by "W-ℓ system" and "$D^* - D$ system".

Form factors $V(q^2)$, $A_1(q^2)$ and $A_2(q^2)$ are related to helicity form factors $H_0(q^2)$, $H_+(q^2)$ and $H_-(q^2)$, which correspond to the three allowed polarization state of D^* (one longitudinal and two transverse). A_1 contributes to all three helicity components, A_2 contributes only to the helicity-zero component and V contributes only to the helicity ± 1 components

$$H_+(q^2) = (m_B + m_{D^*})A_1(q^2) - \frac{\sqrt{(q^2 - m_B^2 - m_{D^*}^2)^2 - 4m_B^2 m_{D^*}^2}}{m_B + m_{D^*}} V(q^2) \tag{648}$$

$$H_-(q^2) = (m_B + m_{D^*})A_1(q^2) + \frac{\sqrt{(q^2 - m_B^2 - m_{D^*}^2)^2 - 4m_B^2 m_{D^*}^2}}{m_B + m_{D^*}} V(q^2) \tag{649}$$

$$\begin{aligned} H_0(q^2) = \frac{1}{2m_{D^*}\sqrt{q^2}} \Big[&(m_B^2 - m_{D^*}^2 - q^2)(m_B + m_{D^*})A_1(q^2) \\ &- \frac{(q^2 - m_B^2 - m_{D^*}^2)^2 - 4m_B^2 m_{D^*}^2}{m_B + m_{D^*}} A_2(q^2) \Big] \end{aligned} \tag{650}$$

Differential decay rate is given in terms of the helicity form factors,

$$\begin{aligned} \frac{d\Gamma(B \to D^* \ell\nu)}{dw d\cos\theta_V d\cos\theta_\ell d\chi} = & \frac{3G_F^2}{4(4\pi)^4} |V_{cb}|^2 m_B m_{D^*}^2 \sqrt{w^2-1}(1 - 2wr + r^2) \times \\ & [(1 - \cos\theta_\ell)^2 \sin^2\theta_V |H_+(w)|^2 \\ & +(1 + \cos\theta_\ell)^2 \sin^2\theta_V |H_-(w)|^2 \\ & +4\sin^2\theta_\ell \cos^2\theta_V |H_0(w)|^2 \\ & -4\sin\theta_\ell(1 - \cos\theta_\ell)\sin\theta_V\cos\theta_V\cos\chi H_+(w)H_0(w) \\ & +4\sin\theta_\ell(1 + \cos\theta_\ell)\sin\theta_V\cos\theta_V\cos\chi H_-(w)H_0(w) \\ & -2\sin^2\theta_\ell \sin^2\theta_V \cos 2\chi H_+(w)H_-(w)] \end{aligned} \tag{651}$$

$H_i(w)$ are

$$H_i = -m_B \frac{R^*(1 - r^2)(w + 1)}{2\sqrt{1 - 2wr + r^2}} h_{A_1}(w) \widetilde{H}_i(w) \tag{652}$$

$h_{A_1}(w)$ is

$$h_{A_1}(w) = h_{A_1}(1) \left[1 - \rho^2(w - 1)\right] \tag{653}$$

where ρ^2 is the form factor slope, and $\widetilde{H}_i(w)$ are

$$\begin{aligned} \widetilde{H}_\pm(w) &= \tfrac{\sqrt{1-2wr+r^2}}{1-r} \left(1 \mp \sqrt{\tfrac{w-1}{w+1}} R_1(w)\right) \\ \widetilde{H}_0(w) &= 1 + \tfrac{w-1}{1-r}\left(1 - R_2(w)\right) \end{aligned} \tag{654}$$

where R_1 and R_2 are the form factor ratios.

$$R_1 = \frac{h_V}{h_{A_1}}, \quad R_2 = \frac{h_{A_3} + r h_{A_2}}{h_{A_1}} \tag{655}$$

To make the notation simple, we define

$$
\begin{aligned}
& c_L \equiv \cos\theta_\ell \\
& c_V \equiv \cos\theta_V \\
& \tilde{h}_\pm(w) \equiv (1-r)\widetilde{H}_\pm(w) = \sqrt{1-2wr+r^2}\left(1 \mp \sqrt{\tfrac{w-1}{w+1}}R_1\right) \\
& \tilde{h}_0(w) \equiv (1-r)\widetilde{H}_0(w) = (1-r) + (w-1)\,(1-R_2)
\end{aligned}
\tag{656}
$$

then

$$
\frac{d\Gamma(B \to D^*\ell\nu)}{dw dc_V dc_L d\chi} = f(w)\ \ [h_{A_1}(w)]^2\, g(w) \tag{657}
$$

where

$$
\begin{aligned}
f(w) &\equiv \frac{3G_F^2}{4(4\pi)^4}|V_{cb}|^2 m_B m_{D^*}^2 \sqrt{w^2-1}(1-2wr+r^2) \times \\
&\qquad\qquad \left[m_B \frac{2\sqrt{m_B m_{D^*}}}{m_B+m_{D^*}} \frac{(1-r^2)(w+1)}{2\sqrt{1-2wr+r^2}} \frac{1}{(1-r)}\right]^2 \\
&= \frac{3G_F^2}{4(4\pi)^4}|V_{cb}|^2 \frac{m_B^4 m_{D^*}^3}{(m_B+m_{D^*})^2}(1+r)^2(w+1)^2\sqrt{w^2-1} \\
&= \frac{3G_F^2|V_{cb}|^2}{1024\pi^4}\frac{m_B^5 r^3}{(1+r)^2}(1+r)^2(w+1)^2\sqrt{w^2-1} \\
&= \frac{G_F^2|V_{cb}|^2 m_B^5}{48\pi^3} r^3 (w^2-1)^{1/2} \times \frac{9}{64\pi}(w+1)^2
\end{aligned}
\tag{658}
$$

and

$$
\begin{aligned}
g(w) \;=\; & [(1-c_L)^2(1-c_V^2)\tilde{h}_+^2 + (1+c_L)^2(1-c_V^2)\tilde{h}_-^2 \\
& +4(1-c_L^2)c_V^2\tilde{h}_0^2 - 2(1-c_L^2)(1-c_V^2)\cos 2\chi \tilde{h}_+\tilde{h}_- \\
& -4\sqrt{1-c_L^2}(1-c_L)\sqrt{1-c_V^2}c_V\cos\chi\tilde{h}_+\tilde{h}_0 \\
& +4\sqrt{1-c_L^2}(1+c_L)\sqrt{1-c_V^2}c_V\cos\chi\tilde{h}_-\tilde{h}_0]
\end{aligned}
\tag{659}
$$

Integrating over c_L, c_V and χ

$$
\int_{-1}^{1} dc_L \int_{-1}^{1} dc_V \int_0^{2\pi} d\chi\ \ g(w) = \left[\frac{8}{3}\frac{4}{3}2\pi\tilde{h}_+^2 + \frac{8}{3}\frac{4}{3}2\pi\tilde{h}_-^2 + 4\frac{4}{3}\frac{2}{3}2\pi\tilde{h}_0^2\right] \tag{660}
$$

Thus

$$
\frac{d\Gamma(B \to D^*\ell\nu)}{dw} = \frac{G_F^2|V_{cb}|^2 m_B^5}{48\pi^3} r^3 (w^2-1)^{1/2}\mathcal{J}_{D^*}(w) \tag{661}
$$

where

$$
\begin{aligned}
\mathcal{J}_{D^*}(w) &= \frac{9}{64\pi}(w+1)^2\,[h_{A_1}]^2\,\frac{64\pi}{9}\left[\tilde{h}_+^2 + \tilde{h}_-^2 + \tilde{h}_0^2\right] \\
&= (w+1)^2\,[h_{A_1}]^2\left[\tilde{h}_+^2 + \tilde{h}_-^2 + \tilde{h}_0^2\right] \\
&= (w+1)^2\,[h_{A_1}]^2\left[(1-2wr+r^2)\left(1 - \sqrt{\frac{w-1}{w+1}}\frac{h_V}{h_{A_1}}\right)^2\right.
\end{aligned}
$$

$$
\begin{aligned}
&+(1-2wr+r^2)\left(1+\sqrt{\frac{w-1}{w+1}}\frac{h_V}{h_{A_1}}\right)^2 \\
&+\left\{(1-r)+(w-1)\left(1-\frac{h_{A_3}+rh_{A_2}}{h_{A_1}}\right)\right\}^2\Bigg] \\
&=(1-2wr+r^2)\left[\left\{(w+1)h_{A_1}-\sqrt{w^2-1}\,h_V\right\}^2\right. \\
&\qquad\left.+\left\{(w+1)h_{A_1}+\sqrt{w^2-1}\,h_V\right\}^2\right] \\
&\quad+[(1-r)(w+1)h_{A_1} \\
&\qquad+(w^2-1)\{(h_{A_1}-(h_{A_3}+rh_{A_2})\}]^2 \\
&=2(1-2wr+r^2)\left[(w+1)^2h_{A_1}^2+(w^2-1)h_V^2\right] \\
&\quad+\left[(w-r)(w+1)h_{A_1}-(w^2-1)(h_{A_3}+rh_{A_2})\right]^2
\end{aligned}
\tag{662}
$$

Thus, we recovered equation (524).

H.5 Leibovich Ligeti Stewart Wise (LLSW) model

Details of LLSW model is described in [42][43]. We will summarize the part which is related to our analysis.
Kinematic variables are w and θ. This θ is the angle between the charged lepton and the charmed meson in the rest frame of the virtual W boson. Thus $\theta = \pi - \theta_\ell$,

$$\cos\theta = \cos(\pi - \theta_\ell) = -\cos\theta_\ell \tag{663}$$

In the paper [43], they use different approximations : Approximation A and B. In Approximation A, they treat $w-1$ as order $\Lambda_{\mathrm{QCD}}/m_Q$ and expand decay rates in these parameters. In Approximation B, they keep the known order $\Lambda_{\mathrm{QCD}}/m_Q$ contributions to form factors as well as the full w-dependence of decay rates.
In the paper some parameters are defined as follows

$$\varepsilon_b \equiv \frac{1}{2m_b}, \quad \varepsilon_c \equiv \frac{1}{2m_c} \tag{664}$$

with numerical values

$$
\begin{aligned}
m_b &= 4.8\mathrm{GeV} \\
m_c &= 1.4\mathrm{GeV}
\end{aligned}
\tag{665}
$$

The difference between a hadron mass and a heavy quark mass in the first order :

$$
\begin{aligned}
&\bar{\Lambda} \text{ for ground state doublet } (D \text{ and } D^*) \\
&\bar{\Lambda}' \text{ for exited } \tfrac{3}{2}^+ \text{ doublet } (D_1 \text{ and } D_2^*) \\
&\bar{\Lambda}^* \text{ for exited } \tfrac{1}{2}^+ \text{ doublet } (D_0^* \text{ and } D_1')
\end{aligned}
\tag{666}
$$

with numerical values

$$\begin{aligned}\bar{\Lambda} &= 0.4\text{GeV}\\ \bar{\Lambda}' - \bar{\Lambda} &= 0.39\text{GeV}\\ \bar{\Lambda}^* - \bar{\Lambda} &= 0.35\text{GeV}\end{aligned} \tag{667}$$

In the paper, they also used the branching fraction

$$\mathcal{B}(B \to D_1 e\bar{\nu}_e) = 0.0060 \tag{668}$$

H.5.1 $B \to D_1\ell\nu$

The matrix elements are

$$\frac{< D_1(v',\varepsilon)|V^\mu|B(v) >}{\sqrt{m_{D_1}m_B}} = f_{V_1}\varepsilon^{*\mu} + (f_{V_2}v^\mu + f_{V_3}v'^\mu)(\varepsilon^*\cdot v) \tag{669}$$

$$\frac{< D_1(v',\varepsilon)|A^\mu|B(v) >}{\sqrt{m_{D_1}m_B}} = if_A\epsilon^{\mu\alpha\beta\gamma}\varepsilon^*_\alpha v_\beta v'_\gamma \tag{670}$$

The differential decay rate is

$$\begin{aligned}\frac{d^2\Gamma_{D_1}}{dwd\cos\theta} = 3\Gamma_0 r_1^3\sqrt{w^2-1}\{&\sin^2\theta[(w-r_1)f_{V_1} + (w^2-1)(f_{V_3}+r_1 f_{V_2})]^2\\ &+(1-2r_1w+r_1^2)[(1+\cos^2\theta)(f_{V_1}^2+(w^2-1)f_A^2)\\ &-4\cos\theta\sqrt{w^2-1}f_{V_1}f_A]\}\end{aligned} \tag{671}$$

where

$$\Gamma_0 = \frac{G_F^2|V_{cb}|^2m_B^5}{192\pi^3} \tag{672}$$

and

$$r_1 = \frac{m_{D_1}}{m_B} \tag{673}$$

In approximation B, the form factors are given by

$$\begin{aligned}\sqrt{6}f_A &= -(w+1)\tau - \varepsilon_b\{(w-1)[(\bar{\Lambda}'+\bar{\Lambda})\tau - (2w+1)\tau_1 - \tau_2] + (w+1)\eta_b\}\\ &\quad -\varepsilon_c[4(w\bar{\Lambda}'-\bar{\Lambda})\tau - 3(w-1)(\tau_1-\tau_2) + (w+1)(\eta_{\text{ke}} - 2\eta_1 - 3\eta_3)]\\ \sqrt{6}f_{V_1} &= (1-w^2)\tau - \varepsilon_b(w^2-1)[(\bar{\Lambda}'+\bar{\Lambda})\tau - (2w+1)\tau_1 - \tau_2 + \eta_b]\\ &\quad -\varepsilon_c[4(w+1)(w\bar{\Lambda}'-\bar{\Lambda})\tau - (w^2-1)(3\tau_1 - 3\tau_2 - \eta_{\text{ke}} + 2\eta_1 + 3\eta_3)]\\ \sqrt{6}f_{V_2} &= -3\tau - 3\varepsilon_b[(\bar{\Lambda}'+\bar{\Lambda})\tau - (2w+1)\tau_1 - \tau_2 + \eta_b]\\ &\quad -\varepsilon_c[(4w-1)\tau_1 + 5\tau_2 + 3\eta_{\text{ke}} + 10\eta_1 + 4(w-1)\eta_2 - 5\eta_3)]\\ \sqrt{6}f_{V_3} &= (w-2)\tau + \varepsilon_b\{(2+w)[(\bar{\Lambda}'+\bar{\Lambda})\tau - (2w+1)\tau_1 - \tau_2] - (2-w)\eta_b\}\\ &\quad +\varepsilon_c[4(w\bar{\Lambda}'-\bar{\Lambda})\tau + (2+w)\tau_1 + (2+3w)\tau_2\\ &\quad +(w-2)\eta_{\text{ke}} - 2(6+w)\eta_1 - 4(w-1)\eta_2 - (3w-2)\eta_3]\end{aligned} \tag{674}$$

where τ is the leading $m_Q \to \infty$ Isgur-Wise function, which is assumed to be a linear form:

$$\tau(w) = \tau(1)[1 + \hat{\tau}'(w-1)] \tag{675}$$

where

$$\tau' = \frac{d\tau}{dw}, \quad \hat{\tau}' = \frac{\tau'}{\tau(1)} \tag{676}$$

The uncertainty in the $\Lambda_{\rm QCD}/m_Q$ corrections is parameterized by τ_1 and τ_2.
In Approximation $\rm B_1$,

$$\begin{aligned} \tau_1 &= 0 \\ \tau_2 &= 0 \end{aligned} \tag{677}$$

In Approximation $\rm B_2$,

$$\begin{aligned} \tau_1 &= \bar{\Lambda}\tau \\ \tau_2 &= -\bar{\Lambda}'\tau \end{aligned} \tag{678}$$

These are the two end values of τ_1 and τ_2. True τ_1 and τ_2 reside somewhere in between. η_i comes from the correction to the HQET Lagrangian. In Approximation B,

$$\eta_1 = \eta_2 = \eta_3 = 0 \tag{679}$$

Also, in this Approximation, $\eta_1^{(b)} = \eta_2^{(b)} = \eta_3^{(b)} = 0$. Thus

$$\eta_b \equiv \eta_{\rm ke}^{(b)} + 6\eta_1^{(b)} - 2(w-1)\eta_2^{(b)} + \eta_3^{(b)} = \eta_{\rm ke}^{(b)} \tag{680}$$

Hence, the form factors are

$$\begin{aligned}
\sqrt{6}f_A &= -(w+1)(\tau + \varepsilon_c\eta_{\rm ke} + \varepsilon_b\eta_{\rm ke}^{(b)}) - \varepsilon_b(w-1)[(\bar{\Lambda}' + \bar{\Lambda})\tau - (2w+1)\tau_1 - \tau_2] \\
&\quad -\varepsilon_c[4(w\bar{\Lambda}' - \bar{\Lambda})\tau - 3(w-1)(\tau_1 - \tau_2)] \\
\sqrt{6}f_{V_1} &= (1-w^2)(\tau + \varepsilon_c\eta_{\rm ke} + \varepsilon_b\eta_{\rm ke}^{(b)}) - \varepsilon_b(w^2-1)[(\bar{\Lambda}' + \bar{\Lambda})\tau - (2w+1)\tau_1 - \tau_2] \\
&\quad -\varepsilon_c[4(w+1)(w\bar{\Lambda}' - \bar{\Lambda})\tau - 3(w^2-1)(\tau_1 - \tau_2)] \\
\sqrt{6}f_{V_2} &= -3(\tau + \varepsilon_c\eta_{\rm ke} + \varepsilon_b\eta_{\rm ke}^{(b)}) - 3\varepsilon_b[(\bar{\Lambda}' + \bar{\Lambda})\tau - (2w+1)\tau_1 - \tau_2] \\
&\quad -\varepsilon_c[(4w-1)\tau_1 + 5\tau_2] \\
\sqrt{6}f_{V_3} &= (w-2)(\tau + \varepsilon_c\eta_{\rm ke} + \varepsilon_b\eta_{\rm ke}^{(b)}) + \varepsilon_b(2+w)[(\bar{\Lambda}' + \bar{\Lambda})\tau - (2w+1)\tau_1 - \tau_2] \\
&\quad +\varepsilon_c[4(w\bar{\Lambda}' - \bar{\Lambda})\tau + (2+w)\tau_1 + (2+3w)\tau_2]
\end{aligned} \tag{681}$$

$\eta_{\rm ke}$ and $\eta_{\rm ke}^{(b)}$ can be absorbed into τ by the replacement of τ by

$$\tilde{\tau} = \tau + \varepsilon_c\eta_{\rm ke} + \varepsilon_b\eta_{\rm ke}^{(b)} \tag{682}$$

Thus, the form factors are

$$\begin{aligned}
\sqrt{6}f_A &= -(w+1)\tilde{\tau} - \varepsilon_b(w-1)[(\bar{\Lambda}'+\bar{\Lambda})\tau - (2w+1)\tau_1 - \tau_2] \\
&\quad -\varepsilon_c[4(w\bar{\Lambda}' - \bar{\Lambda})\tau - 3(w-1)(\tau_1-\tau_2)] \\
\sqrt{6}f_{V_1} &= (1-w^2)\tilde{\tau} - \varepsilon_b(w^2-1)[(\bar{\Lambda}'+\bar{\Lambda})\tau - (2w+1)\tau_1 - \tau_2] \\
&\quad -\varepsilon_c[4(w+1)(w\bar{\Lambda}' - \bar{\Lambda})\tau - 3(w^2-1)(\tau_1-\tau_2)] \\
\sqrt{6}f_{V_2} &= -3\tilde{\tau} - 3\varepsilon_b[(\bar{\Lambda}'+\bar{\Lambda})\tau - (2w+1)\tau_1 - \tau_2] \\
&\quad -\varepsilon_c[(4w-1)\tau_1 + 5\tau_2] \\
\sqrt{6}f_{V_3} &= (w-2)\tilde{\tau} + \varepsilon_b(2+w)[(\bar{\Lambda}'+\bar{\Lambda})\tau - (2w+1)\tau_1 - \tau_2] \\
&\quad +\varepsilon_c[4(w\bar{\Lambda}' - \bar{\Lambda})\tau + (2+w)\tau_1 + (2+3w)\tau_2]
\end{aligned} \tag{683}$$

Other τ can also be replaced by $\tilde{\tau}$ in the same order of approximation. For simplicity, we omit $\tilde{}$, then

$$\begin{aligned}
\sqrt{6}f_A &= -(w+1)\tau - \varepsilon_b(w-1)[(\bar{\Lambda}'+\bar{\Lambda})\tau - (2w+1)\tau_1 - \tau_2] \\
&\quad -\varepsilon_c[4(w\bar{\Lambda}' - \bar{\Lambda})\tau - 3(w-1)(\tau_1-\tau_2)] \\
\sqrt{6}f_{V_1} &= (1-w^2)\tau - \varepsilon_b(w^2-1)[(\bar{\Lambda}'+\bar{\Lambda})\tau - (2w+1)\tau_1 - \tau_2] \\
&\quad -\varepsilon_c[4(w+1)(w\bar{\Lambda}' - \bar{\Lambda})\tau - 3(w^2-1)(\tau_1-\tau_2)] \\
\sqrt{6}f_{V_2} &= -3\tau - 3\varepsilon_b[(\bar{\Lambda}'+\bar{\Lambda})\tau - (2w+1)\tau_1 - \tau_2] \\
&\quad -\varepsilon_c[(4w-1)\tau_1 + 5\tau_2] \\
\sqrt{6}f_{V_3} &= (w-2)\tau + \varepsilon_b(2+w)[(\bar{\Lambda}'+\bar{\Lambda})\tau - (2w+1)\tau_1 - \tau_2] \\
&\quad +\varepsilon_c[4(w\bar{\Lambda}' - \bar{\Lambda})\tau + (2+w)\tau_1 + (2+3w)\tau_2]
\end{aligned} \tag{684}$$

In Approximation A, the differential decay rate can be expanded in powers of $w-1$

$$\begin{aligned}
\frac{d^2\Gamma_{D_1}}{dw\,d\cos\theta} &= \Gamma_0\tau^2(1)r_1^3\sqrt{w^2-1}\sum_n(w-1)^n \\
&\quad \{\sin^2\theta s_1^{(n)} + (1-2r_1w+r_1^2)[(1+\cos^2\theta)t_1^{(n)} - 4\cos\theta\sqrt{w^2-1}u_1^{(n)}]\}
\end{aligned} \tag{685}$$

where

$$\begin{aligned}
&s_1^{(0)} = 32\varepsilon_c^2(1-r_1)^2(\bar{\Lambda}'-\bar{\Lambda})^2 + \ldots \\
&s_1^{(1)} = 32\varepsilon_c(1-r_1^2)(\bar{\Lambda}'-\bar{\Lambda}) + \ldots \\
&s_1^{(2)} = 8(1+r_1)^2 + \ldots \\
&t_1^{(0)} = 32\varepsilon_c^2(\bar{\Lambda}'-\bar{\Lambda})^2 + \ldots \\
&t_1^{(1)} = 4 + 8\varepsilon_c[4(\bar{\Lambda}'-\bar{\Lambda}) + \hat{\eta}_{\text{ke}} - 2\hat{\eta}_1 - 3\hat{\eta}_3] + 8\varepsilon_b\hat{\eta}_b + \ldots \\
&t_1^{(2)} = 8(1+\hat{\tau}') + \ldots \\
&u_1^{(0)} = 8\varepsilon_c(\bar{\Lambda}'-\bar{\Lambda}) + \ldots \\
&u_1^{(1)} = 2 + \ldots
\end{aligned} \tag{686}$$

where

$$\hat{\eta}_i = \frac{\eta_i}{\tau(1)} \tag{687}$$

We use the same tricks for ηs, then

$$
\begin{aligned}
s_1^{(0)} &= 32\varepsilon_c^2(1-r_1)^2(\bar{\Lambda}'-\bar{\Lambda})^2 \\
s_1^{(1)} &= 32\varepsilon_c(1-r_1^2)(\bar{\Lambda}'-\bar{\Lambda}) \\
s_1^{(2)} &= 8(1+r_1)^2 \\
t_1^{(0)} &= 32\varepsilon_c^2(\bar{\Lambda}'-\bar{\Lambda})^2 \\
t_1^{(1)} &= 4+8\varepsilon_c[4(\bar{\Lambda}'-\bar{\Lambda})] \\
t_1^{(2)} &= 8(1+\hat{\tau}')+... \\
u_1^{(0)} &= 8\varepsilon_c(\bar{\Lambda}'-\bar{\Lambda}) \\
u_1^{(1)} &= 2
\end{aligned}
\tag{688}
$$

The differential decay rate can be integrated over $\cos\theta$ to give

$$
\frac{d^2\Gamma_{D_1}}{dw} = \Gamma_0\tau^2(1)r_1^3\sqrt{w^2-1}\sum_n(w-1)^n\left[\frac{4}{3}s_1^{(n)}+(1-2r_1w+r_1^2)\frac{8}{3}t_1^{(n)}\right] \tag{689}
$$

$$
\begin{aligned}
\frac{d^2\Gamma_{D_1}}{dw} &= \frac{G_F^2|V_{cb}|^2m_B^5}{192\pi^3}r_1^3(w^2-1)^{1/2}\,\tau^2(1)\sum_n(w-1)^n\left[\frac{4}{3}s_1^{(n)}+(1-2r_1w+r_1^2)\frac{8}{3}t_1^{(n)}\right] \\
&= \frac{G_F^2|V_{cb}|^2m_B^5}{48\pi^3}r^3(w^2-1)^{1/2}\,\mathcal{J}_{D_1}(w)
\end{aligned}
\tag{690}
$$

where

$$
\mathcal{J}_{D_1}(w) = \frac{1}{3}\tau^2(1)\sum_n(w-1)^n\left[s_1^{(n)}+2(1-2r_1w+r_1^2)t_1^{(n)}\right] \tag{691}
$$

Numerical values used in the LLSW paper are

$$
\begin{aligned}
\tau(1)\left[\frac{6.0\times10^{-3}}{\mathcal{B}(B\to D_1e\bar{\nu}_e)}\right]^{1/2} &= 0.71 \text{ for Approximation B1} \\
&= 0.75 \text{ for Approximation B2} \\
&= 0.60 \text{ for Approximation A}
\end{aligned}
\tag{692}
$$

and

$$
\hat{\tau}' = -1.5 \tag{693}
$$

H.5.2 $B \to D_2^*\ell\nu$

The matrix elements are

$$
\frac{< D_2^*(v',\varepsilon)|V^\mu|B(v) >}{\sqrt{m_{D_2^*}m_B}} = ik_V\epsilon^{\mu\alpha\beta\gamma}\varepsilon^*_{\alpha\sigma}v^\sigma v_\beta v'_\gamma \tag{694}
$$

$$
\frac{< D_2^*(v',\varepsilon)|A^\mu|B(v) >}{\sqrt{m_{D_2^*}m_B}} = k_{A_1}\varepsilon^{*\mu\alpha}v_\alpha+(k_{A_2}v^\mu+k_{A_3}v'^\mu)\varepsilon^*_{\alpha\beta}v^\alpha v^\beta \tag{695}
$$

The differential decay rate is

$$\frac{d^2\Gamma_{D_2^*}}{dw d\cos\theta} = \tfrac{3}{2}\Gamma_0 r_2^3 (w^2-1)^{3/2}\{\tfrac{4}{3}\sin^2\theta[(w-r_2)k_{A_1} + (w^2-1)(k_{A_3} + r_2 k_{A_2})]^2 \\ +(1-2r_2 w + r_2^2)[(1+\cos^2\theta)(k_{A_1}^2 + (w^2-1)k_V^2) - 4\cos\theta\sqrt{w^2-1}k_{A_1}k_V]\} \tag{696}$$

where

$$r_2 = \frac{m_{D_2^*}}{m_B} \tag{697}$$

In Approximation B, the form factors are given by

$$\begin{aligned} k_V &= -\tau - \varepsilon_b[(\bar{\Lambda}' + \bar{\Lambda})\tau - (2w+1)\tau_1 - \tau_2 + \eta_b] - \varepsilon_c(\tau_1 - \tau_2 + \eta_{\mathrm{ke}} - 2\eta_1 + \eta_3) \\ k_{A_1} &= -(1+w)\tau - \varepsilon_b\{(w-1)[(\bar{\Lambda}' + \bar{\Lambda})\tau - (2w+1)\tau_1 - \tau_2] + (1+w)\eta_b\} \\ &\qquad -\varepsilon_c[(w-1)(\tau_1 - \tau_2) + (w+1)(\eta_{\mathrm{ke}} - 2\eta_1 + \eta_3)] \\ k_{A_2} &= -2\varepsilon_c(\tau_1 + \eta_2) \\ k_{A_3} &= \tau + \varepsilon_b[(\bar{\Lambda}' + \bar{\Lambda})\tau - (2w+1)\tau_1 - \tau_2 + \eta_b] \\ &\qquad -\varepsilon_c(\tau_1 + \tau_2 - \eta_{\mathrm{ke}} + 2\eta_1 - 2\eta_2 - \eta_3) \end{aligned} \tag{698}$$

We use the same tricks for ηs, then

$$\begin{aligned} k_V &= -\tau - \varepsilon_b[(\bar{\Lambda}' + \bar{\Lambda})\tau - (2w+1)\tau_1 - \tau_2] - \varepsilon_c(\tau_1 - \tau_2) \\ k_{A_1} &= -(1+w)\tau - \varepsilon_b(w-1)[(\bar{\Lambda}' + \bar{\Lambda})\tau - (2w+1)\tau_1 - \tau_2] \\ &\qquad -\varepsilon_c(w-1)(\tau_1 - \tau_2) \\ k_{A_2} &= -2\varepsilon_c\tau_1 \\ k_{A_3} &= \tau + \varepsilon_b[(\bar{\Lambda}' + \bar{\Lambda})\tau - (2w+1)\tau_1 - \tau_2] - \varepsilon_c(\tau_1 + \tau_2) \end{aligned} \tag{699}$$

In Approximation B_1,

$$\begin{aligned} \tau_1 &= 0 \\ \tau_2 &= 0 \end{aligned} \tag{700}$$

In Approximation B_2,

$$\begin{aligned} \tau_1 &= \bar{\Lambda}\tau \\ \tau_2 &= -\bar{\Lambda}'\tau \end{aligned} \tag{701}$$

These are the two end values of τ_1 and τ_2. True τ_1 and τ_2 reside somewhere in between. In Approximation A, the differential decay rate can be expanded in powers of $w-1$

$$\frac{d^2\Gamma_{D_2^*}}{dw d\cos\theta} = \tfrac{3}{2}\Gamma_0\tau^2(1) r_2^3 (w^2-1)^{3/2}\sum_n (w-1)^n \\ \{\tfrac{4}{3}\sin^2\theta s_2^{(n)} + (1-2r_2 w + r_2^2)[(1+\cos^2\theta)t_2^{(n)} - 4\cos\theta\sqrt{w^2-1}u_2^{(n)}]\} \tag{702}$$

where

$$
\begin{aligned}
s_2^{(0)} &= 4(1-r_2)^2[1+2\varepsilon_b\hat{\eta}_b+2\varepsilon_c(\hat{\eta}_{\rm ke}-2\hat{\eta}_1+\hat{\eta}_3)]+...\\
s_2^{(1)} &= 4(1-r_2)^2(1+2\hat{\tau}')+...\\
t_2^{(0)} &= 4+8\varepsilon_b\hat{\eta}_b+8\varepsilon_c(\hat{\eta}_{\rm ke}-2\hat{\eta}_1+\hat{\eta}_3)+...\\
t_2^{(1)} &= 2(3+4\hat{\tau}')+...\\
u_2^{(0)} &= 2+...
\end{aligned}
\tag{703}
$$

We use the same tricks for ηs, then

$$
\begin{aligned}
s_2^{(0)} &= 4(1-r_2)^2\\
s_2^{(1)} &= 4(1-r_2)^2(1+2\hat{\tau}')\\
t_2^{(0)} &= 4\\
t_2^{(1)} &= 2(3+4\hat{\tau}')\\
u_2^{(0)} &= 2
\end{aligned}
\tag{704}
$$

The differential decay rate can be integrated over $\cos\theta$

$$
\frac{d^2\Gamma_{D_2^*}}{dw} = \frac{3}{2}\Gamma_0\tau^2(1)r_2^3(w^2-1)^{3/2}\sum_n(w-1)^n\left[\frac{4}{3}\frac{4}{3}s_2^{(n)}+(1-2r_2w+r_2^2)\frac{8}{3}t_2^{(n)}\right] \tag{705}
$$

Thus,

$$
\begin{aligned}
\frac{d^2\Gamma_{D_2^*}}{dw} &= \frac{3}{2}\frac{G_F^2|V_{cb}|^2m_B^5}{192\pi^3}r_2^3(w^2-1)^{3/2}\tau^2(1)\\
&\quad\sum_n(w-1)^n\left[\frac{16}{9}s_2^{(n)}+(1-2r_2w+r_2^2)\frac{8}{3}t_2^{(n)}\right]\\
&= \frac{G_F^2|V_{cb}|^2m_B^5}{48\pi^3}r^3(w^2-1)^{3/2}\,\mathcal{J}_{D_2^*}(w)
\end{aligned}
\tag{706}
$$

where

$$
\mathcal{J}_{D_2^*}(w) = \frac{1}{3}\tau^2(1)\sum_n(w-1)^n\left[2s_2^{(n)}+3(1-2r_2w+r_2^2)t_2^{(n)}\right] \tag{707}
$$

Numerical values used in the LLSW paper are

$$
\begin{aligned}
\tau(1)\left[\frac{6.0\times10^{-3}}{\mathcal{B}(B\to D_1e\bar{\nu}_e)}\right]^{1/2} &= 0.71 \text{ for Approximation B1}\\
&= 0.75 \text{ for Approximation B2}\\
&= 0.60 \text{ for Approximation A}
\end{aligned}
\tag{708}
$$

and

$$
\hat{\tau}' = -1.5 \tag{709}
$$

H.5.3 $B \to D_0^*\ell\nu$

The matrix elements are

$$\frac{< D_0^*(v',\varepsilon)|V^\mu|B(v) >}{\sqrt{m_{D_0^*}m_B}} = 0 \tag{710}$$

$$\frac{< D_0^*(v',\varepsilon)|A^\mu|B(v) >}{\sqrt{m_{D_0^*}m_B}} = g_+(v^\mu + v'^\mu) + g_-(v^\mu - v'^\mu) \tag{711}$$

The differential decay rate is

$$\frac{d^2\Gamma_{D_0^*}}{dwd\cos\theta} = 3\Gamma_0 r_0^{*3}(w^2-1)^{3/2}\sin^2\theta[(1+r_0^*)g_+ - (1-r_0^*)g_-]^2 \tag{712}$$

where

$$r_0^* = \frac{m_{D_0^*}}{m_B} \tag{713}$$

In Approximation B, the form factors are given by

$$\begin{aligned} g_+ &= \varepsilon_c\left[2(w-1)\zeta_1 - 3\zeta\tfrac{w\bar{\Lambda}^*-\bar{\Lambda}}{w+1}\right] - \varepsilon_b\left[\tfrac{\bar{\Lambda}^*(2w+1)-\bar{\Lambda}(w+2)}{w+1}\zeta - 2(w-1)\zeta_1\right] \\ g_- &= \zeta + \varepsilon_c\left[\chi_{\rm ke} + 6\chi_1 - 2(w+1)\chi_2\right] + \varepsilon_b\chi_b \end{aligned} \tag{714}$$

We can use the same tricks for χs as ηs, then

$$\begin{aligned} g_+ &= \varepsilon_c\left[2(w-1)\zeta_1 - 3\zeta\tfrac{w\bar{\Lambda}^*-\bar{\Lambda}}{w+1}\right] - \varepsilon_b\left[\tfrac{\bar{\Lambda}^*(2w+1)-\bar{\Lambda}(w+2)}{w+1}\zeta - 2(w-1)\zeta_1\right] \\ g_- &= \zeta \end{aligned} \tag{715}$$

where

$$\zeta(w) = \frac{w+1}{\sqrt{3}}\tau(w) \tag{716}$$

Thus,

$$\begin{aligned} \zeta(1)[1+\hat{\zeta}'(w-1)] &= \tfrac{2+(w-1)}{\sqrt{3}}\tau(1)[1+\hat{\tau}'(w-1)] \\ &\simeq \tfrac{1}{\sqrt{3}}\tau(1)[2+2\hat{\tau}'(w-1)+(w-1)] \\ &= \tfrac{2}{\sqrt{3}}\tau(1)\left[1+\left(\hat{\tau}'+\tfrac{1}{2}\right)(w-1)\right] \end{aligned} \tag{717}$$

Hence

$$\begin{aligned} \zeta(1) &= \tfrac{2}{\sqrt{3}}\tau(1) \\ \hat{\zeta}' &= \tfrac{1}{2} + \hat{\tau}' = -1 \end{aligned} \tag{718}$$

In Approximation B_1,

$$\begin{aligned} \zeta_1 &= 0 \\ \zeta_2 &= 0 \end{aligned} \tag{719}$$

In Approximation B_2,

$$\begin{aligned} \zeta_1 &= \bar{\Lambda}\zeta \\ \zeta_2 &= -\bar{\Lambda}^*\zeta \end{aligned} \tag{720}$$

These are the two end values of ζ_1 and ζ_2. True ζ_1 and ζ_2 reside somewhere in between. In Approximation A, the differential decay rate can be expanded in powers of $w-1$

$$\frac{d^2\Gamma_{D_0^*}}{dw\,d\cos\theta} = 3\Gamma_0\zeta^2(1)r_0^{*3}(w^2-1)^{3/2}\sin^2\theta\sum_n(w-1)^n s_0^{(n)} \tag{721}$$

where

$$\begin{aligned} s_0^{(0)} &= (1-r_0^*)^2[1+2\varepsilon_c(\hat\chi_{\rm ke}+6\hat\chi_1-4\hat\chi_2)+4\varepsilon_b\hat\chi_b] \\ &\qquad +3(\varepsilon_c+\varepsilon_b)(1-r_0^{*2})(\bar\Lambda^*-\bar\Lambda)+... \\ s_0^{(1)} &= 2(1-r_0^*)^2\hat\zeta'+... \end{aligned} \tag{722}$$

We can use the same tricks for χs, then

$$\begin{aligned} s_0^{(0)} &= (1-r_0^*)^2+3(\varepsilon_c+\varepsilon_b)(1-r_0^{*2})(\bar\Lambda^*-\bar\Lambda) \\ s_0^{(1)} &= 2(1-r_0^*)^2\hat\zeta' \end{aligned} \tag{723}$$

The differential decay rate can be integrated over $\cos\theta$

$$\frac{d^2\Gamma_{D_0^*}}{dw} = 3\Gamma_0\zeta^2(1)r_0^{*3}(w^2-1)^{3/2}\frac{4}{3}\sum_n(w-1)^n s_0^{(n)} \tag{724}$$

Thus

$$\begin{aligned} \frac{d^2\Gamma_{D_0^*}}{dw} &= 3\frac{G_F^2|V_{cb}|^2m_B^5}{192\pi^3}r_0^{*3}(w^2-1)^{3/2}\zeta^2(1)\frac{4}{3}\sum_n(w-1)^n s_0^{(n)} \\ &= \frac{G_F^2|V_{cb}|^2m_B^5}{48\pi^3}r^3(w^2-1)^{3/2}\,\mathcal{J}_{D_0^*}(w) \end{aligned} \tag{725}$$

where

$$\mathcal{J}_{D_0^*}(w) = \zeta^2(1)\sum_n(w-1)^n s_0^{(n)} \tag{726}$$

Numerical values used in the LLSW paper are

$$\begin{aligned} \tau(1)\left[\frac{6.0\times10^{-3}}{\mathcal{B}(B\to D_1e\bar\nu_e)}\right]^{1/2} &= 0.71 \text{ for Approximation B1} \\ &= 0.75 \text{ for Approximation B2} \\ &= 0.60 \text{ for Approximation A} \end{aligned} \tag{727}$$

and

$$\hat\tau' = -1.5 \tag{728}$$

H.5.4 $B \to D_1^* \ell\nu$

The matrix elements are

$$\frac{< D_1^*(v',\varepsilon)|V^\mu|B(v) >}{\sqrt{m_{D_1^*} m_B}} = g_{V_1}\varepsilon^{*\mu} + (g_{V_2} v^\mu + g_{V_3} v'^\mu)(\varepsilon^* \cdot v) \tag{729}$$

$$\frac{< D_1^*(v',\varepsilon)|A^\mu|B(v) >}{\sqrt{m_{D_1^*} m_B}} = i g_A \epsilon^{\mu\alpha\beta\gamma} \varepsilon^*_\alpha v_\beta v'_\gamma \tag{730}$$

The differential decay rate is

$$\begin{aligned} &\tfrac{d^2\Gamma_{D_1^*}}{dw d\cos\theta} = 3\Gamma_0 r_1^{*3}\sqrt{w^2-1}\{\sin^2\theta[(w-r_1^*)g_{V_1} + (w^2-1)(g_{V_3} + r_1^* g_{V_2})]^2 \\ &+(1-2r_1^* w + r_1^{*2})[(1+\cos^2\theta)(g_{V_1}^2 + (w^2-1)g_A^2) - 4\cos\theta\sqrt{w^2-1}g_{V_1} g_A]\} \end{aligned} \tag{731}$$

where

$$r_1^* = \frac{m_{D_1^*}}{m_B} \tag{732}$$

In Approximation B, the form factors are given by

$$\begin{aligned} g_A &= \zeta + \varepsilon_c\left[\tfrac{w\bar{\Lambda}^* - \bar{\Lambda}}{w+1}\zeta + \chi_{\rm ke} - 2\chi_1\right] - \varepsilon_b\left[\tfrac{\bar{\Lambda}^*(2w+1) - \bar{\Lambda}(w+2)}{w+1}\zeta - 2(w-1)\zeta_1 - \chi_b\right] \\ g_{V_1} &= (w-1)\zeta + \varepsilon_c\left[(w\bar{\Lambda}^* - \bar{\Lambda})\zeta + (w-1)(\chi_{\rm ke} - 2\chi_1)\right] \\ &\qquad -\varepsilon_b\left[(\bar{\Lambda}^*(2w+1) - \bar{\Lambda}(w+2))\zeta - 2(w^2-1)\zeta_1 - (w-1)\chi_b\right] \\ g_{V_2} &= 2\varepsilon_c(\zeta_1 - \chi_2) \\ g_{V_3} &= -\zeta - \varepsilon_c\left[\tfrac{w\bar{\Lambda}^* - \bar{\Lambda}}{w+1}\zeta + 2\zeta_1 + \chi_{\rm ke} - 2\chi_1 + 2\chi_2\right] \\ &\qquad +\varepsilon_b\left[\tfrac{\bar{\Lambda}^*(2w+1) - \bar{\Lambda}(w+2)}{w+1}\zeta - 2(w-1)\zeta_1 - \chi_b\right] \end{aligned} \tag{733}$$

where

$$\zeta(w) = \frac{w+1}{\sqrt{3}}\tau(w) \tag{734}$$

We use the same tricks for χs, then

$$\begin{aligned} g_A &= \zeta + \varepsilon_c\left[\tfrac{w\bar{\Lambda}^* - \bar{\Lambda}}{w+1}\zeta\right] - \varepsilon_b\left[\tfrac{\bar{\Lambda}^*(2w+1) - \bar{\Lambda}(w+2)}{w+1}\zeta - 2(w-1)\zeta_1\right] \\ g_{V_1} &= (w-1)\zeta + \varepsilon_c(w\bar{\Lambda}^* - \bar{\Lambda})\zeta \\ &\qquad -\varepsilon_b\left[(\bar{\Lambda}^*(2w+1) - \bar{\Lambda}(w+2))\zeta - 2(w^2-1)\zeta_1\right] \\ g_{V_2} &= 2\varepsilon_c\zeta_1 \\ g_{V_3} &= -\zeta - \varepsilon_c\left[\tfrac{w\bar{\Lambda}^* - \bar{\Lambda}}{w+1}\zeta + 2\zeta_1\right] \\ &\qquad +\varepsilon_b\left[\tfrac{\bar{\Lambda}^*(2w+1) - \bar{\Lambda}(w+2)}{w+1}\zeta - 2(w-1)\zeta_1\right] \end{aligned} \tag{735}$$

In Approximation B_1,

$$\begin{aligned} \zeta_1 &= 0 \\ \zeta_2 &= 0 \end{aligned} \tag{736}$$

In Approximation B_2,

$$\begin{aligned}\zeta_1 &= \bar{\Lambda}\zeta \\ \zeta_2 &= -\bar{\Lambda}^*\zeta\end{aligned} \tag{737}$$

These are the two end values of ζ_1 and ζ_2. True ζ_1 and ζ_2 reside somewhere in between. In Approximation A, the differential decay rate can be expanded in powers of $w-1$

$$\begin{aligned}&\tfrac{d^2\Gamma_{D_1^*}}{dw d\cos\theta} = 3\Gamma_0\zeta^2(1)r_1^{*3}\sqrt{w^2-1}\sum_n(w-1)^n \\ &\{\sin^2\theta s_1^{(n)} + (1-2r_1^*w+r_1^{*2})[(1+\cos^2\theta)t_1^{(n)} - 4\cos\theta\sqrt{w^2-1}u_1^{(n)}]\}\end{aligned} \tag{738}$$

where

$$\begin{aligned}s_1^{(0)} &= (\varepsilon_c - 3\varepsilon_b)^2(1-r_1^*)^2(\bar{\Lambda}^* - \bar{\Lambda})^2 + ... \\ s_1^{(1)} &= -2(\varepsilon_c - 3\varepsilon_b)(1-r_1^{*2})(\bar{\Lambda}^* - \bar{\Lambda}) + ... \\ s_1^{(2)} &= (1+r_1^*)^2 + ... \\ t_1^{(0)} &= (\varepsilon_c - 3\varepsilon_b)^2(\bar{\Lambda}^* - \bar{\Lambda})^2 + ... \\ t_1^{(1)} &= 2 + 4(\varepsilon_c - 3\varepsilon_b)(\bar{\Lambda}^* - \bar{\Lambda}) + 4\varepsilon_c(\hat{\chi}_{\rm ke} - 2\hat{\chi}_1) + 4\varepsilon_b\hat{\chi}_b + ... \\ t_1^{(2)} &= 2(1+2\hat{\zeta}') + ... \\ u_1^{(0)} &= (\varepsilon_c - 3\varepsilon_b)(\bar{\Lambda}^* - \bar{\Lambda}) + ... \\ u_1^{(1)} &= 1 + ...\end{aligned} \tag{739}$$

We use the same tricks for χs, then

$$\begin{aligned}s_1^{(0)} &= (\varepsilon_c - 3\varepsilon_b)^2(1-r_1^*)^2(\bar{\Lambda}^* - \bar{\Lambda})^2 \\ s_1^{(1)} &= -2(\varepsilon_c - 3\varepsilon_b)(1-r_1^{*2})(\bar{\Lambda}^* - \bar{\Lambda}) \\ s_1^{(2)} &= (1+r_1^*)^2 \\ t_1^{(0)} &= (\varepsilon_c - 3\varepsilon_b)^2(\bar{\Lambda}^* - \bar{\Lambda})^2 \\ t_1^{(1)} &= 2 + 4(\varepsilon_c - 3\varepsilon_b)(\bar{\Lambda}^* - \bar{\Lambda}) \\ t_1^{(2)} &= 2(1+2\hat{\zeta}') \\ u_1^{(0)} &= (\varepsilon_c - 3\varepsilon_b)(\bar{\Lambda}^* - \bar{\Lambda}) \\ u_1^{(1)} &= 1\end{aligned} \tag{740}$$

The differential decay rate can be integrated over $\cos\theta$

$$\frac{d^2\Gamma_{D_1^*}}{dw} = 3\Gamma_0\zeta^2(1)r_1^{*3}\sqrt{w^2-1}\sum_n(w-1)^n\left[\frac{4}{3}s_1^{(n)} + (1-2r_1^*w+r_1^{*2})\frac{8}{3}t_1^{(n)}\right] \tag{741}$$

Thus

$$\begin{aligned}\frac{d^2\Gamma_{D_1^*}}{dw} &= \frac{G_F^2|V_{cb}|^2m_B^5}{192\pi^3}r_1^{*3}(w^2-1)^{1/2}\zeta^2(1) \\ &\qquad \sum_n(w-1)^n\left[4s_1^{(n)} + 8(1-2r_1^*w+r_1^{*2})t_1^{(n)}\right] \\ &= \frac{G_F^2|V_{cb}|^2m_B^5}{48\pi^3}r^3(w^2-1)^{1/2}\,\mathcal{J}_{D_1'}(w)\end{aligned} \tag{742}$$

where

$$\mathcal{J}_{D_1'}(w) = \zeta^2(1) \sum_n (w-1)^n \left[s_1^{(n)} + 2(1 - 2r_1^* w + r_1^{*2}) t_1^{(n)} \right] \tag{743}$$

Numerical values used in the LLSW paper are

$$\begin{aligned} \tau(1) \left[\frac{6.0 \times 10^{-3}}{\mathcal{B}(B \to D_1 e \bar{\nu}_e)} \right]^{1/2} &= 0.71 \text{ for Approximation B1} \\ &= 0.75 \text{ for Approximation B2} \\ &= 0.60 \text{ for Approximation A} \end{aligned} \tag{744}$$

and

$$\hat{\tau}' = -1.5 \tag{745}$$

H.6 GoityRoberts model

In GoiryRoberts model [45], the "soft-pion" domain was studied in the framework of the chiral Lagrangian approach combined with the $1/m_Q$ expansion.

H.6.1 $B \to D\pi\ell\nu$

The amplitude for this process has the general form

$$T = \kappa j_\mu \Omega^\mu \tag{746}$$

Here j_μ is the V-A charged leptonic current and the Ω^μ is the hadronic part of the amplitude. To evaluate Ω^μ, these six diagrams are considered to get the amplitude (matrix element)

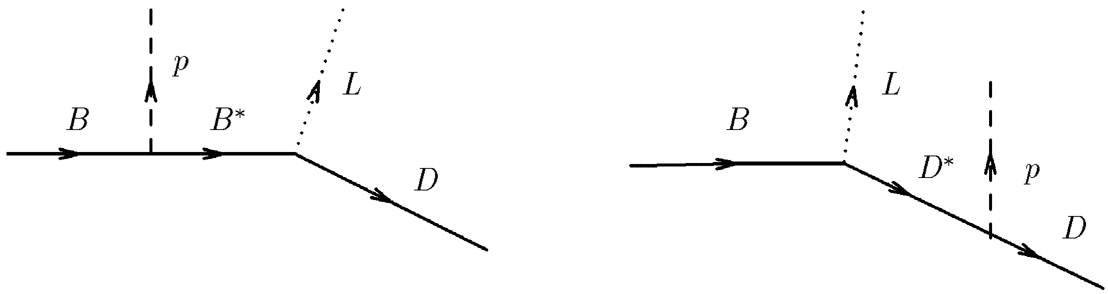

(a)

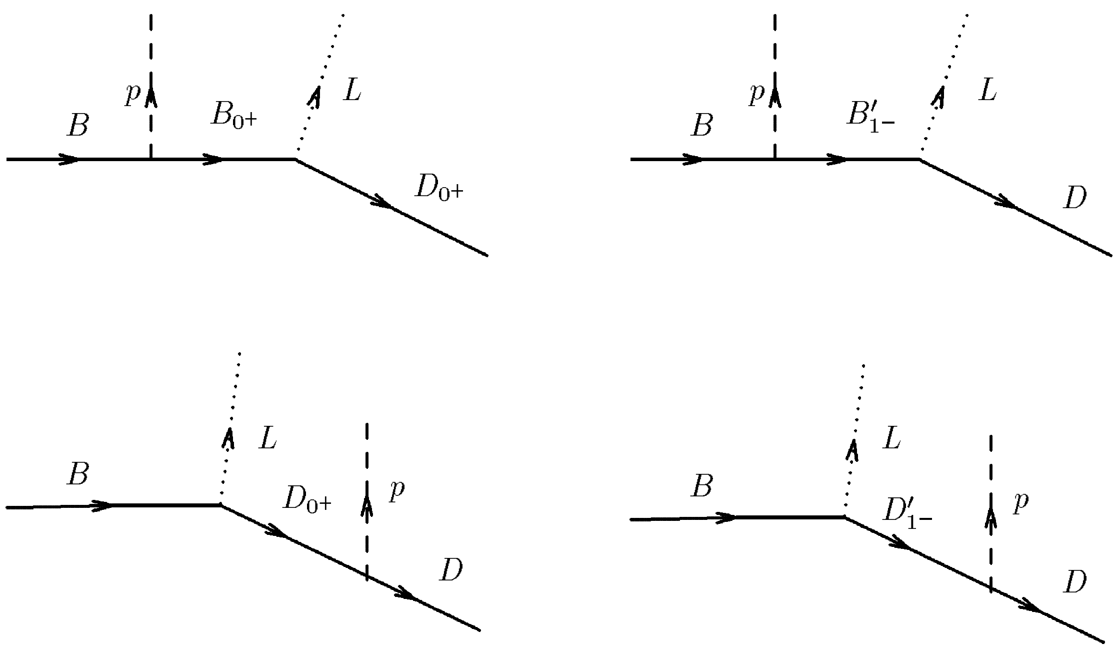

(b)

(a) shows two non-resonant decays , (b) shows four resonant decays. The non-resonant portion of Ω^{μ} is

$$\begin{aligned} \Omega_{\mu}^{NR} \;=\; & \tfrac{g}{F_0}\xi(\nu)p_{\nu}\Big\{\tfrac{\Theta^{\nu\rho}(v)}{-2(p\cdot v-\delta m_B)+i\varepsilon}\left[iv^{\alpha}v'^{\beta}\epsilon_{\mu\alpha\beta\rho}+g_{\mu\rho}(1+\nu)-v_{\mu}v'_{\rho}\right] \\ & +\tfrac{\Theta^{\nu\rho}(v')}{2(p\cdot v'-\delta m_D)+i\varepsilon}\left[iv^{\alpha}v'^{\beta}\epsilon_{\mu\alpha\beta\rho}+g_{\mu\rho}(1+\nu)-v_{\rho}v'_{\mu}\right]\Big\} \end{aligned} \tag{747}$$

where $\delta m_D = m_{D^*} - m_D$ and $\delta m_B = m_{B^*} - m_B$, and

$$\Theta^{\mu\nu}(v) = g^{\mu\nu} - v^{\mu}v^{\nu} \tag{748}$$

The resonant portion of Ω^μ is

$$\begin{aligned}
\Omega^R_\mu \;=\;& \frac{\alpha_1}{F_0}\rho_1(\nu)(v-v')_\mu\left[-\frac{p\cdot v}{2(-p\cdot v-\delta\tilde m_1)}+\frac{p\cdot v'}{2(p\cdot v'-\delta\tilde m_1)}\right]\\
&+\frac{\alpha_2}{3F_0}\rho_2(\nu)p_\rho\Big\{\frac{\Theta^{\nu\rho}(v)}{2(-p\cdot v-\delta\tilde m_2)}\left[i\epsilon_{\mu\nu\alpha\beta}v^\alpha v'^\beta(\nu-1)+g_{\mu\nu}(\nu^2-1)\right.\\
&\qquad\qquad\left.-v'_\nu\left(v_\mu(2+\nu)-3v'_\mu\right)\right]\\
&+\frac{\Theta^{\nu\rho}(v')}{2(p\cdot v'-\delta\tilde m_2)}\left[i\epsilon_{\mu\nu\alpha\beta}v^\alpha v'^\beta(\nu-1)+g_{\mu\nu}(\nu^2-1)\right.\\
&\qquad\qquad\left.-v_\nu\left(v'_\mu(2+\nu)-3v_\mu\right)\right]\Big\}\\
&+\frac{\alpha_3}{F_0}\xi^{(1)}(\nu)p_\nu\Big\{\frac{\Theta^{\nu\rho}(v)}{-2p\cdot v-\delta\tilde m_3}\left[i\epsilon_{\mu\alpha\beta\rho}v^\alpha v'^\beta+g_{\mu\rho}(\nu+1)-v_\mu v'_\rho\right]\\
&+\frac{\Theta^{\nu\rho}(v')}{2p\cdot v'-\delta\tilde m_3}\left[i\epsilon_{\mu\alpha\beta\rho}v^\alpha v'^\beta+g_{\mu\rho}(\nu+1)-v_\rho v'_\mu\right]\Big\}
\end{aligned}\tag{749}$$

Here we denote $\delta\tilde m-j=\delta m_j-i\Gamma_j/2$, where Γ_j is the total width of the resonance. Contribution from other resonances are small. Isgur-Wise functions are given by

$$\begin{aligned}
&\xi(\nu)=\exp\left[\tfrac{\bar\Lambda^2}{4\beta^2}(\nu^2-1)\right]\\
&\xi^{(1)}(\nu)=-\sqrt{\tfrac{2}{3}}\left[\tfrac{\bar\Lambda^2}{4\beta^2}(\nu^2-1)\right]\exp\left[\tfrac{\bar\Lambda^2}{4\beta^2}(\nu^2-1)\right]\\
&\rho_1(\nu)=\tfrac{1}{\sqrt2}\tfrac{\bar\Lambda}{\beta}\left(\tfrac{2\beta\beta'}{\beta^2+\beta'^2}\right)^{5/2}\exp\left[\tfrac{\bar\Lambda^2}{2(\beta^2+\beta'^2)}(\nu^2-1)\right]\\
&\rho_2(\nu)=\tfrac{1}{2\sqrt2}\left(\tfrac{\bar\Lambda}{\beta}\right)^2\left(\tfrac{2\beta\beta'}{\beta^2+\beta'^2}\right)^{7/2}\exp\left[\tfrac{\bar\Lambda^2}{2(\beta^2+\beta'^2)}(\nu^2-1)\right]
\end{aligned}\tag{750}$$

where β and β' are the harmonic oscillator parameters of the ground and excited states, respectively. $\bar\Lambda$ is defined by

$$M_{(0^-,1^-)}=m_Q+\bar\Lambda\tag{751}$$

Ω_μ can be, in general, expressed as

$$\Omega_\mu=-ihm_Bm_D\epsilon_{\mu\nu\rho\sigma}v^\nu v'^\rho p^\sigma_\pi+A_1p_{\pi\mu}+A_2m_Bv_\mu+A_3m_Dv'_{mu}\tag{752}$$

where h, A_1, A_2 and A_3 are the form factors and p_π is the 4-momentum of the pion. The non-resonant contribution to the form factors are

$$\begin{aligned}
&h_{NR}=\tfrac{g}{2F_0}\tfrac{\xi(\nu)}{m_Bm_D}\left(\tfrac{1}{p_\pi\cdot v+\delta m_B-i\varepsilon}-\tfrac{1}{p_\pi\cdot v'-\delta m_D+i\varepsilon}\right)\\
&A_{1NR}=-\tfrac{g}{2F_0}\xi(\nu)(1+\nu)\left(\tfrac{1}{p_\pi\cdot v+\delta m_B-i\varepsilon}-\tfrac{1}{p_\pi\cdot v'-\delta m_D+i\varepsilon}\right)\\
&A_{2NR}=\tfrac{g}{2F_0}\tfrac{\xi(\nu)}{m_B}\left(\tfrac{p_\pi\cdot v+p_\pi\cdot v'}{p_\pi\cdot v+\delta m_B-i\varepsilon}\right)\\
&A_{3NR}=-\tfrac{g}{2F_0}\tfrac{\xi(\nu)}{m_D}\left(\tfrac{p_\pi\cdot v+p_\pi\cdot v'}{p_\pi\cdot v'-\delta m_D+i\varepsilon}\right)
\end{aligned}\tag{753}$$

In SP5/SP6, the contribution from $B \to D^*\ell\nu \to D\pi\ell\nu$ was removed. Hence

$$\begin{aligned}
h_{NR} &= \tfrac{g}{2F_0}\tfrac{\xi(\nu)}{m_B m_D}\left(\tfrac{1}{p_\pi\cdot v+\delta m_B-i\varepsilon}\right)\\
A_{1NR} &= -\tfrac{g}{2F_0}\xi(\nu)(1+\nu)\left(\tfrac{1}{p_\pi\cdot v+\delta m_B-i\varepsilon}\right)\\
A_{2NR} &= \tfrac{g}{2F_0}\tfrac{\xi(\nu)}{m_B}\left(\tfrac{p_\pi\cdot v+p_\pi\cdot v'}{p_\pi\cdot v+\delta m_B-i\varepsilon}\right)\\
A_{3NR} &= 0
\end{aligned} \tag{754}$$

The resonant contribution to the form factors are

$$\begin{aligned}
h_R &= \frac{\alpha_2\rho_2(\nu)}{6F_0 m_B m_D}(\nu-1)\left(\frac{1}{p_\pi\cdot v+\delta\tilde{m}_2}-\frac{1}{p_\pi\cdot v'-\delta\tilde{m}_2}\right)\\
&\quad+\frac{\alpha_3\xi^{(1)}(\nu)}{2F_0 m_B m_D}\left(\frac{1}{p_\pi\cdot v+\delta\tilde{m}_3}-\frac{1}{p_\pi\cdot v'-\delta\tilde{m}_3}\right)
\end{aligned} \tag{755}$$

$$\begin{aligned}
A_{1R} &= -\frac{\alpha_2\rho_2(\nu)}{6F_0}(\nu^2-1)\left(\frac{1}{p_\pi\cdot v+\delta\tilde{m}_2}-\frac{1}{p_\pi\cdot v'-\delta\tilde{m}_2}\right)\\
&\quad-\frac{\alpha_3\xi^{(1)}(\nu)}{2F_0}(1+\nu)\left(\frac{1}{p_\pi\cdot v+\delta\tilde{m}_3}-\frac{1}{p_\pi\cdot v'-\delta\tilde{m}_3}\right)
\end{aligned} \tag{756}$$

$$\begin{aligned}
A_{2R} &= \frac{\alpha_1\rho_1(\nu)}{2F_0 m_B}\left(\frac{p_\pi\cdot v}{p_\pi\cdot v+\delta\tilde{m}_1}+\frac{p_\pi\cdot v'}{p_\pi\cdot v'-\delta\tilde{m}_2}\right)\\
&\quad+\frac{\alpha_2\rho_2(\nu)}{F_0 m_B}\Big\{\frac{1}{p_\pi\cdot v+\delta\tilde{m}_2}\left[\frac{1}{6}(\nu p_\pi\cdot v'-p_\pi\cdot v)+\frac{1}{3}(p_\pi\cdot v'-\nu p_\pi\cdot v)\right]\\
&\quad+\frac{1}{2}\frac{1}{p_\pi\cdot v'-\delta\tilde{m}_2}(p_\pi\cdot v-\nu p_\pi\cdot v')\Big\}\\
&\quad+\frac{\alpha_3\xi^{(1)}(\nu)}{2F_0 m_B}\left(\frac{p_\pi\cdot(v+v')}{p_\pi\cdot v+\delta\tilde{m}_3}\right)
\end{aligned} \tag{757}$$

$$\begin{aligned}
A_{3R} &= -\frac{\alpha_1\rho_1(\nu)}{2F_0 m_D}\left(\frac{p_\pi\cdot v}{p_\pi\cdot v+\delta\tilde{m}_1}+\frac{p_\pi\cdot v'}{p_\pi\cdot v'-\delta\tilde{m}_1}\right)\\
&\quad-\frac{\alpha_2\rho_2(\nu)}{F_0 m_D}\Big\{\frac{1}{p_\pi\cdot v'-\delta\tilde{m}_2}\left[\frac{1}{6}(\nu p_\pi\cdot v-p_\pi\cdot v')+\frac{1}{3}(p_\pi\cdot v-\nu p_\pi\cdot v')\right]\\
&\quad+\frac{1}{2}\frac{1}{p_\pi\cdot v+\delta\tilde{m}_2}(p_\pi\cdot v'-\nu p_\pi\cdot v)\Big\}\\
&\quad-\frac{\alpha_3\xi^{(1)}(\nu)}{2F_0 m_D}\left(\frac{p_\pi\cdot(v+v')}{p_\pi\cdot v'-\delta\tilde{m}_3}\right)
\end{aligned} \tag{758}$$

In SP5/SP6 contributions from D^{**} was removed

$$\begin{aligned}
h_R &= \tfrac{\alpha_2\rho_2(\nu)}{6F_0 m_B m_D}(\nu-1)\left(\tfrac{1}{p_\pi\cdot v+\delta\tilde{m}_2}\right) + \tfrac{\alpha_3\xi^{(1)}(\nu)}{2F_0 m_B m_D}\left(\tfrac{1}{p_\pi\cdot v+\delta\tilde{m}_3}\right)\\
A_{1R} &= -\tfrac{\alpha_2\rho_2(\nu)}{6F_0}(\nu^2-1)\left(\tfrac{1}{p_\pi\cdot v+\delta\tilde{m}_2}\right) - \tfrac{\alpha_3\xi^{(1)}(\nu)}{2F_0}(1+\nu)\left(\tfrac{1}{p_\pi\cdot v+\delta\tilde{m}_3}\right)\\
A_{2R} &= \tfrac{\alpha_1\rho_1(\nu)}{2F_0 m_B}\left(\tfrac{p_\pi\cdot v}{p_\pi\cdot v+\delta\tilde{m}_1}\right)\\
&\quad+\tfrac{\alpha_2\rho_2(\nu)}{F_0 m_B}\left\{\tfrac{1}{p_\pi\cdot v+\delta\tilde{m}_2}\left[\tfrac{1}{6}(\nu p_\pi\cdot v'-p_\pi\cdot v)+\tfrac{1}{3}(p_\pi\cdot v'-\nu p_\pi\cdot v)\right]\right\}\\
&\quad+\tfrac{\alpha_3\xi^{(1)}(\nu)}{2F_0 m_B}\left(\tfrac{p_\pi\cdot(v+v')}{p_\pi\cdot v+\delta\tilde{m}_3}\right)\\
A_{3R} &= -\tfrac{\alpha_1\rho_1(\nu)}{2F_0 m_D}\left(\tfrac{p_\pi\cdot v}{p_\pi\cdot v+\delta\tilde{m}_1}\right)\\
&\quad-\tfrac{\alpha_2\rho_2(\nu)}{F_0 m_D}\left\{\tfrac{1}{2}\tfrac{1}{p_\pi\cdot v+\delta\tilde{m}_2}(p_\pi\cdot v'-\nu p_\pi\cdot v)\right\}
\end{aligned} \tag{759}$$

Numerical values used in SP5/SP6 are

$$\begin{aligned}
&g = 0.5\\
&\alpha_1 = -1.430\\
&\alpha_2 = -0.140\\
&\alpha_3 = 0.690\\
&F_0 = 0.093\\
&\delta m_B = 0.0460 - \tfrac{0.00001}{2}i\\
&\delta m_D = 0.1421 - \tfrac{0.00006}{2}i\\
&\delta\tilde{m}_1 = 0.392 - \tfrac{1.040}{2}i\\
&\delta\tilde{m}_2 = 0.709 - \tfrac{0.405}{2}i\\
&\delta\tilde{m}_3 = 0.563 - \tfrac{0.191}{2}i\\
&\beta = 0.285\\
&\beta' = 0.280 \quad \text{for} \quad \rho_1(\nu)\\
&\beta' = 0.260 \quad \text{for} \quad \rho_2(\nu)\\
&\bar{\Lambda} = 0.750
\end{aligned} \tag{760}$$

H.6.2 $B \to D^*\pi\ell\nu$

The amplitude for this process has the general form

$$T = \kappa j_\mu \Omega^{\mu\nu}\varepsilon_{D^*\nu} \tag{761}$$

where $\varepsilon_{D^*\nu}$ is the polarization vector of the D^*.

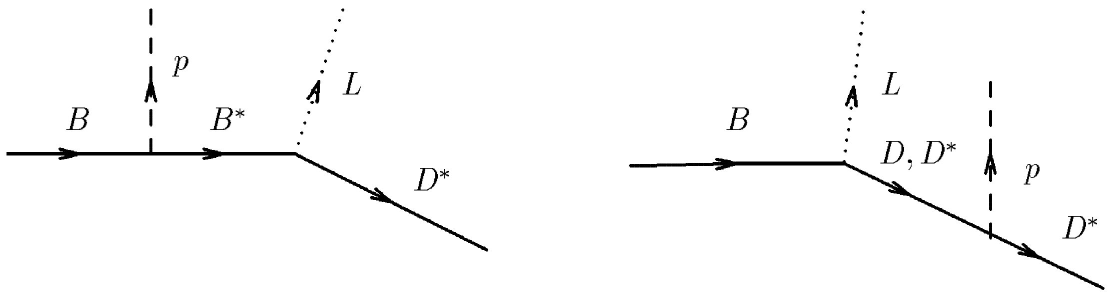

(a)

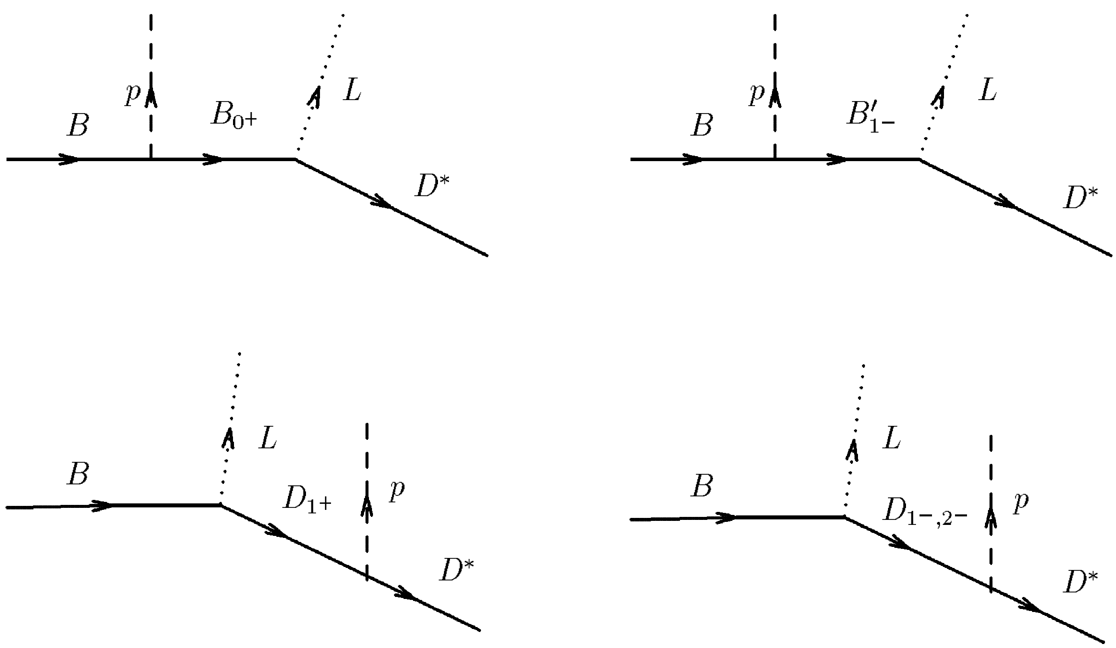

(b)

(a) shows two non-resonant decays , (b) shows four resonant decays. The non-resonant portion of $\Omega_{\mu\nu}$ is

$$
\begin{aligned}
\Omega^{NR}_{\mu\nu} \;\; = \;\; & \tfrac{g}{2F_0}\xi(\nu)\Big\{(v+v')_\mu \tfrac{p_\nu}{p\cdot v'+\delta m_D+i\varepsilon} \\
& -p^\rho \tfrac{\Theta_{\rho\sigma}(v)}{-(p\cdot v+\delta m_B)+i\varepsilon}\left[g_{\nu\sigma}(v+v')_\mu - g_{\mu\sigma}v_\nu - g_{\mu\nu}v'_\sigma + i\epsilon_{\mu\alpha\sigma\nu}(v+v')^\alpha\right] \qquad (762) \\
& +\tfrac{\Theta_{\rho\delta}(v')}{p\cdot v'+i\varepsilon}\left[-i\epsilon_{\mu\rho\alpha\beta}v'^\alpha v^\beta + g_{\mu\rho}(1+\nu) - v_\rho v'_\mu\right] i\epsilon_{\omega\nu\gamma\delta}p^\gamma v'^\omega\Big\}
\end{aligned}
$$

The resonant portion of $\Omega_{\mu\nu}$ is

$$
\begin{aligned}
\Omega^R_{\mu\nu} \;=\; & \tfrac{\alpha_1}{F_0}\rho_1(\nu)\left[-g_{\mu\nu}(\nu-1)+v'_\mu v_\nu - i\epsilon_{\mu\nu\alpha\beta}v^\alpha v'^\beta\right]\left[-\tfrac{p\cdot v}{2(-p\cdot v-\delta\tilde{m}_1)}+\tfrac{p\cdot v'}{2(p\cdot v'-\delta\tilde{m}_1)}\right] \\
& -\tfrac{\alpha_2}{3F_0}\rho_2(\nu)\Big\{p_\rho\tfrac{\Theta^{\rho\sigma}(v)}{2(-p\cdot v-\delta\tilde{m}_2)}\left[-g_{\nu\sigma}(v+v')_\mu(\nu-1)+3v_\nu v'_\mu v'_\sigma-2g_{\mu\nu}v'_\sigma(\nu-1)\right. \\
& \left.+g_{\mu\sigma}v_\nu(\nu-1)+i\epsilon_{\mu\sigma\alpha\nu}(v-v')^\alpha(1+\nu)+2i\epsilon_{\sigma\nu\alpha\beta}v'^\alpha v^\beta v'_\mu+i\epsilon_{\mu\nu\alpha\beta}v'_\sigma v'^\alpha v^\beta\right] \\
& +3p^\gamma\tfrac{\Theta^{\sigma\rho}_{\gamma\nu}(v')}{2(p\cdot v'-\delta\tilde{m}_2)+i\varepsilon}\left[v_\delta g_{\rho\mu}(\nu-1)-v_\delta v_\rho v'_\mu+i\epsilon_{\mu\delta\alpha\beta}v_\rho v^\alpha v'^\beta\right] \\
& +\tfrac{i}{2}\tfrac{\Theta^{\sigma\rho}(v)}{2(p\cdot v'-\delta\tilde{m}_2)}\epsilon_{\rho\delta\gamma\nu}p_\pi^\delta v'^\gamma \\
& \quad\times\left[i\epsilon_{\mu\sigma\alpha\beta}v^\alpha v'^\beta(\nu-1)+g_{\mu\sigma}(\nu^2-1)-v_\alpha\left(v'_\mu(2+\nu)-3v_\mu\right)\right]\Big\} \\
& +\tfrac{\alpha_3}{F_0}\xi^{(1)}(\nu)\Big\{(v+v')_\mu\tfrac{p_\nu}{2(p\cdot v'-\delta\tilde{m}_3)} \\
& +p^\rho\tfrac{\Theta_{\rho\sigma}(v)}{-2(-p\cdot v-\delta\tilde{m}_3)}\left[g_{\nu\sigma}(v+v')_\mu-g_{\mu\sigma}v_\nu-g_{\mu\nu}v'_\sigma+i\epsilon_{\mu\alpha\sigma\nu}(v+v')^\alpha\right] \\
& +\tfrac{\Theta_{\rho\delta}(v')}{2(p\cdot v'-\delta\tilde{m}_3)}\left[-i\epsilon_{\mu\rho\alpha\beta}v'^\alpha v^\beta+g_{\mu\rho}(1+\nu)-v_\rho v'_\mu\right]i\epsilon_{\omega\nu\gamma\delta}p^\gamma v'^\omega\Big\}
\end{aligned}
\tag{763}
$$

The tensor $\Omega_{\mu\nu}$ can be expressed as

$$
\begin{aligned}
\Omega_{\mu\nu} \;=\; & \tfrac{i}{2}\epsilon_{\mu\nu\rho\sigma}\left[h_1 m_B m_D v^\rho v'^\sigma + h_2 m_B v^\rho p_\pi^\sigma + h_3 m_D v'^\rho p_\pi^\sigma\right] \\
& +f_1 m_B v_\mu p_{\pi\nu}+f_2 m_D v'_\mu p_{\pi\nu}+f_3 p_{\pi\mu}p_{\pi\nu}+f_4 m_B^2 v_\mu v_\nu \\
& +f_5 m_B m_D v'_\mu v_\nu + f_6 m_B p_{\pi\mu}v_\nu \\
& +k g_{\mu\nu} \\
& +\tfrac{i}{2}\epsilon_{\mu\delta\rho\sigma}v^\delta v'^\rho p_\pi^\sigma(g_1 p_{\pi\nu}+g_2 m_B v_\nu) \\
& +\tfrac{i}{2}\epsilon_{\nu\delta\rho\sigma}v^\delta v'^\rho p_\pi^\sigma(g_3 m_B v_\mu + g_4 m_D v'_\mu + g_5 p_{\pi\mu})
\end{aligned}
\tag{764}
$$

The non-resonant contribution to the form factors are

$$
\begin{aligned}
h_{1NR} &= -\tfrac{g\xi(\nu)}{F_0 m_B m_D} \tfrac{p_\pi \cdot v}{p_\pi \cdot v + \delta m_B - i\varepsilon} \\
h_{2NR} &= -\tfrac{g\xi(\nu)}{F_0 m_B} \tfrac{1}{p_\pi \cdot v + \delta m_B - i\varepsilon} \\
h_{3NR} &= -\tfrac{g\xi(\nu)}{F_0 m_D} \left(\tfrac{1}{p_\pi \cdot v + \delta m_B - i\varepsilon} - \tfrac{1+\nu}{p_\pi \cdot v' + i\varepsilon} \right) \\
f_{1NR} &= -\tfrac{g\xi(\nu)}{2F_0 m_B} \left(\tfrac{1}{p_\pi \cdot v + \delta m_B - i\varepsilon} - \tfrac{1}{p_\pi \cdot v' + \delta m_D + i\varepsilon} \right) \\
f_{2NR} &= \tfrac{m_B}{m_D} f_{1NR} \\
f_{3NR} &= 0 \\
f_{4NR} &= 0 \\
f_{5NR} &= -\tfrac{g\xi(\nu)}{2F_0 m_B m_D} \left(1 + \tfrac{p_\pi \cdot v}{p_\pi \cdot v + \delta m_B - i\varepsilon} \right) \\
f_{6NR} &= -\tfrac{g\xi(\nu)}{2F_0 m_B} \left(\tfrac{1}{p_\pi \cdot v + \delta m_B - i\varepsilon} - \tfrac{1}{p_\pi \cdot v' + i\varepsilon} \right) \\
k_{NR} &= \tfrac{g\xi(\nu)}{2F_0} \left(\tfrac{p_\pi \cdot v' - \nu p_\pi \cdot v}{p_\pi \cdot v + \delta m_B - i\varepsilon} + \tfrac{p_\pi \cdot v - \nu p_\pi \cdot v'}{p_\pi \cdot v' + i\varepsilon} \right) \\
g_{1NR} &= 0 \\
g_{2NR} &= 0 \\
g_{3NR} &= 0 \\
g_{4NR} &= \tfrac{g\xi(\nu)}{F_0 m_D} \tfrac{1}{p_\pi \cdot v' + i\varepsilon} \\
g_{5NR} &= 0
\end{aligned}
\tag{765}
$$

The resonant contribution to the form factors are

$$
\begin{aligned}
h_{1R} &= \tfrac{\alpha_1\rho_1(\nu)}{F_0 m_B m_D}\left(\tfrac{p_\pi\cdot v}{-p_\pi\cdot v-\delta\tilde{m}_1} - \tfrac{p_\pi\cdot v'}{p_\pi\cdot v'-\delta\tilde{m}_1}\right)\\
&\quad + \tfrac{\alpha_2\rho_2(\nu)}{3F_0 m_B m_D}\left(\tfrac{p_\pi\cdot v(1+2\nu)-p_\pi\cdot v'}{p_\pi\cdot v+\delta\tilde{m}_2} + \tfrac{3}{2}\tfrac{\nu p_\pi\cdot v'-p_\pi\cdot v}{p_\pi\cdot v'-\delta\tilde{m}_2}\right)\\
&\quad - \tfrac{\alpha_3\xi^{(1)}(\nu)}{F_0 m_B m_D}\tfrac{p_\pi\cdot v}{p_\pi\cdot v+\delta\tilde{m}_3}\\
h_{2R} &= \tfrac{\alpha_2(1+\nu)\rho_2(\nu)}{3F_0 m_B}\tfrac{1}{-p_\pi\cdot v-\delta\tilde{m}_2} - \tfrac{\alpha_3\xi^{(1)}(\nu)}{F_0 m_B}\tfrac{1}{p_\pi\cdot v+\delta\tilde{m}_3}\\
h_{3R} &= \tfrac{\alpha_2\rho_2(\nu)}{3F_0 m_D}\left(\tfrac{1+\nu}{p_\pi\cdot v+\delta\tilde{m}_2} - \tfrac{\nu^2-1}{2(p_\pi\cdot v'-\delta\tilde{m}_2)}\right) - \tfrac{\alpha_3\xi^{(1)}(\nu)}{F_0 m_D}\left(\tfrac{1}{p_\pi\cdot v+\delta\tilde{m}_3} - \tfrac{1+\nu}{p_\pi\cdot v'-\delta\tilde{m}_3}\right)\\
f_{1R} &= -\tfrac{\alpha_2\rho_2(\nu)(\nu-1)}{6F_0 m_B}\left(\tfrac{1}{p_\pi\cdot v+\delta\tilde{m}_2} - \tfrac{1}{p_\pi\cdot v'-\delta\tilde{m}_2}\right) - \tfrac{\alpha_3\xi^{(1)}(\nu)}{2F_0 m_B}\left(\tfrac{1}{p_\pi\cdot v+\delta\tilde{m}_3} - \tfrac{1}{p_\pi\cdot v'-\delta\tilde{m}_3}\right)\\
f_{2R} &= \tfrac{m_B}{m_D} f_{1R}\\
f_{3R} &= 0\\
f_{4R} &= 0\\
f_{5R} &= -\tfrac{\alpha_1\rho_1(\nu)}{2F_0 m_B m_D}\left(\tfrac{p_\pi\cdot v}{p_\pi\cdot v+\delta\tilde{m}_1} + \tfrac{p_\pi\cdot v'}{p_\pi\cdot v'-\delta\tilde{m}_1}\right)\\
&\quad + \tfrac{\alpha_2\rho_2(\nu)}{2F_0 m_B m_D}\left(\tfrac{p_\pi\cdot v'-\frac{1}{3}p_\pi\cdot v(1+2\nu)}{p_\pi\cdot v+\delta\tilde{m}_2} + \tfrac{p_\pi\cdot v-\frac{1}{3}p_\pi\cdot v'(1+2\nu)}{p_\pi\cdot v'-\delta\tilde{m}_2}\right)\\
&\quad + \tfrac{\alpha_3\xi^{(1)}(\nu)}{F_0 m_B m_D}\left(\tfrac{p_\pi\cdot v}{p_\pi\cdot v+\delta\tilde{m}_3} + \tfrac{p_\pi\cdot v'}{p_\pi\cdot v'-\delta\tilde{m}_3}\right)\\
f_{6R} &= \tfrac{\alpha_2\rho_2(\nu)(\nu-1)}{6F_0 m_B}\left(\tfrac{1}{p_\pi\cdot v+\delta\tilde{m}_2} - \tfrac{1}{p_\pi\cdot v'-\delta\tilde{m}_2}\right) + \tfrac{\alpha_3\xi^{(1)}(\nu)}{2F_0 m_B}\left(\tfrac{1}{p_\pi\cdot v+\delta\tilde{m}_3} - \tfrac{1}{p_\pi\cdot v'-\delta\tilde{m}_3}\right)\\
k_R &= -\tfrac{\alpha_1\rho_1(\nu)(\nu-1)}{2F_0}\left(\tfrac{p_\pi\cdot v}{p_\pi\cdot v+\delta\tilde{m}_1} + \tfrac{p_\pi\cdot v'}{p_\pi\cdot v'-\delta\tilde{m}_1}\right)\\
&\quad - \tfrac{\alpha_2\rho_2(\nu)(\nu-1)}{3F_0}\left(\tfrac{p_\pi\cdot v'-\nu p_\pi\cdot v}{p_\pi\cdot v+\delta\tilde{m}_2} + \tfrac{p_\pi\cdot v-\nu p_\pi\cdot v'}{p_\pi\cdot v'-\delta\tilde{m}_2}\right)\\
&\quad + \tfrac{\alpha_3\xi^{(1)}(\nu)}{2F_0}\left(\tfrac{p_\pi\cdot v'-\nu p_\pi\cdot v}{p_\pi\cdot v+\delta\tilde{m}_3} + \tfrac{p_\pi\cdot v-\nu p_\pi\cdot v'}{p_\pi\cdot v'-\delta\tilde{m}_3}\right)\\
g_{1R} &= 0\\
g_{2R} &= -\tfrac{\alpha_2\rho_2(\nu)}{2F_0 m_B}\tfrac{1}{p_\pi\cdot v'-\delta\tilde{m}_2}\\
g_{3R} &= -g_{2R}\\
g_{4R} &= \tfrac{\alpha_2\rho_2(\nu)}{3F_0 m_D}\left(\tfrac{2}{p_\pi\cdot v+\delta\tilde{m}_2} - \tfrac{1+\frac{1}{2}\nu}{p_\pi\cdot v'-\delta\tilde{m}_2}\right) + \tfrac{\alpha_3\xi^{(1)}(\nu)}{F_0}\tfrac{1}{p_\pi\cdot v'-\delta\tilde{m}_3}\\
g_{5R} &= 0
\end{aligned}
\tag{766}
$$

In SP5/SP6 contributions from D^{**} was removed

$$
\begin{aligned}
h_{1R} &= \tfrac{\alpha_1\rho_1(\nu)}{F_0 m_B m_D}\left(\tfrac{p_\pi\cdot v}{-p_\pi\cdot v-\delta\tilde{m}_1}\right)+\tfrac{\alpha_2\rho_2(\nu)}{3F_0 m_B m_D}\left(\tfrac{p_\pi\cdot v(1+2\nu)-p_\pi\cdot v'}{p_\pi\cdot v+\delta\tilde{m}_2}\right)\\
&\quad -\tfrac{\alpha_3\xi^{(1)}(\nu)}{F_0 m_B m_D}\tfrac{p_\pi\cdot v}{p_\pi\cdot v+\delta\tilde{m}_3}\\
h_{2R} &= \tfrac{\alpha_2(1+\nu)\rho_2(\nu)}{3F_0 m_B}\tfrac{1}{-p_\pi\cdot v-\delta\tilde{m}_2}-\tfrac{\alpha_3\xi^{(1)}(\nu)}{F_0 m_B}\tfrac{1}{p_\pi\cdot v+\delta\tilde{m}_3}\\
h_{3R} &= \tfrac{\alpha_2\rho_2(\nu)}{3F_0 m_D}\left(\tfrac{1+\nu}{p_\pi\cdot v+\delta\tilde{m}_2}\right)-\tfrac{\alpha_3\xi^{(1)}(\nu)}{F_0 m_D}\left(\tfrac{1}{p_\pi\cdot v+\delta\tilde{m}_3}\right)\\
f_{1R} &= -\tfrac{\alpha_2\rho_2(\nu)(\nu-1)}{6F_0 m_B}\left(\tfrac{1}{p_\pi\cdot v+\delta\tilde{m}_2}\right)-\tfrac{\alpha_3\xi^{(1)}(\nu)}{2F_0 m_B}\left(\tfrac{1}{p_\pi\cdot v+\delta\tilde{m}_3}\right)\\
f_{2R} &= \tfrac{m_B}{m_D}f_{1R}\\
f_{3R} &= 0\\
f_{4R} &= 0\\
f_{5R} &= -\tfrac{\alpha_1\rho_1(\nu)}{2F_0 m_B m_D}\left(\tfrac{p_\pi\cdot v}{p_\pi\cdot v+\delta\tilde{m}_1}\right)+\tfrac{\alpha_2\rho_2(\nu)}{2F_0 m_B m_D}\left(\tfrac{p_\pi\cdot v'-\frac{1}{3}p_\pi\cdot v(1+2\nu)}{p_\pi\cdot v+\delta\tilde{m}_2}\right)\\
&\quad +\tfrac{\alpha_3\xi^{(1)}(\nu)}{F_0 m_B m_D}\left(\tfrac{p_\pi\cdot v}{p_\pi\cdot v+\delta\tilde{m}_3}\right)\\
f_{6R} &= \tfrac{\alpha_2\rho_2(\nu)(\nu-1)}{6F_0 m_B}\left(\tfrac{1}{p_\pi\cdot v+\delta\tilde{m}_2}\right)+\tfrac{\alpha_3\xi^{(1)}(\nu)}{2F_0 m_B}\left(\tfrac{1}{p_\pi\cdot v+\delta\tilde{m}_3}\right)\\
k_R &= -\tfrac{\alpha_1\rho_1(\nu)(\nu-1)}{2F_0}\left(\tfrac{p_\pi\cdot v}{p_\pi\cdot v+\delta\tilde{m}_1}\right)-\tfrac{\alpha_2\rho_2(\nu)(\nu-1)}{3F_0}\left(\tfrac{p_\pi\cdot v'-\nu p_\pi\cdot v}{p_\pi\cdot v+\delta\tilde{m}_2}\right)\\
&\quad +\tfrac{\alpha_3\xi^{(1)}(\nu)}{2F_0}\left(\tfrac{p_\pi\cdot v'-\nu p_\pi\cdot v}{p_\pi\cdot v+\delta\tilde{m}_3}\right)\\
g_{1R} &= 0\\
g_{2R} &= 0\\
g_{3R} &= -g_{2R}\\
g_{4R} &= \tfrac{\alpha_2\rho_2(\nu)}{3F_0 m_D}\left(\tfrac{2}{p_\pi\cdot v+\delta\tilde{m}_2}\right)\\
g_{5R} &= 0
\end{aligned}
\tag{767}
$$

Numerical values used in SP5/SP6 are

$$\begin{aligned}
&g = 0.5\\
&\alpha_1 = -1.430\\
&\alpha_2 = -0.140\\
&\alpha_3 = 0.690\\
&F_0 = 0.093\\
&\delta m_B = 0.0460 - \tfrac{0.00001}{2} i\\
&\delta m_D = 0.1421 - \tfrac{0.00006}{2} i\\
&\delta \tilde{m}_1 = 0.392 - \tfrac{1.040}{2} i\\
&\delta \tilde{m}_2 = 0.709 - \tfrac{0.405}{2} i\\
&\delta \tilde{m}_3 = 0.563 - \tfrac{0.191}{2} i\\
&\beta = 0.285\\
&\beta' = 0.280 \quad \text{for} \quad \rho_1(\nu)\\
&\beta' = 0.260 \quad \text{for} \quad \rho_2(\nu)\\
&\bar{\Lambda} = 0.750
\end{aligned} \tag{768}$$

References

[1] N. Cabbibo, *"Unitary Symmetry and Leptonic Decays"*, Phys. Rev. Lett. **10**, 531 (1963).

[2] M. Kobayashi and T. Maskawa, *"CP-Violation in the Renormalizable Theory of Weak Interaction"*, Prog. Theor. Phys. **49**, 652 (1973).

[3] BABAR Collaboration, *"Measurement of the Relative Branching Fractions of $\bar{B} \to D/D^*/D^{**}\ell^-\bar{\nu}_\ell$ Decays in Events with a Fully Reconstructed B Meson"*, Phys. Rev. D - Rapid Communications **XX**, xxxx (2008), hep-ex/0703027, BAD1687.

[4] BABAR Collaboration, *"A Measurement of the Branching Fractions of Exclusive $\bar{B} \to D^{(*)}(\pi)\ell^-\bar{\nu}_\ell$ Decays in Events with a Fully Reconstructed B Meson"*, Phys. Rev. Lett. **XX**, xxxx (2008), arXiv:0712.3503v1 [hep-ex], BAD1889.

[5] BELLE Collaboration, K. Abe *et al.*, *"Determination of $|V_{cb}|$ using the semileptonic decay $\bar{B}^0 \to D^{*+}e^-\bar{\nu}$"*, Phys. Lett. B**526**, 247 (2002), hep-ex/0111060.

[6] DELPHI Collaboration, P. Abreu *et al.*, *"Measurement of V_{cb} from the decay process $\bar{B}^0 \to D^{*+}\ell^-\bar{\nu}$"*, Phys. Lett. B**510**, 55 (2001), hep-ex/0104026.

[7] BABAR Collaboration, B. Aubert *et al.*, *"Measurement of the $\bar{B}^0 \to D^{*+}l^-\bar{\nu}_l$ Decay Rate and $|V_{cb}|$"*, Phys. Rev. D**71**, 051502 (2005), hep-ex/0408027.

[8] OPAL Collaboration, G. Abbiendi *et al.*, *"Measurement of $|V_{cb}|$ using $B^0 \to D^*l\nu$ decays"*, Phys. Lett. B**482**, 15 (2000), hep-ex/0003013.

[9] ALEPH Collaboration, D. Buskulic *et al.*, *"Measurements of $|V_{cb}|$, form-factors and branching fractions in the decays $\bar{B}^0 \to D^{*+}l^-\bar{\nu}_l$ and $\bar{B}^0 \to D^+l^-\bar{\nu}_l$"*, Phys. Lett. B**395**, 373 (1997).

[10] DELPHI Collaboration, J. Abdallah *et al.*, *"Measurement of $|V_cb|$ using the semileptonic decay $\bar{B}^0_d \to D^{*+}l^-\bar{\nu}_l$"*, European. Phys. J. C**33**, 213 (2004), hep-ex/0401023.

[11] CLEO Collaboration, N. E. Adam *et al.*, *"Determination of the $\bar{B} \to D^*l\bar{\nu}$ Decay Width and $|V_{cb}|$"*, Phys. Rev. D**67**, 032001 (2003), hep-ex/0210040.

[12] Particle Data Group, W. M. Yao *et al.*, *"Review of Particle Physics"*, J. Phys. G**33**, 1 (2006); URL: http://pdg.lbl.gov (2007).

[13] BELLE Collaboration, K. Abe *et al.*, *"Measurement of $\mathcal{B}(\bar{B} \to D^+l^-\bar{\nu})$ and Determination of $|V_{cb}|$"*, Phys. Lett. B**526**, 258 (2002), hep-ex/0111082.

[14] CLEO Collaboration, J. Bartelt *et al.*, *"Measurement of the $B \to D\ell\nu$ Branching Fractions and Form Factor"*, Phys. Rev. Lett.**82**, 3746 (2003), hep-ex/9811042.

[15] BABAR Collaboration, B. Aubert *et al.*, *"Measurement of Semileptonic B Decays into Orbitally-Excited Charmed Mesons with BaBar Detector at SLAC"*, BAD1565 (2006).

[16] DELPHI Collaboration, J. Abdallah *et al.*, *"Determination of heavy quark non-perturbative parameters from spectral moments in semileptonic B decays"*, European. Phys. J. C**45**, 35 (2006), hep-ex/0510024.

[17] BELLE Collaboration, Liventsev, D. *et al.*, *"Measurement of the branching fractions for* $B^- \to D^{(*)+}\pi^- l^- \bar{\nu}$ *and* $\bar{B}^0 \to D^{(*)0}\pi^+ l^- \bar{\nu}$*"*, Phys. Rev. D**72**, 051109 (2005), hep-ex/0507060.

[18] BABAR Collaboration, Semileptonic Analysis Working Group, http://www.slac.stanford.edu/BFROOT/www/Physics/Analysis/AWG/Semileptonic/Reweighting2007.html.

[19] BABAR Collaboration, B. Aubert *et al.*, *"The BABAR Detector"*, Nucl. Instrum. Meth. **A479**, 1 (2002), hep-ex/0105044.

[20] *"PEP-II Conceptual Design Report"*, SLAC-0418 (2002).

[21] D. J. Lange, *"The EvtGen particle decay simulation package"*, Nucl. Instrum. Meth. **A462**, 152 (2001).

[22] Geant 4 Collaboration, S. Agostinelli *et al.*, *"GEANT4: A Simulation toolkit"*, Nucl. Instrum. Meth. **A506**, 250 (2003).

[23] W. D. Hulsbergen, *"Decay Chain Fitting with a Kalman Filter"*, Nucl. Instrum. Meth. **A552**, 566 (2005).

[24] BABAR Collaboration, B. Aubert *et al.*, *"Observation of the Semileptonic Decays* $B \to D^* \tau \bar{\nu}_\tau$ *and Evidence for* $B \to D \tau \bar{\nu}_\tau$*"*, Phys. Rev. D **76**, 051104 (2007), arXiv:0709.1698v1 [hep-ex].

[25] BELLE Collaboration, A. Matyia *et al.*, *"Observation of* $B^0 \to D^{*-}\tau^+\nu_\tau$ *decay at Belle"*, arXiv:0706.4429 [hep-ex].

[26] Heavy Flavor Averaging Group (HFAG), http://www.slac.stanford.edu/xorg/hfag/index.html.

[27] Babar Collaboration, B. Barate*et al.*, *"Study of inclusive charm production in B meson decays with the BaBar experiment"*, Babar Analysis Document 1234, (2006).

[28] Babar Collaboration, B. Barate*et al.*, *"Study of Inclusive* B^- *and* $\bar{B}^0$ *Decays to Flavor-Tagged* D*,* D_s *and* Λ_c^+*"*, Phys. Rev. D **75**, 072002 (2007), hep-ex/0606026.

[29] BELLE Collaboration, K. Abe *et al.*, *"Observation of the* $D_1(2420) \to D\pi^+\pi^-$ *decays"*, Phys. Rev. Lett. **94**, 221805 (2005), hep-ex/0410091.

[30] Babar Collaboration, B. Aubert *et al.*, *"Measurement of the Absolute Branching Fraction of $D^0 \to K^-\pi^+$ Decays"*, Phys. Rev. Lett. , (2007), arXiv:0704.2080v2 [hep-ex].

[31] CLEO Collaboration, S. Dobbs *et al.*, *"Measurement of Absolute Hadronic Branching Fractions of D Mesons and $e^+e^- \to D\bar{D}$ Cross Sections at the* $\psi(3770)$ ", Phys. Rev. D , (2007), arXiv:0709.3783v2[hep-ex].

[32] XX *et al.*, *"Beam energy"*, BADxxxx.

[33] D. Scora and N. Isgur., Phys. Rev. D**52**, 2783 (1995), *"Semileptonic Meson Decays in the Quark Model: An Update"*, hep-ph/9503486.

[34] N. Isgur, D. Scora, B. Grinstein and M. B. Wise., *"Semileptonic Meson Decays in the Quark Model"*, Phys. Rev. D**39**, 2783 (1989).

[35] M. Neubert, *"Heavy Quark Symmetry"*, Phys. Rept. **245**, 259 (1994), hep-ph/9306320.

[36] J. D. Richman and P. R. Burchat., *"Leptonic and Semileptonic Decays of Charm and Bottom Hadrons"*, Rev. Mod. Phys. **67**, 893 (1995), hep-ph/9508250.

[37] M. Okamoto *et al.*, *"Semileptonic $D \to \pi/K$ and $B \to \pi/D$ decays in 2+1 flavor lattice QCD"*, Nucl. Phys. Proc. Suppl. **140**, 461 (2005), hep-lat/0409116.

[38] I. Caprini, L. Lellouch and M.Neubert., *"Dispersive Bounds on the Shape of $B \to D^{(*)} l\nu$ Form Factors"*, Nucl. Phys. B**530**, 153 (1998), hep-ph/9712417.

[39] S. Hashimoto *et al.*, *"Lattice calculation of the zero recoil form-factor of $\bar{B} \to D^*\ell\bar{\nu}$: Toward a model independent determination of $|V_{cb}|$"*, Phys. Rev. D**66**, 014503 (2002), hep-ph/0110253.

[40] BABAR Collaboration, B. Aubert *et al.*, *"Measurements of the B to D^* Form Factors Using the Decay $B^0 \to D^* e\nu_e$"*, Phys. Rev. D**74**, 092004 (2006), hep-ex/0602023; BAD 482.

[41] BABAR Collaboration, B. Aubert *et al.*, *"Determination of the Form Factors for the Decay $B^0 \to D^{*-}\ell^+\nu_\ell$ and of the CKM Matrix Element $|V_{cb}|$"*, Phys. Rev. D**77**, 032002 (2008), arXiv:0705.4008v2 [hep-ex], hep-ex/0607076.

[42] A. K. Leibovich, Z. Ligeti, I. W. Stewart, M. B. Wise., *"Model independent results for $B \to D_1(2420)\ell\bar{\nu}$ and $B \to D_2^*(2460)\ell\bar{\nu}$ at order $\Lambda_{QCD}/m_{c,b}$"*, Phys. Rev. Lett.**78**, 3995 (1997), hep-ph/9703213.

[43] A. K. Leibovich, Z. Ligeti, I. W. Stewart, M. B. Wise., *"Semileptonic B decays to excited charmed mesons"*, Phys. Rev. D**57**, 308 (1998), hep-ph/9705467.

[44] J. L. Goity, *"Chiral perturbation theory for SU(3) breaking in heavy meson systems"*, Phys. Rev. D**46**, 3929 (1992), hep-ph/9206230.

[45] J. L. Goity and W. Roberts., *"Soft Pion Emission in Semileptonic B-Meson Decays"*, Phys. Rev. D**51**, 3459 (1995), hep-ph/9406236.

[46] BABAR Collaboration, B. Aubert *et al.*, *"Measurements of the Decay $B^- \rightarrow D^{*0} e^- \bar{\nu}_e$"*, Phys. Rev. Lett.**XX**, xxxx (2008), arXiv:0712.3493v2 [hep-ex].

[47] Babar Collaboration, B. Aubert *et al.*, *"Measurement of the Electron Energy Spectrum and its Moments in Inclusive $B \rightarrow Xe\nu$ Decays"*, Phys. Rev. D**69**, 111104 (2004), hep-ex/0403030.

[48] CLEO Collaboration, B. Bartelt *et al.*, *"Observation of the radiative decay $D^{*+} \rightarrow D^+\gamma$"*, Phys. Rev. Lett. **80**, 3919 (1998), hep-ex/9711011.

[49] F. Bernlochner *et al.*, *"On the Effects of Additional Bremsstrhlung due Detector Geometry Uncertainties on Monte Carlo Simulatated Electron Energy Spectra"*, Babar Analysis Document 1911.

[50] Babar Analysis Document 1465.

[51] *"$B \rightarrow D_s K \ell \nu$"*.

[52] BABAR Collaboration, P. F. Harrison, ed. *et al.*, *"The BABAR Physics Book"*, (1997), SLAC-R-504.